LEABHARLANN CHOLÁISTE NA TRÍONÓIDE, BAILE ÁTHA CLIATH | TRINITY COLLEGE LIBRARY DUBLIN
Ollscoil Átha Cliath | The University of Dublin

Terms and Conditions of Use of Digitised Theses from Trinity College Library Dublin

Copyright statement

All material supplied by Trinity College Library is protected by copyright (under the Copyright and Related Rights Act, 2000 as amended) and other relevant Intellectual Property Rights. By accessing and using a Digitised Thesis from Trinity College Library you acknowledge that all Intellectual Property Rights in any Works supplied are the sole and exclusive property of the copyright and/or other IPR holder. Specific copyright holders may not be explicitly identified. Use of materials from other sources within a thesis should not be construed as a claim over them.

A non-exclusive, non-transferable licence is hereby granted to those using or reproducing, in whole or in part, the material for valid purposes, providing the copyright owners are acknowledged using the normal conventions. Where specific permission to use material is required, this is identified and such permission must be sought from the copyright holder or agency cited.

Liability statement

By using a Digitised Thesis, I accept that Trinity College Dublin bears no legal responsibility for the accuracy, legality or comprehensiveness of materials contained within the thesis, and that Trinity College Dublin accepts no liability for indirect, consequential, or incidental, damages or losses arising from use of the thesis for whatever reason. Information located in a thesis may be subject to specific use constraints, details of which may not be explicitly described. It is the responsibility of potential and actual users to be aware of such constraints and to abide by them. By making use of material from a digitised thesis, you accept these copyright and disclaimer provisions. Where it is brought to the attention of Trinity College Library that there may be a breach of copyright or other restraint, it is the policy to withdraw or take down access to a thesis while the issue is being resolved.

Access Agreement

By using a Digitised Thesis from Trinity College Library you are bound by the following Terms & Conditions. Please read them carefully.

I have read and I understand the following statement: All material supplied via a Digitised Thesis from Trinity College Library is protected by copyright and other intellectual property rights, and duplication or sale of all or part of any of a thesis is not permitted, except that material may be duplicated by you for your research use or for educational purposes in electronic or print form providing the copyright owners are acknowledged using the normal conventions. You must obtain permission for any other use. Electronic or print copies may not be offered, whether for sale or otherwise to anyone. This copy has been supplied on the understanding that it is copyright material and that no quotation from the thesis may be published without proper acknowledgement.

Analysis and development of the recombinant Semliki Forest virus vector as a cancer gene therapy agent

---

Thesis submitted to the

University of Dublin,

Trinity College

for the Degree of

Doctor of Philosophy

by

Anne Marie Murphy

Department of Microbiology,

Moyne Institute of Preventive Medicine,

Trinity College, Dublin

October 2000

TRINITY COLLEGE
27 APR 2001
LIBRARY DUBLIN
Thesis
6129

FOR MY PARENTS

Declaration

This thesis is submitted by the undersigned to the University of Dublin, Trinity College for the examination of Doctorate of Philosophy. The work herein is entirely my own work and has not been submitted as an exercise for a degree to any other university. The librarian of Trinity College Dublin has my permission to lend or copy this thesis upon request.



Anne Marie Murphy

Table of Contents

	Page #
Acknowledgements	*(i)*
Abbreviations	*(ii)*
Summary	*(iii)*
1. General Introduction	**1**
1.1 Apoptosis	**3**
1.1.1 Death receptors, the direct physical activators of apoptosis	4
1.1.2 Role of the mitochondrion in apoptosis induction	7
1.1.3 Caspases, the executioners of apoptotic cell death	8
1.1.3.1 Known caspase substrates	11
1.1.4 Regulation of apoptosis; the p53 signalling pathways	13
1.1.5 Regulation of apoptosis; the Bcl-2 family	14
1.1.6 Viral infection and apoptosis induction	18
1.2 Cancer gene therapy	**20**
1.2.1 Molecular chemotherapy	20
1.2.2 Genetic immunomodulation	23
1.2.3 Mutation compensation	25
1.2.3.1 Ablation of activated oncogenes	26
1.2.3.2 Augmentation of tumour suppressor genes	27

1.3 Vectors for cancer gene therapy **30**

1.3.1 Viral vectors 30

1.3.1.1 Adenovirus vectors 31

1.3.1.2 Retrovirus vectors 33

1.3.1.3 Adeno-associated virus and other DNA viruses 34

1.3.2 Non-viral (synthetic) gene therapy 35

1.4 Semliki Forest virus **37**

1.4.1 Structure of the SFV virion 37

1.4.2 Genome structure and organisation 38

1.4.3 The Alphavirus replication cycle 39

1.4.3.1 Viral entry 39

1.4.3.2 Viral RNA replication 40

1.4.3.3 Translation of subgenomic RNA and viral release 43

1.4.4 Effects of alphaviral replication in infected cells 45

1.4.5 Pathogenesis of SFV 49

1.5 Alphaviral expression systems **52**

1.5.1 SFV vectors in vaccine development and gene therapy 56

1.6 Objectives of study **58**

2. Recombinant SFV particle production, expression and apoptosis induction in the BHK-21 cell line **59**

2.1 Introduction 59

2.2 Experimental procedures 61

2.3 Results 83

2.4 Discussion 94

3. rSFV-mediated inhibition of human lung carcinoma cell growth *in vitro*, by apoptosis induction. **99**

3.1 Introduction 99

3.2 Experimental procedures 101

3.3 Results 112

3.4 Discussion 126

4. Therapeutic efficiency of rSFV vector particles using an *in vivo* lung cancer model **132**

4.1 Introduction 132

4.2 Experimental procedures 134

4.3 Results 144

4.4 Discussion 154

5. SFV-mediated overexpression of pro-apoptotic Bax further enhances the cytotoxic potential of the vector for treatment of apoptosis-resistant cancer **162**

5.1 Introduction 162

5.2 Experimental procedures 164

5.3 Results 179

5.4 Discussion 201

6. General discussion 212

7. References 223

8. Publications and Presentations 266

First and foremost, I'd like to thank my supervisor Prof. Greg Atkins, for his excellent supervision and assistance, ideas and encouragement especially when work was not going according to plan! Thanks for everything.

Huge thanks also to Prof. Brian Sheahan, University College, Dublin, for his never-ending encouragement, enthusiasm for my work and for all his help with pathology.

To all in the virology lab, past and present. To Mags and Sareen, two excellent post-docs who have helped me to get the work done, and who have been such a brilliant laugh, both in and out of the lab. Also to Bronagh, Lisa, Jamie, Christopher, Brian and Alan for lots of fun and interesting discussions! Now that the boys are taking over the lab next year, I think its a good job that I'm out of there! A special thanks to Dot, for being so wonderful with everything, and I'm only waiting to hear from you on my 35th birthday!

Thanks to the Health Research Board and the Irish Cancer Society for funding me over the past three years.

A special thanks to everyone in the Moyne, for your friendship and for making the Moyne such a fun place to work in.

To everyone in the prep-room, particularly Joe and Paddy for help with all those cages, for always being in top form and for cheering everyone up on those dreary Monday mornings.

To the people in Bioresources, especially Peter, Cormac and Caroline.

To everyone in Peter Liljeström's lab in Stockholm, Sweden, for putting up with me over those 2 weeks in November 1998. A special word of thanks to Dr. Marina Fleeton, who provided me with all I needed to know about particles, and without whose assistance I would not be writing this thesis.

For all my friends at home in Cork, especially Tina (who is in Dublin!), Moira, Brian, Louise, Chris and Ellie and all the lads, for the best nights out and for your never-ending support and friendship. Thanks also to Dr. Kate Fitzgerald, for your help and encouragement and for the loan of your excellent thesis.

To my parents, Vincent and Sheila Murphy, for everything, and to Catriona, Aidan and Karen, and Uncle DanJoe, for all your love and encouragement, both at home and in Dublin.
Yes lads, I'm coming home for good!

Most especially, I would like to thank Pat, the reason I do anything, for your love, patience, support, (help in the lab!), and for being an unending source of happiness.

Ad – adenovirus

ASO – antisense oligonucleotides

ATCC – American type culture collection

BHK – baby hamster kidney

bp – base pair

CEA – carcinoembryonic antigen

CMV – cytomegalo virus

CNS - central nervous system

cpe – cytopathic effect

cpm – counts per minute

DAB – diaminobenzidine

DAPI – 4, -6, diamidino-2-phenylindole

ddNTP – dideoxynucleoside triphosphates

dNTP – deoxynucleoside triphosphates

dsRNA – double stranded ribonucleic acid

DTT – Dithiotreitol

EBV – Epstein Barr virus

ECACC – European collection of animal cultures

EDTA - ethylenediaminetetra-acetic acid

ELISA – enzyme linked immunosorbent assay

ER – endoplasmic reticulum

FADD – Fas-associated death domain

FITC – fluorescein isothiocyanate

g - gravitational force

H & E – Haematoxylin and Eosin

HCV – Hepatitis C virus

hepes – N-2-hydroxyethyl-piperazine-N'-2-ethanesulphonic acid

HIV - human immunodeficiency virus

HLA – human lymphotrophic antigen

HPV – Human Papilloma virus

h.p.i. – hours post infection

HRP – horseradish peroxidase

ICC - immunocytochemistry

Ig – immunoglobin

IκB – Inhibitor binding protein κB

IL - interleukin

IPTG – isopropyl- -D-galactopyranoside

M - molar

MAb – monoclonal antibody

MCS – multiple cloning site

MHC – major histocompatibility complex

Moi - multiplicity of infection

mRNA – messenger RNA

NFκB – Nuclear factor kappa B

NK – Natural killer cells

NSCLC – non-small cell lung cancer

NTR – nontranslated region

PBS – phosphate buffered saline

PCa – prostate cancer

PCD – programmed cell death

PCR – polymerase chain reaction

PDGF – platelet-derived growth factor

p.e. – post-electroporation

PFU – plaque forming units

p.i. – post-infection

PI – propidium iodide

PKR – interferon-inducible dsRNA-activated protein kinase

pSFV-EGFP – recombinant EGFP-expressing plasmid DNA

r – recombinant

rSFV-EGFP – recombinant EGFP-expressing SFV virus particles

RCV – replication-competent virus

RNase – ribonuclease

SC – subcutaneously

SCLC – small cell lung cancer

SFV – Semliki Forest virus

SV – Sindbis virus

TCA – trichloroacetic acid

TNF – Tumour necrosis factor

TRADD – TNF receptor-associated death domain

TRITC – rhodamine isothiocyanate

TRAF – TNF receptor associated factor

VEE – Venezuelan equine encephalitis

X-gal – 5-bromo-4-chloro-3-indolyl-D-galactopyranoside

Increased understanding of the molecular pathogenesis of cancer has shown that its accumulation is the result of multiple genetic alterations. Cancer is a disease of altered genes, with the most predominantly altered appearing in a number of dominant cellular proto-oncogenes and tumour suppressor genes. Disruption of these proteins and their associated pathways leads to deregulation of crucial pathways involved in the maintenance of cell growth and division, homeostasis and induction of programmed cell death or apoptosis. In fact, many of the oncogenes and anti-oncogenes mutated or deleted in carcinogenesis play crucial roles in the regulation and execution of the normal cell suicide pathways in the cell.

The objective of cancer gene therapy is to correct these lesions at the molecular level sufficiently to abrogate tumourigenicity and mediate a therapeutic effect. Mutation compensation can take the form of tumour suppressor gene replacement, with wild-type *p53* gene replacement the most common, or oncogene ablation, commonly using antisense technology, which target the activated oncogene products for degradation. For many B cell malignancies and in prostate cancers, the oncogene most frequently targeted for gene therapy is the anti-apoptotic *Bcl-2* gene, which is known to be upregulated in these malignancies.

In terms of delivery, the heterologous gene for cancer therapy must reach the target cell population, transduce the cell, facilitate transcription and translation of its protein product and mediate its therapeutic effect, either in cytosol or in the nucleus. Viral vector delivery systems represent the best available system to date for cancer gene therapy, although non-viral vectors have had limited success. Retroviral and adenoviral delivery systems are routinely used, primarily due to their naturally high transfection efficiencies. However, neither vector is without its limitations, a disadvantage which has greatly limited the therapeutic potential of gene therapy-based regimes in cancer treatment.

In this study, we introduce the recombinant Semliki Forest virus vector (rSFV) as a cancer therapy agent for the treatment of both lung and prostate malignancies. rSFV infectious particles, derived from a 12 kb positive-sense RNA virus, facilitates the expression of the heterologous gene when 3' one-third of the viral genome, containing viral structural proteins, is replaced with the foreign gene of choice, and is expressed at high levels. SFV helper RNA molecules facilitate the packaging of recombinant RNA molecules in the cell following co-trasnfection with RNAs that supply the structural proteins *in trans*. In contrast to other cancer therapy vectors, rSFV particles have the major advantage of containing a potent pro-apoptotic function, and induces programmed cell death in infected cells, a function which has been mapped to the non-structural region of the viral genome, or as a consequence of viral replication.

rSFV vector particles, containing the non-cytotoxic reporter gene, *enhanced green fluorescent protein* (*EGFP*), were shown to greatly inhibit the growth and proliferation of the non-tumourigenic BHK-21 cell line and the non-small cell lung cancer (NSCLC) cell line, H358a *in vitro*. Inhibition of cell growth was shown to be a result of apoptosis induction in both cell lines. H358a cells lack functional *p53* activity, and rSFV-EGFP virus-induced apoptotic cell death was therefore *p53*-independent. Growth of H358a cells as three-dimensional multicellular tumour spheroids, an *in vitro* model of tumour growth, was shown to be significantly inhibited following infection of these masses with rSFV-EGFP virus particles.

The potent pro-death efficiencies of rSFV for the H358a cell line *in vitro* was reproduced *in vivo*. rSFV-EGFP virus treatment of H358a NSCLC tumours in nude mice greatly inhibited tumour growth compared to controls, and the effects were dose-dependent. rSFV-EGFP virus treatment mediated significant tumour regression, and in a number of cases, the subcutaneous tumours completely regressed. Pathological analysis revealed large areas of apoptotic cell death in the early stages following treatment, followed 2-3 days later with large areas of necrotic cell death.

In an attempt to further enhance the cytotoxicity of the vector, pro-apoptotic *Bax*, known to be a potent inhibitor of the Bcl-2 oncoprotein, was cloned into the SFV expression system. A *Bcl-2*-overexpressing cell line AT3-Bcl-2, derived from a rat prostatic adenocarcinoma, was shown to resist apoptotic cell death induced by replication-competent SFV-4 virus for at least 2 days before succumbing to cell death. Overexpression of *Bax* in the AT3-Bcl-2 cells by electroporation of SFV-Bax RNA, was shown to inhibit *Bcl-2*-mediated suppression of SFV-induced cell death and induce apoptosis without a delay. The potent pro-apoptotic abilities of the SFV-Bax RNA construct however, proved to be disadvantageous in the generation of rSFV-Bax virus particles, and titres remained 200-fold lower than standard rSFV-EGFP virus concentrations. Thus, the cytotoxicity of this vector was somewhat underestimated due to lower viral infections, resulting in less dramatic growth inhibitory effects on the AT3-Bcl-2 cell line *in vitro* and *in vivo*. In the nude mouse xenograft however, there was a significant inhibition of AT3-Bcl-2 tumour growth over the rSFV-EGFP virus particles despite the lower titres.

Thus, the potent pro-apoptotic capabilities of rSFV particles can be used as effective gene therapy agents for the elimination of malignant cells. A strategy to increase rSFV-Bax viral titres, and a targeted tumour-specific delivery mechanism may serve to produce a cancer therapy system which is more potent and efficient than any of the conventional systems used to date.

List of figures

Chapter 1

1.1 Pro-apoptotic and pro-survival signalling by death factors.

1.2 Role of mitochondria in apoptosis induction.

1.3 Proteolytic processing and activation of caspases.

1.4 Phylogenetic relationship of the mammalian caspase family.

1.5 Classification of Bcl-2 family members based on domain organisation.

1.6 Model of Bcl-2 family regulation of mitochondrial function and apoptosis induction.

1.7 Structure of the SFV virion.

1.8 Schematic representation of the SFV genome.

1.9 Processing of SFV structural proteins and viral release.

1.10 Alphaviral vectors.

1.11 Schematic of rSFV particle production.

1.12 Schematic of rSFV constructs utilised in this study.

Chapter 2

2.1 Construction of the pSFV1-EGFP expression clone.

2.2 Preparation of SFV expression vector and EGFP PCR product for ligation.

2.3 *In vitro* RNA transcription of putative pSFV1-EGFP clones.

2.4 SFV-4 virus-induced apoptotic cell death in BHK-21 cells, as assessed by morphological analysis.

2.5 Apoptosis induction in BHK-21 cells following infection with infectious SFV-4 virus, as assessed by DNA fragmentation, using agarose gel electrophoresis.

2.6 SFV-4-mediated apoptosis in BHK-21 cells, as assessed by chromosomal DNA fragmentation, using TUNEL.

2.7 Screening for pSFV1-EGFP recombinant clones by restriction digestion.

2.8 The orientation of *EGFP* inserts within the pSFV-1 vector, determined by *Not1* digestion

2.9 Screening for EGFP expression from recombinant clones by direct epifluorescence in BHK-21 cells.

2.10 Apoptosis induction in BHK-21 cells following transfection with *in vitro*-transcribed SFV1-EGFP RNA.

2.11 *In vitro* RNA transcription for rSFV-EGFP virus particle production.

2.12 Optimisation of *in vitro* SP6 RNA transcription for rSFV virus particle production.

2.13 Dual detection of β-galactosidase and SFV E2 proteins in particle-producing cells.

2.14 Transduction efficiency of rSFV-EGFP virus particles in BHK-21 cells.

2.15 Growth and viability of BHK-21 cells following infection with rSFV virus particles, as determined by trypan blue exclusion.

2.16 Effect of multiple rSFV virus particle infections on BHK-21 cell viability, as determined by trypan blue exclusion.

2.17 Growth and viability of BHK-21 cells following infection with rSFV virus particles, as determined by ^{3}H incorporation.

2.18 Apoptosis induction in BHK-21 cells following infection with rSFV recombinant particles, as assessed by DNA fragmentation, using agarose gel electrophoresis.

2.19 rSFV virus particle-mediated apoptosis in BHK-21 cells, as assessed by chromosomal DNA fragmentation, using TUNEL.

Chapter 3

3.1 Growth and morphology of NCI-H358a cells.

3.2 Infectious SFV-4 virus-mediated apoptosis in H358a cells, as assessed by chromosomal DNA fragmentation, using agarose gel electrophoresis.

3.3 SFV-4 virus-mediated apoptosis in H358a cells, as assessed by chromosomal DNA fragmentation, using TUNEL.

3.4 Transfection with recombinant SFV RNA induces apoptotic cell death in H358a cells.

3.5 The SFV vector backbone, and not reporter gene expression, mediates H358a apoptosis.

3.6 Infection efficiency of rSFV-EGFP virus particles in H358a cells.

3.7 Optimisation of SRB colorimetric analysis for the H358a cell line *in vitro*.

3.8 Optimisation of One Solution cell proliferation assay for the H358a cell line.

3.9 Cell viability of H358a cells following infection with rSFV virus particles, as determined by trypan blue exclusion.

3.10 Cell viability of H358a cells following infection with rSFV virus particles, as determined by sulphorhodamine B colorimetric analysis.

3.11 Cell viability of H358a cells following infection with rSFV virus particles, as determined by ^{3}H thymidine incorporation.

3.12 Cytopathic effect in H358a cell monolayers following infection with rSFV-EGFP virus particles.

3.13 rSFV virus particle-induced programmed cell death in H358a cells, as assessed by chromosomal DNA fragmentation, using agarose gel electrophoresis.

3.14 rSFV virus particle-induced programmed cell death in H358a cells, as assessed by chromosomal DNA fragmentation, using TUNEL.

3.15 rSFV virus particle-induced programmed cell death in H358a cells, as assessed by morphological analysis, using DAPI.

3.16 H358a cell monolayers develop into 3-D multicellular tumour spheroid masses.

3.17 Morphology of H358a spheroids *in vitro*.

3.18 rSFV virus particles can infect H358a three-dimensional cultures.

3.19 Proliferation of H358a spheroids following infection with rSFV-EGFP virus particles, as assessed by ^{3}H thymidine incorporation.

3.20 Proliferation of H358a spheroids following infection with rSFV-EGFP virus particles, as assessed by the One Solution cell proliferation assay.

3.21 rSFV virus particle infection inhibits initial *in vitro* three-dimensional H358a spheroid formation.

Chapter 4

4.1 H358a tumour formation *in vivo*.

4.2 Immunohistochemical analysis of H358a tumours *in vivo*, using an anti-cytokeratin antibody.

4.3 Immunohistochemical analysis of H358a tumours, using anti-CA-19-9 antibody.

4.4 TUNEL reactivity within H358a tumours *in vivo*.

4.5 *In vitro* RNA transcription for high titre rSFV-EGFP virus particle production.

4.6 Effects of rSFV-EGFP virus particle treatment on NSCLC growth *in vivo.*

4.7 Effects of two cycles of rSFV-EGFP virus particle treatment on NSCLC growth *in vivo*.

4.8 Subcutaneous H358a tumour growth as a *nu/nu* mouse xenograft and following rSFV virus particle therapeutic intervention.

4.9 Two cycles of rSFV-EGFP virus particle treatment induce complete regression of *in vivo* H358a tumours.

4.10 Expression of EGFP within H358a tumours *in vivo*.

4.11 Histology of H358a tumours following treatment with rSFV virus particles.

4.12 Histology of H358a tumours, 30 days following treatment with rSFV virus particles.

4.13 TUNEL reactivity within H358a tumours following treatment with rSFV virus particles.

4.14 Composite representation of EGFP expression and TUNEL reactivity following one intratumoural rSFV-EGFP virus injection.

Chapter 5

5.1 Construction of the pSFV-1-Bax-α expression clone.

5.2 PCR amplification of *HABax* and *Bax* gene constructs from pSG5-HABax and pSG5-bax plasmids, respectively.

5.3 Preparation of *HABax* and *Bax* gene fragments for ligation .

5.4 Construction of the pSFV1-HABax-α expression clone.

5.5 *In vitro* transcription of pSFV1-Bax-α clones by SP6 RNA polymerase.

5.6 *In vitro* transcription of pSFV1-HABax-α by SP6 RNA polymerase.

5.7 Nucleotide and deduced aa sequence of human *Bax-α* from the pSG5-Bax plasmid.

5.8 Amino acid sequence alignment of the Bax-α protein with others from the database.

5.9 Screening for pSFV1-Bax-α recombinant clones using the rapid screening procedure.

5.10 Screening for recombinant pSFV1-Bax-α clones by restriction digestion.

5.11 Screening for Bax-α protein overexpression from recombinant SFV clones by ICC.

5.12 Screening for Bax-α overexpression in the *Bax*-null cell line, HL-60, by ICC.

5.13 Nucleotide and deduced aa sequence of human HA-tagged *Bax-α* from the pSG5-HABax plasmid.

5.14 Amino acid sequence alignment of the haemagglutinin epitope tag and Bax-α protein with others from the database.

5.15 Rapid colony screening for pSFV1-HABax-α recombinant clones.

5.16 Screening for pSFV1-HABax-α recombinant clones by *Xma1* restriction digestion.

5.17 Determination of *HABax-α* insert orientation in pSFV-1 by *BamH1* restriction digestion.

5.18 Screening for HABax protein expression from recombinant SFV clones by ICC.

5.19 Cytopathic effects following transfection of SFV-HABax RNA, in BHK-21 cells.

5.20 Induction of apoptosis following transfection with SFV-HABax and SFV-EGFP RNA constructs, in BHK-21 cells.

5.21 Optimisation of rSFV-HABax particle production.

5.22 rSFV-HABax particle-producing BHK-21 cells undergo rapid cell death.

5.23 Bcl-2 overexpression in NSCLC cell lines, as detected by ICC.

5.24 Growth and morphology of AT3-Neo and AT3-Bcl-2 cells.

5.25 Bcl-2 overexpression in AT3-Bcl-2 cells.

5.26 Growth of AT3-Neo and AT3-Bcl-2 cell lines as *in vivo* sc tumours.

5.27 Gross examination of *in vivo* AT3 sc tumours.

5.28 Histological examination of AT3-Neo and AT3-Bcl-2 sc tumours.

5.29 Immunohistochemical analysis of an *in vivo* AT3-Bcl-2 sc tumour.

5.30 Viability of AT3-Neo and AT3-Bcl-2 cells following infection with infectious SFV-4 virus, as determined by trypan blue exclusion.

5.31 Viability of AT3-Neo and AT3-Bcl-2 cells following infection with SFV-4 virus, as determined by sulphorhodamine B colorimetric analysis.

5.32 Viability of AT3-Neo and AT3-Bcl-2 cells following infection with SFV-4 virus, as determined by ^{3}H thymidine incorporation.

5.33 Apoptosis induction in AT3-Neo and AT3-Bcl-2 cells following infection with infectious SFV-4 virus.

5.34 Infection efficiency and effect of increasing concentrations of rSFV-EGFP virus particles in AT3-Neo and AT3-Bcl-2 cell lines.

5.35 Growth and viability of AT3-Neo and AT3-Bcl-2 cells following infection with rSFV particles, as determined by trypan blue exclusion.

5.36 Growth and viability of AT3-Neo and AT3-Bcl-2 cells following infection with rSFV particles, as determined by sulphorhodamine B colorimetric analysis.

5.37 Apoptosis induction in AT3-Neo and AT-Bcl-2 cells following infection with rSFV virus particles.

5.38 Effects of rSFV-EGFP virus vector treatment on AT3 tumour growth *in vivo*.

5.39 Subcutaneous AT3-Neo tumour growth in the *nu/nu* mouse xenograft model following rSFV-EGFP virus therapeutic intervention.

5.40 Subcutaneous AT3-Bcl-2 tumour growth in the *nu/nu* mouse xenograft model following rSFV-EGFP virus therapeutic intervention.

5.41 rSFV-EGFP virus-treated AT3 tumours regrow following cessation of treatment.

5.42 Histology of AT3 tumours following treatment with rSFV-EGFP virus.

5.43 TUNEL reactivity within AT3 tumours following treatment with rSFV-EGFP virus.

5.44 Viability of AT3-Neo and AT3-Bcl-2 cells following infection with rSFV-HABax virus particles, as determined by trypan blue exclusion.

5.45 Viability of AT3-Neo and AT3-Bcl-2 cells following infection with rSFV-HABax virus particles, as determined by sulphorhodamine B colorimetric analysis.

5.46 Viability of AT3-Neo and AT3-Bcl-2 cells following infection with rSFV-HABax virus particles, as determined by ^{3}H thymidine incorporation.

5.47 Effects of rSFV-HABax virus treatment on AT3 tumour growth *in vivo*.

5.48 Histology of AT3-Neo tumours following treatment with rSFV-HA-Bax particles.

5.49 Histology of AT3-Bcl-2 tumours following treatment with rSFV-HABax particles.

5.50 Cytopathic effect in AT3-Neo cells following transfection with SFV-HABax RNA.

5.51 Cytopathic effect in AT3-Bcl-2 cells following transfection with SFV-HABax RNA.

5.52 Viability of AT3-Neo and AT3-Bcl-2 cells following transfection with SFV-HABax RNA, as determined by trypan blue exclusion.

5.53 Viability of AT3-Neo and AT3-Bcl-2 cells following transfection with SFV-HABax RNA, as determined by sulphorhodamine B colorimetric analysis.

5.54 Viability of AT3-Neo and AT3-Bcl-2 cells following transfection with SFV-HABax RNA, as determined by ^{3}H thymidine incorporation.

5.55 Apoptosis induction in AT3-Neo and AT3-Bcl-2 cells following transfection with SFV-HABax RNA.

5.56 SFV-HABax-induced programmed cell death in AT3-Neo cells, as assessed by chromosomal DNA fragmentation, using TUNEL.

5.57 SFV-HABax-induced programmed cell death in AT3-Bcl-2 cells, as determined by chromosomal DNA fragmentation, using TUNEL.

List of Tables

1.1 Protein substrates of caspases.

1.2 Viral protein inducers and inhibitors of apoptosis.

1.3 Comparison of gene transfer vectors.

2.1 Oligonucelotide primers used in PCR amplification of EGFP.

4.1 Effects of rSFV-EGFP virus treatment on *in vivo* H358a tumour growth.

5.1 Oligonucleotide primers used in PCR amplification of *Bax-α* and *HABax-α*.

Chapter 1

General Introduction

1 INTRODUCTION

Cancer is generally regarded as a disease of uncontrolled cell growth. Although there are more than 200 different types of malignancies, they all appear to share the common denominators of uncontrolled growth and lack of differentiation. Accelerated cell growth may be attributed to an increase in mitotic rate and cell proliferation, which is independent of the normal cellular restraints required for adequate homeostasis. However, for many malignancies, the mitotic index appears to be quite low, with the number of replicating cells in some instances, even lower than in the tissues of origin. Thus, the development of neoplasia is due not only to an increase in cell proliferation, but also to a diminished rate of cell depletion.

The maintenance of normal tissue homeostasis is intimately controlled by a programmed cell death pathway known as apoptosis. When this crucial checkpoint control is lost, hyperplasia results. Specific genes, identified as proto-oncogenes and tumour suppressor genes, shown to be mutated or deleted in a myriad of malignancies, are known to also play a critical role in the regulation and execution of apoptotic cell death.

The mainstay of cancer treatment is surgical resection of the primary tumour, but this is often unsatisfactory because of advanced disease at presentation, or because of the development of metastases. This is so for around two-thirds of cancer patients, for which a more systemic form of treatment is required. Chemotherapeutic and radiotherapeutic regimes, either alone or in combination, have provided the only alternative or adjuvant to surgery. Increased understanding of the molecular pathogenesis of these regimes in cancer treatment has revealed that their damaging action on hyperproliferative cells is mediated directly or indirectly by the induction of apoptosis. Thus, the ability of malignant cells to become refractory to the cytotoxic effects of these regimes, is closely

related to their ability to escape apoptotic cell death. Thus, apoptosis is not only important in the progression of cancer, but is also intimately associated with cancer treatment.

Strategies to induce an apoptotic pathway in such malignancies could only serve to reverse the malignant phenotype, while also enhancing the sensitivity of the tumour cells to current anti-cancer regimes. The continuing characterisation of genes involved in the control of apoptosis presents an opportunity to utilise these genetic elements as targets for the treatment of cancer. Approximately two-thirds of the 300 approved clinical protocols involving a genetic element this year, are directed at cancer treatment, indicating the enormous potential of this technique, or reflecting the lack of success with alternative strategies.

This chapter will begin with an outline of the apoptotic pathway and its associated genes, which are known to be mutated in cancer. This is followed by an analysis of the 'gene therapy' strategies currently utilised for cancer treatment. Of crucial importance, is the vehicle used to deliver such genetic components. These gene therapy vectors are described and compared. As this study is aimed at exploiting a new viral vector system as a cancer therapy agent, the Semliki Forest virus (SFV) itself is described, together with an outline of the development of the SFV recombinant vector and its potential for gene therapy.

1.1 APOPTOSIS

Apoptosis or programmed cell death (PCD), is a naturally occurring process of cell suicide that plays a crucial role in the development and maintenance of metazoans for eliminating superfluous or unwanted cells (Vaux & Korsmeyer, 1999). In addition, apoptosis also plays an important role in immune responses, viral infections and various pathologies. Inappropriate regulation of apoptosis is associated with a variety of diseases including cancer, AIDS, neurodegenerative disorders and ischemic stroke (Thompson, 1995).

Apoptosis refers to the morphological alterations exhibited by actively dying cells that include cell shrinkage, membrane blebbing and phagocytosis of 'apoptotic bodies' by neighbouring cells. Apoptosis is referred to as the physiological form of cell death, is genetically regulated, and culminates in the efficient removal of a cell population without the induction of an inflammatory response (Jacobson *et al*, 1997). In contrast, necrosis, sometimes referred to as 'accidental cell death', is defined by swelling and lysis of cells, due to acute cell injury or exposure to toxic stimuli. Necrotic cell death lacks a genetic element, and is accompanied by inflammatory responses. Other investigators define a third mechanism of cell death, namely oncosis, as a pre-lethal type of reaction that precedes necrosis (Trump *et al*, 1997; Manjo & Joris, 1995).

Although the morphological features of PCD are well described, the molecular mechanisms behind apoptotic cell death are only now being slowly elucidated (Song & Steller, 1999). Much of the knowledge on the genetic regulation of cell death has emerged from using the nematode *Caenorhabditis elegans* as a model organism (Ellis & Horvitz, 1986). In this worm, 1090 cells are generated during development, of which 131 die by a precisely controlled apoptotic paradigm. Genetic analysis has identified 14 genes that function at different stages of PCD in the nematode. The three well-known genes, *ced-3*, *ced-*

4 and *ced-9*, are crucial for the regulation and execution of apoptotic cell death. Whereas *ced-3* and *ced-4* are required for cell death induction, *ced-9* is a cell death antagonist. The discovery that a lack-of-function *ced-9* mutation can be partly compensated with a mammalian *ced-9* homologue *Bcl-2* (Vaux *et al*, 1992) revealed that apoptotic cell death pathways are highly conserved, from nematode to mammal. Similarly, analysis of *ced-3* has revealed that its product is similar to certain members of the mammalian cysteinyl-aspartate protease family, the executioners of apoptotic cell death (Yuan *et al*, 1993), whereas *ced-4* is analogous to the mammalian *Apaf-1* gene, an essential component of the mitochondrial facet of PCD induction (Zou *et al*, 1997).

The induction of apoptosis is largely determined by a complex of signal transduction pathways, starting with the initiation of a death signal at the plasma membrane, and following through to the execution of cell death, mediated by a variety of activated cellular proteases, caspases, which actively facilitate cellular demise. Enmeshed with this is the pro-apoptotic role of the mitochondrion, which also directly initiates the caspase cascade. All stages of the process are regulated by an intricate series of nuclear and cytoplasmic control checkpoints, where complexes of pro- and anti-apoptotic factors, such as the *p53* tumour suppressor and *Bcl-2* superfamily of regulators, function to facilitate or deter cell death. Finally, the role of viral infection in the induction and inhibition of the PCD pathway in infected cells is discussed.

1.1.1 Death receptors, the direct physical activators of apoptosis.

Probably the best characterised pathways for the induction of apoptotic cell death involves the binding of specific extracellular death ligands, such as TNFα, TRAIL (TNF-related apoptosis-inducing ligand), Apo-3L and FasL

proteins to members of the tumour necrosis factor receptor 1 (TNFR1) family, including TNFR1, DR(Death Receptor)4/5, DR3 and Fas (CD95), respectively (Nagata, 1997) (*Figure 1.1*). Binding of ligands such as FasL to the CD95 receptor functions in the removal of activated T lymphocytes by apoptosis, at the end of the immune response (Nagata & Golstein, 1995). Each death receptor is located at the cell surface and contains an N-terminal cytoplasmic domain of approximately 80 amino acids, designated the Death Domain (DD) (Tartaglia *et al*, 1993), which is critical for caspase activation. Caspases, as described below, function as downstream activators of apoptotic cell death.

Binding of extracellular ligands induces trimerisation of its cognate receptor (Ashkenazi & Dixit, 1998). By virtue of their cytoplasmic DD, activated Fas and TNFR1 can recruit intracellular adaptor proteins; FADD (for Fas-associated death domain protein) (Chinnaiyan *et al*, 1995) and TRADD (for TNFR1-associated death domain protein) (Hsu *et al*, 1995), to the plasma membrane. For FasL-induced apoptosis, FADD serves as the link between initial signal activation, and the apoptotic executioners, the caspases (Chinnaiyan *et al*, 1996). The C terminal of FADD contains a DD similar to that of the Fas receptor, and DD protein-protein interactions mediate the binding of Fas to this adaptor. In addition to its C-terminal DD, FADD also contains an N-terminal Death Effector Domain (DED), which in turn, functions to recruit and bind to analogous DEDs, repeated in tandem within the zymogen form of the apical apoptotic protease, pro-caspase-8 (Muzio *et al*, 1996; Boldin *et al*, 1996). The DED is part of a larger group of homophillic interaction domains termed CARD (caspase recruitment domain) (Hofmann *et al*, 1997), and are located in the prodomains of several caspases, including caspase-2, -8, -9 and –10. Fas/FasL, FADD and pro-caspase-8 form a multimeric complex known as the Death-Inducing Signal Complex or DISC (Kischkel *et al*, 1995). Upon Fas –mediated recruitment by FADD, caspase-8 oligomerisation drives its own activation by self-cleavage, and goes on

Figure. 1.1. Pro-apoptotic and pro-survival signalling by death factors.

A) Fas-induced apoptosis. Binding of FasL to the Fas receptor induces trimerisation of Fas, which recruits pro-caspase-8 (FLICE/MACH) via the adaptor protein FADD/MORT1 and is mediated by DD protein-protein interactions. The oligomerisation of FLICE results in self-activation of the caspase, which then triggers downstream caspase activation.

B) TNFα-induced apoptosis. TNFα binds to TNFR1, and trimerisation of the receptor facilitates recruitment of pro-caspase-8 via the docking protein, TRADD by virtue of their DD. TRADD recruits pro-caspase-8 via its interaction with FADD. TRADD also interacts with the DD of RIP to transduce an apoptotic signal. Conversely, TRADD-RIP interactions, together with TRAF2, activate NFκB and c-Jun pathways via NIK and MEKK pathways, respectively. This may induce the expression of survival genes.

DD; Death Domain, DED; Death Effector Domain, FADD; Fas-associated Death Domain, TRADD; TNF-associated Death Domain, RIP; Receptor-interacting protein, TRAF2; TNF receptor-associated factor. (Adapted from Nagata, 1997; Ashkenazi & Dixit, 1998).

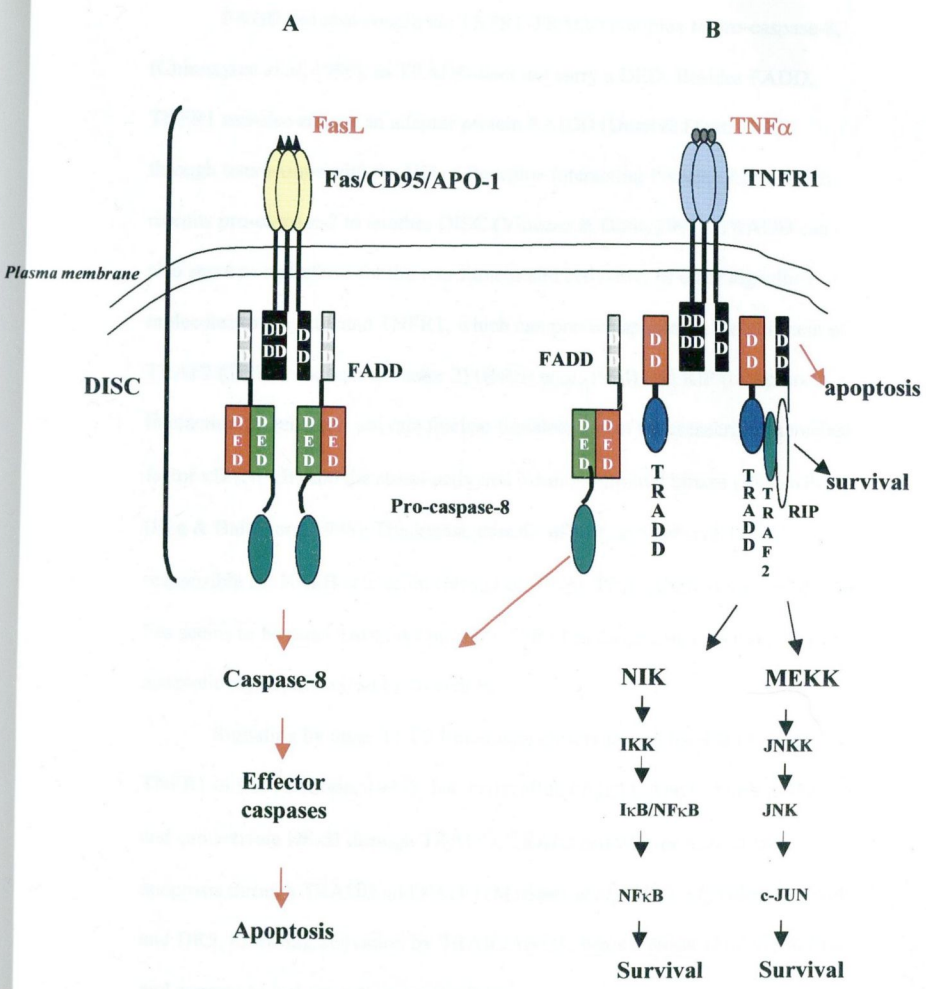


Figure 1.1- Pro-apoptotic and pro-survival signalling by death factors.

to cleave downstream caspase zymogens such as pro-caspase-3 (Muzio *et al*, 1998) (*see below*).

FADD can also couple the TNFR1-TRADD complex to pro-caspase-8, (Chinnayian *et al*, 1996), as TRADD does not carry a DED. Besides FADD, TNFR1 can also engage an adaptor protein RAIDD (Duan & Dixit, 1997), through interactions with the DD of Receptor-Interacting Protein (RIP), which recruits pro-caspase-2 to another DISC (Vincenz & Dixit, 1997). TRADD can also serve as a platform for the recruitment and activation of other signalling molecules to the activated TNFR1, which can prevent apoptosis. Recruitment of TRAF2 (TNFR1-associated factor 2) (Rothe *et al*, 1994) and RIP (receptor-interaction protein) can activate nuclear translocation of the transcription nuclear factor κB (NFκB) and the stress-activated c-Jun N-terminal kinase (JNK/AP-1) (Beg & Baltimore, 1996). The kinase domain of RIP, and not its DD, is responsible for NKκB activation (Hsu *et al*, 1996). Thus, whereas the signal from Fas seems to be restricted to apoptosis, TNFR1 has the potential to transduce an apoptotic signal, as well as to prevent it.

Signaling by other TNFR1 members closely resembles that of either TNFR1 or Fas (Golstein, 1997). The extracellular ligand, Apo3L binds to DR3, and can activate NFκB through TRADD, TRAF2 and RIP, or may trigger apoptosis through TRADD and FADD (Marsters *et al*, 1998). Signalling by DR4 and DR5, following activation by TRAIL/Apo2L, bears a closer similarly to Fas, and appears to lack an anti-apoptotic facet.

Finally, several decoy receptors, which share homologous extracellular domains with specific death receptors but lack the cytoplasmic DED domain (Pan *et al*, 1998; Pan *et al*, 1997), can compete for ligand binding, to reduce the effectiveness of specific death ligands, and thus prevent apoptosis. Deregulation in both Fas- and TNFα-mediated signalling has also been observed in many

tumour cell lines of both hematologic and non-hematologic origin (Laucet *et al*, 1995).

1.1.2 Role of the mitochondrion in apoptosis induction.

Mitochondria have been implicated in apoptosis ever since the discovery that the *Bcl-2* family of proteins are located in the outer mitochondrial membrane (*see below*). One of the crucial mitochondrial events in the early stages of apoptosis is mitochondrial transmembrane depolarisation (MMD) (Bernardi *et al*, 1999), which initiates the opening of a large conductance channel known as the mitochondrial PT pore (*Figure 1.2*). Opening of this inner membrane channel allows for the equilibration of ions within the matrix and inner mitochondrial membranous space and thus, uncoupling of the respiratory chain. A correlation between MMD and apoptosis was identified by Susin *et al* (1999), as a 57kDa flavoprotein, AIF (apoptosis inducing factor). Release of AIF from the mitochondrion to the cytoplasm depends on this dissipation of the proton and electrical gradients over the inner mitochondrial membrane, which releases soluble proteins, including AIF, from the intermembranous space. AIF is translocated to the nucleus where it induces caspase-independent chromatin condensation in isolated nuclei and forces the nucleus to adopt an apoptotic morphology. AIF may also act on other mitochondria to compromise their membrane function, releasing other apoptogenic factors. More recently, AIF has been shown to process purified pro-caspase-3 *in vitro*, thus introducing a caspase-dependent function of AIF, and also raising the possibility that AIF may itself, be another caspase (Green & Reed, 1998).

In addition to AIF, three other proteins have been identified that are required for mitochondrion-induced apoptosis. The first protein is the mature

Figure 1.2- Role of mitochondria in apoptosis induction.

Upon receipt of an apoptotic stimulus, a decrease in mitochondrial transmembrane potential ($\Delta\psi_m$) mediates the opening of mitochondrial megapores, to release a number of caspase-activating proteins, such as AIF and cytochrome *c*. Disruption of the outer mitochondrial membrane as a consequence of matrix swelling, also facilitates the release of these apoptogenic factors. Release of cytochrome *c* induces the activation of Apaf-1 in the cytosol, which recruits pro-caspase-9 to the site of activation by virtue of its CARD domain. Pro-caspase-9 cleavage and activation facilitates the activation of downstream caspases, such as pro-caspase-3. AIF is also responsible for pro-caspase-3 activation, whereas release of ROS, and a decrease in the hydrolysable form of ATP induces a necrotic cell death phenotype.

CARD; caspase activation recruitment domain, AIF; apoptosis inducing factor, Apaf-1; apoptosis protease inducing factor, ROS; reactive oxygen species.

(Adapted from Green & Douglas, 1998).

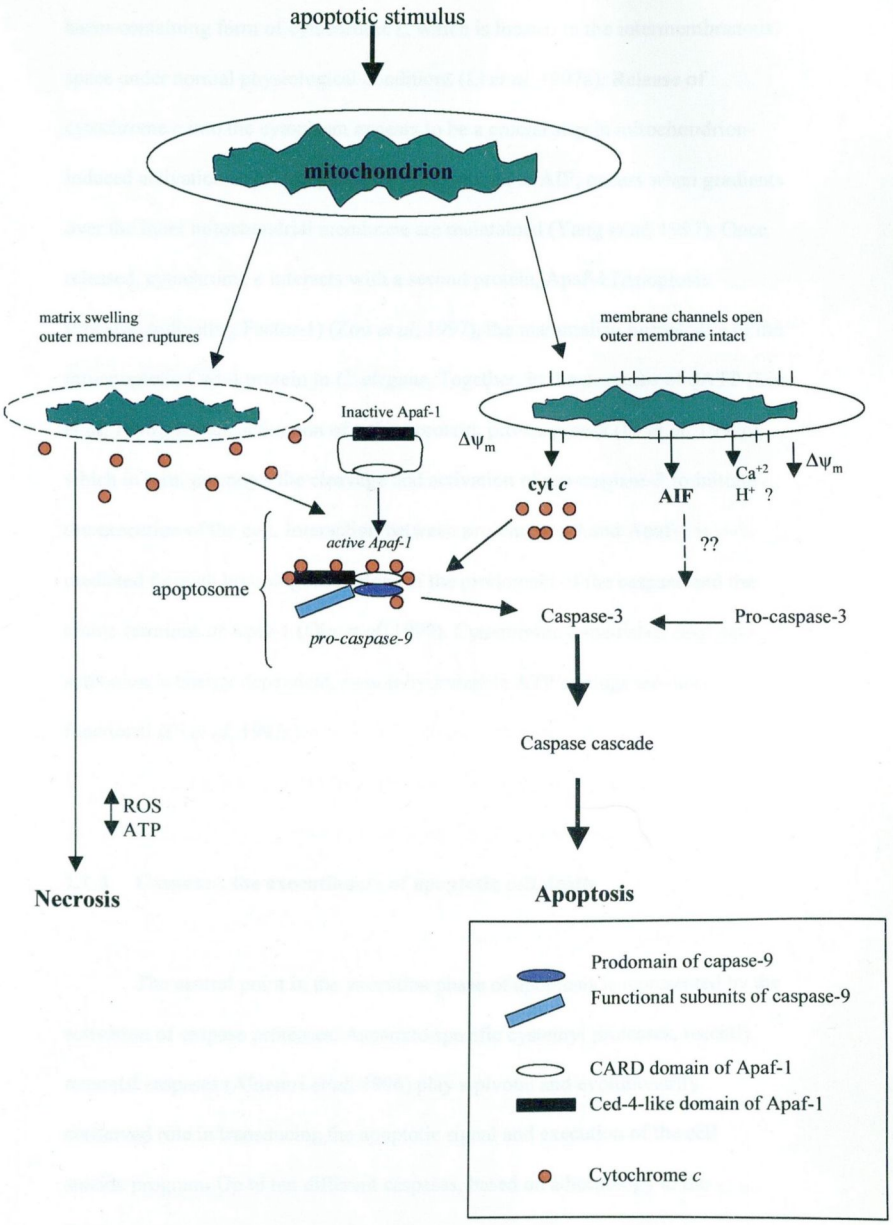


Figure 1.2- Role of mitochondria in apoptosis induction.

haem-containing form of cytochrome *c*, which is located in the intermembranous space under normal physiological conditions (Li *et al*, 1997a). Release of cytochrome *c* into the cytoplasm appears to be a crucial step in mitochondrion-induced activation of pro-caspase-3, and in contrast to AIF, occurs when gradients over the inner mitochondrial membrane are maintained (Yang *et al*, 1997). Once released, cytochrome *c* interacts with a second protein, Apaf-1 (Apoptosis Protease-Activating Factor-1) (Zou *et al*, 1997), the mammalian homologue of the pro-apoptotic Ced-4 protein in *C. elegans*. Together, in the presence of dATP (Liu *et al*, 1996), induce activation of a third protein, pro-caspase-9 (Li *et al*, 1997c), which in turn, promotes the cleavage and activation of pro-caspase-3 to initiate the execution of the cell. Interaction between pro-caspase-9 and Apaf-1 is mediated through homologous regions in the prodomain of the caspase and the amino terminus of Apaf-1 (Qin *et al*, 1999). Cytochrome *c*-mediated caspase-3 activation is energy dependent, as non-hydrolzable ATP analogs are non-functional (Li *et al*, 1997c).

1.1.3 Caspases, the executioners of apoptotic cell death.

The central point in the execution phase of apoptosis is represented by the activation of caspase proteases. Aspartate-specific cysteinyl proteases, recently renamed caspases (Alnemri *et al,* 1996) play a pivotal and evolutionarily conserved role in transducing the apoptotic signal and execution of the cell suicide program. Up to ten different caspases, based on a homology to the mammalian pro-inflammatory prototypical caspase, interleukin-1β-converting enzyme (ICE) or caspase-1, and the nematode cell death protein Ced-3, have now been identified (Yuan *et al*, 1993). All share a predilection for cleavage of their substrates after an aspartate residue at the P_1 position (*Figure 1.3*). All caspases

contain an active site pentapeptide of general structure QACXG (where X is R, Q, or G), and includes the amino acids Cys-285 and His-237 (in ICE), essential for proteolytic activity (Cohen, 1997). All caspases are synthesised as inactive proenzymes, composed of a prodomain and an enzymatic region. For activation, the caspase zymogen is cleaved at specific aspartate residues to active enzyme, containing two self-associating large (p20) and small (p10) heterodimers. Because this cleavage site is a unique characteristic of caspases (with the exception of the serine protease Granzyme B), activation can occur only through auto- or trans-activation by another caspases or Granzyme B.

Heterogeneity exists regarding the structure of the prodomain, suggesting that this region may define important functional or regulatory differences between caspases. Caspase-1, -2, -4, -5, -8, -9 and –10 contain a long prodomain of approximately 20 kDa compared with <5 kDa in caspase-3, -6 and –7 (Criekinge *et al*, 1996). Recent evidence suggests that the prodomain of caspase-9 mediates its own binding to Apaf1 (Irmler *et al*, 1997a). Casapse-8 and –10 also contain long prodomains that may facilitate delivery of the inactive proenzyme to the Fas and TNFR DISC complexes via protein-protein interaction motifs (Boldin *et al*, 1996). Substrate specificity is determined by both tissue-specific distribution, and by residues adjacent to active site cysteine residues (P2-P4), which form the binding pocket of the active site (Walker *et al*, 1994). Based on phylogenetic analysis, mammalian caspases have been classified into 3 subfamilies (*Figure 1.4*), an ICE subfamily, a caspase-3/CPP32 subfamily, and a caspase-2/ICH-1 subfamily (Thornberry & Lazebnik, 1998).

The role of caspases in the execution phase of apoptosis is supported by genetic, biochemical and physiological evidence. Specific mutations within the catalytic cysteine residue, and constructs devoid of either large or small subunits are unable to induce apoptosis (Miura *et al*, 1993). Caspase-3/CPP32 is one of the key executioners of apoptosis induced by a wide variety of stimuli, and is widely

Figure 1.3- **Proteolytic processing and activation of caspases.**

Caspase zymogens are activated by auto- or trans-proteolysis at aspartate (D) residues resulting in release of the N-terminal prodomain and two enzyme subunits, p20 and p10. The enzymes heterodimers self-associate to form an active protease tetramer. The conserved pentapeptide QACXG, including the conserved cysteine residues, indicates the catalytic centre of the enzyme.

Figure 1.4- Phylogenetic relationship of the mammalian caspase family.

Based on their amino acid sequence similarities, three subfamilies can be delineated; a caspase-3/CPP32 subfamily, including caspase-3, -6, -7, -8, and –10 ; a caspase-2 subfamily including caspase-2 and –9, and an ICE subfamily, including caspase-1, -4 and –5. Relationships are based on full-lenght pro-enzymes, which is appropriate as the prodomains play a functional role. Previous nomenclature of each caspase is indicated in parentheses. (Adapted from Cryns & Yuan, 1998; Cohen, 1997).

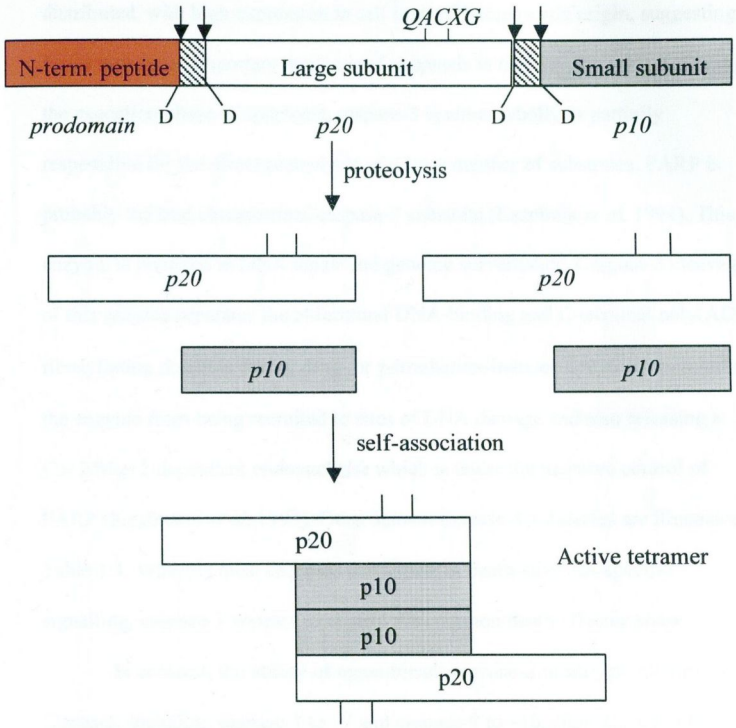


Figure 1.3- Proteolytic processing and activation of caspases

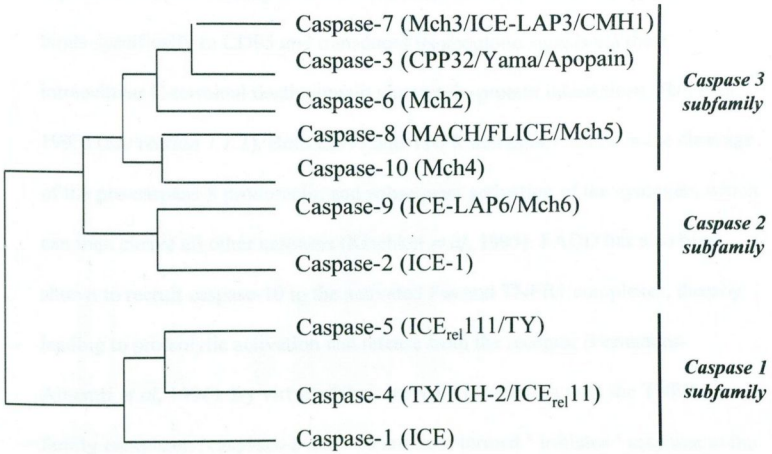


Figure 1.4- Phylogenetic relationship of the mammalian caspase family.

distributed, with high expression in cell lines of lymphocytic origin, suggesting that it may be an important mediator of apoptosis in the immune system. During the execution phase of apoptosis, caspase-3 is either wholly or partially responsible for the direct proteolysis of a large number of substrates. PARP is probably the best characterised caspase-3 substrate (Lazebnik *et al*, 1994). This enzyme is involved in DNA repair and genome surveillance. Caspase-3 cleavage of this enzyme separates the N-terminal DNA-binding and C-terminal poly(ADP-ribosyl)ating domains during drug- or γ-irradiation-induced apoptosis, precluding the enzyme from being recruited to sites of DNA damage and also releasing a Ca+2/Mg+2-dependent endonuclease which is under the negative control of PARP (Kaufmann *et al*, 1993). Other known caspase-3 substrates are illustrated in Table 1.1. Whereas most caspases participate in death-stimulus-specific signalling, caspase-3 appears to control the common death effector phase.

In contrast, the ability of recombinant caspase-8 to activate all known caspases, including caspase-1 to –7 and caspase-9 to –10, suggests that it lies at the apex of the apoptotic cascade, at least during Fas- and TNFα-induced apoptosis. Pro-caspase-8 contains a long N-terminal prodomain which has two regions of marked identity with the N-terminal DED of FADD /MORT1, which binds specifically to CD95 and transduces its apoptotic signals via their intracellular C-terminal death domain via protein-protein interactions (Hsu *et al*, 1995) (*see section 1.1.1*). Both CD95 and TNFR activation results in the cleavage of the pro-caspase-8 prodomain, and subsequent activation of the zymogen, which can then cleave all other caspases (Kischkel *et al*, 1995). FADD has also been shown to recruit caspase-10 to the activated Fas and TNFR1 complexes, thereby leading to proteolytic activation and release from the receptor (Fernandes-Alnemri *et al*, 1996). By virtue of their intimate association with the TNFR1 family complexes, caspases-8 and –10 are thus, termed ' initiator ' caspases at the apex of the casapse proteolytic cascade. Clearly there are many gaps in the

Protein substrate	Caspase(s)	Substrate function	Reference
PARP	3, 7	DNA repair	Lazebnik *et al*, 1994 Kaufmann *et al*, 1993
Bcl-2	3	Apoptosis inhibition	Grandgirard *et al*, 1998
DNA-PK_{CS}	3	DNA repair	Song *et al*, 1996
ICAD/DFF45	3	DNA fragmentation	Enari *et al*, 1998 Liu *et al*, 1997
Lamins	6 ?	Nuclear envelope protein	Neamati *et al*, 1995
α-fodrin	6	Cytoskeletal protein	Cryns *et al*, 1996 Vanags *et al*, 1996
U1-70 kDa	3	Small nuclear riboprotein	Casiola-Rosen *et al*, 1994
pRB	3	Tumour suppressor protein	Tan *et al*, 1997
Gelsolin	3	Actin-modulating protein	Kothakota *et al*, 1997

Table 1.1- Protein substrates of caspases. (Adapted from Cohen, 1997).

understanding of the events in this proteolytic cascade and much previous evidence is based on *in vitro* data.

1.1.3.1 Known caspase substrates.

Many, if not all of the proteins that are known to undergo proteolysis during cell death are substrates of one or more of the caspases. These include nuclear, signal transduction and cytoskeletal proteins and a number of these are presented in Table 1.1. Cleavage of important cytoskeletal proteins, including β-actin, α-fodrin and Gas-2 (Vanags *et al*, 1996; Cryns *et al*, 1996) may contribute to degradation of the cell. Intracellular actin depolymerisation may lead to cytoplasmic shrinkage and membrane blebbing, the characteristic morphological features of apoptotic cell death. The actin-modulating protein, gelsolin, which is the most prominent direct substrate of murine caspase-3 is also a possible *in vivo* target (Kothakota *et al*, 1997). Nuclear structural proteins are also targeted. Lamin B binds directly to regularly spaced matrix attachment regions (MARs) in chromatin. Its degradation may directly promote large DNA fragment formation and unfolding, sufficient for endonuclease attack (Neamati *et al*, 1995). DNA repair enzymes such as PARP and DNA-PK are also cleaved, abolishing the function of these crucial DNA repair activities. Cleavage of U1-70kDa blocks cellular repair pathways dependent on new RNA synthesis (Casciola-Rosen *et al*, 1994). pRB tumour suppressor protein, a critical regulator of cell cycle progression, and Bcl-2, a major anti-apoptotic protein are also direct caspase targets. Proteolysis of these key cell cycle and cell death regulators facilitates cell death. In addition to these, signal transduction molecules including PKCδ and proteins involved in JNK pathway activation, are also cleaved.

Cleavage of nuclear chromatin to oligonucleosomal fragments can be considered as the end-point of apoptosis, ensuring cell death of the affected cell prior to budding as apoptotic bodies. Several nucleases were suggested as candidates, including DNase-1, DNase-2, cyclophillins or perhaps any available nuclease. Enari *et al*, (1998) have described a novel factor, CAD (for caspase-activated DNase), which appears to be activated specifically during apoptosis via caspase-3-mediated cleavage of a second protein, ICAD (inhibitor CAD), which releases the active endonuclease. ICAD is closely homologous to the protein DFF45, which was also shown to induce endonuclease activity upon cleavage with caspase-3 (Liu *et al*, 1997). Thus, the disruption of homeostatic repair processes and the simultaneous activation of endonucleases such as CAD, together with the collapse of nuclear and cytoskeletal structure, is likely to commit the cell to apoptosis.

The anti-apoptotic Bcl-2 protein is a negative upstream regulator of caspase activation (Chianniyian *et al*, 1996) and is found to be overexpressed in a wide variety of human cancers (*see below*). More recently, overexpression of an endogeous inhibitor of certain caspases, the FLIP protein, has been demonstrated in malignant melanomas (Irmler *et al*, 1997b). Similarly, *survivin*, a novel member of the 'inhibitor of apoptosis' family, is overexpressed in a number of human cancers and has been postulated as a suppressor of caspase activation (Deveraux *et al*, 1997). Thus, inactivation of caspases may be a crucial determinant in the development of neoplasia and suggests that the major caspase proteases, particularly caspase-3, could be used as a potenial therapeutic target for cancer gene therapy.

1.1.4 Regulation of apoptosis; the *p53* signalling pathway.

One of the most important controls of cell cycle progression and apoptosis induction is the tumour suppressor *p53* gene product. The p53 protein has been defined as a nuclear phosphoprotein which functions as a transcription factor for the activation of a variety of cell cycle- and apoptosis-related genes (Levine *et al*, 1991). As a consequence, pertubations in *p53* expression and function are associated with a broad array of malignancies (Hollstein *et al*, 1991). Also, the evolution of varied strategies to modify *p53*-dependent apoptosis pathway signals the importance of *p53* in the host cell defence against viral infection (*see below*).

Genotoxic stress inducers of apoptosis, including UV- and γ-irradiation, and chemotherapeutic drugs are dependent on *p53* induction (Kuerbitz *et al*, 1992; Lowe *et al*, 1993). In addition, when cells are induced to proliferate by deregulated expression of certain viral and cellular oncogenes, they undergo *p53*-dependent apoptosis, unless rescued by pro-survival *Bcl-2*-like gene products (Symonds *et al*, 1994; Levine, 1997). Recent evidence suggests that oncogene expression and DNA damage use different mechanisms to induce *p53*-dependent apoptosis (Prives, 1998). Overexpression of oncogenes, such as *E2F-1*, *c-myc*, *E1A* or oncogenic versions of *ras*, results in the accumulation of $p19^{ARF}$, which in turn, leads to promotion of p53 stability and function (Palmero *et al*, 1998; Zindy *et al*, 1998). Genotoxic damage activates *p53* transcription, and post-translation modifications result in its accumulation in the nucleus.

Known downstream targets of p53 transcriptional activation include $p21^{CIP1/WAF1}$ (Dulic *et al*, 1994), which in turn, leads to inactivation of cyclin-dependent kinase (CDK)-cyclin complexes (Slebos *et al*, 1994), causing $p105^{Rb}$ dephosphorylation, which prevents the release of the potent oncogene *E2F*, and blocks G_1-S cell cycle transition. Degradation of p53 leads to a reduction in p21

levels, hyperphosphorylation of pRB, and continuation through the S phase of the cell cycle. Cell cycle arrest allows the cell time to repair its DNA. If repair is not possible, p53 induces programmed cell death (Chen *et al*, 1990). The pro-apoptotic effects of *p53* have been linked to the *p53*-induced expression of Fas, Bax and IGF binding protein 2 (Ludwig *et al*, 1996; Miyashita & Reed, 1995). *p53* has also been shown to upregulate expression by 10-fold, of key genes involved in cellular redox reactions (Polyak *et al*, 1997). Other genes transcriptionally activated by sequence-specific p53-DNA binding include *GADD45*, whose product appears to play a role in DNA repair, and *mdm2*, a negative regulator of *p53* expression (Guo *et al*, 2000).

1.1.5 Regulation of apoptosis; The Bcl-2 family

Whereas *p53* can promote apoptosis, the Bcl-2 protein is a potent repressor of the process. *Bcl-2*, the mammalian homolog of the *ced-9* negative regulatory protein for apoptosis in *C. elegans* (Vaux *et al*, 1992 ; Hengartner & Horvitz, 1994), was initially discovered by virtue of a t(14 ;18) translocation breakpoint, that is common in many B-cell lymphomas (Hockenbery *et al*, 1990). As a result of this translocation, *Bcl-2* comes under the control of the immunoglobulin heavy chain enhancer, and is constitutively expressed in B cells (Adams & Cory, 1998). The resulting protection from cell death permits the survival and accumulation of aberrant B cells and the development of neoplasia. Thus, the Bcl-2 protein was defined as unique, because it contributed to malignant cell expansion primarily by prolonging cell survival, rather than by increasing the rate of cellular proliferation (Yang & Korsmeyer, 1996).

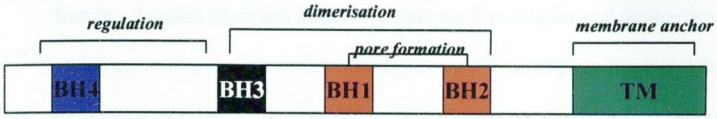
Overexpression of *Bcl-2* contributes not only to the origins of cancer, but also to difficulties in treating it (Reed, 1997b). Similar results have recently been

observed following overexpression of a Bcl-2-like protein, Bcl-X_L (Boise *et al*, 1993). Both Bcl-2 and Bcl-X_L proteins have been found to protect against apoptotic cell death in a variety of cell types, including the negative selection of mature $CD4^-$ $CD8^-$ double-negative cells (Sentman *et al*, 1991), and in cytokine-dependent cell lines following withdrawal of IL-3, IL-4 and GM-CSF (Nunez *et al*, 1990). Bcl-2 has also been shown to protect against neuronal cell death following withdrawal of nerve growth factors NGF, BDNF and NT-3 (Davies, 1995). *Bcl-2* may therefore, be required to save progenitor and long-lived cells in a variety of cell lineages. However, the specific mechanisms by which Bcl-2-like proteins extend cell survival remains rather enigmatic.

At least 15 *Bcl-2* family members have been identified in mammalian cells, each possessing either pro- or anti-apoptotic activities (*Figure 1.5*). All members possess at least one of the four conserved motifs, known as Bcl-2 homology (BH) domains (Oltavi *et al*, 1993), and a C-terminal transmembrane domain that targets the proteins predominantly to the outer mitochondrial membrane, endoplasmic reticulum and plasma membrane (Krajewski *et al*, 1993). Classification of *Bcl-2* family members is based on domain organisation (Kelekar & Thompson, 1998). The pro-survival cohort contains the Bcl-2 and Bcl-X_L proteins, which contain all four BH domains, whereas the pro-apoptotic subgroups contain Bax and Bcl-X_S proteins, which vary in domain composition (Yin *et al*, 1994; Chittenden *et al*, 1995). Analysis of sequence and structural similarities between members of the pro- and anti-apoptotic subgroups indicates potential implications for the general mechanisms of programmed cell death regulation (*Figure 1.5*).

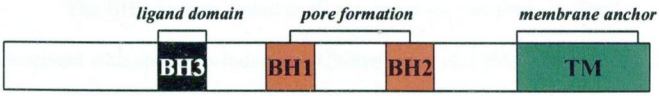
Residues within the BH1 and BH2 domains are essential for the survival function of the death suppressors *Bcl-2* and *Bcl-X_L*, and for interactions of these proteins with death agonists such as *Bax* and *Bak* (Yin *et al*, 1994). In an effort to relate structure to function, the three-dimensional structure of Bcl-X_L BH1 and

PRO-SURVIVAL



Bcl-2	Hockenbery *et al*, (1990)
Bcl-X_L	Boise *et al*, (1993)
Mcl-1	Kozopas *et al*, (1993)
Bcl-w	Gibson *et al*, (1996)
A1/Bfl-1	Choi *et al*, (1995)
(E1B-19K)	Farrow *et al*, (1995)
(BHRF1)	Henderson *et al*, (1993)
(KS-Bcl-2)	Cheng *et al*, (1997)

PRO-APOPTOTIC



Bax	Oltavi *et al*, (1993)
Bak	Chittenden *et al*, (1995)
*Bad	Gajewski & Thompson, (1996)
*Bik	Boyd *et al*, (1995)
*Bid	Wang *et al*, (1996)
*Bcl-X_S	Minn *et al*, (1996)
*Hrk	Inohara *et al*, (1997)
*Bim	O'Connor *et al*, (1998)

Figure 1.5- Classification of Bcl-2 family members based on domain organisation.

Bcl-2 homology domains (BH) and transmembrane (TM) domains are indicated, as are the related functions of each domain region. Of potential relevance to certain types of cancers, three homologues of Bcl-2 have also been discovered in viruses, which are indicated in parentheses.

* Contain BH3 domain only. (Adapted from Adams & Cory, 1998; Kelekar & Thompson, 1998).

BH2 domains (Muchmore *et al*, 1996) revealed a striking similarity to the pore-forming domains of certain bacterial toxins, such as colicins and diptheria toxin, which act as channels for ions or small proteins (Reed, 1997a). The Bcl-2 family of proteins may insert themselves into lipid bilayers via the carboxy terminus, allowing the BH1 and BH2 domains to act as conductance channels for small molecule traffic (*Figure 1.6*). Bcl-2 family members localise predominantly within mitochondrial membranes, where alterations in Ca^{+2}, H^{+}, and in permeability transition, herald the onset of cytochrome *c* release and apoptosis induction (Green & Kroemer, 1998). However it is unlikely that BH1 and BH2 domains are solely responsible for the regulation of apoptosis induction, as other pro-apoptotic members, such as *Bcl-X$_S$*, lack BH1 and BH2 domains, and do not form ion-selective channels (Minn *et al*, 1996).

The BH3 domain, found in all pro-apoptotic members, is closely associated with apoptosis induction (Chittenden *et al*, 1995). Ultrastructural analysis of a complex between Bcl-X_L and Bak, which is comprised of a BH3 domain only (Sattler *et al*, 1997), indicates a hydrophobic pocket created by BH1, BH2 and BH3 domains, of the Bcl-X_L protein, which binds with high affinity to the amphipathic BH3 α-helical structure within Bak. Bcl-X_L has also been shown to homodimerise and heterodimerise with high affinity, to other members of the *Bcl-2* family, establishing a form of hierarchy of binding (Kelekar *et al*, 1997).

Thus, if *Bcl-2*-like proteins act as ion channels to maintain mitochondrial homeostasis and integrity, BH3-domain-containing pro-apoptotic members may function to antagonise their function, by binding to the hydrophobic pocket of the anti-apoptotic protein, or by displacing anti-apoptotic homodimers with dysfunctional or nonfuctional pro-apoptoptic heterodimers (Pawlowski & Kraft, 2000). Alternatively, competitive displacement of anti-apoptotic proteins by Bax homodimers may allow for formation of their own channels, thereby committing the cell to apoptotic degradation (Adams & Cory, 1998).

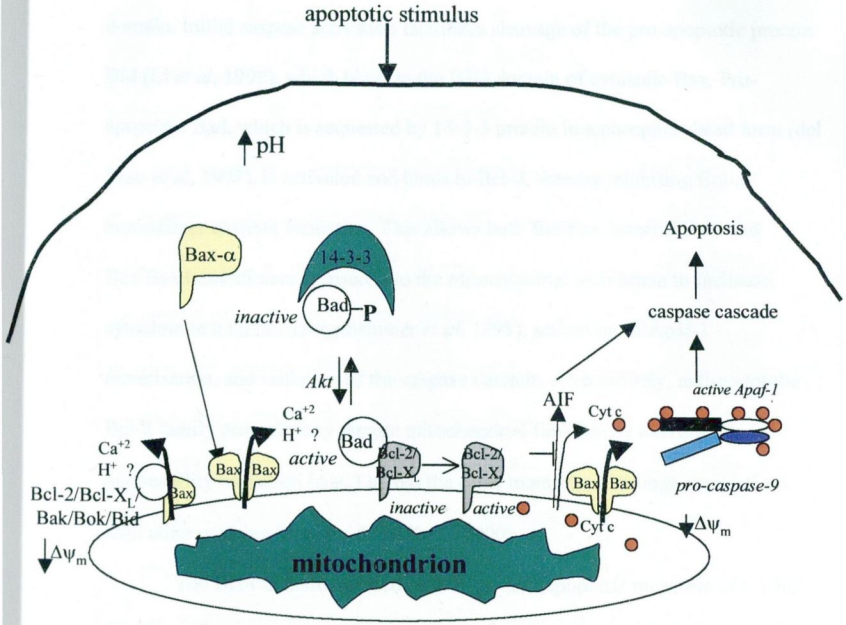


Figure 1.6- Model of Bcl-2 family regulation of mitochondrial function and apoptosis induction. Upon receipt of an apoptotic stimulus, a transient increase in intracellular pH facilitates Bax-α translocation from the cytosol to the outer mitochondrial membrane. Pro-apoptotic Bad, which is sequestered by 14-3-3 protein, is activated by Akt phosphatase, and binds and inactivates Bcl-2/Bcl-X_L homo/heterodimers, residing in the mitochondrial membrane. Homo/heterodimerisation of pro-apoptotic family members facilitates mitochondrial disruption, by release of cytochrome *c* and ions and other small molecules, and by decreasing the mitochondrial transmembrane potential. Cytochrome *c* release triggers Apaf-1 dimerisation and pro-caspase-9 activation, thus initiating the downstream caspases and apoptosis induction. (Adapted from Kelekar & Thompson, 1998).

In a model suggested by Khaled *et al*, (1999), the Bax protein resides in the cell cytoplasm and responds to various apoptotic stimuli by migration to mitochondria (Wolter *et al*, 1997), where it inserts itself via its C-terminal domain. Initial caspase activation facilitates cleavage of the pro-apoptotic protein Bid (Li *et al*, 1998), which binds to the BH3 domain of cytosolic Bax. Pro-apoptotic Bad, which is sequested by 14-3-3 protein in a phosphorylated form (del Peso *et al*, 1997), is activated and binds to Bcl-2, thereby inhibiting Bcl-2 homodimer channel formation. This allows both Bid/Bax heterodimers and Bax/Bax homodimers to insert into the mitochondrial membrane to facilitate cytochrome c release (Jurgensmeier *et al*, 1998), activation of Apaf-1 dimerisation, and initiation of the caspase cascade. Alternatively, anti-apoptotic Bcl-2 family proteins may disrupt mitochondrial function by altering the permeability transition ($\Delta\psi_m$) across the outer membrane, through interactions with other proteins (Pawlowski & Kraft, 2000).

The BH4 domain, located only in the anti-apoptotic members of the Bcl-2 family, may serve as a regulatory region, interacting with regulatory proteins outside the Bcl-2 family, such as c-myc (Bissonnette *et al*, 1992), Raf-1 (Wang *et al*, 1994a) and ced-4 (Huang *et al*, 1998). An unstructured, flexible loop lies between the BH4 and BH3 domains of Bcl-2 and Bcl-X_L only. This structure is believed to serve as a site of negative regulation, but is not essential for anti-apoptotic function (Chang *et al*, 1997). Bcl-2 may be converted into a death promoter as a consequence of the loss of the BH4 domain, by cleavage of putative caspase sites within this loop region (Cheng *et al*, 1997).

Bax, which is transcriptionally upregulated by *p53* tumour suppressor gene (Miyashita & Reed, 1995; Cregan *et al*, 1999) has also been suggested to act as a G_1/S checkpoint of cell cycle progression, as *Bax*-overexpressing cells proceed through S phase more rapidly than *Bcl-2*-overexpressing cells (Brady *et al*, 1996). The obvious complexity and hierarchies involved in *Bcl-2* family

protein-protein interactions allow for the intricate modulation of the apoptotic response.

1.1.6 Viral infection and apoptosis induction

Apart from the important role in development and normal tissue homeostasis, apoptosis also plays a key role in viral infection and host cell responses (Razvi & Welsh, 1996). In virus-infected cells, the induction of early cell death may severely limit viral production and reduce the dissemination of progeny virus to surrounding cells. Also, cellular perturbation caused by virus infection can inadventantly trigger cellular detectors to initiate an innate apoptotic response (Everett & McFadden, 1999). Thus, several animal viruses have evolved genes encoding proteins which effectively evade or delay apoptosis induction (*Table 1.2*). On the other hand, a number of viruses replicate very efficiently, leading to massive viral infection in the absence of anti-apoptotic effects (Gillet & Brun, 1996).

The proteins which these viruses encode to induce or inhibit apoptosis appear to target levels such as viral entry, or key effector molecules within the host-cell apoptotic cascade (Teodoro & Branton, 1997). HIV-1 and Reovirus cell surface molecules induce apoptosis in infected cells by functioning as 'superligands', to engage cellular pro-death receptors (Kaplan & Sieg, 1998), whereas others function as new members of the TNF receptor superfamily (Brojatsch *et al*, 1996).

Following influenza and HIV-1 infection, the host cell-encoded interferon-inducible, double-stranded (ds)-RNA-dependent protein kinase (PKR), is activated. The pro-apoptotic functions of PKR, which include Fas ligand-pathway activation (Balachandran *et al*, 1998) and protein synthesis inhibition

Virus	*Protein*	*Mechanism*	*Ref*
INDUCERS			
HIV-1	gp120, gp41	receptor signalling	Kaplan & Sieg, (1998)
	Tar mRNA	PKR induction	Clemens & Elia, (1997)
Reovirus	σ1	receptor signalling	Tyler *et al*, (1995)
	S1 mRNA	PKR induction	
Sindbis virus	E2	receptor signalling	Ubol *et al*, (1994)
Adenovirus	E1A	p53 potentiation	Teodoro *et al*, (1995)
HPV	E7	p53 potentiation	Nevins, (1992)
INHIBITORS			
Adenovirus	E1B-19K	Bcl-2 homolog	Farrow *et al*, (1995)
	E1B-55B	p53 antagonist	Rao *et al*, (1992)
EBV	BHRF-1	Bcl-2 homolog	Henderson *et al*, (1993)
	LMP-1	Fas/TNFα pathway inhibition	Wyllie, (1995)
HHV-8	KS-*Bcl-2*	Bcl-2 homolog	Cheng *et al*, (1997)
Cowpox virus	CrmA	caspase inhibition	Ray *et al*, (1992)
HCV	5A	PKR inhibition	Gale *et al*, (1997)
HIV-1	tat	PKR inhibition	Roy *et al*, (1990)
Vaccinia virus	E3L, K3L	PKR inhibition	Beattie *et al*, (1991)
HPV	E6/E7	$p53/p105^{Rb}$ inhibition	Nevins, (1992)
Baculovirus	p35/IAP	caspase inhibition	Manji *et al*, (1997)
SV40	T antigen	$p53/p105^{Rb}$ inhibition	Nevins, 1992
Mollucum contagiosum	MCO66L	anti-oxidant	Shisler *et al*, (1997)

Table 1.2- Viral protein inducers and inhibitors of apoptosis.

Abbreviations; HIV-1, Human Immunodeficiency virus-1; HPV, human papilloma virus; EBV, Epstein Barr virus; HHV-8, Human Herpesvirus-8; HCV; Hepatitis C virus; PKR, ds-RNA-dependent protein kinase.

(Adapted from Everett & McFadden, 1999; Gillet & Brun, 1996).

(Lee & Esteban, 1994), become manifest only in the presence of dsRNA intermediates, which are frequently present in the cytosol of infected cells as an intermediate of viral replication (Jacobs & Langland, 1996). The effectiveness of PKR activation as a cellular defence against viral spread is reflected by the fact that numerous other viruses appear to have developed strategies to suppress this kinase, including EBV, HIV-1, HCV and Adenovirus (*Table 1.2*). Vaccinia virus encodes at least two proteins, E3L and K3L, to ensure suppression of PKR (Beattie *et al*, 1991).

The caspase family of apoptotic proteases are also targeted (Gillet & Brun, 1996). Both Cowpox virus-encoded CrmA and Baculovirus-encoded p35 proteins, act as serine protease inhibitors, or serpins, to act as competitive inhibitors of the *ced-3*-like proteases in mammalian cells. Viral modulation of host cell death also occurs at the level of the endoplasmic reticulum (Pahl & Baeuerle, 1997) and mitochondrion (Tschopp *et al*, 1998). Numerous Bcl-2-like proteins have been identified in viruses such as Adenovirus, EBV, African Swine Fever virus, and Human Herpesvirus-8. Although Adenoviral E1B-19K protein bears no significant homology with Bcl-2, it binds to and inactivates both Bax and Bak proteins *in vivo*, thereby inhibiting their death-promoting activities (Boulakia *et al*, 1996).

Small oncogenic DNA viruses, including Adenovirus, HPV and SV40, all share the common property of being able to induce active DNA synthesis in quiescent host cells. Central to this is the activity of the tumour suppressor *p53* and $p105^{Rb}$ gene products (Teodoro & Branton, 1997). Each virus has adopted a different strategy to induce active cellular proliferation. HPV encodes two proteins, E6 and E7, which cooperate to induce cell tranformation. E6 targets p53 to proteolytic degradation and E7 inactivates $p105^{Rb}$, thereby releasing free E2F-1 and promoting extensive cell proliferation (Nevins, 1992). Adenoviral E1A protein also binds to $p105^{Rb}$ to induce cell transformation (Debbas & White,

1993). E1A is also a potent inducer of apoptosis, the response from which is dependent on the activity of *p53* (Teodoro *et al*, 1995), which is inhibitable by the adenoviral E1B-55K gene product (Rao *et al*, 1992).

The susceptibility of a given infected cell to the execution phase of apoptosis therefore depends on multiple factors, primarily the pre-existing thresholds established by host-cell anti-apoptotic modulators, and a variety of virally-encoded apoptotic modulators, to facilitate adequate viral replication and dissemination, or host-cell transformation.

1.2 CANCER GENE THERAPY

Increased knowledge of the gene-based mechanisms in the development of cancer, prompted the use of 'gene therapy' based regimes as a more rational treatment strategy, and which would also provide an adjunct to conventional treatments. The current strategies employed in gene therapy of neoplastic disease can be divided into 3 main areas; molecular chemotherapy, genetic immunomodulation and mutation compensation.

1.2.1 Molecular chemotherapy

The self-renewing nature of malignant disease dictates that tumour cells be cleared as efficiently as possible. Thus, one of the first cancer gene therapy strategies proposed, and the most frequently used, were designed to kill cells directly using toxic or prodrug therapy (Davis *et al*, 1996). This so called 'suicide gene' therapy approach involves the selective transduction of an enzyme, whose product can convert a relatively non-toxic prodrug, administered systematically,

to a toxic metabolite in the cancer cell. Enzyme gene transfer is usually achieved through a vector delivery system (*see below*), and selective expression may be accomplished by transductional targeting, where the gene is specifically delivered to the tumour; or by transcriptional targeting, where tissue- or tumour-specific activators are employed to turn on the gene selectively in the tumour (Moolten *et al*, 1994).

In the first protocol to be approved using this strategy, brain tumours were targeted with a retroviral vector expressing the Herpes Simplex virus *thymidine kinase* gene (HSV*tk*) (Jia *et al*, 1994). The HSV*tk* phosphorylates the systematically delivered antiviral drug, gancyclovir into an intermediary metabolite, which is then converted by cellular kinases into a potent inhibitor of DNA polymerase, leading to cell death. Normal cells remain unaffected by the drug. Studies in a rat glioma model showed that marked tumour regression occurred when only a small fraction (10%) of the cells were positively transduced by the vector (Freeman *et al*, 1993). This 'bystander effect' appears to be mediated principally by the transfer of gancyclovir-generated toxic metabolites into non-transduced cells via gap junctions, or by phagocytosis of apoptotic bodies of dead tumour cells by live tumour cells (Bi *et al*, 1993). Investigators have recently used recombinant viral vectors to deliver high levels of HSV*tk* to tumours such as lung carcinoma (Osaki *et al*, 1994), melanoma (Vile *et al*, 1994), mesothelioma (Hwang *et al*, 1995) and squamous cell carcinoma of the head and neck (O'Malley *et al*, 1995). Using this system *in vivo*, they reported significant tumour regression over a wide range of vector doses and clinically translatable gancyclovir levels.

Other prodrug therapy combinations include the bacterial enzyme cytosine deaminase (CD) and the anti-fungal and anti-neoplastic agent 5'Fluorocytosine (5'-FC); and nitroreductase which converts the non-functional CB19554 prodrug into a potent bifunctional alkylating agent (Austin & Huber,

1993; Green *et al*, 1997). When colorectal cancer xenografts were transfected with the *CD* gene, they became very susceptible to 5'-FC, with an IC_{50} of 25 μM compared with 26,000 μM for wild-type cells, resulting in 100% regression and 75% cure rate (Huber *et al*, 1994). The CD/5'-FC combination has also been shown to be ~8 times more potent than HSV*tk*/gancyclovir, and also demonstrates profound bystander effects.

In an opposite scenario, current strategies also include the molecular chemotherapy of normal cells to augment existing cancer treatments. Current protocols are attempting to introduce certain drug resistance genes into hematopoietic cells to provide increased protection from commonly used myelosuppressive chemotherapeutic agents (Sorrentino *et al*, 1992). Gene transfer of multidrug resistance gene (MDR)-1 allows for the production of P-glycoprotein, which functions as a cellular efflux pump, which expels a range of toxic metabolites from the cell. Mickisch *et al*, (1992), and other investigators showed that MDR-1 gene transfer provided resistance to a wide range of chemotherapeutic agents, including paclitaxel, anthracyclines and bisanthrene. The potential advantage of this approach is to allow high doses of chemotherapy to be administered to the patient with less associated toxicity, and approved MDR-1 clinical protocols already exist for the treatment of patients with breast and ovarian cancers who are receiving paclitaxel (Roth & Cristiano, 1997). Other potential genes include dihydrofolate reductase (May *et al*, 1995) and O^6-methylguanine-DNA methyltransferase, an efficient DNA repair enzyme, which was shown to protect mouse hemotopoietic cells from nitrosourea-induced toxicity (Moritz *et al*, 1995).

1.2.2 Genetic immunomodulation.

The majority of cancer gene therapy protocols have been aimed at immunostimulation. The major advantage of this approach is the potential to generate a systemic, rather than a local immune reaction against the tumour and any associated metastases. Many cancers can be recognised and destroyed by a tumour-specific immune response, usually mediated through cytotoxic T cells or natural killer cells (NKC). The activation of this process requires three synergistic signals; (1) presentation of tumour-associated antigens to T cells in conjugation with MHC class I and MHC class II molecules, which transport the tumour antigens to the cell surface, (2) additional costimulatory molecules, such as B7-1 and B7-2, which are required for effective induction of the efferent arm of the immune response, and (3) cytokines secreted by the helper T cell population following stimulation by the antigen presenting cell (APC). Many cancers may be defective in any one of the above pathways, which may contribute to T cell anergy to the tumour antigens (Harding *et al*, 1992). Also, tumour-mediated upregulation of immunosuppressive cytokines, such as IL-10 and TGFβ, may prevent an inflammatory response and lead to tumour tolerance (Todryk & Lemoine, 1998). Gene therapy based restoration of tumour antigen presentation pathways may enhance tumour cell destruction.

One of the major advances in cancer gene therapy has been the cloning and identification of tumour-associated antigens from human tumours, such as melanoma, which are recognised by both helper and cytotoxic T cells, providing defined targets for tumour vaccinations. One such tumour-associated antigen, carcinoembryonic antigen (CEA), a cell surface glycoprotein with a putative role in cell adhesion, is expressed in very low levels in normal adult tissues, but is overexpressed in the foetus and in 90% of colorectal, lung, ovarian and pancreatic cancers (Chung-Faye *et al*, 2000). A number of vector-based strategies, whereby

plasmid DNA and mRNA transcripts from CEA antigen have been used as a vaccine for *in vivo* anti-tumour activity, lead to CEA-specific humoral and cell-mediated immune responses, and growth inhibition of CEA^+ colon cancer cells in syngenic mice (Conry *et al*, 1995). In a human study, vector-based CEA immunisation of patients with early stage gastrointestinal malignancies revealed primary CEA-specific T cell responses (Kantor *et al*, 1992). However, molecular vaccination will require a 'cocktail' approach where multiple antigen cDNAs are employed, as tumours are highly heterogenous and unlikely to express only one dominant antigen on the surface of all cells.

Clinical trials reveal encouraging signs that cytokine-modified vaccines can generate significant tumour immune responses in patients with minimal toxicity. Many of the first clinical protocols for cancer gene therapy involved the *ex vivo* modification of freshly isolated tumour cells, tumour infiltrating lymphocytes (TIL's) or fibroblasts with cytokines such as IL-2 (Fearon *et al*, 1990) and TNFα (Asher *et al*, 1991). It was initially believed that TIL's had a propensity to traffic specifically and concentrate cytokines to tumour cells, and thus avoid the toxicity associated with systemically administered cytokines. Subsequently, this was disproved by a study which showed that tumours did not significantly take up the TIL's *in vivo* (Nerrouche *et al*, 1995). Successful experiments have been reported which have challenged murine melanoma, human colorectal and rat prostatic cancers with vaccines expressing IL-4 (Golumbek *et al*, 1991), IL-7 (Hock *et al*, 1991), IL-12 and IFNγ (Gansbacher *et al*, 1990). Granulocyte macrophage-colony stimulating factor (GM-CSF) stimulates the proliferation of granulocyte and macrophage precursors and activators. Murine melanoma cells transfected with the murine GM-CSF gene, showed markedly decreased growth and high levels of GM-CSF expression following injection into mice, and tissue sections revealed neutrophil, macrophage and T cell migration to

the site of the tumour (Gunji *et al*, 1996). A phase 1 trial of autologous tumour cell and IL-12-transduced fibroblast immunisation in patients with metastatic colon cancer is ongoing.

Enhancement of costimulatory molecules B7-1 and B7-2 may also facilitate greater T cell stimulation. Vaccination with B7-2-transduced colorectal tumours has been shown to generate anti-tumoural protection in 50% of cases compared to controls when injected into syngenic mice. Cotransfection of B7 and another immunogenic gene seems to generate better immunity than with B7 alone. Vaccination with B7 and IL-7, or B7 and IL-12, enhanced rejection of parental tumours compared with tumour cells carrying only one of the two genes (Chong *et al*, 1998). One substantial difficulty with this approach is the heterogeneity and unpredictability of loss of costimulatory molecules in human cancers.

1.2.3 Mutation compensation.

Due to the gene-based mechanisms of tumourigenicity, mutation compensation has become the most important strategy in cancer gene therapy. The identification of specific genes that contribute to the development of cancer, including dominant protooncogenes and tumour suppressor genes, presents an opportunity to use these genes as prevention and treatment targets. Based on this realisation, the introduction of a functional tumour suppressor gene, or the downregulation of an activated oncogene, could eventually lead to the destruction of the malignant cell. One would assume that for most cancers, this goal is elusive, because malignant transformation is usually accompanied by a series of genetic mutations. However, some of these mutated genes occupy pivotal roles in the execution and regulation of cell growth arrest, homeostasis and apoptotic cell

death, and are thus, crucial for the maintenance and propagation of the malignant phenotype.

1.2.3.1. Ablation of activated oncogenes

A variety of strategies have been designed to abrogate the expression of dominant oncogenes responsible for the inhibition of apoptosis and malignant transformation of cells. Antisense technology involves the introduction into the cell of a gene construct that has a base sequence complementary to the RNA sequence targeted for inhibition. The advantage of this is the potential to achieve ablation of oncogene activity at the proximal level of mRNA splicing, transport or translation. This strategy has been used effectively for the downregulation of mutant K-*ras* protein in NSCLC cell lines (Georges *et al*, 1993; Mukhopadhyay *et al*, 1991). K-*ras*, a member of the GTPase family of oncoproteins, is frequently mutated early on in lung, colorectal and other cancers (Marshall, 1991). In colon cancer cell lines, antisense oligonucleotides (ASO's) complementary to K-*ras* inhibited cell growth, colony formation and K-*ras* expression in a dose-dependent manner (Sakakura *et al*, 1995).

In recent years, the efficiency of these ASO compounds has been enhanced through advances in oligonucleotide chemistry. Phosphorthioated ASO molecules targeted towards the potent anti-apoptotic factor *Bcl-2*, has been used in a limited number of patients with non-Hodgkins lymphoma, with low systemic toxicity and promising responses (Webb *et al*, 1997). Expression of Bcl-X_L, a close anti-apoptotic homologue of *Bcl-2*, was similarly downregulated using a 2'methoxy-ethoxy-modified ASO in a number of small cell lung cancer cell lines (Leech *et al*, 2000). Other oncogenes targeted include the cAMP-dependent protein kinase A (Nesterova *et al*, 1995), and TGFα (Laird *et al*, 1994).

More recently, a catalytic antisense RNA, or ribozyme strategy, has been developed, which allows for highly specific cleavage and degradation of target mRNA (Gibson *et al*, 2000). Ribozymes have the added advantage that following degradation of the target mRNA molecule, the molecule becomes free to bind to another molecule, thereby increasing the levels of oncogene ablation. Hammerhead ribozymes specific for *Bcl-2* mRNA have been shown to sensitise prostate cancer cells to apoptotic cell death induction (Dorai *et al*, 1997). Finally, single-chain antibody targeting offers an attractive alternative to ASO's. These antibody molecules can specifically recognise proteins such as Bcl-2 or epidermal growth factor receptor (EGFR), the CD19 antigen, bind specifically to them, neutralise their activities, reverse the malignant phenotype and induce cell death in a variety of lymphomas and B cell leukemias (Piche *et al*, 1998; Bejcek *et al*, 1995). Although promising, it remains to be determined which of these strategies will be successful in inducing tumour regression.

1.2.3.2. Augmentation of mutated tumour suppressor genes

The replacement of tumour suppressor gene function has also gained importance in cancer gene therapy. The inactivation of certain genes, such as *p53* and, $p105^{Rb}$ may contribute to tumour progression (Takahashi *et al*, 1989). The fact that both copies of the gene must be mutated or deleted to eradicate the growth suppressive functions of the protein, means replacement of a functional copy of the gene in malignant cells could restore normal growth or induce cell death. Uncontrolled tumour growth is often caused by loss of the *p53*-regulated checkpoint in the cell cycle. Missense mutations or deletions in the *p53* gene are observed in a myriad of cancer types, and are essential for their transforming ability (Hollstein *et al,* 1991). The restoration of wt-*p53* is sufficient to cause

programmed cell death or growth arrest, despite many other genetic abnormalities which may be present in the cell. As a result, a multitude of studies, using many different methods of delivery, have proven successful in replacing wt-*p53* activity in malignant cell, leading to growth inhibition due to cell cycle arrest, or apoptosis induction, followed by tumour regression *in vivo* (Quazilbash *et al*, 1997; Fujiwara *et al*, 1993; Rizk *et al*, 1999). Cell mixing experiments *in vitro* and *in vivo* have also shown that transduction with wt-*p53* induced cell death in non-transduced neighbouring tumour cells, owing to a bystander effect as described for molecular chemotherapy (Bouvet *et al*, 1998). As *p53* is inactivated in up to 70% of human lung malignancies, a significant number of wt-*p53* gene replacement protocols have been applied to lung cancers (Fujiwara *et al*, 1994b). More recently however, this strategy has been applied to a myriad of other human cancer cell lines, including, squamous head and neck (Liu *et al*, 1995; Frederick *et al*, 1999), ovarian (Hamada *et al*, 1996), colorectal (Harris *et al*, 1996), prostate and nasopharyngeal carcinomas (Li *et al*, 1997b), with the successful induction of programmed cell death in culture and in subcutaneous mouse xenograph and orthotopic (intratracheal) cancer models (Fujiwara *et al*, 1994a). Numerous human clinical trials have also proven effective (Schuler *et al*, 1998; Roth *et al*, 1996), with one recent study indicating therapeutic activity, including partial responses in 8% of patients, and disease stabilisation in 64% of the 25 evaluable patients (Swisher *et al*, 1999).

p53 has not been unique in gene replacement applications. Other tumour suppressor genes, including *pRB*, demonstrate a dose-dependent reduction in tumour size of retinoblastoma mutant cell lines (Xu *et al*, 1996). Others, such as the colon-specific *APC* gene, *plasminogen activator factor-2* and *p16* (Jin *et al*, 1995), and other potent pro-apoptotic proteins, such as caspase-3 (Yamabe *et al*, 2000), Bcl-X_S (Sumantran *et al*, 1995) and Bax (Tai *et al*, 1999) have all proved

effective at reducing tumour burden by inducing a programmed cell death pathway.

Although the *Bax* gene product functions primarily as a pro-death factor, investigators have shown that this protein also has tumour suppressor functions (Brady *et al*, 1996). Vector-based strategies to overexpress this protein in NSCLC and other malignancies have demonstrated high levels of Bax expression and extensive apoptosis induction in tumours, regardless of their *p53* status (Kagawa *et al*, 2000; Xiang *et al*, 2000). Bax overexpression may also facilitate apoptosis induction in more resistant cell lines, particularly those which overexpress key apoptosis inhibitors, such as *Bcl-2*.

As oncogene and tumour suppressor gene status has a profound influence on the chemotherapeutic and radiotherapeutic sensitivities of a malignant cell population, mutation compensation strategies, such as those described above, may be used in conjunction with conventional therapies as an adjunct, thereby increasing the overall effectiveness of cancer therapy. This has already been demonstrated using vector-based wt-*p53* overexpression and cisplatin treatment (Fujiwara *et al*, 1994b), which proved much more effective at reducing tumour burden *in vivo* than either therapy alone.

There are however, limitations to the mutation compensation approach, the majority of which appear to be due to inadequacies in vector delivery, and will be discussed below.

1.3 VECTORS FOR CANCER GENE THERAPY.

The success of cancer gene therapy depends largely on an efficient gene delivery system. Therapeutic effects demand that the delivery system chosen must reach the target tumour cell population, transduce them, translate the therapeutic protein(s), deliver the protein(s) to the site of action and express it in such a way as to have the desired effect. There are two main types of gene-delivery vector for cancer therapy; viral and non-viral, both of which will be discussed separately below.

1.3.1 Viral vectors for gene delivery.

Currently, viruses represent the best available system for gene delivery *in vivo*, particularly in cancer gene therapy applications, and this is primarily due to their naturally high transfection efficiencies (Vile *et al*, 2000). Viral vectors are modified viruses in which the genes required for viral replication have been either partially or completely removed, and replaced with the therapeutic gene(s). The viral proteins which are encoded for by the missing viral genes are supplied *in trans*, using a 'helper' virus(es) (Smerdou & Liljeström, 1999) or a packaging cell line (Markowitz *et al*, 1988). Both helper species supply the remainder of the viral genome and produce all proteins necessary for assembly of the recombinant viral particles. When released, the replication-defective vector will then transport the therapeutic gene to the target cell instead of its own genetic information. Since the vector particles only carry a therapeutic gene and not the complete viral genome, only therapeutic proteins and no viral particles are produced in the target cells (Klein & Günzberg, 1997). This scenario is mirrored in all viral vector systems, and many different viruses have been adapted as vectors. The three most widely

used viruses, particularly for cancer therapy purposes, are Retrovirus, Adenovirus and Adeno-associated virus. These are described below and are summarised in Table 1.3.

1.3.1.1 Adenovirus vectors

The natural affinity of adenovirus for the respiratory epithelium initially led to the development of adenovirus vectors (Ad) for use in the genetic treatment of cystic fibrosis and emphysema (Rosenfeld *et al*, 1991). The majority of cancer therapy studies that have given the most encouraging results to date, have utilised this Ad system as the delivery agent (Sobol & Scanlon, 1995). It is clear that for a variety of cancer types, Ad vectors give more efficient gene transfer compared with any other system, particularly *in vivo*. Most first generation Ad vectors were based on the Ad5 serotype (Li *et al*, 1993), since this dsDNA vector was capable of transducing cells at very high titres, regardless of their mitotic status, to give high levels of expression of the therapeutic gene (Mehtali *et al*, 1996). Ad5 vectors have capacity for up to 7.5kb of heterologous DNA, following homologous recombination with the E1 and/or E3 regions of the Ad genome. This results in a dependence on the embryonic kidney cell line 293, that provide the essential E1 gene products *in trans*.

However, the initial enthusiasm over Ad vectors has been tempered by the realisation that host immune responses and inflammation against existing Ad proteins severely limits the time of episomal gene expression or the efficiency of repetitive vector administration (Kaplan *et al*, 1996). Recent studies indicate that 55% of adult humans have pre-existing anti-Ad antibodies capable of neutralising even initial *in vivo* infections by Ad5-derived vectors (Chirmule *et al*, 1999). These observations have stimulated a tremendous number of studies that have sought to attenuate the host responses, including the introduction of temperature-

Feature	Retrovirus	Adenovirus	Adeno-associated virus (AAV)	non-viral
Capacity (kb)	7	7-10	4.5	no limit
Target cells	replicating	replicating & quiescent	replicating & quiescent	replicating & quiescent
Average Titre (Particles/ml)	10^6-10^7	10^{11}	10^{12}	-
Stability	Low	High	High	Low
Efficiency	Low	High	High	Low
Integration	Integrates randomly	Episomal	Integrates 70% Chromsome 19	Episomal
Expression	Long-term	Transient	Long-term	Very transient
Host response	Complement-mediated lysis	Host Immune reactions & inflammation	Humoral response	No response detected
Biosafety	Insertional mutagenesis	Human Pathogen & RCV	Random Integration & Helper virus contamination	Good safety profile
Retargeting	Difficult	Efficient retargeting transfection demonstrated	Efficient retargeting transfection demonstrated	Moderately difficult
Cost & ease of manufacture	Manufacture, strorage, QC extremely difficult	Manufacture, strorage, QC moderately difficult	Manufacture, strorage, QC extremely difficult	Manufacture, strorage, QC simple & cheap

Table 1.3- Comparision of gene transfer vectors. Abbreviations, RCV; replication-competent virus, QC; quality control. (Adapted fron Klein & Güzburg, 1997).

sensitive *E2a* gene mutations, to bring about minimal viral late gene expression to blunt the immune response (Engelhardt *et al*, 1994), or the deletion of most or all of the Ad proteins, to produce 'gutless' vectors (Schnieder *et al*, 1998), which can accommodate up to 30 kb of foreign DNA. Strategies to overcome pre-existing Ad antibodies include the use of IL-12 overexpression to downregulate the T_H2 subset of T helper cells which are necessary for antibody production (Yang *et al*, 1995a), macrophage deletion (Stein *et al*, 1998), and the administration of immunosuppressive drugs to decrease anti-Ad inflammatory responses (Fang *et al*, 1995). Finally, since Ad has 47 different serotypes, some investigators have proposed that distinct serotypes, or different Ad capsid proteins, be sequentially administered to patients, in an attempt to circumvent the neutralising effects (Mastrangeli *et al*, 1996). In stark contrast to this, Vile *et al,* (2000) proposed that the immunogenicity afforded with Ad vectors probably offers an added adjuvant bonus in the context of cancer treatment, although this remains to be proven.

The development of 2nd generation Ad vectors also pose increased manufacture and stability problems, as well as the added reservation of replication-competent virus (RCV) contamination (Fallaux *et al*, 1998), which arises through recombination between viral sequences in the vector and the chromosome of packaging producer cells. Also Ad is a human pathogen (Horwitz, 1990), causing mild upper and lower respiratory tract infections. Toxic effects in patients have also been reported after administration of an Ad vector expressing the *CFTR* and *wt-p53* genes (Mountain, 2000).

Nonetheless, the majority of mutation compensation studies for cancer gene therapy have utilised these vectors. The most advanced of these is *wt-p53* delivery for induction of apoptosis and tumour cell killing (Rizk *et al*, 1999; Li *et al*, 1997b; Frederik *et al*, 1999). A series of Phase II studies are underway, and a number of clinical trials have published encouraging reports of tumour treatment using the Ad-*wt-p53* construct alone, or in combinantion with chemotherapies for

the local management of various cancers (Schuler *et al*, 1998; Swisher *et al*, 1999).

1.3.1.2 Retroviral vectors

In terms of cancer gene therapy, more clinical experience has been obtained so far with retroviruses (Rv) than with any other vector. Up until very recently, the majority of approved gene-transfer protocols for cancer therapy used Rv systems (Sorbol & Scanlon, 1995), as the propensity for Rv to integrate into rapidly proliferating cells appeared to be an advantage (Fujiwara *et al*, 1994c). The initial rationale of the use of Rv vectors to target exclusively dividing tumour cells on the background of quiescent tissue is being gradually superseded however, by the realisation that human tumours generally cycle much more slowly than the rodent cell lines on which this strategy was based (Vile *et al*, 2000). Rv unlike Ad, transfect cells by integrating the transgene into the target cell chromosome (Miller *et al*, 1990). This results in more prolonged expression, but at much reduced levels. In contrast to Ad systems, most 1st generation Rv do not express residual viral proteins, and thus are much less immunogenic than Ad (Roth & Cristiano, 1997; Ghazizadeh *et al*, 1997). For cancer gene therapy, Rv has been most useful where prolonged gene expression was required, such as the delivery of antisense mRNAs or anti-angiogenic factors (Chung-Faye *et al*, 2000). In terms of gene replacement therapy, numerous *in vivo* xenograft studies and clinical trials have revealed apoptosis induction and tumour regression following Rv-mediated exogenous *wt-p53* delivery (Fujiwara *et al*, 1994a; Roth *et al*, 1996).

However, Rv has presented serious manufacturing challenges, with difficulties in achieving high titres and retention of infectivity through concentration and storage. Additional problems with RPV, through recombination

with cryptic Rv's that are resident in the tumour genome, have since been largely rectified with the onset of packaging cell lines that split the packaging signals between 2 plasmids (Markowitz *et al*, 1988). Also, the intrinsically limited host range of Rv may now be overcome following pseudotyping studies, whereby the packaging cell line, in which envelope proteins having the desired host range are substituted for endogenous Rv proteins, have also become available (Yam *et al*, 1995).

1.3.1.3 Adeno-associated virus and other DNA viruses.

Work in the field of virology has identified a large number of viruses that have unique characteristics useful for their application in gene therapy. The small linear ssDNA Adeno-associated virus (AAV) poses several advantages for gene therapy, including low pathogenicity, low immunogenicity, a broad host range and stable expression of foreign proteins (Monaghan & Samulski, 2000). AAV vectors can be generated in which most of the viral genome has been replaced with the therapeutic gene, and as a result, there is less chance of developing an immune response to the vector. In terms of pre-existing antibodies, limited data suggests that 32% of adult humans possess pre-existing antibodies that will neutralise transfection *in vitro* of the AAV2 serotype, from which most AAV vectors are derived (Chirmule *et al*, 1999). AAV have an integrative capacity for a specific region of chromosome 19 (Samulski *et al*, 1991), although this appears to be lost or randomised for the recombinant virus. However, transgenes appear to persist, either as genuine integrants and/or stable episomes, both of which may be actively transcribed (Mountain, 2000). AAV vectors expressing *wt-p53* have shown great promise in mediating human lung tumour regression both *in vitro* and *in vivo* (Quazilbash *et al*, 1997), and have also been utilised in various other

anti-cancer strategies for exogenous expression of anti-angiogenic and pro-apoptotic factors (Nguyen *et al*, 1998).

The main disadvantage of AAV concerns insert size and manufacture. Production requires the use of a helper virus such as Ad or Herpes virus, to provide the missing viral genes, and as a result, contamination of preparations with helper virus can frequently occur (Ferrari *et al*, 1997). Production difficulties also affect particle titres, which are quite low at 10^4 I.U./ml, compared with what is required for the treatment of large tumours (Vile *et al*, 2000).

In addition, Herpes Simplex virus has received some attention as a vector because of its ability to establish latent infection in the brain (Latchman, 1994). Also poxviruses, particularly Vaccinia virus, have been studied intensely as an efficient delivery system (Hodge *et al*, 1994). Baculovirus, an insect virus system, is also being considered for gene therapy, primarily due to high levels of protein expression (Forstova *et al*, 1995). Finally, substantial effort has gone into the develoment of lentiviral vectors, such as Simian Immunodeficiency virus and HIV. Unlike their Rv predecessors, these viruses can infect both dividing and non-dividing cells (Trono, 2000).

1.3.2 Non-viral (synthetic) gene therapy.

The second main type of gene delivery for cancer therapy are non-viral vectors. Non-viral approaches fall into three main categories; (1) naked DNA, (2) DNA complexed with cationic lipids and (3) DNA condensed with cationic polymers. Non-viral therapies were initially developed due to their ease of manufacture and lower toxicity and immunogenicity compared with their viral counterparts (Ledley, 1994). The simplest of delivery systems have been achieved

by mechanical means, such as direct injection of DNA or high velocity bombardment of tissues with DNA attached to gold particles. However, naked DNA results in only very transient gene expression, is rapidly degraded and effects are only limited to the site of injection (Li & Hunag, 2000). In terms of cancer therapy however, this technology has been applied in three clinical protocols for the generation of vaccines against colon cancer and melanoma (Sobol & Scanlon, 1995).

In cationic lipids/polymer delivery, the nucleic acid is complexed with molecules that facilitate its delivery to cells by way of electrostatic interactions (Felgner *et al*, 1987). Although expression is transient, helper lipids such as cholesterol and polyethyleneglycol-conjugates, have been successful in ligand receptor-mediated targeting and nuclear localisation *in vitro* (Thierry *et al*, 1997). Several studies have employed cationic lipid-DNA formulations, injected directly into tumour masses as successful tumour vaccines (Conry *et al*, 1995), and due to the lack of immunogenicity, these systems are amenable to repetitive administration (Plautz *et al*, 1993). However, problems such as instability and relatively poor transduction efficiencies have limited their use *in vivo*. The requirement for an endosomal lysis agent to mediate nuclear entry prior to degradation, have recently utilised a lipid-DNA-Ad chimera, where the endosome-disrupting properties of Ad were utilised effectively (Curiel *et al*, 1992).

The fact that neither synthetic nor viral vector systems alone demonstrate all the required necessities as a cancer therapy vector, several investigators have proposed hybrid or chimeric systems (Bilbao *et al*, 1997; Feng *et al*, 1997), which aim to mix and match the DNA-binding and protection from host responses afforded by the synthetic component, with the endosomal escape, efficiency of delivery and long-term persistence mediated by the viral component.

1.4 SEMLIKI FOREST VIRUS

Semliki Forest virus (SFV) belongs to the genus Alphavirus, and is a member of the *Togaviridae* family, which also includes Venezuelan equine encephalitis virus (VEE), Western equine encephalitis virus and Eastern equine encephalitis virus (EEE) and Sindbis virus (SV), the prototypical alphavirus. The alphaviruses are arthropod-borne, neurotropic viruses, which may also infect mammalian and avian species. Much of the information regarding the structure and replication of alphaviruses has been obtained from studies with both SFV and SV.

1.4.1 Structure of the SFV virion.

SFV is a simple, spherical virus with a diameter of approximately 69 nm. The virion is composed of iscosahedral protein lattices with an associated membrane bilayer, which in SV, is approximately 4 nm thick (Renkonen *et al*, 1971) (*Figure 1.7*). The nucleocapsid core contains a single RNA molecule of about 11.4 kb, in association with 240 copies of the viral capsid (C) or core protein. The C protein (approx. 30 kDa) contains an N-terminal RNA-binding domain and a conserved chymotrypsin-like serine protease COOH terminal domain, which facilitates capsid autocleavage from the nascent viral polypeptide (Melancon & Garoff, 1987; Owen & Kuhn, 1996). Due to its fenestrated structure, the RNA within the nucleocapsid is RNase sensitive, and has a diameter of approximately 40 nm (Soderland *et al*, 1979).

Both the nucleocapsid and host membrane-derived viral envelope are organised into T=4 icosahedral lattices (Choi *et al*, 1991; von Bonsdorff & Harrison, 1975). Each viral spike consists of three copies each of the

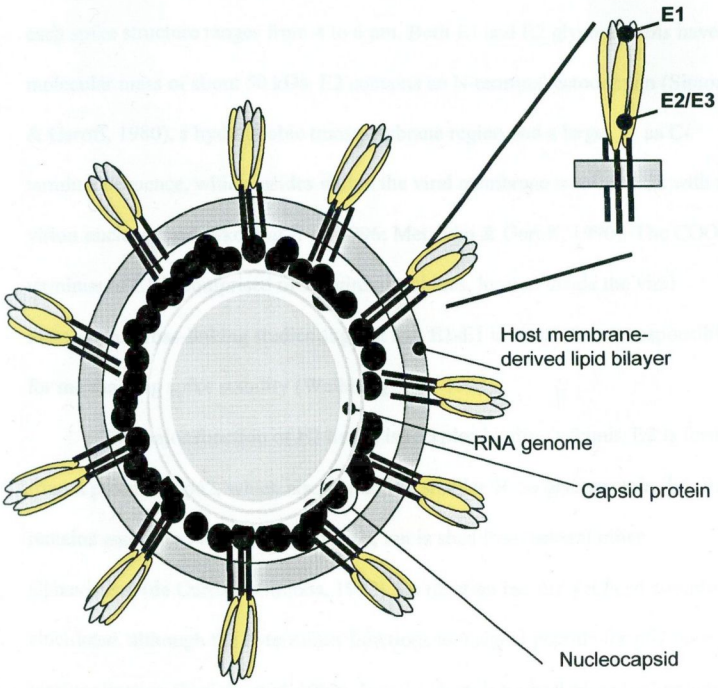


Figure 1.7- Structure of the SFV virion.

The SFV virion consists of a nucleocapsid containing a single-stranded RNA molecule of positive polarity, encapsidated with 240 copies of the C protein. The host-derived lipid bilayer contains 80 spikes, each of which are composed of three copies of the E1, E2 and E3 glycoproteins. Only the C terminal tail of the E2 glycoprotein is in contact with the nucleocapsid core.

glycoproteins E1/E2/E3. Three heterotrimers interact to give 240 heterotrimers on the surface, assembled into 80 spikes (Garoff *et al*, 1974). The distance between each spike structure ranges from 4 to 6 nm. Both E1 and E2 glycoproteins have a molecular mass of about 50 kDa. E2 contains an N-terminal ectodomain (Simons & Garoff, 1980), a hydrophobic transmembrane region and a large, 31 aa C-terminal sequence, which resides within the viral membrane and interacts with the virion nucleocapsid (Skoging *et al*, 1996; Metsikko & Garoff, 1990). The COOH-terminus of E1 is comprised of 2 arginine residues, located inside the viral membrane. Cross-linking studies suggest that E1-E1 interactions are responsible for maintaining spike stability (Walhberg *et al*, 1992).

The major function of E2 lies in is receptor-binding subunit. E2 is formed from a precursor, p62, which also contains a smaller 66 aa glycoprotein, E3. E3 remains associated with the SFV virion, but is shed from several other alphaviruses (de Curtis & Simons, 1998). Its function has not yet been completely elucidated, although the N-terminus functions as a signal peptide for p62 during viral replication (Sariola *et al*, 1995). Finally, there is a small 66 aa hydrophobic peptide, 6K, found in submolar quantities in the SFV virion. Although also of unknown function, it may be involved in viral budding (Liljeström *et al*, 1991; Lusa *et al*, 1991).

1.4.2 Genome structure and organisation.

The structure of the SFV genome is illustrated in Fig. 1.8. Approximately 11.4 kb in length, the SFV genome consists of a single strand of positive-sense RNA, with an overall sedimentation coefficient of 42S (Strauss & Strauss, 1994). The genome is arranged into two modules, both of which are capped with a 5' 7-methylguanosine residue, and a 3' polyadenylated tail (Sawicki & Gamatos,

Figure 1.8- Schematic representation of the SFV genome.

The 5' two-thirds of the genome encode the non-structural proteins (nsPs), which are translated as the polyprotein P1234. P1234 is subsequently processed to nonstructural proteins nsP1-nsP4, through the action of the nsP2 and nsP4 autoproteases. The structural proteins are also transcribed and translated as a polyprotein, and is also post-translationally cleaved. (Adapted from Strauss & Strauss, 1994).

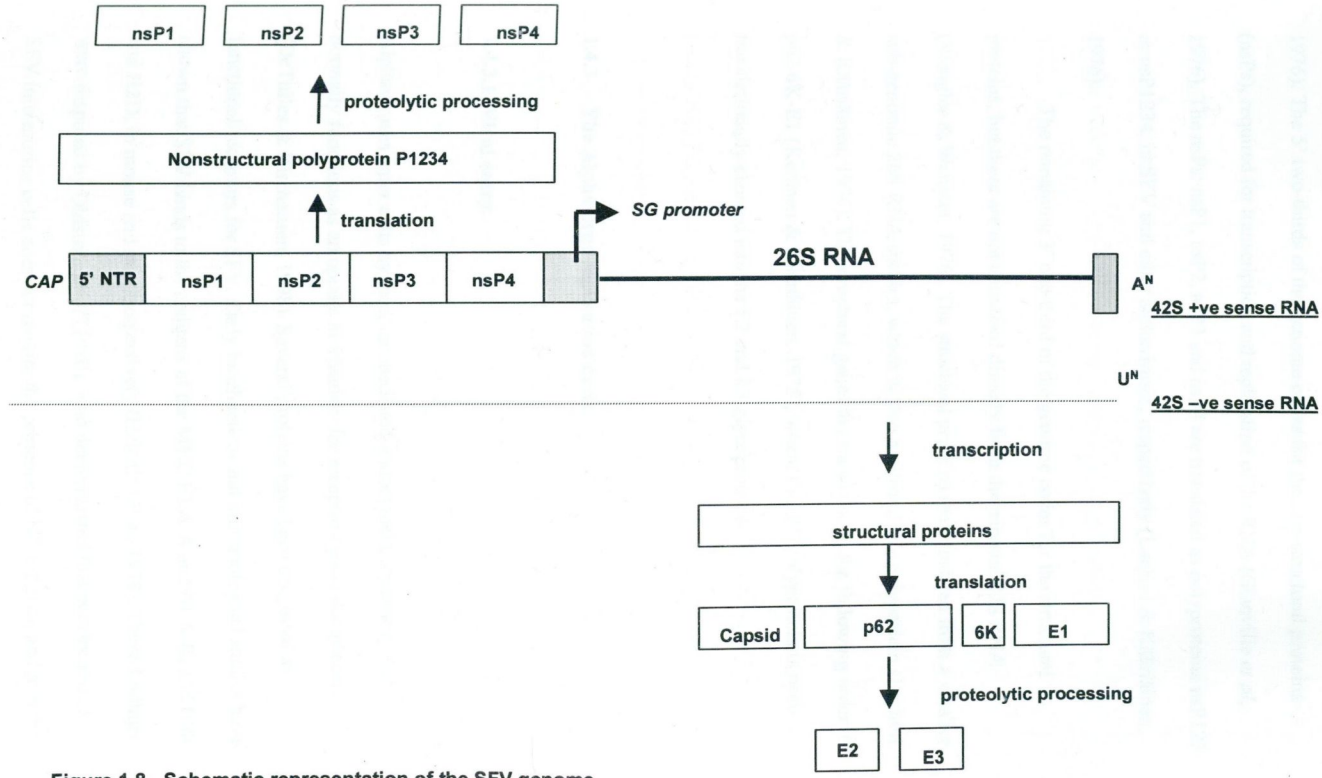


Figure 1.8- Schematic representation of the SFV genome.

1976). The 5' two-thirds of the genome codes for the non-structural proteins (nsPs), required for transcription and replication of the RNA (Glanville *et al*, 1976). The nsPs: nsP1, nsP2, nsP3 and nsP4 are translated as polyproteins nsP123 or nsP1234, in SFV and other alphaviruses, respectively (Lachmi & Kääriäinen, 1976).

The remaining 3' one-third of the genome codes for the structural proteins, but these are not translated directly from the parental 42S RNA (Wengler & Wengler, 1976). The structural proteins are translated from a smaller sub-genomic 26S RNA species, which is also produced as a polyprotein (Lachmi & Kääriäinen, 1976). The structural genes are translated in the following order: C-p62-6K-E1 (Keränen & Kääriäinen, 1975), where the p62 polyprotein is post-translationally cleaved into the E2 and E3 glycoproteins.

1.4.3 The Alphavirus replication cycle.

1.4.3.1 Viral entry.

Alphaviruses enter cells by receptor-mediated endocytosis, a pathway that normally functions as an uptake mechanism for receptor-ligand complexes (DeTulles & Kirchausen, 1998). Several proteins have been suggested as functional receptors for SFV. Early biochemical and immunological studies have shown that SFV binds to the antigens of the MHC HLA-A and HLA-B, and H2K and H2D, in mouse and man, respectively (Helenius et al, 1978). These findings were disputed by Oldstone *et al* (1980), who demonstrated that penetration of SFV into murine cells does not require the presence of H2 antigens, and that the MHC antigens are not a specific receptor for SFV. In contrast, for SV, a 67 kDa laminin receptor has been identified as the putative mammalian receptor (Wang *et*

al, 1992), although other molecules may also facilitate SV entry. Consistent with its broad host range and its ability to replicate in many different cell types, it is possible that SFV utilizes a variety of surface receptors with varying affinities (Strauss & Strauss, 1994). The E2 subunit of the SFV spike has been shown to interact with the cell surface and to facilitate viral entry (Dubuisson & Rice, 1993).

Following internalisation, a reduction in endosomal pH induces a conformational change in the viral spike proteins, resulting in E1-E2 heterooligomeric dissociation as well as conformational changes within individual E1 and E2 subunits (Wahlberg *et al*, 1992). E2 dissociation stimulates E1 homotrimerisation at the centre of the spike. This E1 homotrimer directly mediates fusion of the viral membrane with the endosomal membrane (Wahlberg *et al*, 1992). The fusion process itself is cholesterol-dependent. Sphingolipids also support SFV viral membrane fusion (Jan *et al*, 2000), where only the D-*erythroid* sphinglipid (the naturally occurring stereoisomer) is necessary (Strauss & Strauss, 1994).

Following fusion, the nucleocapsid is released into the cytoplasm where it is uncoated by host cell ribosomes (Singh & Helenius, 1992). This culminates in the release of viral RNA into the cytoplasm.

1.4.3.2. Viral RNA replication.

RNA replication occurs exclusively in the cell cytoplasm, more specifically, in approximately 2 μm-wide type-1 cytoplasmic vacuoles (CPV-1), derived from endosomes and lysosomes (Froshauer et al, 1988; Peränen & Kääriäinen, 1991). Alphaviral RNA is 5' capped and 3' polyadenylated, and thus can function directly as an mRNA.

In the early phase of infection, the 5' two-thirds of the genome corresponding to the non-structural proteins of the virus are translated to form the polyprotein precursor P1234 (Lachmi & Kääriäinen, 1976). An AUG codon in the 5' NTR of SFV is the initiation site for translation (Kääriäinen *et al*, 1987). Autoproteolysis of the polyprotein precursor into non-structural proteins nsP1-nsP4, follows two alternative pathways (Peränen *et al*, 1988; Takkinen *et al*, 1991). For SV and other alphaviruses, an opal termination codon, 3' of the nsP3 gene is used to generate two alternative polyprotein intermediates, P123 and P1234 (Strauss *et al*, 1983; Hardy & Strauss, 1988). These are then cleaved by the COOH-terminal proteinase activity of the nsP2 protein (Ding & Schlesinger, 1989). P34 is cleaved by nsP4-mediated autoproteolysis (Takkinen *et al*, 1990). The four non-structural proteins function during infection as polyproteins as well as cleaved final products.

Functional analysis of the four non-structural proteins was derived mainly from studies of conserved sequence motifs and the study of temperature-sensitive (*ts*) mutants. SV *ts* mutants that fail in RNA replication are divided into four different complementation groups, all of which have mutations in one of the 4 non-structural proteins. nsP1 has been implicated in the synthesis of minus-strand RNA (Wang *et al*, 1991). Other functions including a methyl-transferase activity and an ability to anchor the replication complex to intracellular membrane structures have also been shown (Peränen *et al*, 1988). Alphaviruses utilise a novel mechanism for the methylation of the 5' terminal CAP structure on both 42S and 26S RNA. GTP is firstly methylated to yield 7-methyl-GTP and is then translocated to the 5' end of viral RNA by nsP1 guanyltransferase activity (Ahola *et al*, 1995).

nsP2 appears to be involved in the regulation of 42S and 26S RNA synthesis (Sawicki & Sawicki, 1985). nsP2 contains a COOH-terminal NLS p^{648}RRRV, and approximately 50% of nsP2 appears to be localised in the host-

cell nucleolus (Peränen *et al*, 1990). The nuclear localisation of nsP2 is still unresolved but mutational analysis demonstrates that abolishing nuclear localisation does not abrogate viral growth. nsP2 has also been postulated as an RNA helicase (Gorbalenya & Koonin, 1989), but more importantly has been shown to contain an autoproteinase activity in its COOH-terminus, which functions both *in cis* and *in trans*, to cleave the nsP1/nsP2 bond during viral replication (Ding & Schlersinger, 1989).

Although phosphorylated by an autophosphorylase or cellular kinase (Peränen, 1991), the function of nsP3 in viral replication is not well understood. Replication complexes have been shown to contain heavily phosphorylated nsP3, in association with nsP1 (Peränen *et al*, 1988), and may be required in some capacity for RNA synthesis (LaStarza *et al*, 1994). More recently, specific deletions in the COOH-terminal of the nsP3 gene have significantly reduced the neuropathogenicity of the virus in rodents (S. Galbraith, *personal communication*).

nsP4 is postulated as the RNA polymerase of alphaviruses (Argos, 1988). It contains a GDD sequence motif characteristic of RNA-dependent RNA polymerases, and this is supported by nsP4 *ts* mutants with total cessation of viral RNA synthesis (Hahn *et al*, 1989). The concentration of nsP4 is tightly regulated. This is primarily due to the presence of the opal termination codon following nsP3 in most alphaviruses, leading to an underproduction of nsP4 relative to other non-structural proteins. The NH_2-terminal amino acid of nsP4 is tyrosine and is thus, rapidly degraded by the ubiquitin-dependent N-rule pathway (Strauss & Strauss, 1994). The N-rule pathway relates the half-life of the protein to its N-terminal residue. Although the bulk of nsP4 is rapidly degraded, the fraction complexed with the viral RNA replicase is protected from degradation, which may thus, facilitate viral RNA replication and transcription. In addition, nsP4

contains an autoproteinase activity responsible for nsP3/nsP4 cleavage (Takkinen *et al*, 1990).

Replication begins with translation of the 5' two-thirds of the viral genome, coding for the non-structural polyprotein. Following autoproteolytic cleavage, the replication complex assembles, and catalyses the formation of full length minus-strand 42S RNA (Sawicki & Sawicki, 1985). This intermediate RNA species serves as the template for synthesis of new positive-strand 42S RNA, and for the production of subgenomic 26S RNA, by virtue of its internal subgenomic promoter (Sawicki *et al*, 1978). Following translation, the subgenomic polyprotein is cleaved to yield viral structural proteins (Welch *et al*, 1981; Welch & Sefton, 1980).

1.4.3.3 Translation of subgenomic RNA and viral release.

The polyprotein encoded by the 26S subgenomic RNA encompasses all viral structural proteins in the order NH_2-C-p62(E3/E2)-6K-E1-COOH. Translation of subgenomic 26S RNA occurs early (2-3 h p.i.) in the replication cycle. The efficiency of translation is explained by the secondary structure of the 5' NTR, and a translational enhancer sequence present in the first 102 nucleotides of the capsid-encoding region (Frolov & Schlesinger, 1994; Sjöberg & Garoff, 1996). Host-cell components are also involved in structural polyprotein synthesis.

The first sequences to be translated encode the viral capsid polypeptide (*Figure 1.9*). Once the C protein is synthesised, it folds to create at its COOH-terminus, a serine-protease catalytic site, and is autoproteolytically cleaved from the nascent polypeptide co-translationally (Aliperti & Schlesinger, 1978; Melancon & Garoff, 1987). The newly-formed C protein interacts specifically with the 42S RNA in the cytoplasm, and subsequently multimerises to form the

viral nucleocapsid (Forsell *et al*, 1995). This occurs in association with the large ribosomal subunits (Ulmanen *et al*, 1976). The presence of an encapsidation signal within the non-structural region of the viral RNA is required for viral packaging. In SV, the *nsP1* gene is thought to contain the packaging signal (Levis *et al*, 1986), whereas for SFV, the signal is located within the *nsP2* gene (White *et al*, 1998).

Cleavage of the C protein from the polypeptide exposes the N-terminus of the p62 polypeptide precursor, which functions as a signal sequence to facilitate translocation into the endoplasmic reticulum (ER) (Garoff *et al*, 1990). The p62, E1 and 6K proteins appear to move as a cohort following synthesis, through the ER, to their ultimate location on the host-cell plasma membrane. The p62 signal sequence remains intact and is glycosylated in the ER lumen. Other signal peptidase sequences are located at the COOH-terminus of the p62 and 6K proteins, to promote 6K and E1 translocation, respectively (Liljeström & Garoff, 1991; Melancon & Garoff, 1986). Subsequent cleavage by host cell peptidases generates p62, 6K and E1 proteins (Barth *et al*, 1995).

Rapidly after synthesis, p62 and E1 associate in the ER to form a heterodimeric complex, which is resistant to low pH, and interacts with 6K. The heterodimer is transported, via the Golgi apparatus (GA), to the cell surface, where 6K dissociates (Lusa *et al*, 1991). Due to a requirement for cholesterol in viral assembly, 6K may function to select specific lipids for insertion into the membrane bilayer, to facilitate efficient viral budding (Marquart *et al*, 1993). Another function of 6K may be to promote the correct folding of the E1 protein in its heterodimeric form (Strauss & Strauss, 1994). During migration to the plasma membrane, the p62 precursor is palmitylated (Ivanova & Schlesinger, 1993), and cleaved into E2 and E3 glycoprotein subunits, presumably mediated by a host-cell furin, located in the trans-Golgi vesicle (deCurtis & Simons, 1988; Sariola *et al*, 1995; Smeekens, 1993). Cleavage of p62 renders the viral spike sensitive to low

Figure 1.9- Processing of SFV structural proteins and viral release.

Capsid protein is released cotranslationally by autoproteolysis, and assembles with genomic RNA to form nucleocapsids. The p62, 6K and E1 proteins are translocated to the ER. A NH_2-terminal sequence in p62 is thought to be the translocation signal. Co-translational cleavage of the remaining polypeptide occurs in the ER, aswell as N-glycosylation and further proteolytic processing. P62 is further cleaved into E2 and E3 subunits during transport to the Golgi apparatus. E2 associates with E1 to form heterodimers necessary for viral infectivity. Interaction of capsid proteins with the COOH-terminal of E2 drives the budding process, and releases infectious progeny. (Adapted from Schlesinger & Schlesinger, 1996).

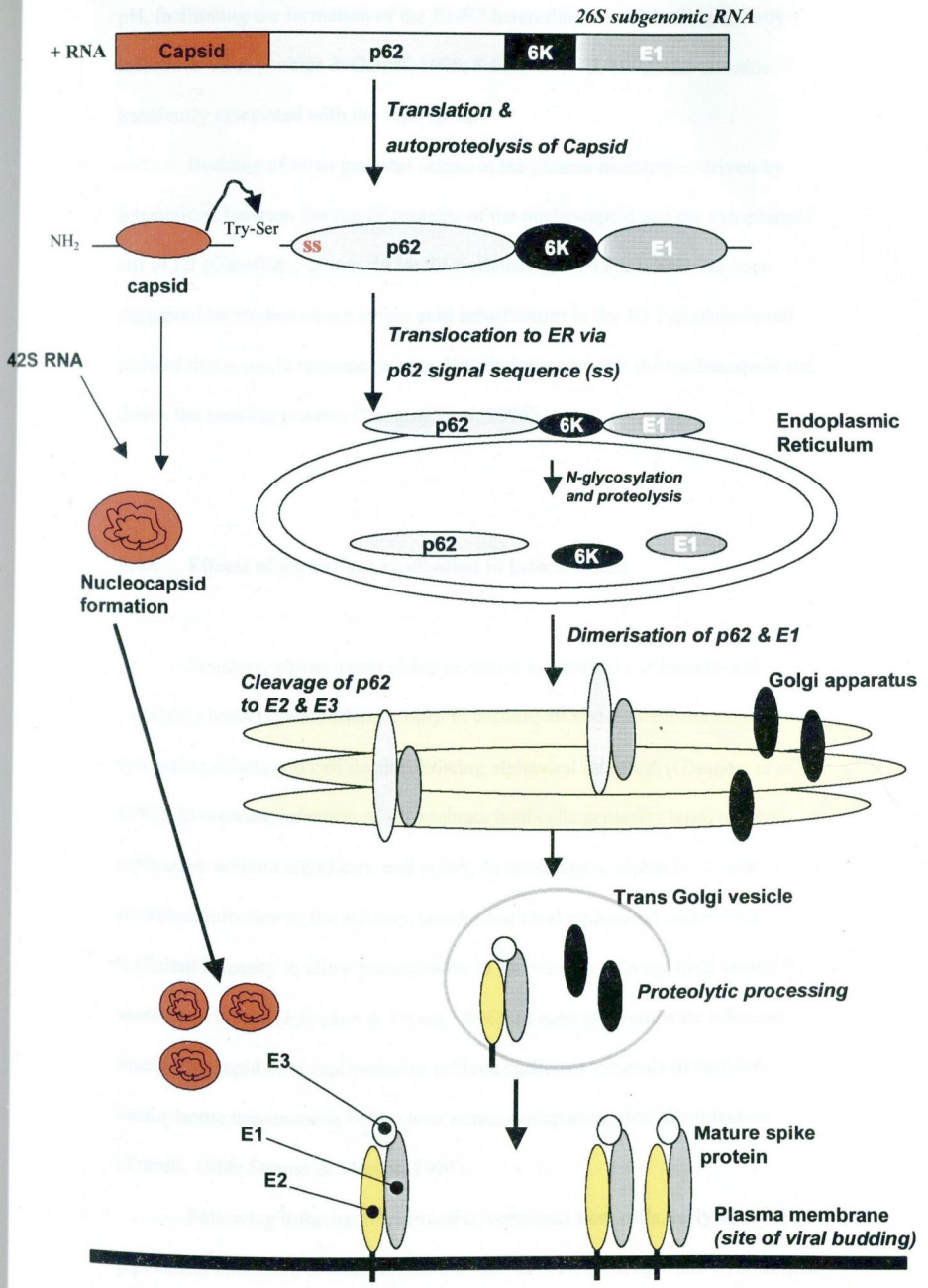


Figure 1.9- Processing of SFV structural proteins and viral release.

pH, facilitating the formation of the E1-E2 heterodimers, and leading to fully infectious virus (Lobigs & Garoff, 1990; Salminen *et al*, 1992). E3 remains transiently associated with the viral spike.

Budding of virus particles occurs at the plasma membrane, driven by interactions between the capsid proteins of the nucleocapsid and the cytoplasmic tail of E2 (Garoff & Simons, 1974; Suomalainen *et al*, 1992). This has been suggested by studies where amino acid substitutions in the E2 cytoplasmic tail showed that a single tyrosine residue directly interacts with the nucleocapsid and drives the budding process (Skoging *et al*, 1996).

1.4.4 Effects of alphaviral replication in infected cells.

In nature, alphaviruses alternate between growth in arthropod and vertebrate hosts (Chamberlain, 1980). In culture, all vertebrate hosts exhibit cytopathic effects and cell death following alphaviral infection (Glasgow *et al*, 1997). In contrast, infection of invertebrate host cells generally leads to viral replication without significant cell injury. In mosquitoes, alphaviruses establish a persistent infection of the salivary glands, and viral replication occurs to a sufficient intensity to allow transmission of the virus in salivary fluid during the vector's next feed (Johnston & Peters, 1996). In contrast, vertebrate infection must allow rapid viral replication to achieve sufficient viraemia to facilitate vector-borne transmission before host immune responses clear the infection (Turrell, 1988; Strauss & Strauss, 1994).

Following infection of permissive vertebrate host cells, early viral RNA replication inhibits host macromolecular synthesis facilitating a take-over of host-cell translational machinery. At 6 hours after infection, only viral structural proteins are synthesised, with approximately 10^4 virus particles released per cell,

per day (Liljeström & Garoff, 1991). It is during this process that infected cells show dramatic signs of CPE and die rapidly from infection (Glasgow *et al*, 1997). As with other cytolytic viruses, it was assumed cell death was attributed exclusively to the shut-off in host macromolecular synthesis and a general disruption of cellular function. Recently however, it has been clearly shown that cell death following alphaviral infection can be attributed to the induction of apoptosis (Glasgow *et al*, 1997; Scallan *et al*, 1997; Levine *et al*, 1993). Some cell types naturally resistant to PCD, such as neurons and fully differentiated macrophages, are instead killed by necrosis (Atkins *et al*, 1990; Balluz *et al*, 1993).

A number of cellular factors have been suggested as crucial in modulating the outcome of alphaviral infection, including ras (Hsu *et al*, 1995), caspases (Nava *et al*, 1998), nitric oxide (Tucker *et al*, 1996) and NF-κB (Lin *et al*, 1998; Lin *et al*, 1995). Overexpression of the anti-apoptotic Bcl-2 oncoprotein in AT3-Bcl-2 cells, protected against apoptosis induced by SV, and allowed the establishment of a persistently infected cell line (Levine *et al*, 1993). Also, SV infection of explanted dorsal root ganglia cells showed elevated levels of Bcl-2 expression that were inversely correlated with SV-induced lytic effects. Similar to SV, the overexpression of *Bcl-2* restricts SFV multiplication and delays the onset of apoptosis in AT3-Bcl-2 cells (Scallan *et al*, 1997). AT3-Bcl2 monolayers were able to survive following infection with both A7 and L10 strains of SFV, and persistently infected cells lines could be readily maintained after infection. A similar result was obtained in *Bcl-2*-overexpressing RIN cells infected with the SFV vector (Lundstrom *et al*, 1997). In contrast to these results however, Grandgirard *et al*, (1998) demonstrated that although there is a delay in SFV replication in *Bcl-2*-overexpressing cells, both SFV and SV were capable of overcoming this, and induced apoptosis by a caspase-3-mediated cleavage of the N-terminus of the Bcl-2 protein, thereby inhibiting its pro-survival functions. In a

separate study, SFV- and SV-induced apoptosis was accompanied by cytochrome *c* release from mitochondria into the cytoplasm, where it participates with Apaf-1 and caspase-9 to activate caspase-3 (Grandigirard *et al*, 2000). In this system, cells overexpressing *Bcl-2* still undergo apoptosis. Hence inactivation of *Bcl-2* occurs before it could confer its protective effects on cellular mitochondria.

Although the cellular factors governing alphaviral-induced apoptosis are well examined, the virally-encoded factors responsible for cell death remain obscure. The mechanisms of SV-induced apoptosis have been shown to be closely related to the synthesis of viral structural proteins, as SV-induced cell death is delayed in BHK cells that are transfected with RNA lacking these proteins (Despres *et al*, 1995). More recently, Joe *et al* (1998) localised the apoptosis-inducing function of SV to the transmembrane domains of E1 and E2 glycoproteins in the AT3-Bcl-2 cell line. The glycoproteins may induce the apoptotic phenotype by modulating the signal transduction pathways involving the apoptosis-related factor NFκB (Lin *et al*, 1998) or by interacting with Bcl-2 at the level of intracellular membrane insertion (Joe *et al*, 1998), or by suppression of the Bcl-2-activated, anti-apoptotic protein Beclin (Liang *et al*, 1998). Ubol *et al*, (1994) showed that a single amino acid substitution of His 55-Gln 55 in the E2 glycoprotein of SV, overcomes the protective effect of Bcl-2 and restores viral apoptotic potential, whilst also conferring neurovirulence (*see below*). The most recent data however, suggests that SV induces apoptosis in the absence of viral replication and synthesis of viral glycoproteins (Jan & Griffin, 1999), and that this process is mediated by an interaction between viral glycoproteins and the cell surface receptor on the cell membrane at the level of viral entry. More specifically, Jan *et al* (2000) have localised this trigger to acid-induced conformational changes in viral surface glycoproteins and sphingomyelin-dependent fusion of the virus envelope with the endosomal membrane. This is followed by sphingomyelin degradation and release of ceramide into the cytosol.

Ceramide-induced apoptosis is well established (Griffin, 1998), and treatment with caspase inhibitors inhibits both ceramide- and SV-induced apoptosis (Jan *et al*, 2000).

Unlike SV, deletion of all SFV structural proteins does not abrogate the cytopathic effects of the virus in infected cells (Glasgow *et al*, 1998). Thus, for SFV, it is the non-structural proteins and/or viral replication itself that act as the apoptotic trigger. Deletion of the *nsP2* gene abrogates both apoptosis induction and viral replication for both wild type SFV and the basic SFV vector, in which all structural proteins have been removed (Glasgow *et al*, 1998). SFV may also indirectly trigger the cell death pathway as a consequence of viral replication and the induction of dsRNA-dependent protein kinase (PKR) (Favre *et al*, 1996; Grandgirard *et al*, 1998), which has been shown to mediate a number of pro-apoptotic effects in a virally-infected cell, including the inhibition of protein synthesis and upregulation of the Fas/TNFR pathways (Balachandran *et al*, 1998; Lee & Esteban, 1994). SFV-induced apoptosis has also been shown to occur independently of *p53* expression, as H358 cells, containing a homozygous deletion in the *p53* gene, readily undergo apoptosis following SFV infection (Glasgow *et al*, 1998). It appears that alphaviral-induced apoptosis is multifaceted, involving the interaction of several apoptotic proteins and pathways, which may or may not be mutually exclusive.

1.4.5 Pathogenesis of SFV

Experimental infection of mice with SFV illustrates a variety of pathologies, ranging form asymptomatic infection to fatal encephalitic disease. The outcome is largely dependent on the strain of virus and the age of the host. The first isolation of SFV dates back to 1944, from mosquitoes in Uganda (Smithburn & Haddow, 1944), and there have been a number of subsequent isolations. Following the original isolation, the virus was passaged several times in the brains of weanling and suckling mice and was designated L10 (Bradish *et al*, 1971). This original isolate shows complete virulence in both neonatal and adult mice, causing fatal encephalitis whether it is administered peripherally or intracranially. Although serologically indistinguishable from L10, another SFV strain, A7, differs markedly in its virulence for mice. This avirulent strain (A7), was isolated from mosquitoes in Mozambique (McIntosh *et al*, 1961). Subsequently, an SFV A7(74) strain was derived from A7 after two plaque purifications in primary chick cells, to further select for avirulence (Bradish *et al*, 1971). The A7 strain is fatal in neonatal mice, whereas all adult mice survive infection. The original cDNA clone of SFV, designated pSP6-SFV4 appears to be derived from the L10 strain, although it has lost some of its virulence due to continuous passage in cell culture (Glasgow *et al*, 1991). Virus transcribed from this infectious clone, designated SFV4, also shows complete virulence in both neonatal and adult mice when infected intranasally.

The virulence of SFV strains in mice is determined by their ability to replicate in neurons. Intraperitoneal infection with both A7 and L10 strains of SFV result in similar levels of viremia, attributed mainly to replication within mouse muscle, which subsequently leads to CNS invasion (Fazakerley *et al*, 1993). The avirulent A7 virus enters the CNS by infecting vascular endothelial cells as indicated by foci of infection surrounding brain capillaries, by

immunohistochemistry and electron microscopy (Soilu-Hänninen *et al*, 1994). In the CNS, both L10 and A7 strains infect neurons and oligodendrocytes, but differ in respect to the kinetics of viral spread and subsequent neuronal damage (Fazakerley *et al*, 1993; Smyth *et al*, 1990). Whereas A7(74) infection remains in small, delimited foci surrounding cerebral capilliaries, L10 initiates an effective infection from small perivascular foci to a disseminated infection (Oliver *et al*, 1997). In virulent strains, virus titre increases in the brain until death, unlike avirulent strains, where the A7 titre peaks and then declines (Balluz *et al*, 1993).

The determining factors governing viral replication and virulence are still unresolved. However, the direct cytocidal effects of SFV in culture illustrate a basis for alphaviral pathogenesis *in vivo,* which appears to be mediated by a complex interplay of host cell and virally encoded factors. Ubol *et al* (1994) showed that a single amino acid change in the E2 glycoprotein of SV, which overcomes Bcl-2 inhibition of cell death, also confers an ability to replicate in mature neurons and induce apoptosis. Thus, an interplay of pro- and anti-apoptotic factors may function to modulate neuronal infection and cell death (Levine *et al*, 1993; Griffin & Harwick, 1997; Levine *et al*, 1996; Griffin, 1998).

Replication of A7 in the brains of adult mice appears to occur predominantly in oligodendrocytes, resulting in subacute demyelinating disease (Amor *et al*, 1996). Both virulent and avirulent strains induce demyelination, although the former is obscured by death (Atkins *et al*, 2000). Intraperitoneal infection of adult Balb/C mice with A7(74) is accompanied by an infiltration of mononuclear cells and lesions of demyelination, reaching maximum levels at 14 days p.i., at the time when virus is cleared from the CNS (Amor *et al*, 1996; Kelly *et al*, 1982). In SJL mice, lesions appear to persist for up to a year, suggesting that secretion of the negative regulatory cytokines IFNγ and TNFα may have a role in the progression of the disease (Donnelly *et al*, 1997; Mokhtarian *et al*, 1996). $CD8^+$ T cells have been postulated as the mediators of demyelination *in vivo*

(Atkins *et al*, 2000). It appears that myelin debris, released by destruction of oligodendrocytes, is phagocytosed by mononuclear cells and is subsequently presented to the immune system, which in turn leads to degradation of myelin by activated $CD8^+$ T cells. Demyelination appears to occur as discrete plaques and has been suggested as a model for human demyelinating diseases such as subacute sclerosing panencephalitis (SSPE), caused by measles virus, and multiple sclerosis (Fazakerley & Buchmeier, 1993; Atkins *et al*, 2000).

SFV infection of mice can also be used as a model for virus-induced teratogenesis (Atkins *et al*, 2000). Although the A7 strain is avirulent for adult mice, peripheral infection of pregnant females results in foetal death. Infection of the foetus occurs following an initial replication in the placenta, followed by spread to the embryo itself. Thus foetal death can be attributed to the rapidity of A7 replication in the foetus before humoral intervention via maternal antibodies can occur. Due to its limited replication capacity, the SFV vector fails to cross the placental barrier, as assessed by PCR analysis of vector RNA (Morris-Downes *et al*, 2000).

1.5 ALPHAVIRAL EXPRESSION SYSTEMS.

The development of alphaviral expression vectors is based on the following characteristics of the viral replicon; (a) a high level of alphaviral replication and interference of the virus with host cellular functions leads to production of very large amounts of expressed protein. Also, the time window between virus replication and host cell death is optimal to allow for exogenous protein expression; (b) the presence of *cis*-acting elements in the RNA genome to facilitate viral replication and packaging reside exclusively in the 5' non-structural region of the viral genome. The gene products encoded by the subgenomic RNA are not required for intracellular RNA replication. This allows for the subgenomic RNA to be manipulated, or replaced without affecting the replication capacity of the system; (c) the alphavirus genome functions directly as mRNA and replication is exclusively cytoplasmic.

Infectious clones of many of the alphaviruses, including SFV (Liljeström *et al*, 1991), SV (Rice *et al*, 1987), and VEE (Davis *et al*, 1989) have been generated by cloning viral cDNA under the control of a prokaryotic DNA-dependent RNA polymerase promoter, such as SP6 or T7, to allow viral mRNA to be transcribed *in vitro*. The RNA transcripts are fully infectious, and transfection of cells by electroporation or lipofection with this RNA is sufficient to initiate intracellular replication and propagation of progeny virus particles. Due to the inherent toxicity of these viruses for infected cells, vectors have been developed from the infectious clones as transient-based expression systems, for synthesis of desired proteins (Liljeström *et al*, 1991; Berglund *et al*, 1996), construction of novel vaccines (Berglund *et al*, 1997; Mossman *et al*, 1996) and gene therapy (Asselin-Paturel *et al*, 1998).

In the SFV system, several approaches to vector design have been explored, and these are illustrated in Fig.1.10. In the original vector system, the

Fig. 1. 10- Alphaviral vectors.

(*A*) represents the organisation of the parental SFV genome. (*B-C*) are replication and transcription-competent alphavirus replicons, in which the heterologous protein is cloned under a second subgenomic promoter placed 3' or 5' of the viral structural genes. (*D-F*) are suicidal vectors that do not result in productive replication because the structural genes of the virus are absent. (*E-F*) contain the capsid translational enhancer (Cenh), either as the full-lenght capsid protein with autoproteolytic activity, or as a fusion protein containing the first 48 amino acids of the capsid protein, with the 2A protease from Foot and Mouth disease virus as linker or filler region between enhancer and heterologous gene regions. (*G-J*) are the helper constructs, with the majority of the complete replicase deleted. Helper vectors supply the structural proteins *in trans* to encapsidate the recombinant molecule. Helpers lack the viral nsP2-derived packaging signal, allowing for the production of helper-free virus stocks. Helper-2 (*H*) contains a mutation in the *p62* gene, abolishing E2/E3 self-cleavage abilities. The split helper constructs (*I & J*) are composed of two separate RNA molecules, one encoding the capsid protein, the other for viral spike proteins. An additional serine-219 to alanine-219 mutation in pSFV-Capsid abolishes the self-cleaving activity of capsid and is labelled pSFV-CS219A. The spike helper, labelled pSFV-S2 contains the Cenh in order to produce similar levels of expression comared to pSFV-CS219A during translation.
(*K*) The layered DNA-RNA vector system. cDNA from the non-structural region of SFV is cloned into a DNA vector, under the control of the CMV eukaryotic promoter. Transcription of the full-lenght construct occurs in the cell nucleus, followed by translocation to cell cytoplasm, for translation of replicase and foreign proteins.
(Adpated from Berglund *et al*, 1996; Smerdou & Liljeström, 1999).

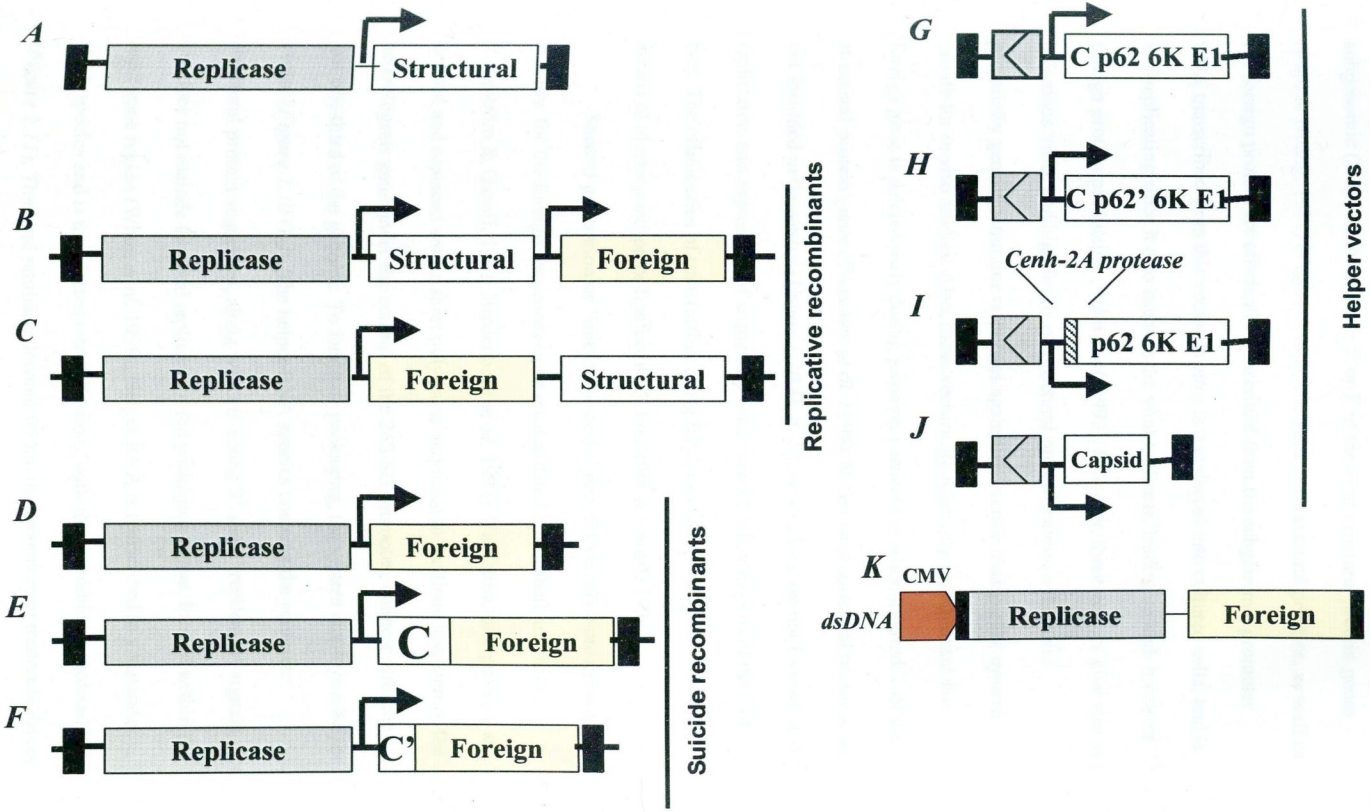


Figure 1.10- Alphaviral vectors.

heterologous gene of interest is inserted under the control of the viral 26S subgenomic (SG) promoter, either 5' or 3' of the viral structural protein genes (Raju & Huang, 1991) (*Figure 1.10 B, C*). Thus, the structural proteins, as well as the foreign protein are efficiently transcribed from the subgenomic promoter. RNA transcribed from this vector *in vitro* is transfected into cultured cells, and is self-replicating since it also encodes the viral replicase, leading to high levels of foreign protein production (Hahn *et al*, 1992). However, these vectors give rise to infectious virus, and high levels of structural protein synthesis may also potentially generate immune responses against the vector, making the system unsafe for *in vivo* studies. Also, these vectors are relatively unstable and the foreign gene is deleted early during passage, particularly when inserted 3' of the structural protein genes (Pugachev *et al*, 1995). When viral structural proteins are not included in the vector (*Figure 1.10 D, E, F*), new virions are not formed, and replication and expression of sequences continues for a few days until the cell dies. The efficiencies of transfection using RNA can consistently be 90-100% by means of electroporation or lipofection (Liljeström & Garoff, 1994).

Second-generation or "suicide"-based alphaviral vectors were developed to allow for the foreign sequences to be encapsidated into infectious virions (Liljeström & Garoff, 1991; Bredenbeek *et al*, 1993). Viral structural proteins are deleted and replaced with a short polylinker sequence to facilitate insertion of the heterologous gene under the control of the 26S SG promoter, colinear with the last one-third of the genome. To facilitate packaging, the system employs a helper vector (*Figure 1.10 G-J*). The helper RNA species contains the complete structural protein sequences, along with *cis*-acting 5' and 3' replication signals, but does not include the viral replicase or the packaging signal, located within the *nsp2* gene region (White *et al*, 1998). Helper RNA is transcribed as a separate RNA species and is transfected into cells along with the recombinant molecule (*Figure 1.11*). The viral replicase, located within the recombinant molecule drives

Fig. 1.11- Schematic of rSFV particle production.

SFV structural proteins are replaced with the foreign gene in the recombinant plasmid. Structural proteins are supplied in two separate helper plasmids. Helper molecules lack the majority of viral non-structural sequences (nsP1'-nsP4'), except those essential for translation of viral structural proteins. *In vitro*- transcribed RNA from all 3 SFV constructs are used to co-transfect, where the rRNA-encoded replicase amplifies both RNA species in BHK-21 cells. The helper molecules supply viral structural proteins *in trans*. The capsid protein only packages the rRNA molecule, as both helper molecules lack the SFV packaging signal (▭). Recombinant particles are produced and released. These particles are used to infect new cells, and high-level expression of the foreign protein results. As the infecting RNA lacks the structural genes of the virus, new infectious virions are not formed, and are thus, suicide rSFV particles. (Adapted from Berglund *et al*, 1996).

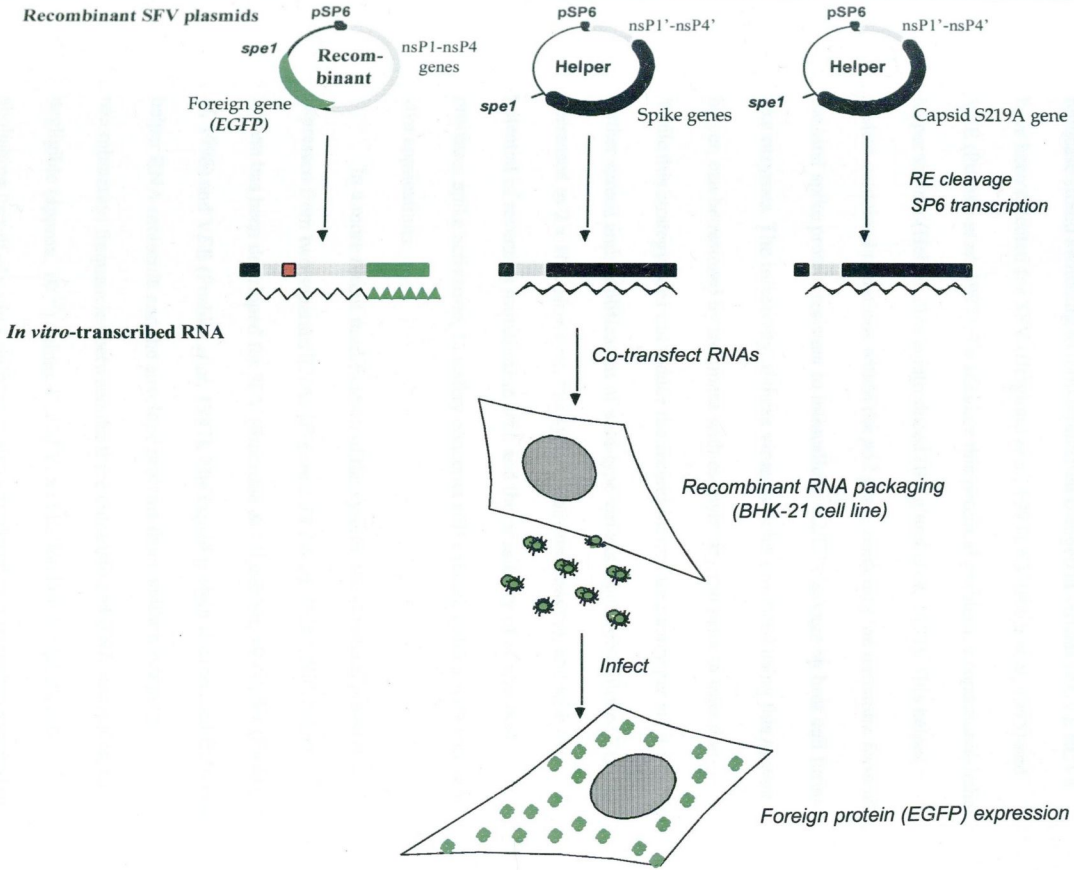


Figure 1.11- Schematic of rSFV particle production.

the synthesis of both RNA species in cotransfected cells. Structural proteins, supplied *in trans* by the helper vector, encpasidate the recombinant RNA (rRNA), resulting in the production of recombinant particles.

A problem, at least in the case of *in vivo* applications is recombination by replicase strand switching to form replication competent viruses (RCV). RCVs have been detected for SFV (Berglund *et al*, 1993), SV (Raju *et al*, 1995) and VEE (Pushko *et al*, 1997). To alleviate this potential problem, a conditional-lethal helper variant (Helper 2) was introduced (Berglund *et al*, 1993). This helper system contained mutations within the *p62* gene, rendering the immature form of the viral spike protein resistant to intracellular E2/E3 cleavage by host cell furin-like enzymes. The infectivity of these virus particles produced using this mutant helper, can be restored by treatment with α-chymotrypsin prior to infection. While this strategy does not reduce the recombination frequency per se, it inhibits further spread and amplification of wild-type virions. The probability of RCV is decreased to 2×10^{-6}. However, this system was cumbersome, and with the potential of reversion mutations in *p62*, and the possibility of *in vivo* host proteases spike activation, biosafety concerns still existed, at least with regard *in vivo* applications.

In a more recent modification of the system, the structural proteins are expressed from two separate RNAs (*Figure 1.10 I & J*). This "split" helper system has been developed for SFV (Smerdou & Liljeström, 1999), SV (Frolov *et al*, 1996) and VEE (Pushko *et al*, 1997). The capsid protein is expressed from one helper RNA molecule and the envelope proteins from another, bringing recombination frequencies between the three cotransfected RNA molecules, to negligible (approx. 10^{-12}) values. For SFV, a mutation in the *capsid* gene, abolishing its self-cleaving abilities, is also introduced as a secondary precaution. Thus, if recombinant virus was to be generated, virus particles could not assemble within infected cells. When released from the cell, the packaged particles are

infectious and contain RNA encoding the heterologous gene. However, the viral genome no longer contains structural genes, and are thus prevented from further replication. Hence, these particles are labelled "suicide" particles.

Recent modifications to the alphavirus expression system have included taking advantage of a translational enhancer (Cenh) sequence, located in the N-terminal region of the C-protein (Sjöberg *et al*, 1994). This enhancer, which appears to be active only in the context of the alphaviral replicon, has been mapped to the first 226 nucleotides of SV (Frolov & Schlesinger, 1994) and the first 102 nucleotides in SFV C-protein (Sjöberg *et al*, 1996). This C-enh induced up to 10-fold more β-galactosidase expression when *LacZ* was cloned in-frame at the 3' end of the *capsid* gene. The autoproteolytic activity of the C-protein enables it to cleave itself from the nascent fusion protein chain during translation. Alternatively, the inclusion of only the first 48 aa of the C-protein results in high-level synthesis of uncleaved fusion proteins. This C-enh is included upstream of the envelope protein genes in the "split" helper system in order to produce equal levels of capsid and spike proteins following transfection (Smerdou & Liljeström, 1999).

For biosafety reasons, and because of the large expense involved in *in vitro* RNA production, the SFV vector system was further developed as a layered DNA-RNA vector (Berglund *et al*, 1998). In this system, which is independent of helper vectors (*Figure 1.10 K*), the full-length SFV expression cassette cDNA, under the control of the eukaryotic Cytomegalovirus (CMV) immediate early promoter is directly delivered into the cell by conventional DNA transfection. Host-cell RNA polymerases transcribe the complete unit, along with the foreign gene, into RNA within the host-cell nucleus. RNA is subsequently transported to the host-cell cytoplasm, where as a result of its positive polarity, functions directly as mRNA, and replicates as does infectious virus, to give high-level transient protein expression.

Additional modifications to alphavirus expression systems are continuously being developed. Recently, Polo *et al* (1999) developed a series of packaging cell lines (PCLs) for the production of SV and SFV recombinant particles. These cell lines are stably transformed with expression cassettes that constitutively produce RNA transcripts encoding alphaviral structural proteins under the regulation of their native SG RNA promoter. Although of a lower efficiency, these PCLs result in the production of biologically active vector particles in the absence of detectable contaminating RCVs. The inherent cytotoxicity of alphaviral vectors however, precludes the development of these PCL's. Further modifications, including the development of an inducible system may be very useful. Finally, non-cytopathic vectors based on SV and more recently, SFV, are currently being developed. In SV, a mutation in the *nsP2* gene resulted in the establishment of a persistently infected cell line with prolonged expression *in vivo* (Ubol *et al*, 1994). In SFV, the *E2* and *nsP3* genes are currently being manipulated to assess pathogenicity determinants of the virus, which will be introduced into the vector also (Santigati *et al*, 1995; Tuittila et al, 2000; S. Galbraith, *personal communication*).

1.5.1 SFV vectors in vaccine development and gene therapy.

The SFV expression vector has been primarily utilised for the expression of foreign proteins and vaccine delivery. The lack of anti-SFV antibodies in humans is one major advantage of this system as a vaccine delivery agent. SFV-based vaccines against viral pathogens, such as influenza virus, HIV and simian immunodeficiency virus (SIV), have generated good immune responses in mice and larger animals. The broad host range of SFV also allowed the construction of novel vaccines, including infectious pancreatic necrosis virus in fish (Vaughan *et*

al, 1998) and infectious bursal disease virus in chickens (Phenix *et al*, 1999). More recently, an SFV-based vaccine construct generated protective immunity against challenge with louping ill virus, in both mice and sheep (Fleeton *et al*, 1999).

A limited number of studies have been initiated with regard to gene therapy, using the SFV system as a delivery agent. In terms of cancer gene therapy, rSFV-mediated overexpression of IL-12 in a murine tumour model inhibited tumour growth, based on the anti-angiogenic effects of the cytokine (Asselin-Paturel *et al*, 1998). Also, both naked RNA and rSFV particles have recently been shown to augment anti-tumour immune responses, by expression of immunogenic proteins (Ying *et al*, 1999; Colmenero *et al*, 1999).

1.6 *Objectives of study.*

The development of recombinant Semliki Forest virus particles (rSFV) as a vector for foreign gene expression and vaccine delivery is well established. However, at the onset of this study, the potential of rSFV as a gene therapy agent, particularly for treatment of neoplastic disease was unexplored. The potent cytotoxic effects of replication-competent SFV and recombinant SFV RNA molecules in cultured cells had been established. This offered and immediate advantage over the conventional cancer gene therapy viral vectors, that relied exclusively on the choice of foreign gene to mediate its cytotoxic effects within tumours.
Therefore, the objectives of this study were as follows:

(1) To optimise production of rSFV particles, using the reporter gene *LacZ*, and later *Enhanced Green Fluorescent protein* (*EGFP*), as the foreign gene for expression.

(2) To examine the cytotoxic effects of rSFV, initially in the non-tumourigenic cell line BHK-21, and the NCI-H358a non-small cell lung cancer (NSCLC) cell line. Also, to delineate whether the cytotoxic effects of rSFV *in vitro* were due to the induction of apoptosis.

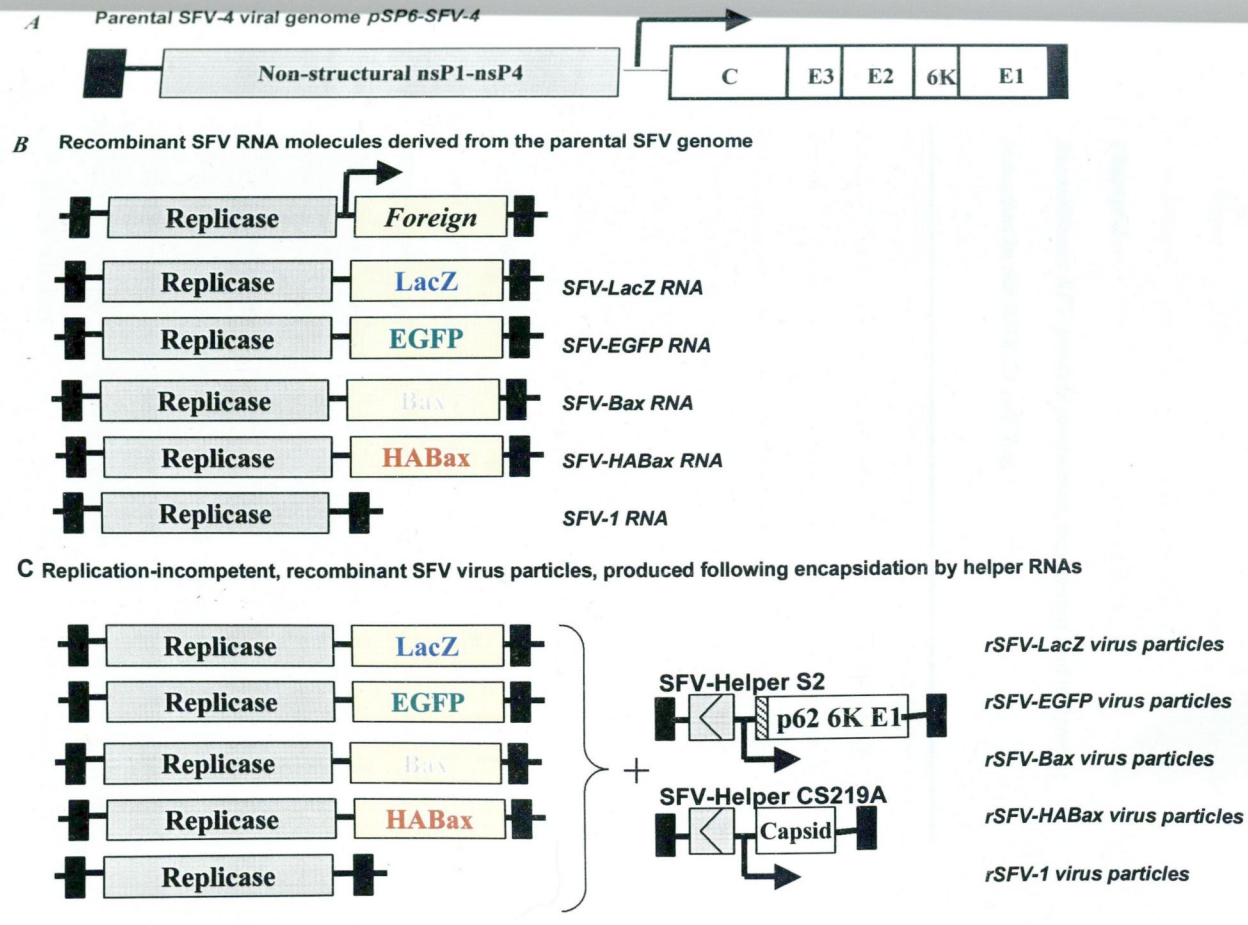
(3) To examine the ability of rSFV-EGFP to induce apoptosis and facilitate regression of solid NSCLC tumours *in vivo*, using the nude mouse xenograft model.

(4) To enhance the cytotoxicity of rSFV for the more apoptosis-resistant cell line AT3-Bcl-2, by overexpression of pro-apoptotic Bax, *in vitro* and *in vivo*.

A schematic representation of the recombinant SFV constructs used in this study are illustrated in comparison to the wild-type SFV-4 cDNA clone of SFV (*Figure 1.12*).

Figure 1.12- Schematic of recombinant SFV constructs used in this study.

(A) is a representation of the linearised cDNA from the parental pSP6-SFV-4 viral genome, from which all other vectors were derived. RNA *in vitro*-transcribed from this cDNA is labelled SFV-4 virus. (B) is a representation of the recombinant RNA molecules derived by manipulation of the parental SFV-4 genome. Structural genes under the control of the subgenomic promoter were replaced with foreign genes; LacZ, EGFP, Bax and HABax. RNA derived from this manipulation are labelled SFV-LacZ, SFV-EGFP, SFV-Bax and SFV-HABax, respectively. An RNA construct which lacks any foreign gene, and contains the 5' structural genes only is labelled SFV-1 RNA. (C) Replication-incompetent, infectious SFV particles were produced by co-transfection of recombinant SFV RNA molecules (B), with helper RNA molecules SFV-CapsidS219A and SFV-S2. Infectious particles are labelled rSFV-LacZ, rSFV-EGFP, rSFV-Bax, rSFV-HABax and rSFV-1 virus vector particles, respectively.


A
Parental SFV-4 viral genome pSP6-SFV-4
Non-structural nsP1-nsP4
C
E3
E2
6K
E1
B
Recombinant SFV RNA molecules derived from the parental SFV genome
Replicase
Foreign
Replicase
LacZ
SFV-LacZ RNA
Replicase
EGFP
SFV-EGFP RNA
Replicase
Bax
SFV-Bax RNA
Replicase
HABax
SFV-HABax RNA
Replicase
SFV-1 RNA
C Replication-incompetent, recombinant SFV virus particles, produced following encapsidation by helper RNAs
Replicase
LacZ
Replicase
EGFP
Replicase
Bax
Replicase
HABax
Replicase
SFV-Helper S2
p62 6K E1
SFV-Helper CS219A
Capsid
rSFV-LacZ virus particles
rSFV-EGFP virus particles
rSFV-Bax virus particles
rSFV-HABax virus particles
rSFV-1 virus particles

Chapter 2

Recombinant SFV particle production, expression and apoptosis induction in the BHK-21 cell line.

2.1 INTRODUCTION

The ability of Alphaviruses (SFV and SV) to induce programmed cell death in cultured cells is well established (Glasgow *et al*, 1997; Scallan *et al*, 1997). Recombinant SFV particles (rSFV), derived from genetic manipulation of the viral RNA genome, have been widely utilised as an effective vector for heterologous gene expression and delivery (Berglund *et al*, 1996). As an expression system, foreign proteins are efficiently delivered and expressed in cells which have been infected with encapsidated, rSFV RNA. These rSFV particles are produced by dual electroporation of cultured cells with 'helper' RNAs which supply the viral structural proteins *in trans*. A recent report by Glasgow *et al*, 1998, demonstrated that recombinant SFV RNA, induced apoptosis in cultured cells when transfected by electroporation. However, the pro-apoptotic capabilities of the recombinant SFV vector particles remain to be elucidated.

In this study, the cytotoxicity of encapsidated rSFV particles for cultured cells was examined *in vitro*. The BHK-21 cell line was chosen, as it was previously demonstrated that the infectious clone of the SFV virus, SFV-4, induces cell death in these cells following infection. Furthermore, these cells are used for routine viral propagation and rSFV particle production, as they are efficiently infected with the virus. This cell line will prove useful as a positive infection control in later chapters.

For the detection of the vector *in situ*, the reporter gene *LacZ*, which codes for the enzyme β-galactosidase, was used initially. More recently, this was replaced following the cloning of the reporter gene *Green Fluorescent Protein* (*GFP*), which was found to have several advantages over LacZ expression, particularly for *in vivo* analyses in later chapters.

In this chapter, the cytotoxicity of the rSFV virus vector system for BHK-21 cells in culture is investigated. This was performed primarily through cell viability assays. This study will conclude that the decrease in BHK-21 cell viabilty upon infection with the vector is primarily due to the induction of apoptosis.

2.2 EXPERIMENTAL PROCEDURES

2.2.1 MATERIALS

2.2.1.1 *Cell Lines*

The Baby Hamster Kidney 21 (BHK-21) cell line was obtained from the American Type Culture Collection (ATCC) (Maryland, USA). The BHK cell line, sBHK, was a gift from Prof. P. Liljeström, (Microbiology and Tumorbiology centre, Karolinska Institute, Stockholm, Sweden). BHK medium (Glasgow MEM) and heat-inactivated fetal calf serum (FCS), penicillin-streptomycin-L-glutamine solution were from Life Technologies, Inc. (Paisley, Scotland).

2.2.1.2 *Expression Vectors*

The SFV expression vector, pSFV-1, pSFV-LacZ, pSFV-EGFP, and helper vectors, pSFV-Helper S2 and pSFV-Helper CS219A were a gift Prof. P. Liljeström. pSFV-1 contains the 4 non-structural SFV proteins and a 3' MCS to facilitate insertion of the heterologous gene (*see Figure 1.12*).

2.2.1.3 *Molecular Biology Reagents*

Primers used for PCR amplification were from MWG Biotech AG (Germany). Restriction enzymes *BamH1, Not 1* and *Spe1*, *Taq* DNA polymerase, High efficiency T4 DNA Ligase, recombinant RNasin ribonuclease inhibitor and PCR molecular weight markers were from Promega (Promega, Wisconsin, USA). The

PCR cleanup, *nucleotide extraction* and *gel extraction* kits were from Qiagen Ltd. (West Sussex, UK). Plasmid purification kits for *mini-* and *midi*-preps were from Qiagen Ltd. SP6 RNA polymerase, cloned FPLC pure, $m^7G(5')ppp(5')G$, Sodium and nucleoside 5'-triphosphate mix were from Amersham Pharmacia Biotech (Uppsala, Sweden).

2.2.1.4 *Antibodies*

Polyclonal anti-SFV E2 protein and anti-SFV replicase antibodies were a gift from Prof. P. Liljeström. Monoclonal anti-β-galactosiadse was obtained from Boehringer Mannheim (GmbH, Mannheim, Germany). Rabbit anti-mouse IgG FITC-conjugated and goat anti-rabbit IgG TRITC-conjugated antibodies were from DAKO (Glostrup, Denmark). Goat and rabbit serum were from Vector laboratories Inc. and Sigma (St. Louis, MO, USA).

2.2.1.5 *In Vitro Studies*

Diamino-2-phenylindole (DAPI), Trypan Blue, RnaseA and Proteinase K were from Sigma. 5-bromo-4-chloro-3-indoyly-β-D-galactopyranoside (X-gal) was from Biosynth AG (Switzerland). Sodium Lauryl Sarcosinate (SLS) was from NBS biologicals (UK). [Methyl-^{3}H] thymidine (76 Ci/mmol) was from Amersham Pharmacia Biotech. Terminal deoxynucleotidyl Transferase (TdT), conjugated to peroxidase, and diaminobenzidine substrate were from Boehringer Mannheim.

2.2.1.6 *Miscellaneous*

Lambda molecular weight markers and 10X loading dye and Phenol ;Chloroform : isoamyl alcohol were from Promega. Mowiol was from Calbiochem Novabiochem Ltd (Nottingham, UK). 1, 4-diazabicyclo-[2.2.2]octane (DABCO) was from Sigma.

Electroporation cuvettes were from BTX (San Diego, USA). Solvents were mainly from BDH Ltd. All other chemicals were of AnalaR or molecular biology grade as required and were purchased from Sigma or BDH Ltd (Poole, UK).

2.2.2 METHODS

2.2.2.1 Cell Culture

BHK-21 cells were used for SFV-4 virus growth and recombinant SFV particle production. Cells were cultured in BHK medium, supplemented with 5% (v/v) newborn calf serum (NCS), 5% (v/v) tryptose phosphate broth, 100 U/ml penicillin, 100 μg/ml streptomycin and 200 mM L-glutamine, and maintained at 37°C in a humidified atmosphere of 5% CO_2, in 75 cm^2 culture flasks. For particle production, BHK medium contained 10% (v/v) FCS and 2% (v/v) 1M Hepes in addition to tryptose phosphate broth, L-glutamine and antibiotics. Cells were seeded at 1 x 10^5 ml^{-1} for growing (ATCC recommendation) in a total volume of 15 ml medium, and passaged when confluent as follows : Cell monolayers were washed with phosphate buffered saline (PBS, pH6.7) and incubated with 0.25% (w/v) trypsin/EDTA at 37°C until detachment was evident (1-2 min), the flask tapped to complete detachment and medium added to terminate trypsinization. Cells were then centrifuged (170g, 5 min), and the pellet resuspended in 1ml medium. Cell number and viability were determined by mixing a 10 μl aliquot of resuspended cells with 10 μl 0.4% (w/v) trypan blue solution, and applying 10 μl of this mixture to a haemocytometer. The dye trypan blue is excluded from viable cells, and under bright field microscopy membrane-damaged cells stain blue-violet, whereas undamaged cells appear translucent. Cell viability was always greater than 95%.

A second BHK cell line (sBHK), utilised for recombinant SFV particle titration, were cultured in Glasgow MEM BHK medium, containing 10% (v/v) FCS, 100 U/ml penicillin, 100 μg/ml streptomycin and 2 mM L-glutamine, 2% (v/v) 1M Hepes, 5% (v/v) tryptose phosphate broth. Cells were maintained at 37°C in a

humidified atmosphere of 5% CO_2. Cells were seeded at 1 x 10^5 ml^{-1} for growing in a total volume of 15 ml (75 cm^2 flasks) or 2 ml per well in 6-well dishes.

2.2.2.2 Virus

The infectious clone of SFV, pSP6-SFV-4, contains the full coding and non-coding genomic cDNA sequence of virulent SFV (Liljeström *et al*, 1991). Working stock SFV-4 virus was obtained by allowing seed stock SFV-4 to adsorb onto subconfluent BHK-21 cells in a 75 cm^2 flask for 1 hour, with rocking movements every 15 min to achieve a homogenous infection. The virus inoculum was removed from the monolayer and cells were incubated with fresh BHK medium. The virally infected cells were subsequently incubated at 37°C in a humidified atmosphere of 5% CO_2 until full cytopathic effect was observed (approximately 24 h). To harvest the virus, the medium was removed, centrifuged at 700*g* for 10 min to remove cellular debris, filtered through 0.45 μm filters, and stored in 1 ml aliquots at -70°C. Titration of virus stocks by plaque assay was necessary prior to use. Virus titres of 1-5 x 10^9 pfu/ml was routinely obtained. Virus at 1 x 10^4 pfu/ml was used to infect cell lines. For *in vitro* SFV-4 infection experiments, BHK-21 cells were grown in 75 cm^2 tissue culture flasks until ~80% confluent, the medium removed and replaced with infection medium (minimal essential medium, 0.2% (v/v) bovine serum albumin, 20 mM Hepes, 2 mM L-glutamine, and antibiotics), containing SFV-4 virus or medium alone, as a mock-infection control, for 1 h , and the medium was replaced. Cells were incubated for indicated timepoints prior to analysis (*see below*).

2.2.2.3 Preparation of recombinant SFV plasmids

2.2.2.3.1 *Preparation of competent E. coli DH5α cells*

Cells used for transformation of recombinant SFV and 'helper' SFV plasmids was *Escherchia coli* strain DH5α. Preparation of competent DH5α cells for transformation proceeded using the *Clontech E. coli transformation kit.*

2.2.2.3.2 *Transformation of Bacterial Cells*

Competent DH5α cells were transformed with recombinant and Helper SFV plasmids, pSFV-Helper S2 and pSFV-Helper CS219A using the *Clontech E. coli transformation kit* according to manufacturers instructions.

2.2.2.3.3 *Isolation of plasmid DNA from E. coli DH5α*

Plasmid DNA was purified from E. coli DH5α cells using the *Qiagen Midi Plasmid Purification Kit* according to manufacturers instructions. The plasmid concentration was assessed by mixing a 1 µl aliquot of plasmid DNA with 1µl loading buffer (33% (v/v) glycerol, 0.05% (w/v) bromophenol blue, 0.05% (w/v) xylene cyanole FF) and running this on a 0.8% (w/v) agarose gel (0.8% agarose, 2.0µl 10 mg/ml ethidium bromide in 100 ml TBE) in TBE at 75 mA. The concentration of plasmid was estimated from this gel be comparing band intensity with that of 5 and 10 µl *Lambda* molecular weight marker [5 µl Lambda (*Hind111* & *EcoR1*), 20 µl loading buffer, 75µl TBE]. *Midi-prep* plasmid concentrations were further estimated on a GeneQuant DNA/RNA spectrophotometer.

2.2.2.4 Production of RNA from recombinant SFV plasmid DNA

2.2.2.4.1 *SpeI linearisation of plasmid DNA*

For the production of SFV viral RNA, the pSFV1-LacZ plasmid was first linearised with the *SpeI* restriction enzyme. This is a unique restriction site in the infectious clone proceeding the non-structural protein genes. A total of 10 µg SFV plasmid DNA was linearised in final reaction volumes of 20 µl, containing 2 µl *SpeI* buffer (50 mM NaCl, 10 mM Tris-HCL, 10 mM $MgCl_2$, 1 mM DTT, pH7.9), and 15 U *SpeI*. Following 16-18 h digestion at 37°C, linearised plasmid DNA was pooled and brought to a final volume of 100 µl. The DNA was cleaned using the *Qiagen nucleotide extraction kit*, and plasmid DNA was resuspended in a final volume of 40 µl sterile dH_2O. Plasmid DNA concentration was assessed by mixing a 1 µl aliquot with 1 µl loading buffer and running this on a 0.8% (w/v) agarose gel. The concentration of plasmid was estimated from this gel by comparing band intensity with that of 5 and 10 µl *Lambda* (*Hind111* and *EcoR1*) DNA molecular weight markers.

2.2.2.4.2 *In vitro SP6 RNA transcription*

SP6 RNA polymerase was used to initiate RNA production from Spe I-linearised recombinant SFV plasmid DNA. Standard reaction mixtures contained 0.5 µg DNA template, 1 x SP6 buffer [40 mM N-2-hydroxyrthyl-piperazine-N'-2-ethansulphonic acid-KOH (Hepes-KOH), pH7.4, 6 mM MgOAc, 2 mM spermidine-HCL], 1 mM $m^7G(5')ppp(5')G$, 5 mM dithiotreitol, 1 mM each rATP, rCTP, rUTP, 500 µM rGTP, and 10 U recombinant RNasin. The reactions were

incubated at 37°C for 1 h and transcripts were analysed by electrophoresis on a 0.6% (w/v) agarose gel.

2.2.2.4.3 *Electroporation*

BHK-21 cells were propagated as described in section 2.2.2.1 For electroporation, BHK-21 cells were grown in 75 cm^2 tissue culture flasks until ~80% confluent. Cell monolayers were washed twice with PBS, incubated with 0.25% (w/v) trypsin/EDTA at 37°C until detachment was evident, the flask tapped to complete detachment and 6 ml medium added to terminate trypsinisation and to resuspend the cells. Cells were centrifuged (170*g*, 10 min), and pellet resuspended in 6 ml PBS. The cells were centrifuged (170*g*, 10 min) and resuspended in a final volume of 700 µl PBS. *In vitro* transcribed SFV RNA was then added to suspended cells, and the mixture incubated on ice for 15 min in a 0.4 µm electroporation cuvette. The cuvette was then electroporated at 0.85 kV and 25 µF capacitance, using a BioRad Gene Pulser 11. Following 2 pulses, cells were replaced on ice for a further 15 min, before resuspension in 20 ml BHK medium at 37°C. The cells were immediately placed into 6-well plates, each containing one 18 x 18 mm glass coverslip, and maintained at 37°C in a humidified atmosphere of 5% CO_2 for the indicated timepoints.

2.2.2.4.4 *Detection of expression*

Following 16 h incubation, cells electroporated with RNA transcribed from the pSFV-LacZ plasmid (SFV-LacZ), were fixed in ice cold methanol for 5-7 min at -20°C. The cells were washed twice with PBS and incubated with β-galactosidase staining solution (5 mM $K_4Fe(CN)_6.3H_2O$, 5 mM $K_3Fe(CN)_6$, 2 mM $MgCl_2$, 1

mg/ml 5-bromo-4-chloro-3-indoyly-β-D-galactopyranoside ; dimethylformamide), in PBS for 2-6 h at 37°C. The coverslips were washed and mounted onto glass slides using Mowiol/DABCO solution. Cells were examined for LacZ expression using bright field microscopy. Cells expressing the LacZ protein exhibited a blue staining reaction, whereas negative control cells remain yellow.

2.2.2.5 SFV-EGFP cloning

A strategy for cloning the *enhanced green fluorescent protein* (*EGFP*) gene into the SFV expression vector, SFV-1, was designed using the unique *BamH1* restiction site in the pSFV-1 MCS. This strategy is illustrated in Figure 2.1.

2.2.2.5.1 *DNA Amplification*

To facilitate cloning of *EGFP* into the SFV-1 vector, the forward primer was designed to include the first 18 nucleotides of the *EGFP* gene. In addition, this primer also incorporated the native SFV ribosome-binding site (RBS) sequence, and both forward and reverse primers contained a *BamH1* restriction site, to facilitate ligation with pSFV-1. The sequence of the reverse primer included the final 27 nucleotides, specific for a region of the pEGFP-N1 plasmid backbone, 49 nucleotides downstream of the *EGFP* gene sequence, and also included a *BamH1* restriction site. The sequence of primers used in *EGFP* amplification are as follows, with the *BamH1* sites in *italics*, the RBS sequence underlined, and the *EGFP* start codon in bold:

Figure 2.1- **Construction of the pSFV1-EGFP expression clone.** The *EGFP* gene was PCR-amplified from the pEGFP-N1 plasmid backbone, using primers specific for the 5' region of the *EGFP* gene, and a 3' region of pEGFP-N1 plasmid, ~50 nucleotides downstream of the *EGFP* gene. The PCR product was cloned into the MCS of the SFV expression vector, pSFV-1, using the unique *BamH1* restriction enzyme site. Red arrows indicate 5' and 3' primers for *EGFP* amplification.

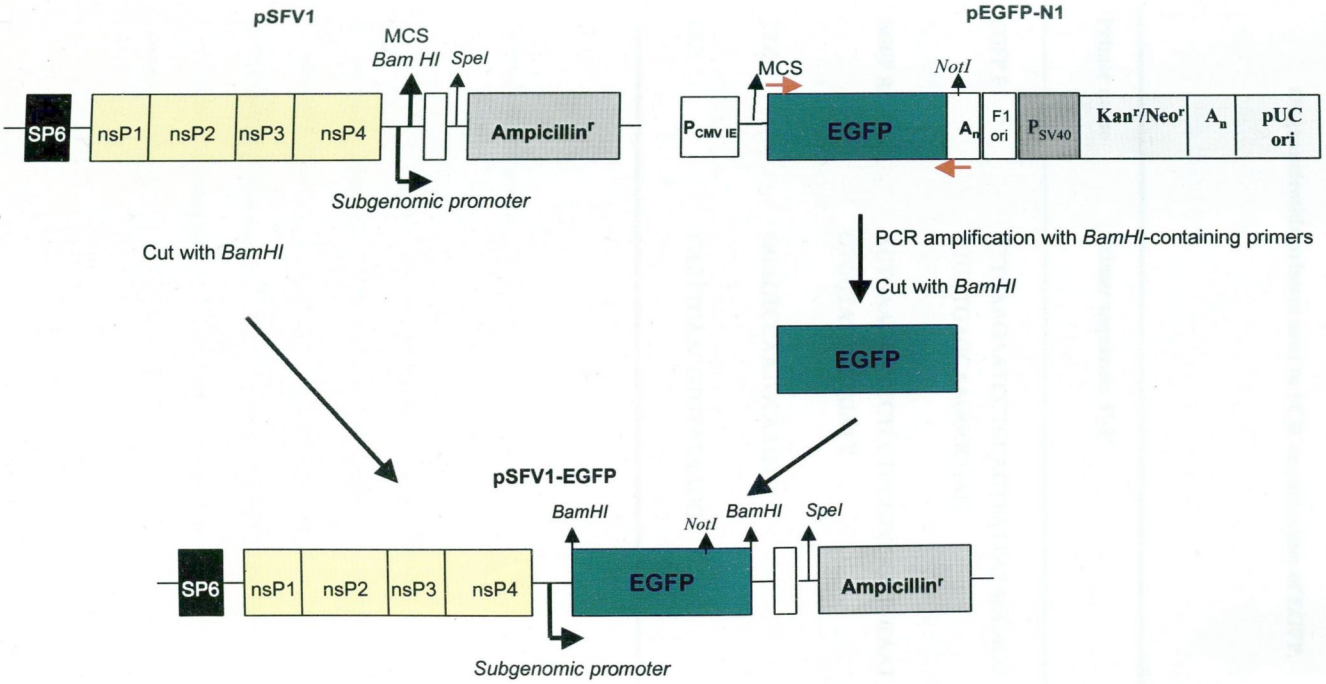


Figure 2.1. Construction of pSFV1-EGFP expression clone.

Table 2.1

Oligonucleotide primers used in PCR amplification of EGFP.

Primer name	Primer sequence: 5'-3'
EGFP F1	GTTGAAGAATCCTCCACTTATTATAGCACC ATGGTGAGCAAGGGCGAG
EGFP R1	ACTGAAGAATCCTCCTCGGTCGGATCCAAT GTGGTATGGCTGATT
ZZZ	GGAGTCCAATGCAAGTG
EEE	CACTTCAACGTGTATAAGGC

BaxF2 5'-GTTGAA*GAATCC*TCCACTTATTATAGCACC**ATG**GTGA
GCAAGGGCGAG-3'

BaxR2 3'-ACTGAA*GAATCC*TCCTCGGTCGGATCCAATGTGGTATG
GCTGATT-5'

Standard PCR reaction mixtures contained 1.5 mM $MgCl_2$, 1 X thermophillic DNA polymerase, 200 μM each of dATP, dCTP, dGTP and dTTP, and 0.5 μM each of forward and reverse primers, and 0.5-1.0 μg DNA template. The reaction was performed in an automated DNA thermal cycler (Crocodile, Oncor), programmed for 30 cycles of denaturation at 96°C for 1 min, annealing at 55°C for 1 min and polymerisation at 72°C for 1.5 min. The final cycle included a polymerisation step at 72°C for 10 min. The reaction always included a 96°C 'hotstart' for 10 min before the addition of 2.5units *Taq* polymerase. PCR products were analysed by electrophoresis of a 2 μl aliquot on a 0.8% (w/v) agarose gel. The primer pair ZZZ and EEE was used as a positive PCR control, and amplified a 300 bp fragment from the plasmid pSP6-SFV-4.

2.2.2.5.2 *Preparation of the EGFP insert*

Following PCR amplification, the 799 bp *EGFP* fragment was purified using the *Qiagen PCR purification* and *gel extraction* kits, eluted in 30 μl sterile dH_2O, and digested with BamH1 to create the necessary 'sticky' ends. These digestion reactions were pooled and further purified using the *Qiagen nucleotide removal* kit. Inserts were analysed by electrophoresis of a 2 μl aliquot on a 0.8% (w/v) agarose gel (*Figure 2.2*).

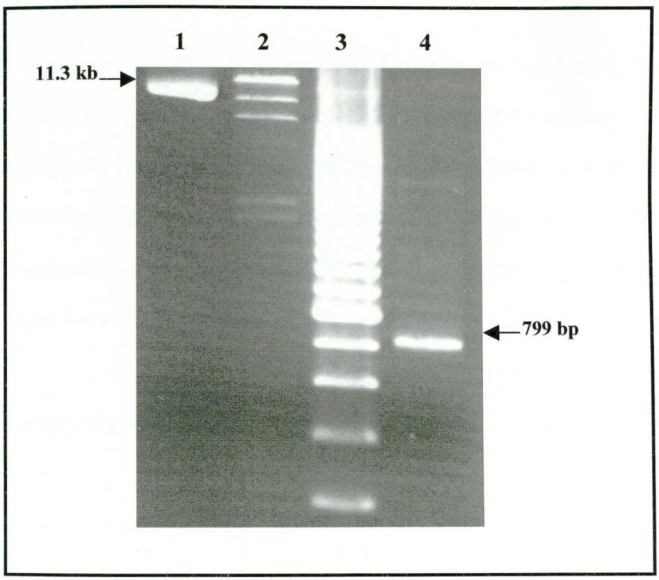


***Figure 2.2-* Preparation of SFV expression vector and EGFP PCR product for ligation.** Primers were designed to amplify the 799 bp EGFP gene from the pEGFP-N1 plasmid, digested with *BamH1*, to release the necessary 'sticky' ends and cleaned. The SFV expression vector, pSFV-1, was also digested with *BamH1* and cleaned. Both products were analysed by running 2 µl aliquots on a 0.8% (w/v) agarose gel, stained with ethidium bromide. *Lane 1*; pSFV-1, cut with *BamH1*. *Lane 2*; λ (*Hind111*) DNA molecular weight markers. *Lane 3*; 200 bp DNA molecular weight ladder. *Lane 4*; EGFP PCR product, digested with *BamH1*.

2.2.2.5.3 *Preparation of the SFV expression vector*

The 11.3 kbp plasmid pSFV-1 vector contains a MCS (*BamH1-Xma1-Sma1*) for use in the construction of recombinant plasmids, and an ampicillin resistance site for bacterial screening. Prior to cloning, pSFV1 *midi-prep* plasmid was digested with *BamH1*, which linearised the circular plasmid, and was purified using the *Qiagen nucleotide removal kit*. The plasmid was analysed by electrophoresis of a 2 µl aliquot on a 0.8% (w/v) agarose gel (*Figure 2.2*).

2.2.2.5.4 *DNA Ligation*

Ligation of the linearised pSFV-1 plasmid to the purified *EGFP* PCR product was carried out at a ratio of 1:20 vector to insert. A ligation mixture containing approximately 20 µl of *EGFP* PCR fragment and 1 µl of pSFV1 were combined in a total volume of 50 µl, including 5 µl high efficiency T4 DNA ligase buffer and 500 U T4 DNA ligase. The ligation mix was incubated overnight at 18°C.

2.2.2.5.5 *Screening for recombinant plasmids.*

pSFV-1 transformants were selected on ampicillin agar plates. To confirm the presence of pSFV1-EGFP recombinants, putative positive clones were selected using a procedure that allows for the rapid screening of uncut plasmid DNA directly from transformed colonies on agar plates (Le Gouill & Deiry, 1991). Putative positive clones are differentiated from negative clones, on the basis of size, by agarose gel electrophoresis of DNA extracted from cells transformed with the ligation mix, alongside DNA extracted from colonies transformed with pSFV-

1 only. Restriction digestion of plasmid DNA, was then used to confirm the presence and orientation of the inserts.

2.2.2.5.5.1 *Rapid colony screening procedure*

Putative positive transformed colonies, growing on ampicillin plates were picked using a sterile pipette and placed on a fresh ampicillin agar plate before the remainder of the colony was resuspended in 8 µl lysis buffer [9 volumes 0.25% (w/v) bromophenol blue, 0.25% (w/v) xylene cyanol, 25% (w/v) Ficoll type 400], 11 volumes water and 40 volumes [0.2 M NaOH, 1% (w/v) sodium dodecyl sulphate (SDS)]. 1.5 µl of buffer 2 (3 M potassium acetate, 1.8 M formic acid) was placed on the wall of the eppendorfs and centrifuged at 10,000*g* for four minutes. Supernatants were then loaded into 0.8% (w/v) agarose gels, with pSFV1 used as negative controls.

2.2.2.5.5.2 *Screening for recombinant pSFV1-EGFP clones by restriction digestion*

To confirm the presence of inserts and their orientation in the vector, putative positive colonies, selected by the rapid screening technique, were inoculated into 10 ml L broth containing 100 µg/ml ampicillin and incubated shaking at 37°C overnight. Plasmids were purified using the *Qiagen mini-prep* procedure, and size compared to pSFV-1 by agarose gel electrophoresis. Putative positive plasmids, containing the EGFP insert, were digested with *BamH1* and *Not1,* and run on 0.8% (w/v) agarose gels.

2.2.2.6 Detection of expression

2.2.2.6.1 *In vitro SP6 RNA transcription*

Spe1-linearisation, cleanup and *in vitro* RNA transcription from pSFV1-EGFP plasmid DNA, was performed as outlined for the transcription of SFV-LacZ, in sections 2.2.2.4.1 and 2.2.2.4.2, respectively. Negative transcription control included PBS only, instead of DNA template. Recombinant SFV1-EGFP RNA transcripts were analysed by agarose gel electrophoresis, on a 0.6% (w/v) agarose gel (*Figure 2.3*).

2.2.2.6.2 *Electroporation*

Electroporation of *in vitro*-transcribed RNA from the SFV1-EGFP clones into ~80% confluent BHK-21 cells, was performed as outlined in section 2.2.2.4.3. Transfected cells were maintained at 37°C, 5% CO_2 for 10-18 h, or until fluorescence was evident.

2.2.2.6.3 *Detection of pSFV-EGFP recombinant clones by direct epifluorescence*

Following 16 h incubation, cells transfected with RNA transcribed from putative positive pSFV1-EGFP plasmids were fixed in 4% (w/v) paraformaldehyde in PBS for 20 min. Cells were washed in PBS and dH_2O and mounted onto glass slides, using Mowiol/DABCO solution. Cells were examined using a fluorescent microscope, fitted with a specfic EGFP filter, at a wavelenght of 488 nm. Green fluorescing cells were scored as positive for EGFP expression. Background

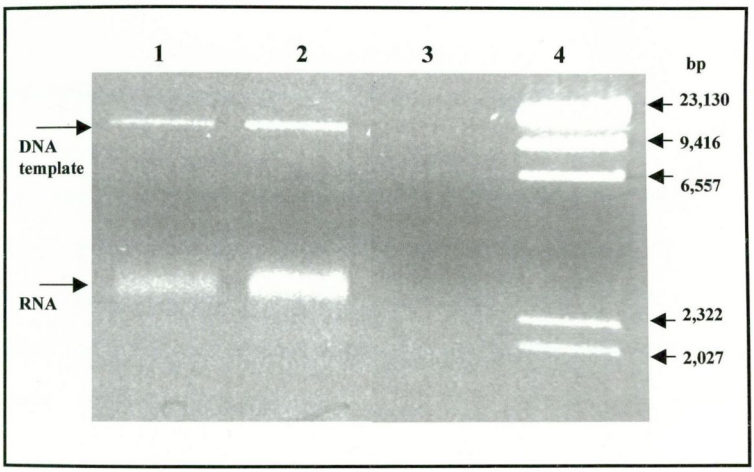


***Figure 2.3- In vitro* RNA transcription of putative pSFV1-EGFP clones.**

Plasmid DNA from putative positive pSFV1-EGFP clones #3 and #5, were *Spe1*-linearised, cleaned, and RNA was transcribed *in vitro*, using SP6 RNA polymerase. The negative transcription control included PBS instead of DNA template. *Lanes 1 to 2; in vitro*-transcribed RNA from potential pSFV1-EGFP clones, #3 and #5, respectively. *Lane 3*; negative RNA transcription control. *Lane 4*; λ (*Hind111*) DNA molecular weight marker. 0.6% (w/v) agarose gel, stained with ethidium bromide.

epifluorescence was accounted for using cells that had been mock-transfected with PBS only.

2.2.2.7 Production of recombinant SFV vector particles (rSFV particles)

The production of recombinant, encapsidated SFV particles (rSFV) involves the *in vitro*-transcription of the recombinant RNA molecules SFV-LacZ or SFV-EGFP, as described in section 2.2.2.4.2. *In vitro*-transcribed RNA from SFV 'helper' plasmids also occurs simultaneously, with modifications as described below.

2.2.2.7.1 *Isolation of plasmid DNA from E. coli DH5α*

Recombinant plasmid DNA and plasmid DNA from 'helper' plasmids, pSFV-Helper S2 and pSFV-Helper CS219A, were isolated from transformed *E. coli* DH5α using the *Qiagen Midi Plasmid Purification Kit*, as described in section 2.2.2.3.3.

2.2.2.7.2 *SpeI-linearisation of plasmid DNA*

Both recombinant and helper plasmids were *SpeI*-linearised prior to *in vitro* RNA transcription. A total of 20 µg SFV plasmid DNA was linearised in final reaction volumes of 100 µl containing, 5 µl *SpeI* buffer, and 35 U *SpeI* enzyme. Following overnight digestion at 37°C, linearised DNA was pooled and brought to final reaction volumes of 200 µl. A 10% volume of 3 M NaOAc was added, and plasmid DNA was precipitated twice in an equal volume of

Phenol:Chloroform:isoamyl-alcohol solution. DNA within the supernatants were back-extracted with four volumes diethyl ether and centrifuged (13,000*g*, 2 min, 4°C). Supernatants were then aspirated and DNA precipitated in 2.5 volumes absolute ethanol, overnight at -20°C. Tubes were centrifuged (20,000*g*, 40 min, 4°C), the ether layer aspirated and DNA pellets washed twice in ice-cold 70% (v/v) ethanol. Pellets were then air-dried for 5 min and redissolved in sterile dH_2O (100 µl/tube). Plasmid concentrations for both recombinant and helper plasmids, were assessed by mixing a 1 µl aliquot with 1 µl loading buffer, and running these on a 0.8% (w/v) agarose gel. The concentration of plasmid DNA was estimated from this gel by comparing band intensities with that of 5 and 10 µl *Lambda* (*Hind111*) DNA molecular weight markers.

2.2.2.7.3 *In vitro RNA transcription from recombinant SFV plasmids for particle production*

For the production of recombinant and helper SFV RNAs suitable for particle production, 1.5 µg each of *Spe1*-linearised recombinant and helper plasmid DNA was used to initiate independent RNA transcription reactions, in total volumes of 50 µl each. Standard reaction mixtures contained 1 x SP6 buffer [40 mM N-2-hydroxyethyl-piperazine-N'-2-ethansulphonic acid-KOH (Hepes-KOH), pH 7.4, 6 mM MgOAc, 2 mM spermidine-HCL], 1 mM $m^7G(5')ppp(5')G$, 5 mM dithiothreitol, 1 mM each of rATP, rCTP, rUTP, 500 µM rGTP, 25 U recombinant Rnasin and 100 U SP6 RNA polymerase. The reactions were incubated at 37°C for 1.5 h, and transcripts were analysed and quantified by mixing a 2 µl aliquot of RNA with 3 µl loading buffer, in a total volume of 20 µl. Concentrations of each RNA sample were analysed by running 5 and 10 µl

aliquots of each RNA mixture alongside that of 5 and 10 µl *Lambda* (*Hind111*) DNA molecular weight markers mixture, on a 0.6% (w/v) agarose gel.

2.2.2.7.4 *Electroporation*

BHK-21 cells were propagated as described in section 2.2.2.1 For particle production, electroporation was performed as described in section 2.2.2.6.2 with the following modifications; *in vitro* transcribed RNA from SFV recombinant and helper reactions were pooled and the transcription mix was added to suspended cells in a 0.4 µm gap electroporation cuvette. Following 2 pulses, cells were immediately resuspended in 20 ml normal BHK medium at 37°C, placed in a 75 cm^2 tissue culture flask, and maintained at 37°C in a humidified atmosphere of 5% CO_2. At 24 h post-electroporation, the culture supernatant, containing recombinant, encapsidated SFV particles, was removed and centrifuged (170*g*, 15 min, 4°C), to remove cellular debris, and placed on ice. Cytopathic effects were visible at this timepoint and particle production was at a maximum. Particles were then aliquoted into 1 ml volumes, on ice, and rapidly frozen using dry-ice-cooled ethanol or liquid nitrogen, before storing at -70°C.

2.2.2.7.5 *rSFV Particle titration*

For particle titration, the sBHK cell line was seeded at 1 x 10^5 cm^{-1} onto glass coverslips, contained within each well of a 6-well plate, and incubated until confluent. Serial dilutions (10 µl, 1 µl , 0.1 µl) of rSFV-EGFP or rSFV-LacZ particles, in duplicate, were used to infect successive wells of confluent sBHK cell monolayers, in a total volume of 500 µl infection medium for 1 h, with rocking movements every 15 min to achieve a homogenous infection. The cells

were then replaced with fresh BHK medium and incubated at 37°C in a humidified atmosphere of 5% CO_2. Following 18 h incubation with rSFV-EGFP particles, medium was removed, the coverslips washed twice in PBS and the cells were fixed in 4% (w/v) paraformaldehyde for 20 min. Coverslips were again washed twice with PBS, and mounted onto glass slides in Mowiol-DABCO solution. Cells were examined microscopically for the presence of EGFP fluorescence using a specific EGFP filter at a wavelenght of 488nm. Following infection with rSFV-LacZ virus particles, cells were fixed in ice-cold methanol for 5-7 min at -20°C. The cells were washed twice with PBS and incubated with β-galactosidase staining solution, as outlined in section 2.2.2.4.4. The coverslips were washed and mounted onto glass slides using Mowiol/DABCO solution. Cells were examined for LacZ expression using bright field microscopy. Particle titres were calculated at a magnification of x 400, and expressed as I.U./ml.

2.2.2.7.6 Optimisation of rSFV particle production

To optimise rSFV virus particle production, a double labelling experiment was performed to detect recombinant SFV RNA (SFV-LacZ/SFV-EGFP) and SFV-Helper S2 RNA simultaneously in particle-producing cells. SFV-Helper CS219A RNA could not be detected as an anti-capsid antibody was not available. Approximately 6 ml of BHK-21 cells, transfected with each RNA, were placed onto glass coverslips, contained within 6-well plates and incubated for 24 h. The cells were washed with PBS and fixed in ice-cold methanol, at -20°C for 6 min. Methanol was removed and cells were washed as before. Blocking buffer [0.5% (w/v) gelatin/0.25 (w/v) BSA in PBS-eisen] was added to the cell monolayers and left at room temperature for 1 h. Primary antibodies included a mixture of mouse

anti-β-galactosidase (1:20 dilution) and rabbit anti-spike (1 :200 dilution), for rSFV-LacZ particle-producing cells; and a mixture of mouse anti SFV replicase (1:4 dilution) and rabbit anti-spike (1:200 dilution) for rSFV-EGFP particle-producing cells, in blocking buffer. Primary antibody mixtures were incubated with appropriate cell monolayers for 1 h at 37°C, in a dark humidified chamber. The cells were washed with PBS and a mixture of secondary antibodies (FITC-conjugated anti-mouse; 1:100 dilution, and TRITC-conjugated anti-rabbit; 1:200 dilution) were added, and incubated under the same reaction conditions as primary antibodies, for 2 h. Cells were washed with PBS containing 0.25% (w/v) Tween solution, and PBS alone, before mounting onto glass slides with Mowiol/DABCO solution. FITC- and TRITC-specific expression of recombinant and spike proteins were visualised using fluorescent microscopy, at 450 and 510 nm, respectively.

2.2.2.8 Calculation of rSFV virus particle infection efficiency

To determine the infection efficiency of rSFV virus particles, BHK-21 cells were seeded at 1 x 10^4 ml^{-1} in 6-well plates (2 ml/well). Cells were then infected with rSFV-EGFP virus at a range of mois: moi 1-moi 400, in a total volume of 500 µl infection medium, for 1 hour, with rocking movements every 15 min. Infection medium alone was used in mock-infected controls, or moi=0. The cells were replenished with fresh BHK medium, and incubated at 37°C in a humidified atmosphere of 5% CO_2, for 18 h. The cells were washed in PBS, fixed in 4% (w/v) paraformaldehyde for 20 min, and stained with 2.5 µl/ml DAPI solution for 30 min. The cells were washed in PBS and mounted in Mowiol-DABCO. Cells were observed by fluorescent microscopy for EGFP expression. DAPI-stained

cells were visualised using a DAPI-specific filter at 360nm. DAPI staining is cell nucleus-specific. Infection efficiencies were calculated as the number of EGFP-expressing cells as a percentage of the total number of DAPI-positive cells, in each microscopic field. Up to 600 cells were scored, and each moi was calculated as the mean of triplicate samples.

2.2.2.9 Analysis of cell viability

To measure growth in cultured cells following rSFV virus infection, BHK-21 cells were seeded at 1 x 10^4 ml^{-1} in 6-well plates. Cells were infected at moi 10 rSFV-LacZ and rSFV-EGFP virus, in a total volume of 500 µl infection medium, for 1 hour with rocking movements every 15 min to achieve a homogenous infection. Infection medium alone was used as a mock-infection control. The cells were replenished with fresh BHK medium, incubated at 37°C in a humidified atmosphere of 5% CO_2, and subsequently analysed for cellular viability by trypan blue exclusion (section 2.2.2.9.1) and methyl-^{3}H thymidine incorporation (section 2.2.2.9.2).

2.2.2.9.1 *Trypan blue exclusion assay*

The viability of rSFV virus- and mock-infected BHK-21 cells was determined by trypan blue exclusion.. At 24 h intervals, the medium from rSFV- and mock-infected control cells was removed from 6-well plates and cell monolayers washed twice in PBS. Cells were then trypsinised and 500 µl complete BHK medium added to terminate trypsinisation, in a total volume of 1 ml. A 100 µl aliquot of each sample was removed and added to 100 µl trypan blue solution. A

100 µl aliquot of this mixture was applied to a haemocytometer, and viable, trypan blue-excluding cells were enumerated. Cells were harvested and analysed daily over a period of 10 days, and each sample was performed and analysed in triplicate.

2.2.2.9.2 *methyl-^{3}H thymidine incorporation*

To determine the prolifertion rate and viability of rSFV virus- and mock-infected control BHK-21 cells, measurement of radiolabelled [methyl-^{3}H]thymidine incorporation, which is directly related to the rate of cellular proliferation, was analysed. At 24 h intervals following infection, BHK growth medium was removed from cells and replaced with medium containing [methyl-^{3}H]thymidine (1 µCi/ml) in 6-well plates (2 ml/well). Following 24 h incubation with radiolabelled thymidine, growth medium was removed, cells were washed twice in PBS, and 1% (v/v) sodium dodecyl sulphate in PBS was added (2 ml/well) to lyse the cells, transferred to 5 ml glass bijous, and stored at -70°C. Samples were processed for scintillation counting as follows: 10% (v/v) trichloroacetic acid (TCA) was added to each sample and incubated on ice for at least 15 min, to precipitate large molecules including cellular DNA. The cells were transferred to filter mats, washed twice with 5% (v/v) TCA and air-dried. The mats were subsequently placed in plastic scintillation vials, mixed with 4 ml scintillation fluid and counted using a Tricarb 1500 scintillation counter (3 min count/sample). Counts per minute (cpm) was directly proportional to the rate of proliferation of cells in culture. Cells were analysed daily over a period of 7 days, and each sample was performed and analysed in triplicate.

2.2.2.10 Detection of apoptosis

3.2.2.10.1 *DNA fragmentation detection using agarose gel electrophoresis*

To detect the internucleosomal DNA fragments characteristic of apoptosis (Fernandes & Cotter, 1993), 80-90% confluent BHK-21 cells in 75 cm^2 tissue culture flasks were infected with rSFV-LacZ and rSFV-EGFP virus particles at moi 100 in a total volume of 1 ml infection medium for 1 h, with rocking movements every 15 min to achieve a homogenous infection. Infection medium alone was used as mock-infection controls. Cells were replenished with 15 ml complete BHK-21 medium, and incubated at 37°C in a humidified atmosphere of 5% CO_2. At 24, 48 and 72 h p.i., DNA was isolated from rSFV- and mock-infected cells as follows : supernatants containing cell debris were centrifuged (170g, 5 min), the pellets resuspended in 1 ml lysis buffer (20 mM EDTA, 100 mM Tris, pH8, 0.8% (w/v) sodium lauryl sarcosinate) and added to the remaining monolayers in the 75 cm^2 flask, to a final volume of 1 ml lysis buffer. Following a 1 h incubation at 37°C, cells were treated with 10 mg/ml ribonuclease A at 37°C for 2 h, and 20 mg/ml proteinase K for 18 h. DNA samples were analysed by electrophoresis of extracted DNA, on 1.5% (w/v) agarose gels, containing 1 mg/ml ethidium bromide, for 4 h at 55 V, and visualised using autoradiography.

2.2.2.10.2 *DNA fragmentation detection using TUNEL*

Detection of DNA fragmentation at the single-cell level was also performed using the Terminal deoxynucleotidyl transferase (TdT)-mediated dUTP-biotin nick-end labelling (TUNEL) technique (Gavrieli *et al*, 1992). In this TUNEL technique, digoxigenin-dUTP is added to 3'OH ends of double- and single-stranded DNA fragments, generated by the downstream apoptosis effector nucleases, by the

enzyme TdT. DNA fragments which have been labelled with the digoxygenin nucleotide are then allowed to bind an anti-digoxygenin antibody which is conjugated to horse-radish peroxidase (POD). The bound peroxidase antibody conjugate enzymatically generates a permanent localised stain from the chromogenic substrate, DAB. BHK-21 cells were seeded at 1 x 10^5 ml^{-1} into 6-well culture plates and infected with rSFV-LacZ and rSFV-EGFP virus particles at moi 100 as described in section 2.2.2.9. At 24, 48 and 72 h p.i., cells were fixed in 4% (w/v) paraformaldehyde for 1 h, permeabilised with 0.1% (w/v) Triton X-100 in 0.1% NaOAc for 2 min, and incubated with TdT enzyme in a humidified atmosphere at 37°C for 1 h, according to manufacturers instructions. Cells were washed and incubated with converter-POD solution for 30 min, and finally with 10% (v/v) DAB substrate for 10 min. Cells were counterstained with 5% (w/v) methyl green, washed, dehydated in N-butanol solution and mounted onto glass slides using DPX. Cells were observed by light microscopy for the presence of brown-stained apoptotic nuclei within a background of methyl green-stained intact nuclei.

2.2.2.11 Statistical analyses

For statistical analyses, data was presented as the mean values for a 95% confidence interval. Statistical comparisons were performed using the Student's paired t test, with $P<0.05$ considered to be statistically significant.

2.3 RESULTS

2.3.1 Infectious SFV-4 virus induces apoptosis in the BHK-21 cell line.

Initial apoptosis experiments began with an analysis of programmed cell death induced by replication-competent SFV-4 virus in the BHK-21 cell line. These experiments were a reproduction of studies published earlier by Glasgow *et al*, (1996), and were necessary in order to optimise cell viability and apoptosis studies for all subsequent recombinant SFV virus particle work. BHK-21 cells were seeded into 75 cm^2 tissue culture flasks and grown until ~80% confluent. Cell monolayers were then infected with SFV-4 virus (moi 0.1), or with medium alone, as a mock-infection control. We utilised morphological and DNA fragmentation criteria as indicators of apoptotic cell death. Chromosomal DNA was extracted from infected and mock-infected cells at 24 h intervals, and analysed for the presence of 180-200bp oligonucleosomal DNA fragments and their multiples, indicative of apoptotic cell death, by agarose gel electrophoresis. At 18 h p.i. with the virus, BHK-21 cells begin to reveal initial signs of virus-induced cytopathic effect (cpe), including rounding up of cells and nuclear shrinkage, in comparison to healthy, mitotic mock-infected controls (*Figure 2.4.A*). Virus-induced cpe becomes more pronounced at 48 h p.i. (*Figure 2. 4. C*), at which time DNA fragmentation was clearly observed by agarose gel electrophoresis (*Figure 2.5*). By 72 h p.i. with the virus, the BHK-21 cell monolayer was completely obliterated (*not shown*) and DNA fragmentation was even more pronounced. Neither cpe nor apoptotic DNA fragmentation were observed within mock-infected control BHK-21 cell monolayers, which grew normally until 100% confluent (*Figure 2.4 B, D*).

Figure 2.4- **SFV-4 virus-induced apoptotic cell death in BHK-21 cells, as assessed by morphological analysis.** BHK-21 cells were seeded at densities of 1 x 10^5 cells/well, in 6-well plates, and incubated with SFV-4 virus (moi 0.1), for 1 h. Medium alone was used as a mock-infection control. BHK-21 cells 18 h p.i. with SFV-4 (*A*) or medium alone (*B*). Note initial indications of apoptotic cell death within BHK-21 cell monolayers, including rounding up of cells and nuclear shrinkage. *C*, *D*; SFV-4- and mock-infected BHK-21 cells at 48 h p.i., respectively. Cells infected with the virus reveal signs of late-stage apoptotic cell death, with many dying cells floating from the monolayer. Mock-infected controls remained normal. Photographed at x 100 magnification.

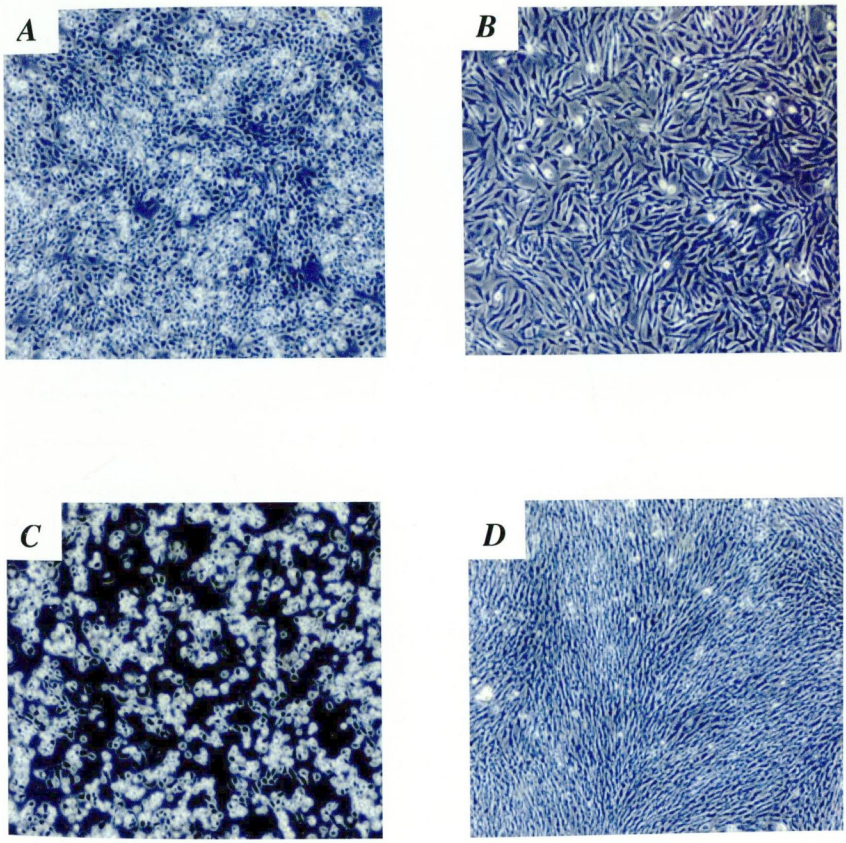


Figure 2.4- SFV-4 virus-induced apoptotic cell death in BHK-21 cells, as assessed by morphological analysis.

Figure 2.5- **Apoptosis induction in BHK-21 cells following infection with infectious SFV-4 virus, as assessed by DNA fragmentation, using agarose gel electrophoresis.** BHK-21 cells were incubated at densities of 1 x 10^6 cells/well in 75 cm^2 flasks, and infected with SFV-4 virus (moi 0.1) or medium alone as a control. At 24 h intervals following infection, cells were lysed and DNA was released by enzymatic digestion. Cellular DNA for SFV-4- and mock-infected cells was analysed for fragmentation into oligonucleosomal-size fragments, and their multiples, indicative of cell death, by agarose gel electrophoresis. *Lanes 1 and 2;* DNA from SFV-4- and mock-infected BHK-21 cells, respectively, at 24 h p.i. *Lanes 3 and 4*; DNA from SFV-4- and mock-infected BHK-21 cells, respectively, at 48 h p.i. *Lanes 5 and 6*; DNA from SFV-4- and mock-infected BHK-21 cells, respectively, at 72 h p.i. *Lane 7*; *Lambda* (*Hind 111*) DNA molecular weight markers.

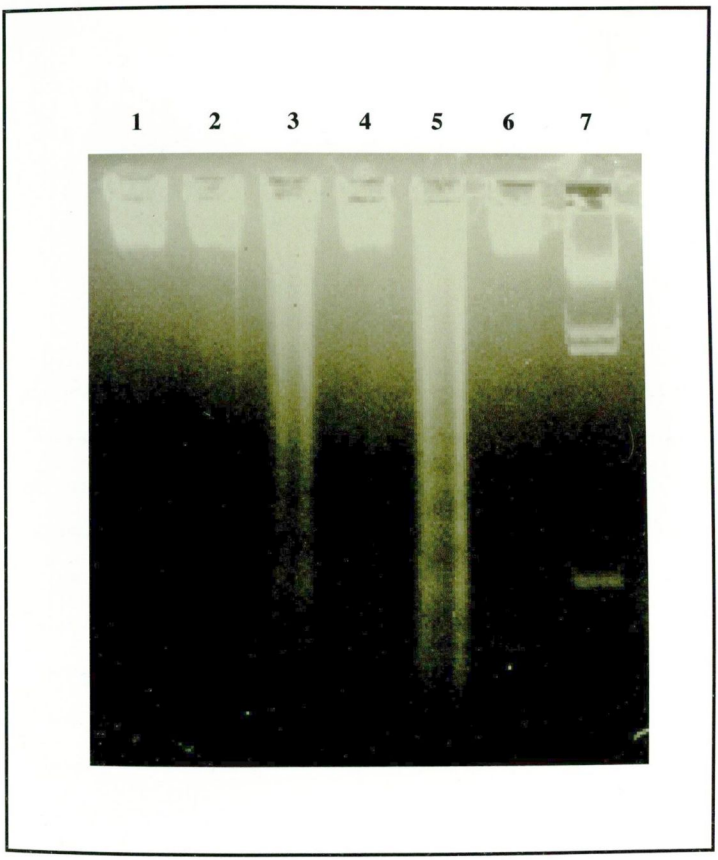


Figure 2.5- Apoptosis induction in BHK-21 cells following infection with infectious SFV-4 virus, as assessed by DNA fragmentation, using agarose gel electrophoresis.

Figure 2.6- **SFV-4 virus-mediated apoptosis in BHK-21 cells, as assessed by chromosomal DNA fragmentation, using TUNEL.** BHK-21 cells were seeded onto glass coverslips in 6-well plates and grown until ~80% confluent. Monolayers were infected with SFV-4 virus (moi 0.1) or medium alone as a mock-infection control. At 48 h p.i., cell monolayers were fixed and fragmented chromosomal DNA labelled with TdT and horse-radish peroxidase. Colorimetric detection was performed using diaminobenzidine. Normal cells were counterstained with methyl green. *A*; BHK-21 cells, 48 h following infection with SFV-4. *B*; Mock-infected BHK-21 cells. Note extensive brown TUNEL-positive peroxidase staining within apoptotic nuclei (*arrows*) in the SFV-4-infected cell monolayer (*A*), in contrast to healthy and dividing mock-infected control cells (*B*). Photographed at x 200 magnification.

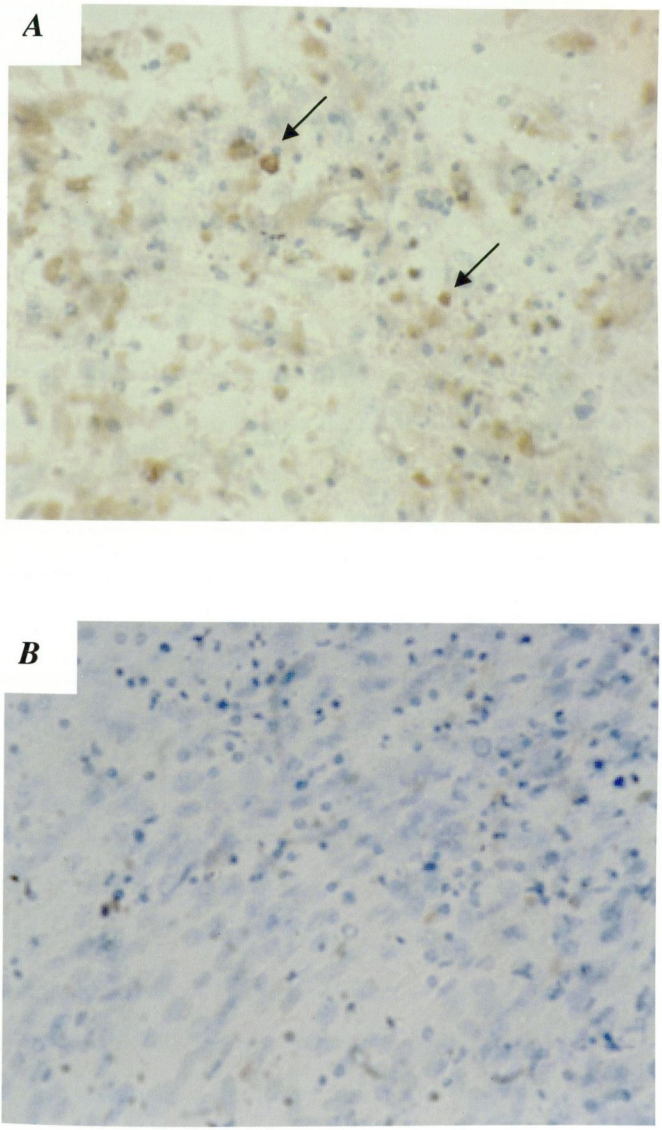


Figure 2.6- SFV-4-mediated apoptosis in BHK-21 cells,

as assessed by chromosomal DNA fragmentation, using TUNEL.

Chromosomal DNA fragmentation may also be detected within apoptotic nuclei, *in situ*, using the TUNEL procedure. The Terminal deoxynucleotidyl transferase (TdT)-mediated dUTP-biotin nick-end labelling (TUNEL) technique (Gavrieli *et al*, 1992) is used to detect free 3'OH ends of cleaved DNA within apoptotic cells. In this method, dioxygenin-dUTP is added to 3'OH ends of double-and single-stranded DNA, by the enzyme TdT. An anti-dioxygenin Fab antibody, with conjugated peroxidase, is used to immunostain nuclei that have high concentrations of 3'OH ends, which are generated when endogenous endonucleases are activated. Colorimetric detection was performed using diaminobenzidine (DAB). Normal, intact nuclei were counterstained with methyl green. BHK-21 cells were seeded onto glass coverslips, placed in 6-well plates, and were grown until ~80% confluent. Monolayers were then infected with SFV-4 virus or medium alone, as indicated above. At 24 h intervals following infection, cells were fixed and processed for TUNEL. The results for TUNEL-mediated detection of apoptosis, a 48 h, are illustrated in Figure 2.6. The presence of brown, TUNEL-positive apoptotic nuclei in SFV-4 virus-infected BHK-21 cell monolayers confirms DNA fragmentation observed by agarose gel electrophoresis, in Figure 2.5. TUNEL-positive cells also exhibited other indications of apoptosis, including nuclear shrinkage or pyknosis and the formation of cytoplasmic/membrane blebs, in contrast to mock-infected BHK-21 cell monolayers, which contained mainly intact, methyl green-stained, round to oval nuclei. Apoptotic TUNEL-positive cells were also detected at 24 and 72 h p.i. with the virus, but to a slightly lesser extent (*not shown*). At 24 h p.i., infected cells appeared to initiate an apoptotic response, but the majority of these cells remain TUNEL-negative, with little DNA fragmentation, indicating initial stages of apoptosis only. At 72 h p.i. with the virus, the majority of infected cells had lifted from the monolayer and were thus, refractory to analysis. Infection with

SFV-4 virus was used as a positive apoptosis control in all subsequent experiments.

2.3.2 Cloning and expression of the Enhanced Green Fluorescent Protein in the SFV expression vector.

To facilitate cloning of the *enhanced green fluorescent protein* (*EGFP*) gene into the SFV expression system, SFV-1, the gene was amplified from the pEGFP-N1 plasmid, using primers specific for the 5' and 3' end regions of the *EGFP* gene. Primer sequences were designed from pEGFP-N1 sequence analysis. The 5' primer also included the native SFV ribosome binding site (RBS), and both 5' and 3' primers contained an exogenous *BamH1* enzyme site, for ligation with the pSFV-1 plasmid. The resulting PCR product was cloned into the SFV expression vector, and recombinant clones were selected by rapid colony screening (*not shown*). Putative positive colonies were selected, and the presence of the *EGFP* gene was confirmed by *BamH1*- restriction analysis (*Figure 2.7*). The orientation of *EGFP* inserts were determined by *Not1*- (*Figure 2.8*) and *Nco1*-(*not shown*) restriction analysis. Three clones were obtained, two in the correct orientation (clones pSFV1-EGFP #3 and #5), the other (clone pSFV1-EGFP #9), in the opposite orientation.

Expression of *EGFP* from the recombinant SFV expression system was determined by direct epifluorescence. Plasmid DNA from putative positive pSFV1-EGFP clones #3 and #5 were linearised, and *in vitro*-transcribed RNA from both clones were electroporated into BHK-21 cells, placed on glass coverslips in 6-well plates, and incubated. Following overnight incubation, fixed cells were analysed by fluorescent microscopy, using a specific EGFP filter, at a

***Figure 2.7*- Screening for pSFV1-EGFP recombinant clones by restriction digestion.** Putative positive clones were screened for the presence of EGFP inserts by *BamH1* restriction analysis. *Lanes 1 and 8*; 200bp DNA molecular weight ladder. *Lane 2*; 799 bp EGFP PCR product. *Lanes 3 to 6*; putative recombinant pSFV1-EGFP clones #3, #5, #9 and #11, respectively, digested with *BamH1*. *Lane 7*; pSFV-1 digested with *BamH1*. Plasmid digests were run on a 0.8% (w/v) agarose gel, stained with ethidium bromide.

***Figure 2.8*- The orientation of EGFP inserts within the pSFV-1 vector, determined by *Not1* restriction digestion of putative positive clones.** *Lanes 1 to 4*; Putative recombinant pSFV1-EGFP clones #3, #5, #9 and #11, respectively, digested with *Not1*. *Lane 5*; pSFV-1 digested with *Not1*. *Lane 6*; 500bp DNA molecular weight ladder. pSFV1-EGFP clones with correct insert orientation were determined by a 2 kb fragment, following *Not1* digestion. Those with the EGFP insert in the incorrect orientation were determined by a 1.32 kb fragment, following *Not1* digestion. Plasmid digests were run on a 0.8% (w/v) agarose gel, stained with ethidium bromide.

Figure 2.7

Screening for pSFV1-EGFP recombinant clones by restriction digestion

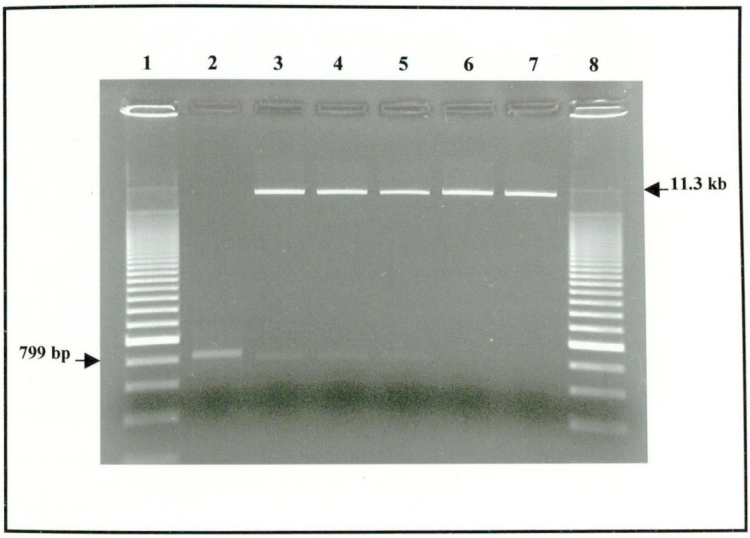


Figure 2.8

The orientation of EGFP inserts within the SFV-1 vector, determined by *Not1* digestion

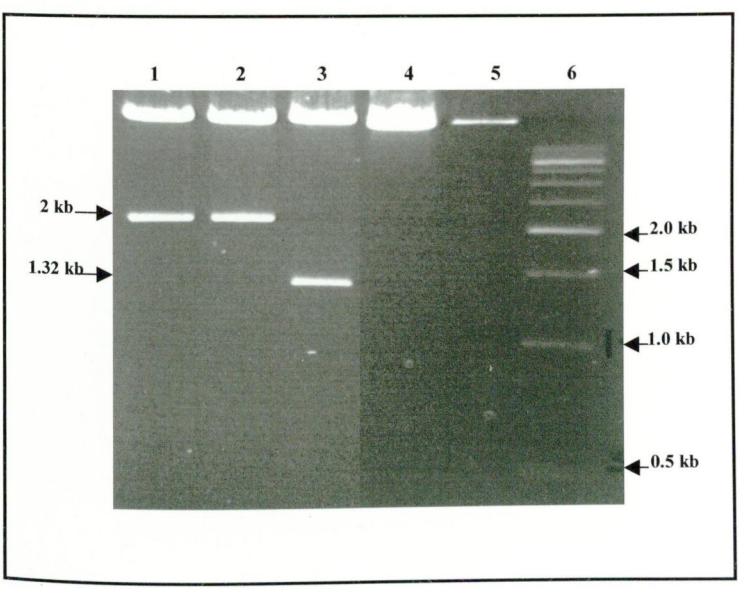


Figure 2.9- **Screening for EGFP expression from recombinant clones by direct epifluorescence in BHK-21 cells.** *In vitro*-transcribed RNA from pSFV1-EGFP plasmids #3 and #5, were electroporated into ~80% confluent BHK-21 cells and incubated on glass coverslips in 6-well plates, for 18 h p.e. PBS was used as a negative electroporation control. Cells were fixed, mounted onto glass slides, and analysed for EGFP expression by direct epifluorescence, using an EGFP-specific filter, at 488 nm. Note bright green EGFP-positive appearance of BHK-21 cells, transfected with RNA from pSFV1-EGFP clones #3 (*A*) and #5 (*B*). Mock-transfected cells were completely negative for EGFP fluorescence (*not shown*). Electroporation with RNA from the pSFV1-EGFP clone produced in Stockholm (*C*), produced a higher intensity of fluorescence compared to pSFV1-EGFP clones #3 and #5. Photographed at x 400 magnification.

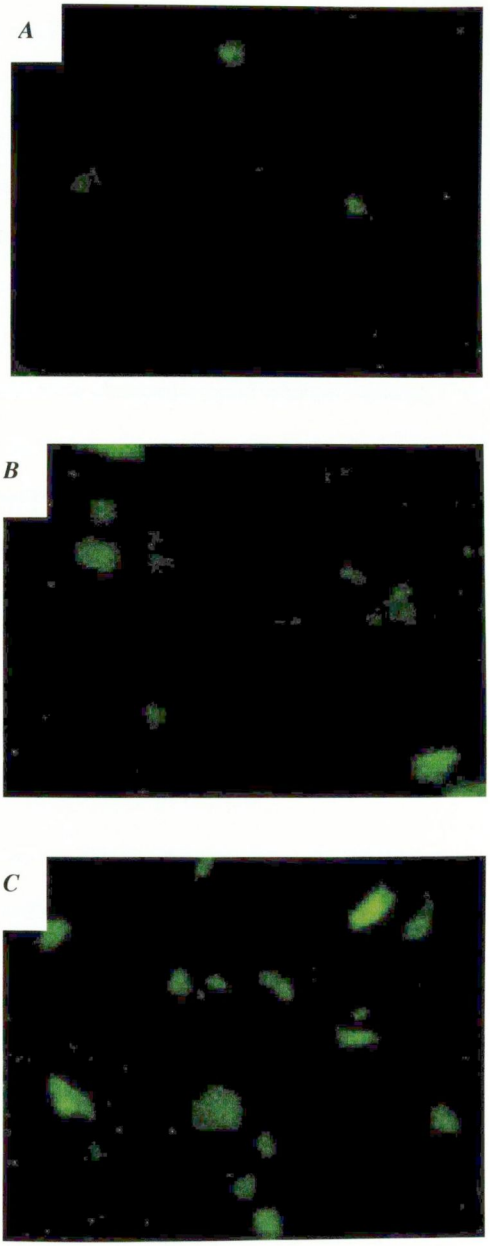


Figure 2.9- Screening for EGFP expression from recombinant clones by direct epifluorescence in BHK-21 cells.

wavelength of 488 nm. Results are illustrated in Figure 2.9. EGFP-expressing BHK-21 cells were detected following electroporation with RNA from both pSFV1-EGFP clones (*Figure 2.9 A, B*). BHK-21 cells that received PBS alone were completely negative for EGFP expression (*not shown*). At the time of cloning, collaborators in Stockholm had also been successful with the *EGFP* cloning procedure. This pSFV1-EGFP clone (*Figure 2.9 C*) showed a higher intensity of EGFP fluorescence following transfection, than with either clone #3 or #5. The Stockholm clone contained a capsid enhancer sequence, 5' of the *EGFP* gene, resulting in higher levels of reporter gene expression (*P. Liljeström, personal communication*). This pSFV-EGFP plasmid was subsequently utilised in all subsequent experiments.

2.3.3 Transfection with *in vitro*-transcribed RNA from recombinant SFV plasmids induces apoptosis in the BHK-21 cell line.

To determine whether transfection with recombinant SFV RNA induces apoptosis in BHK-21 cells, recombinant SFV RNA molecules, transcribed from plasmids pSFV-LacZ and pSFV-EGFP were utilised. BHK-21 cells were grown until ~80% confluent, trypsinised and electroporated with *in vitro*-transcribed SFV-LacZ or SFV-EGFP RNA. PBS alone was used as a mock-transfection control. Transfected cells were incubated on glass coverslips, in 6-well plates and assessed for efficient viral RNA transfection by analysis for reporter gene expression. *LacZ* expression was detected following methanol-fixation and staining with *X-gal* solution, for 6 h (*not shown*). Detection of EGFP was performed by direct epifluorescence on paraformaldehyde-fixed cell monolayers. At 18 h p.e. with either RNA construct, reporter gene expression was evident in up to 100% of

BHK-21 cells analysed (*Figure 2.10.A*). Cells transfected with PBS alone, were negative for both *EGFP* and *LacZ* reporter gene expression (*not shown*).

Transfected cells were analysed for apoptosis induction, using DNA fragmentation criteria, as for SFV-4 virus infection studies (*see section 2.3.1*). Analysis of chromosomal DNA fragmentation *in situ* using TUNEL, at 48 h p.e. with either SFV-LacZ (*not shown*), or SFV-EGFP (*Figure 2.10.B*) RNA constructs, revealed numerous apoptotic TUNEL-positive cells. Note however that the number of TUNEL-positive cells does not adequately reflect the number of cells transfected with SFV RNA. This is due to the fact that not all transfected cells may be undergoing apoptosis at any one time. DNA fragmentation was confirmed by agarose gel electrophoresis of cellular DNA, extracted from SFV RNA- and mock-transfected cells. Figure 2.10.*C* indicates features of cellular DNA fragmentation, at days 2 and 3 p.e. with the EGFP-expressing RNA construct. Mock-transfected cells failed to reveal signs of cpe or DNA fragmentation at any of the indicated time-points.

Thus, transfection with recombinant SFV RNA molecules, initiated correct translation of the reporter gene, followed later by apoptosis induction within transfected cells. Apoptosis could therefore, occur in the absence of SFV structural proteins and occured independently of the choice of heterologous gene. By confirming structural gene-independent apoptosis induction, it is reasonable to assume that recombinant, encapsidated SFV virus particles (rSFV), containing these recombinant RNA molecules, are likely to produce a similar, and more powerful apoptotic phenotype in infected cell lines.

Figure 2.10- **Apoptosis induction in BHK-21 cells following transfection with *in vitro*-transcribed recombinant SFV-EGFP RNA.** BHK-21 cells were seeded into 75 cm^2 culture flasks and grown until ~80% confluent. Cell monolayers were trypsinised, resuspended in PBS and mixed with RNA *in vitro*-transcribed from the recombinant pSFV-EGFP plasmid. Following electroporation, cells were placed onto glass coverslips, contained within 6-well plates and incubated. *A*; Analysis of reporter gene, EGFP expression at 18 h p.e. Cells were fixed and mounted onto glass slides. Positive EGFP expression within the BHK-21 cell monolayer was visualised using direct epifluorescence, at 488 nm. Photographed at x 400 magnification. *B*; BHK-21 cells were assessed for apoptosis induction by DNA fragmentation analysis, using TUNEL. At 72 h p.e., SFV-EGFP RNA-transfected and mock-transfected (*not shown*) BHK-21 cells were fixed, and processed for TUNEL. Note brown, $TUNEL^+$ staining within nuclei of SFV-EGFP-transfected cells, indicative of apoptotic cell death (*arrows*) Note cells in (B) appear to form islands of cells, which was due to inadequate mounting in DPX solution. Photographed at x 400 magnification. Note that the number of cells transfected with the vector are not represented by the number of TUNEL positive cells. *C*; BHK-21 cells were assessed for apoptosis by DNA fragmentation analysis, using agarose gel electrophoresis of extracted cellular DNA. At 24 h intervals following transfection, cellular DNA from both mock- and SFV-EGFP RNA-transfected cells, were extracted and analysed for DNA fragmentation on a 1.5% (w/v) agarose gel. *Lanes 1, 3, and 5*; DNA extracted from pSFV-EGFP-transfected BHK-21 cells at 24, 48 and 72 h p.e., respectively. *Lanes 2, 4 and 6*; DNA extracted from mock-transfected BHK-21 cells at 24, 48 and 72 h p.e., respectively. *Lane 7*; *Lambda* (*Hind111*) DNA molecular weight markers.

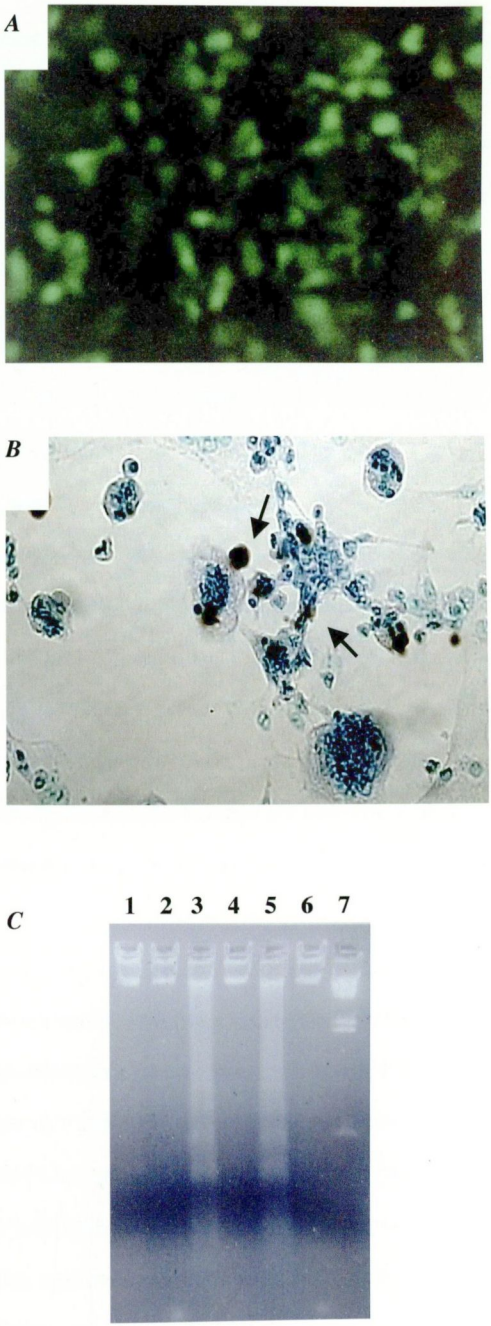


Figure 2.10- Apoptosis induction in BHK-21 cells following transfection with *in vitro*-transcribed recombinant SFV-EGFP RNA.

2.3.4 Recombinant SFV virus particle production in the BHK-21 cell line.

Recombinant SFV particles (rSFV), expressing both *EGFP* and *LacZ* reporter genes, were prepared using the simultaneous electroporation procedure, as outlined by Berglund *et al*, (1993). *In vitro*-transcribed recombinant SFV-LacZ and SFV-EGFP RNA molecules were encapsidated into infectious virus particles by electroporation with two *in vitro*-transcribed 'helper' RNA species, SFV-Helper S2 and SFV-Helper CS219A, in BHK-21 cells *in vitro* (*Figure 2.11*). Following electroporation of all three RNA species into BHK-21 cells, the helper RNA constructs efficiently translate viral structural proteins, which are used to encapsidate the recombinant RNA molecules. Infectious, *EGFP*- or *LacZ*-expressing particles were subsequently released and harvested. rSFV virus particle titres were calculated by infecting sBHK cell monolayers with serial dilutions of the virus. rSFV-EGFP particle titres were determined at 18 h p.i. with recombinant particles. Following paraformaldehyde fixation, cells were assessed for *EGFP* expression by direct epifluorescence and enumerated. rSFV-LacZ virus particles were enumerated using light microscopy of *X-gal*-stained sBHK cell monolayers.

Particle production was optimised during a visit to the Karolinska Institute, Stockholm, Sweden. rSFV virus particle titres were increased by up to 7 logs from previous attempts, to 2-5 x 10^8 I.U./ml. Initial attempts at particle production involved the *in vitro* transcription of recombinant and helper RNA constructs, using the techniques described in section 2.2.2.4. Following amendments to transcription reaction conditions and constituents, RNA production was increased 5-fold. Figure 2.12 illustrates clearly that RNA production and quality were the major determinants of particle production efficiency. Factors such as quality of plasmid DNA for *in vitro* RNA transcription, source of reagents and subtle

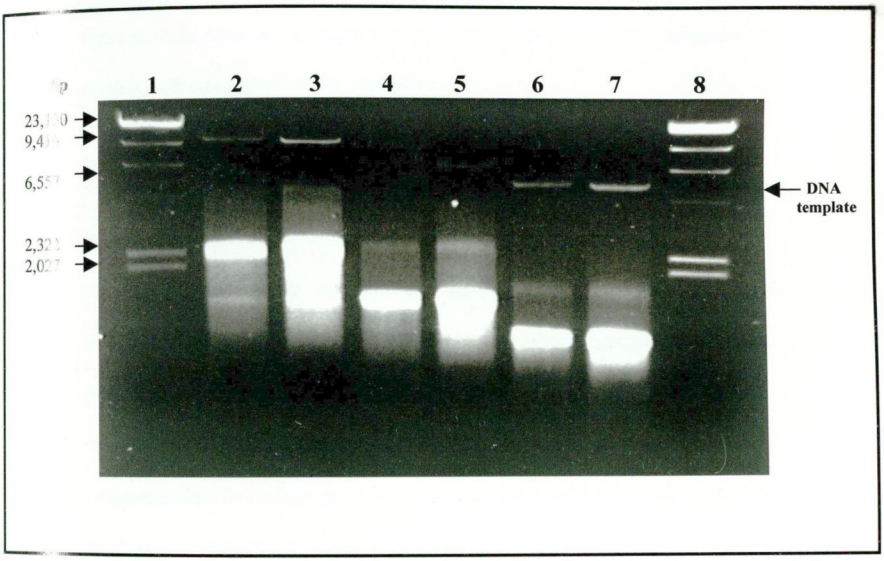


***Figure 2.11- In vitro* RNA transcription for rSFV-EGFP virus particle production.** 0.6% (w/v) agarose gel, stained with ethidium bromide. *Lanes 1* and *8*; 5 µl and 10 µl *Lambda* (*Hind111*) DNA marker, respectively. *Lanes 2* and *3*; 0.5 µl and 1.0 µl each of RNA *in vitro* transcribed from the pSFV-EGFP plasmid. *Lanes 4* and *5*; 0.5 µl and 1.0 µl each of SFV-Helper S2 RNA. *Lanes 6* and *7*; 0.5 µl and 1.0 µl each of SFV-Helper CS219A RNA. Arrow indicates *Spe1*-linearised DNA template.

differences in the electroporation and titration procedures also increased rSFV virus particle titres (*not shown*). This procedure was consistently reproduced and is now well established in the laboratory.

To optimise particle production, it was necessary to monitor levels of expression of each of the RNA constructs within particle-producing cells during the procedure. In this way, it was possible to determine which construct was limiting and to determine the cause of particle production failure. Samples of BHK-21 cells were placed into 6-well plates immediately following electroporation of recombinant SFV-LacZ and helper RNA constructs, and incubated for 24 h. Following fixation, cells were double-labelled for detection of both LacZ and SFV spike E2 proteins, indicative of SFV-LacZ and SFV-Helper S2 RNA molecules, respectively (*Figure 2.13*). An antibody for SFV capsid protein was unavailable. Both proteins were detected by incubating the cells with a mixture of anti-LacZ and anti-SFV E2 antibodies, and subsequently with TRITC- and FITC-conjugated secondary antibodies. The transfection efficiencies of both SFV RNA constructs were then detected by analysis for the expressing protein, using fluorescent microscopy with TRITC- and FITC-specific filters at 510 and 450 nm, respectively. FITC-specific staining of β-galactosidase-expressing cells in figure 2.13.*A* indicated upwards of 100% transfection efficiency for the recombinant SFV-LacZ RNA molecule. Double-labelling with TRITC-specific SFV E2 antibody however (*Figure 2.13.B*), indicated SFV-Helper S2 RNA uptake was up to 20% less than that of LacZ. Following this analysis, the ratio of SFV-Helper S2 to recombinant SFV-LacZ RNA species was marginally increased to ensure 100% transfection of BHK-21 cells with both RNA molecules, ensuring particle titre was at maximum. This experiment was reproduced for *EGFP* expressing rSFV virus particle production, using an antibody directed to the non-structural proteins of SFV, or by direct epifluorescence, for SFV-EGFP RNA detection (*not shown*).

Figure 2.12- **Optimisation of *in vitro* SP6 RNA transcription for rSFV virus particle production.** *A*; *In vitro* SP6 RNA transcription of SFV-Helper constructs prior to optimisation. Transcription reaction conditions are outlined in section 2.2.2.4. *Lane 1*; 2 µl *in vitro*-transcribed SFV-Helper CS219A RNA. *Lane 2*; 2 µl *in vitro*-transcribed SFV-Helper S2 RNA. *Lane 3*; *Lambda* (*Hind111*) DNA molecular weight markers. *B*; *In vitro* SP6 RNA transcription of SFV-Helper constructs following optimisation. Transcription reaction conditions are outlined in section 2.2.2.7. *Lanes 1 and 2*; 0.5 µl and 1.0 µl each of SFV-Helper S2 RNA. *Lanes 3 and 4*; 0.5 µl and 1.0 µl each of SFV-Helper CS219A RNA. *Lane 5*; *Lambda* (*Hind111* and *EcoR1*) DNA molecular weight markers. 0.6% (w/v) agarose gels, stained with ethidium bromide.

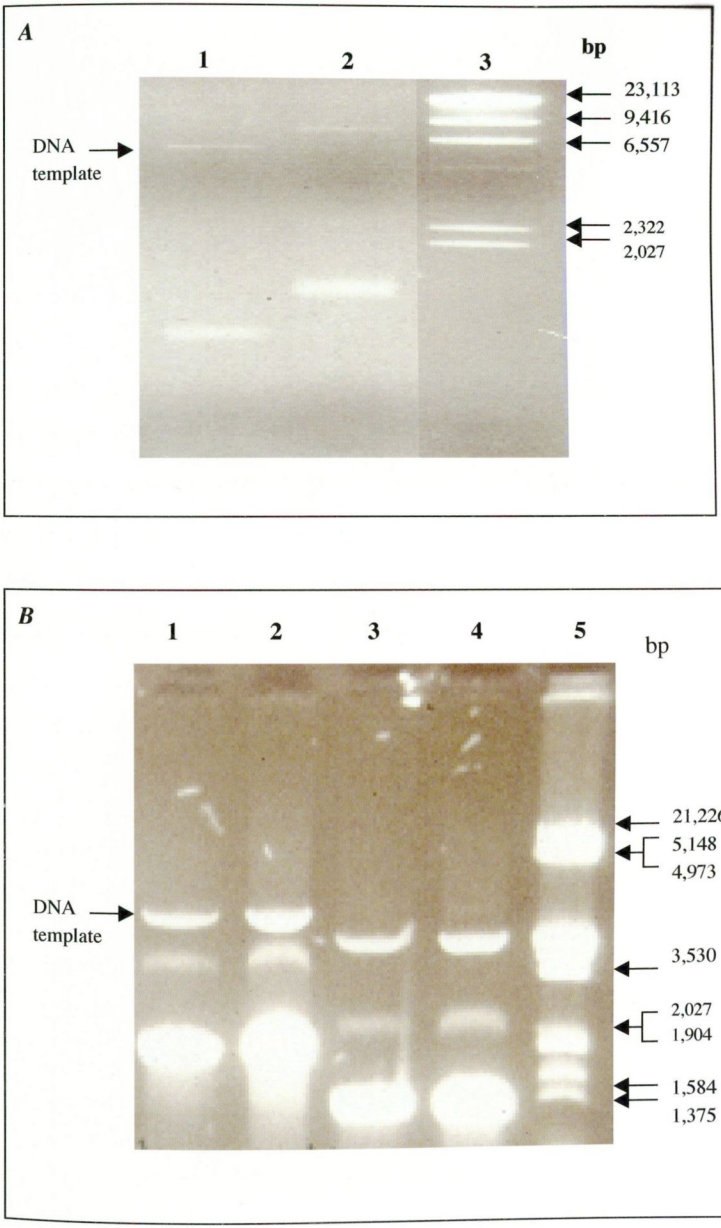


Figure 2.12- Optimisation of *in vitro* SP6 RNA transcription for rSFV virus particle production.

Figure 2.13- **Dual detection of β-galactosidase and SFV E2 proteins in particle-producing cells.** BHK-21 cells were seeded into 75 cm^2 culture flasks and grown until ~80% confluent. The cells were trypsinised, resuspended in PBS and transfected with a mixture of recombinant SFV-LacZ and Helper (SFV-Helper S2 and SFV-Helper CS219A) RNAs. Cells were immediately resuspended in BHK-21 medium and placed onto glass coverslips contained in 6-well plates. Following 18 h incubation, cells were assessed for β-galactosidase (*A*) and SFV E2 (*B*) protein expression using a double-labeling procedure. Following fixation, cells were incubated with a mixture of mouse anti-β-galactosidase and rabbit anti-SFV spike antibodies, and subsequently with a mixture of FITC-conjugated anti-mouse and TRITC-conjugated anti-rabbit IgG antibodies. Cells were visualised by fluorescent microscopy at 450 and 510 nm for FITC and TRITC expression, respectively. Arrowheads indicate a single cell transfected with SFV-LacZ RNA (*A*) but not with SFV-Helper S2 (*B*), as assessed by antibody reactions. This specific cell will not produce packaged particles. This system allowed us to monitor limiting quantities of individual RNA species within particle-producing cells. Photographed at x 400 magnification.

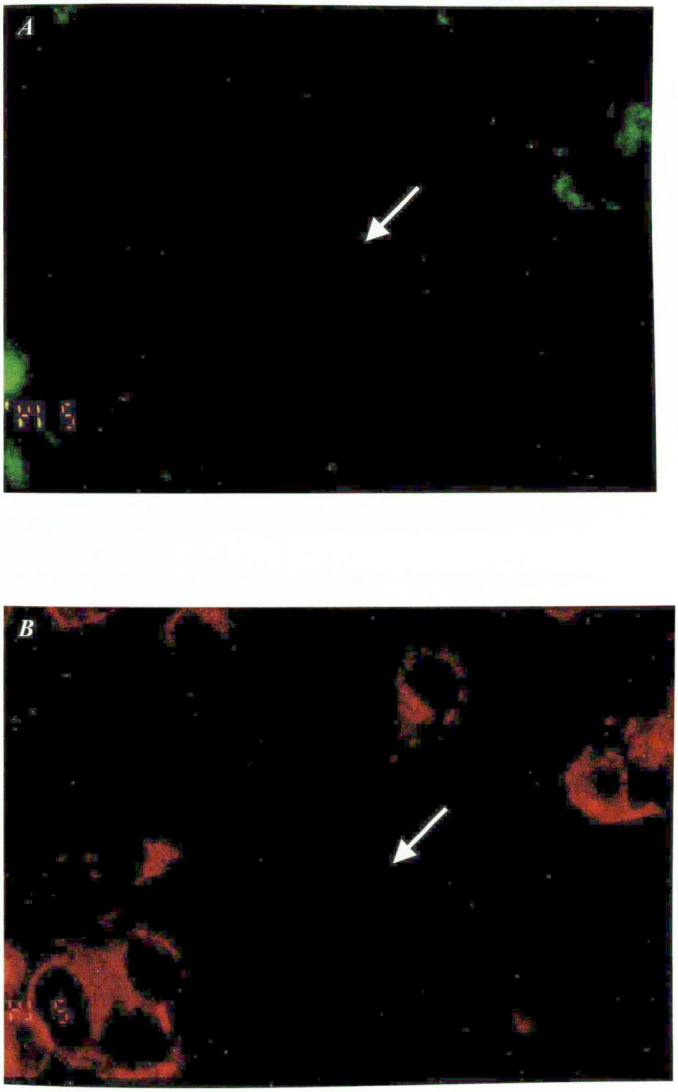


Figure 2.13- Dual detection of β-galactosidase and SFV E2 proteins in particle-producing cells.

2.3.5 Infection efficiency of rSFV virus particles in the BHK-21 cell line.

Prior to initiating rSFV virus infection studies on the BHK-21 cell line, the conditions for optimal rSFV virus particle infection were determined. This was necessary to calculate the optimum number of rSFV particles to infect the majority of BHK-21 cells in the monolayer. rSFV virus infection efficiencies were calculated using rSFV-EGFP particles. BHK-21 cells were seeded in triplicate, into 6-well plates and infected with increasing concentrations (moi) of rSFV-EGFP particles in infection medium. Following overnight incubation, cells were fixed and stained with a DNA-specific fluorochrome, DAPI, which labels all nuclei present in the monolayer, and is representative of the total cell population. Both EGFP expression and DAPI staining were detected by direct epifluorescence. Cells were examined for virus vector infection by expressing the number of EGFP-positive cells as a percentage of the number of DAPI positive cells per field. Results are presented in Figure 2.14. At moi 0.01 to 10, an apparent exponential relationship existed between the number of virus-infected cells and the moi of virus used. Upwards from moi 40 to 100, infection efficiencies approached maximum levels. Infection efficiencies of *LacZ* virus particles were identical to that of rSFV-EGFP (*data not shown*). Thus, rSFV virus infection at moi=10, was calculated as optimal for rSFV infection of BHK-21 cells *in vitro*, and was used in all subsequent infection studies unless otherwise indicated.

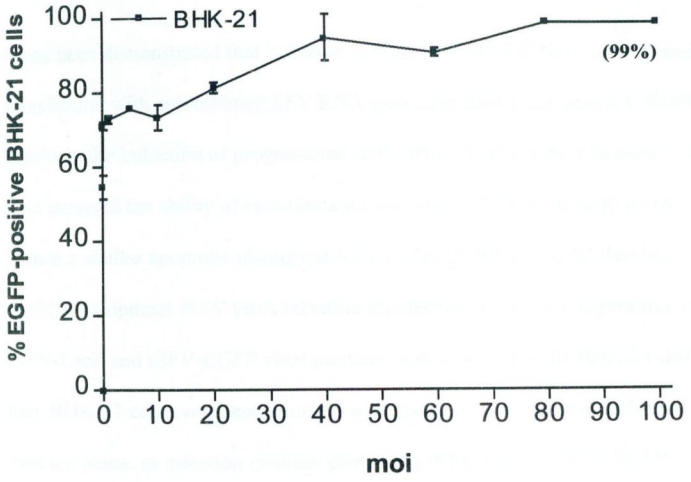


Figure. 2.14- Infection efficiency of rSFV-EGFP virus particles in BHK-21 cells. BHK-21 cells were seeded onto glass coverslips in 6-well plates at densities of 1 x 10^5 cells/well, and infected, in triplicate, with increasing concentrations (moi = 0.01, 0.1, 1, 10, 20, 40, 60, 80 and 100) of rSFV-EGFP virus particles (1 x 10^8 I.U./ml), or medium alone as control, (moi=0), for 1 h. At 18 h p.i., cells were fixed, stained with DAPI for 20 min, and analysed for EGFP expression by fluorescent microscopy at 488 nm (EGFP) and 350 nm (DAPI). EGFP-expressing cells were scored, and calculated as a percentage of the number of DAPI-stained cells in each field. Percentage infection efficiency is indicated in parentheses. *Points*; means, *bars*; SD, for a single experiment.

2.3.6 Infection with rSFV virus particles inhibits the growth and viability of BHK-21 cells *in vitro*.

It has been demonstrated that infection with replicative SFV virus, SFV-4, and transfection with recombinant SFV RNA molecules SFV-LacZ and SFV-EGFP, results in the induction of programmed cell death of BHK-21 cells in culture. We next assessed the ability of recombinant encapsidated SFV virus particles to induce a similar apoptotic phenotype within infected BHK-21 cells. Having established optimal rSFV virus infection efficiencies, the cytotoxic potential of rSFV-LacZ and rSFV-EGFP virus particles were assessed in the BHK-21 cell line. BHK-21 cells were seeded into 6-well plates and infected with infection medium alone, or infection medium containing rSFV-LacZ or rSFV-EGFP particles (moi 10). Reporter gene expression from both recombinant viruses could be detected at 18 h p.i. Cell growth and viability of BHK-21 cells following infection, were determined by trypan blue exclusion and methyl-^{3}H thymidine incorporation, daily for 10 days p.i. Trypan blue analysis (*Figure 2.15*) indicated that survival of BHK-21 cells at 24 h p.i. with either rSFV-LacZ or rSFV-EGFP particles appeared to be greatly reduced compared to mock-infected control cells, which continued to grow and proliferate at an exponential rate, at all indicated timepoints. At 5 days p.i. with rSFV virus, cells showed approximately 20% the viability that of mock-infected controls ($P<0.05$). Figure 2.16 illustrates how a second infection with rSFV-EGFP virus particles inhibited BHK-21 cell growth by a further 15-20% than a single infection alone, with negligible cell survival at the end of analysis (Day 10, $P<0.001$).

The effects of rSFV-EGFP virus particles on BHK-21 cell viability were further confirmed by methyl-^{3}H thymidine incorporation analyses. Measurement of cellular ^{3}H thymidine uptake in culture is a direct reflection of active cellular

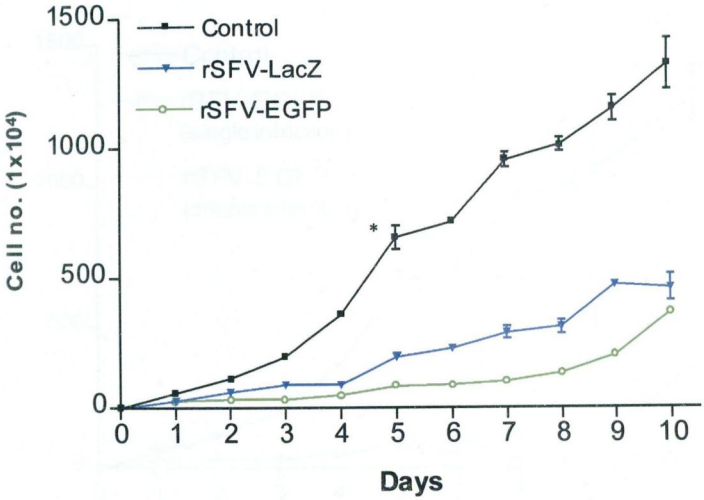


Figure 2.15- Growth and viability of BHK-21 cells following infection with rSFV virus particles, as determined by trypan blue exclusion. BHK-21 cells were incubated at densities of 1 x 10^5 cells/well in 6-well plates, and infected with rSFV-EGFP virus (moi 10), rSFV-LacZ virus (moi 10) or medium alone as a control, for 1 h. At each indicated time-point p.i., triplicate wells, for were typsinised and counted using trypan blue exclusion criteria. *Points*; means, *bars*; SD, for a single experiment, and is representative of 2 independent experiments.

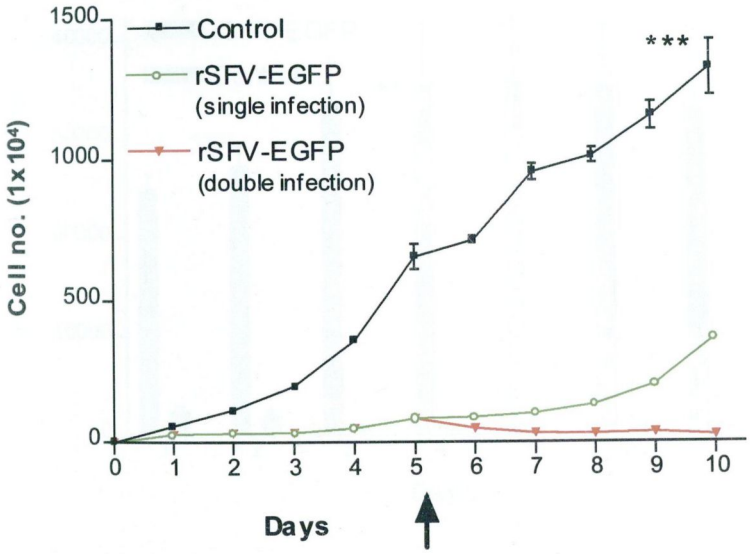


Figure 2.16- Effect of multiple rSFV virus particle infections on BHK-21 cell viability, as determined by trypan blue exclusion. BHK-21 cells were incubated at densities of 1 x 10^5 cells/well in 6-well plates, and infected with rSFV-EGFP virus (moi 10) or medium alone as a control, for 1 h. On day 5 p.i. (*arrow*), cells were reinfected with rSFV-EGFP particles (moi 10). At each indicated time-point p.i., triplicate wells were typsinised and counted using trypan blue exclusion criteria. *Points*; means, *bars*; SD, for a single experiment.

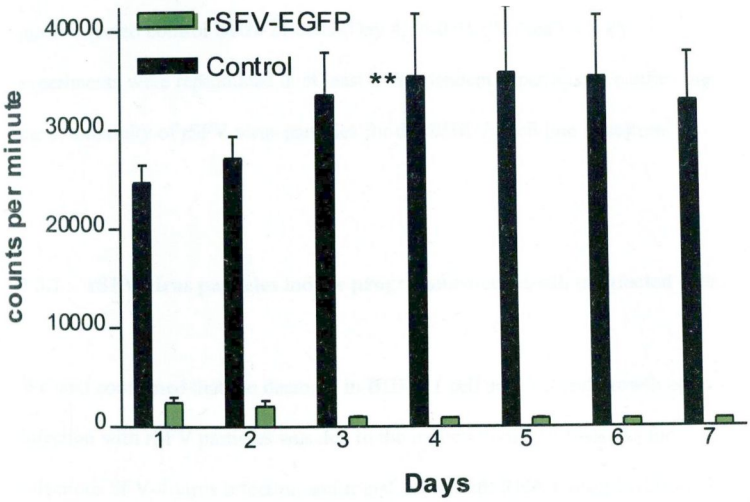


Figure 2.17- Growth and viability of BHK-21 cells following infection with rSFV virus particles, as determined by ^{3}H incorporation. BHK-21 cells were incubated at densities of 1 x 10^{5} cells/well in 6-well plates, and infected with rSFV-EGFP virus (moi 10), rSFV-LacZ virus (moi 10) or medium alone as a control for 1 h. At each indicated time-point p.i., medium from triplicate wells was replaced with medium containing methyl-^{3}H thymidine. Following a 24 h incubation, cells were removed and ^{3}H incorporation was measured using a liquid scintillation counter. *Points*; means, *bars*; SD, for a single experiment, and is representative of 2 independent experiments.

proliferation and division, and is measured directly from cellular DNA by liquid scintillation counting. As illustrated in Figure 2.17, BHK-21 cell proliferation greatly decreased as early as 24 h p.i. with the rSFV-EGFP vector. For the duration of the experiment, cell viability remained at approximately 3-5% that of mock-infected control BHK-21 cells (Day 4, $P<0.01$). Values for both experiments were reproduced in at least 2 independent experiments, confirming the cytotoxicity of rSFV virus particles for the BHK-21 cell line in culture.

2.3.7 rSFV virus particles induce programmed cell death in infected cells.

We next confirmed that the decrease in BHK-21 cell survival and growth upon infection with rSFV particles was due to the induction of apoptosis. As for infectious SFV-4 virus infection and transfection with RNA transcribed from the recombinant pSFV-LacZ and pSFV-EGFP plasmids, we analysed for apoptosis induction using DNA fragmentation criteria. BHK-21 cells were infected with medium alone, or medium containing rSFV-LacZ or rSFV-EGFP virus particles (moi 50), for 1 h. DNA was extracted from treated cells at 24 h intervals, for 3 days and analysed for DNA fragmentation by agarose gel electrophoresis. The results are illustrated in Figure 2.18. At 48 and 72 h p.i. with both rSFV virus vector constructs, cells revealed dramatic DNA fragmentation, in comparison to mock-infected contols. The 'laddering' effect observed at 48 h p.i. with rSFV-LacZ virus (*Lane 4*) was slightly less compared to that of rSFV-EGFP virus (*Lane 5*). This was due to a slightly lower rSFV-LacZ virus particle titre, when later examined (*not shown*).

Morphological and TUNEL analyses at 48 h p.i. confirmed apoptosis induction (*Figure 2.19*). TUNEL-positive cells, with intrinsic features of apoptotic

Figure 2.18- **Apoptosis induction in BHK-21 cells following infection with rSFV virus particles, as assessed by DNA fragmentation, using agarose gel electrophoresis.** BHK-21 cells were incubated at densities of 1 x 10^6 cells/well in 75 cm^2 flasks, and infected with rSFV-EGFP (moi 50), rSFV-LacZ (moi 50) particles or medium alone as a control. At 24 h intervals following infection, cells were lysed and DNA was released by enzymatic digestion. Cellular DNA for rSFV particle- and mock-infected cells was analysed for fragmentation into oligonucleosomal-size fragments, indicative of cell death, by agarose gel electrophoresis. *Lanes 1, 4 and 7;* DNA from rSFV-LacZ particle-infected BHK-21 cells at 24, 48 and 72 h, respectively. *Lanes 2, 5 and 8;* DNA from rSFV-EGFP particle-infected BHK-21 cells, at 24, 48 and 72 h, respectively. *Lanes 3, 6 and 9*; DNA from mock-infected BHK-21 cells, at 24, 48 and 72 h, respectively. *Lane 10*; *Lambda* (*Hind 111*) DNA molecular weight markers.

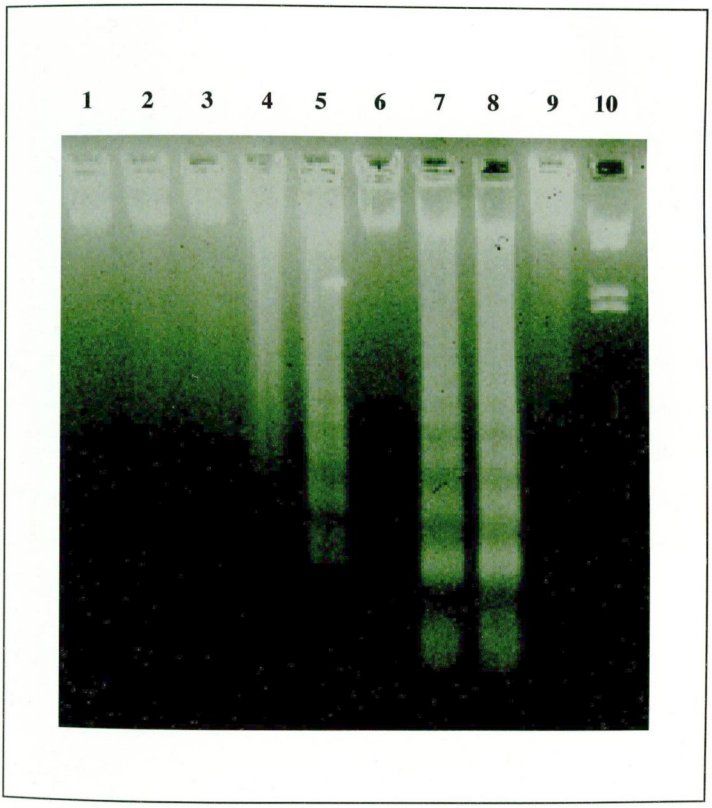


Figure 2.18- Apoptosis induction in BHK-21 cells following infection with rSFV recombinant particles, as assessed by DNA fragmentation, using agarose gel electrophoresis.

Figure 2.19- **rSFV virus particle-mediated apoptosis in BHK-21 cells, as assessed by chromosomal DNA fragmentation, using TUNEL.** BHK-21 cells were seeded onto glass coverslips in 6-well plates and grown until ~80% confluent. Monolayers were infected with rSFV-EGFP particles (moi 50) (*A*) or medium alone (*B*) as a mock-infection control. At 48 h p.i., cell monolayers were fixed and fragmented chromosomal DNA labelled with TdT and horse-radish peroxidase. Colorimetric detection was performed using DAB and normal, intact nuclei were counterstained with methyl green. Note brown, TUNEL-positive peroxidase staining within apoptotic nuclei (*arrows*) and apoptotic bodies in the rSFV-EGFP virus-infected cell monolayers (*A*), in contrast to healthy and dividing mock-infected control cells (*B*). Similar results were obtained with rSFV-LacZ virus-infected BHK-21 cell monlayers (*not shown*). Photographed at x 400 magnification.

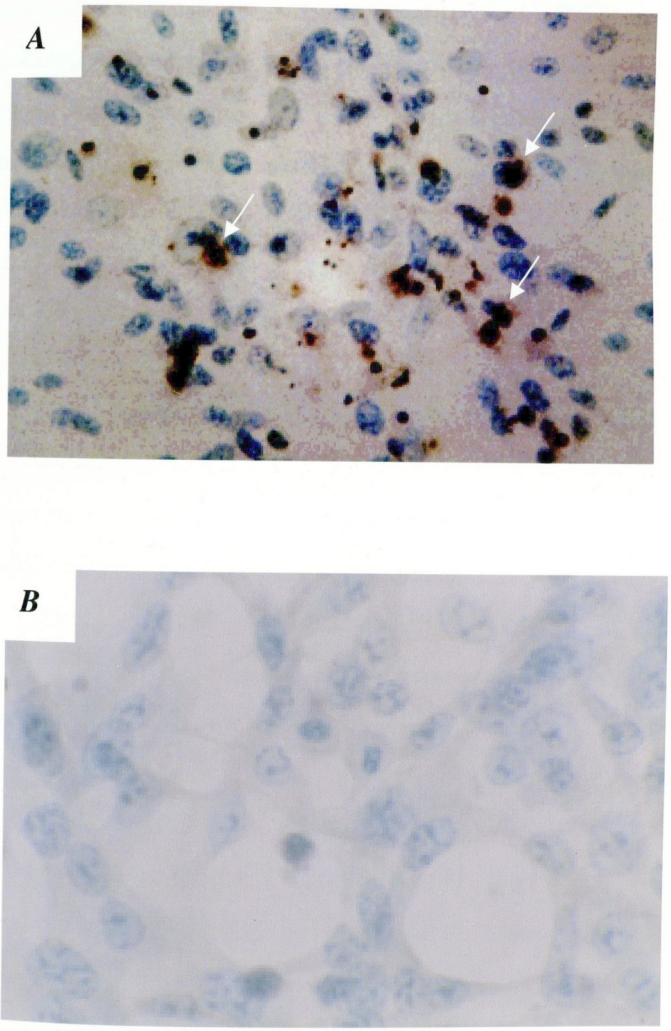


Figure 2.19- rSFV virus particle-mediated apoptosis in BHK-21 cells, as assessed by chromosomal DNA fragmentation, using TUNEL.

morphology, including nuclear shrinkage or pyknosis, and the formation of apoptotic bodies, were observed in rSFV-EGFP virus- (*Figure 2.19.A*) and rSFV-LacZ virus- (*not shown*) infected BHK-21 cells. This was not observed in mock-transfected BHK-21 cells (*Figure 2.19.B*), and coincided directly with the DNA ladder formation, observed by agarose gel electrophoresis (*Figure 2.18*). Thus, rSFV virus particles infect and replicate within BHK-21 cells, and as a consequence, inhibit cell proliferation by inducing programmed cell death.

2.4 DISCUSSION

Alphaviral infection of mammalian cells results in a drastic inhibition of cellular proliferation (Glasgow *et al*, 1997). Viral-induced shut-down of host macromolecular synthesis allows for sufficient intracellular virus replication and release. It is now well established that the cytopathological consquences that ensue following infection with SFV, are due to the induction of apoptosis (Scallan *et al*, 1997). SFV replication is believed to trigger an apoptotic pathway(s) within infected cells and engage host-cell death machinery (Grandgirard *et al*, 1998). *In vivo*, cell death induction is believed to be advantageous to the host, preventing further viral propagation and release, and the onset and extent of SFV-induced apoptosis is cell type and virus strain specific. Previous studies indicate that infectious SFV virus strains A7 and L10, induce apoptosis in both BHK-21 and CHIK cells *in vitro* (Glasgow *et al*, 1997; Atkins *et al*, 2000).

In the analysis of SFV-induced apoptosis, we utilised BHK-21 cells, routinely used for SFV propagation, and the virulent strain of SFV, SFV-4. SFV-4 bears closest similarity to the SFV strain L10, and is produced by electroporation of *in vitro*-transcribed RNA from the *Spe1*-linearised plasmid pSP6-SFV-4 (Liljeström *et al*, 1991). Following 8-10 hours incubation with the virus, BHK-21 cells revealed initial cytopathogical changes that were characteristic of apoptosis. These included the rounding up of cells, and cell and nuclear shrinkage. At later timepoints following infection, numerous apoptotic bodies were detected, and cell monolayers were completely obliterated after one day, thereby confirming data from previous studies indicated above.

Similar to Sindbis virus, it was initially believed that viral structural proteins were responsible for apoptosis induction (Ubol *et al*, 1994; Despres *et al*, 1995). The SFV capsid protein was hypothesised as the major pro-apoptotic protein, primarily due to its chymotrypsin-like self-cleavage abilities (Grandgirard

et al, 1998), which may mimic upstream caspase protease activities and lead to apoptosis induction. As in the previous study by Glasgow *et al*, (1998), it was reproducibly demonstrated that deletion of SFV structural proteins does not abrogate the pro-apoptotic abilities of the virus. The recombinant SFV vector system, which is largely derived from manipulation of the infectious cDNA clone of SFV, SFV-4 (Berglund *et al*, 1993), lacks all SFV structural protein genes, which are instead replaced with a short polylinker sequence, containing a multicloning site to facilitate insertion of the heterologous gene. Transfection with *in vitro*-transcribed RNA from the recombinant SFV plasmids pSFV-LacZ and pSFV-EGFP, induced a similar apoptotic phenotype in transfected BHK-21 cells, to infection with SFV infectious virus. Deletion of the non-structural *nsP2* gene however, abrogates both viral RNA synthesis and apoptosis induction (Glasgow *et al*, 1998). Thus, viral RNA synthesis is required for the cytopathological effects. It was obvious that the cytopathology of BHK-21 cells following infectious SFV-4 virus infection was more immediate and dramatic, than transfection with recombinant SFV RNA molecules transcribed from the SFV plasmids pSFV-LacZ and pSFV-EGFP, which lack both viral structural proteins and an ability to produce infectious progeny virions. Perhaps as with Sindbis virus (Ubol *et al*, 1994), SFV structural proteins are necessary for full cytopathic effect.

In initial SFV vector expression studies, the reporter gene *LacZ* was used to facilitate detection of the vector *in situ* (Berglund *et al*, 1993). Incubation of recombinant SFV-LacZ RNA-transfected cells with *X-gal* substrate revealed positive blue staining, whereas mock-transfected cells remained yellow. For the detection of recombinant SFV constructs within fixed tumour tissue, discussed in future chapters, a more favourable reporter system was necessary. *Green Fluorescent Protein* (*GFP*), from the jellyfish *Aequorea victoria*, is now the reporter gene of choice in many experimental systems (Chalfie *et al*, 1994), and

offers several advantages for *in situ* tumour analysis. *GFP* may be detected in many heterologous systems using UV light, and unlike *LacZ*, does not require fixation or staining methods prior to detection, and requires no additional proteins, substrates or cofactors.

For the cloning of this reporter gene into the SFV expression vector, we utilised an optimised variant of the protein termed *'enhanced' GFP* or *EGFP*. *EGFP* encodes a protein which fluoresces about 35 times more intensely than wild-type GFP when excited at 488 nm. The EGFP protein was cloned into the MCS of the SFV expression vector, pSFV-1 and positive EGFP-expressing clones were selected by direct epifluorescence of transfected cells. Fluorescence was still quite low however, when compared to a SFV-EGFP clone produced using a similar system in Stockholm, Sweden (P. Liljeström, *unpublished results*). This SFV-EGFP clone utilised the sequence from the SFV capsid translational enhancer (Sjöberg *et al*, 1994) to amplify EGFP expression further, and produce a higher intensity of fluorescence.

The production of packaged recombinant SFV virus particles (rSFV) was also optimised in Stockholm, Sweden. rSFV particles were produced using the 'split helper' vector system developed by Smerdou & Liljeström (1999). Recombinant RNA molecules were encapsidated into fully infectious vector particles by cotransfection with two 'helper' RNA molecules, which supply the SFV capsid and spike proteins *in trans*. The recombinant RNA molecule was preferentially encapsidated as both helper RNA species lack a packaging signal. Infectious, recombinant particles were then released and harvested.

Initial difficulties with rSFV particle production were rectified, increasing rSFV-LacZ and rSFV-EGFP virus particle titres by up to 7 logs from previous attempts. Many factors contributed to titre discrepancies, particularly the quality and quantity of recombinant and helper RNAs produced during *in vitro* RNA

transcription reactions. The initial ratio of recombinant-to-helper RNA species within transfected cells were also critical to particle titre, and double labeling experiments to detect both recombinant and helper protein expression, were necessary for efficient rSFV particle production. rSFV particle stocks of 2-5 x 10^8 I.U./ml are now successfully produced in the laboratory, and this is increased by 10- to 50-fold using the large particle preparation procedure (*see Chapter 4*).

Following rSFV particle production, and determination of rSFV virus infection efficiencies for the BHK-21 cell line, we next assessed the effects of rSFV virus particle infection for cytopathology and apoptosis induction. Results from this study indicate clearly the extensive cytotoxicity of rSFV particles for BHK-21 cells in culture. rSFV virus infection inhibited BHK-21 cell proliferation as early as 24 h p.i. with the vector, while also allowing sufficient time for reporter gene expression. Cell survival was further decreased to negligible values following a second infection at a later timepoint.

The extensive cytopathological changes following rSFV virus particle infection, closely resembled that of infection with virulent SFV-4 virus infection and was proven to be a consequence of apoptosis induction. As with SFV-4 virus infection and recombinant SFV RNA transfection, rSFV virus particle-infected BHK-21 cells revealed morphological alterations characteristic of apoptosis, including cell and nuclear shrinkage and chromatin condensation and fragmentation.

Thus, in contrast to other recombinant viral vectors derived from adeno and retroviruses, which are used extensively for apoptotic cancer gene therapy, rSFV encodes its own inherent PCD system, localised either within the SFV non-structural protein region or as a consequence of viral replication. rSFV virus-mediated apoptosis induction is consistent, with up to 100% infection and cytotoxic efficiencies in BHK-21 cells, and occurs independently of heterologous

protein expression. Infection with recombinant retroviral particles is non-cytopathic (Fujiwara *et al*, 1993) resulting in a persistently infected cell line. In adenovirus vectors, the pro-apoptotic *E1A* gene, is commonly deleted to facilitate insertion of the heterologous gene (Teodoro *et al*, 1995). Thus, whereas for pro-apoptotic gene therapy, the latter two vectors rely exclusively on heterolgous protein expression to mediate a therapeutic effect, this report clearly demonstrates that rSFV particles induce their own endogenous cell death pathway, and the MCS can be used for other purposes. In this and subsequent chapters, the MCS contains the reporter gene *EGFP* to facilitate detection of the vector *in situ*.

The efficiency of rSFV virus infection of BHK-21 cells, the 100% electroporation efficiencies of recombinant SFV viral RNA, and the consistency of PCD induction, makes the BHK-21 cell line an ideal positive control for rSFV virus particle studies on the cancerous cell lines utilised in subsequent chapters.

Chapter 3

rSFV-mediated inhibition of human lung cancer cell growth in vitro, by apoptosis induction.

3.1 INTRODUCTION

Transformation of a normal to a malignant cell involves the accumulation of multiple genetic alterations (Bishop, 1992). Mutations within the *p53* tumour suppressor gene are amongst the most common abnomalities yet identified in human cancers (Takahashi *et al*, 1989). The documented functions of p53 include cell cycle checkpoint regulation (Kuerbitz *et al*, 1992) and the induction of apoptosis (Symonds *et al*, 1994).

Several previous studies, using recombinant retrovirus and adenovirus vectors have indicated that *p53* gene replacement strategies can suppress tumour growth and induce apoptosis in a number of human cancers (Fujiwara *et al*, 1994a ; Fujiwara *et al*, 1994b). These vectors however, are non-cytopathic, and rely exclusively on exogenous *p53* gene delivery to mediate the apoptotic effects.

The cytotoxic abilities of the recombinant SFV vector were introduced in Chapter 2. This viral vector was shown to induce programmed cell death independently of the heterologous gene. In chapter 3, the cytotoxicity of rSFV particles is further exploited as a potential cytotoxic gene therapy agent for the elimination of malignant cells. The human non-small cell lung cancer (NSCLC) cell line, H358a, was chosen for this study. This cell line contains a homozygous deletion in the *p53* gene (Takahashi *et al*, 1989).

rSFV-mediated cellular cytotoxicity and apoptosis induction were monitored *in vitro*, in H358a monolayer cultures. It is well-documented however, that tumour cell growth as two-dimensional (2-D) monolayer cultures, does not adequately reflect the considerable heterogeneity observed within solid tumours *in vivo*. Thus, as a prerequisite to *in vivo* studies, an *in vitro* three-dimensional (3-D) multicellular tumour spheroid (MTS) model was developed. MTS have been previously shown to approximate the 3-D configuration of primary and metastatic

tumours in culture (Sutherland, 1988), and were utilised to further assess the cytotoxicity of rSFV *in vitro*.

This chapter clearly illustrates the potential of the rSFV vector system as a cytotoxic cancer gene therapy agent. rSFV virus particle infection of the NSCLC cell line was shown to greatly inhibit tumour cell proliferation and induce apoptosis in the *p53*-deleted cell line. The vector was also shown to infect and penetrate multiple layers of H358a cells, growing as solid *in vitro* tumour masses, and thereby conferring therapeutic effects.

3.2 EXPERIMENTAL PROCEDURES

3.2.1 MATERIALS

3.2.1.1 *Cell Lines*

NCI-H358a human non-small cell lung carcinoma cell line, containing a homozygous *p53* deletion (Takahashi *et al*, 1989), was a gift from Prof. J. A. Roth, (Department of Thoracic Surgery, M. D. Anderson Cancer Centre, University of Texas, Houston, Texas). RPMI-1640 medium was from Life Technologies, Inc. (Paisley, Scotland).

3.2.1.2 *In Vitro Studies*

[3-(4, 5-dimethylthiazol-2-yl)-5-(3-carboxymethoxyphenyl)-2-2(4-sulfophenyl)-2H-tetrazolium, inner salt (MTS) was from Promega (Wisconsin, USA). Sulphorhodamine B and Poly(2-hydroxyethyl methacrylate)(polyHEME) were from Sigma (St. Louis, MO, USA).

3.2.2 METHODS

3.2.2.1 Cell Culture

NCI-H358a cells were cultured in RPMI-1640 medium supplemented with 10% (v/v) FCS, 100 U/ml ampicillin, 100 µl/ml streptomycin and 2 mM L-glutamine, and maintained at 37°C in a humidified atmosphere of 5% CO_2, in 25 or 75 cm^2 culture flasks. Cells were seeded at 1 x $10^5 ml^{-1}$ for growing (ATCC recommendation) in a total volume of 8 ml (25 cm^2 flask) or 15 ml (75 cm^2 flask), and passaged when confluent as described for BHK-21 cell amintenance in section 2.2.2.1

3.2.2.2 Virus

The production of SFV4 virus was described in section 2.2.2.2. Virus titres of between 1 and 5 x 10^9 pfu/ml was routinely obtained. Virus at 1 x 10^4 pfu/ml was used to infect cell lines, as described in section 2.2.2.2.

3.2.2.3 Preparation of recombinant SFV RNA

Preparation of recombinant SFV plasmids, and *in vitro* transcription for SFV-LacZ and SFV-EGFP RNA, were performed as outlined in sections 2.2.2.3-2.2.2.4 and section 2.2.2.6, respectively.

3.2.2.4 Recombinant SFV virus particle production

Recombinant rSFV-LacZ and rSFV-EGFP virus particle production was performed as described in section 2.2.2.7. 'Empty' rSFV-1 vector particles, which lack a reporter gene, were also prepared as indicated above. As no antibody was available for titration of rSFV-1 virus particles, each batch of rSFV-1 particles were produced in parallel with rSFV-EGFP particles, and thus rSFV-1 virus titres were calculated indirectly, by reference to rSFV-EGFP virus titres.

3.2.2.5 Calculation of rSFV virus particle infection efficiency

To determine the infection efficiency of rSFV virus particles in lung carcinoma cells, NCI-H358a cells were seeded at 1 x 10^4 ml^{-1} in 6-well plates (2 ml/well). Cells were then infected with rSFV-EGFP virus at a range of mois: moi 1-moi 400, in a total volume of 500 µl infection medium (minimal essential medium, 0.2% (v/v) BSA, 20 mM Hepes, 2 mM L-Glutamine and antibiotics), for 1 hour, with rocking movements every 15 min. Infection medium alone was used in mock-infected controls, or moi=0. Infection efficiencies were subsequently determined as dascribed for the BHK-21 cell line in section 2.2.2.8. Up to 600 H358a cells were scored, and each moi was calculated as a mean of triplicate samples.

3.2.2.6 Optimisation of cytotoxicity assays for H358a cells

3.2.2.6.1 *Sulphorhodamine B assay*

Sulphorhodamine B (SRB) colorimetric analysis of cell viability was optimised for the H358a cell line by SRB staining of increasing numbers of H358a cells and its relatedness to the initial H358a cell number. SRB is a bright pink aminoxanthene dye which binds to protein basic amino acid residues under mildly acidic conditions, in trichloroacetic acid (TCA)-fixed cells, to provide a sensitive index of cellular protein content over a cell density range of at least 2 orders of magnitude (Skehan *et al*, 1990). In order to optimise this assay for the H358a cell line, 6-well plates were seeded in triplicate with increasing numbers of H358a cells (1, 2.5, 5, 10, 20, 40, 80 and 160 x 10^4) in a total volume of 2 ml, and allowed to adhere to the bottom of the plates. Cells were fixed in 5% (v/v) ice-cold TCA for 1 h. The cells were washed in tap-water and air-dried for 2 h. Cells were then stained with 1 ml 0.4% (w/v) SRB in 1% (v/v) acetic acid, for 20 min. At the end of the staining period, SRB was removed and cultures were quickly rinsed four times with 1% (v/v) acetic acid, to remove unbound dye. Following rinsing, the cultures were air-dried until no standing moisture was visible. Bound dye was solubilised with 10 mM unbuffered Tris base (pH 10.5), for 5 min on a gyratory shaker. The dye was removed from the cell monolayers and 200 µl aliquots added to wells of a 96-well plate. Colorimetric detection was performed using a Labsystems Multiscan plus ELISA plate reader at 570 nm. Background optical densities were measured in wells incubated with growth medium without cells. Absorbance values were determined and correlated with initial cell numbers in culture.

3.2.2.6.2 *MTS assay*

The CellTitre 96® AQ_{ueous} One Solution Cell Proliferation Assay was also used to determine cell viability, and was also optimised for the H358a cell line. This system contains a novel tetrazolium compound [3-(4, 5-dimethylthiazol-2-yl)-5-(3-carboxymethoxyphenyl)-2-2(4-sulfophenyl)-2H-tetrazolium, inner salt (MTS) and the electron-coupling agent, phenazine ethosulphate (PES). Assays were performed by adding a small amount of this reagent directly to culture wells and incubating for 1-4 h. In order to optimise this assay for the H358a cell line, 96-well plates were seeded in triplicate with increasing numbers of H358a cells (1, 2.5, 5, 10, 20, 40, 80 and 160 x 10^3) in a total volume of 200 µl RPMI medium, and allowed to adhere to the bottom of plates. A 20 µl volume MTS reagent was directly added to each well, and incubated at 37°C in a humidified atmosphere of 5% CO_2, for 4 h. MTS is bioreduced by cells into a coloured formazan product, which is soluable in tissue culture medium, and was measured at 492 nm using a Labsystems Multiscan Plus 96-well plate reader. Background optical densities were measured in wells incubated with growth medium without cells. The quantity of formazan product produced by cultured cells, detected at 492 nm, was correlated to the initial H358a cell inoculum.

3.2.2.7 Analysis of H358a cell viability

To measure growth and cytotoxicity in cultured cells, NCI-H358a cells were seeded at 1 x 10^4 ml^{-1} in 6-well plates (2 ml/well) prior to infection. Cells were infected at moi 100 rSFV-1 and rSFV-EGFP virus particles, unless otherwise indicated, in a total volume of 500 µl infection medium, for 1 hour, with rocking

movements every 15 min to achieve a homogenous infection. Infection medium alone was used as a mock-infected control. The cells were replenished with fresh RPMI-1640 medium, and incubated at 37°C in a humidified atmosphere of 5% CO_2 for the indicated timepoints, and subsequently analysed for cell viability by trypan blue exclusion (section 3.2.2.7.1), sulphorhodamine B colorimetric (section 3.2.2.7.2), and [methyl-^{3}H]thymidine incorporation (section 3.2.2.7.3) assays.

3.2.2.7.1 *Trypan blue exclusion assay*

The viability of rSFV- and mock-infected NCI-H358a cells was determined by trypan blue exclusion, as outlined for BHK-21 cells in section 2.2.2.9.1. Cells were harvested and analysed daily over a period of 7 days, and each sample was taken and analysed in triplicate.

3.2.2.7.2 *Sulphorhodamine B assay*

The cytotoxicity of both vector constructs was assessed using a sulphorhodamine B (SRB) colorimetric assay. SRB staining, optimised for the H358a cell line in section 3.2.2.6.1, provides a sensitive index of cellular protein content and therefore, cell survival. At 24 h intervals following rSFV virus particle infection, cells were fixed in 5% (v/v) ice-cold TCA for 1 h and stained with 1 ml 0.4% (w/v) SRB in 1% (v/v) acetic acid, for 20 min. Following rinsing with 1% (v/v) acetic acid, the cultures were air-dried until no standing moisture was visible. Bound dye was solubilised with 10 mM unbuffered Tris base (pH 10.5), for 5 min on a gyratory shaker and colorimetric detection was performed on 200 µl aliquots, using a Labsystems Multiscan plus ELISA plate reader, at 570 nm. Background optical densities were measured in wells incubated with growth medium without cells. Absorbance values were directly proportional to the total number of

surviving cells. Cells were analysed daily over a period of 7 days, and each sample was performed and analysed in triplicate.

3.2.2.7.3 *[methyl-^{3}H]thymidine incorporation*

To determine the prolifertaion rate and viability of rSFV- and mock-infected control H358a cells, measurement of radiolabelled [methyl-^{3}H]thymidine incorporation, as described for BHK-21 cells in section 2.2.2.9.2. Cells were analysed daily over a period of 7 days, and each sample was performed and analysed in triplicate.

3.2.2.8 Detection of apoptosis

3.2.2.8.1 *DNA fragmentation detection using agarose gel electrophoresis*

To detect the internucleosomal DNA fragments characteristic of apoptosis, approximately 80-90% confluent H358a cells in 75 cm^2 tissue culture flasks, were infected with rSFV-1 and rSFV-EGFP virus particles at moi 400 in a total volume of 1 ml infection medium for 1 h, with rocking movements every 15 min to achieve a homogenous infection. Infection medium alone was used as mock-infection controls. Cells were replenished with 15 ml complete RPMI-1640 medium, and incubated at 37°C in a humidified atmosphere of 5% CO_2. At 24, 48 and 72 h p.i. DNA was extracted from rSFV- and mock-infected cells and analysed for DNA fragmentation as described in section 3.2.2.10.1.

3.2.2.8.2 *DNA fragmentation detection using TUNEL*

Detection of DNA fragmentation at the single-cell level, performed using the Terminal deoxynucleotidyl transferase (TdT)-mediated dUTP-biotin nick-end labelling (TUNEL) technique, was performed as outlined in section 2.2.2.10.2. H358a cells were seeded at 1 x 10^5 ml^{-1} into 6-well culture plates containing 18 x 18 mm glass coverslips, and infected with rSFV-1 and rSFV-EGFP virus particles at moi 400, and analysed at 24, 48 and 72 h p.i.

3.2.2.8.3 *DNA fragmentation analysis by DAPI staining*

H358a cells were seeded onto glass coverslips, in 6-well plates and infeted with rSFV-EGFP particles (moi 100) in infection medium, or medium alone as a mock-infection control. At 24 h intervals following infection, adherent H358a cells were washed with PBS, fixed with 2% (w/v) paraformaldehyde for 1 h, washed and stained with the DNA-specific dye, DAPI (1 :40 dilution), for 20 min at room temperature. Cells were washed, mounted onto glass slides using Mowiol-DABCO solution, and visualised by direct epifluorescence at 488 nm (EGFP-specific) and 350 nm (DAPI-specific). Fragmented or condensed nuclei were scored as apoptotic. Intact or mitotic nuclei were scored as normal.

3.2.2.9 Spheroid culture

3.2.2.9.1 *Production of H358a multicellular spheroids*

Multicellular spheroids were prepared by the liquid overlay technique (Korff & Augustin, 1998). Tissue culture plates were coated with 1% (w/v) serum-free medium agar in 96-well plates (50 µl/well), 24-well plates (100 µl/well) and 60 mm^2 plates (3 ml/well), allowed to solidify and form a gentle meniscus at the bottom of the plates (H. Lichenbeld, *personal communication*). Alternatively, plates were coated with 2% (w/v) polyHEME solution (S. Mann, *personal communication*). H358a spheroids were initiated from a cell suspension by seeding the dishes at 1 x 10^4 ml^{-1}, 1 x 10^5 ml^{-1} or 5 x 10^5 ml^{-1} in complete RPMI-1640 medium, in 96-well, 24-well and 60 mm^2 plates, respectively. Cells were swirled gently to allow for cell-to-cell contact, and incubated undisturbed at 37°C in a humidified atmosphere of 5% CO_2. After 2-3 days in culture, emerging spheroids were observed using stereo microscopy. In 60 mm^2 plates, spheroids of varying sizes were formed and were isolated from single cells by sedimentation rate in a 10 ml pipette. Perpendicular diameters were measured using a Nikon inverted microscope and image analysis system. Spheroid medium was replaced every 48 h, and following 2-6 days in culture, spheroids of approximately 100-200 µm in diameter were isolated by sedimantation rate in a 10 ml pipette. In 96- and 24-well plates, all suspended cells contibute to the formation of a single spheroid of equal diameter following 2-4 days in culture.

3.2.2.9.2 *rSFV virus particle infection of H358a spheroids*

To assess the ability of rSFV-EGFP particles to infect H358a spheroids, cells were plated in 1% (w/v) medium agar-precoated 60 mm^2 culture plates for 2 days to allow for spheroid formation, and then infected with rSFV-EGFP particles (~ moi 100), in a total volume of 1 ml infection medium, for 1 h. Infection medium alone was used as a control. Spheroids were then resuspended in complete RPMI-1640 medium and transferred back to the 60 mm^2 plates, and incubated at 37°C, in a humidified atmosphere of 5% CO_2. Following 18 h in culture, infected spheroids were analysed for EGFP expression by direct epifluorescence, on a fluorescent inverted microscope. To assess the ability of rSFV virus particles to inhibit initial H358a spheroid formation, cells were plated in 1% (w/v) medium agar-precoated 60 mm^2 culture plates, swirled to ensure cell-to-cell contact, and immediately infected with rSFV-EGFP virus (moi 100) for 1 h. Infection medium alone was used as a control. Spheroids were then resuspended in complete RPMI-1640 medium and incubated at 37°C, 5% CO_2. Following 24-48 h in culture, infected spheroids were analysed for spheroid formation and EGFP expression by direct epifluorescence at 488 nm.

3.2.2.9.3 *The effect of rSFV virus infection on H358a spheroid proliferation*

To determine the proliferation rate of H358a spheroids following infection, cells were plated at densities of 1 x 10^5 cells ml^{-1}, in 2% (w/v) polyHEME-precoated 24-well plates for 36 h, to allow for spheroid formation, and then infected with rSFV-EGFP virus particles (~ moi 100) in a total volume of 200 µl infection medium for 1 h. Spheroids were replenished with complete RPMI-1640 medium, and incubated as before. Infection medium was used as a control. At 24 h

intervals following infection, spheroids were then incubated with RPMI-1640 medium containing [methyl-^{3}H]thymidine (2 μCi/well in 200μl), for 24 h. Spheroids were washed twice in PBS under a stereo microscope, lysed in 500μl 1% (w/v) SDS, transferred to glass bijous and stored at -70°C. Samples were processed for scintillation counting as indicated in section 3.2.2.7.3. Spheroids were analysed daily over a period of 7 days, and each sample was performed and analysed in triplicate.

To further determine the effects of rSFV virus infection on the viability of H358a spheroids, the MTS assay was used (optimised in section 3.2.2.6.2). Cells were plated at a density of 1 x 10^4 ml^{-1} in 96-well plates (100 μl/well) for 36 h to allow for spheroid formation. Spheroids were infected with rSFV-EGFP virus (~ moi 100) for 1 h, in a total volume of 200 μl infection medium. Infection medium alone was used as a control. Spheroids were then returned to wells containing 100 μl complete RPMI-1640 medium, and incubated at 37°C in a humidified atmosphere of 5% CO_2. At 24 h intervals following infection, a 20 μl volume MTS reagent was added directly into culture wells and incubated at 37°C and 5% CO_2 for 4 h. MTS was also added to wells containing medium alone to correct for background absorbance. Following incubation, absorbance values were obtained using a Labsystems Multiscan plus 96-well ELISA reader, at 492 nm. Absorbance is directly related to spheroid viability. Spheroids were analysed daily over a period of 7 days, and each sample was performed and analysed in triplicate.

3.3 RESULTS

3.3.1 Growth and morphology of H358a cells.

The NCI-H358a cell line was found to proliferate rapidly in culture, reaching ~80% confluence in 2-3 days, depending on the seeding density (5×10^4-5×10^5 cells ml^{-1}). In all experiments, cells were used when 80-90% confluent rather than completely confluent (*Figure 3.1*).

3.3.2 Infectious SFV-4 virus induces *p53*-independent apoptotic cell death in the NSCLC cell line, NCI-H358a.

The NSCLC cell line H358a contains a homozygous deletion in the *p53* gene, previously shown to be a direct contributing factor in its malignancy (Takahashi *et al*, 1989). In a reproduction of studies performed by Glasgow *et al* (1997), it was determined whether lack of p53 expression in this tumour cell line would retard the SFV-induced apoptotic process, observed in non-malignant BHK-21 cells, in Chapter 2. As with Glasgow *et al* (1997), the infectious cDNA clone of SFV, SFV-4, was used to investigate SFV-induced *p53*-independent cell death. H358a cells were seeded into 75 cm^2 flasks and infected with infectious SFV-4 virus (moi 1) or with medium alone as a mock-infection control. Chromosomal DNA was extracted from treated cells at 24 h p.i. and analysed for fragmentation into 180-200bp oligonucleosomal fragments and their multiples, by agarose gel electrophoresis. The results are illustrated in Figure 3.2. SFV-4 virus mediated H358a chromosomal DNA fragmentation was observed at 48 h p.i. This correlates precisely with the onset of cpe in infected cultures, such as the rounding up of cells and formation of membrane blebs, when growing in culture (*not shown*).

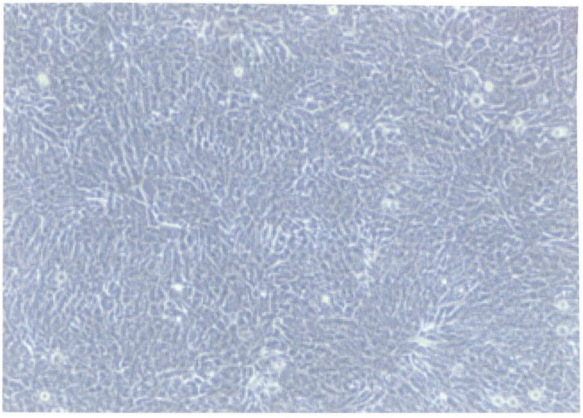


Figure 3.1- Growth and morphology of NCI-H358a cells.

Human non-small cell lung cancer cells NCI-H358a, were seeded at 1 x 10^4 cells/well in 6-well plates and incubated until confluent. Photographed at x 100 magnification.

DNA fragmentation continued to be observed within infected H358a cells at 72 h p.i. with the virus. The presence of cytopathology and chromosomal DNA fragmentation was not observed within mock-infected control H358a cells, at any of the indicated timepoints.

These results were confirmed by TUNEL staining. The TUNEL procedure labels 3'OH nicks within fragmented chromosomal DNA, commonly found within apoptotic nuclei. H358a cells were seeded onto glass coverslips in 6-well plates, grown until ~80% confluent, and infected with infectious SFV-4 virus (moi 1) or medium alone, as above. At 48 h p.i. (*Figure 3.3*), cells were fixed and labelled for DNA fragmentation with TdT and horse-radish peroxidase. Colorimetric detection was performed using DAB. At 48 h following infection with the virus (*Figure 3.3 A*), brown TUNEL-positive apoptotic H358a nuclei were detected in approximately 8-10% of the total cell population at any one time. These cells also displayed the morphological features characteristic of apoptotic cell death, including nuclear shrinkage or pyknosis, and formation of membrane blebs. The intensity of apoptosis appeared to increase marginally by 72 h p.i. with the virus (*not shown*). Following 72 h of incubation, the majority of SFV-4 virus-infected cells had lifted from the monolayer (*not shown*), and were thus, refractory to analysis. Mock-infected cells remained TUNEL-negative (*Figure 3.3 B*), and lacked the cytopathology observed within infected H358a cells.

Thus, infectious SFV-4 virus induces a *p53*-independent apoptotic pathway within the NSCLC cell line H358a, as indicated by the morphological characteristics of PCD and chromosomal DNA fragmentation, following infection with the virus.

Figure 3.2- **Infectious SFV-4 virus-mediated apoptosis in H358a cells, as assessed by chromosomal DNA fragmentation, using agarose gel electrophoresis.** H358a cells were incubated at densities of 1 x 10^6 cells in 75 cm^2 flasks, and infected with SFV-4 virus (moi 1) or medium alone as a control. At 24 h intervals following infection, cells were lysed and DNA was released by enzymatic digestion. Cellular DNA for SFV-4- and mock-infected cells was analysed for fragmentation into oligonucleosomal-sized fragments, indicative of cell death, by agarose gel electrophoresis. *Lanes 1, 3 and 5;* DNA from SFV-4 virus-infected H358a cells at 24, 48 and 72 h p.i., respectively. *Lanes 2, 4, and 6*; DNA from mock-infected control H358a cells at 24, 48 and 72 h p.i., respectively. *Lane 7;* λ (*Hind 111*) DNA molecular weight markers. Prominent DNA fragmentation is detectable at 48 and 72 h p.i. with the SFV-4 virus.

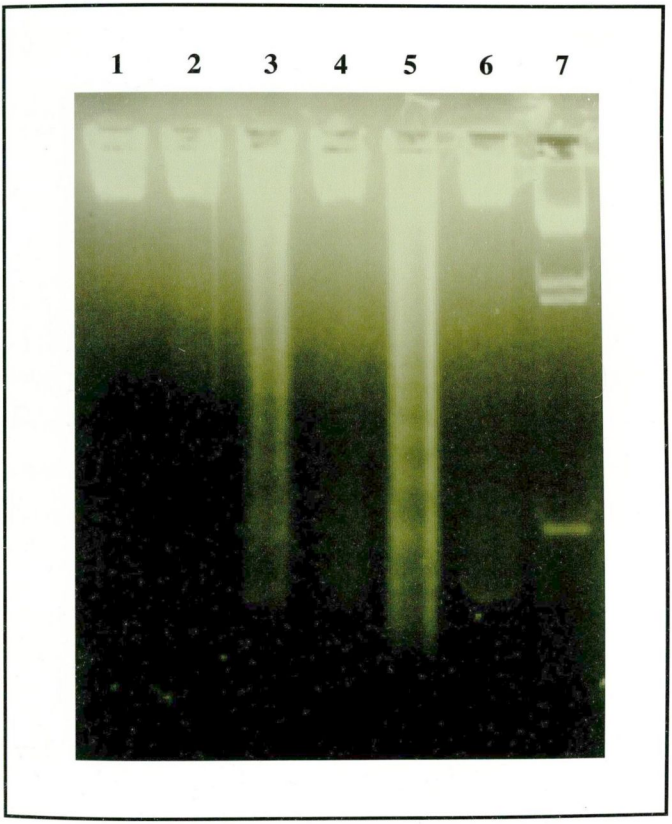


Figure 3.2- **Infectious SFV-4 virus mediated apoptosis in H358a cells, as Assessed by chromosomal DNA fragmentation, using agarose gel electrophoresis.**

Figure 3.3- **SFV-4 virus-mediated apoptosis in H358a cells, as assessed by chromosomal DNA fragmentation, using TUNEL.** H358a cells were grown on glass coverslips in 6-well plates until ~80% confluent, and infected with SFV-4 virus (moi 1) or medium alone as a mock-infection control. At 48 h p.i., cell monolayers were formalin-fixed, and fragmented chromosomal DNA labelled with TdT and horse-radish peroxidase. Colorimetric detection was performed using DAB. Normal cells were counterstained with methyl green. *A*; H358a cells, 48 h following infection with the SFV-4 virus. *B*; Mock-infected H358a cells. Note brown, $TUNEL^{+}$ peroxidase staining within apoptotic nuclei (*arrows*). Photographed at x 100 magnification.

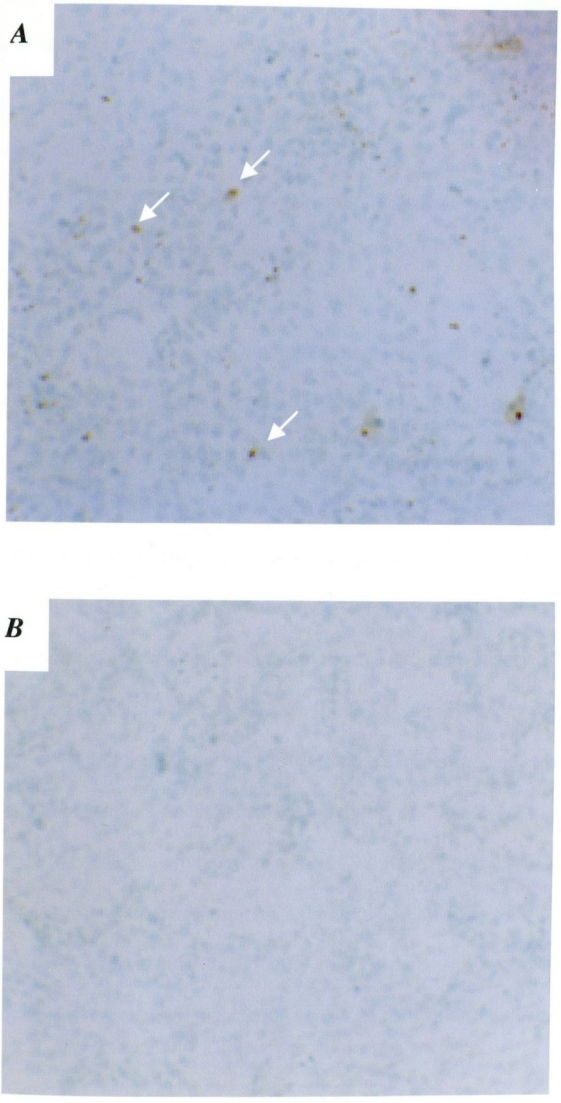


Figure 3.3- SFV-4 virus-mediated apoptosis in H358a cells, as assessed by chromosomal DNA fragmentation, using TUNEL.

3.3.3 Transfection with recombinant SFV RNA molecules induces apoptosis in the NSCLC cell line, NCI-H358a.

Earlier studies on the cytopathogenicity of SFV for infected cells implicated the non-structural region of the SFV genome (Chapter 2, Glasgow *et al*, 1998) as an important mediator of SFV-induced apoptosis. Infectious SFV-4 virus has been shown to induce programmed cell death in H358a cells by a *p53*-independent pathway. To determine whether *p53*-independent apoptosis can occur in the absence of SFV structural proteins, H358a cells were transfected with *in vitro*-transcribed SFV vector RNA, derived from transcription of the recombinant SFV plasmid pSFV-EGFP. The SFV constructs chosen, contained the reporter gene *EGFP* in place of the viral structural proteins, to facilitate detection of the vector within transfected cells. H358a cells were grown in 75 cm^2 flasks until ~80% confluent, trypsinised and electroporated with *in vitro*-transcribed RNA from the linearised pSFV-EGFP plasmid, or PBS alone, as a mock-transfection control, and incubated for the indicated timepoints. Reporter gene expression, indicative of SFV RNA transfection was detected at 18 h p.e. Figure 3.4 *A* illustrates an example of H358a cells, transfected with SFV-EGFP RNA. The SFV-EGFP RNA construct successfully transfected the NSCLC cell line, with transfection efficiencies usually approaching 60-70% (*data not shown*). Similar transfection efficiencies were obtained using the *LacZ*-expressing SFV construct (*not shown*), whereas cells transfected with PBS alone were negative for both reporter genes (*not shown*).

At 48 h p.e., transfected cells were assessed for possible apoptosis induction by DNA fragmentation analysis *in situ*. TUNEL staining of transfected H358a cells revealed brown, TUNEL-positive apoptotic cells, 2 days following transfection with SFV-EGFP (*Figure 3.4 B*) RNA. Apoptotic cell death following SFV-LacZ RNA transfection was also observed at similar levels to SFV-EGFP RNA (*not*

Figure 3.4- **Transfection with recombinant SFV RNA induces apoptotic cell death in the H358a cell line.** H358a cells were grown until ~80% confluent, trypsinised and electroporated with RNA *in vitro*-transcribed from the recombinant plasmid pSFV-EGFP, or PBS alone as a control. Cells were placed onto glass coverslips in 6-well plates and analysed at indicated timepoints. *A*; Cells were assessed for reporter gene expression at 18 h p.e. EGFP expression was determined by direct epifluorescence of paraformaldehyde-fixed cells. *B*; Transfected cells were assessed for apoptosis induction, at 48 h p.e. Cells were formalin-fixed and labelled with TdT enzyme and horse-radish peroxidase. Colorimetric detection was performed using DAB. Normal cells were counterstained with methyl green. Note brown, $TUNEL^{+}$ peroxidase staining within apoptotic nuclei (*arrows*), following transfection with SFV RNA. Photographed at x 400 magnification.

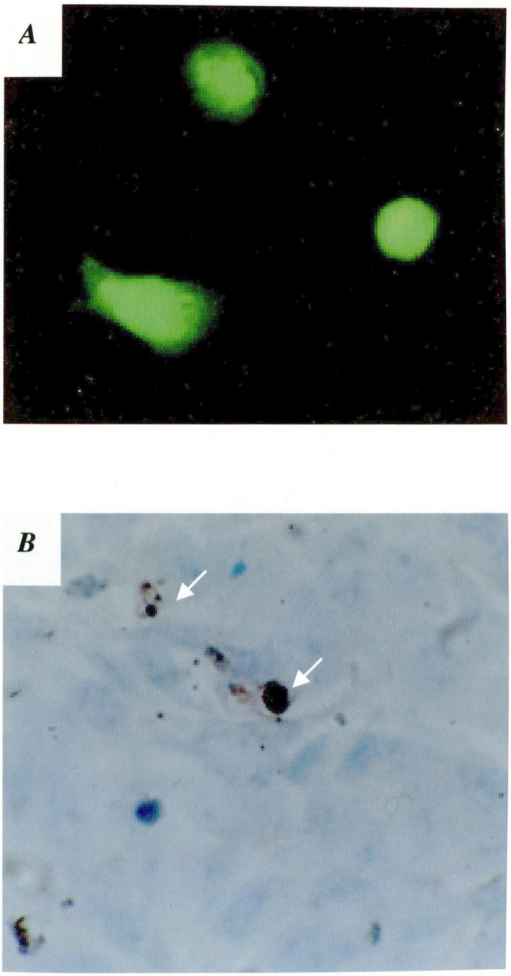


Figure 3.4- Transfection with recombinant SFV RNA induces apoptotic cell death in the H358a cell line.

Figure 3.5- **The SFV vector backbone, and not reporter gene expression, mediates H358a apoptotic cell death.** H358a cells were incubated until ~80% confluent, trypsinised and electroporated with RNA *in vitro*-transcribed from the linearised pSFV-1 plasmid, or medium alone as a control. This recombinant SFV plasmid contains the non-structural SFV genes only, and does not contain a reporter gene. At 24 h intervals following electroporation of RNA, cells were lysed and DNA was released by enzymatic digestion. Cellular DNA from SFV-1 RNA- and PBS-transfected cells were analysed for fragmentation, by agarose gel electrophoresis. *Lane 1*; λ (*Hind 111*) DNA molecular weight marker. *Lanes 2 and 4*; DNA from SFV-1 RNA-transfected H358a cells, at 24 and 28 h p.e., respectively. *Lanes 3 and 5*; DNA from mock-transfected H358a control cells, at 24 and 48 h p.e., respectively. DNA fragmentation is evident at 48h p.e. with SFV-1 RNA.

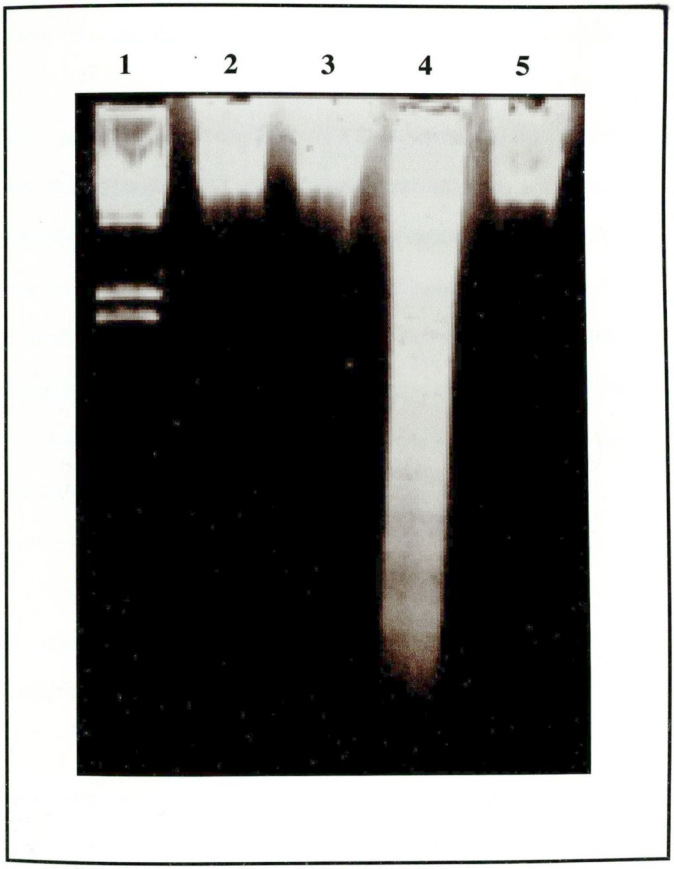


Figure 3.5- The SFV vector backbone, and not reporter gene expression, mediates H358a apoptotic cell death.

shown). The quantity of apoptotic cells per field was however, marginally lower than that with direct infection with infectious SFV-4 virus (*see figure 3.3*).

Finally, transfection with recombinant SFV RNA, transcribed from the linearised 'empty' recombinant pSFV-1 plasmid, also induced apoptosis, as illustrated by chromosomal DNA fragmentation by agarose gel electrophoresis at 48 h p.e. (*Figure 3.5*). This indicated clearly that apoptosis induction, detected in H358a cells transfected with either SFV-LacZ and SFV-EGFP RNAs, could not be attributed to reporter gene expression. The cytotoxic effects of the SFV vector in the *p53*-deleted H358a cell line was instead, directly attributed to a function within the SFV virus vector backbone.

3.3.4 Infection efficiency of rSFV virus vector particles in the NSCLC cell line, H358a.

The *p53*-independent pro-apoptotic properties of encapsidated, recombinant SFV particles in H358a cells *in vitro* were subsequently investigated. As with BHK-21 cells, the conditions for optimal rSFV virus particle infection of the H358a cell line was determined using rSFV-EGFP virus particles. H358a cells were seeded in duplicate, into 6-well plates at a density of 1 x 10^4 cells/well and infected with increasing concentrations (moi) of rSFV-EGFP virus particles in infection medium. Following overnight incubation, cells were fixed and examined for EGFP expression. Results are presented in Figure 3.6. A linear relationship existed between the number of infected cells and the moi of virus used up to moi 100, in which 35% of the total H358a cell population were infected with the vector. At moi 400, almost 50% of the cells were positive for the vector and this could be increased marginally using multiple infections (*not shown*). This is in

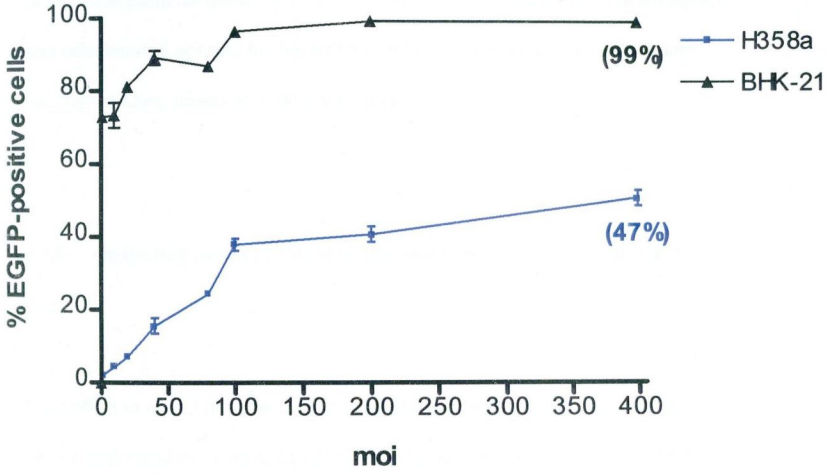


Figure 3.6- Infection efficiency of rSFV-EGFP virus particles in H358a cells in comparison to BHK-21 cells. H358a (■) and BHK-21 (▲) cells were seeded onto glass coverslips in 6-well plates at densities of 1 x 10^4 cells/well, and infected, in duplicate, with increasing concentrations (moi = 1, 10, 20, 40, 80, 100, 200 and 400) of rSFV-EGFP virus particles (1 x 10^8 I.U./ml), or medium alone as control, (moi=0), for 1 h. At 18 h p.i., cells were fixed, stained with DAPI for 20 min, and analysed for EGFP expression by fluorescent microscopy, at 488 nm (EGFP) and 350 nm (DAPI). EGFP-expressing cells were scored, and calculated as a percentage of the number of DAPI-stained cells in each field. Percentage infection efficiencies for both cell lines are indicated in parentheses. *Points*; means, *bars*; SD, and is representative of two independent experiments.

contrast to much higher rSFV virus infection efficiencies in standard BHK-21 cells, with up to 75% of cells infected with the vector at moi 1 (*see Chapter 2*). Infection efficiencies of *LacZ*-expressing particles were identical to that of rSFV-EGFP virus particles (*data not shown*). Thus, rSFV virus infection at moi 100-400 was calculated as optimal for the NSCLC cells, and was used in all subsequent infection studies, unless otherwise indicated.

3.3.5 Optimisation of cellular viability analyses for the H358a cell line *in vitro*.

In an effort to assess the effects of rSFV particle infection on H358a tumour cell growth and viability *in vitro*, an additional two new methods of analysis were developed and optimised for the H358a cell line. The dye sulphorhodamine B (SRB), binds to protein basic amino acid residues on adherent cells under mildly acidic conditions, to provide a sensitive index of cellular content and thus, survival. The dye, which displays a bright pink fluorescence, can be measured colorimetrically using an ELISA reader, and is considered to be directly related to total cell viability. The assay was optimised using increasing numbers of H358a cells, seeded in triplicate into 6-well plates. Cells were fixed with trichloroacetic acid (TCA), stained with SRB and the absorbance values were determined and correlated with the initial cell inoculum. As illustrated in Figure 3.7, SRB absorbance was found to be directly proportional to the initial number of H358a cells in culture, up to a cell number of 7×10^5, where the linear relationship ceased. Thus, for the SRB viability assay, H358a cells were initially seeded at densities of between 1×10^4 and 5×10^5 cells per well, unless otherwise indicated.

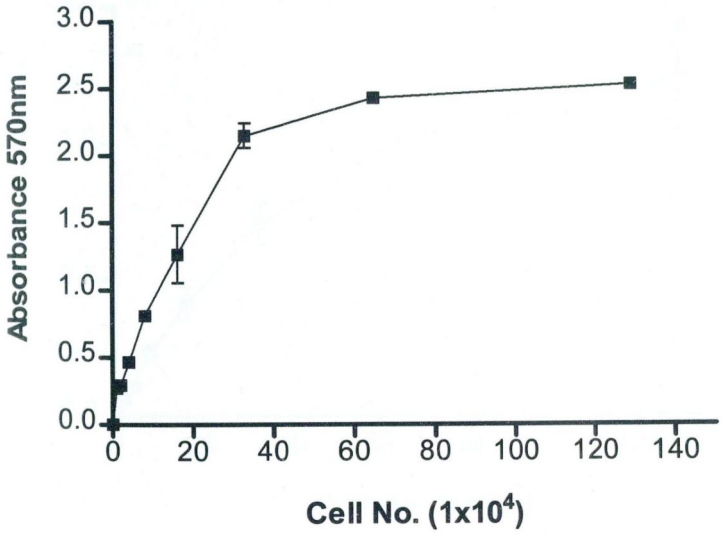


Figure 3.7- Optimisation of sulphorhodamine B (SRB) colorimetric analysis for the H358a cell line *in vitro*. Various numbers of H358a cells (1, 2.5, 5, 10, 20, 35, 70, 130 x 10^4), in normal medium, were seeded in triplicate, into 6-well plates and allowed to equilibrate. Cells were fixed in 5% TCA and air-dried before staining with 0.4% (w/v) SRB. The cells were rinsed and the bound dye solubilised and measured colorimetrically at 570 nm, using an ELISA reader. Background absorbance was measured in wells incubated with growth medium without cells. Cell viability was directly proportional to the number of viable H358a cells in culture. *Points*; means, *bars*; SD for a single experiment.

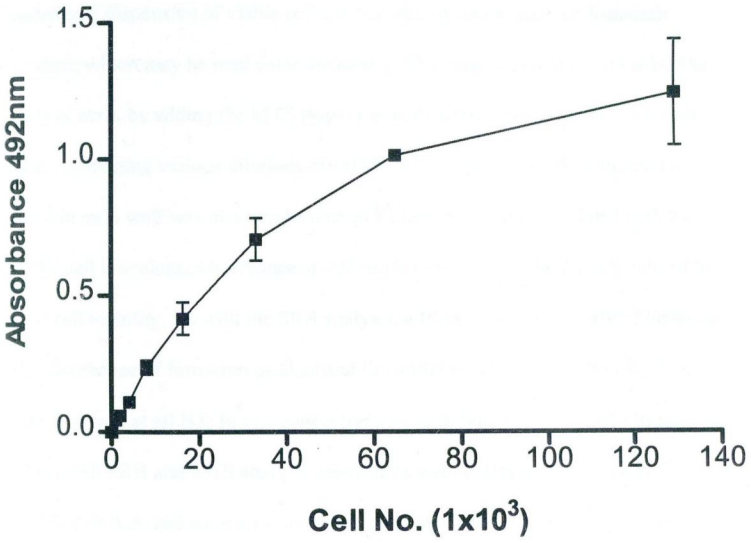


Figure 3.8- Optimisation of Cell Titre® AQ_{ueous} One Solution cell proliferation (MTS) assay for the H358a cell line. Various numbers of H358a cells (1, 2.5, 5, 10, 20, 35, 70, 130 x 10^4), in normal medium, were seeded into triplicate wells of 96-well plates and allowed to equilibrate. A 10% volume of MTS reagent was added to the cell medium and incubated at 37°C, 5% CO_2 for 4 h. MTS was bioreduced by viable cells, into a coloured formazan product, which was measured colorimetrically at 492 nm, using an ELISA reader. Background absorbance was measured in wells incubated with growth medium without cells. H358a cell viability was directly proportional to the quantity of bioreduced formazan. *Points*; means, *bars*; SD for a single experiment, and is representative of three independent experiments.

A second cell viability assay, the Cell Titre® AQ_{ueous} One Solution Cell Proliferation (MTS) assay, was also used for analysis of H358a cell viability. This one solution assay contains a novel tetrazolium compound, MTS, which when added to a suspension of viable cells, is bioreduced into a coloured formazan product, which may be read colorimetrically. The assay was optimised for H358a cells *in vitro*, by adding the MTS reagent directly to triplicate wells of a 96-well plate, containing various dilutions of H358a cells (*Figure 3.8*). Bioreduction of MTS in each well was measured using an ELISA reader and correlated with the initial cell inoculum. Absorbance at 492 nm is considered to be directly related to total cell viability. As with the SRB analysis, a linear relationship existed between the absorbance of formazan product and the initial number of H358a cells. This was observed at all H358a cell concentrations, with no detectable upper limit. Thus, both SRB and MTS analysis procedures were optimised specifically for the H358a cell line, and were now amenable for downstream viability experiments.

3.3.6 Growth and viability of H358a cells following infection with rSFV-EGFP virus particles.

We have shown that infection with replication competent SFV-4 infectious virus, and transfection with recombinant SFV RNA molecules resulted in apoptosis induction in the H358a tumour cell line *in vitro*. We next examined whether this cytotoxicity could be reproduced in the tumour cells following direct infection with recombinant SFV particles. Having established optimal infection efficiencies, H358a cells were seeded into 6-well plates and infected with rSFV-EGFP (moi 100) or rSFV-1 (moi ~100) particles. rSFV-1 virus particles lack a reporter gene and contain the vector backbone only. rSFV-1 particles were used as a vector control to ensure that the effects on H358a cell growth were due to the

infection with the vector itself, and not as a consequence of reporter gene EGFP expression. Cells were also mock-infected with medium alone, as a negative control. Cell growth and viability of H358a cells were estimated by trypan blue exclusion (*Figure 3.9*), SRB colorimetric analysis (*Figure 3.10*) and methyl-^{3}H thymidine incorporation (*Figure 3.11*), daily, for 7 days p.i.
H358a cell survival was detected using trypan blue exclusion criteria. Results are illustrated in Figure 3.9. rSFV-EGFP virus-infected cells were shown to be drastically reduced in number, with less than 50% survival after one day, and less than 10% after one week. Tumour cell growth was similarly inhibited upon infection with rSFV-1 (Day 7, $P<0.01$).

The cytotoxic effects of rSFV virus particles on H358a cell viability were confirmed by SRB colorimetric analysis (*Figure 3.10*). As early as 24 h p.i. with both rSFV-EGFP and rSFV-1 particles, H358a cell viability was reduced by 50%, and remained at negligible levels following one week of infection (Day 7, $P<0.01$).

Finally, cellular proliferation was assessed by measurement of methyl-^{3}H thymidine incorporation (*Figure 3.11*). By day 3 p.i., cells infected with rSFV-EGFP virus showed less than 10% the viability of mock-infected controls.

In comparison to rSFV-EGFP virus particles, infection with rSFV-1 virus resulted in slightly higher levels of H358a cell survival (Day 3, $P<0.05$), particularly when viability was assessed by ^{3}H thymidine incorporation (*Figure 3.11*). This can be attributed to the fact that titres of these 'empty' particles are obtained indirectly, by comparison to rSFV-EGFP particles, which were produced in parallel with rSFV-1 virus particle batches. The use of multiple infections of rSFV-EGFP virus on days 0, 1 and 2, failed to accentuate the vector's inhibitory effects beyond that

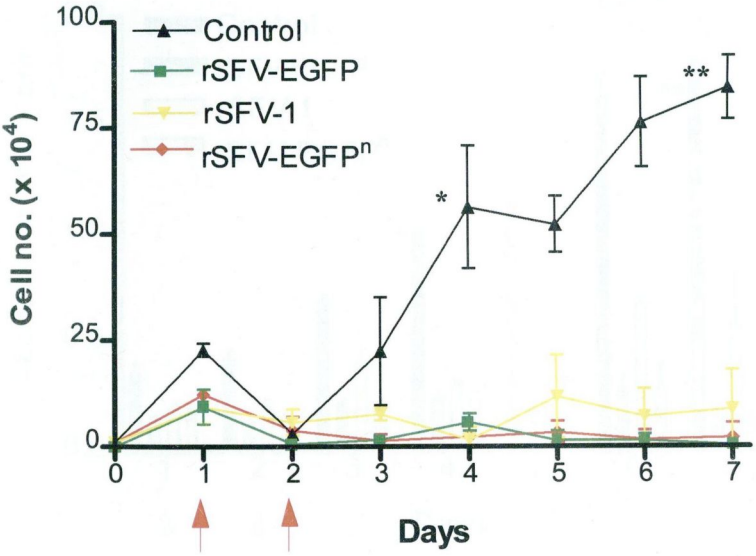


Figure 3.9- Cell viability of H358a cells following infection with rSFV virus particles, as determined by trypan blue exclusion. H358a cells were incubated at densities of $1x10^4$ cells/well in 6-well plates, and infected at day 0, with rSFV-EGFP virus (moi 100), rSFV-1 virus (~moi 100) or medium alone as a control. Red arrows indicate any other subsequent infections. At each indicated time-point p.i., triplicate wells were trypsinsied and counted by trypan blue exclusion criteria. *n*; three infections, *points*; means, *bars*; SD for a single experiment, and is representative of four independent experiments.

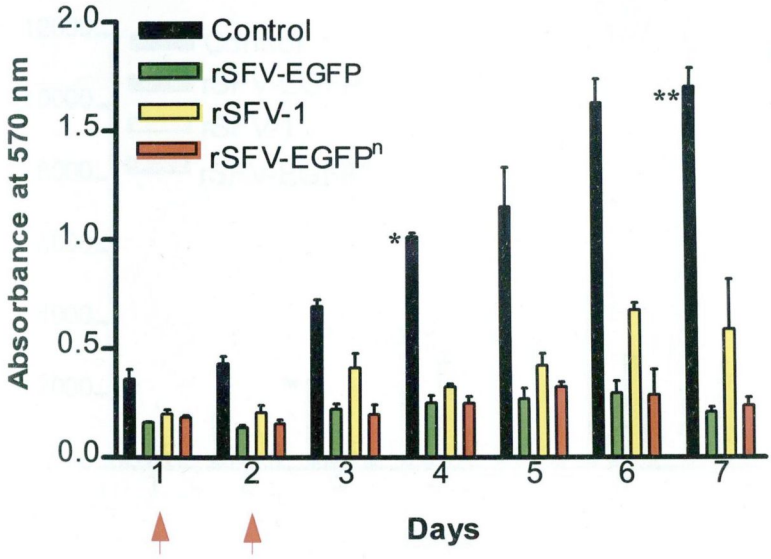


Figure 3.10- Cell viability of H358a cells following infection with rSFV virus particles, as determined by sulphorhodamine B colorimetric analysis. H358a cells were incubated at densities of $1x10^4$ cells/well in 6-well plates, and infected at day 0, with rSFV-EGFP virus (moi 100), rSFV-1 virus (~moi 100) or medium alone as a control. Red arrows indicate any other subsequent infections. At each indicated time-point p.i., cells from triplicate wells were fixed in TCA, stained with sulphorhodamine B, and the surviving cells measured colorimetrically using an ELISA reader, at 570 nm. *N;* three infections, *Points*; means, *bars*; SD for a single experiment, and is representative of four independent experiments.

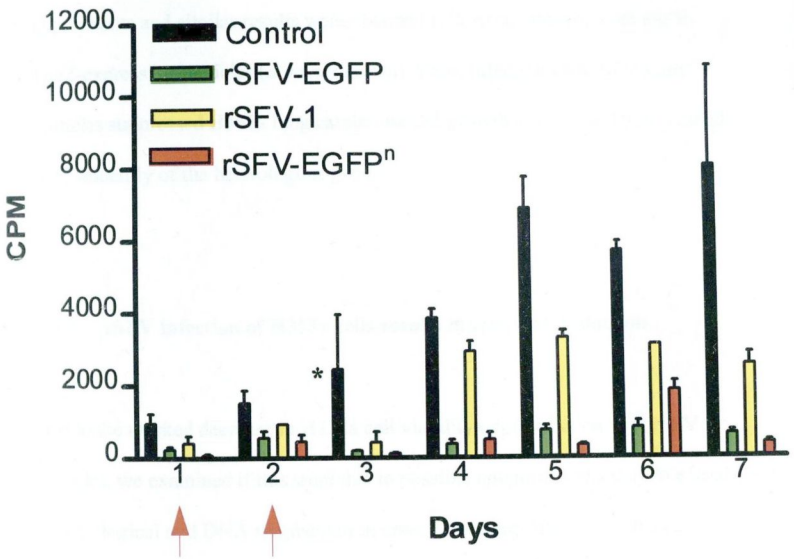


Figure 3.11- Cell viability of H358a cells following infection with rSFV virus particles, as determined by ^{3}H thymidine incorporation. H358a cells were incubated at densities of $1x10^{4}$ cells/well in 6-well plates, and infected at day 0, with rSFV-EGFP virus (moi 100), rSFV-1 virus (~moi 100) or medium alone as a control. Red arrows indicate any other subsequent infections. At each indicated time-point p.i., medium from triplicate wells was replaced with medium containing methyl-^{3}H thymidine. Following 24 h incubation, cells were removed, and ^{3}H thymidine incorporation was measured by liquid scintillation counting. Results are presented as counts per minute (cpm). *n;* three infections, *Points*; means, *bars*; SD for a single experiment, and is representative of four independent experiments.

of one infection alone. Multiple infections were not in fact necessary, as a single infection was sufficient to eliminate up to 90% of the tumour cells alone by 7 days. Values for all three assays were reproduced in at least 4 independent experiments and similar results were obtained following infection with rSFV-LacZ-expressing particles (*data not shown*). Thus, infection with rSFV virus particles suppressed H358a lung carcinoma cell growth *in vitro*, and this occured independently of the heterologous gene.

3.3.7 rSFV infection of H358a cells results in apoptosis induction.

Due to the marked decrease in H358a cell viability upon infection with rSFV particles, we examined if this were due to possible apoptosis induction. We used morphological and DNA fragmentation criteria for apoptotic cell death detection. H358a cells were grown until 80% confluent, and infected with rSFV-EGFP virus (moi 400) or medium alone as a control. rSFV-EGFP virus-mediated H358a cell death in culture was evident as early as 36 h p.i. H358a cells ceased division, rounded up and revealed the classical characteristics of apoptosis, including cell shrinkage and membrane blebbing, at 72 h p.i. (*Figure 3.12 B*). Mock-infected controls however, continued to grow and proliferate at normal rates (*Figure 3.12 A*), reaching confluence after 4 days. Analysis of rSFV-EGFP virus-infected H358a cells for reporter gene expression (*Figure 3.12 C*) indicated approximately 40% of cells positive for the vector, confirming that cell death was in fact due to infection with the vector.

Further analysis of rSFV-EGFP virus-infected H358a chromosomal DNA (*Figure 3.13*), revealed the appearance of 180-200bp DNA fragments and their multiples, formed by internucleosomal cleavage, by agarose gel electrophoresis. This was

Figure 3.12- **Cytopathic effect in H358a cell monolayers following infection with rSFV-EGFP virus particles.** H358a cells were seeded at densities of 1 x 10^4 cells/well, into 6-well plates, and grown until ~80% confluent. Cell monolayers were infected with rSFV-EGFP virus (moi 400) or medium alone as a mock-infection control, for 1 h and the medium replaced. Phase contrast micrographs of H358a cell monolayers, 3 days following infection with (*A*) medium alone, and (*B*) medium containing rSFV-EGFP virus particles. Note the lack of cell growth and cytopathic effects in rSFV-EGFP virus-infected cells (*B*), in comparison to control cells (*A*), which show normal growth with no morphological abnormalities. *C*; rSFV virus-infected cells were analysed for EGFP expression, by direct epifluorescence. H358a cells express the reporter gene with approximately 40% infection efficiency. Photographed at x 100 magnification.

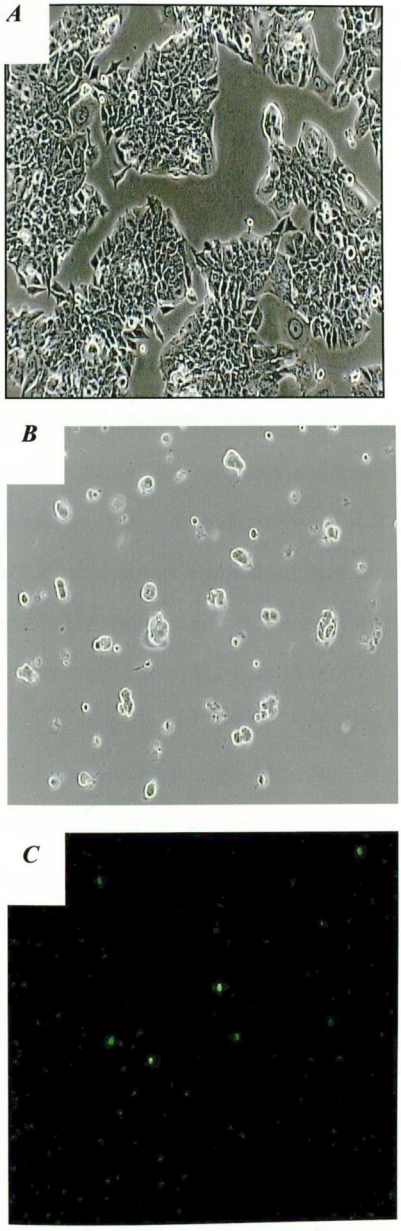


Figure 3.12- Cytopathic effect in H358a cell monolayers following infection with rSFV-EGFP virus particles.

demonstrated at 24 and 48 h p.i. with rSFV-EGFP particles, but not in DNA extracted from mock-infected controls. Chromosomal DNA fragmentation continued to be detected at later timepoints following rSFV virus infection (*not shown*).

These results were confirmed by TUNEL staining *in situ*, (*Figure 3.14*). For TUNEL analysis, H358a cells were grown on glass coverslips and infected with rSFV-EGFP particles or medium alone as above. Reporter gene EGFP expression was confirmed at 18 h p.i., as described previously (*not shown*). At 24 h intervals p.i., cells were formaldehyde-fixed, and individual nuclei labelled using TdT and horse-radish peroxidase. Colorimetric detection was performed using DAB. At 48 h p.i., rSFV-EGFP particles were observed to trigger apoptosis in the H358a cell line, as characterised by the appearance of nuclear shrinkage and brown peroxidase staining, indicative of oligonucleosomal DNA cleavage (*Figure 3.14.A*). By 72 h p.i., the number of $TUNEL^{+}$ cells marginally increased (*not shown*), and at all subsequent timepoints, the majority of rSFV-EGFP virus-infected cells had lifted from the monolayer and were thus, refractory to analysis. Detection of apoptosis in rSFV-EGFP virus-infected cells *in situ* correlated with the detection of oligonucleosomal fragmention detection by agarose gel electrophoresis (*Figure 3.13*). Mock-infected control cells failed to show these morphological changes or oligonucleosomal DNA fragmentation at any of the above timepoints (*Figure 3.14 B*).

To unequivocally illustrate that rSFV virus particle infection directly induces apoptosis induction in the H358a cell line, cells were grown on glass coverslips and infected as indicated above. At 24 h p.i., cells were fixed and stained with the DNA-specific fluorochrome DAPI, and mounted. Cells were analysed using fluorescent microscopy. Fragmented or condensed nuclei, observed using DAPI,

Figure 3.13- **rSFV virus particle-induced programmed cell death in H358a cells as assessed by chromosomal DNA fragmentation, using agarose gel electrophoresis.** H358a cells were incubated at densities of 1 x 10^6 cells/ml in 75 cm^2 flasks, and infected with rSFV-EGFP virus particles (moi 400) or medium alone as a mock-infection control. At 24 h intervals following infection, cells were lysed and DNA was released by enzymatic digestion. Cellular DNA form rSFV-EGFP virus- and mock-infected H358a cells was then analysed for DNA fragmentation into 180-200bp oligonucleosomal fragments and their multiples, by agarose gel electrophoresis. *Lane 1*; λ (*Hind111*) DNA molecular weight markers. *Lane 2*; DNA from mock-infected control H358a cells, at 48 h pi. *Lanes 3-4*; DNA from rSFV-EGFP virus-infected H358a cells, at 24 and 48 h p.i., respectively. Prominent DNA fragmentation was detected at 24 and 28 h p.i. with rSFV-EGFP virus particles.

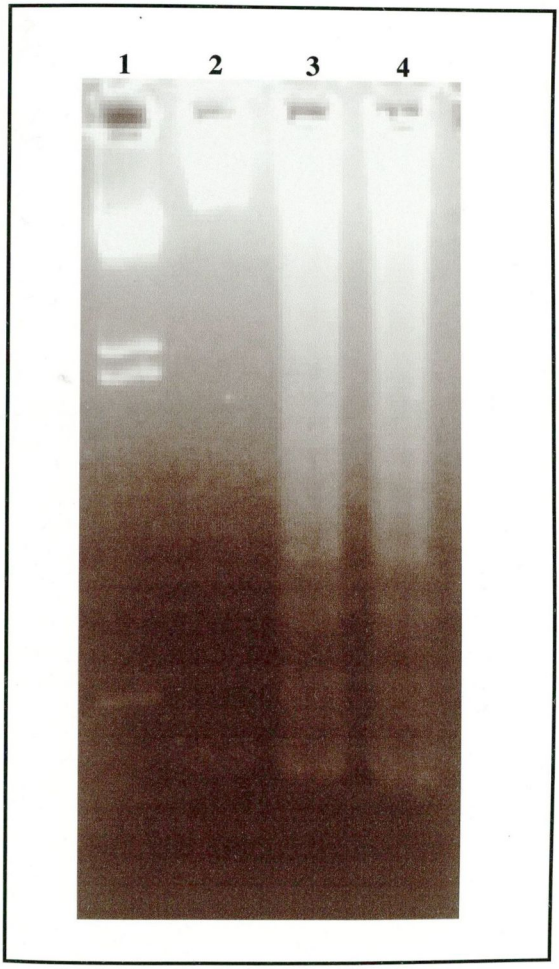


Figure 3.13- rSFV virus particle-induced programmed cell death in H358a cells, as assessed by chromosomal DNA fragmentation, using agarose gel electrophoresis.

Figure 3.14- **rSFV virus particle-induced programmed cell death in H358a cells, as assessed by chromosomal DNA fragmentation, using TUNEL.** H358a cells were grown on glass coverslips in 6-well plates until ~80% confluent, and infected with rSFV-EGFP virus (moi 400) or medium alone as a mock-infection control. At 48 h p.i., cell monolayers were fixed and fragmented chromosomal DNA labelled with TdT and horse-radish peroxidase. Colorimetric detection was performed using DAB. Normal cells were counterstained with methyl green. *A*; H358a cells, 48 h following infection with rSFV-EGFP virus particles. *B*; Mock-infected H358a cells. Note brown, $TUNEL^{+}$ peroxidase staining within apoptotic nuclei (*arrows*) in the rSFV-EGFP infected cell monolayer. Photographed at x 400 magnification.

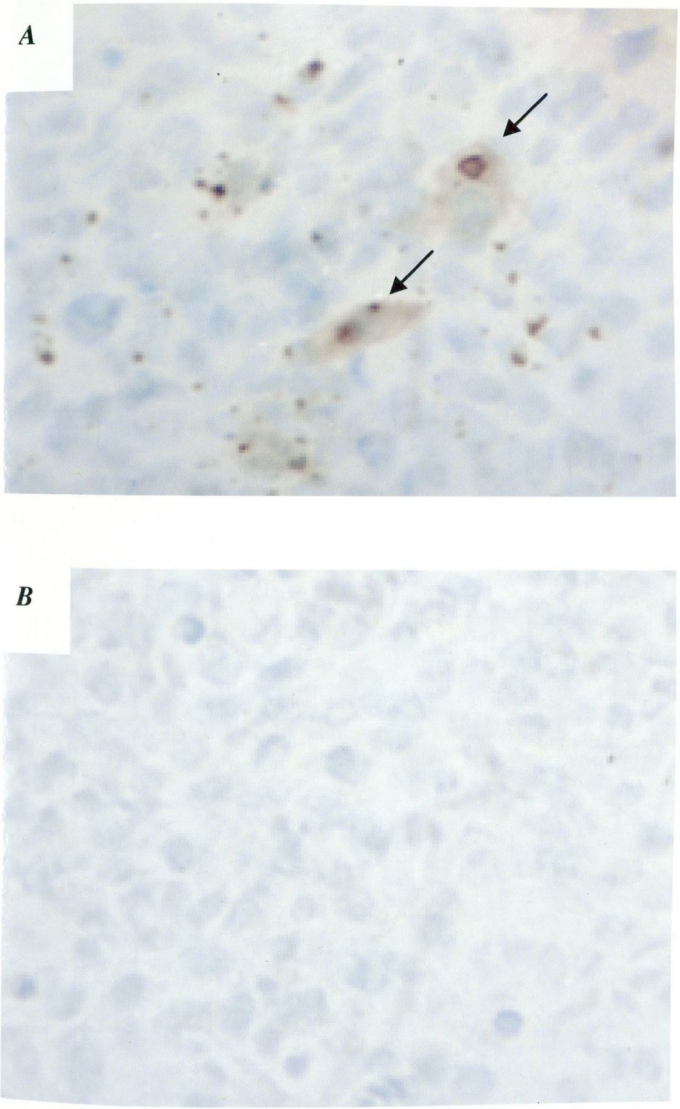


Figure 3.14- rSFV virus particle-induced programmed cell death in H358a cells, as assessed by chromosomal DNA fragmentation, using TUNEL.

Figure 3.15- **rSFV virus particle-induced programmed cell death in H358a cells, as assessed by morphological analysis, using DAPI.** H358a cells were incubated on glass coverslips in 6-well plates, and infected with rSFV-EGFP virus (moi 100), for 1 h. Following 24 h incubation, cells were fixed and stained with DAPI, a DNA-specific fluorochrome, for 20 min. Cells were analysed for EGFP reporter gene expression by direct epifluorescence at 488 nm (*A*), and for morphological features of apoptosis within infected nuclei, at 350 nm (*B*). Illustrated are single H358a cells, one of which (*arrow*), was infected with rSFV-EGFP virus and expresses the protein at 488 nm (*A*). When analysed with DAPI at 350 nm (*B*), the cell nucleus displays characteristic features of apoptotic cell death, including nuclear shrinkage and chromatin condensation, in comparison to round/oval nuclei within surrounding uninfected H358a cells. Photographed at x 400 magnification.

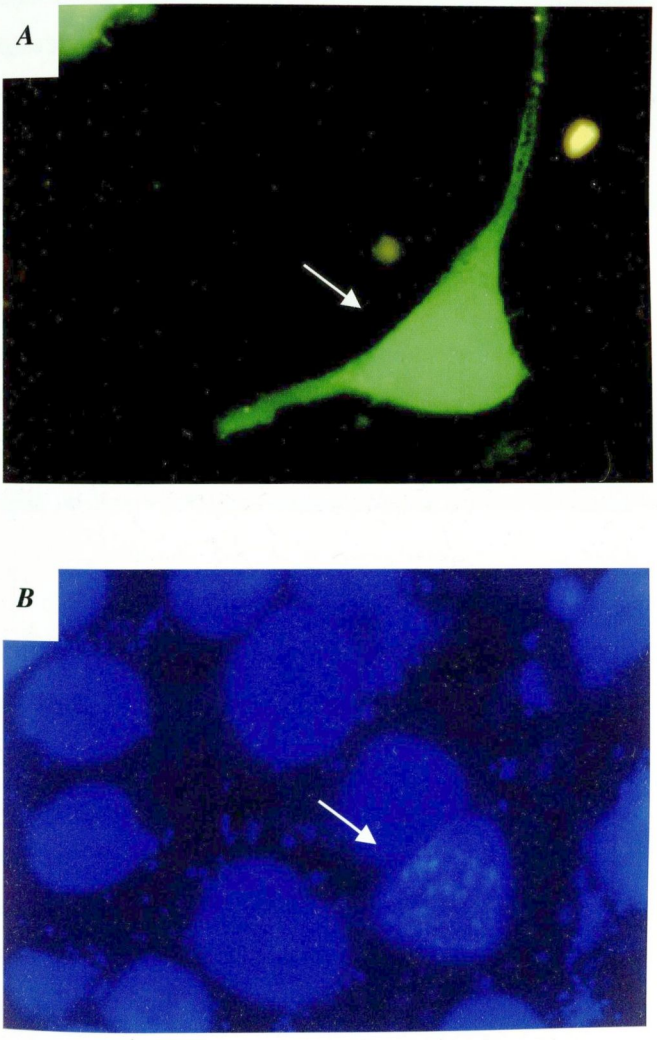


Figure 3.15- rSFV virus particle-induced programmed cell death in H358a cells, as assessed by morphological analysis, using DAPI.

were scored as apoptotic, whereas intact or mitotic nuclei were scored as normal. Figure 3.15 illustrates one such H358a cell, which was analysed for both rSFV-EGFP virus infection (*Figure 3.15 A*) and DNA fragmentation within the nucleus (*Figure 3.15 B*). Note the appearance of nuclear shrinkage and chromatin condensation in the rSFV-EGFP virus-infected cell compared to the surrounding cells, which remained uninfected, and failed to show these morphological changes within the nucleus.

Thus, one round of rSFV virus replication was sufficient to cause a marked decrease in human lung carcinoma cell growth, a phenomenon which can be directly attributed to rSFV virus-mediated *p53*-independent apoptosis induction.

3.3.8 Multicellular tumour spheroids can be prepared from H358a monolayer cultures and are infected with rSFV virus particles

As a prerequisite to *in vivo* analysis we next assessed the pro-apoptotic capabilities of rSFV virus on the H358a cell line growing as multicellular tumour spheroids (MTS), *in vitro*. MTS are composed of tumour cells growing in a 3-D structure, simulating the growth and microenvironmental conditions of solid tumours *in vivo* (Sutherland, 1988). Many tumour cell lines, particularly those derived from NSCLC, develop from monolayer cultures into 3-D spheroids *in vitro* (Fujiwara *et al*, 1994b). However, there is no well-documented or set procedure for the preparation of NSCLC spheroids. At least three independent methods were used in an attempt to initiate H358a spheroid growth from monolayer cultures, including growth on bacteriological plates (Freyer *et al*, 1980) and in spinner flasks (Sutherland *et al*, 1986) (*not shown*). Only one method, the liquid overlay technique, was successful. Spheroids were initiated

from 2-D H358a monolayer culture by seeding a defined number of suspended cells onto 60 mm^2 tissue culture plates, which were pre-coated with 1% medium agar. Cells were swirled gently to allow cell-to-cell contact and, inhibited from adhering to the base of the plate, adhere to one another to develop into a solid 3-D mass. Figure 3.16 illustrates a number of developing H358a spheroids prepared using this technique. Following 2 days in culture, these spheroidal aggregates had an average diameter of 100 µm, measured using an image analyser (*Figure 3.17 A*). Spheroid medium was changed every 2 days, and following 2 weeks in culture, proliferating spheroids appear to develop large necrotic centres, as in figure 3.17 *B*, simulating the situation in an underperfused solid tumour *in vivo*. Spheroids with diameters of between 100-200µm, were chosen as optimal for rSFV studies.

In an effort to assess the ability of rSFV virus particles to infect these 3-D H358a spheroids, those with an average diameter of 100-200 µm, were incubated in medium containing rSFV-EGFP particles (~10^8 I. U.), for 1 h and the medium replaced. Following 18 h incubation, individual MTS were selected under a stereo microscope and assessed for rSFV virus infection by reporter gene expression. EGFP was detected by direct epifluorescence using a fluorescent inverted microscope. Figure 3.18 illustrates clearly that rSFV particles could indeed infect individual cells within 3-D H358a spheroids. The majority of these spheroids contained cells at the periphery of the 3D mass which are positive for the vector, whereas in other spheroids, much larger areas were positive for rSFV virus infection. Thus, it may be possible that cells within the underlying layers of the spheroids are also infected, and that rSFV particles could penetrate the 3D mass. Successful rSFV virus infection of 3-D *in vitro* tumour masses was a positive indication that rSFV virus infection would also occur within solid tumours *in vivo*.

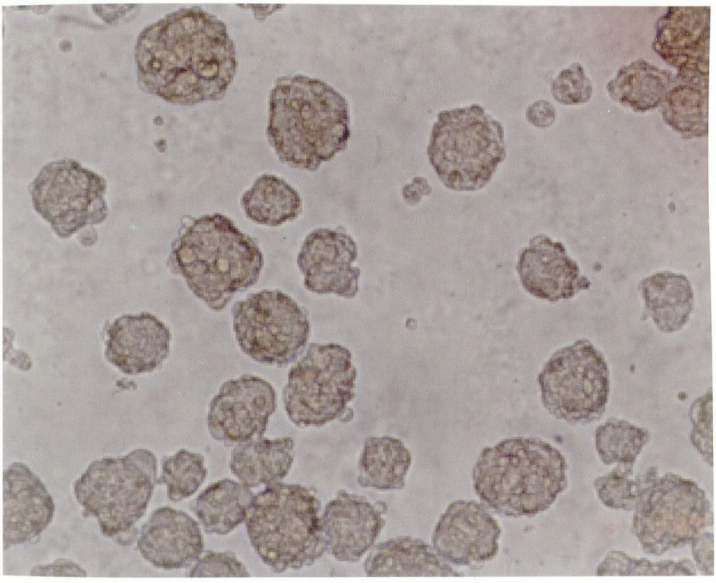
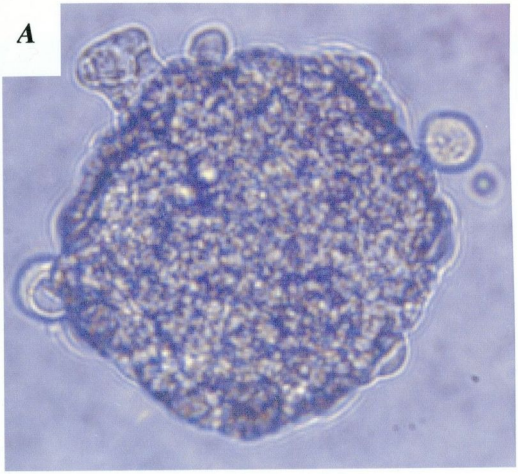


Figure 3.16- H358a cell monolayers develop into three-dimensional multicellular tumour spheroid masses. H358a cells (1 x 10^4) were seeded onto 60 mm^2 tissue culture plates, pre-coated with 1% medium agar. Cellular adhesion to the bottom of the tissue culture dish is prevented by the thin layer of agarose, forcing the cells to remain in suspension, forming solid, three-dimensional H358a spheroidal aggregates. Photographed at x 100 magnification.

Figure 3.17- Morphology of H358a spheroids *in vitro*. H358a cells (1×10^4) were seeded onto 60 mm^2 tissue culture plates, pre-coated with 1% medium agar to form *in vitro* multicellular tumour spheroids. Spheroid diameter was determined as a geometric mean of two orthogonal diameters, measured using an image analyser. *A*; H358a spheroid of ~100μm diameter, after 3 days in culture, before the development of central necrosis. Spheroids of this size were chosen as optimal for *in vitro* rSFV virus particle studies. *B*; H358a spheroid after 2 weeks in culture. Note the presence of a large necrotic centre, surrounded by a viable rim of cells, simulating the situation in an underperfused solid tumour *in vivo*. Photographed at x 200 magnification.



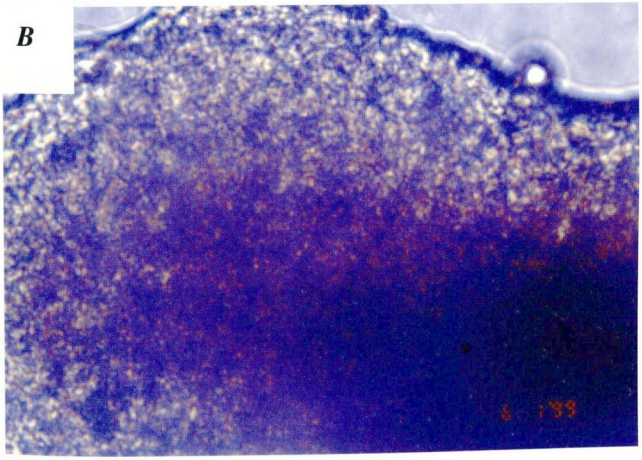


Figure 3.17- Morphology of H358a spheroids *in vitro*.

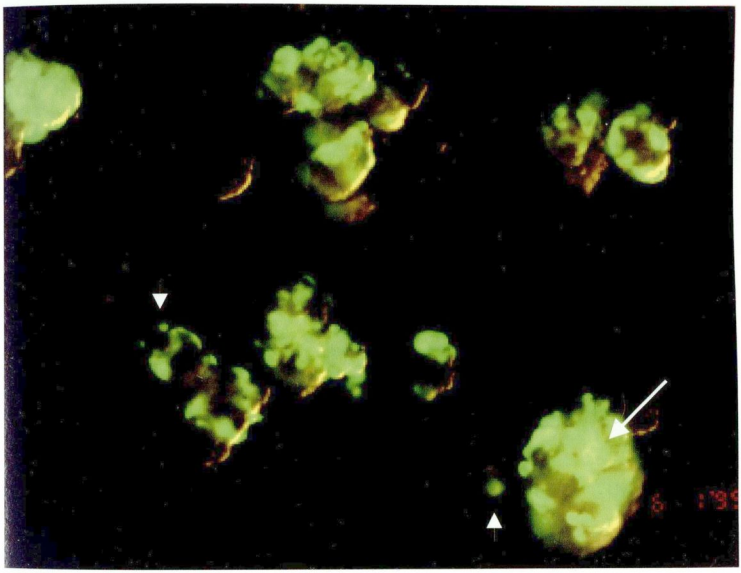


Figure 3.18- rSFV virus particles can infect H358a three-dimensional cultures. H358a spheroids with an average diameter of 50-200μm were placed in medium containing rSFV-EGFP (~ moi 400), for 1 h. Spheroids were analysed for EGFP expression at 18 h p.i., using an inverted fluorescent microscope, at 488 nm. H358a spheroids, with a number of rSFV-EGFP virus-infected cells at the periphery, are indicated by small arrows. Complete sections of a H358a spheroid, positive for infection with the vector, are indicated by large arrow. It is reasonable to assume that individual infected cells within the spheroid would be triggered to undergo apoptosis. Photographed at x 100 magnification.

3.3.9 rSFV virus particle infection inhibits proliferation of H358a MTS and also inhibits initial MTS formation from 2-D cell monolayers.

We next assessed the proliferation of H358a multicellular aggregates following infection with rSFV particles. The heterogeneity in size of individual H358a spheroids upon preparation however, made proliferation studies difficult. To assess inhibition of individual MTS, the aggregates were prepared in individual wells of 24- and 96-well plates prior to infection. Cellular proliferation within these aggregates was measured by tritiated thymidine incorporation and One Solution Cell Proliferation assays.

H358a cells (1×10^4), were seeded in triplicate, into individual wells of a 24-well plate, precoated with 2% polyHEMA. Medium agar interfered with tritiated thymidine measurements (S. Mann, *personal communication*). The plates were swirled gently to allow for cell-to-cell contact, allowing one spheroid to form in each well, with all suspended cells contributing to the formation of the spheroid. Using stereo microscopy, spheroids (200 μm diameter) were placed into wells containing rSFV-EGFP particles (~ moi 400) or medium alone as a mock-infection control. At 24 h intervals following infection, spheroids were pulse-labelled with ^{3}H thymidine for 24 h, harvested, and thymidine incorporation was measured, daily, for one week. Figure 3.19. illustrates these results. RSFV virus-mediated inhibition of spheroid growth was observed as early as 24 h p.i., and at 7 days following infection, mock-infected spheroids incorporated up to 10 times the amount of ^{3}H thymidine compared to those which had been infected with the vector ($P<0.01$).

rSFV virus particle-mediated inhibition of H358a spheroid proliferation was confirmed using a One Solution Cell Proliferation assay. This assay was

previously optimised for analysis of the H358a cell line in section 3.3.5. H358a cells (1×10^3) were seeded into polyHEMA-coated wells of a 96-well plate and infected as above. At 24 h intervals following infection, a 10% volume of MTS reagent was added to spheroid-containing medium, and incubated for 4 h. MTS contains a novel tetrazolium compound and electron-coupling reagent, and is bioreduced by viable cells, to a brown formazan product that can be measured colorimetrically at 492 nm. Figure 3.20 also clearly illustrates a rSFV-EGFP-mediated reduction in H358a spheroid proliferation. Spheroid proliferation was shown to be reduced as early as 24 h p.i., compared to mock-infected controls, and revealed up to a 70% reduction in viability at 6 days p.i. with the vector ($P<0.001$).

Both MTS and tritiated thymidine incorporation assays indicated a higher proliferation of H358a spheroids at 24 h p.i. for both control and infected spheroids. This was observed in at least 4 independent experiments and could be attributed to higher proliferation activities from individual H358a cells, which have not yet joined the compact 3-D spheroidal cluster. At later timepoints, fully compact 3-D spheroids have formed, with a much-reduced viability than that of day 1 p.i.

Finally, we assessed the ability of rSFV virus particles to inhibit initial spheroid formation. H358a cells were seeded onto polyHEMA-coated wells at densities of 1×10^4 cells/well and immediately infected with rSFV-EGFP virus or medium alone. At 48 h after infection, control wells formed highly cohesive spheroids, with essentially all suspended cells contributing to the single spheroid (*Figure 3.21 A*). This compaction increased with time. In marked contrast, rSFV virus-infected cells failed to initiate spheroids at 48 h p.i. (*Figure 3.21 B*), and at all other analysed timepoints (*not shown*). Any loose aggregates which did form in rSFV virus-infected wells, were easily disrupted by mechanical pipetting. As

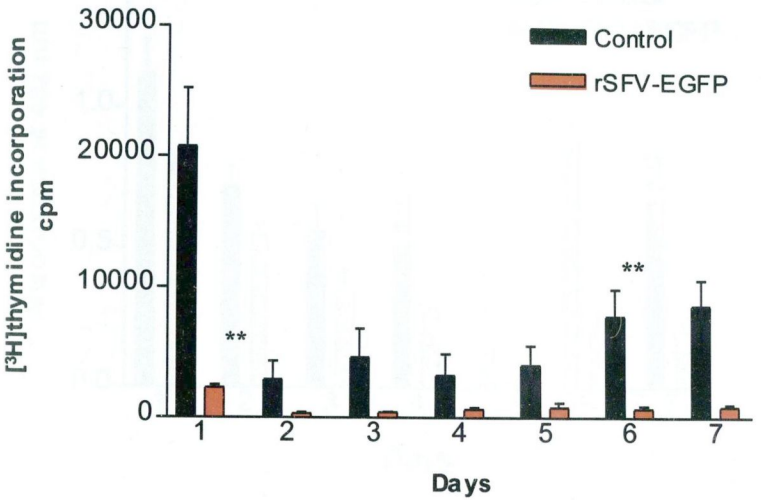


Figure 3.19- Proliferation of H358a spheroids following infection with rSFV-EGFP virus particles, as assessed by ^{3}H thymidine incorporation. H358a cells were seeded onto polyHEMA-coated 24-well plates at densities of 1 x 10^{4} cells/well, and spheroids were allowed to initiate. At 48 h post-plating, emerging spheroids were infected with rSFV-EGFP virus (~moi 400) or medium alone, as a mock-infection control. Spheroids were washed in PBS, vigorously lysed by mechanical pipeting in 1% SDS solution, and harvested onto filter mats. [^{3}H] thymidine incorporation was measured by liquid scintillation counting. *Column*; means of six replicates, *bars*; SD, for a single experiment, and is representative of four independent experiments.

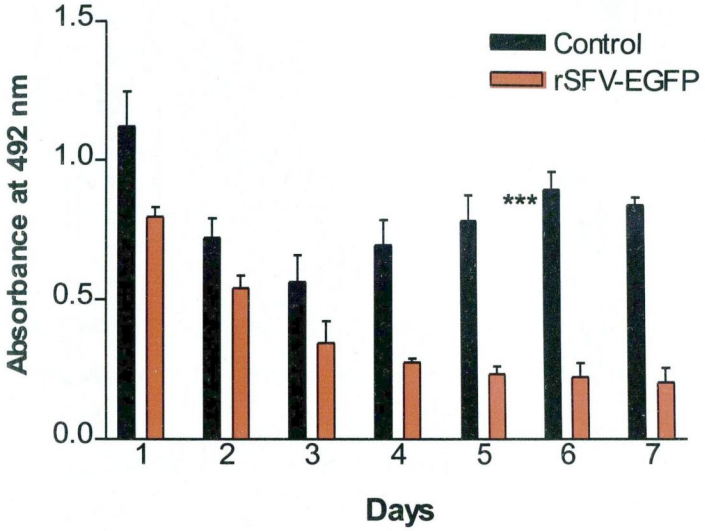


Figure 3.20- Proliferation of H358a spheroids following infection with rSFV-EGFP virus particles, as assessed by the AQ_{ueous} One Solution Cell Proliferation assay. H358a cells were seeded onto polyHEMA-coated 96-well plates at densities of 1 x 10^3 cells/well, and spheroids were allowed to initiate. At 48 h after plating, emerging spheroids were infected with rSFV-EGFP virus (~moi 400) or medium alone, as a mock-infection control. At 20µl aliquot of MTS reagent was added to medium in each well and incubated for 4 h. MTS is bioreduced into a brown formazan product, an indicator of cellular viability, which may be measured colorimetrically, at 492 nm. *Columns*; means of eight replicates, *bars*; SD, for a single experiment and is representative of three independent experiments.

Figure 3.21- **rSFV virus particle infection inhibits initial *in vitro* three-dimensional H358a spheroid formation.** H358a cells (1 x 10^4) were seeded onto 1% medium agar-coated 24-well plates. Cells were immediately mock-infected with medium alone (*A*), or with medium containing rSFV-EGFP virus particles (~moi 400) *(B-C)*. Cells were analysed for their ability to form compact three-dimensional H358a spheroidal aggregates. At 48 h post-plating, mock-infected H358a cells readily formed compact 3-D spheroids in each well (*A*), whereas those infected with rSFV-EGFP virus fail to form cohesive spheroids (*B*). The vast majority of these cells were also positive for infection with the vector (*C*), as observed by EGFP expression by direct epifluorescence. Photographed at x 100 magnification.

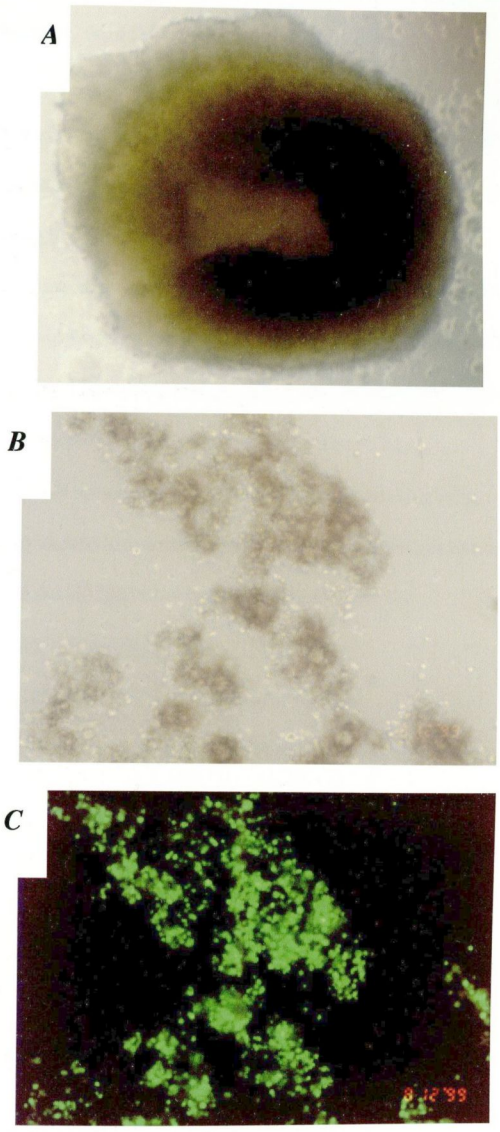


Figure 3.21- rSFV virus patricle infection inhibits *in vitro* three-dimensional H358a spheroid formation.

illustrated in figure 3.21 *C*, the vast majority of these cells were positive for EGFP expression, and therefore, were infected with the vector.

Thus, H358a cells readily formed solid 3-D tumour masses *in vitro*. These aggregates could be readily infected and penetrated by the rSFV virus vector, concomitantly leading to inhibition of 3-D spheroid development and proliferation, in comparison to mock-infected controls. rSFV particle also inhibited initial spheroid formation from 2-D H358a monolayer cultures. The inhibition of 3-D spheroid formation and growth, offers a favourable insight into the effects of rSFV particles on solid tumours *in vivo*. The ability of rSFV particles to penetrate 3-D tumour masses, and to infect surrounding cells, may provide the necessary capabilities to allow rSFV to infect, inhibit growth and induce apoptosis in solid H358a tumours *in vivo* (*see Chapter 4*).

3.4 DISCUSSION

Expression of the transcription factor p53 in normal cells is well documented to participate in the regulation of cell proliferation (Guo & Hay, 1999), genetic integrity (Lowndes & Murguia, 2000) and apoptosis induction following exposure to various stress stimuli (Symonds *et al*, 1994). Inactivation of the *p53* gene by missense mutation or deletion is the most common genetic alteration observed in human cancers (Hollstein *et al*, 1991 ; Levine *et al*, 1991). Following genotoxic insult, intracellular levels of p53 are elevated, inhibiting cell cycle progression at G_1 phase (Kastan *et al*, 1992), and thus, allowing time for DNA repair. If optimal repair is impossible, programmed cell death ensues. Whether the cell enters growth arrest or undergoes apoptosis, depends on the final integration of incoming signals with antagonistic effects on cell growth. Whereas wild-type *p53*-induced growth arrest is partially mediated by p21 inhibition of cyclin-Cdk complexes, necessary for S phase entry (Dulic *et al*, 1994) and a Rb/ E2F balance (Slebos *et al*, 1994), *p53*-dependent apoptosis involves the interplay of apoptosis-regulating genes, such as *Bcl-2* (Strasser *et al*, 1994) and *Bax*. Also, in terms of cancer treatment, it has been shown that chemotherapeutic (Lowe *et al*, 1993) and radiotherapeutic (Lee *et al*, 1993) responsiveness is largely affected by the *p53* status of affected cells, as the tumour-specific cytotoxicity of these agents has been attributed to their genotoxic effects on actively proliferating cells.

p53 is thus, a tumour suppressor gene, a rate-limiting step in malignant transformation and thus, an important determinant in the efficacy of many cancer treatment protocols. The transfer of wild-type *p53* to malignant cells to replace the defective gene, is therefore, an attractive therapetuic avenue for cancer gene therapy. Numerous *in vitro* studies have indicated growth inhibition, restoration of chemotherapy sensitivity and the induction of apoptosis upon wild-type *p53* transfer (Reviewed by Vile *et al*, 2000). In contrast, several previous studies have

demonstrated that not all forms of apoptosis requires p53 expression (Clarke *et al*, 1993). Strasser *et al*, (1994), showed that $p53^{-/-}$ lymphoid cells remained highly sensitive to ionising radiation and chemotherapeutic drugs, such as etoposide and cisplatin. Thus, cells that sustain sufficient damage may undergo apoptosis regardless of their *p53* status.

In chapter 2, the pro-apoptotic properties of the rSFV vector system were assessed using a standard, non-tumorigenic cell line, BHK-21. Apoptosis rapidly ensued following rSFV virus particle infection and occured in the absence of viral structural proteins. The inherent cytotoxictiy of rSFV particles thus, offers significant potential as a cytotoxic cancer gene therapy agent. In this assessment, the NCI-H358a cell line was utilised. This NSCLC cell line contains a homozygous *p53* deletion (Takahashi *et al*, 1989). The *p53* status of this cell line was further confirmed using preliminary blotting experiments (G. M. Glasgow, *personal communication*).

Initial studies, using infectious SFV-4 virus, indicated positive apoptosis induction in the H358a cell line, regardless of *p53* expression, a confirmation of a separate study by Glasgow *et al* (1998). As with BHK-21 apoptosis, the non-structural region of the virus was sufficient to mediate the pro-apoptotic effects, as transfection with recombinant SFV RNA induced a similar apoptotic phenotype. Cell death following RNA tranfection was less immediate and dramatic, than with infectious virus. This was primarily due to lower transfection efficiencies (~60%), as assessed by reporter gene expression, and the lack of replicative capacity within transfected H358a cells, when compared to infectious SFV-4 virus.

Despite rather low infection efficiencies, infection with recombinant, encapsidated SFV virus particles was shown to greatly inhibit the growth and proliferation of the *p53*-deleted cell line *in vitro*. Extensive rSFV virus-mediated cellular cytotoxicity, confirmed using trypan blue, sulphorhodamine B and ^{3}H thymidine incorporation analyses, indicated that inhibition of H358a cell growth

occured independently of the heterologous gene (*LacZ/EGFP*), as infection with 'empty' rSFV-1 virus particles mediated a similar effect. rSFV-1 particle inhibition was marginally lower than with rSFV-EGFP particles however. This was attributed to the fact that rSFV-1 particles could not be adequately titrated, as they lack a detectable reporter gene. rSFV-1 particle titres and therefore, the appropriate moi for H358a infection studies, were calculated indirectly, by preparing rSFV-1 particle batches in parallel to rSFV-EGFP. rSFV-1 titres may have therefore, been underestimated, resulting in lower cytotoxicity for H358a cell line *in vitro*.

All three viability studies included independent aspects of H358a cell viability. The higher ^{3}H thymidine counts from rSFV virus-infected H358a cells in comparison to low cell number assessed by trypan blue exclusion may be attributed to the fact that increases in DNA replication can be detected more rapidly than an increase in total cell number.

The extensive rSFV-EGFP virus-mediated inhibition of H358a cell growth was attributed to apoptosis induction. Infected H358a monlayers clearly revealed morphological alterations consistent with apoptosis induction, when assessed *in situ*, using TUNEL and DAPI-staining of infected nuclei. Chromatin condensation and fragmentataion were also demonstrated.

Up until now, apoptosis induction within the H358a cell line was mediated exclusively by restoration of wild-type *p53* function, using adenoviral (Fujiwara *et al*, 1994b), retroviral (Fujiwara *et al*, 1994a) and adeno-associated viral (Quazilbash *et al*, 1997) vectors. In the absence of *p53* however, these viral vectors remain non-cytopathic and facilitate gene delivery only. AAV-mediated wt-*p53* delivery resulted in a 50% reduction in H358a cell proliferation, as determined by trypan blue exclusion and SRB assays after 7 days, at which time it is reasonable to assume that surviving cells remain and the monolayer recovers. Adenoviral-mediated wt-*p53* expression alone, could not promote DNA

fragmentation in the H358a cell line without simultaneous exposure to the chemotherapeutic egent, cisplatin. Thus, whereas adenoviral and AAV vectors serve only to limit *in vitro* H358a tumour cell growth, rSFV infection reduced H358a proliferation to negligible values compared to controls, and induced programmed cell death, without exogenous wt-*p53* delivery, or with the use of multiple infections.

Although the cytotoxicity of rSFV virus particles for human lung cancer cells *in vitro* has been clearly demonstrated, it is reasonable to assume that H358a cell growth in conventional monolayer cell culture conditions does not adequately reflect the considerable heterogeneity of solid tumours *in vivo*. Cellular gene expression and function, as well as susceptibility to chemotherapeutic agents have been shown to be significantly altered by three-dimensional (3D) growth (Sutherland, 1988). Where the ultimate goal was to apply rSFV virus cytotoxicity to solid *in vivo* tumours, the *in vitro*/*in vivo* discrepancy was resloved using the 3D multicellular tumour spheroid (MTS) system (Reviewed by Mueller-Kleiser, 1997).

Since their introduction in the seventies by Sutherland *et al*, (1971), MTS have gained fundamental significance in experimental cancer research. In addition to therapeutically-oriented investigations (Frankel *et al*, 1997), spheroids have been used to study other areas of tumour biology, including angiogenesis (Shweiki *et al*, 1995), neovascularisation (Abramovitch *et al*, 1995) and intracellular communication (Freyer & Sutherland, 1980). Although lacking stromas and vasculatures, spheroids are considered to mimic the *in vivo* micromileu of primary tumours, micrometastases and intercapillary tumour microregions (Hamilton, 1998). These solid 3D aggregates also preserve *in vitro*, specific biochemical and morphological features similar to corresponding *in vivo* tumours, and can be maintained in culture for many weeks.

H358a MTS were created using the liquid overlay technique. By preventing cellular attachment at the base of the tissue culture plate, the tumour cells form cell-cell contacts and grow as spherical aggregates in suspension. This has been previously documented for other lung, ovarian, bladder and colon carcinoma cell lines (Dangles *et al*, 1997; Sutherland *et al*, 1986). However, H358a MTS do not grow as vigorously as other NSCLC spheroids, even following the addition of TGFα (Fujiwara *et al*, 1993). Thus, analysis of an rSFV-mediated relative change in spheroid volume, was impossible.

Analysis of H358a cell viability within individual 3D MTS structures, using ^{3}H thymidine incorporation and metabolic assays, revealed a highly significant decrease in proliferation as early as 24 h p.i. with the vector, and this was maintained over a 7 day period. The high proliferative activity of both control and treated spheroids at 24 h p.i. relative to subsequent timepoints, could be directly attributed to the contribution of individual H358a cells which have not yet joined the 3D structure, and was observed in all repeat experiments. At least 48hrs are required for uninfected H358a cells to form an intact spheroid. The high counts at 24h suggest that aggregation into these spheroidal clusters, does not necessarily offer a growth advantage to individual cells, in contrast to monolayer cell culture systems (Lieubeau-Teillet *et al*, 1998). At 48 h p.i., fully compact spheroids were established, with much lower overall proliferation rates. Finally, rSFV virus infection of H358a cells at the time of spheroid formation was shown to markedly inhibit the ability of cells to form these 3D aggregates.

Fujiwara *et al*, (1993) indicated the ability of a retroviral vector, expressing wt-*p53*, to penetrate solid 3D H322a spheroids and induce apoptosis. However, it is well known that the centres of these spheroids contain layers of non-proliferating and necrotic cells, due to gradual gradations in oxygen and nutrient concentrations, aswell as other metabolites and catabolites (Freyer & Sutherland, 1980). Retroviral vectors can only penetrate cells that are actively

replicating at the time of infection, as the vector requires chromosomal integration for recombinant gene expression. As the SFV vector does not have this limitation, it is possible that rSFV particles could penetrate the non-proliferating cell layers within the 3-D tumour mass. Further spheroid studies should confirm this.

rSFV virus particles have therefore, proved highly successful in the inhibition of human NSCLC cell growth *in vitro*, both as monolayer cultures and as solid 3D spheroidal aggregates. Infected cells clearly manifested apoptosis, which was shown to occur independently of endogenous and exogenous p53 activity, and occurred as a function of the SFV vector backbone, and not reporter gene expression. The impressive pro-apoptotic activities of the rSFV virus vector system for the NSCLC cell line *in vitro*, provides a favourable insight for the application of rSFV to solid tumours *in vivo* (*Chapter 4*).

Chapter 4

Therapeutic efficiency of rSFV vector particles using an in vivo lung cancer model.

4.1 INTRODUCTION

Mutations in the *p53* gene constitute one of the most frequent alterations in non-small cell lung cancer (NSCLC) (Levine *et al*, 1991). Structural alterations within the *p53* gene are detected in about 50-70% in tumours of NSCLC patients and are associated with poor prognosis (Takahashi *et al*, 1989). Loss of wild-type *p53* function impairs cell cycle arrest as well as repair mechanisms involved in the response to DNA damage, and abrogate apoptosis induced by several cytotoxic agents or radiation (Lowe *et al*, 1993). At present, high dose radiation therapy and chemotherapy are the standard treatments for patients with locally or regionally advanced NSCLC (Belani *et al*, 1993; Dillman *et al*, 1996), despite a 5-year survival rate of only 3-10% following such therapies. Thus, restoration of functional *p53* represents an attractive target for gene therapy of NSCLC.

Previous studies using recombinant retro-, adeno- and adeno-associated viruses, have indicated human NSCLC growth inhibition *in vivo* following the transduction of tumour cells with wild-type *p53*, both in animal models (Fujiwara *et al*, 1994a, Fujiwara *et al*, 1994b, Quazilbash *et al*, 1997), and in patients with advanced and incurable NSCLC (Swisher *et al*, 1999, Roth *et al*, 1996). The animal model, or nude mouse/tumour xenograft model, is an extremely useful tool for cancer research, and was exploited in the studies mentioned above. Lack of cell-mediated immunity makes the nude mouse amenable to induced tumour growth and therapeutic intervention studies (Sharkey & Fogh, 1984).

In Chapter 3, the pro-apoptotic properties of recombinant SFV vector particles for the *p53*-deleted H358a NSCLC cell line, were studied *in vitro* as cells in culture and as three-dimensional solid tumour spheroids. In this chapter, the

cytotoxicty of rSFV virus particles are further examined and exploited *in vivo*, using the H358a cell line as solid tumours in nude mice. The reporter gene, *EGFP* was utilised to detect the vector within the tumours *in situ*. This study shows that the NSCLC cell line forms solid compact tumours when implanted subcutaneously, and grows at an exponential rate. Therapeutic intervention studies, using high titre (10^{10} I.U./ml) rSFV virus particles, clearly indicated a tumour growth inhibitory effect, which was shown to be dose-dependent.

4.2 EXPERIMENTAL PROCEDURES

4.2.1 MATERIALS

4.2.1.1 *Mice*

Female Balb/C0/attsd-*nu* (nude) mice were obtained from Shaw Farm, Blackthorne, Oxon, UK. Mice were maintained in accordance with the principles outlined in S1 17/94 European Communities regulations 1994, for care and use of laboratory animals. Syringes (1.0 ml and 0.5 ml microfine insulin) and needles, (21G and 29G), were from Becton Dickenson, (Le pont de Claix), France.

4.2.1.2 *Particle production*

Ultracentrifuge tubes and the SW40Ti rotor were from Beckman-Coulter Instruments Inc. (CA, USA). Sucrose was from Sigma (St. Louis, MO, USA).

4.2.1.3 Antibodies

Monoclonal mouse anti-human cytokeratin, clone MNF116 and monoclonal mouse anti-CA 19-9, clone 116-NS-19-9 were obtained from DAKO A/S (Glostrup, Denmark). FITC-conjugated rabbit anti-mouse immunoglobulin was from DAKO. Normal rabbit serum and propidium iodide were from Sigma.

4.2.1.4 *Histological and pathological studies*

A CM 1900 cryostat was from Leica Microsystems (Nussloch, Germany). OCT compound and DABCO were from Sigma. Isopentane, neutral buffered formalin (NBF), acetone, haematoxylin and eosin and DPX solution were from BDH Ltd (Poole, UK). Cork discs were purchased from Raymond Lamb (East Sussex, UK). TUNEL analysis kit and colorimetric substrate diaminobenzidine (DAB) were from Boehringer Mannheim (GmBH, Mannheim, Germany). Mowiol was from Calbiochem Novabiochem (Nottingham, UK).

4.2.2 METHODS

4.2.2.1 Mice

The cytotoxic effect of rSFV virus particles on H358a cell growth was analysed *in vivo* using a *nu/nu* mouse xenograft model. Pathogen-free, female Balb/c *nu/nu* (nude) mice, of 6-8 weeks of age, were maintained under barrier conditions (conventional autoclaved cages with filter tops and sterilised bedding, in a negative air pressure cabinet), at 23°C, with sterilised food and water supplied *ab libitum.* All mice were allowed to settle for 7 days before use.

4.2.2.2 H358a tumour formation *in vivo*

To assess the potential of a tumour xenograft model for H358a tumour formation, and thus, rSFV virus-mediated cytocidal analysis, H358a cells were harvested during the exponential phase of growth, suspended in complete RPMI-1640 medium and injected subcutaneously (sc) into the right flank of each mouse, using a 1 ml syringe and 21G gauge needle, at a concentration of 1×10^6 cells/mouse. Mice were examined daily for signs of sc tumour formation. Tumour diameters were measured using a sterile linear calipers, in 2 perpendicular directions, and tumour volume was calculated by assuming a spherical shape ($4/3\ pr^3$), with the average tumour diameter calculated as the product of the square-root of cross-sectional diameters (Hamada *et al*, 1996). A total of 20 mice were utilised for this assessment. Tumour diameters were measured twice-weekly over a period of 10 weeks to assess H358a tumour formation and tumour growth kinetics. H358a tumours were excised at varying time intervals, and processed for histological examination as follows: tumour-bearing mice were sacrificed by cervical

dislocation and tumours were excised from the subcutaneous region for gross and histologic examination.

4.2.2.3 H358a tumour histology

4.2.2.3.1 *Preparation of H358a cryosections*

To facilitate histological analysis on frozen H358a tumour sections, excised tumours were immediately embedded in OCT compound on cork discs, and rapidly frozen in liquid-nitrogen-cooled isopentane, before storing at -70°C for histologic sectioning and staining. Frozen tumour sections were prepared using a Leica CM 1900 cryostat. Four to six μm thick tumour sections were placed on glass slides that were pre-coated with 0.5% (w/v) gelatin. Sections were fixed in acetone, 10% (v/v) NBF or 4% (w/v) paraformaldehyde solutions as required.

4.2.2.3.2 *Paraffin embedding and sectioning*

Paraffin embedding and sectioning of H358a tumours was performed by Ms. Marie Moore (Veterinary Pathology Laboratory, University College, Dublin). Excised tumours were immediately fixed in 10% NBF prior to paraffin embedding. Tumour samples were dehydrated in a graded alcohol series of washes; 50% (v/v) alcohol for 60 min, 70% (v/v) alcohol for 60 min and 90% (v/v) alcohol for 60 min, before being placed into two absolute alcohol washes, for 40 min each. Tumour samples were then immersed in a 1:1 solution of absolute alcohol: xylene solution, for 60 min, before being washed 3 times in absolute xylene, for 40 min each. This was followed by four individual immersions in paraffin wax, for 40 min each. Tumours were then mounted onto

blocks prior to sectioning. Six to eight μm thick paraffin sections were prepared using a microtome, placed onto standard slides and acetone fixed for routine histological analysis.

4.2.2.3.3 *Routine histology*

For routine histology, acetone-fixed cryosections and paraffin sections were stained with haematoxylin and eosin (H & E), for 1 min each, rinsed in PBS and dH_2O, dehydrated in a series of N-butanol and xylene washes and mounted onto coverslips using DPX solution.

4.2.2.3.4 *Immunohistochemistry and TUNEL in vivo*

For immunohistochemical analysis, H358a tumour cryosections were stained for the presence of human lung carcinoma cell markers, human cytokeratin and human CA-19-9 pentasacharride. The optimal dilution for each antibody was previously determined using a antibody dilution series on H358a cell smears. Cryosections were fixed in acetone and incubated with 0.5 mg/ml normal rabbit antiserum at 37°C, for 10 min. Sections were then incubated with mouse monoclonal anti-human cytokeratin (1:50 dilution) or mouse monoclonal anti-human CA-19-9 (1:50 dilution), in a dark humidified chamber at 37°C, for 1 h. Sections were washed twice in PBS containing 0.5% (v/v) Tween, twice in PBS alone for 5 min, and then incubated for a further 30 min at 25°C with rabbit anti-mouse FITC-conjugated secondary antibody (1:20 dilution), in a dark humidified chamber. Sections were washed in PBS, counterstained with 0.1 ng/ml propidium iodide (10 sec, 25°C), washed in PBS and dH_2O and mounted using Mowiol-DABCO solution. Negative controls included sections stained with and without 1°

or 2° antibodies. Sections were observed using fluorescent microscopy, using FITC- and PI-specific filters at 450 and 510 nm, respectively.

For TUNEL analysis, tumour cryosections were fixed in 4% (w/v) paraformaldehyde solution for 1 h, permeabilised with 0.1% (w/v) Triton X-100 and stained for the presence of nuclear DNA fragmentation using the apoptosis detection system described in section 2.2.2.10.2.

4.2.2.4 High titre rSFV virus particle production

To achieve a more enhanced response to treatment, and a greater cytocidal effect within *in vivo* tumour tissue, it was necessary to produce rSFV-EGFP particles of up to 10-fold higher concentrations, than for *in vitro* experiments (*see Chapter 3*). The production of recombinant, encapsidated SFV particles of high titre, for *in vivo* experiments, proceeded as described in section 2.2.2.7, with the following modifications.

4.2.2.4.1 *In vitro SP6 RNA transcription*

Plasmid production and preparation for *in vitro* RNA transcription from recombinant SFV plasmids pSFV-EGFP, pSFV-Helper S2 and pSFV-Helper CS219A proceeded as described in sections 2.2.2.7.1-2.2.2.7.3. For *in vitro* RNA transcription, standard reactions for each recombinant and helper plasmid, were performed in total reaction volumes of 250 µl, with five times the volume of each reagent, added as indicated in section 2.2.2.6.4. RNA concentrations were analysed by running 5 and 10 µl aliquots of each RNA reaction alongside that of 5

and 10 µl *Lambda* (*Hind111* and *EcoR1*) DNA molecular weight markers, on a 0.6% (w/v) agarose gel.

4.2.2.4.2 *Electroporation*

BHK-21 cells were electroporated for rSFV particle production, as described in section 2.2.2.7.4, with the following modifications: five 75 cm^2 tissue culture flasks, containing ~80% confluent BHK-21 cells were used for electroporation. The *in vitro*-transcribed RNA reactions were divided into five 150 µl aliquots, with each tube containing 50 µl each SFV-EGFP, SFV-Helper S2 and SFV-Helper CS219A RNA. One flask BHK-21 cells was used per electroporation, and all five reactions were placed in five 75 cm^2 culture flasks and incubated at 37°C, 5% CO_2, for 24 h.

4.2.2.4.3 *Harvesting high titre rSFV virus particles*

Twenty-four fours following electroporation, tissue culture supernatants, containing rSFV-EGFP particles were removed from the five culture flasks and pooled (100 ml) in a glass conical flask at 4°C. The supernatant was centrifuged (6,000g, 30 min, 4°C) to remove cellular debris, and further clarified by centrifugation (6,000g, 15 min, 4°C), before being pooled into a glass conical flask at 4°C. An aliquot was taken as a titration sample and quickly frozen at -70°C. Ten ml aliquots of particle supernatant were placed in 4 Beckman SW40Ti ultracentrifuge tubes. A 20% (w/v) sucrose cushion was carefully placed beneath this solution, and the tubes topped up and balanced with a further 3 ml rSFV supernatant. The tubes were placed into 4 SW40Ti swing buckets, balanced and the rSFV virus centrifuged (25,000*g*, 1.5 h, 4°C). Following ultracentrifugation,

the supernatant was immediately removed, the sides of the tubes dried with sterile cotton tips, and each pellet was resuspended in 150 µl TNE buffer (50 mM Tris-HCL, pH 7.4, 100 mM NaCl, 0.1 mM EDTA). This ultracentrifugation and resuspension step was then repeated for the remaining 50 ml rSFV supernatant. Ultracentrifugation supernatant samples were taken and quickly frozen for titration later. The rSFV pellets were incubated on ice at 4°C. Following overnight resuspension, particles were further resuspended by gentle pipetting, and each tube washed with a further 100 µl TNE buffer. rSFV virus resuspensions were pooled into a final volume of 2 ml, which were then aliquoted into 50-200 µl volumes, on ice, and rapidly frozen using dry-ice-cooled ethanol or liquid nitrogen, before storing at -70°C.

4.2.2.4.5 *High titre rSFV virus particle titration*

High titre rSFV particle titration was performed as described in section 2.2.2.7.5, with the following modifications: Serial dilutions (5 µl, 0.5 µl, 0.05 µl, 0.005 µl, 0.0005 µl) of rSFV-EGFP particles were used to infect successive wells of confluent sBHK cell monolayers, in a total volume of 500 µl infection medium. Infection medium alone was used as a control. Also, rSFV particle titres of samples taken during the harvesting procedure were used to infect sBHK monolayers, with serial dilutions (10 µl, 1 µl, 0.1 µl). Following overnight incubation, particle titres were obtained by direct epifluorescence at 488 nm. Particle titres were calculated at a magnification of x 400 and expressed as I.U/ml.

4.2.2.5 rSFV virus-mediated inhibition of H358a tumour growth *in vivo*

To assess rSFV-EGFP virus-mediated inhibition of tumour growth *in vivo*, H358a cells were harvested at the exponential phase of growth, and 1 x 10^6, in 0.4 ml complete RPMI-1640 medium, were injected sc into the right flank of each mouse to form H358a tumour xenografts as before. Mice were examined daily for signs of sc tumour formation, and tumour diameters were measured using a sterile linear calipers, in 2 perpendicular diameters. On reaching a diameter of 4 mm (approximately 7-20 days), 50 µl TNE buffer alone or TNE containing rSFV-EGFP particles (1 x 10^{10} I.U. ml^{-1}), were injected intratumourally, using a 0.5 ml insulin syringe and 21G_ gauge needle. The direction of injection ensured that solutions were targeted towards the centre of the tumour, and not into surrounding normal tissue. Three separate analyses were performed; one with a single injection (day 1), three injections (days 1, 2 and 3) and six injections (days 1, 2, 3 and days 7, 8 and 9). Five to seven mice were used per treatment group. To assess the rate of tumour growth, tumours were measured every second day for 135 days with sterile linear calipers, and tumour volume was calculated by assuming a spherical shape, as described in section 4.2.2.2.

4.2.2.6 Pathological examination of H358a tumours following administration of rSFV virus particles

Tumours that received one injection of rSFV virus particles or buffer only, were harvested from 8 h to 8 days after injection for pathological examination. Tumours that received higher numbers of injections, were harvested at various times for pathological examination also. Routine histology was performed on H&E stained, formalin-fixed, paraffin-embedded sections, as described in section

4.2.2.3.2-4.2.2.3.3, and observed by light microscopy. EGFP expression was observed by direct epifluorescence on frozen H358a 4-6 μm tumour cryosections. TUNEL analysis to detect apoptotic cells *in situ*, was performed on 4% (w/v) paraformaldehyde-fixed cryosections, as described in section 4.2.2.3.4.

4.3 RESULTS

4.3.1 H358a tumour formation *in vivo*.

As a prerequisite for rSFVvirus particle-mediated H358a cell death analysis *in vivo*, it was necessary to first obtain information on the ability of the NSCLC cell line to induce solid tumour formation *in vivo*, to determine tumour growth rate and to characterise these tumours *in vivo*. For this analysis, the *nu/nu* (nude) mouse xenograft model was utilised. Congenitally athymic nude mice are amenable for these studies as they lack cell-mediated immunity and therefore, are extremely susceptible to induced tumour formation, compared to immunocompetent mice (Pritchard & Micklem, 1974). Because of their short life span, mice were used as early as 6-8 weeks of age. To assess the ability of the H358a NSCLC cell line to induce the formation of solid tumours, a total of 10^6 H358a cells were injected subcutaneously (sc) into the right flank of 10 female mice and monitored for tumour development. Subcutaneous H358a tumour formation was observed at approximately 7 to 10 days following injection, and after 20 days, 70% of mice had detectable tumours at the injection site. Tumour diameters were measured using a sterile linear calipers, and tumour volume was calculated by assuming a spherical shape, as described in section 4.2.2.2. Tumour measurements were taken once-weekly for 6 weeks, and the results are illustrated in figure 4.1. During the first 30 days of growth, tumour volume was observed to increase exponentially, and then gradually formed a plateau. Identical results were observed in a repeat experiment (*not shown*). Small metastases were noted at small distances from the primary tumour in at least 6 of the mice, at approximately 25-30 days following injection. The gradual decrease in tumour growth rate could be explained following histochemical examination (*see below*).

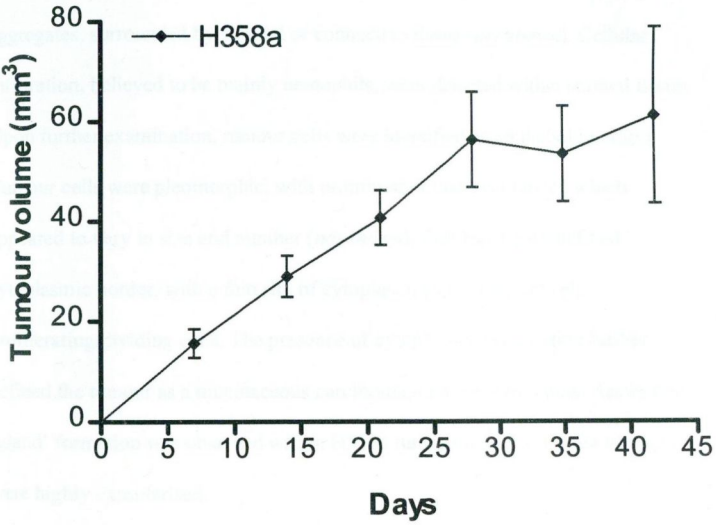


Figure 4.1- H358a tumour formation *in vivo*.

Ten female Balb/C nude mice were injected sc with H358a cell suspensions (1 x 10^6 cells, in normal medium). Tumour nodules were detected at the injection site between 7-15 days following injection. Tumour diameters were measured in 2 orthogonal directions with linear calipers, and volume was calculated by assuming a spherical shape, with the average diameter calculated as the square root of the product of cross-sectional diameters. *Points*; means, *bars*; SD.

Six weeks following injection, mice were sacrificed and tumours were excised and processed for histochemical examination.

Upon gross histologic examination, H358a tumours appeared to form lobular aggregates, surrounded by stromal or connective tissue (*not shown*). Cellular infiltration, believed to be mainly neutophils, were detected within stromal tissue. Upon further examination, tumour cells were identified as epithelial in origin. Tumour cells were pleomorphic, with prominent round/oval nuclei, which appeared to vary in size and number (*not shown*). Cell had a well-defined cytoplasmic border, with a thin rim of cytoplasm, suggesting actively proliferating/dividing cells. The presence of cytoplasmic vacuolation further defined the tumour as a mucinaceous carcinoma, or adenocarcinoma. Ascinar or 'gland' formation was observed within H358a tumour sections. H358a tumours were highly vascularised.

4.3.2 Immunohistochemical characterisation of *in vivo* H358a tumours.

Human NSCLC are of epithelial origin (Janeway *et al*, 1999). Epithelial cells of normal or malignant origin contain intracellular cytokeratin polypeptides (Moll *et al*, 1982), and carcinomas from various tissues, including squamous cell carcinoma, small cell carcinoma and adenocarcinoma, react positively with antibodies directed against a wide range of cytokeratins (Goddard *et al*, 1991). Acetone-fixed H358a NSCLC cryosections were incubated with a mouse anti-human cytokeratin antibody and subsequently with a FITC-conjugated rabbit anti-mouse antibody (*Figure 4.2*). The presence of positive FITC staining within the cytoplasm of individual H358a cells indicated a positive reaction, confirming that the tumours are of epithelial origin.

Figure 4.2- **Immunohistochemical analysis of H358a tumours *in vivo*, using an anti-cytokeratin antibody.** Subcutaneous H358a tumours were grown to volumes of approximately 60 mm^3, excised and rapidly frozen in liquid nitrogen-cooled isopentane, and 4-6 μm cryosections were prepared. Acetone-fixed cryosections were incubated with monoclonal mouse anti-human cytokeratin antibody for 1 h. Sections were subsequently incubated with an anti-mouse FITC-conjugated secondary antibody and visualised using fluorescent microscopy, at 460 nm. Note positive FITC cytoplasmic staining of cytokeratin protein within H358a tumour cells *in vivo*. Photographed at x 200 magnification.

Figure 4.3- **Immunohistochemical analysis of H358a tumours, using anti-CA-19-9 antibody.** Subcutaneous H358a tumours were grown to volumes of approximately 60 mm^3, excised and rapidly frozen in liquid nitrogen-cooled isopentane, and 4-6 μm cryosections were prepared. Acetone-fixed cryosections were incubated with monoclonal mouse anti-human CA-19-9 antibody, for 1 h. Sections were subsequently incubated with an anti-mouse FITC-conjugated secondary antibody, and counterstained using propidium iodide (PI). Sections were visualised by fluorescent microscopy, using a FITC- and PI-specific filter, at 460 nm. Note positive FITC cytoplasmic staining of CA-19-9 tumour marker within H358a tumour cells *in vivo*. Photographed at x 400 magnification.

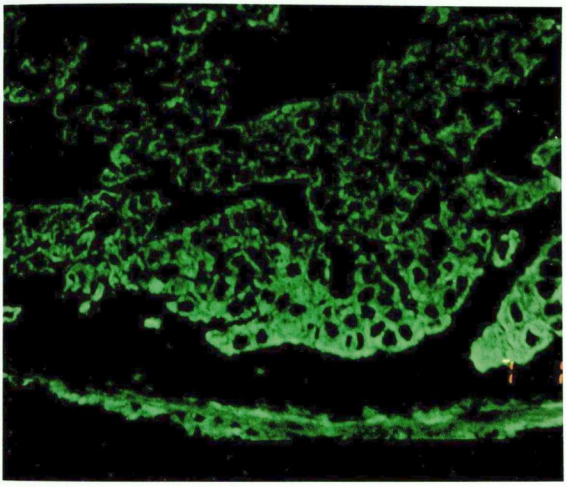


Figure 4.2- Immunohistochemical analysis of H358a tumours *in vivo*, using an anti-cytokeratin antibody.

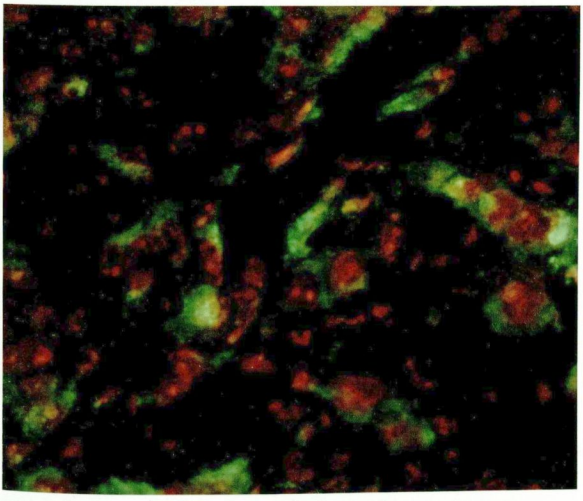


Figure 4.3- Immunohistochemical analysis of H358a tumours, using an anti-CA-19-9 antibody.

H358a tumour cryosections also displayed a positive reaction for the presence of the CA-19-9 pentasaccharide (*Figure 4.3*). Human lung carcinomas, including adenocarcinomas, bronchioalveolar carcinomas, squamous cell carcinomas and small cell anaplastic carcinomas, stain positively with an anti-CA-19-9 antibody (Gatalica & Miettinen, 1994). Monoclonal anti-CA-19-9 antibodies react with the sialylated Le^a-active pentasaccharide (sialylated lacto-N-fucopentaose 11), which is enzymatically synthesised by sialylation of type-1 carbohydrate chains (Hanai *et al*, 1990). Sections were counterstained with propidium iodide, to identify tumour cell nuclei.

Similar results were also obtained with acetone-fixed H358a cell smears from culture (*not shown*). Although these smears were primarily used for antibody titrations, it also confirmed that the H358a tumour cells *in vitro*, induced tumour formation observed *in vivo*. H358a cells have been well-characterised by other authors (Gazdar *et al*, 1980; Brower *et al*, 1986), as a human non-small cell lung adenocarcinoma of bronchioalveolar origin. The *p53* gene deletion within this cell line, was demonstrated by other authors (Takahashi *et al*, 1989; Quazilbash *et al*, 1997), and in preliminary blotting experiments by G. M. Glasgow (*personal communication*).

4.3.3 Cell death analysis *in vivo*.

The fact that tumour growth rate decreased after approximately 30 days of growth (*Figure 4.1*), suggested that rapid cellular growth and proliferation led to a concomitant reduction in nutrient and oxygen concentrations, as observed with other solid tumours (Gazdar, 1994), and in the *in vitro* H358a multicellular tumour spheroid model (*see Chapter 3*). Hypoxia and decreasing metabolite

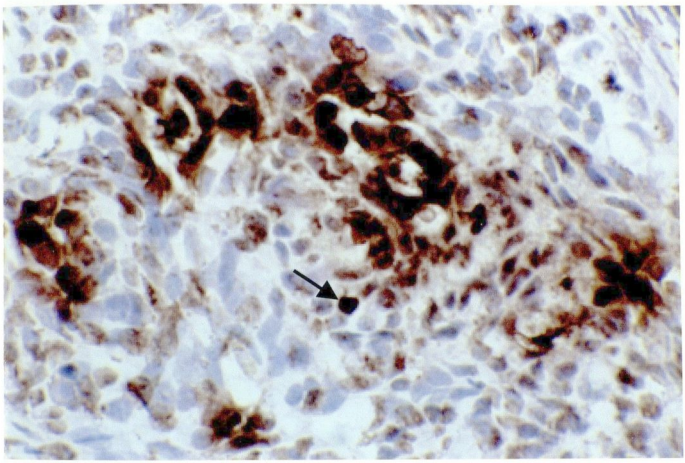


Figure 4.4- TUNEL reactivity within H358a tumours *in vivo*. Subcutaneous H358a tumours were grown to volumes of 7.5 mm^3 (20 days), excised and rapidly frozen in liquid nitrogen-cooled isopentane. Six μm cryosections were prepared and fixed with 4% paraformaldehyde solution, permeabilised in Triton X-100 solution and stained for apoptotic DNA fragmentation, using TdT and horse-radish peroxidase. Colorimetric detection was performed using diaminobenzidine, and normal nuclei were couterstained with methyl green. Arrow indicates TUNEL positive apoptotic cells, detected *in situ*, within the H358a tumour section. Photographed at x 400 magnification.

concentrations has also been shown to induce both necrotic and apoptotic cell death (Shimizu *et al*, 1995). Ischemic injury or needle tracts may lead to necrotic areas within the tumour mass (*B. J. Sheahan, personal communication*), where cells lacking nuclei, or 'ghost' cells are observed (*not shown*).

In contrast to necrosis, apoptotic cell death was also observed in the absence of inflammation, and was characterised by cell shrinkage and nuclear pyknosis (*not shown*). Quantitation of indigenous apoptotic cell death within H358a tumours was performed on frozen tissue sections, using the TUNEL procedure. This *in situ* apoptosis detection system was outlined and utilised in *in vitro* analyses in Chapter 3, and was optimised and applied to paraformaldehyde-fixed cryosections at 30 days following initial tumour injection. Figure 4.4 illustrates an area of indigenous apoptotic cell death within the tumour tissue. The number of TUNEL positive cells were calculated by scoring 100 cells in several fields, using duplicate samples, for up to three different tumours. In other areas of the tumour TUNEL reactivity was much less pronounced, yet it was important to standardise the reaction *in vivo*, prior to rSFV virus-mediated apoptotic therapy in subsequent experiments.

4.3.4 High titre recombinant SFV virus particle production and titration in BHK-21 cells.

Due to limited volume restrictions for direct intratumoural injections *in vivo* (~50µl/tumour), titres in excess of 1 x 10^{10} I.U./ml were necessary to achieve maximum effect. Recombinant EGFP-expressing particles were used for high titre particle preparations for *in vivo* use. For the production of rSFV-EGFP particles at ~10^{10} I.U./ml, *in vitro*-transcribed RNA from recombinant pSFV-EGFP, pSFV-

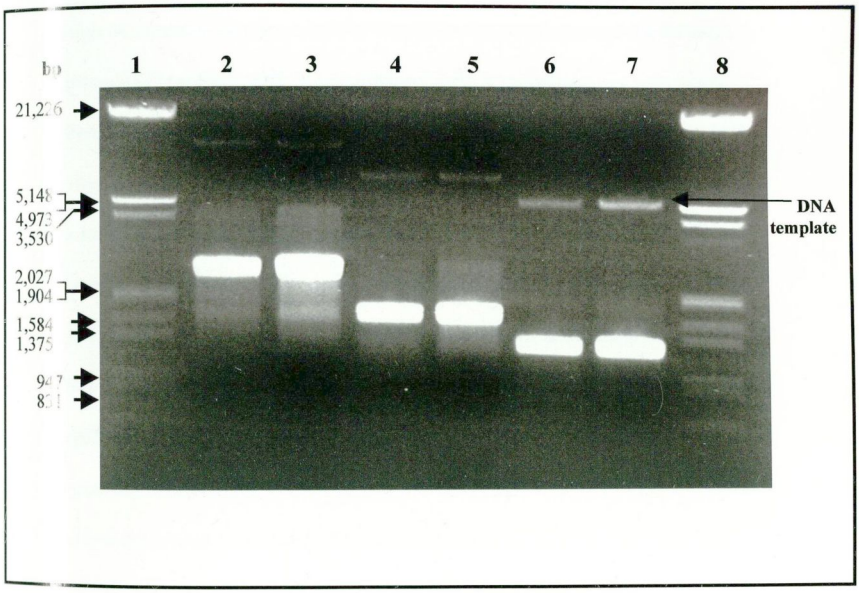


Figure 4.5- *In vitro* RNA transcription for high titre rSFV-EGFP virus particle production. 0.6% (w/v) agarose gel, stained with ethidium bromide. *Lanes 1* and *8*; 5 µl and 10 µl *Lambda* (*Hind111 and EcoR1*) DNA marker, respectively. *Lanes 2* and *3*; 0.5 µl and 1.0 µl each of *in vitro* transcribed SFV-EGFP RNA. *Lanes 4* and *5*; 0.5 µl and 1.0 µl each of SFV-Helper S2 RNA. *Lanes 6* and *7*; 0.5 µl and 1.0 µl each of SFV-Helper CS219A RNA. Arrow indicates *Spe1*-linearised DNA template.

Helper S2 and pSFV-Helper CS219A plasmids, were electroporated in equimolar amounts, into the BHK-21 cell line, as described in section 2.3.5. However, for high titre particle batches, a total of five RNA transcription reactions for each plasmid (*Figure 4.5*), and five simultaneous electroporations, were necessary. Particles were harvested at 24 h p.e. The resulting 100 ml volume of rSFV-EGFP virus particles (~1 x 10^8 I.U./ml), were concentrated to a final volume of 2 ml, by a series of ultracentrifugation and resuspension steps. Particles were finally resuspended in TNE buffer, and were titrated by infecting 80% confluent sBHK cell monolayers, grown on glass coverslips, with serial dilutions of the virus. EGFP expression from infected sBHK cell monolayers, were obtained by direct epifluorescence, and titres of approximately 1 x 10^9-1 x 10^{10} I.U./ml, were routinely obtained. rSFV virus particles at this titre were used exclusively for *in vivo* applications, and TNE buffer alone was used as a mock-infection control.

4.3.5 rSFV virus particle-mediated inhibition of H358a tumour growth *in vivo*.

To address the therapeutic efficiency of rSFV particles *in vivo*, H358a cells were injected subcutaneously into the right flank of immunodeficient mice, and tumours of 4 mm diameter were allowed to develop. Mice received direct intratumoural injections of 50 µl TNE buffer alone, or TNE buffer containing rSFV-EGFP particles (1 x 10^{10} I. U./ml), daily for 3 days. A 50 µl volume of high titre rSFV-EGFP particles was chosen as optimal for intratumoural injections based upon the size of the tumours, and contained at least 5 x 10^8 I.U. of rSFV-EGFP particles per injection. An aliquot of each rSFV-EGFP particle solution was re-titrated using the sBHK cell monolayer, immediately following each treatment. Five mice were used per treatment group. Tumour diameters were

measured, in 2 orthogonal directions, every other day for 30 days, and tumour volume calculated as described in section 4.3.1. Figure 4.6 illustrates the effect of 3 intratumoural injections of rSFV virus particles on the growth of H358a tumours, in comparison to TNE buffer-treated controls. In mice treated with TNE buffer alone, tumours continued to grow rapidly throughout the treatment. At day 30, tumour volumes approached 20% body weight, and the mice were sacrificed. In contrast to controls, mice which received rSFV-EGFP particles showed a significant inhibition of tumour growth rate in less than 1 week ($P<0.05$). Tumour growth remained significantly reduced throughout the experiment (Day 16, $P<0.05$), and at 30 days after injection, tumour volumes were reduced up to 5-fold in comparison to controls (*Table 4.1*). However, an increase in tumour growth was detected in rSFV-EGFP virus-treated mice in the days following the 30-day examination period, indicating that 3 injections with rSFV particles was not adequate for complete tumour growth inhibition, and that following cessation of treatment, surviving tumour cells recover and the tumour survives.

The growth inhibitory effects of rSFV particles on H358a tumour growth was more pronounced following the application of 2 treatment cycles, with 3 injections per cycle (*Figure 4.7*). As before, mice with sc tumours of 4 mm diameter, received direct intratumoural injections with TNE buffer alone, or TNE buffer containing rSFV particles (1×10^{10} I.U./ml). Five to seven mice were used per treatment group. Mice received treatment on days 1, 2, 3 and days 7, 8 and 9. In mice treated with TNE buffer alone, tumours continued to grow rapidly throughout treatment as before, whereas tumour growth in mice treated with rSFV-EGFP particles were reduced even further than those which received three injections (Day 16; $P<0.01$). At day 8 p.i., H358a tumours had visibly reduced in size, and at 30 days following initial treatment, tumours which received rSFV-EGFP particles showed a 95% reduction in tumour volume, compared to TNE

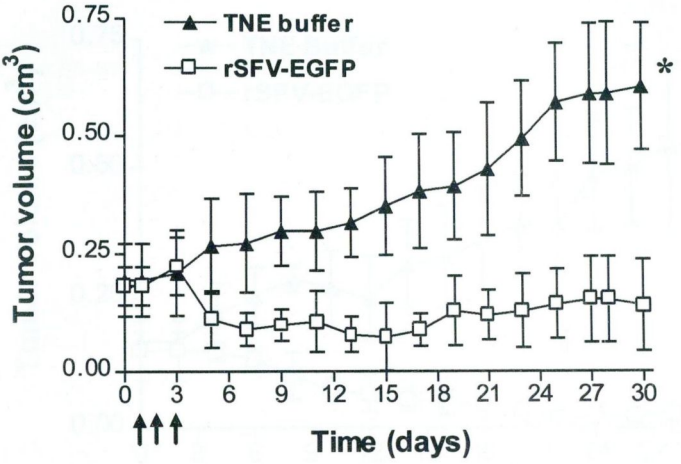


Figure 4.6- Effects of rSFV-EGFP virus particle treatment on NSCLC growth *in vivo*. H358a cells (1×10^6) were injected subcutaneously into Balb/C *nu/nu* mice. On reaching tumour diameters of 4 mm (approximately 20 days), tumours received three intratumoural injections of rSFV-EGFP virus particles (5×10^8 I.U.) or TNE buffer. Five mice were used per treatment group. Arrows indicate days of treatment. Tumour diameters were measured every other day, in two orthogonal directions, and tumour volume was calculated by assuming a spherical shape. *Points*; means, *bars*; SD, for a single experiment.

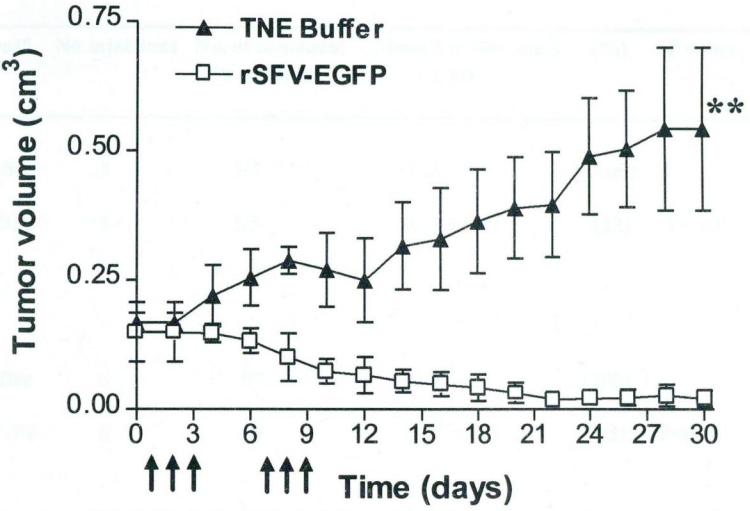


Figure 4.7- Effects of two cycles of rSFV-EGFP virus particle treatment on NSCLC growth *in vivo*. H358a cells (1×10^6) were injected subcutaneously into Balb/C *nu/nu* mice. On reaching tumour diameters of 4 mm (approximately 20 days), tumours received six intratumoural injections of rSFV-EGFP virus particles (5×10^8 I.U.) or TNE buffer. Seven mice were used per treatment group. Arrows indicate days of treatment. Tumour diameters were measured every other day, in two orthogonal directions, and tumour volume was calculated by assuming a spherical shape. *Points*; means, *bars*; SD, for a single experiment and is representative of 2 independent experiments.

Treatment*	No.injections	No. of tumours/ No. of mice	Mean Volume (cm^3) ± SD	(%)	P value
TNE Buffer	3	5/5	0.65 ± 0.1	(100)	
rSFV-EGFP	3	5/5	0.15 ± 0.04	(23)	P<0.05
TNE Buffer	6	7/7	0.54 ± 0.2	(100)	
rSFV-EGFP	6	4/7	0.03 ± 0.01	(5)	P<0.002

* Values at 30 days post-treatment.

Table 4.1- **Effects of rSFV-EGFP virus particle treatment on *in vivo* H358a tumour growth.**

buffer controls ($P<0.002$) (*Table 4.1 & Figure 4.8*). At day 20 following initial treatment, detection of macroscopic tumours in 3 of the 7 rSFV-EGFP-treated mice was virtually impossible. This growth rate experiment was repeated using similar initial tumour volumes and timepoints for rSFV virus injections, and yielded identical results (*not shown*).

As illustrated in Figure 4.7, following 6 intratumoural injections with rSFV-EGFP virus particles, tumours revealed rapid regression rates to the point that macroscopic H358a tumours were non-detectable in 3 of 7 treated mice. In an effort to assess whether rSFV-EGFP virus treatment mediated complete tumour regression, these mice were maintained beyond day 30, and following the elimination of controls. Mice were again examined daily for reappearance of macroscopic tumours. The results are illustrated in figure 4.9. A continuation of results described in figure 4.7, almost half of the rSFV virus-treated mice failed to reveal signs of tumour regrowth, even when maintained for over 135 days after initial rSFV virus injections. Thus, 3 out of 7 mice treated with rSFV-EGFP particles underwent complete tumour regression. The remaining mice continued to reveal small tumour nodules of ~1 mm diameter. When excised for pathology, these nodules were comprised mainly of scar tissue and inflammatory and H358a tumour cells (*see below*). Also, no metastases or secondary tumours were observed in areas beyond the initial injection site, nor within any of the major organs, as assessed by post-mortem analyses (*not shown*).

Figure 4.8- **Subcutaneous H358a tumour growth as a *nu/nu* mouse xenograft and following rSFV virus therapeutic intervention.** Mice received subcutaneous injections of 1 x 10^6 H358a cells. Upon reaching 4 mm diameter, mice received direct intratumoural injections of rSFV-EGFP virus particles (5 x 10^8 I.U.) (*A*) or TNE buffer (*B*), on days 1, 2, 3 and days 7, 8 and 9. Mice were maintained for 50 days, at which time, control mice (*B*) were eliminated. Mice treated with rSFV virus particles showed a 95% reduction in tumour growth (*A*), compared to TNE buffer controls (*B*) (*arrows*).



Figure 4.8- Subcutaneous H358a tumour growth as a *nu/nu* mouse xenograft, following rSFV virus particle therapetic intervention.

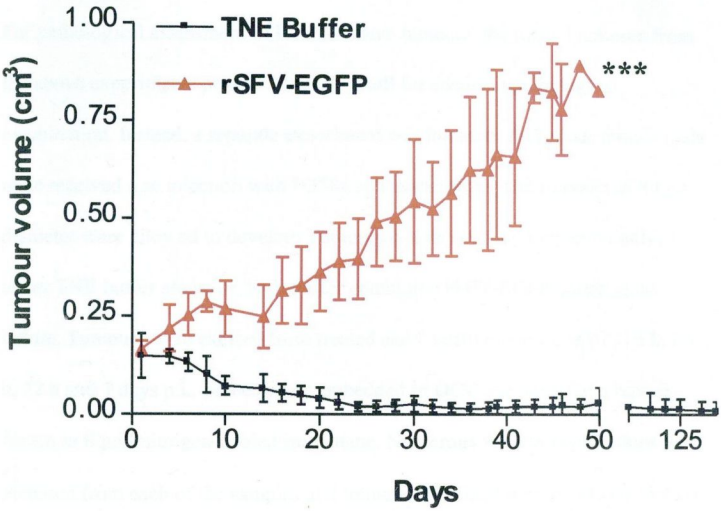


Figure 4.9- Two cycles of rSFV-EGFP virus particle treatment induce complete regression of *in vivo* H358a tumours. H358a cells (1×10^6) were injected subcutaneously into Balb/C *nu/nu* mice. On reaching tumour diameters of 4 mm (approximately 20 days), tumours received six intratumoural injections of rSFV-EGFP virus particles (5×10^8 I.U.) or TNE buffer. Arrows indicate days of treatment. Tumour diameters were measured every other day, in two orthogonal directions, and tumour volume was calculated by assuming a spherical shape. TNE buffer control mice were eliminated at day 50, or when tumour volume reached 20% body weight. Five rSFV-EGFP virus-treated mice were maintained for 137 days after initial rSFV treatment, and tumour diameters were measured as before. *Points*; means, *bars*; SD, for a single experiment.

4.3.6 Pathological examination of H358a tumours following rSFV virus treatment.

For pathological assessment of H358a *in vivo* tumours, the treated tumours from the above experiments proved to be too small for adequate pathological examination. Instead, a separate experiment was initiated. As before, female nude mice received a sc injection with H358a cell suspensions, and tumours of 4 mm diameter were allowed to develop. Tumours received a single injection only, of either TNE buffer alone, or TNE buffer containing rSFV-EGFP particles, as before. Tumours were excised from treated and control tumours, at 8 h, 16 h, 24 h, 72 h and 7 days p.i., immediately embedded in OCT compound and rapidly frozen in liquid nitrogen-cooled isopentane. Numerous 4-6 μm cryosections were prepared from each of the samples and immediately fixed with paraformaldehyde to facilitate detection of the vector *in situ*. Control and treated cryosections were analysed for the presence of EGFP fluorescence by direct epifluorescence. Paraffin-embedding of such tissues destroys EGFP fluorescence, and thus cryosections were used (Prasher *et al*, 1992). EGFP fluorescence was a direct indication of whether the vector was successful in replicating within the tumour cells *in vivo* and was directly responsible for tumour cell death. EGFP expression was also a method to assess vector distribution and persistence within tumour tissue. Results are illustrated in Figure 4.10 and Figure 4.14. The vector was detected within treated tumours no earlier than 16 h after injection, consistent with standard SFV replication kinetics (Atkins *et al*, 2000), and reached maximum levels at 24 h p.i. (*Figure 4.10*). EGFP expression appeared to localise within a defined area of the tumour, probably within regions close to the initial injection site, and persisted for 3 days only, and was not detected at other subsequent timepoints (*Figure 4.14*). These results are consistent with PCR analysis and EGFP fluorescence detection of the rSFV-EGFP virus construct

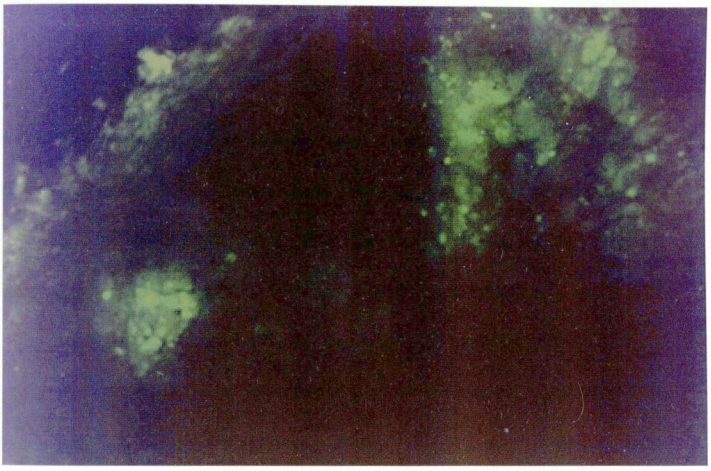


Figure 4.10- **Expression of EGFP within H358a tumours *in vivo*.**

H358a cells (1 x 10^6) were injected subcutaneously into Balb/C *nu/nu* mice. On reaching tumour diameters of 4 mm (approximately 20 days), tumours received one intratumoural injection of rSFV-EGFP particles (5 x 10^8 I.U.). The tumour was excised 24 h following injection and rapidly frozen in liquid nitrogen-cooled isopentane. Ten μm cryosections were prepared and fixed with 4% (w/v) paraformaldehyde. EGFP expression within tumour cryosections was observed by direct epifluorescence, at 488 nm. Note positive EGFP expression occurs in discrete regions within the rSFV virus-treated tumour, encompassing a number of H358a tumour nodules. Photographed at x 100 magnification.

within the tibialis anterior muscle of immunocompetent mice (Morris-Downes *et al*, 2000), in a separate study. Control tumours did not exhibit EGFP fluorescence at any of these timepoints (*not shown*).

Histological examination of tumours was performed on H & E stained, formalin-fixed paraffin-embedded sections. Analysis of tumours which received one injection of TNE buffer alone and excised after 4 days (*Figure 4.11 A*), revealed well-demarcated, densely cellular nodular masses, located in the subcutis. Lobular aggregates and acini of polygonal cells were separated by delicate strands of fibrovascular stroma. The tumour cells had distinct cell borders, various amounts of eosinophillic, frequently vacuolated cytoplasm and oval hyperchromatic nuclei, with prominent nucleoli. Nuclear pleomorphism and mitotic figures were common. Numerous apoptotic figures were observed, together with the occasional small foci of oncotic necrosis. Tumours treated once with rSFV-EGFP particles, and sampled at 4 days after treatment (*Figure 4.11 B*), were characterised by large coalescent areas of oncotic necrosis. Apoptotic necrosis was also common and much more pronounced in treated tumours. Small aggregates of lymphoid cells and neutrophils were present among fibroblastic cells, which partially encircled the tumour nodules. Fibroblastic cells are an indication of scar tissue, whereas the presence of immune cells are an indication of a transient, limited immune response, and occured more predominantly in tumours excised at later timepoints (*Figure 4.12*). No gross lesions were detected in areas surrounding the excised tumours, from both control and treated mice.

TUNEL reactivity within control and treated tumours was assessed on paraformaldehyde-fixed tumour cryosections, from 8 h to 7 days post-treatment. Positive TUNEL reactivity was detected as early as 8 h p.i. (*Figure 4.14*), reaching maximum levels at 24 h (*Figure 4.13 A*) and approached control levels

Figure 4.11- **Histology of H358a tumours following treatment with rSFV virus particles.** Subcutaneous H358a tumours were excised and fixed in 10% neutral buffered formalin. Fixed tissues were dehydrated in graded alcohols, embedded in paraffin, sectioned at 5 μm and stained with haematoxylin and eosin. (*A*) H358a tumour, 4 days following direct intratumoural injection with TNE buffer. Aggregates of tumour cells are observed, separated by thin bands of fibrovascular stroma. Apoptotic bodies (*arrows*) and mitotic forms (*M*) are indicated. Photographed at x 400 magnification. (*B*) H358a tumour, 4 days following direct intratumoural injection with rSFV-EGFP virus particles. An area of oncotic necrosis (*N*) is indicated, surrounded by tumour cells. Photographed at x 200 magnification.

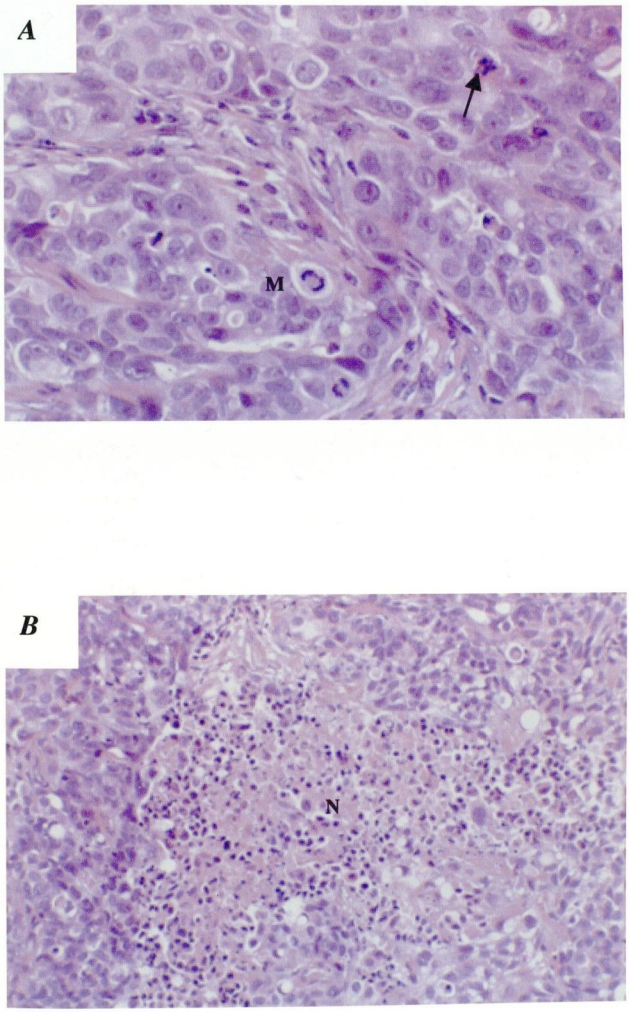


Figure 4.11. Histology of H358a tumours following treatment with rSFV virus particles.

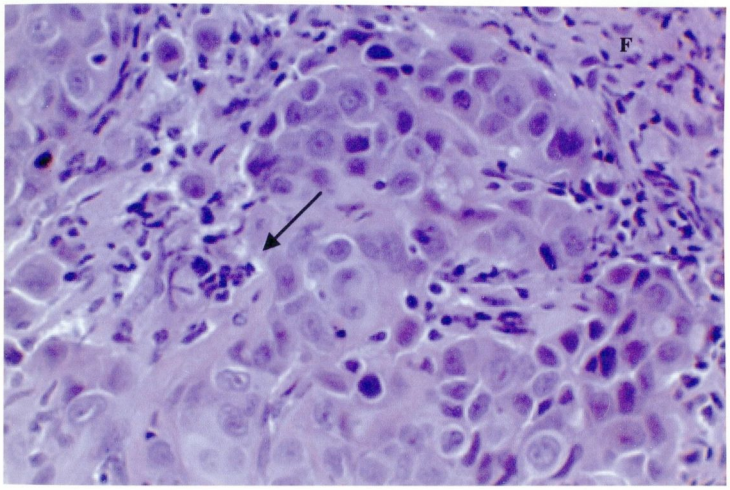


Figure 4.12- **Histology of H358a tumours, 30 days following treatment with rSFV virus particles.** Subcutaneous H358a tumours received at total of 6 injections of rSFV-EGFP particles, on days 1, 2 and 3 and days 4, 5 and 6. At 30 days post-treatment, tumours were excised and fixed in 10% neutral buffered formalin. Fixed tissues were dehydrated in graded alcohols, embedded in paraffin, sectioned at 5 μm and stained with haematoxylin and eosin. Numerous apoptotic figures are observed (*arrow*), together with lymphoid and neutrophilic infiltration, as well as fibroblastic cells (*F*), which partially encircle the tumour nodules. Photographed at x 200 magnification.

Figure 4.13- **TUNEL reactivity within H358a tumours following treatment with rSFV virus particles.** H358a cells (1 x 10^6) were injected subcutaneously into Balb/C *nu/nu* mice. On reaching tumour diameters of 4 mm, tumours received an intratumoural injection of either rSFV-EGFP virus particles (5 x 10^8 I.U.) (*A*) or TNE buffer (*B*). At 24 h post-treatment, tumours were excised, rapidly frozen in liquid nitrogen-cooled isopentane and 6 μm sections prepared. Paraformaldehyde-fixed cryosections were stained for apoptosis using the TUNEL detection method. Colorimetric detection was performed using DAB. No counterstain was applied. (*A*) H358a tumour section, labelled for apoptosis, 24 h following treatment with rSFV-EGFP particles. An area of intense TUNEL reactivity is indicated (*T*), and was not observed at the same intensity within TNE buffer control tumours (*B*). Photographed at x 400 magnification.

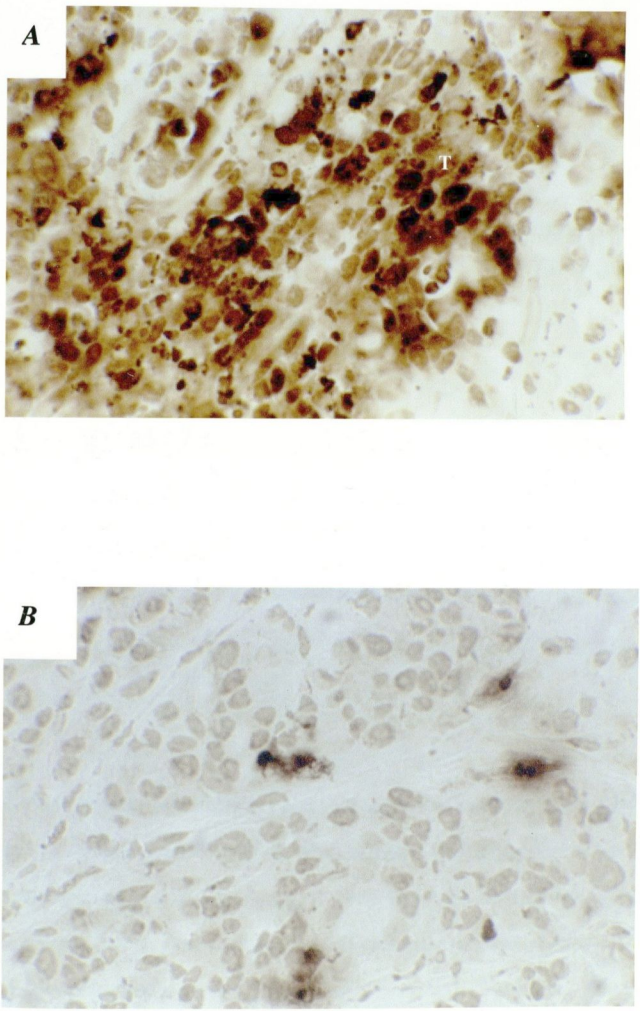


Fig 4.13- TUNEL reactivity within H358a tumours following treatment with rSFV virus particles.

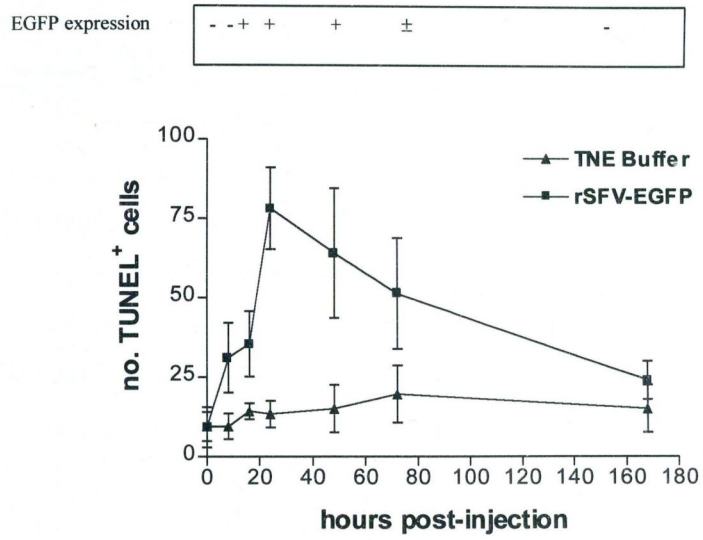


Figure 4.14- Composite representation of EGFP expression and TUNEL reactivity following one intratumoural rSFV-EGFP virus injection. H358a tumours of 4 mm diameter were injected intratumourally with rSFV-EGFP particles (5 x 10^8 I.U.) or TNE buffer, as controls. Tumours were harvested in duplicate, at various time-points post-treatment and rapidly frozen in liquid nitrogen-cooled isopentane. Cryosections from both control and treated samples were prepared. For analysis of EGFP expression, paraformaldehyde-fixed sections were examined by direct epifluorescence, at 488 nm. TUNEL was performed using TdT enzyme, horse-radish peroxidase and DAB colorimetric substrate. The number of $TUNEL^+$ apoptotic cells were obtained by scoring 600 cells, each on duplicate samples. *Points*; means, *bars*; SD, for a single experiment.

after 1 week. Control tumours failed to exhibit TUNEL reactivity above that of indigenous levels observed in pilot *in vivo* studies (*Figure 4.13 B; Figure 4. 14*).

4.4 DISCUSSION

Cancer of the lung is the single greatest cause of cancer-related deaths in the United States. The American Cancer Society revealed that the estimated incidence of lung cancer in the US in 1998 was 172,000, with more than 160,000 deaths. The National Cancer Registry of Ireland designated cancer of the lung as the third most frequent cancer within the Irish population. The World Health Organisation classification of lung cancers describes four major types (Annonymous, 1982), including squamous cell carcinoma, adenocarcinoma, small-cell carcinoma and large-cell undifferentiated carcinoma. Small-cell lung carcinomas (SCLC) are neuroendocrine in origin and express all of the general neuroendocrine cell properties (Baillie-Johnson *et al*, 1985). SCLC metastasise early and are usually associated with poor prognosis. Adenocarcinomas arise form glandular epithelia from peripheral airways, such as bronchioles and alveoli, and are typified by acinar, or gland-formation and secretion of mucin, either extra- or intracellularly (Gazdar & Linnoila, 1988). Because of the major differences in their biological and histological properties, lung cancers are frequently divided into SCLC and nonSCLC or NSCLC types (Gould & Warren, 1989). The latter accounts for 75-80% of all lung cancers (Minna *et al*, 1989). At primary diagnosis, most NSCLC patients present with non-resectable disease, and despite major advances in chemo- and radiation therapies, the 5-year survival rate of stage 111 patients does not exceed 10% (Belani, 1993; Dillman *et al*, 1996). Because of the poor results obtained with conventional therapy alone, additional treatments are required.

p53 gene mutations and deletions have been associated with NSCLC progression, and the development of resistance to chemotherapy and radiation therapy (Lowe *et al*, 1993), and are detected in about 50-70% of tumours of

NSCLC patients (Takahashi *et al*, 1989). Recent reports have demonstrated that growth of several NSCLC cell lines and in tumours of patients, were suppressed by viral vector-mediated transfer of exogenous wild-type *p53* (Quazilbash *et al*, 1997; Schuler *et al*, 1998), by restoring tumour suppressor gene function and inducing apoptosis. In this chapter, the *p53*-independent pro-apoptotic properties of rSFV were exploited in inducing apoptosis within solid NSCLC tumours, and inducing tumour regression *in vivo*. The NSCLC cell line used in this study was the human *p53*-deleted NSCLC H358a cell line (*see Chapter 3*).

Advances in the study of new potential treatment modalities for human lung cancer, can be attributed to the development of animal models for use in these investigations (Sharkey & Fogh, 1984). Athymic nude mouse models have been extensively used for the *in vivo* propagation and study of human pulmonary cancers as well as models for therapeutic intervention. In order to assess the ability of the NSCLC H358a cell line to develop as an *in vivo* nude mouse xenograph, H358a cell suspensions were injected subcutaneously into the mice, and monitored for tumour development. As with previous studies (Fujiwara *et al*, 1994b; Quazilbash *et al*, 1997), H358a tumours developed approximately 2-3 weeks following injection, and continued to grow and proliferate exponentially. Pathological examination of excised tumours indicated the presence of both apoptotic and oncotic necrosis towards the centre of the tumour mass, particularly at the latter stages of tumour growth. This suggested that tumour cell proliferation surpassed the provision of an adequate blood supply, causing cells at the centre of the tumour to undergo cell death due to hypoxia or limiting nutrient supplies (Shweiki *et al*, 1995).

H358 tumour cells have been extensively characterised as a human adenocarcinoma of bronchioalveolar origin (Gazdar *et al*, 1990). The presence of

cytoplasmic cytokeratin proteins (Moll *et al*, 1982) and the bronchioalveolar carcinoma marker, CA-19-9 (Gatalica & Miettinen, 1994), further confirmed this characterisation. The *p53* status of this NSCLC cell line has been previously demonstrated (Takahashi *et al*, 1989; G. M. Glasgow, *personal communication*).

Due to low rSFV virus infection efficiencies for the NSCLC cell line *in vitro* (*see Chapter 3*), and the relatively stringent volume restrictions for direct intratumoural injection, rSFV particle batches were prepared at maximum titre (10^9-10^{10} I.U./ml). This was achieved using a larger, modified rSFV virus particle production procedure, encompassing a series of ultracentrifugation and resuspension steps. The virus was resuspended in a TNE buffer solution at the end of the preparation procedure and was used as the transport medium for intratumoural rSFV particle injections. This obviated any adverse reactions *in vivo*, to the mileu of ingredients contained in normal cell growth medium.

Based on previous NSCLC xenograft studies (Fujiwara *et al*, 1994a, b), tumours of 4 mm diameter were chosen as optimal for therapeutic intervention. Mice received direct intratumoural injections of 50 µl rSFV particles, based upon the size of the tumour, and contained over 5 x 10^8 I.U. per injection. EGFP-expressing rSFV particles were used exclusively, to facilitate detection of the vector *in situ*. Control mice received equal volumes of TNE buffer alone.

rSFV virus-mediated tumour growth inhibition *in vivo* was shown to be dose-related. A total of three injections of rSFV-EGFP particles significantly suppressed H358a tumour growth for up to 30 days following treatment. However, at time-points later than 25-30 days, the treated tumours began to show signs of regrowth. A second cycle of rSFV virus treatment, with three injections per cycle, produced much greater inhibitory effects, suppressing tumour growth by up to 95% of TNE buffer-treated controls, and induced complete tumour

regression in almost 50% of treated mice, when maintained for over 3.5 months after initial treatment. Also, tumours from all remaining mice existed only as minute nodules, which failed to show any signs of regrowth throughout the analysis.

The growth suppressive effects of a single intratumoural injection were not assessed for tumour growth rate experiments, as Asselin-Paturel *et al*, (1998) showed that rSFV-LacZ virus particles failed to have a significant antitumoural effect in a murine tumour xenograft after a single injection, without the addition of exogenous interleukin-12 expression, and its associated anti-angiogenic effects. This, and the fact that other viral vector-based cancer therapy studies used three to six intratumoural injections to achieve tumour growth inhibitory effects (Hamada *et al*, 1996; Fujiwara *et al*, 1994b), prompted us to best assess the feasibility of rSFV-EGFP virus-mediated tumour growth inhibition *in vivo* using multiple intratumoural injections.

Previous studies with the H358a xenograft model using other non-cytopathic recombinant viral vectors (Fujiwara *et al*, 1994a; Fujiwara *et al*, 1994b; Quazilbash *et al*, 1997), facilitated tumour regression only by wild-type *p53* transduction methods, and all failed to induce complete tumour regression, at later time-points after treatment, compared with rSFV particles in this study.

Tumours which received one rSFV virus intratumoural injection were studied for pathological changes in contrast to TNE-treated controls. Histological and TUNEL analyses indicated massive induction of apoptosis within rSFV virus-treated tissue as early as 24 h post-treatment, and persisted for 72 h. This correlated precisely with rSFV-induced apoptosis within H358a cells in culture, in Chapter 3. However, the low infection efficiency of rSFV virus particles for H358a cells *in vitro* and the large extent of oncotic necrosis and infiltration of inflammatory cells, observed from day 4 onwards in rSFV virus-treated tissue,

indicate that rSFV infection and apoptosis induction alone, cannot be responsible for tumour cell death and regression. One possible explanation for this extensive tumour death and regression involves an initial rSFV virus-induced apoptotic response during the early stages following infection, within the treated tissue. This response is enhanced due to the local nature of rSFV virus treatment, and persists for 3 days. The large necrotic regions observed at later timepoints may be due to an effect on tumour angiogenesis. rSFV virus particles may have infected and induced apoptosis in vascular endothelial cells, followed by disruption of vascular function and a reduction in tumour blood supply. Cell debris and inflammation increase due to the large extent of hypoxia-induced necrosis, which increased the extent of lymphoid and neutrophilic infiltration. It is unlikely that tumour regression was mediated exclusively by immune-mediated mechanisms, due to the limited immunogenicity of the rSFV vector system, the types of immune cells observed and the limited immune responses in the nude mouse.

A second possible explanation for the complete tumour regression observed following rSFV virus treatment, is 'bystander killing'. Bystander effects are operative when rSFV-infected H358a cells inhibit growth and induce apoptosis in non-transduced neighbouring H358a cells. A bystander effect in wild-type *p53*- transduced lung cancer cells, have been previously demonstrated both in culture and in *in vivo* applications, for both retroviral and adeno-associated viral apoptotic gene therapy (Cai *et al*, 1993, Quazilbash *et al*, 1997). Suggested mechanisms for this potentially valuable phenomenon include 'metabolic cooperation' via gap junctions (Mesnil *et al*, 1996; Xu *et al*, 1997) and endocytosis of apoptotic bodies (Freeman *et al*, 1993).

The possibility that rSFV virus administration was toxic to normal cells surrounding the tumour is remote, given that no gross lesions or side-effects were

observed following resection of the rSFV virus-treated tumours, indicating a favourable advantage of the rSFV system for tumour treatment. Using EGFP expression to detect the vector *in situ*, it was demonstrated that rSFV particles were present and functional within treated tumour tissue as early as 16 h p.i., and persisted for 3 days only. The limited persistence of rSFV particles *in vivo*, proves advantageous for transient apoptotic gene therapy, eliminating both transduced cells and viral RNA rapidly from the treated tissue, in comparison to non-cytopathic retroviral and adeno-associated viral vectors, which persist within transduced cells following integration of viral DNA into the host cell genome. The persistence and distribution of the rSFV vector has been extensively investigated, using both immunocompetent mice and chickens. Morris-Downes *et al*, (2000), indicated that rSFV-EGFP particles were detected at the injection site of the tibilias anterior (TA) muscle of immunocompetent mice from 2 h to 24 h, using RT-PCR analysis, and up to 72 h using direct epifluorescence for EGFP expression. This correlated precisely with EGFP expression studies in the NSCLC tumours. Due to the episomal properties of rSFV particles, all of the input viral RNA following intratumoural injection with rSFV-EGFP virus, is presumably degraded rapidly following apoptosis induction and host cell death. Morris-Downes *et al*, (2000), also utilised RT-PCR and epifluorescence analyses to study the distribution of the particles from the site of injection, to other organs within the mice. rSFV particles were observed by epifluorescence at the injection site only (TA muscle), and by RT-PCR, in lymphoid organs up to 24 h p.i. only, but failed to disperse throughout other organs in the body. The limited persistence, cytotoxicity for surrounding normal tissues and the suicidal nature of rSFV vector system further accentuates the advantages of rSFV as a cancer therapy agent.

An additional advantage of rSFV-mediated cancer therapy was the relatively high tolerance observed for the vector following repeated injections.

The anti-tumoural effects of six rSFV virus intratumoural injections within the first 9 days of treatment was well tolerated by individual mice, and induced complete tumour regression. Although humoural immune responses towards repeated rSFV viral inoculations were not investigated, rSFV particles have been shown to induce a relatively low level of immune reactivity (Berglund *et al*, 1993), and are thus, well tolerated. This is in stark contrast to adenovirus vectors. One of the major pitfalls in adenovirus-induced apoptotic gene therapy is the profound adenovirus immunogenicity, as several studies have shown. Titres of anti-adenovirus antibodies rise in rhesus monkey plasma within 2 weeks following a single adenoviral inoculation (Zabner *et al*, 1994), suppressing adenovirus-mediated *LacZ* transgene expression (Engelhardt *et al*, 1994). The high levels of immunogenicity prohibits the use of repeated adenoviral intratumoural injections, a scenario which was not observed following repeated administration of rSFV particles, which displayed positive transgene expression at all analysed timepoints following injections. Cell-mediated anti-rSFV immunogenicity should be assessed using an immunocompetent mouse model.

Due to its localised action, negligible toxicity for surrounding tissues and lack of detection within other tissues, rSFV viral vector therapy poses as an ideal candidate for solid tumour therapy within patients with advanced NSCLC. A small number of NSCLC clinical trials, primarily using recombinant adenovirus and retrovirus systems to deliver exogenous wild-type *p53* have demonstrated sufficient levels of wild-type *p53* restoration, to mediate clinically significant tumour regression (Roth *et al*, 1996; Swisher *et al*, 1999). The clinical use of retroviruses is limited, due to difficulties in transducing non-replicating tumour cells, particularly within poorly vascularised tumours, and in producing high titres of virus. On the other hand, adenoviral vector efficiency is complicated by a

limited tolerance in patients and prior exposure to the virus, which may be underestimated in an immunocompromised nude mouse model.

This study indicates that rSFV viral vector treatment for NSCLC *in vivo*, is both extensive and successful, and possesses several advantages over previous viral vector delivery systems. Replacement of the *EGFP* reporter gene with wild-type *p53* at the SFV multicloning site, could only serve to enhance the pro-apoptotic abilities of the virus, particularly with reference to NSCLC, due to the high frequency of *p53* gene mutations.

Chapter 5

SFV-mediated overexpression of pro-apoptotic Bax further enhances the cytotoxic potential of the vector for treatment of apoptosis-resistant prostate cancer.

5.1 INTRODUCTION

A wide range of genetic alterations are associated with the development of prostate cancer (PCa) (Ozen & Pathak, 2000). The conversion of androgen-dependent to androgen-independent PCa has recently been shown to be due in part to mutations and overexpression of key genes involved in the regulation of apoptotic cell death (Berchem *et al*, 1995). Following androgen-ablation therapy, the anti-apoptotic protein Bcl-2 is upregulated, leading to a resistant population of PCa cells, and a disease that is rapidly fatal (McDonnell *et al*, 1992). Novel strategies to downregulate *Bcl-2* expression in PCa are now becoming attractive alternatives for cancer treatment.

In this study, a rat prostatic adenocarcinoma cell line, artificially transfected to overexpress the *Bcl-2* oncogene (Levine *et al*, 1993), is utilised as a model for apoptosis-resistant cancer therapy. This cell line, AT3-Bcl-2, was previously shown to resist apoptotic cell death following infection with both SV (Levine *et al*, 1993) and SFV (Scallan *et al*, 1997). Failure to undergo apoptosis was due to overexpression of the *Bcl-2* oncogene, as the *Bcl-2*-negative control cell line, AT3-Neo, rapidly succumbed to programmed cell death upon infection.

This study strengthens the potential of rSFV vector particles as a cytotoxic therapy agent. Recombinant *EGFP*-expressing SFV particles were shown to overcome *Bcl-2*-mediated cell death inhibitory effects in the AT3-Bcl-2 cell line following a 24-48 h delay, as was shown for the wild-type SFV virus, SFV-4. AT3-Bcl-2 cells underwent apoptotic cell death following infection with the vector *in vitro*, and also induced tumour growth inhibition in vivo, when injected into solid AT3 tumours.

Furthermore, this study introduces the rSFV vector as a valuable *gene* therapy agent for malignant disease. Cloning and rSFV particle-mediated overexpression of the pro-apoptotic protein Bax, known to counteract Bcl-2 activity *in vivo*, abolished *Bcl-2*-mediated inhibition of apoptotic cell death in AT3-Bcl-2 cells, inducing rapid apoptotic cell death, in comparison to the *EGFP*-expressing vector alone. The powerful cytotoxic potential of the *Bax*-expressing SFV vector must be further developed and enhanced as a cytotoxic cancer gene therapy agent for the elimination of more apoptosis-resistant malignancies.

5.2 EXPERIMENTAL PROCEDURES

5.2.1 MATERIALS

5.2.1.1 *Cell Lines*

HL-60 human leukemia cell line was a gift from Prof. T. Cotter (Biochemistry Dept., NUI, Cork, Ireland). The rat prostatic adenocarcinoma cell lines, AT3-Neo and AT3-Bcl2, were a gift from Dr. J. Fazakerley, (Department of Veterinary Pathology, University of Edinburgh, Edinburgh, Scotland). NCI-H520 squamous cell carcinoma, NCI-H596 adenosquamous carcinoma and NCI-H460 large cell lung carcinoma cell lines were from ATCC.

5.2.1.2 *Expression Vectors*

The pSG5-Bax and pSG5-HABax (Hyc185) plasmids containing the *Bax* gene and *HABax* fusion protein genes respectively, were a gift from Dr. J. M. Hardwick (Department of Neurology, John Hopkins University School of Medicine, Maryland, USA).

5.2.1.3 *Molecular Biology Reagents*

Primers used for PCR amplification were from MWG Biotech AG (Germany). Thermosequenase sequencing kits were from Amersham Pharmacia Biotech (Uppsala, Sweden).

5.2.1.4 *Antibodies*

Monoclonal anti-human Bcl-2 oncoprotein antibody was obtained from DAKO (Glostrop, Denmark). Polyclonal antibodies against human Bax protein was obtained from Oncogene Research products (Nottingham, UK). Monoclonal high affinity anti-haemagglutinin (HA) Tag was from Boehringer Mannheim (GmbH, Mannheim, Germany). Rabbit anti-mouse IgG FITC conjugate was from DAKO. Goat anti-rabbit and rabbit anti-mouse IgG peroxidase conjugates were from Vector laboratories Inc. (Burlingame, CA, USA). Goat and rabbit serum were from Vector laboratories Inc. and Sigma (St. Louis, MO, USA).

5.2.2 METHODS

5.2.2.1 Cell Culture

Rat prostatic adenocarcinoma cells AT3-Neo and AT3-Bcl2, were cultured in RPMI-1640 medium supplemented with 10% (v/v) FCS, 200 mM L-glutamine, 100 U/ml penicillin and 100 µg/ml streptomycin, and maintained at 37°C in a humidified atmosphere of 5% CO_2, in 25 and 75 cm^2 flasks. Cells were seeded at 1 x 10^5 ml^{-1} for growing, in a total volume of 6 ml (25 cm^2 flask) or 15 ml (75 cm^2 flask). Medium was replaced daily

5.2.2.2 Virus

The production of wild-type SFV-4 virus was described in section 2.2.2.2. SFV-4 virus titres of between 1 and 5 x 10^9 pfu/ml were routinely obtained. Virus at 10^4 pfu/ml was used to infect cell lines, as described in section 2.2.2.2.

5.2.2.3 SFV-Bax cloning

A strategy for cloning of the *Bax* protein gene into the SFV expression vector, pSFV-1, was designed using the unique *Xmal* restiction site in the pSFV-1 MCS. This strategy is illustrated in Figure 5.1. To facilitate cloning, the *Bax* gene located within the pSG5-Bax vector, was firstly sequenced to facilitate specific primer design, amplification, cloning and expression of the Bax protein.

***Figure 5.1*- Construction of the pSFV1-Bax-α expression clone.**

The Bax-α gene was sequenced directly from the pSG5-Bax plasmid, using primers specific for the pSG5 plasmid backbone, 5' and 3' of the *Bax-α* gene. The *Bax-α* fragment was then PCR-amplified from the pSG5-Bax plasmid, using primers specific for the 5' region of *Bax-α* and a 3' region, downstream of the *Bax-α* gene sequence. This PCR product was cloned into the MCS of the SFV expression vector, pSFV1, using the unique *Xma1* restriction site. Primers for sequencing are indicated by dashed red arrows. Primers for cloning are indicated by full red arrows.

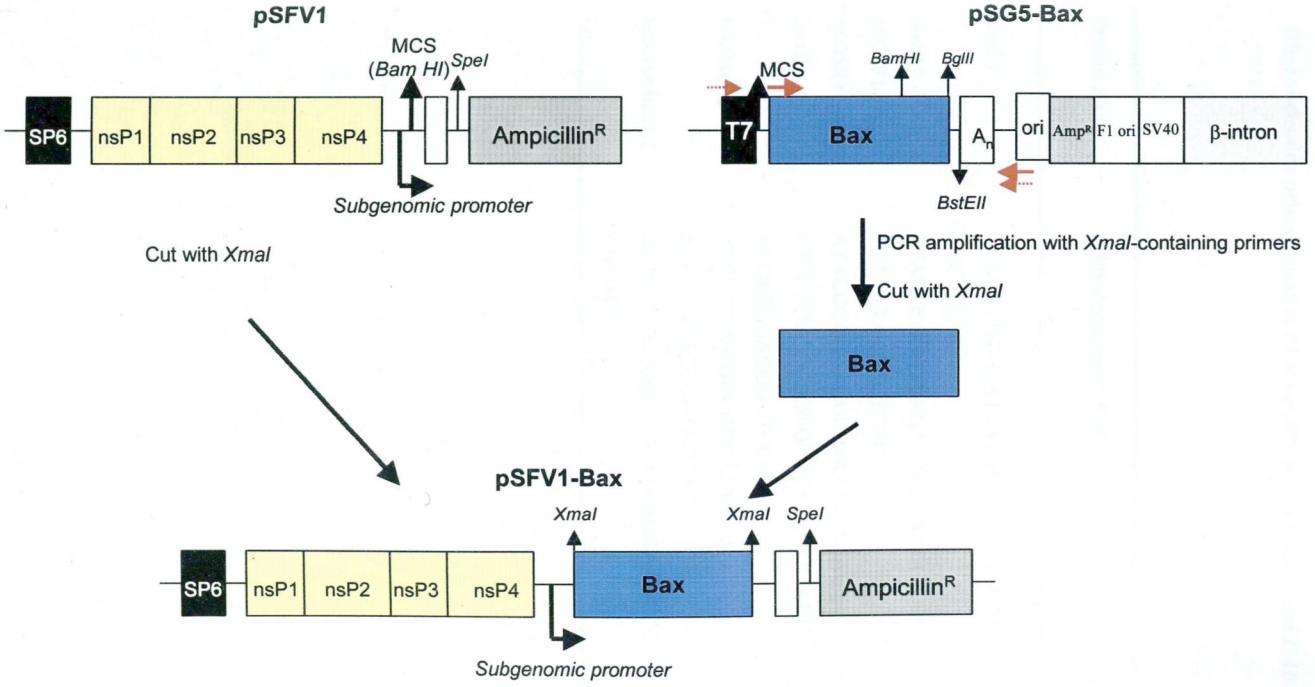


Figure 5.1- Construction of pSFV1-Bax-α expression clone

Table 5.1

Oligonucleotide primers used in PCR amplification of *Bax-α* and *HABax-α*

Primer name	Primer sequence: 5'-3'
BaxF1	ATACCCGGGTATTATAGCACCATGGAC GGGTCCGGG
BaxR1	ATACCCGGGTCAGACACGTAAGGAAA
pSG5F1	TGTAATACGACTCAC
pSG5R1	ATACCCGGGAGGAAGCGGAAGAGT
BaxF2	GTTCCCCCCGGGGGGACTTATTATAGC ACCATGGACGGGTCCGGG
HABaxF2	GTTCCCCCCGGGGGGACTTATTATAGC ACCATGTACCCATACGAT
Bax/HABaxR2	ACTCCCCCCGGGGGGATCAGGAAGCGG AAGAGT

5.2.2.3.1 *Bax sequence analysis*

For DNA sequencing, bacterial colonies transformed with the pSG5-Bax plasmid were grown in 10 ml L broth, supplemented with 100 μg/ml ampicillin, shaking at 70*g*, for 16 h at 37°C. The bacteria were centrifuged at 2000*g* for 10 min and plasmid DNA was isolated from the bacterial cell pellet, using the *Qiagen miniprep* procedure. To facilitate sequencing of the *Bax* gene from pSG5-Bax plasmid, forward and reverse primers (pSG5F1 and pSG5R1) (*Table 5.1* and *Figure 5.1*) were designed to anneal to sequences within the pSG5 vector backbone, flanking the MCS in which the *Bax* gene was located. Sequencing reactions were performed using Thermosequenase *dye terminator sequencing* kit and were performed using an automated thermal cycler and ABI 373A automated DNA sequencer. The sequence was viewed as a computer-generated colour-coded chromatograph. Both strands of DNA were sequenced in three independent reactions and a consensus sequence obtained and compared to *Bax* gene sequences present in GenBank.

5.2.2.3.2 *DNA Amplification*

To facilitate cloning of *Bax* into the pSFV-1 vector, the forward primer was designed, following sequence analysis, to include the first 15 nucleotides of the *Bax* gene (*Table 5.1*). In addition, this primer also incorporated the native SFV RBS sequence, and both forward and reverse primers contained an *XmaI* restiction site, to facilitate ligation with pSFV-1 plasmid. The sequence of the reverse primer includes 15 nucleotides of the pSG5 vector backbone downstream of the *Bax* sequence. The sequence of primers used in *Bax* amplification are as follows, with the *XmaI* sites in *italics*, the RBS sequence underlined, and the *Bax* start codon in bold :

BaxF2 5'-GTTCCC*CCCGGG*GGGACTTATTATAGCACC**ATG**GACGGGTCCGGG-3'

BaxR2 3'-ACTCCC*CCCGGG*GGGATCAGGAAGCGGAAGAGT-5'

Standard PCR reaction mixtures contained 1.5 mM $MgCl_2$, 1X thermophillic DNA polymerase, 200 µM each of dATP, dCTP, dGTP and dTTP, and 0.5 µM each of forward and reverse primers, and 0.5-1.0 µg DNA template. The reaction was performed in an automated DNA thermal cycler, programmed for 30 cycles of denaturation at 96°C for 1 min, annealing at 55°C for 1 min and polymerisation at 72°C for 1.5 min. The final cycle included a polymerisation step at 72°C for 10 min. The reaction always included a 96°C 'hotstart' for 10 min, before the addition of 2.5 U *Taq* polymerase. PCR products were analysed by electrophoresis of a 2 µl aliquot on a 0.8% (w/v) agarose gel (*Figure 5.2*).

5.2.2.3.3 *Preparation of Bax insert*

Following PCR amplification, the 745 bp *Bax* fragment was purified using the Qiagen *PCR purification* and *gel extraction* kits, eluted in 30 µl sterile dH_2O, and digested with *XmaI* to create the necessary 'sticky' ends. These digestion reactions were pooled and further purified using the Qiagen *nucleotide removal* procedure. Inserts were analysed by electrophoresis of a 2 µl aliquot on a 0.8% (w/v) agarose gel (*Figure 5.3*).

5.2.2.3.4 *Preparation of the SFV expression vector*

The 11.3 kbp plasmid pSFV-1 vector contains a MCS (*BamH1-Xma1-Sma1*), for use in the construction of recombinant plasmids, and an ampicillin resistance site for bacterial screening. Prior to cloning, pSFV1 *midi-prep* plasmid was linearised with *XmaI*, and purified using the Qiagen *nucleotide removal* kit. The plasmid was analysed by electrophoresis of a 2 µl aliquot on a 0.8% (w/v) agarose gel (*Figure 5.3*).

Figure 5.2- **PCR amplification of *HABax* and *Bax* gene constructs from pSG5-HABax and pSG5-Bax plasmids, respectively.** Primers were designed to amplify *HABax* and *Bax* sequences directly from the pSG5 plasmid backbone. PCR products were run on a 0.8% (w/v) agarose gel, stained with ethidium bromide. *Lanes 1 and 5*; 200bp ladder. *Lane 2;* 848 bp *HABax* PCR product. *Lane3*; 798 bp *Bax* PCR product. *Lane 4*; negative PCR control.

Figure 5.3- **Preparation of *HABax* and *Bax* gene fragments for ligation with the pSFV-1 expression vector.** PCR-amplified *HABax* and *Bax* gene fragments were digested with *Xma1*and cleaned using the Qiagen *nucleotide removal* procedure. The pSFV-1 plasmid was also digested and cleaned prior to cloning. Fragments were run on a 0.8% (w/v) agarose gel, prior to cloning. *Lane 1*; *Xma1*-digested *HABax* PCR fragment. *Lane 2*; *Xma1*-digested *Bax* PCR fragment. *Lane 3*; 200 bp DNA ladder. *Lane 4*; *Lambda* (*Hind 111*) DNA molecular weight markers. *Lane 5*; *Xma1*-digested pSFV-1 plasmid expression vector.

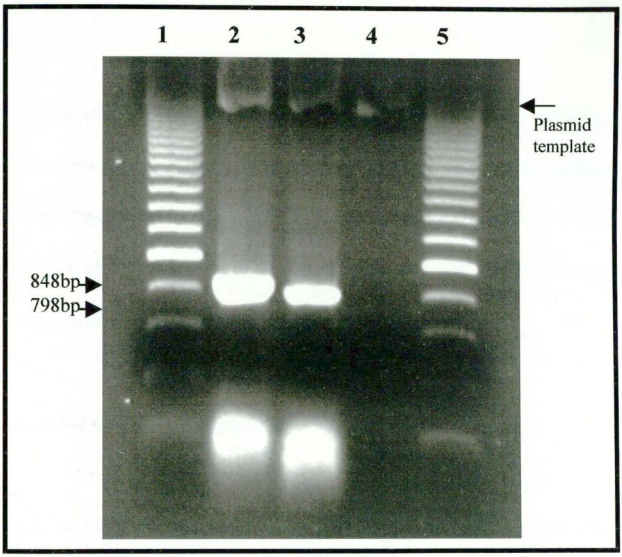


Figure 5.2- PCR amplification of HABax and Bax constructs from pSG5-HABax and pSG5-Bax plasmids, respectively.

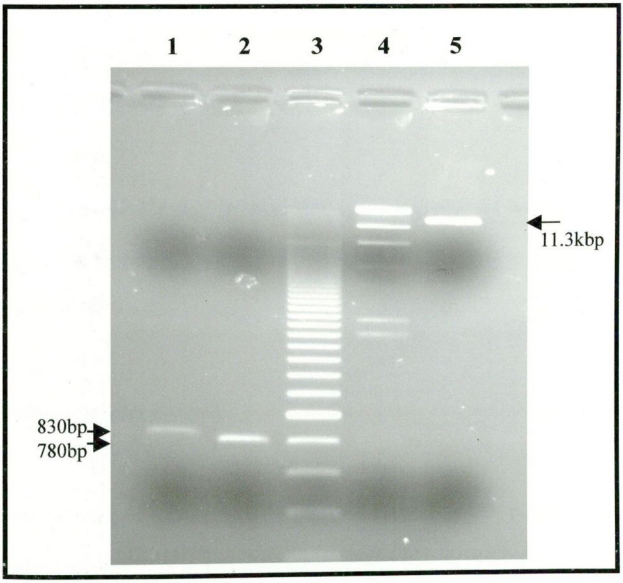


Figure 5.3- Preparation of HABax and Bax gene fragments for ligation with the pSFV-1 expression vector.

5.2.2.3.5 *DNA Ligation*

Ligation of the linearised pSFV-1 vector to the purified *Bax* gene PCR product was carried out at a ratio of 1 :10 vector to insert. A ligation mixture containing approximately 30 µl of *Bax* PCR fragment and 3 µl of pSFV-1, were combined in a total volume of 50 µl, including 5 µl high efficiency T4 DNA ligase buffer and 500U T4 DNA ligase. The ligation mix was incubated overnight at 18°C.

5.2.2.3.6 *Screening for recombinant pSFV1-Bax plasmids.*

The presence of pSFV-Baxα recombinants was performed using the rapid colony screening procedure, followed by restriction digestion with *XmaI* and *BamHI* , as described in sections 2.2.2.5.7.1-2.

5.2.2.4 SFV-HABax cloning

A strategy for cloning the *HA-Bax* fusion protein genes into pSFV-1 was designed using the unique *XmaI* site in the pSFV-1 MCS. This strategy is illustrated in Figure 5.4 and is identical to that of pSFV1-Bax cloning.

5.2.2.4.1 *HABax sequence analysis*

To facilitate sequencing of *HABax* from the pSG5-HABax (Hyc185) plasmid, forward and reverse primers were designed to anneal to sequences in the pSG5 vector backbone, flanking the 5' and 3' ends of the MCS, in which the *HABax* was located. Sequencing reactions were performed as described in section 5.2.2.3.1. Both strands of DNA were

***Figure 5.4*- Construction of the pSFV1-HABax-α expression clone.**

The HA-Bax-α genes were sequenced directly from the pSG5-HABax plasmid, using primers specific for the pSG5 plasmid backbone, 5' and 3' of the *HABax-α* genes. The *HABax-α* fragment was then PCR-amplified from the pSG5-HABax plasmid, using primers specific for the 5' region of the *HA* epitope and a 3' region, downstream of the *Bax-α* sequence. This PCR product was cloned into the MCS of the SFV expression vector, pSFV1, using the unique *Xma1* restriction site. Primers for sequencing are indicated by dashed red arrows. Primers for cloning are indicated by full red arrows.

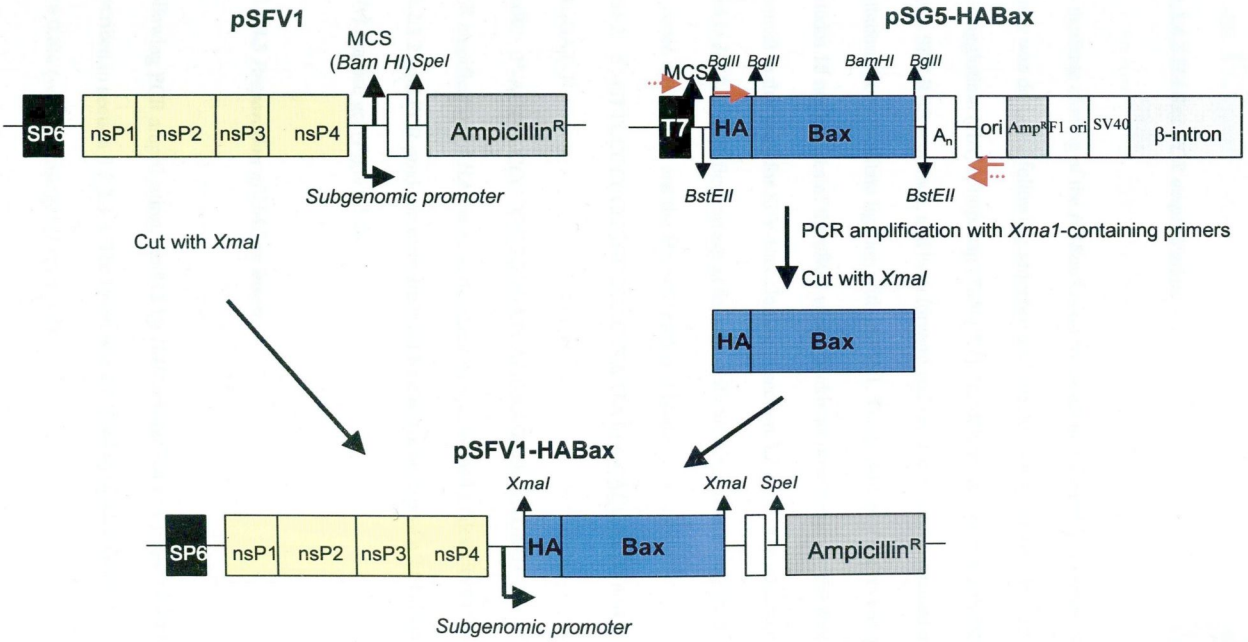


Figure 5.4- Construction of pSFV1-HABax expression clone

sequenced in three independent reactions, and a consensus sequence obtained and compared to *HA epitope* and *Bax* gene sequences in GenBank.

5.2.2.4.2 *HABax PCR amplification*

To facilitate cloning of the *HABax* fusion construct into the pSFV-1 vector, the forward primer was designed following sequence analysis, to include the first 15 nucleotides of the haemagglutinin (HA) epitope tag (*Table 5.1*). In addition, this primer also incorporated the native SFV RBS sequence, and both forward and reverse primers contained an *XmaI* restiction site to facilitate ligation with pSFV-1. The sequence of the reverse primer includes 15 nucleotides of the pSG5 vector backbone downstream of the *Bax* sequence, identical to that used for SFV-Bax cloning in section 5.2.2.3.2. The sequence of primers used in *HABax* amplification are as follows, with the *XmaI* sites in italics, the RBS sequence underlined, and the HA start codon in bold:

BaxF2 5'-GTTCCC*CCCGGG*GGGACTTATTATAGCACC**ATG**TACCCA TACGAT-3'

BaxR2 3'-ACTCCC*CCCGGG*GGGATCAGGAAGCGGAAGAGT-5'

PCR ampification of *HABax* gene fragment was performed as described in section 5.2.2.3.2, and PCR products were analysed by electrophoresis of a 2 µl aliquot on a 0.8% (w/v) agarose gel (*Figure 5.2*).

5.2.2.4.3 *Preparation of HABax insert*

Following PCR ampification, the 812 bp *HABax* fragment was prepared for ligation, as described in section 5.2.2.3.3. The insert was analysed by electrophoresis of a 2 µl aliquot on a 0.8% (w/v) agarose gel (*Figure 5.3*).

5.2.2.4.4 *Screening for recombinant plasmids*

Screening for recombinant plasmids was carried out initially by the rapid colony screening procedure outlined in section 5.2.2.3.8.1. The presence of pSFV1-HABax recombinant plasmids were confirmed by *XmaI* and *BamHI* restriction digests of plasmid DNA, as described in section 5.2.2.3.8.2.

5.2.2.5 Detection of expression

5.2.2.5.1 *In vitro SP6 RNA transcription*

For the production of recombinant viral RNA from the recombinant pSFV1-Bax and pSFV1-HABax plasmids, 20 µg plasmid DNA was first linearised with *SpeI* restriction enzyme, at 37°C for 18 h. Following linearisation, plasmid DNA was purified by phenol precipitation and ether extraction as described in section 2.2.2.7.2. 1.5 µg linearised SFV plasmid DNA was used to initiate *in vitro* RNA transcription from each of the clones, in total reaction volumes of 20 µl each, as described in section 2.2.2.7.3. Transcripts were analysed by electrophoresis on 0.6% (w/v) agarose gels (*Figure 5.5* and *Figure 5.6*).

5.2.2.5.2 *Electroporation*

BHK-21 cells were electroporated with putative positive SFV1-Bax and SFV1-HABax RNA, as described in section 2.2.2.6.2. Negative electroporation controls, using PBS alone, were also prepared. Cells were maintained at 37°C, 5% CO_2 for 10-18h or until cytopathic effect was evident.

***Figure 5.5- In vitro* transcription of recombinant pSFV1-Baxα clones by SP6 RNA polymerase.** 0.6% (w/v) agarose gel, stained with ethidium bromide. *Lanes 1 and 6*; *Lambda* (*Hind111* & *EcoR1*) DNA molecular weight marker. *Lanes 2-3*; 0.5 μl and 1.0 μl, each of *in vitro*- transcribed RNA from putative recombinant pSFV1-Baxα clone #15. *Lanes 4-5*; 0.5 μl and 1.0 μl each, of *in vitro*-transcribed putative recombinant pSFV1-Baxα clone #21.

***Figure 5.6- In vitro* transcription of recombinant pSFV1-HABaxα clones by SP6 RNA polymerase.** 0.6% (w/v) agarose gel, stained with ethidium bromide. *Lane 1*: *Lambda* (*Hind111* & *EcoR1*) DNA molecular weight marker. *Lanes 2 to 5*: *in vitro*-transcribed RNA from putative recombinant pSFV1-HABaxα clones #1 (*Lane2*), #6 (*Lane 3*), #21 (*Lane 4*) and #29 (*Lane 5*). An arrow indicates the *Spe1*-linearised plasmid DNA template.

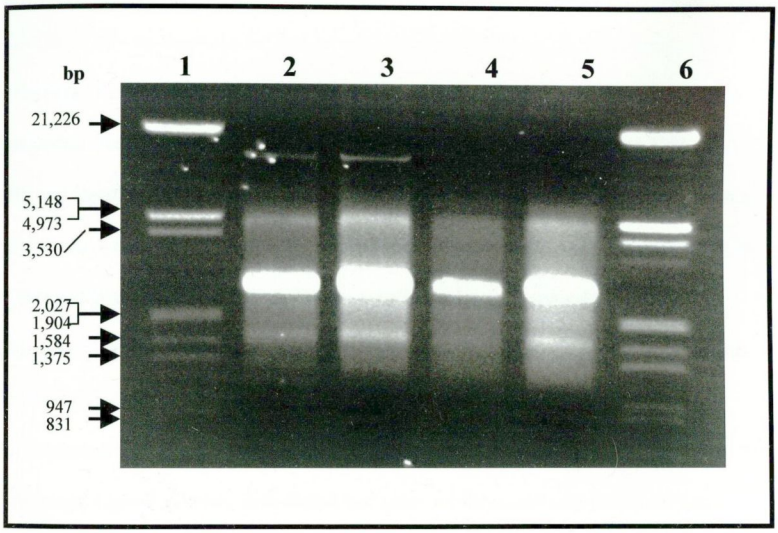


Figure 5.5- ***In vitro*** **transcription of pSFV1-Baxα clones by SP6 RNA polymerase.**

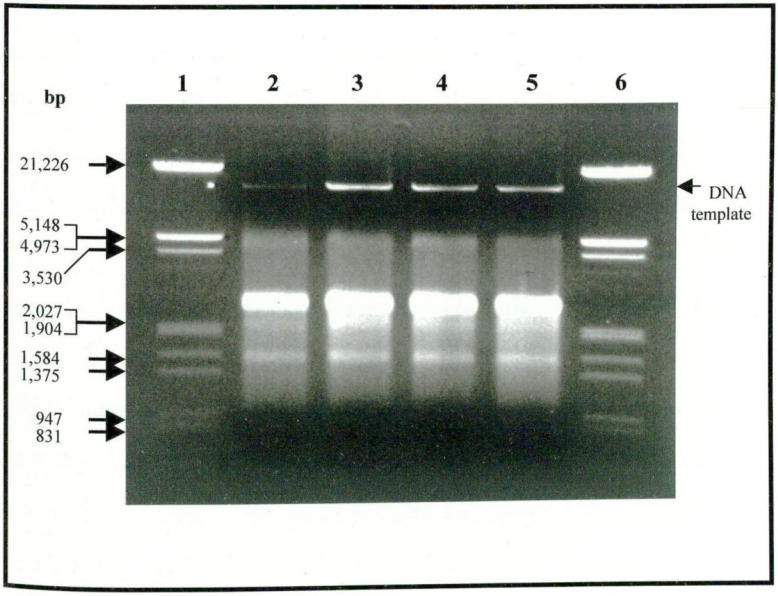


Figure 5.6- ***In vitro*** **transcription of pSFV1-HABaxα clones by Sp6 RNA polymerase.**

5.2.2.5.3 *Detection of SFV-Bax by Immunocytochemistry*

Following 16 h incubation, electroporation control cells and cells transfected with RNA transcribed from putative positive pSFV-Bax clone, SFV-Bax, were fixed in 10% (v/v) NBF and incubated with 1 mg/ml normal goat antiserum, followed by 1 h at 37°C with a 1 :5 dilution of rabbit anti-human Bax polyclonal antibody. Cells were washed in PBS for 10 min and incubated for a further 30 min at 25°C with a goat anti-rabbit, biotin-conjugated antibody. Cells were washed in PBS and incubated for a further 30 min with the Vectastain *Elite* Avidin-Biotin complex (ABC), washed and incubated with diaminobenzidine (DAB) substrate for a further 2 min. Cells were counterstained with 5% (w/v) methyl green solution, dehydrated in a series of N-butanol and xylene washes, and mounted onto glass slides using DPX. Cells were examined by light microscopy, for the presence of Bax-specific DAB staining. For the detection of Bax expression in the *Bax*-null leukemia cell line, HL-60, cells were incubated in suspension until ~80% confluent and resuspended in 1 ml infection medium, containing recombinant rSFV-Bax virus particles (*see section 5.2.2.6*). At 18 h p.i., HL-60 cells were cytospun onto glass slides at 700*g*, fixed in acetone and stained with rabbit anti-human Bax antibody as above. Cells were counterstained with methyl green and expression visualised using light microscopy.

5.2.2.5.4 *Detection of SFV-HABax by immunocytochemistry*

Following 16 h incubation, negative electroporation control cells and cells transfected with RNA transcribed from putative positive pSFV-HABax clones, SFV-HABax, were fixed in 10% (v/v) NBF, and incubated with 1 mg/ml normal rabbit antiserum, followed by 1 h at 37°C with a 1:10 dilution of rat anti-haemagglutinin epitope tag antibody. Cells were washed in PBS for 10 min and incubated for a further 30 min at 25°C, with a rabbit anti-rat biotin-conjugated antibody. Cells were washed in PBS and incubated for a further

30 min with the Vectastain *Elite* ABC complex, followed by a 2 min incubation with DAB substrate. Cells were counterstained with 5% (w/v) methyl green solution for 10 min, dehydrated as before and mounted using DPX. Cells were examined using light microscopy, for the presence of HA epitope-specific DAB staining.

5.2.2.6 Production of rSFV-HABax virus particles

Recombinant SFV-HABax particle production was performed, using an identical preocedure to rSFV-EGFP particle production, as described in section 2.2.2.7. Equimolar amounts of SFV-HABax, SFV-Helper S2 and SFV-Helper CS219A *in vitro*-transcribed RNAs were electroporated into BHK-21 cells as described in sections 2.2.2.7.3-2.2.2.7.4. Cells were incubated at 33° or 37°C, 5% CO_2 for 10 h, 14 h, 24 h or 36 h p.e. Particles within the supernatant were centrifuged at 700*g* for 15 min, aliquoted and rapidly frozen in ethanol-dry ice solution, before storing at -70°C. rSFV-HABax virus particles were titrated by infecting ~80% confluent sBHK cell monolayers grown on 18 x 18mm glass coverslips, with serial dilutions of rSFV-HABax, as described in section 2.2.2.7.5. The coverslips were fixed in 10% (v/v) NBF, and incubated with rat anti-HA epitope Tag and rabbit anti-rat, biotin-conjugated antiseum, as described in section 5.2.2.5.4. Cells were examined microscopically for the presence of specific DAB staining, and titres (I.U./ml) were calculated at a magnification of x400.

5.2.2.7 High titre rSFV virus particle production

To achieve an enhanced response to treatment, and a greater cytocidal effect within tumour tissue, it was necessary to produce both rSFV-EGFP and rSFV-HABax virus particles of up to 10-fold higher concentrations, than for *in vitro* experiments. The

production of recombinant, encapsidated SFV particles of high titre for *in vivo* experiments proceeded as described in section 4.2.2.4. rSFV-HABax particles were produced at 33°C instead of 37°C.

5.2.2.8 Bcl-2 expression determined using immunocytochemistry

Both NSCLC and AT3 tumour cells were grown on glass coverslips, in 6 well plates until ~90% confluent. The cells were washed with PBS and fixed in acetone, for 30 min. Acetone was removed and cells were washed with dH_2O and PBS and blocked with 0.1 mg/ml normal rabbit serum, for 20 min. Cells were immediately incubated with mouse anti-human Bcl-2 oncoprotein antibody (1 :20 dilution), in a dark humidified chamber, for 1 h at 37°C,. The cells were washed with PBS and the rabbit anti-mouse FITC-conjugated secondary antibody added (1 :20 dilution). Following a 30 min incubation, cells were washed with PBS containing 0.25% (w/v) Tween solution, and PBS alone, before mounting onto glass slides with Mowiol/DABCO solution. FITC-specific expression of Bcl-2 oncoprotein was visualised by fluorescent microscopy, at 460 nm. Negative controls included AT3-Bcl-2 cells, incubated either with or without primary or secondary antibodies.

5.2.2.9 Calculation of rSFV virus infection efficiency

To determine the infection efficiency of rSFV virus particles in both AT3 cell lines, AT3-Neo and AT3-Bcl-2 cells were seeded at 1 x $10^4 ml^{-1}$ in 6-well plates and infected with rSFV-EGFP virus at a range of mois: moi 1-moi 1000, in a total volume of 500 µl infection medium for 1 hour, with rocking movements every 15 min. Infection medium alone was used in mock-infected controls. The cells were replenished with fresh RPMI-

1640 medium, and incubated at 37°C in a humidified atmosphere of 5% CO_2 for 18 h. Determination of rSFV-EGFP virus infection efficiency was performed using an identical method to that described in section 3.2.2.5. Each moi was calculated as a mean of triplicate samples.

5.2.2.10 Analysis of AT3 cell viability

To measure growth and cytotoxicity in cultured cells following infection with SFV-4 infectious virus and rSFV-EGFP, rSFV-1 and rSFV-HABax virus particles, both AT3-Neo and AT3-Bcl-2 cells were seeded at 1 x 10^4 ml^{-1} in 6-well plates (2 ml/well) prior to infection. Cells were infected at moi 500 rSFV-1 and rSFV-EGFP, and moi 100 rSFV-HABax virus particles, unless otherwise indicated, in a total volume of 500 µl infection medium. For recombinant SFV-HABax RNA transfection efficiency studies, both AT3-Neo and AT3-Bcl-2 cells were grown in 25 cm^2 flasks until ~80% confluent, trypsinised and electroporated with 50 µl *in vitro*-transcribed RNA, from either pSFV-EGFP or pSFV1-HABax clone #1 plasmids, as described in section 5.2.2.5.2. PBS alone was used as a mock electroporation control. Cells were resuspended in normal RPMI-1640 medium, plated onto 6-well dishes and incubated for the indicated time-points.

The viability of AT3-Neo and AT3-Bcl-2 cells following infection and transfection were determined by trypan blue, sulphorhodamine B and methyl-^{3}H thymidine incorporation studies, as described previously.Cells were analysed daily and each sample was performed and analysed in triplicate.

5.2.2.11 AT3 tumour formation *in vivo*

The cytotoxic effects of rSFV particles on AT3 cell growth, were analysed *in vivo* using a *nu/nu* mouse xenograph model. To assess the potential of a tumour xenograph model for AT3 cell tumour formation, and thus, rSFV virus-mediated cytocidal analysis, both AT3-Neo and AT3-Bcl-2 cells were harvested during the exponential phase of growth and injected subcutaneously (sc) into the right flank of each mouse, using a 1 ml syringe and 21G gauge needle, at a concentration of 5×10^5 cells/mouse, in 0.4 ml complete RPMI-1640 medium. Mice were examined daily for signs of sc tumour formation. Tumour diameters were measured using a sterile linear calipers, in 2 perpendicular directions, and tumour volume was calculated by assuming a spherical shape as described in section 4.2.2.2. A total of 10 mice were utilised for each cell line. Tumour diameters were measured every other day, over a period of 14 days to assess AT3 tumour formation and growth kinetics. Both AT3-Neo and AT3-Bcl-2 tumour-bearing mice were processed following 2 weeks of growth, or when tumour size reached 20% body weight, and processed for histological examination.

5.2.2.12 AT3 tumour histology

Histological analysis of AT3 tumour sections proceeded as described in section 4.2.2.3.

5.2.2.12.1 *Bcl-2 oncoprotein overexpression in vivo by immunocytochemistry*

For immunohistochemical analysis, AT3 tumour cryosections were stained for the presence of human Bcl-2 oncoprotein. Both AT3-Neo and AT3-Bcl-2 cryosections were fixed in acetone and stained for Bcl-2 oncoprotein, as described in section 5.2.2.8.

Negative controls included sections stained with and without 1° or 2° antibodies. Sections were observed using fluorescent microscopy, using a FITC-specific filter, at 460 nm.

5.2.2.13 rSFV-EGFP virus-mediated inhibition of AT3 tumour growth *in vivo*

To assess rSFV-EGFP virus particle-mediated inhibition of tumour growth *in vivo*, AT3-Neo and AT3-Bcl-2 cells were harvested at the exponential phase of growth, and 5 x 10^5, in 0.2 ml complete RPMI-1640 medium, were injected sc into the right flank of each mouse to form solid AT3-Neo and AT3-Bcl-2 tumour xenografts, respectively. Mice were examined daily for signs of sc tumour formation, and on reaching a diameter of 4 mm (approximately 4 days), 50-100µl TNE buffer alone or TNE containing rSFV-EGFP particles (1 x 10^{10} I.U. ml^{-1}), were injected intratumourally, using a 0.5 ml insulin syringe and 21G gauge needle. Mice received 6 intratumoural injections, each on days 1, 2, 3 and days 7, 8 and 9. Up to seven mice were used per treatment group. To assess the rate of tumour growth, tumours were measured every day for up to 14 days with sterile linear calipers, and tumour volume was calculated by assuming a spherical shape. At intervals following treatment, mice were selected randomly and harvested for pathology. Routine histology was performed on H&E stained, formalin-fixed, paraffin-embedded sections, and observed by light microscopy. EGFP expression was observed by direct epifluorescence on frozen AT3-Neo and AT3-Bcl-2 tumour cryosections at 488 nm, and TUNEL analysis was performed on 4% (w/v) paraformaldehyde-fixed cryosections. Apoptotic cells were observed by light microscopy.

5.2.2.14 rSFV-HABax virus-mediated inhibition of AT3 tumour growth *in vivo*

In an identical scenario to that described in section 5.2.2.14, AT3 tumours of 4 mm diameter were selected and received direct intratumoural injections of rSFV-HABax or rSFV-EGFP virus particles (5 x 10^6 I.U./ml), or TNE buffer as controls, each on days 1, 2, 3 and days 7, 8 and 9. Five mice were used per treatment group. To assess the rate of tumour growth, tumours were measured every day for up to 16 days with sterile linear calipers, and tumour volume was calculated by assuming a spherical shape. At intervals following treatment, mice were selected randomly and harvested for pathology as described above.

5.3 RESULTS

5.3.1 SFV-Bax cloning and expression

To facilitate the cloning of the *Bax-α* gene into the SFV expression system, pSFV-1, the gene was amplified from the pSG5-Bax plasmid using primers specific for 5' and 3' flanking regions within the pSG5 plasmid backbone (*Figure 5.1*). Attempts to amplify the *Bax-α* fragment directly, using consensus nucleotide sequences from Genbank, had failed (*not shown*). Both 5' and 3' primers were used to directly sequence the fragment in each orientation (*Figure 5.7*), compared to the consensus in GenBank (*Figure 5.8*), and utilised to design a *Bax-α-* specfic 5' primer for direct cloning into the pSFV-1 plasmid. The 5' primer incorporated the first 15 bp of the *Bax-α* gene and included the native SFV RBS, and an exogenous *XmaI* restiction enzyme site, for ligation with pSFV-1. The 3' primer also included an *XmaI* site and was specific for the *SalI* restriction site region within the pSG5 plasmid backbone, 174 bp downstream of the Bax-α sequence (*Table 5.1*). The resulting 798 bp PCR product was cloned into the SFV expression vector and the recombinant clones were screened using the rapid colony screening procedure (*Figure 5.9*). The presence of a 798 bp insert were confirmed by *XmaI* digestion of plasmid DNA, and the orientation of inserts was determined by *BamHI* digestion (*Figure 5.10*). Two clones were obtained, one in the correct orientation (clone pSFV1-Baxα #15), the other in the opposite orientation, (clone pSFV1-Baxα #21).

Expression of Bax protein from the SFV expression system was determined by ICC. *In vitro*-transcribed RNA from both pSFV1-Bax clones were electroporated into BHK-21 cells and incubated for 18 h. Cells were subsequently analysed for Bax overexpression using a rabbit anti-human Bax antibody and an anti-rabbit biotin-conjugated secondary antibody. The results are illustrated in figure 5.11. Heavy, brown DAB-positive staining

tag ggc gaa cct gat cac ggt cac cgt cca tcc atc caa atc ccg

amb g e p d h g h r p s i q i p

ATG GAC GGG TCC GGG GAG CAG CCC AGA GGC GGG GGG CCC ACC AGC TCT GAG CAG ATC ATG

M D G S G E Q P R G G G P T S S E Q I M

AAG ACA GGG GCC CTT TTG CTT CAG GGT TTC ATC CAG GAT CGA GCA GGG CGA ATG GGG GGG

K T G A L L L Q G F I Q D R A G R M G G

GAG GCA CCC GAG CTG GCC CTG GAC CCG GTG CCT CAG GAT GCG TCC ACC AAG AAG CTG AGC

E A P E L A L D P V P Q D A S T K K L S

GAG TGT CTC AAG CGC ATC GGG GAC GAA CTG GAC AGT AAC ATG GAG CTG CAG AGG ATG ATT

E C L K R I G D E L D S N M E L Q R M I

GCC GCC GTG GAC ACA GAC TCC CCC CGA GAG GTC TTT TTC CGA GTG GCA GCT GAC ATG TTT

A A V D T D S P R E V F F R V A A D M F

TCT GAC GGC AAC TTC AAC TGG GGC CGG GTT GTC GCC CTT TTC TAC TTT GCC AGC AAA CTG

S D G N F N W G R V V A L F Y F A S K L

GTG CTC AAG GCC CTG TGC ACC AAG GTG CCG GAA CTG ATC AGA ACC ATC ATG GGC TGG ACA

V L K A L C T K V P E L I R T I M G W T

TTG GAC TTC CTC CGG GAG CGG CTG TTG GGC TGG ATC CAA GAC CAG GGT GGT TGG GAC GGC

L D F L R E R L L G W I Q D Q G G W D G

CTC CTC TCC TAC TTT GGG ACG CCC ACG TGG CAG ACC GTG ACC ATC TTT GTG GCG GGA GTG

L L S Y F G T P T W Q T V T I F V A G V

CTC ACC GCC TCG CTC ACC ATC TGG AAG AAG ATG GGC TGA

L T A S L T I W K K M G *OPA*

Figure 5.7- Nucleotide and deduced amino acid sequence of human *Bax-α* from the pSG5-Bax plasmid. The *Bax-α* initiation methionine is indicated in red type face. Flanking pSG5 plasmid sequence is indicated in small type-face. For the cloning of Bax-α into pSFV-1, the 5' primer was chosen to include the first 15 nucleotides of the deduced *Bax-α* sequence. The 3' primer was specific for a region of the pSG5 vector backbone, downstream of *Bax* (*not shown*).

```
Bax (pSG5)   1 MDGSGEQPRGGGPTSSEQIMKTGALLLQGFIQDRAGRMGGEAPELALDPV
L22473       1 .....................................................
NM 004324    1 .....................................................

Bax (pSG5)  51 PQDASTKKLSECLKRIGDELDSNMELQRMIAAVDTDSPREVFFRVAADMF
L22473      51 .....................................................
NM 004324   51 .....................................................

Bax (pSG5) 101 SGNFNWGRVVALFYFASKLVLKALCTKVPELIRTIMGWTLDFLRERLLGWI
L22473     101 .....................................................
NM 004324  101 .....................................................

Bax (pSG5) 151 QDQGGWDGLLSYFGTPTWQTVTIFVAGVLTASLTIWKKMG----------
L22473     151 .....................................----------
NM 004324  151 ..... VRLLKPPHPHHRALTTAPAPPSLPPATPLGPWAFWSRSQWCPLPI

Bax (pSG5) 201 ----------------
L22473     201 ----------------
NM 004324  201 FRSSDVVYNAFSLRV
```

Figure 5.8 - Amino acid sequence alignment of the Bax-α protein with others from the database. L22473: Human Bax alpha mRNA, complete cds, NM 004324: *Homo sapiens* BCL2-associated X protein (Bax) mRNA.

Figure 5.9- **Screening for pSFV1-Baxα recombinant clones using the rapid colony screening.** Putative positive pSFV1-Baxα clones were initially screened by running plasmid DNA, isolated directly from transformed bacterial colonies, on 0.8% (w/v) agarose gels, stained with ethidium bromide. Plasmid DNA isolated from known pSFV-1 transformants were run alongside that of ligation transformants. *Lanes 1 and 30*; pSFV-1 vector only transformants. *Lanes 2-29*; plasmid DNA isolated from ligation transfomants. *Lanes 16* (clone #15) and *22* (clone #21) contain plasmid DNA that is of a slightly higher molecular weight that pSFV-1 plasmid DNA, and thus, may contain the recombinant plasmid.

Figure 5.10- **Screening for recombinant pSFV1-Baxα clones by restriction digestion.** Putative positive colonies as determined by rapid colony screening were subjected to restriction analysis with *Xma1* to confirm the presence of 798 bp *Bax-α* gene inserts. *Lane 1*; pSFV1 vector; digested with *Xma1*. *Lanes 2-3*; recombinant clones #15 (*Lane 2*) and #21 (*Lane 3*); digested with *Xma1*. Note presence of 798 bp Bax-α insert. *Lane 4*; 200bp ladder. Recombinant plasmids were subsequently digested with *BamH1* to confirm orientation of inserts. *Lane 5*; pSFV1 vector; digested with *BamH1*. *Lane 6*; clone #15; digested with *BamH1*, with an insert in the correct orientation (473 bp). *Lane 7*; clone #21; digested with *BamH1*, with an insert in the incorrect orientation (307 bp). Digested plasmids were run on a 0.8% (w/v) agarose gel, stained with ethidium bromide.

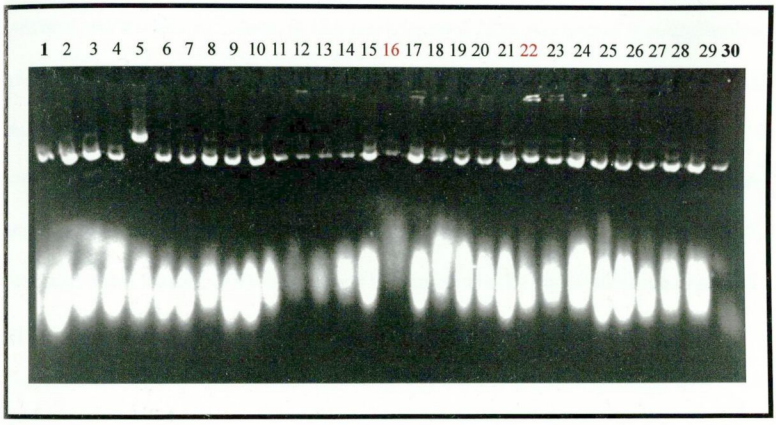


Figure 5.9- Screening for recombinant pSFV1-Baxα clones using the rapid colony screening procedure.

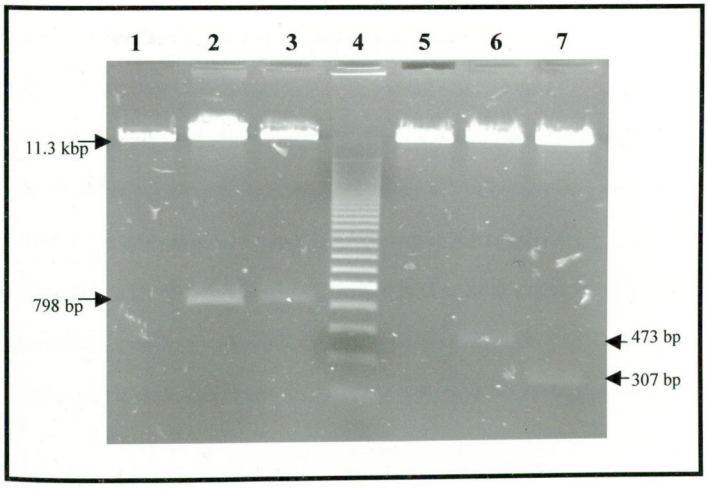


Figure 5.10- Screening for recombinant pSFV1-Baxα clones by restriction digestion.

was observed in BHK-21 cells, transfected with RNA transcribed from the putative positive pSFV1-Bax #15 clone, at 18 h p.e. (*Figure 5.11A*). Analysis of Bax expression in mock- and SFV1-Bax #21-transfected cells also revealed positive Bax staining within the nuclear membrane and cytoplasmic regions (*Figure 5.11 B, C*). However, staining intensity was far less, compared to SFV1-Bax #15-transfected cells, suggesting that this staining was specific for endogenous cellular Bax protein in transfected control cells. It was also noted that all SFV1-Bax clone #15-tranfected cells displayed a high degree of cpe at this timepoint, which was later shown to be apoptotic cell death, by TUNEL analysis (*not shown*). Cells mock-transfected with PBS, and cells transfected with SFV1-Bax #21 RNA, (the antisense version of the *Bax* gene), did not show this degree of cpe or apoptotic cell death at 18 h p.e. (*Figure 5.11 B, C*).

To confirm that the pSFV1-Bax #15 clone overexpressed exogenous Bax protein, and to alleviate the possibility that the anti-Bax antibodies were reacting to endogenous Bax only, a *Bax*-null leukemia cell line, HL60, was utilised. Transfection of HL-60 cells with RNA derived from the pSFV1-Bax #15 clone did not result in cellular Bax expression (*not shown*). This was primarily due to very low electroporation efficiencies for this cell line. Instead, HL-60 cells were infected with rSFV1-Bax #15 infectious, encapsidated particles for 1 h (moi ~1), and analysed for Bax expression 24 h.p.i. (*Figure 5.12*). Cells infected with recombinant rSFV-Bax virus particles displayed positive Bax staining following ICC with the anti-Bax antibody (*Figure 5.12 A*). rSFV1-Bax #21 particles (*not shown*) and mock-infected HL-60 cells (*Figure 5.12 B*) were both negative for Bax expression.

Thus, the pro-apoptotic protein Bax-α, successfully cloned into the SFV expression system, overexpressed the protein in its correct conformation, sufficiently to execute its pro-apoptotic function *in vitro*. However, the presence of endogenous cellular Bax would complicate downstream expression studies, particularly rSFV1-Bax particle titrations. It

Figure 5.11- **Screening for Bax-α protein overexpression from recombinant SFV clones by immunocytochemistry.** *In vitro*-transcribed RNA from pSFV1-Baxα plasmid #15 and pSFV1-Baxα plasmid #21 were electroporated into ~90% confluent BHK-21 cells, and incubated on glass coverslips in 6-well plates for 18 h p.e. PBS was used as an electroporation control. Cells were analysed for Bax overexpression by incubation with monoclonal rabbit anti-human Bax antibody, for 1 h, and subsequently with goat anti-rabbit, biotin-conjugated antibody. Cells were visualised using DAB substrate, counterstained in methyl green and observed by light microscopy. Note dark brown/black DAB-positive Bax-specific staining (*arrows*) in cells transfected with RNA from pSFV1-Bax clone #15 (*A*). Note also, DAB-positive Bax-specific staining in cells transfected with RNA transcribed from pSFV1-Bax clone #21 (*B*) or with PBS (*C*). However, staining appears to be at a much less intensity in *B* and *C*, reflecting endogenous cellular Bax expression. Also note presence of extensive cytopathic effects in SFV-Bax clone #15-transfected cells (*A*), most of which have already lifted from the cell monolayer, in comparison to normal, healthy cells in *B* and *C*. Photographed at x 400 magnification.

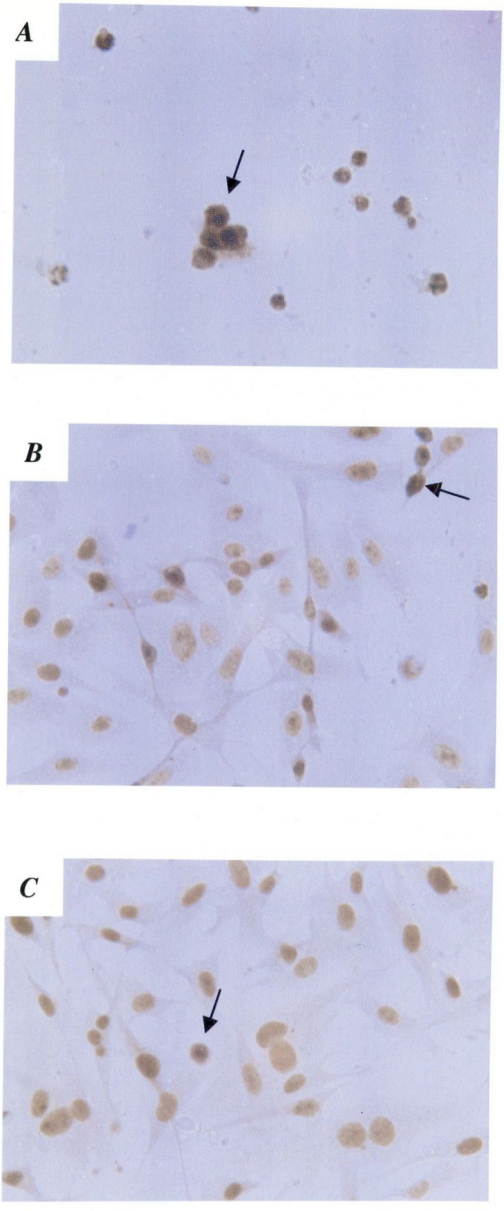


Figure 5.11- Screening for Bax-α protein expression from recombinant pSFV-Bax clones, by immunocytochemistry.

Figure 5.12- **Screening for Bax overexpression in the *Bax*-null cell line, HL-60, by immunocytochemistry.** Recombinant rSFV1-Baxα #15 virus particles were produced by co-transfection of pSFV1-Baxα clone #15 *in vitro*-transcribed RNA, with RNA from SFV helper plasmids, to produce rSFV1-Baxα #15 infectious particles. rSFV1-Bax #15 particles were used to infect the *Bax*-null leukaemia cell line, HL-60, growing as suspension cultures, for 1 h (moi ~1). At 18 h p.i., cells were cyto-spun onto glass slides and were analysed for Bax overexpression by ICC, as described in the legend to figure 5.11. Note presence of brown DAB-positive Bax-specific staining within rSFV1-Bax #15 virus-infected HL-60 cells (*A*, *arrows*). This DAB-positive staining was not detected in mock-infected PBS control HL-60 cells (*B*). The low efficiency of rSFV virus infection in HL-60 cells is reflective of the low initial rSFV1-Baxα #15 virus titres (*see section 5.3.3*). Photographed at x 400 magnification.

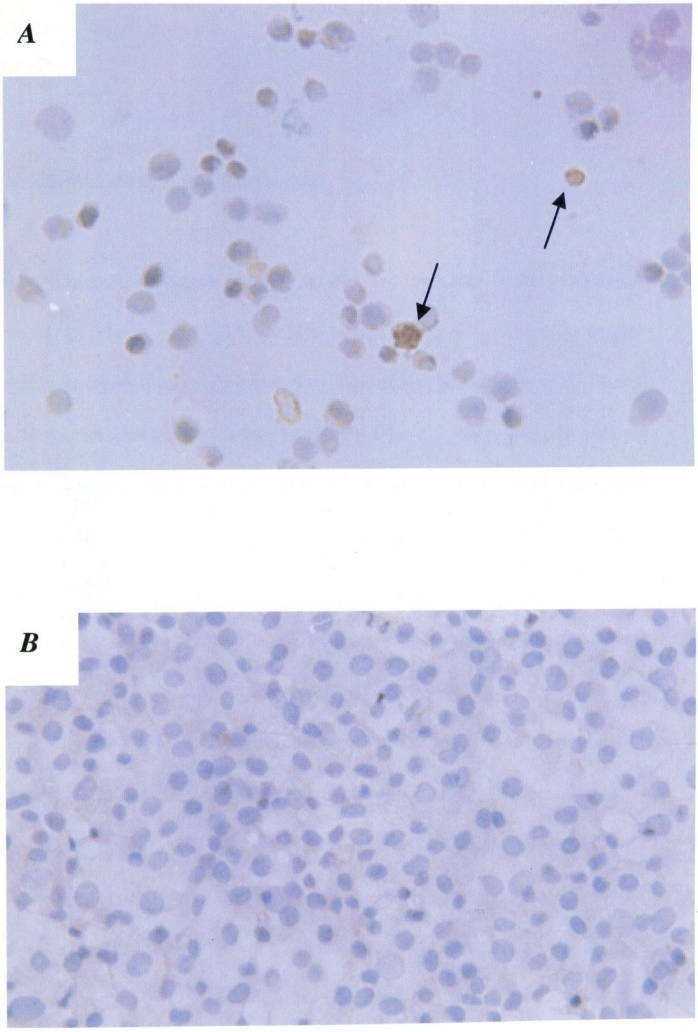


Figure 5.12- Screening for Bax overexpression in the *Bax*-null cell line, HL-60, by immunocytochemistry.

was accepted that the inclusion of a 'tag' protein was necessary to obviate these complications in further analyses.

5.3.2 SFV-HA-Bax cloning and expression

The haemagglutinin (HA)-tagged form of the *Bax* gene was also available within a SG5 plasmid vector backbone, pSG5-HABax. The presence of a HA epitope tag would unequivocally facilitate the simultaneous detection of Bax protein, since HA is not expressed in mammalian cells, and may be detected by ICC, using anti-HA epitope antibodies. To facilitate the cloning of the *HABax-α* fusion protein gene into the SFV expression system, pSFV-1, the gene was amplified from pSG5-HABax using primers specific for 5' and 3' flanking regions within the pSG5 plasmid backbone (*Figure 5.4*). In a similar situation to *Bax-α* cloning in section 5.3.1, the sequence of the HA epitope was determined prior to cloning. Attempts to amplify the *HABax* fragment directly using consensus *HA* nucleotide sequnces from Genbank, had failed (*not shown*). Both 5' and 3' primers were used to directly sequence the fragment in each orientation (*Figure 5.13*), compared to the *HA* and *Bax-α* consensus sequences in GenBank (*Figure 5.14*), and utilised to design a HA-specific 5' primer for direct cloning of *HABax* into pSFV-1. The 5' primer incorporated the first 15 bp of the *HA* epitope sequence and included the native SFV RBS, and an exogenous *XmaI* restriction enzyme site. The 3' primer also included an *XmaI* site and was specific for the *SalI* restriction site regions within the pSG5 plasmid backbone, 174 bp downstream of the *Bax-α* sequence. The resulting 848 bp PCR product was cloned into the SFV expression vector and the recombinant clones were screened using the rapid colony screening procedure (*Figure 5.15*). The presence and orientation of the 848 bp insert were confirmed by *XmaI* (*Figure 5.16*) and *BamHI* (*Figure 5.17*) digestion, respectively. Four clones were obtained, three in the correct orientation (clones

tcc atc caa atc ccg ATG TAC CCA TAC GAT GTT CCA GAT TAC GCT AGC TTG GGA GAT CGA AGA

s i q i p **M Y P Y D V P D Y A S L G D R R**

TCT GAC GGG TCC GGG GAG CAG CCC AGA GGC GGG GGG CCC ACC AGC TCT GAG CAG ATC ATG

M D G S G E Q P R G G G P T S S E Q I M

AAG ACA GGG GCC CTT TTG CTT CAG GGT TTC ATC CAG GAT CGA GCA GGG CGA ATG GGG GGG

K T G A L L L Q G F I Q D R A G R M G G

GAG GCA CCC GAG CTG GCC CTG GAC CCG GTG CCT CAG GAT GCG TCC ACC AAG AAG CTG AGC

E A P E L A L D P V P Q D A S T K K L S

GAG TGT CTC AAG CGC ATC GGG GAC GAA CTG GAC AGT AAC ATG GAG CTG CAG AGG ATG ATT

E C L K R I G D E L D S N M E L Q R M I

GCC GCC GTG GAC ACA GAC TCC CCC CGA GAG GTC TTT TTC CGA GTG GCA GCT GAC ATG TTT

A A V D T D S P R E V F F R V A A D M F

TCT GAC GGC AAC TTC AAC TGG GGC CGG GTT GTC GCC CTT TTC TAC TTT GCC AGC AAA CTG

S D G N F N W G R V V A L F Y F A S K L

GTG CTC AAG GCC CTG TGC ACC AAG GTG CCG GAA CTG ATC AGA ACC ATC ATG GGC TGG ACA

V L K A L C T K V P E L I R T I M G W T

TTG GAC TTC CTC CGG GAG CGG CTG TTG GGC TGG ATC CAA GAC CAG GGT GGT TGG GAC GGC

L D F L R E R L L G W I Q D Q G G W D G

CTC CTC TCC TAC TTT GGG ACG CCC ACG TGG CAG ACC GTG ACC ATC TTT GTG GCG GGA GTG

L L S Y F G T P T W Q T V T I F V A G V

CTC ACC GCC TCG CTC ACC ATC TGG AAG AAG ATG GGC TGA

L T A S L T I W K K M G *OPA*

Figure 5.13- Nucleotide and deduced amino acid sequence of human HA-Tagged *Bax-α* from the pSG5-HABax plasmid. The *HA* epitope initiation methionine is indicated in blue type-face, and the epitope sequence is indicated in bold. The HA-human *Bax-α* fusion sequence is indicated in red type-face. Flanking pSG5 plasmid sequence is indicated in small type-face. For the cloning of *HA-Bax* into pSFV-1, the 5' primer was chosen to include the first 15 nucleotides of the deduced *HA* sequence. The 3' primer was specific for a region of the pSG5 vector backbone, downstream of the *HA-Bax-α* sequence (*not shown*).

Figure 5.14- **Amino acid sequence alignment of the haemagglutinin epitope tag and Bax-α protein with others from the database.** *A*; amino acid sequence alignment of the haemagglutinin epitope tag with others from the database. U46855: HA epitope from cloning vector pAS1-tet, AF134168: HA epitope from Yeast 2-hybrid vector pC-ACT.2, U57443.1: HA epitope from cloning vector pODB8. *B*; amino acid sequence alignment of the Bax-α protein with others from the database. L22473: Human Bax alpha mRNA, complete cds, NM 004324: *Homo sapiens* BCL2-associated X protein (Bax) mRNA.

(A)

```
HA-TAG    1  MYPYDVPDYASLGDRR
U46855    1  -..........------
AF134168  1  -..........------
U57443.1  1  -..........------
```

(B)

```
Bax (pSG5)   1 MDGSGEQPRGGGPTSSEQIMKTGALLLQGFIQDRAGRMGGEAPELALDPV
L22473       1 ............................................................
NM 004324    1 ............................................................

Bax (pSG5)  51 PQDASTKKLSECLKRIGDELDSNMELQRMIAAVDTDSPREVFFRVAADMF
L22473      51 ............................................................
NM 004324   51 ............................................................

Bax (pSG5) 101 SGNFNWGRVVALFYFASKLVLKALCTKVPELIRTIMGWTLDFLRERLLGWI
L22473     101 ............................................................
NM 004324  101 ............................................................

Bax (pSG5) 151 QDQGGWDGLLSYFGTPTWQTVTIFVAGVLTASLTIWKKMG----------
L22473     151 ..................................................----------
NM 004324  151 .........VRLLKPPHPHHRALTTAPAPPSLPPATPLGPWAFWSRSQWCPLPI

Bax (pSG5) 201 ----------------
L22473     201 ----------------
NM 004324  201 FRSSDVVYNAFSLRV
```

Figure 5.14- Amino acid sequence alignment of the haemagglutinin epitope tag and human Bax-α proteins with others from the database.

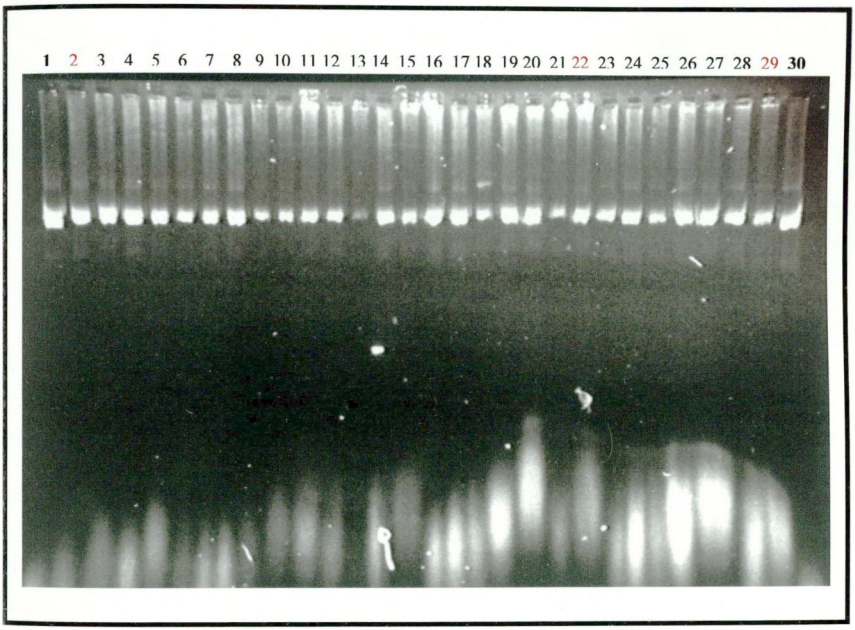


Figure 5.15- Rapid colony screening for pSFV1-HABax recombinant clones.

Putative positive pSFV1-HABaxα clones were initially screened by running plasmid DNA isolated directly from transformant bacterial colonies on 0.8% (w/v) agarose gels, stained with ethidium bromide. Plasmid DNA isolated from known pSFV-1 transformants were run alongside that from ligation transformants. *Lanes 1 and 30*; plasmid DNA from pSFV-1 vector transformants only. *Lanes 2 to 29*; plasmid DNA from ligation transformants. *Lanes 2* (clone #1), *22* (clone #21) and *29* (clone #28) contain plasmid DNA that is of slightly higher molecular weight to pSFV-1 plasmid DNA, and thus, may contain the recombinant plasmid.

***Figure 5.16*- Screening for pSFV1-HABaxα recombinant clones by *Xma1* restriction digestion.** Putative positive clones were screened for the presence of *HABax-α* inserts by *Xma1* restriction analysis. *Lanes 1 and 7*; 200bp ladder. *Lanes 2 and 6*; pSFV-1 digested with *Xma1*. *Lanes 3 to 5*; recombinant pSFV1-HABax clones #1, #6, and #29 respectively, containing the 830 bp *HABax-α* insert; digested with *Xma1*. Plasmid digests were run on a 0.8% (w/v) agarose gel, stained with ethidium bromide.

***Figure 5.17*- Determination of *HABax-α* insert orientation in pSFV-1 by *BamH1* restriction digestion.** The orientation of *HABax-α* inserts within the pSFV-1 vector were determined by *BamH1* restriction digestion of putative positive clones. *Lanes 1 and 7*; 200bp ladder. *Lane 2*; pSFV-1 digested with *BamH1*. *Lanes 3 to 5*; recombinant pSFV1-HABaxα clones #1, #6 and #21 respectively, containing a HABax-α insert in the correct orientation; digested with *BamH1* (523bp). *Lane 6*; recombinant pSFV1-HABaxα clone #29, containing a HABax-α insert in the incorrect orientation; digested with *BamH1* (307bp). Plasmid digests were run on a 0.8% (w/v) agarose gel, stained with ethidium bromide.

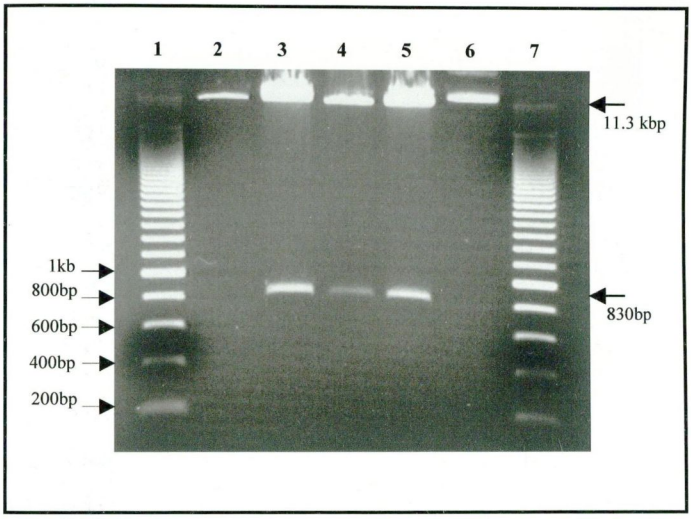


Figure 5.16- Screening for recombinant pSFV1-HABaxα clones by *Xma1* resticion digestion.

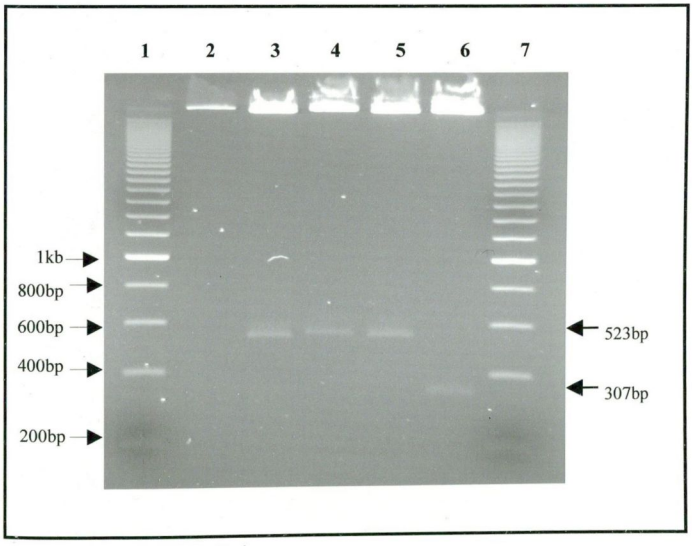


Figure 5.17- Determination of HABax insert orientation in pSFV-1 by *BamH1* restriction digestion

Figure 5.18- **Screening for HABax protein expression from recombinant SFV clones by immunocytochemistry, in BHK-21 cells.** *In vitro*-transcribed RNA from pSFV1-HABax clones; #1, #6, #21 and #29, were electroporated into ~90% confluent BHK-21 cells and incubated on glass coverslips in 6-well plates, for 18 h p.e. PBS was used as an electroporation control. Cells were analysed for HA epitope expression, by incubation with high affinity monoclonal rat anti-haemagglutinin antibody, for 1 h, and subsequently with rabbit anti-rat, biotin-conjugated antibody. Cells were visualised using DAB substrate, counterstained in methyl green and observed by light microscopy. Note dark brown DAB-positive HA-specific staining (*arrows*) in cells transfected with SFV1-HABax clones #1 (*A*), #6 (*B*) and #21 (*C*). BHK-21 cells transfected with SFV1-HABax clone #29 (*D*) or PBS (*E*) are completely negative for HA epitope expression. Photographed at x 400 magnification.

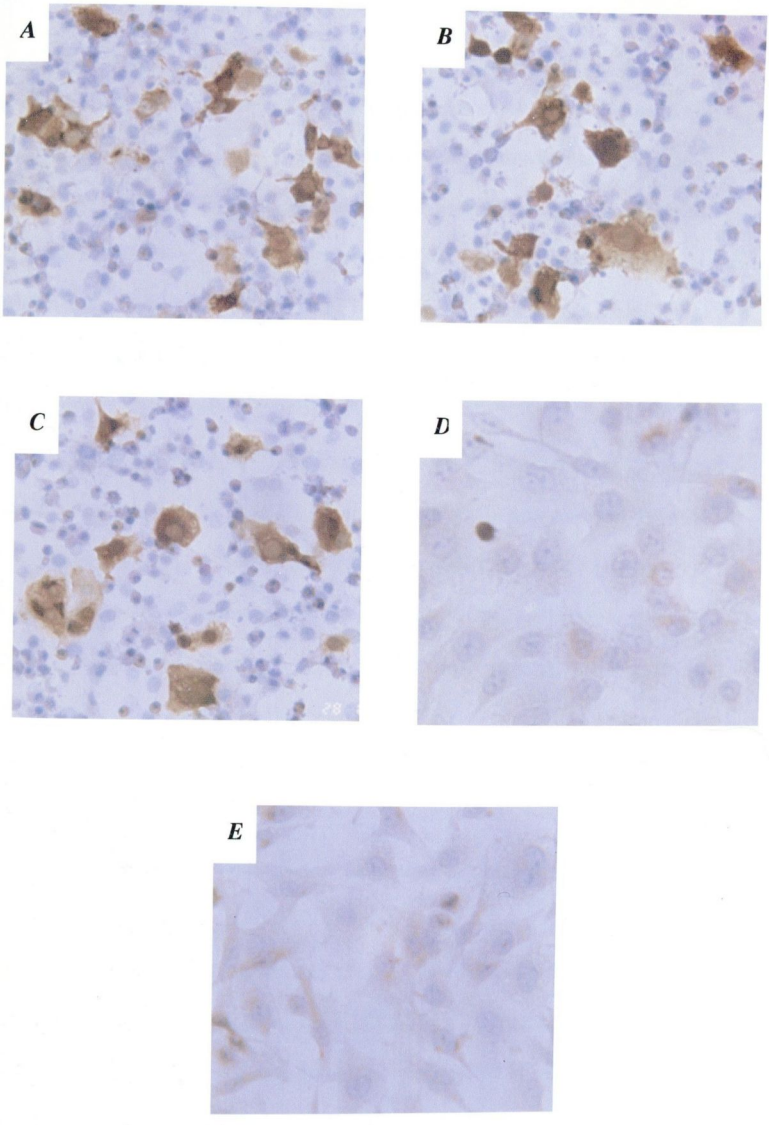


Figure 5.18- Screening for HABaxα protein expression from recombinant SFV clones in BHK-21 cells, by immunocytochemistry.

pSFV1-HABax #1, #6 and #21), the other in the opposite orientation, (clone pSFV1-Bax #29).

Expression of the fusion protein from the SFV expression system was determined by ICC, using a rat anti-HA epitope antibody and rabbit anti-rat biotin-conjugated secondary antibody. The results are illustrated in figure 5.18. Brown DAB-positive staining was observed in the nuclear membrane and cytoplasmic regions of BHK-21 cells, transfected with RNA transcribed from plasmids pSFV1-HABax #1, #6 and #21 18 h p.e (*Figure 5.18 A, B, C*). As with the transfection of SFV1-Bax #15 RNA, all SFV1-HABax-tranfected cells displayed a high degree of apoptotic cell death by TUNEL analysis (*see section 5.3.3*). Cells transfected with SFV1-HABax #29 RNA and PBS were completely negative for HA expression (*Figure 5.18 D, E*). Thus, the use of a HA-tag fusion with the Bax protein serves as a more reliable system for the detection of Bax in SFV1-transfected cells, than with the Bax construct alone. Subsequently, all further studies with SFV-mediated Bax expression concentrate on the SFV-HABax construct, unless otherwise indicated.

5.3.3 SFV-mediated HABax expression induces PCD in transfected cells

To determine the pro-apoptotic efficiency of the SFV1-HABax RNA construct, in comparison the standard SFV-EGFP vector, BHK-21 cells were transfected with *in vitro*-transcribed SFV RNA, and cells were monitored over a period of 24 h. Figure 5.19 illustrates how transfection with SFV-HABax RNA induced a massive cytopathic effect in BHK-21 cells approximately 10 h p.e. (*Figure 5.19 A*), In contrast, cells transfected with RNA from the pSFV-EGFP plasmid appeared normal at 10 h p.e. (*Figure 5.19 B*), and revealed only slight cpe at 24 h p.e. (*Figure 5.19 D*). SFV-HABax-transfected cells lifted from the monolayer as early as 12 h p.e. (*not shown*), and were completely obliterated at

Figure 5.19- **Cytopathic effect following transfection with RNA from recombinant pSFV-HABax clone, in BHK-21 cells.** BHK-21 cells were grown in 75 cm^2 flasks until ~90% confluent, trypsinised and transfected with *in vitro*-transcribed RNA from pSFV1-HABax clone #1 (*A, C*), or with PBS alone as a control (*B, D*). Following electroporation, cells were placed into 6-well dishes and analysed for cytopathic effect, over a period of 24 h. Cells were observed by inverted light microscopy, at 10 h p.e. (*A, B*) and 24 h p.e. (*C, D*). Photographed at x 100 magnification.

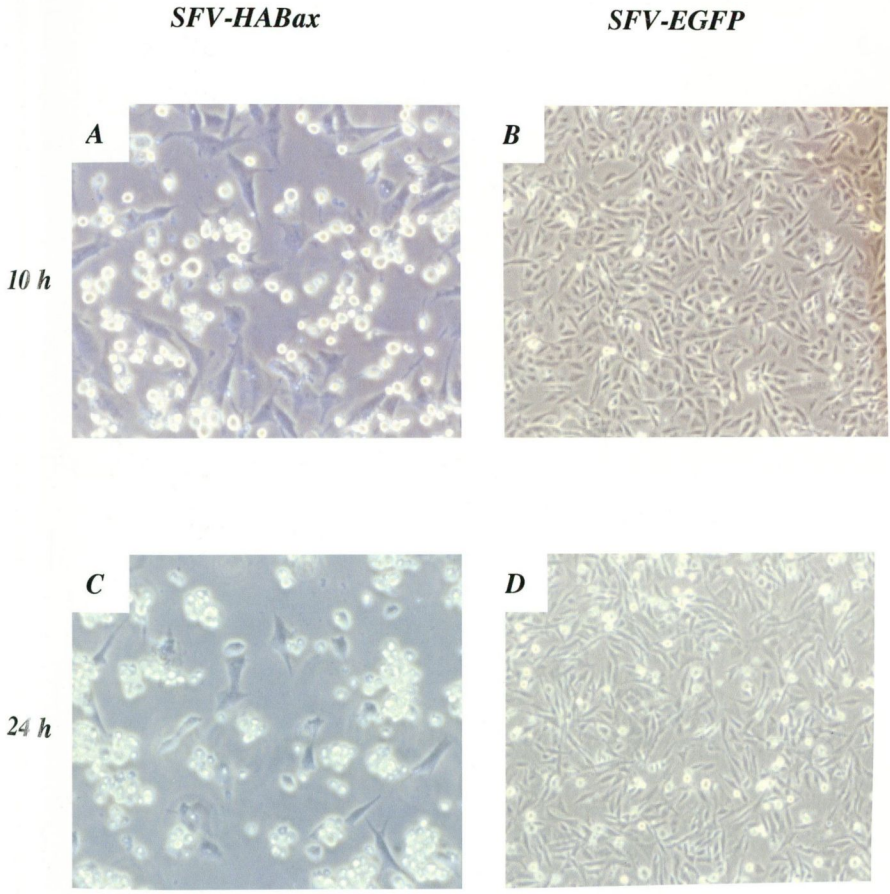


Figure 5.19- Cytopathic effect in BHK-21 cells following transfection with SFV-HABax RNA.

Figure 5.20 - **Induction of apoptosis following transfection with RNA from pSFV1-HABax and pSFV-EGFP recombinant plasmids, in BHK-21 cells.** BHK-21 cells were grown in 75 cm^2 flasks until ~90% confluent, trypsinised and transfected with *in vitro*-transcribed RNA from either pSFV1-HABax (*A*), pSFV-EGFP (*B*) or PBS alone (*C*), as indicated. Following electroporation, cells were placed onto glass coverslips in 6-well plates, and analysed for apoptosis induction by TUNEL, at 10 h p.e. (*A*) and 24 h p.e. (*B, C*). Photographed at x 100 magnification.

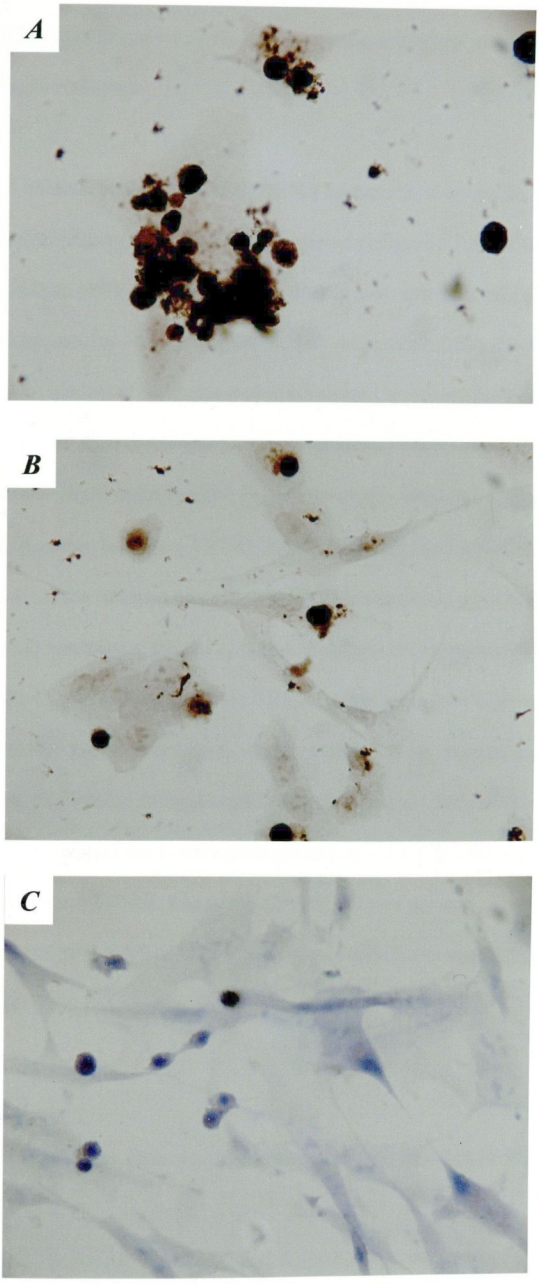


Figure 5.20- Induction of apoptosis following transfection with SFV1-HABax and SFV-EGFP RNA constructs, in BHK-21 cells.

all later timepoints (*Figure 5.19 C*). Mock-infected cells grew and proliferated normally throughout (*not shown*).

Cell death induced by the SFV-HABax RNA construct was apoptotic, as determined by morphological (*Figure 5.19*) and TUNEL analysis (*Figure 5.20*). At 10 h p.e. with RNA transcribed from pSFV-HABax clone #1, dark brown, apoptotic nuclei were observed in all remaining transfected cells (*Figure 5.20 A*). In contrast, DNA fragmentation in SFV-EGFP RNA-transfected cells appeared to commence at a much later time-point of 24 h p.e. (*Figure 5.20 B*), and cpe was far less aggressive. PBS-transfected control BHK-21 cells remained negative for cpe and TUNEL reactivity throughout (*Figure 5.20 C*). Thus, apoptosis induction following SFV-EGFP RNA transfection, which occured as a consequence of the inherent properties of the SFV vector, were strengthened considerably following the insertion of the pro-apoptotic *Bax* gene. Exogenous expression of Bax initiated the apoptotic cascade within BHK-21 cells, at least 10 h earlier than SFV-EGFP alone. Also, the degree of cell death which ensued, was far more potent then SFV-EGFP RNA alone, eliminating the majority of cells by 10 h p.e. Cells transfected with RNA from an antisense version of the *HABax* gene (clone pSFV1-HABax #29) displayed similar morphological and TUNEL features to SFV-EGFP (*not shown*), confirming this analysis. The potency of SFV-HABax RNA as an apoptosis-inducing agent can be compared to that of infectious SFV-4 virus, described in section 2.3.1.

5.3.4 rSFV-HABax virus particle production and titration in BHK cells

As with rSFV-EGFP particle production, *in vitro*-transcribed SFV1-HABax clone#1 RNA was electroporated into ~90% confluent BHK-21 cells, along with equimolar quantities of both helper RNA species, for 24 h at 37°C. Resultant particle titres were calculated by infecting ~90% confluent sBHK cell monolayers, grown on glass coverslips, with serial

dilutions of the virus for 1 h, and incubated overnight. Following fixation, cells were assessed for the presence of infectious recombinant HABax particles by incubation with an anti-HA antibody. In stark contrast to rSFV-EGFP particles, titres of between 3-5 x 10^5 I. U./ml rSFV-HABax were produced following each preparation. Attempts to optimise rSFV1-HABax virus production were initiated and conducted in parallel with rSFV-EGFP virus production, as a control. The results are outlined in figure 5.21. Early harvest timepoints (10 h, 14 h), prior to monolayer disintegration, showed no improvement in rSFV1-HABax virus titres, compared with the standard 24 h harvest timepoint. In fact, both rSFV-HABax and rSFV-EGFP titres were considerably reduced. In contrast, incubation of transfected cells at 33°C for 24 h increased the titres of both EGFP- and HABax-expressing particles by at least 5-fold. A further 12 h incubation period continued to enhance rSFV-EGFP particle titres, but had little effect on rSFV-HABax. A 24 h incubation at 33°C was considered optimal for rSFV-HABax particle production, and titres of approximately 1 x 10^6 I.U./ml were routinely obtained and used in subsequent experiments at this titre.

In an effort to definitively explain the low rSFV-HABax particle titres obtained, BHK-21 cells were co-transfected with RNA transcribed from either pSFV-HABax and pSFV-EGFP plasmids, along with equimolar quantities of RNA from both helper species, using the standard method for particle production. Particle-producing BHK-21 cells were incubated and photographed at intervals throughout the 24 h period. The results are illustrated in figure 5.22, and indicated clearly that the low titres of rSFV-HABax virus obtained was directly attributed to the vigorous nature of *Bax*-mediated apoptosis induction within the BHK-21 cells. BHK-21 cell death was evident as early as 7 h p.e. (*Figure 5.22 A*), and by 16 h p.e. (*Figure 5.22 C*), all cells were completely obliterated in comparison to rSFV-EGFP particle-producing cells (*Figure 5.22 B, D, F*). It appeared that the rSFV-HABax particle-producing cells were not allowed sufficient time to produce and

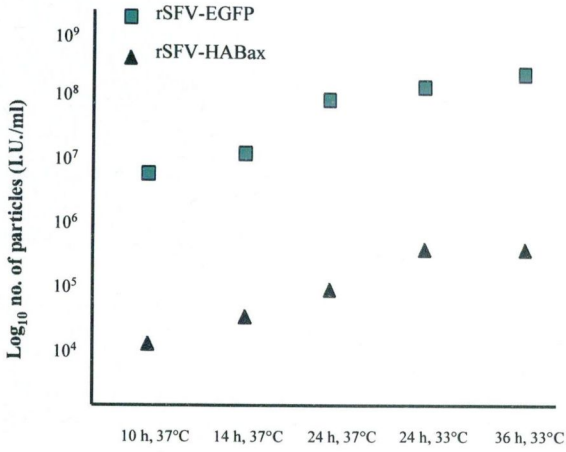


Figure 5.21- Optimisation of rSFV-HABax virus particle production.

rSFV-HABax and rSFV-EGFP virus particles were produced by co-transfection of RNA *in vitro*-transcribed from pSFV-HABax and pSFV-EGFP plasmids, respectively with equimolar quantities of SFV-Helper RNAs, and were incubated for various times and temperatures p.e. rSFV-HABax particles was titrated by ICC, using an anti-HA antibody (▲). rSFV-EGFP particles were titrated by direct epiflourescence at 488 nm (■). The numbers of particles obtained under all incubation conditions are expressed as I.U./ml (*Y axis*).

Figure 5.22- **rSFV-HABax particle-producing BHK-21 cells undergo rapid cell death compared to rSFV-EGFP.** BHK-21 cells were grown in 75 cm^2 flasks until ~80% confluent, trypsinised and cotransfected with RNA *in vitro*-transcribed from recombinant plasmids pSFV-HABax (*A, C, E*) or pSFV-EGFP (*B, D, F*), along with equimolar quantities of SFV helper RNAs, and incubated at 37°C. Cells were monitored for cytopathic effects, at 7 h (*A, B*), 16 h (*C, D*) and 24 h (*E, F*) following initiation of particle production. Photographed at x 100 magnification.

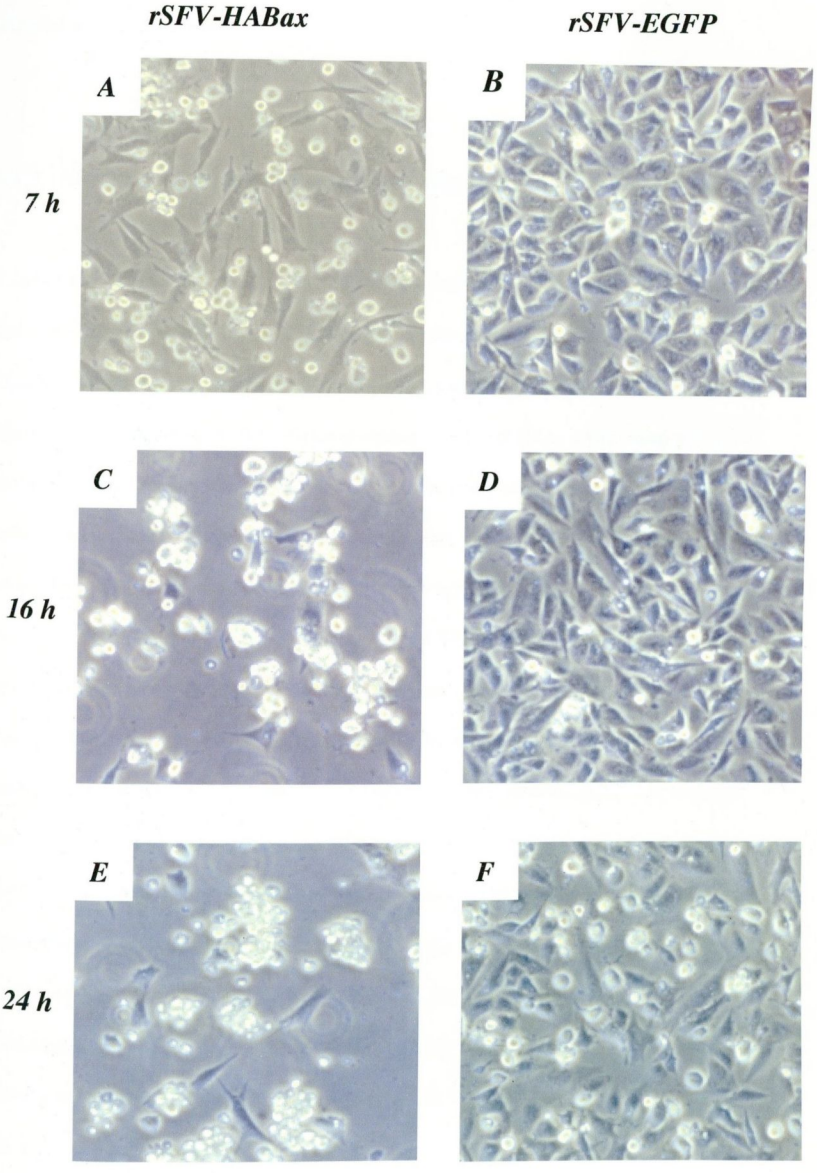


Figure 5.22- rSFV-HABax-α particle-producing BHK-21 cells undergo rapid cell death compared to rSFV-EGFP.

Figure 5.22- **rSFV-HABax particle-producing BHK-21 cells undergo rapid cell death compared to rSFV-EGFP.** BHK-21 cells were grown in 75 cm^2 flasks until ~80% confluent, trypsinised and cotransfected with RNA *in vitro*-transcribed from recombinant plasmids pSFV-HABax (*A, C, E*) or pSFV-EGFP (*B, D, F*), along with equimolar quantities of SFV helper RNAs, and incubated at 37°C. Cells were monitored for cytopathic effects, at 7 h (*A, B*), 16 h (*C, D*) and 24 h (*E, F*) following initiation of particle production. Photographed at x 100 magnification.

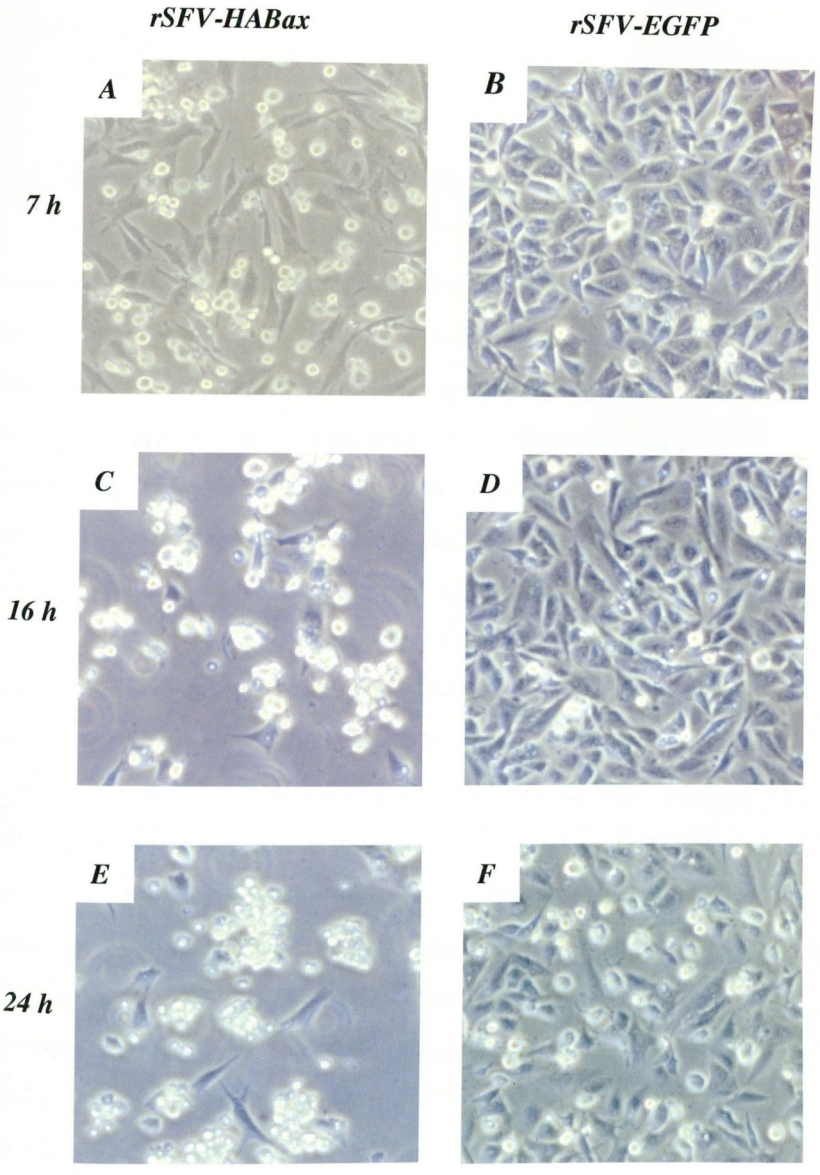


Figure 5.22- rSFV-HABax-α particle-producing BHK-21 cells undergo rapid cell death compared to rSFV-EGFP.

accumulate high levels of the recombinant virus due to the rapid nature of cell death induced by the Bax protein.

5.3.5 Bcl-2 overexpression in non-small cell lung cancer

In order to assess the potential therpeutic efficiency of rSFV-HABax virus particles, a *Bcl-2*-overexpressing cell line was necessary. As with the NCI-H358a system used in Chapters 3 and 4, we wished to focus our attention on human NSCLC. We were unable to specifically locate a natural *Bcl-2*-overexpressing NSCLC cell line, either from ATCC or in the literature. Although evidence suggests that the *Bcl-2* oncogene is expressed in basal cells of normal human lung epithelium (Pezzella *et al*, 1993), there is little data available on the frequency of its expression in lung carcinoma. Instead, four NSCLC cell lines from ATCC (NCI-H358a, NCI-H460, NCI-H520 and NCI-H596) were screened for Bcl-2 overexpression using immunochemical analysis. Also, known, positive and negative *Bcl-2*-expressing cell lines were necessary as controls for this analysis. The rat prostatic adenocarcinoma cell line, AT3, previously transfected with plasmids pZIP-Neo or pZIP-Bcl-2, to produce stably transfected cells lines AT3-Neo and AT3-Bcl-2, respectively (Levine *et al*, 1993), were obtained and used as negative and positive controls, respectively. Both NSCLC and control cell lines were incubated until ~80% confluent and analysed for Bcl-2 overexpression by incubation with a mouse anti-human Bcl-2 monoclonal antibody. Cells were analysed using fluorescent microscopy, at 460 nm. Results are indicated in figure 5.23. AT3-Neo and all 4 NSCLC cell lines were negative for *Bcl-2* overexpression by ICC. Positive control AT3-Bcl-2 cells however, revealed distinctly FITC-positive, Bcl-2-specific staining. As a consequence of this experiment, we decided to divert our attention from human NSCLC, to the AT3 rat PCa cell lines, for SFV-HABax analysis.

Cell Line	Bcl-2 expression
AT3-Neo	-
AT3-Bcl-2	+
NCI-H358a	-
NCI-H460	-
NCI-H520	-
NCI-H596	-

Figure 5.23- Bcl-2 overexpression in NSCLC cell lines, as detected by immunocytochemistry. NSCLC cell lines were obtained from ATCC. All cells were seeded onto glass coverslips and incubated until ~80% confluent. Cells were fixed in acetone and incubated with monoclonal mouse anti-human Bcl2 oncoprotein antibody for 30 minutes, following by rabbit anti-mouse FITC-conjugated secondary antibody. Cells were visualised by fluorescence microscopy at 460 nm, and scored postitive (+) or negative (-) for FITC Bcl-2-specific expression.

5.3.6 Growth, morphology and *Bcl-2*-overexpression in AT3 cells

Both AT3-Neo and AT3-Bcl-2 cells were found to proliferate rapidly in culture, reaching ~80% confluence in 3-6 days, depending on seeding density (1 x 10^4-1 x 10^5 cells ml^{-1}). Growth medium was changed daily due to the vigorous nature of cell growth, and both cell lines were morphologically indistinguishable from each other (*Figure 5.24*). AT3-Bcl2 cells were distinguished from AT3-Neo cells by incubation with anti-human Bcl-2 antibody, as decribed above. As shown in figure 5.25, AT3-Bcl-2 cells revealed distinctly positive cytoplasmic/membranous FITC staining, indicative of Bcl-2 overexpression. AT3-Neo cells failed to reveal a FITC-positive reaction (*not shown*), and were therefore, negative for Bcl-2 overexpression. Both 1° and 2° antibody negative control reactions were also negative for FITC-staining (*not shown*).

5.3.7 Rat adenocarcinoma AT3 cell lines induce *in vivo* sc tumour formation

As a prerequisite for the use of the AT3 cell lines AT3-Neo and AT3-Bcl-2, as the tumour cell model to study the effect of Bcl-2 overexpression on rSFV virus-mediated tumour therapy, it was essential to determine whether both cell lines formed solid subcutaneous tumours in the xenograph *nu/nu* mouse model. A total volume of 0.4 ml each, of AT3-Neo and AT3-Bcl-2 cell suspensions (1 x 10^6 cells ml^{-1}), were injected sc into the right flank of 10 female Balb/C *nu/nu* mice and were monitored daily for sc tumour development. The vigorous rate of AT3 cell growth in culture was reproduced *in vivo*. A solid sc AT3 tumour mass developed in 100% of mice injected with either AT3-Neo or AT3-Bcl-2 cell suspensions (*Figure 5.26*). Subcutaneous tumour nodules were detected at the site of injection as early as 24 h p.i. with each tumour cell line, and reached 20% of mouse body weight in less than 2 weeks, at which time the mice had to be culled. Tumour diameters

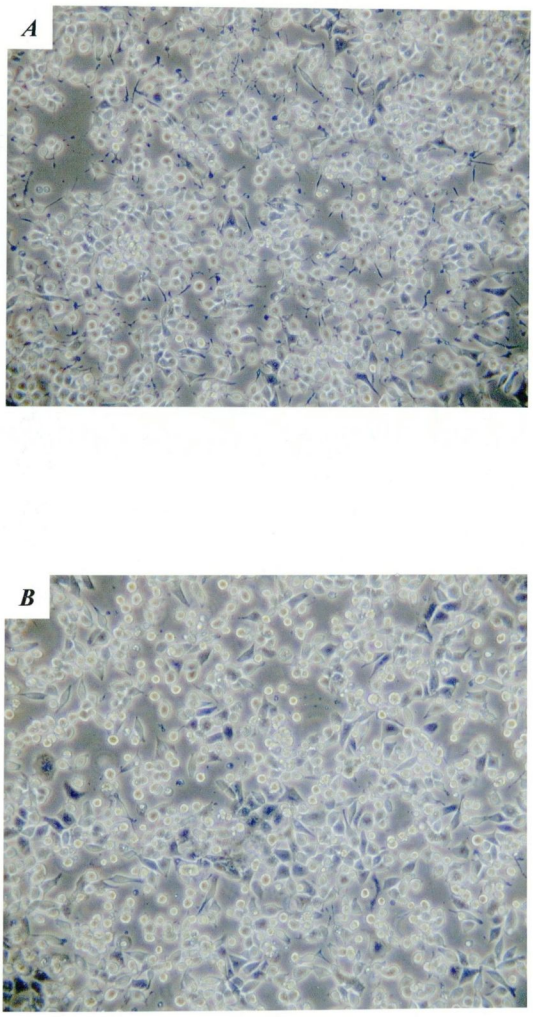


Figure 5.24- Growth and morphology of AT3-Neo and AT3-Bcl-2 cells.

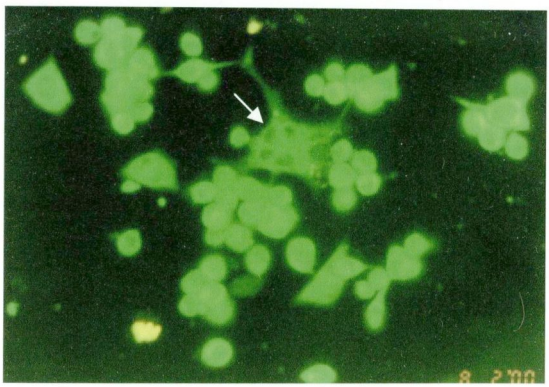


Figure 5.25- Bcl-2 overexpression in AT3-Bcl-2 cells.

AT3-Bcl-2 cells were grown on glass coverslips in 6-well plates until ~80% confluent, fixed in acetone and incubated with monoclonal mouse anti-human Bcl-2 oncoprotein antibody (1 :20 dilution), for 30 minutes. Cells were subsequently stained with rabbit anti-mouse FITC-conjugated secondary antibody (1 :20 dilution), and visualised using fluorescent microscopy, at 460 nm. Note positive FITC staining indicative of *Bcl-2* overexpression. AT3-Neo cells do not reveal this FITC Bcl-2-specific staining (*not shown*). Photographed at x 200 magnification.

were calculated using a linear calipers and volume calculated by assuming a spherical shape. The growth rates of AT3-Neo and AT3-Bcl-2 cell tumours were identical.

Gross pathological examination revealed large, solid, encapsidated sc tumour masses for both tumour types (*Figure 5.27*). Extensive angiogenesis was notable directly under the skin of the AT3-Bcl-2 tumour-containing mouse, in figure 2.27*A*. When resected, the tumours appeared soft and gelatinous, with extensive haemorrhage. The haemorrhaging was probably a consequence of the enormous rate of tumour growth, and the subsequent compression of tumour blood vessels (*B. Sheahan, personal communication*). Histological examination of both AT3-Neo and AT3-Bcl-2 tumours (*Figure 5.28*) revealed expansible, unencapsulated, deeply cellular masses located in the subcutis. Bands of necrosis frequently located towards the ventral aspect of the masses were indicative of compression ischemia against the animal's ribcage (*Figure 5.28 A*). Focal extension of tumour cells into the dermis was sometimes accompanied by ulceration (*Figure 5.28 B*). Bacterial colonies and neutrophils were prominent at the ulcerated surfaces. Both tumours types were morphologically indistinguishable.

Immunohistochemical analysis of frozen AT3-Bcl-2 tumour sections for Bcl-2 overexpression was determined by incubation with monoclonal mouse anti-human Bcl-2 antibody. Sections were visualised using fluorescent microscopy, at 460 nm (*Figure 5.29*). Intense FITC-positive, Bcl-2-specific staining was detected within the AT3-Bcl-2 tumour section. The pattern of tumour cell Bcl-2-specific staining was membranous and cytoplasmic, indicating that the tumour cell line retained its ability to express the oncogene *in vivo*. As with *in vitro* analysis, AT3-Neo tumour cryosections were completely negative for Bcl-2 expression (*not shown*).

Postmortem examination of mice indicated that both tumour types were locally aggressive. Metastases were not detected within any of the major organs, including the

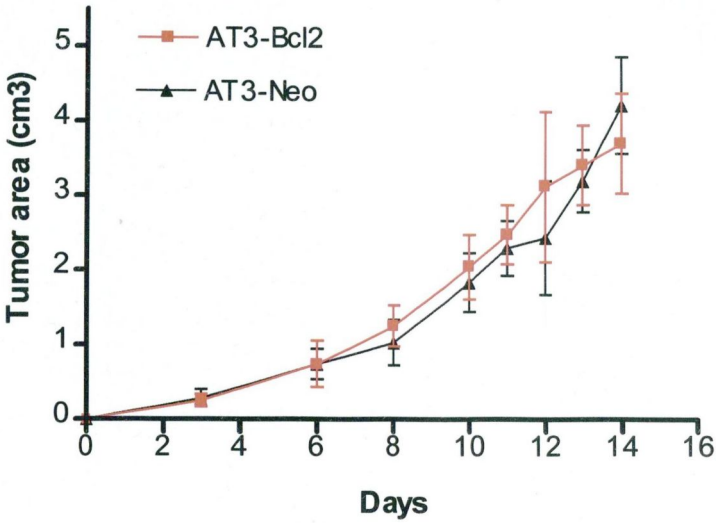


Figure 5.26- Growth of AT3-Neo and AT3-Bcl-2 cell lines as *in vivo* sc tumours.

Mice were injected sc with either AT3-Neo or AT3-Bcl-2 cell suspensions (~5 x 10^5 cells in normal medium). Ten mice were used for each cell line. Tumour nodules were detected in 100% of mice at 24 h p.i. Tumour diameter was measured in 2 orthogonal directions with linear calipers, and volume was calculated by assuming a spherical shape, with the average diameter calculated as the square root of the product of cross-sectional diameters. Tumour volume reached 20% of mouse body weight after 2 weeks, at which time mice were processed for pathological examination. *Points*, means ; *bars*, SD.

***Figure 5.27*- Gross examination of *in vivo* AT3 sc tumours.** Mice were sacrificed at 2 weeks p.i. when tumour size reached 20% body weight. (*A*) Balb/C *nu/nu* mouse with sc AT3-Neo tumour, 2 weeks following injection with an AT3-Neo cell suspension. (*B*) Balb/C *nu/nu* mouse with sc AT3-Bcl-2 tumour, 2 weeks following injection with an AT3-Bcl-2 cell suspension. AT3 tumours are morphologically indistinguishable. Note size and large areas of acute haemorrhage (*large arrow*) within tumour masses. Note also, extensive angiogenic effects of sc tumours (*B*, *small arrow*).

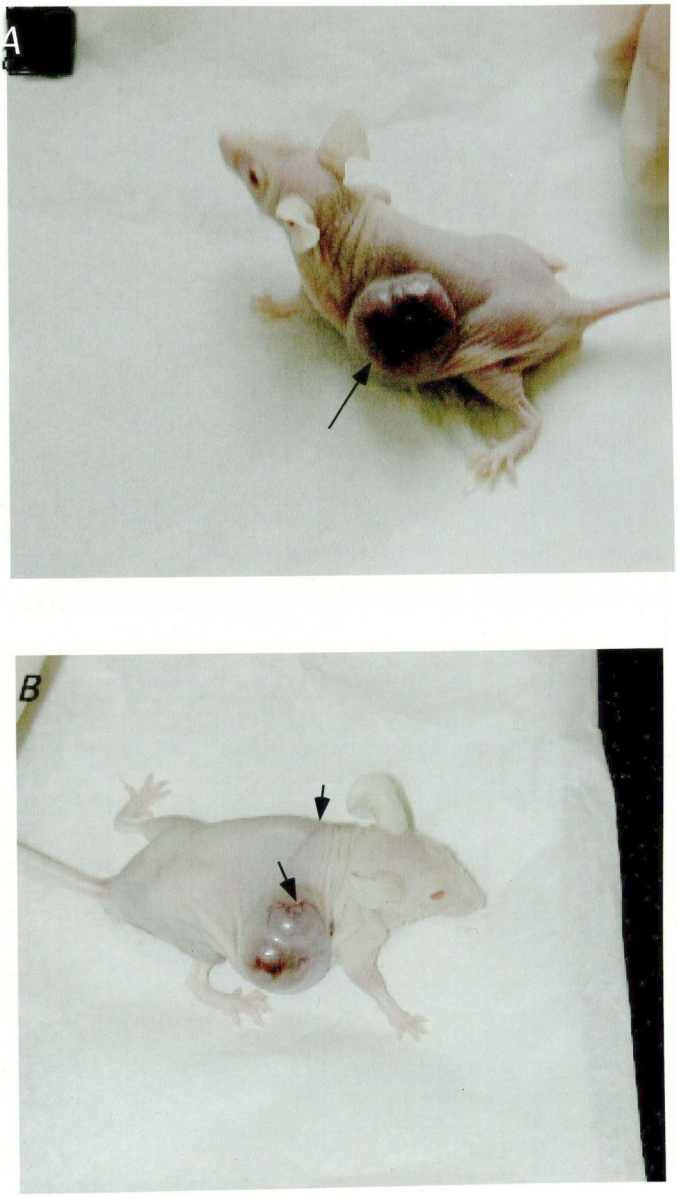


Figure 5.27- Gross examination of *in vivo* AT3 sc tumours.

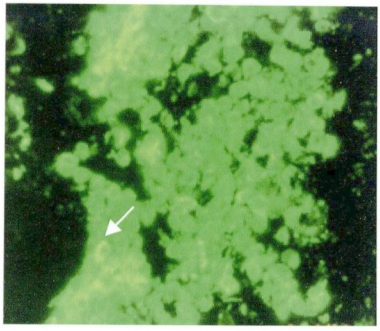


Figure 5.29- Immunohistochemical analysis of an *in vivo* AT3-Bcl-2 sc tumour.

AT3-Bcl-2 cryosections were cut at 6 μm, acetone-fixed and incubated with monoclonal mouse anti-human Bcl-2 oncoprotein antibody, for 30 min. Sections were subsequently incubated with an anti-mouse FITC-conjugated secondary antibody and visualised using fluorescent microscopy, at 460 nm. Note positive FITC, Bcl-2-specific staining within AT3-Bcl-2 tumour cells. Staining appears to be membranous and cytoplasmic (*arrow*). AT3-Neo tumour cryosections were FITC-negative when subjected to an identical analysis (*not shown*). Photographed at x 200 magnification.

heart, lung, kidney and spleen, and at the periphery of the tumours (*not shown*). Although the overexpression of Bcl-2 is artificial, and not inherent to the tumour cell type, its expression was constitutive and localised to regions observed within normal cells. Thus both tumour types were highly amenable to treatment studies. Furthermore, due to the rapid nature of sc tumour cell growth and vascularisation, all subsequent *in vivo* studies would begin with an initial smaller cell inoculum for sc tumour formation.

5.3.8 Infectious SFV-4 virus inhibits the growth and viability of AT3 cells

As a prerequisite to SFV vector analysis, AT3-Neo and AT3-Bcl-2 cell lines were analysed for their ability to survive, following infection with the infectious clone of SFV, SFV-4. Scallan *et al* (1997) demonstrated that Bcl-2 overexpression inhibited apoptosis induction following infection with both A7 and L10 strains of the virus. SFV-4 bears closest similarity to the SFV strain L10. Based on recommendations from Levine *et al*, (1993) and Scallan *et al*, (1997), AT3-Neo and AT3-Bcl-2 cells were grown on 6-well plates and infected with SFV-4 virus (moi 1) or medium alone, for 1 h. Cell viabilities of both cell types were estimated by trypan blue exclusion criteria daily, for 7 days after SFV-4 virus infection. Results are illustrated in figure 5.30. Mock-infected AT3-Neo cells continued to grow and proliferate rapidly in the initial 4 days p.i. (*Figure 5.30 A*), where as the majority of AT3-Neo cells infected with SFV-4 were dead by 24 h p.i. At 48 h p.i. with SFV-4, and in all subsequent time-points, 100% of AT3-Neo cells were eliminated (Day 3 ; $P<0.007$). The viability of mock-infected AT3-Neo cells also showed a marked decrease from day 4 p.i. onwards. This was unequivocally attributed to the rapid nature of cell growth, leading to overconfluence, and subsequent decrease in cellular survival within spent medium. In contrast to AT3-Neo cells, cells overexpressing Bcl-2 show little difference in viability following SFV-4 infection, than with mock-infected AT3-Bcl-2 cells (*Figure 5.30 B*). However, this scenario is true only up until day 2 p.i. with SFV-4.

Figure 5.30- **Viability of AT3-Neo (*A*) and AT3-Bcl-2 (*B*) cells following infection with infectious SFV-4 virus, as determined by trypan blue exclusion.** AT3 cells were incubated at densities of $1x10^4$ cells/well in 6-well plates, and infected with SFV-4 virus (moi 1) or medium alone as a control for 1 h. At each indicated timepoint p.i., triplicate wells for both cell lines, were trypsinsied and counted using trypan blue exclusion criteria. *Points*; means, *bars*; SD for a single experiment, and is representative of two independent experiments.

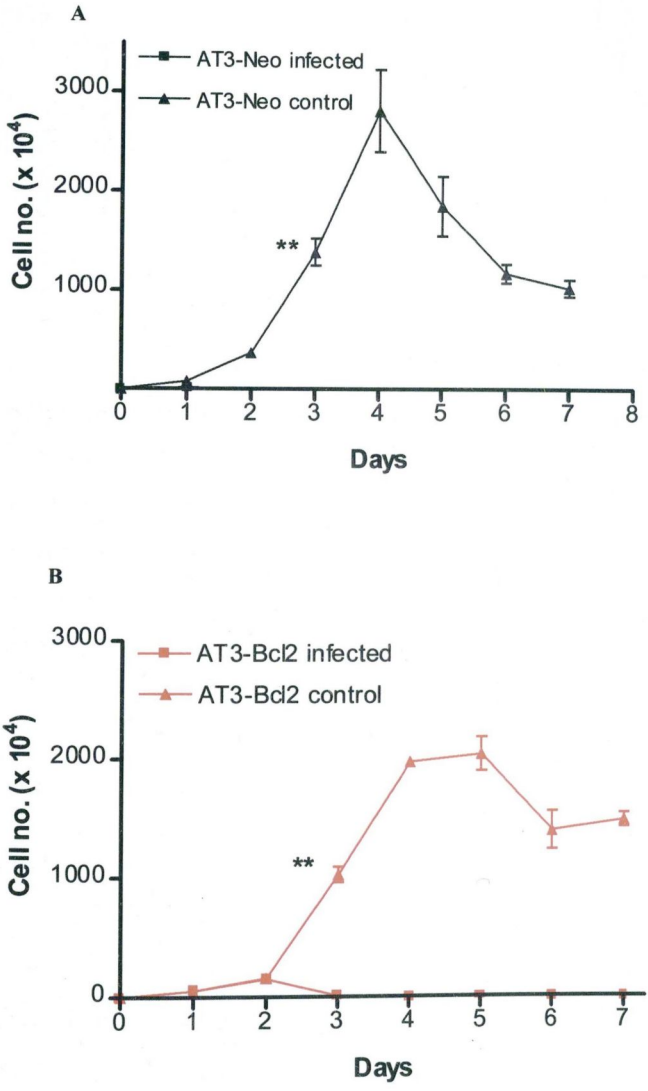


Figure 5.30- Viability of AT3-Neo (*A*) and AT3-Bcl-2 (*B*) cells following infection with SFV-4 virus, as determined by trypan blue exclusion.

Figure 5.30- **Viability of AT3-Neo (*A*) and AT3-Bcl-2 (*B*) cells following infection with infectious SFV-4 virus, as determined by trypan blue exclusion.** AT3 cells were incubated at densities of $1x10^4$ cells/well in 6-well plates, and infected with SFV-4 virus (moi 1) or medium alone as a control for 1 h. At each indicated timepoint p.i., triplicate wells for both cell lines, were trypsinsied and counted using trypan blue exclusion criteria. *Points*; means, *bars*; SD for a single experiment, and is representative of two independent experiments.

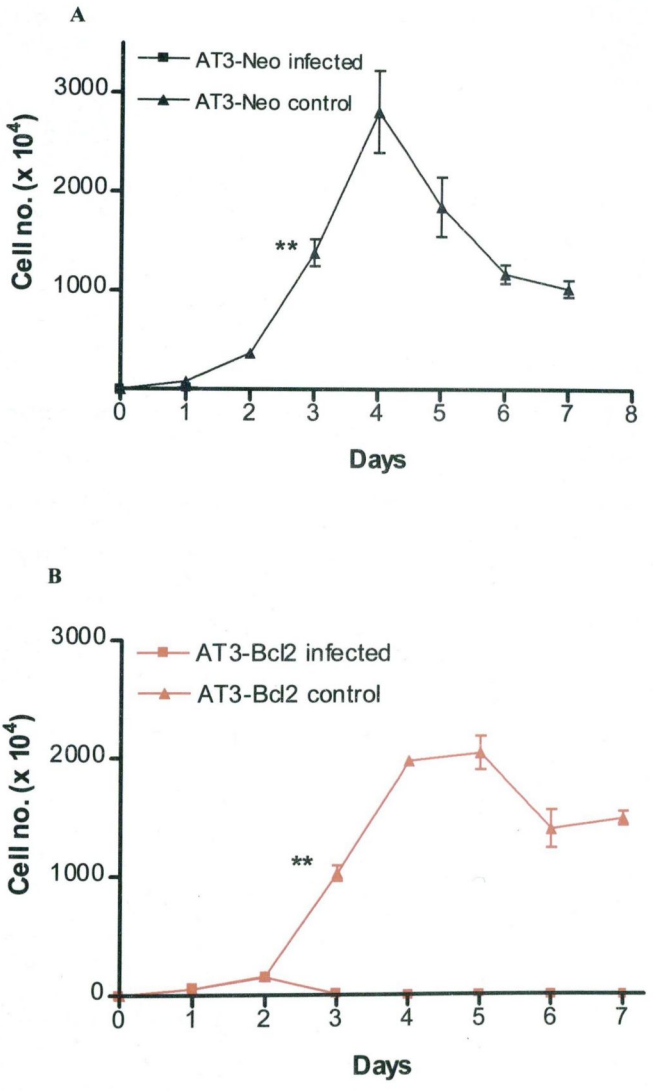


Figure 5.30- Viability of AT3-Neo (*A*) and AT3-Bcl-2 (*B*) cells following infection with SFV-4 virus, as determined by trypan blue exclusion.

Figure 5.31- **Viability of AT3-Neo (*A*) and AT3-Bcl-2 (*B*) cells following infection with infectious SFV-4 virus, as determined by sulphorhodamine B colorimetric analysis.** AT3 cells were incubated at densities of 1 x 10^4 cells/well in 6-well plates, and infected with SFV-4 virus (moi 1) or medium alone as a control. At each indicated timepoint p.i., cells were fixed in TCA, stained with sulphorhodamine B, and the surviving cells were measured colorimetrically using an ELISA reader. *Points*; means, *bars*; SD for a single experiment, and is representative of two independent experiments.

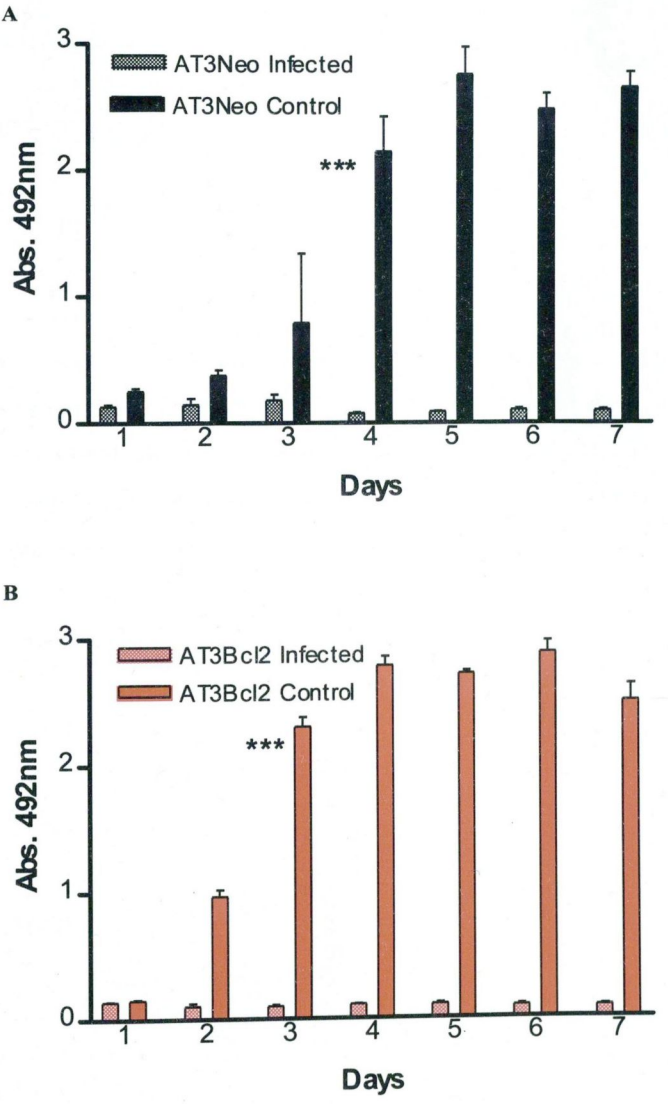


Figure 5.31- Viability of AT3-Neo (*A*) and AT3-Bcl-2 (*B*) cells following infection with SFV-4 virus, as determined by sulphorhodamine B colorimetric analysis.

Figure 5.32- **Viability of AT3-Neo (*A*) and AT3-Bcl-2 (*B*) cells following infection with infectious SFV-4 virus, as determined by ^{3}H thymidine incorporation.** AT3 cells were plated at densities of 1 x 10^{4} cells/well in 6-well plates, and infected with SFV-4 virus (moi 1) or medium alone as a control. At each indicated timepoint p.i., medium from triplicate wells, for both cells lines, was replaced with medium containing methyl-^{3}H thymidine. Following a 24 h incubation, cells were removed, and ^{3}H incorporation was measured using a liquid scintillation counter. *Points*; means, *bars*; SD for a single experiment, and is representative of two independent experiments.

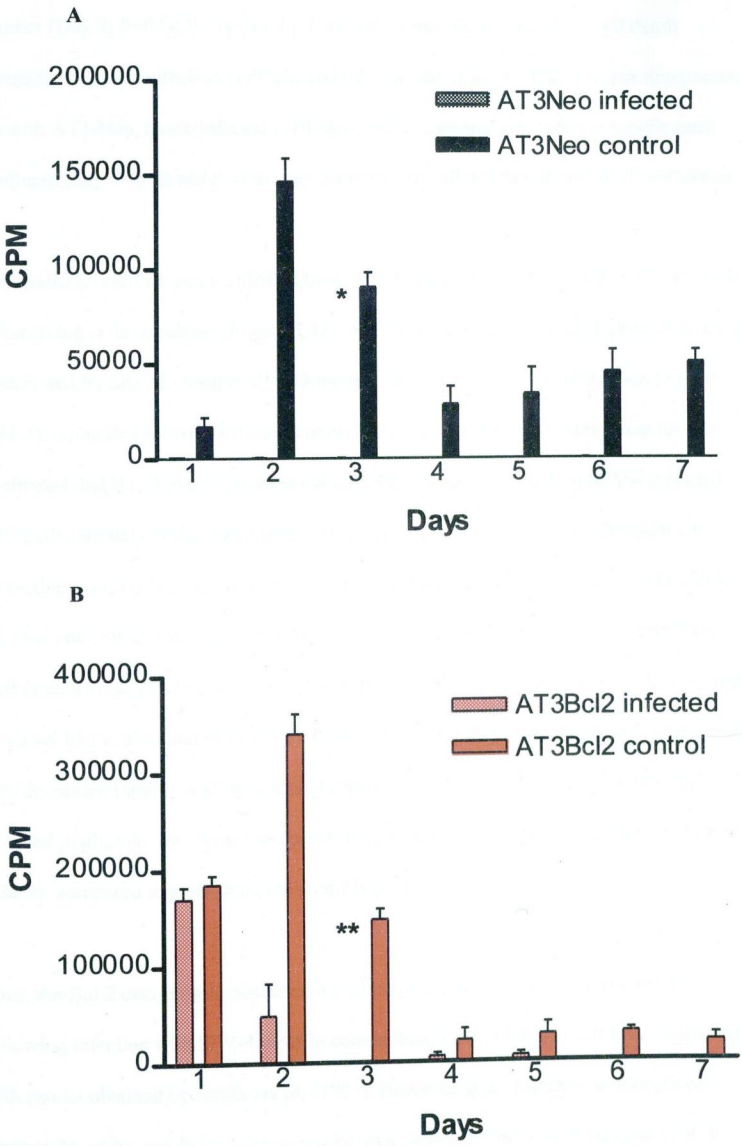


Figure 5.32- Viability of AT3-Neo (*A*) and AT3-Bcl-2 (*B*) cells following infection with SFV-4 virus, as determined by ^{3}H thymidine incorporation.

Figure 5.32- **Viability of AT3-Neo (*A*) and AT3-Bcl-2 (*B*) cells following infection with infectious SFV-4 virus, as determined by ^{3}H thymidine incorporation.** AT3 cells were plated at densities of 1 x 10^{4} cells/well in 6-well plates, and infected with SFV-4 virus (moi 1) or medium alone as a control. At each indicated timepoint p.i., medium from triplicate wells, for both cells lines, was replaced with medium containing methyl-^{3}H thymidine. Following a 24 h incubation, cells were removed, and ^{3}H incorporation was measured using a liquid scintillation counter. *Points*; means, *bars*; SD for a single experiment, and is representative of two independent experiments.

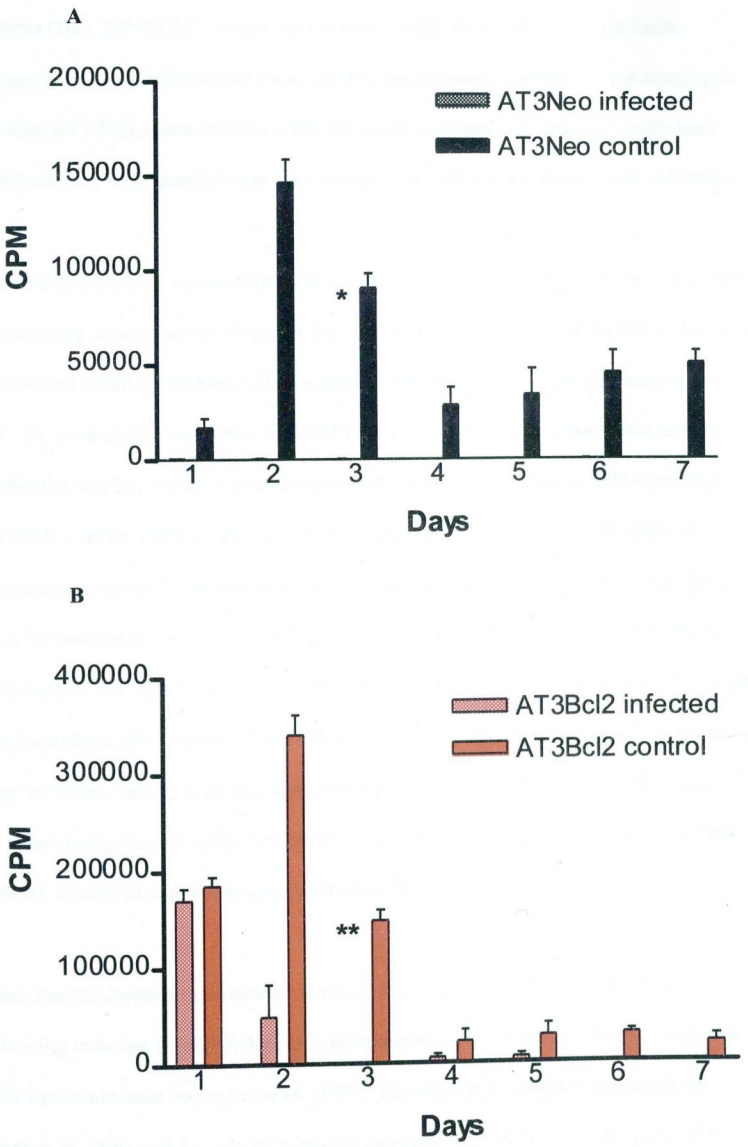


Figure 5.32- Viability of AT3-Neo (*A*) and AT3-Bcl-2 (*B*) cells following infection with SFV-4 virus, as determined by ^{3}H thymidine incorporation.

By day 3 p.i., AT3-Bcl-2 cells revealed the initial signs of cell death and decreased in number (Day 3; $P<0.002$). By day 4 p.i. with the virus, there was ~90% cell death compared to mock-infection controls, and this was repeated in all subsequent timepoints. As with AT3-Neo, mock-infected AT3-Bcl-2 cells continue to proliferate rapidly until confluent (day 4-5), at which time they decreased in cell number, due to overconfluence.

Cell viability analysis was confirmed by sulphorhodamine B (SRB) colorimetric analysis of surviving cells in culture (*Figure 5.31*). AT3-Neo cells displayed negligible viability as determined by SRB staining at all time-points following SFV-4 virus infection (*Figure 5.31 A*), compared to mock-infected controls (day 3, $P<0.006$). This assay also further confirmed that Bcl-2-overexpression conferred a survival advantage in SFV-4-infected AT3 cells, but only in the initial stages of infection (*Figure 5.31 B*). Bcl-2-mediated protection was short-lived, and cell viability was drastically reduced compared to mock-infected controls at 3 days p.i. ($P<0.001$). Cellular methyl[^{3}H]thymidine incorporation, further confirmed this (*Figure 5.32*). The viability of Bcl-2-overexpressing cells remained at a level identical to that of mock-infected controls for 24-36 h p.i. (*Figure 5.32 B*), and then decreased rapidly in all subsequent time-points (day 3, $P<0.004$). AT3-Neo cells revealed negligible thymidine incorporation at all timepoints following infection (*Figure 5.32 A*), compared to mock-infected controls ($P<0.01$).

Thus, the Bcl-2 oncoprotein conferred a protective advantage on AT3-Bcl-2 cells following infection with SFV-4 virus in comparison to the AT3-Neo cell line, consistent with results obtained by Scallan *et al*, (1997). However, this protection is short-lived (approx 24-48 h), and *Bcl-2*-overexpressing cells also succumbed to wild-type SFV-4 infection.

5.3.9 Infectious SFV-4 virus induces apoptotic cell death in AT3 cells lines.

Due to the marked decrease in AT3 cell viability upon infection with SFV-4 virus, we next examined if this were due to the induction of apoptosis. To investigate SFV-4-mediated AT3 cell death, both AT3-Neo and AT3-Bcl-2 cell lines were seeded into 75 cm^2 flasks and infected with SFV-4 (moi 1) or with medium alone. DNA was extracted from treated and control cells at 24 h intervals p.i., for 7 days, and analysed for fragmentation into oligonucleosomal fragments, by agarose gel electrophoresis. The results are illustrated in figure 5.33. As with A7 and L10 strains (Scallan *et al*, 1997), DNA fragmentation was detected in AT3-Neo cells as early as 24 h p.i with SFV-4 (*Figure 5.33 A*). In contrast, AT3-Bcl-2 cells showed no signs of DNA fragmentation in the first 2 days p.i. (*Figure 5.33 B*). However, at day 3 p.i. with SFV-4, DNA oligonucleosomal fragments were observed in AT3-Bcl2 cells. The onset of DNA fragmentation directly coincided with the decrease in AT3-Bcl-2 cell viability shown in figures 5.30-5.32. Mock-infected AT3-Neo and AT3-Bcl-2 cells remained negative for DNA fragmentation, but were detected at later time-points p.i. (*not shown*). DNA fragmentation in control cells directly coincided with the decrease in cellular viability, observed in figures 5.33-5.32, related to overconfluence and cell death in spent medium.

5.3.10 rSFV virus particle infection efficiency of AT3 cell lines *in vitro*.

The conditions for optimal viral infection of the AT3 cell lines with the rSFV virus vector, were determined using rSFV-EGFP particles. AT3-Neo and AT3-Bcl-2 cells (1×10^4 cells/well) were infected with increasing concentrations of rSFV-EGFP particles, and examined for the EGFP expression by direct epifluorescence. Results are presented in Figure 5.34 *A*. In AT3-Neo cells, a linear relationship existed between the number of infected cells and the moi of virus used, up to moi 200. At moi 1000 (~10^7 I.U. rSFV-

Figure 5.33- Apoptosis induction in AT3-Neo (A) and AT3-Bcl-2 (B) cells following infection with infectious SFV-4 virus. AT3 cells were incubated at densities of 1 x 10^6 cells/well in 75 cm^2 flasks, and infected with SFV-4 virus (moi 1) or medium alone as a control. At 24 h intervals following infection, cells were lysed and DNA was released by enzymatic digestion. Cellular DNA for SFV-4 virus- and mock-infected cells was analysed for fragmentation into oligonucleosomal-size fragments, indicative of cell death, by agarose gel electrophoresis. (*A*) AT3-Neo cells. *Lanes 1 and 8*; λ (*Hind 111* and *EcoR1*) DNA molecular weight markers. *Lane 2*; DNA from mock-infected control AT3-Neo cells at 48h p.i. *Lanes 3-9*; DNA from SFV-4 virus-infected AT3-Neo cells at days 1, 2, 3, 4, 5, 6 and 7 p.i., respectively. (*B*) AT3-Bcl-2 cells. *Lanes 1 and 8*; λ (*Hind 111* and *EcoR1*) DNA molecular weight mrkers. *Lane 2*; DNA from mock-infected control AT3-Bcl-2cells at 24h p.i. *Lanes 3-9*; DNA from SFV-4 virus-infected AT3-Bcl-2 cells at days 1, 2, 3, 4, 5, 6 and 7 p.i., respectively.

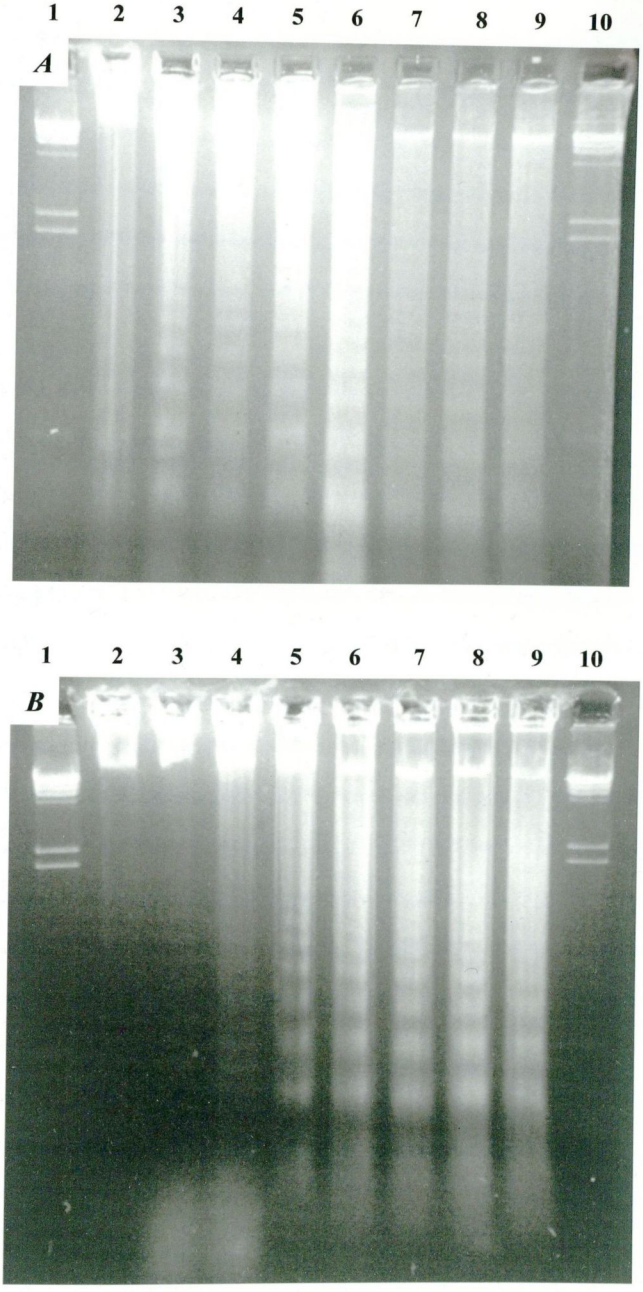


Figure 5.33- Apoptosis induction in AT3-Neo and AT3-Bcl-2 cells following infection with infectious SFV-4 virus.

EGFP), over 90% of AT3-Neo cells were positive for the vector. In contrast to AT3-Neo, the infection efficiency of AT3-Bcl-2 cells with rSFV-EGFP particles was negligible at lower moi's (moi 1-200). At 18 h p.i., less than 11% of AT3-Bcl-2 cells expressed the reporter gene at the maximum moi (moi 1000). Limitations with regard to particle titres, prevented the use of higher moi's for infection. In conclusion, moi 500-1000 was calculated as optimal for infection of both AT3-Neo and AT3-Bcl-2 cell lines.

In an effort to correlate rSFV virus infection with AT3 cell death, cells were analysed for viability, three days following infection with rSFV-EGFP, at the same range of concentrations (*Figure 5.34 B*). The day 3 time-point was analysed due to previous results with infectious SFV-4 virus, in which AT3-Bcl-2 cell viability was not affected until at least 48 h p.i. (*see section 5.3.8*). AT3-Neo cells revealed a linear relationship between rSFV-EGFP virus concentration and percentage cell viability, as determined by SRB staining. At moi 1000, with over 90% infection efficiency, almost 90% of the cells were non-viable compared to the mock-infected control. In AT3-Bcl-2 cells, a linear relationship also existed between the concentration of virus and cell viability, albeit to a much lower degree of efficiency. At maximum moi (moi 1000), with 10% infection efficiencies, up to 40% of the cells were non-viable compared to controls. An examination of whether Bcl-2 overexpression acts to delay rSFV virus infection, or reduces the level of viral replication and EGFP expression remains to be investigated.

5.3.11 rSFV-EGFP particles inhibit the growth and viability of AT3 cells

Having established optimal rSFV viral infection efficiencies, AT3 cells were infected with rSFV-EGFP and rSFV-1 particles. The latter was used as a vector control to ensure that cell death was due to the vector alone, and not as a consequence of reporter gene expression (*see Chapter 3*). Cells were also mock-infected with medium alone as a

Figure 5.34- **Infection efficiency and effect of increasing concentrations of rSFV-EGFP virus particles in AT3Neo and AT3Bcl2 cell lines.** AT3-Neo (■) and AT3-Bcl-2 (▲) cells were seeded onto glass coverslips in 6-well plates at densities of 1 x 10^4 cells/well, and infected, in duplicate, with increasing concentrations (moi = 1, 10, 40, 80, 100, 200, 500 and 1000) of rSFV-EGFP virus particles (1 x 10^8 I.U./ml), or medium alone as control, (moi=0), for 1 h. (*A*) Infection efficiency of rSFV-EGFP virus. At 18 h p.i., cells were fixed, stained with DAPI for 20 min, and analysed for EGFP expression by fluorescent microscopy, at 488 nm (*EGFP*) and 350 nm (*DAPI*). EGFP-expressing cells were scored, and calculated as a percentage of the number of DAPI-stained cells in each field. Percentage infection efficiencies for both cell lines are indicated in parentheses. (*B*) The effect of increasing concentrations of rSFV-EGFP virus on AT3 cell viability. Three days following infection, cells were fixed, stained with sulphorhodamine B, and the surviving cells were determined at 492 nm using an ELISA reader. The percentages of cell viability, indicated in parentheses, were calculated with moi=0 as 100%.

Points; means, *bars*; SD.

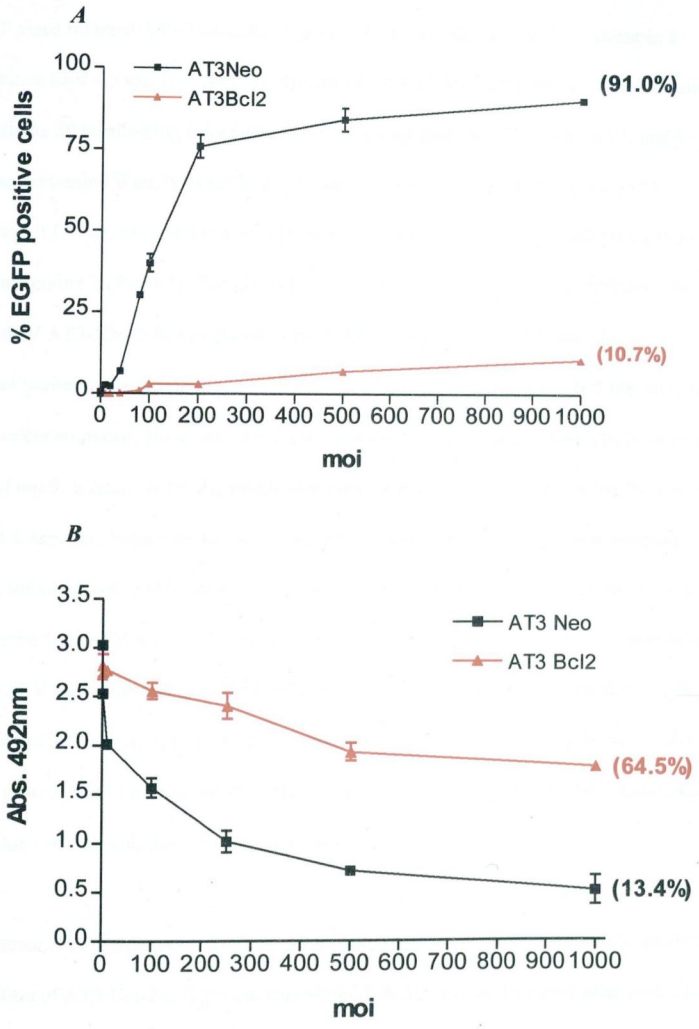


Figure 5.34- Infection efficiency (*A*) and the effect of increasing concentrations (*B*) of rSFV-EGFP virus particles in AT3Neo and AT3Bcl2 cell lines.

negative control. Cell viability, for both cell types, was examined by trypan blue exclusion, daily, for 5 days p.i. Results are illustrated in figure 5.35. Analysis of rSFV-EGFP virus infected AT3-Neo cells (*Figure 5.35 A*) revealed an identical scenario to infectious SFV-4 virus (*Figure 5.30 A*). Growth of AT3-Neo cells was severely curtailed as early as 24 h following infection with rSFV vector particles. This was confirmed by sulphorhodamine B analysis at identical time-points p.i. (*Figure 5.36 A*), and rSFV-infected AT3-Neo cells showed an 80% reduced viability at 3 days p.i. compared to mock-infected controls ($P<0.01$). The rSFV-1 virus vector was less effective at inhibiting the growth of AT3-Neo cells compared to rSFV-EGFP particles. rSFV-1 particles were titrated indirectly, by comparison to rSFV-EGFP production, and thus, viral titre may have been underestimated. However, cell viability of rSFV-1–infected AT3-Neo cells was 40% that of mock-infected controls, which continued to grow and proliferate normally in the initial 4 days p.i., before declining in number due to overconfluence in spent medium. Thus, infection with rSFV particles elicited an identical effect in the AT3-Neo cell line as with infectious SFV-4 virus. The inhibitory effects of rSFV particles were due primarily, to the SFV backbone and not *EGFP* expression, as rSFV-1 particles elicit a similar effect on cell viability. In contrast to wild-type infectious SFV-4 virus infection however, the rapid growth rate of uninfected AT3-Neo cells eventually overcame the rSFV-mediated inhibitory effects, and the cells largely recovered.

In contrast to AT3-Neo cells, Figure 5.35 *B* illustrates clearly that rSFV particle-mediated inhibition of AT3-Bcl-2 cell growth was not inhibited at any of the above time-points p.i. Both rSFV-EGFP- and rSFV-1 virus-infected AT3-Bcl-2 cells showed growth rates and viabilities equal to that of mock-infected control cells, and appeared largely unaffected by infection with the vector when examined by trypan blue exclusion and sulphorhodamine B analysis (*Figure 5.36 B*). This was evident even at later time-points p.i., when a reduction in viability was evident following wild-type SFV-4 virus infection (*Figures 5.30-5.32*). Cellular growth rate for both cell lines was also determined by measurement of methyl-^{3}H

Figure 5.35- **Growth and viability of AT3-Neo (*A*) and AT3-Bcl-2 (*B*) cells following infection with rSFV particles, as determined by trypan blue exclusion.** AT3 cells were incubated at densities of 1 x 10^4 cells/well in 6-well plates, and infected with rSFV-EGFP (moi 500), rSFV-1 (~moi 500) particles or medium alone as a control for 1 h. At each indicated timepoint p.i., triplicate wells, for both cell lines, were trypsinised and counted using trypan blue exclusion criteria. *Points*; means, *bars*; SD, for a single experiment and is representative of 2 independent experiments.

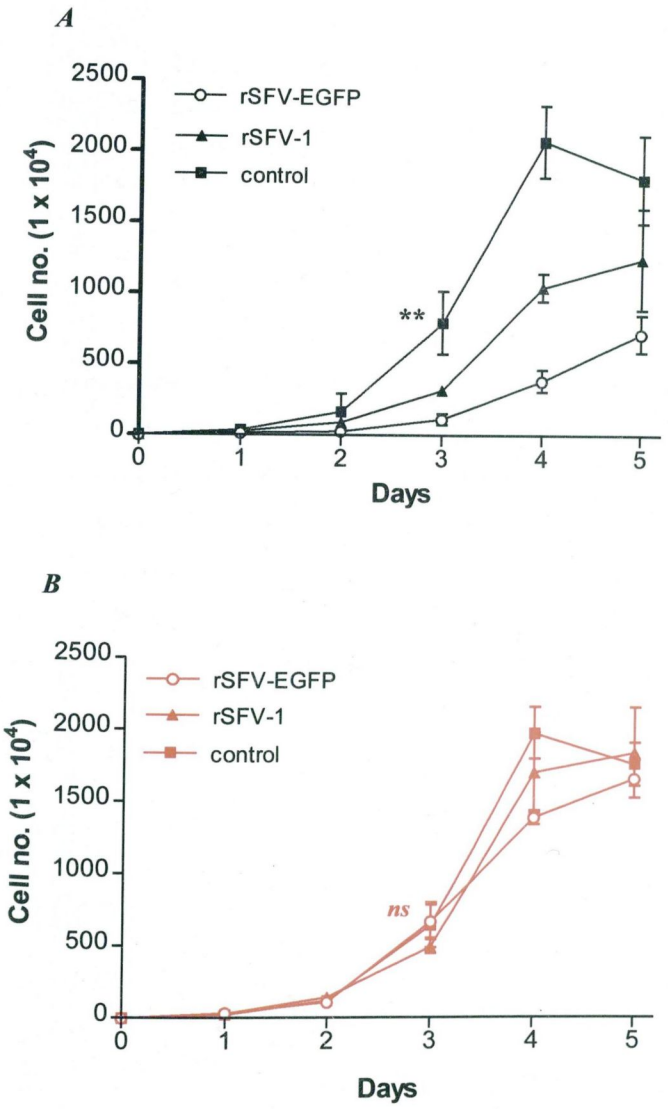


Figure 5.35- Growth and viability of AT3-Neo (*A*) and AT3-Bcl-2 (*B*) cells following infection with rSFV particles, as determined by trypan blue exclusion.

Figure 5.36- **Growth and viability of AT3-Neo (*A*) and AT3-Bcl-2 (*B*) cells following infection with rSFV particles, as determined by sulphorhodamine B colorimetric analysis.** AT3 cells were incubated at densities of 1 x 10^4 cells/well in 6-well plates, and infected with rSFV-EGFP (moi 500), rSFV-1 (~moi 500) particles or medium alone as a control for 1 h. At each indicated timepoint p.i., cells in triplicate wells were fixed in TCA, stained with sulphorhodamine B and the surviving cells measured colorimetrically using an ELISA reader. *Points*; means, *bars*; SD, for a single experiment and is representative of 2 independent experiments.

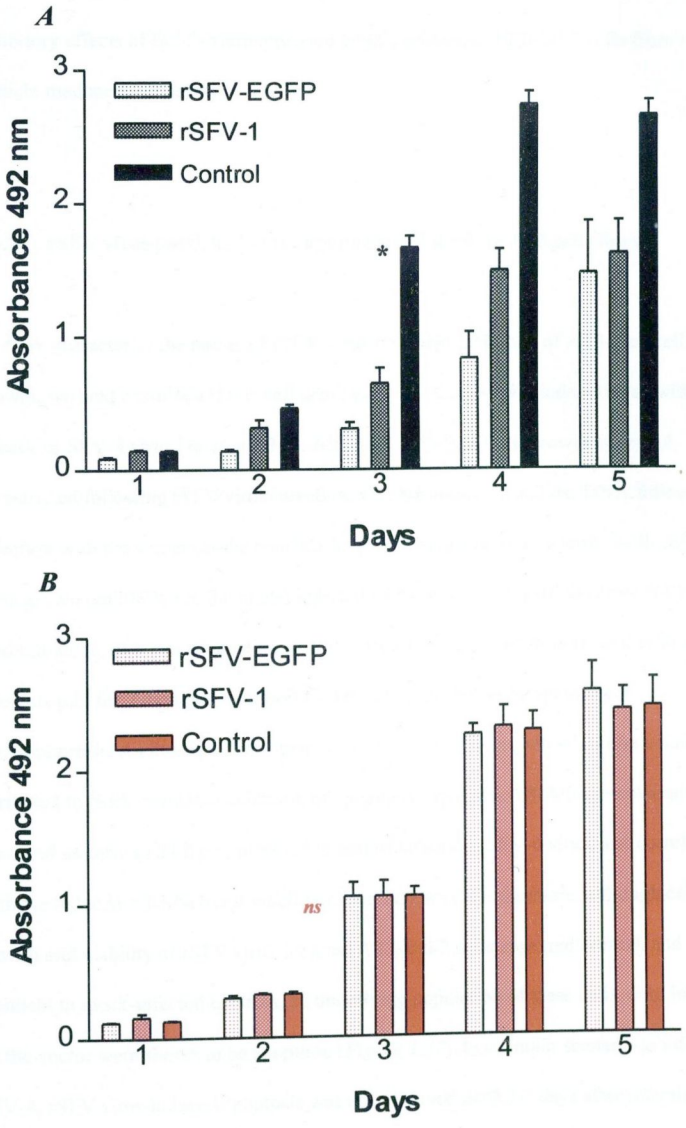


Figure 5.36- Growth and viability of AT3-Neo (*A*) and AT3-Bcl-2 (*B*) cells following infection with rSFV particles, as determined by sulphorhodamine B colorimetric analysis.

thymidine incorporation (*not shown*), confirming the above results, but these results were obscured by cell death in overconfluent plates. Thus, in contrast to infectious virus, the inhibitory effects of Bcl-2-overexpression largely protected AT3-Bcl-2 cells from rSFV-particle mediated cell death.

5.3.12 rSFV virus particles induce apoptotic cell death in AT3 cells lines.

To fully characterise the nature of rSFV virus-mediated inhibition of AT3-Neo cell growth, we next examined if this cell death were due to apoptosis induction, as with infectious SFV-4 virus (*section 5.3.9*). Although AT3-Bcl-2 cell growth appeared unrestricted following rSFV virus infection, we also examined cellular DNA following infection with the vector for the possible low-level induction of apoptosis. Both cell lines were grown until 80% confluent and infected with rSFV-EGFP particles (moi 500) or medium alone, as a mock-infection control. DNA was extracted from treated cells at 24 h intervals p.i., for 7 days and analysed for DNA fragmentation by agarose gel electrophoresis. As illustrated in Figure 5.37, AT3-Neo cell growth inhibition could be attributed to rSFV-mediated induction of apoptosis. Apoptotic DNA fragmentation was observed as early as 24 h p.i., identical to that of infectious SFV-4 virus, and correlated with the reduced AT3-Neo cell viability observed above. Furthermore, although cell growth and viability of rSFV virus-infected AT3-Bcl-2 cells appeared normal, and identical to mock-infected controls, an underlying population of these cells were infected by the vector were shown to be apoptotic (*Figure 5.37*). In a similar scenario to infectious SFV-4, rSFV virus-induced apoptosis was not observed until 2-3 days after infection. This apoptotic phenotype was not observed in mock-infected control cells at these time-points p.i., although it was detected at later time-points.

Figure 5.37- **Apoptosis induction in AT3-Neo (*A*) and AT3-Bcl-2 (*B*) cells following infection with rSFV-EGFP virus particles.** AT3 cells were incubated at densities of 1 x 10^6 cells/well in 75 cm^2 flasks, and infected with rSFV-EGFP particles (moi 500) or medium alone as a control. At 24 h intervals following infection, cells were lysed and DNA was released by enzymatic digestion. Cellular DNA from rSFV virus- and mock-infected cells was analysed for fragmentation into oligonucleosomal-size fragments, indicative of apoptosis, by agarose gel electrophoresis. *Lane 1*; λ (*Hind III*) DNA molecular weight markers. *Lane 2*; DNA from mock-infected control AT3-Neo cells 1day p.i. *Lanes 3-6*; DNA from rSFV-EGFP virus-infected AT3-Neo cells at days 1, 2, 3, 4 p.i., respectively. *Lane 8*; DNA from mock-infected AT3-Bcl-2 cells 1 day p.i. *Lanes 9-12*; DNA from rSFV-EGFP virus-infected AT3-Bcl-2 cells at days 1, 2, 3, 4 p.i., respectively.

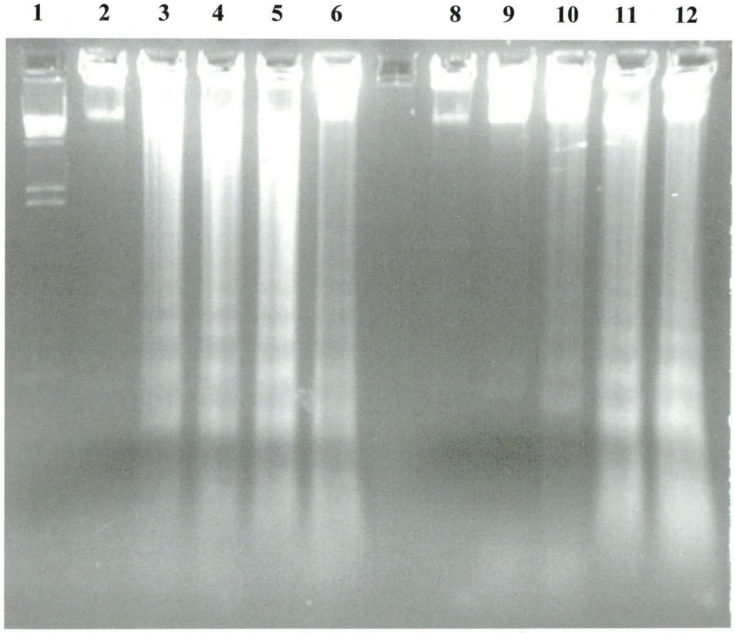


Figure 5.37- Apoptosis induction in AT3-Neo and AT3-Bcl-2 cells following infection with rSFV-EGFP virus particles.

In conclusion, rSFV virus infection of AT3-Bcl-2 cells largely failed to reproduce the cpe and cell growth retardation observed following infection with wild-type SFV-4 virus . A limited number of the AT3-Bcl-2 cells were infected with rSFV particles and underwent apoptosis, but this was obscured by the rapid rate of growth of uninfected cells.

5.3.13 High titre rSFV-EGFP virus-mediated inhibition of AT3 tumour growth *in vivo*.

In the previous section, rSFV-EGFP particles (moi 500) were shown to inhibit the growth and proliferation of AT3-Neo cell lines *in vitro*, and induced apoptosis in both AT3-Neo and AT3-Bcl-2 cell lines. To address the therapeutic potential of rSFV-EGFP particles *in vivo*, both AT3-Neo and AT3-Bcl-2 tumour cell lines were allowed to form sc tumours (~4 mm diameter), using the *nu/nu* mouse xenograft model. Each mouse received direct intratumoural injections of 50-100 µl of TNE buffer alone, or TNE containing rSFV-EGFP particles (1 x 10^{10} I.U./ml), each on days 1, 2, 3 and days 7, 8 and 9. Five to seven mice were used per treatment group. As in Chapter 4, rSFV-EGFP particles were re-titrated using the sBHK cell line, and each mouse received on average, 5 x 10^{8} I.U. per injection. Tumours were measured as before and results from both AT3 cell lines are illustrated in figure 5.38. Tumours treated with TNE buffer only, grew vigorously in size until day 12, when tumour volumes for both AT3-Neo and AT3-Bcl-2 cell lines reached over 20% that of the mouse (*Figures 5.39-5.40*). In contrast, rSFV-EGFP-treated AT3-Neo tumours showed a significant reduction (Day 12, $P<0.009$) in tumour growth, reaching 70% that of control AT3-Neo tumour volumes at this timepoint p.i. AT3-Bcl-2 tumour treatment with rSFV-EGFP particles also indicated a significant inhibition of tumour growth (Day 12, $P<0.025$), compared to TNE buffer-treated controls, reaching 75% of control levels at day 12 p.i.

***Figure 5.38*- Effects of rSFV-EGFP particle treatment on AT3 tumour growth *in vivo*.** AT3-Neo (*A*) and AT3-Bcl-2 (*B*) cell lines (5×10^4) were injected subcutaneously into Balb/C *nu/nu* mice. On reaching tumour diameters of ~4 mm (approximately 4 days), tumours received six intratumoural injections of rSFV-EGFP virus (5×10^8 I.U.) or TNE buffer. Five to seven mice were used per treatment group, for both cell lines. Arrows indicate days of treatment. Tumour diameters were measured in two orthogonal directions, and tumour volume was calculated by assuming a spherical shape. *Points*; means, *bars*; SD, for a single experiment.

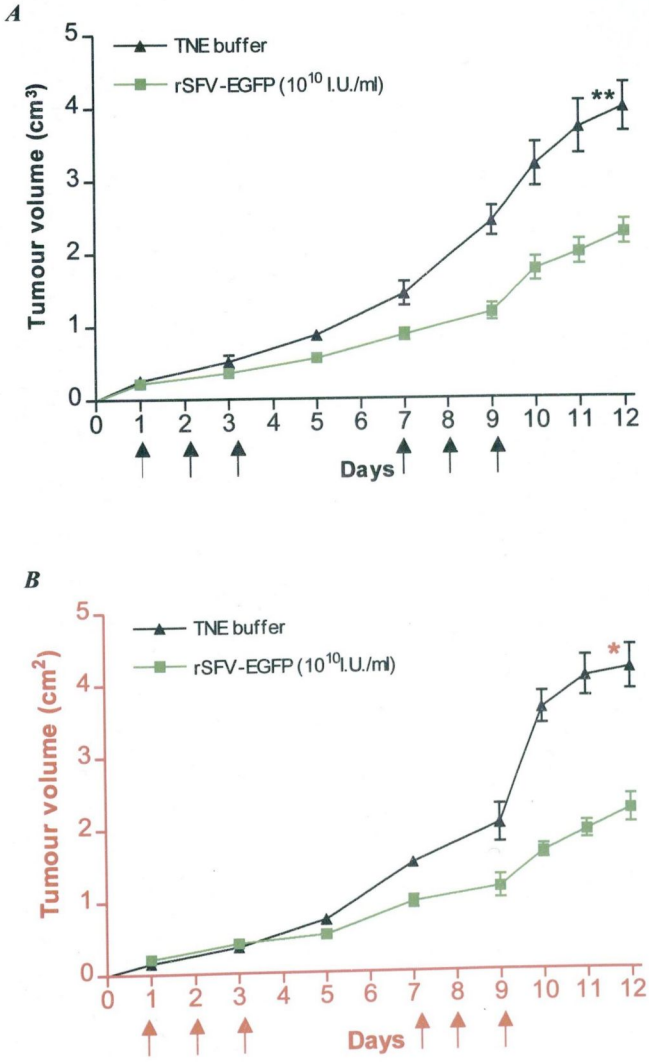


Figure 5.38- Effects of rSFV-EGFP particle treatment on AT3 tumour growth *in vivo*.

***Figure 5.38*- Effects of rSFV-EGFP particle treatment on AT3 tumour growth *in vivo*.** AT3-Neo (*A*) and AT3-Bcl-2 (*B*) cell lines (5 x 10^4) were injected subcutaneously into Balb/C *nu/nu* mice. On reaching tumour diameters of ~4 mm (approximately 4 days), tumours received six intratumoural injections of rSFV-EGFP virus (5 x 10^8 I.U.) or TNE buffer. Five to seven mice were used per treatment group, for both cell lines. Arrows indicate days of treatment. Tumour diameters were measured in two orthogonal directions, and tumour volume was calculated by assuming a spherical shape. *Points*; means, *bars*; SD, for a single experiment.

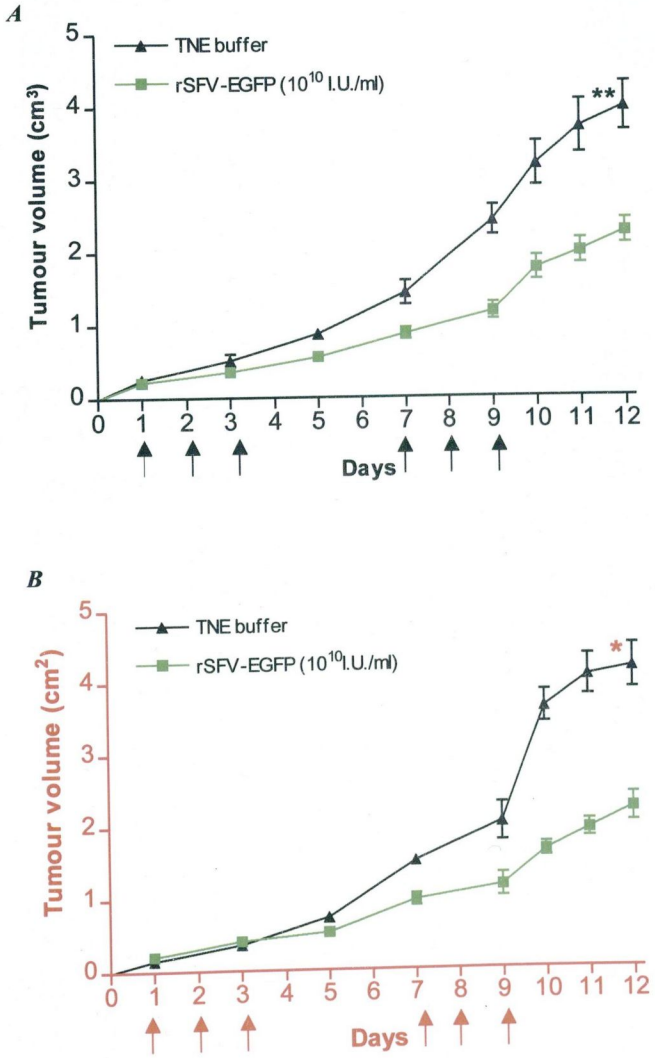


Figure 5.38- Effects of rSFV-EGFP particle treatment on AT3 tumour growth *in vivo*.

Figure 5.39- **Subcutaneous AT3-Neo tumour growth in the *nu/nu* mouse xenograph model following rSFV-EGFP viral therapeutic intervention.** Mice received subcutaneous injections of 5 x 10^4 AT3-Neo cells. Upon reaching 4 mm diameter, mice received direct intratumoural injections of rSFV-EGFP particles (5 x 10^8 I.U.) (*A*) or TNE buffer (*B*), on days 1, 2, 3 and days 7, 8 and 9. Mice were maintained for 12 days, at which time, control mice (*B*) were eliminated.

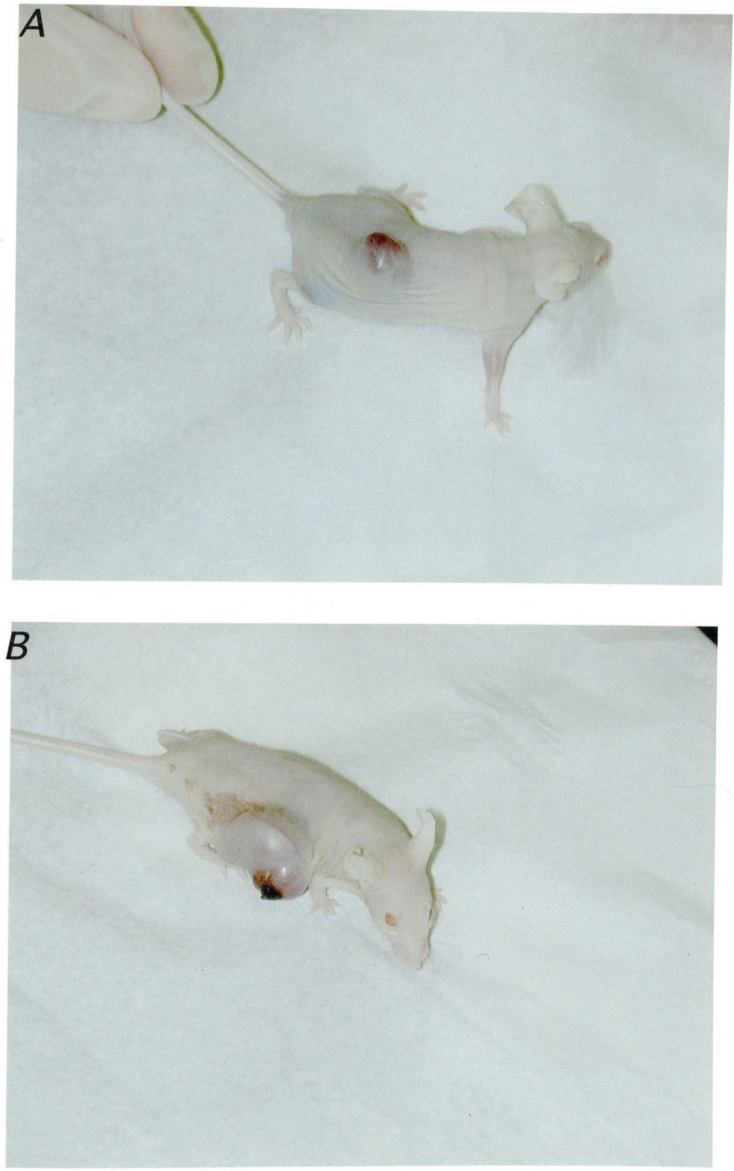


Figure 5.39- Subcutaneous AT3-Neo tumour growth in the *nu/ nu* mouse xenograft model following rSFV-EGFP Virus therapeutic intervention.

Figure 5.40- **Subcutaneous AT3-Bcl-2 tumour growth in the *nu/nu* mouse xenograft model following rSFV-EGFP viral therapeutic intervention.** Mice received subcutaneous injections of 5 x 10^4 AT3-Bcl-2 cells. Upon reaching 4 mm diameter, mice received direct intratumoural injections of rSFV-EGFP particles (5 x 10^8 I.U.) (*A*) or TNE buffer (*B*), on days 1, 2, 3 and days 7, 8 and 9. Mice were maintained for 12 days, at which time, control mice (*B*) were culled.

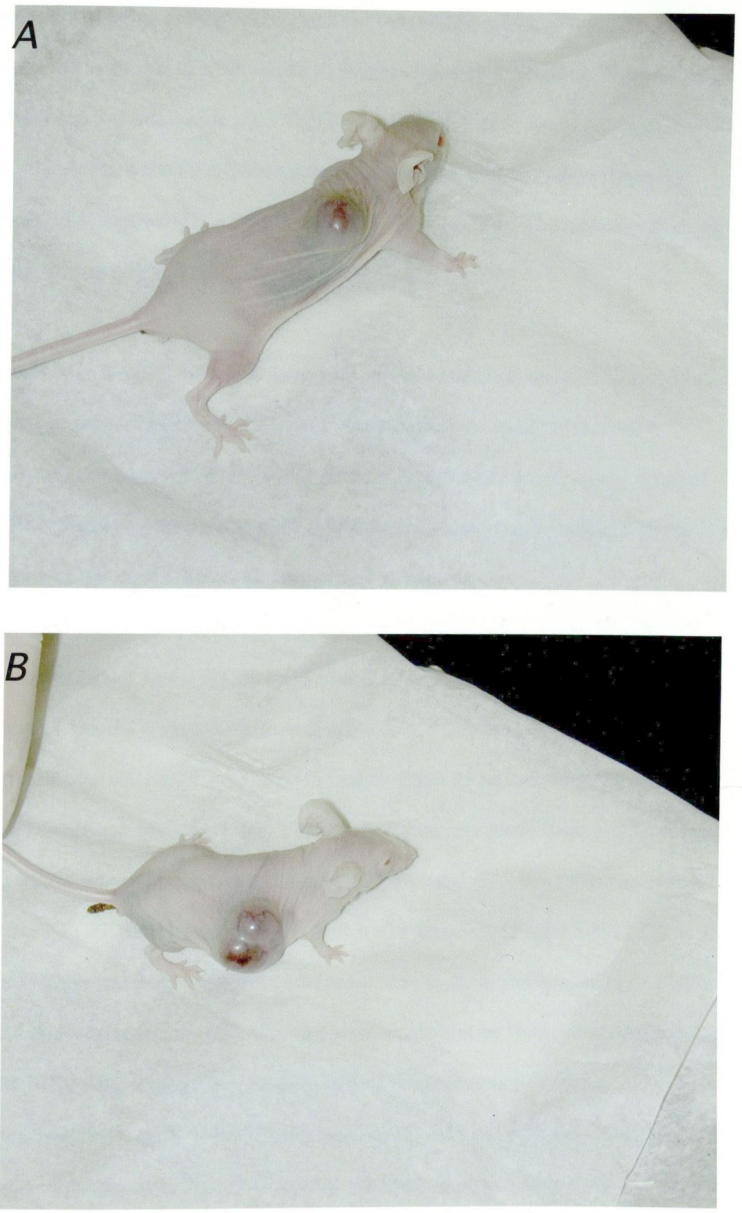


Figure 5.40- Subcutaneous AT3-Bcl-2 tumour growth in the *nu/nu* mouse xenograft model following rSFV-EGFP Virus therapeutic intervention.

In terms of mortality, one control mouse from both AT3-Neo and AT3-Bcl-2 treatment groups, died as a result of tumour burden on days 10 and 11 respectively. Tumour-induced mortality was not observed in rSFV-EGFP virus-treated mice at any of the above time-points. However, when treated mice were maintained for a further 7 days following elimination of controls (*Figure 5.41*), both AT3-Neo and AT3-Bcl-2 tumours regrew to volumes comparable to TNE buffer control levels at day 12.

Tumours were sampled at various timepoints post-treatment and assessed for pathological changes. Frozen AT3-Neo and AT3-Bcl-2 cryosections were analysed for EGFP expression at 24 h p.i. with rSFV-EGFP particles. Both tumour types revealed areas of EGFP-positive expression within rSFV-EGFP treated tumours only, although expression appeared sparse and was absent in many areas (*not shown*).

Histological examination of both AT3-Neo and AT3-Bcl-2 tumours treated with TNE buffer only (*Figure 5.42 A, B*), revealed masses of polygonal tumour cells with moderate amounts of basophilic cytoplasm, located in delicate, highly vascular connective tissue stroma. Tumour cell nuclei were round to oval, and showed prominent nuclei and finely stippled cytoplasm. Multinucleated cells, mitotic figures, apoptotic forms and focal areas of necrosis and haemorrhage were common. AT3-Neo and AT3-Bcl-2 tumours treated with rSFV-EGFP particles and sampled at 24 h after treatment (*Figure 5.42 C, D*), revealed larger and more widespread areas of oncotic necrosis and haemorrhage, distinct from compression necrosis. Necrotic areas were surrounded by layers of rapidly dividing tumour cells, along with small aggregates of lymphoid cells and neutophils.

TUNEL reactivities of rSFV-EGFP virus-treated AT3-Neo and AT3-Bcl-2 tumours were assessed on paraformaldehyde-fixed tumour cryosections, which were sampled at identical timepoints to those processed for routine histology. rSFV-EGFP-treated tumours showed more pronounced TUNEL reactivity in both tumour types, than in TNE buffer-treated controls at 24 h post-treatment, and were concentrated in necrotic areas, as assessed by morphological analysis of $TUNEL^{+}$ cells. Other regions of the rSFV-EGFP virus-treated

Figure 5.41- **rSFV-EGFP virus-treated AT3 tumours regrow following cessation of treatment.** AT3-Neo (*A*) and AT3-Bcl-2 (*B*) cell lines (5×10^4) were injected subcutaneously into Balb/C *nu/nu* mice. On reaching tumour diameters of ~4 mm (approximately 4 days), tumours received six intratumoural injections of rSFV-EGFP virus (5×10^8 I.U.) or TNE buffer, as indicated in figure 5.38. Arrows indicate days of treatment. Control mice were eliminated at day 12, and rSFV-EGFP virus-treated mice were maintained for an additional week post-treatment to assess tumour regrowth. *Points*; means, *bars*; SD, for a single experiment.

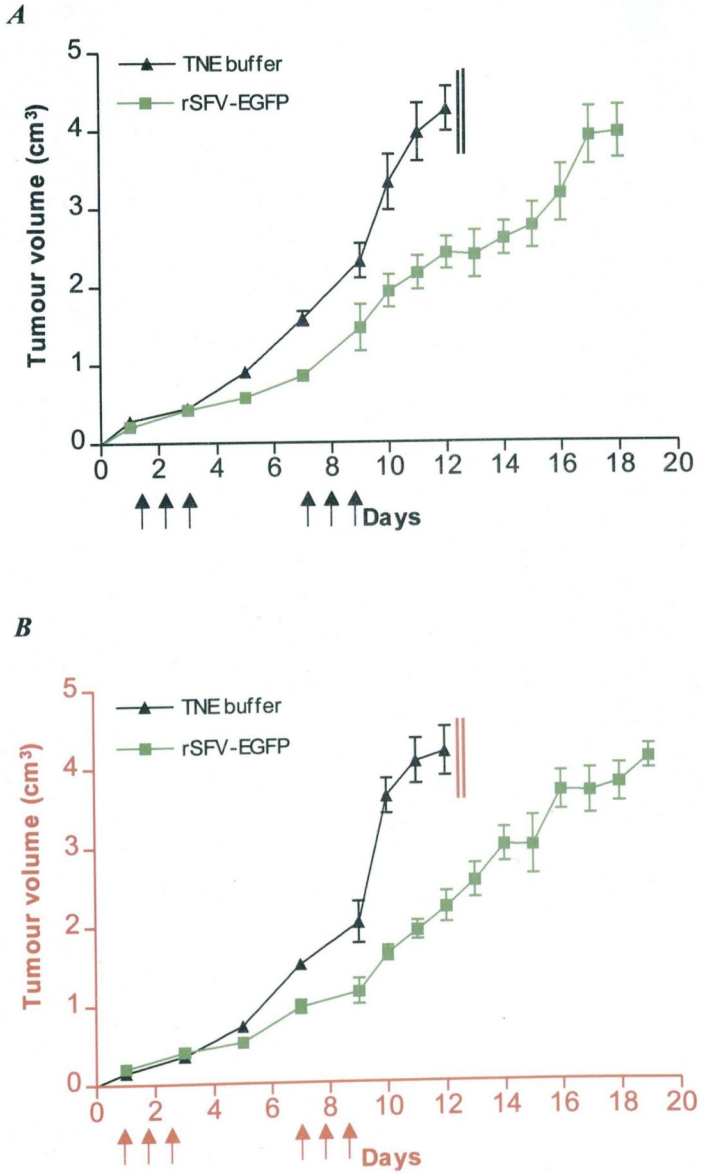


Figure 5.41- rSFV-EGFP virus-treated AT3 tumours regrow following cessation of treatment.

Figure 5.42- **Histology of AT3-Neo and AT3-Bcl-2 tumours following treatment with rSFV-EGFP particles.** (*A, B*) AT3-Neo and AT3-Bcl-2 tumours, 24 h following six daily intratumoural injections with TNE buffer. Aggregates of polyhedral tumour cells, with pleomorphic nuclei and large nucleoli, separated by very delicate, highly vascular strands of connective tissue stroma, were common in both tumour types. Numerous mitotic (M) and apoptotic (A) figures were observed. Photographed at x 200 and x 400, respectively. (*C, D*) AT3-Neo and AT3-Bcl-2 tumours, 24 h following six daily intratumoural injections with rSFV-EGFP virus (5×10^8 I.U./ml). Large areas of necrotic cell death are indicated in both tumour types (N), with cellular debris and anucleated cells, surrounded by layers of actively dividing tumour cells. Photographed at x 100 magnification.

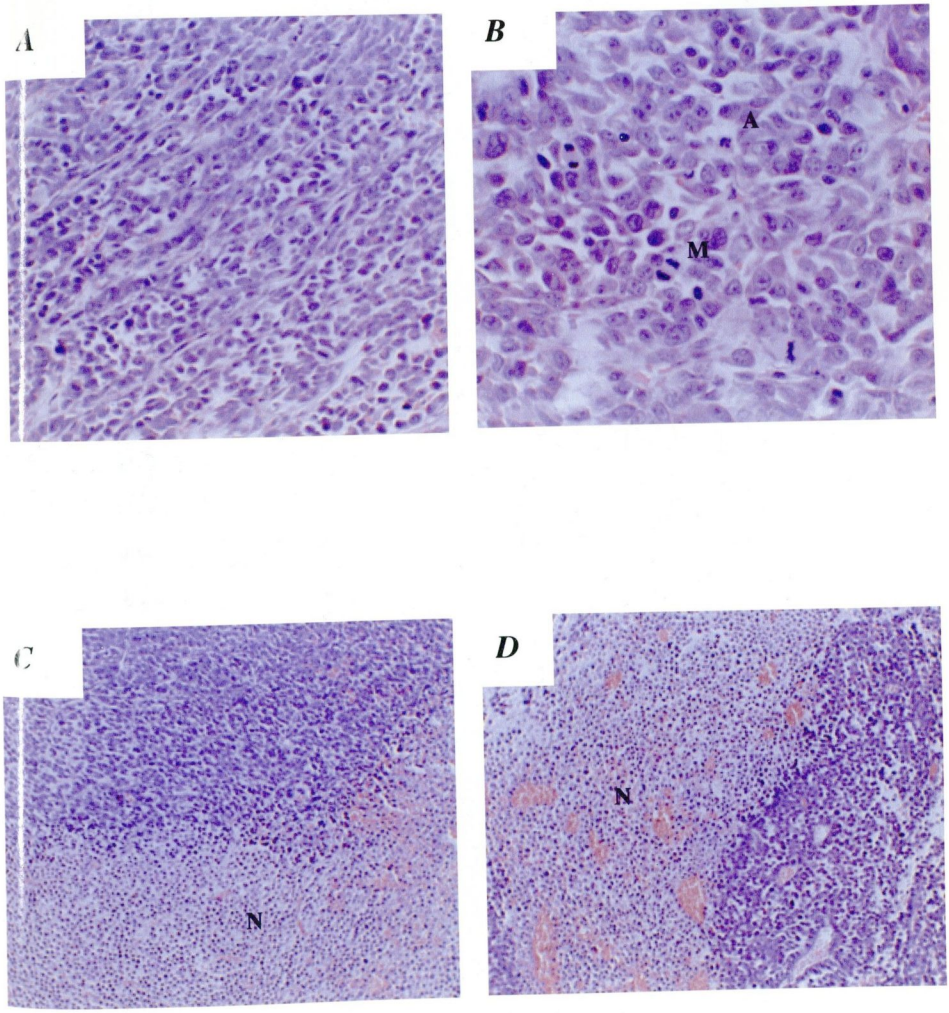


Figure 5.42- Histology of AT3-Neo and AT3-Bcl-2 tumours following treatment with rSFV-EGFP particles.

Figure 5.43- **TUNEL reactivity within AT3 tumours following treatment with rSFV-EGFP virus particles.** TUNEL analysis was performed on paraformaldehyde-fixed 10 μm cryosections. Colorimetric detection was performed using DAB, and normal healthy nuclei were counterstained using methyl green. (*A, B*) AT3-Neo and AT3-Bcl-2 tumours, respectively, 24 h following six daily intratumoural injections with TNE buffer. Both tumour types contained dispersed areas of TUNEL reactivity, particularly in regions of focal necrosis and haemorrhage. (*C, D*) AT3-Neo and AT3-Bcl-2 tumours, respectively, 24 h following six daily intratumoural injections with rSFV-EGFP virus (5×10^8 I. U./ml). Treated tumours contained areas of cell death distinct from endogenous necrosis, observed within controls, and were concentrated within large areas of apoptotic and necrotic cell death, surrounded by TUNEL$^-$, non-transfected tumour cells. Photographed at x 400 magnification.

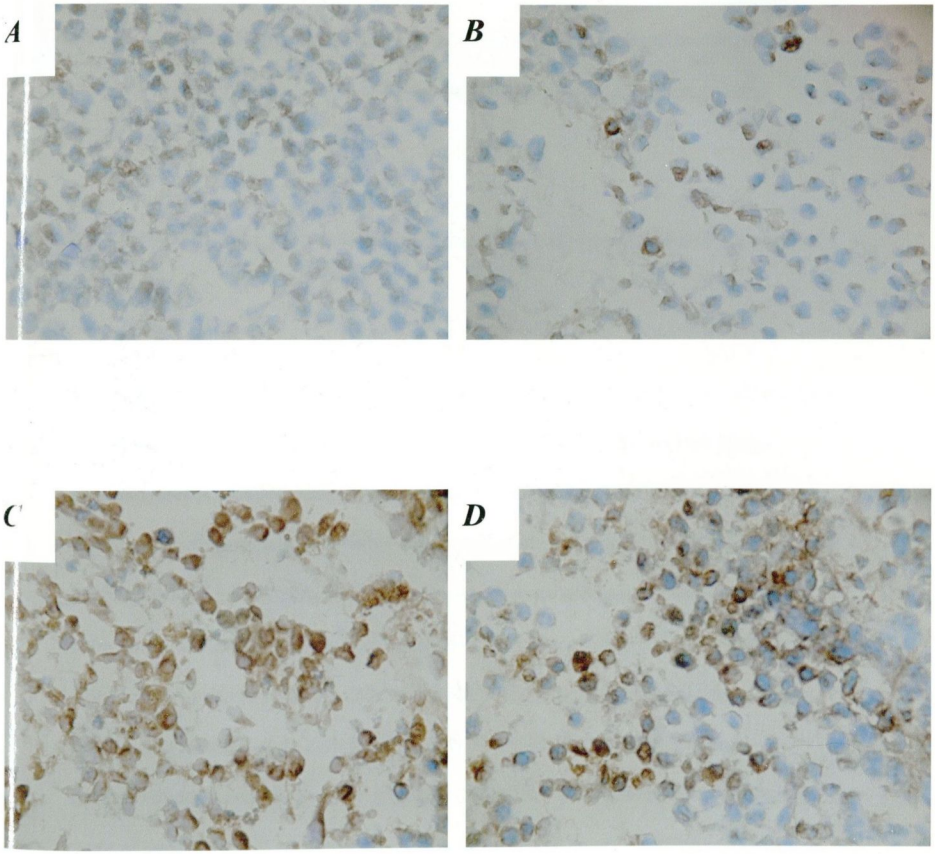


Figure 5.43- TUNEL reactivity within AT3 tumours following treatment with rSFV-EGFP particles.

tumours however, remained TUNEL negative, with lobules of actively proliferating tumour cells, indicating sites within individual tumours that remained inaccessible to rSFV virus treatment, and which were possibly responsible for tumour regrowth.

5.3.14 rSFV-HABax virus infection failed to inhibit the growth and viability of AT3 cells *in vitro*.

Having established optimal rSFV-EGFP virus infection efficiencies for the AT3 cell lines as moi 500-1000 (*section 5.3.10*), and demonstrated the tumour growth inhibitory potential of rSFV-EGFP particles both *in vitro* (*section 5.3.11*) and *in vivo* (*section 5.3.12*), we next assessed the whether the pro-apoptotic potential of the rSFV virus vector could be further enhanced by rSFV virus-mediated overexpression of *Bax* in infected cells. Both AT3-Neo and AT3-Bcl-2 cells were plated at densities of 1×10^4 cells/well, in 6-well plates, prior to infection. Due to low rSFV-HABax particle titres obtained upon harvest (*see section 5.3.4*), cells received only $\sim 10^5$ I.U. particles per infection, corresponding to moi 10-50. rSFV-EGFP virus particles were used as a vector control and were utilised at 10^5 I.U., and medium alone was used as a mock-infection control. Each sample was performed and analysed in triplicate, and cell viability was determined, as in all other analyses, using trypan blue exclusion, sulphorhodamine B and ^{3}H thymidine incorporation criteria. Results are illustrated in Figures 5.44-5.46.

Despite a marginally significant rSFV-HABax virus-mediated reduction in AT3-Neo cell viability early on following infection (Day 3, $P<0.05$), large numbers of uninfected cells appeared to overgrow those infected with the vector, bringing total cell viabilities back to mock-infected control levels by day 5 p.i (*Figures 5.44 A-5.46A*). At this time-point, control cells showed signs of overconfluence and began to die off within exhausted medium. It was assumed that rSFV-HABax virus infection efficiencies for the AT3-Neo cells equated that of rSFV-EGFP virus efficiencies (ie. moi 50;~30% infection), and that

Figure 5.44- **Viability of AT3-Neo (*A*) and AT3-Bcl-2 (*B*) cells following infection with rSFV-HABax particles, as determined by trypan blue exclusion.** AT3 cells were incubated at densities of 1 x 10^4 cells/well in 6-well plates, and infected with rSFV-HABax virus (moi 30), rSFV-EGFP virus (moi 30) or medium alone as a control, for 1 h. At each indicated timepoint p.i., triplicate wells for both cell lines, were trypsinised and counted using trypan blue exclusion criteria. *Points*; means, *bars*; SD for a single experiment.

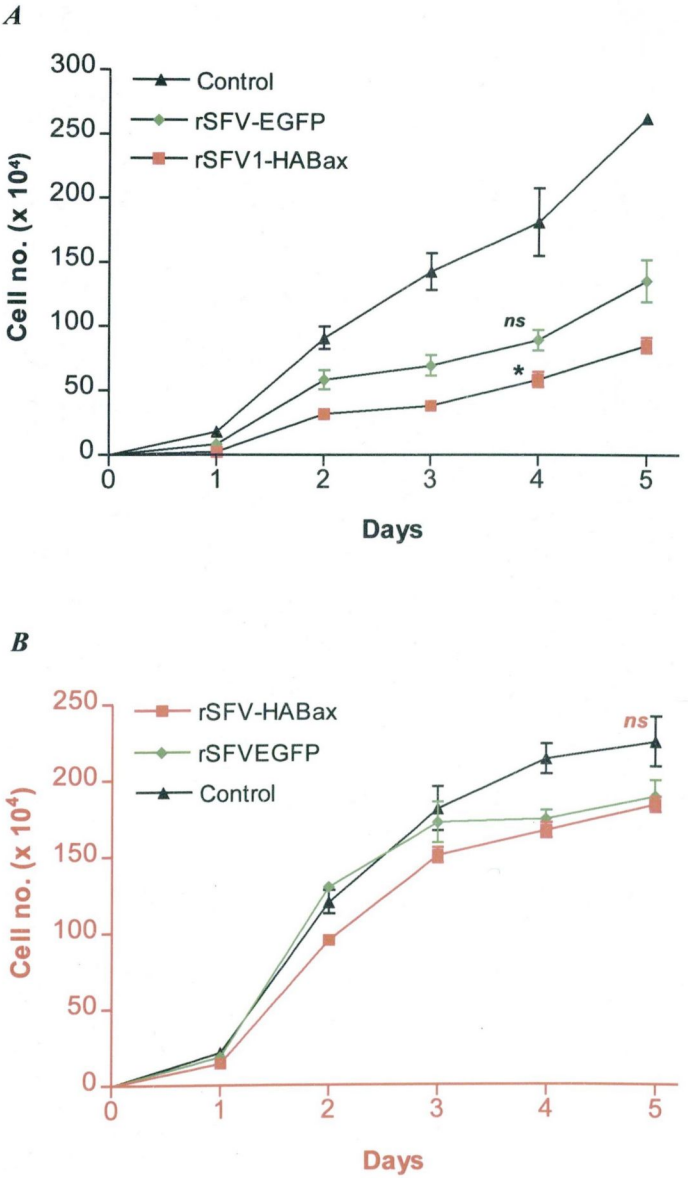


Figure 5.44- Viability of AT3-Neo and AT3-Bcl-2 cells following infection with rSFV-HABax particles, as determined by trypan blue exclusion.

Figure 5.45- **Viability of AT3-Neo (*A*) and AT3-Bcl-2 (*B*) cells following infection with rSFV-HABax particles, as determined by sulphorhodamine B colorimetric analysis.** AT3 cells were incubated at densities of 1 x 10^4 cells/well in 6-well plates, and infected with rSFV-HABax particles (moi 30), rSFV-EGFP particles(moi 30) or medium alone as a control. At each indicated timepoint p.i., cells were fixed in TCA, stained with sulphorhodamine B, and the surviving cells were measured colorimetrically using an ELISA reader. *Points*; means, *bars*; SD for a single experiment.

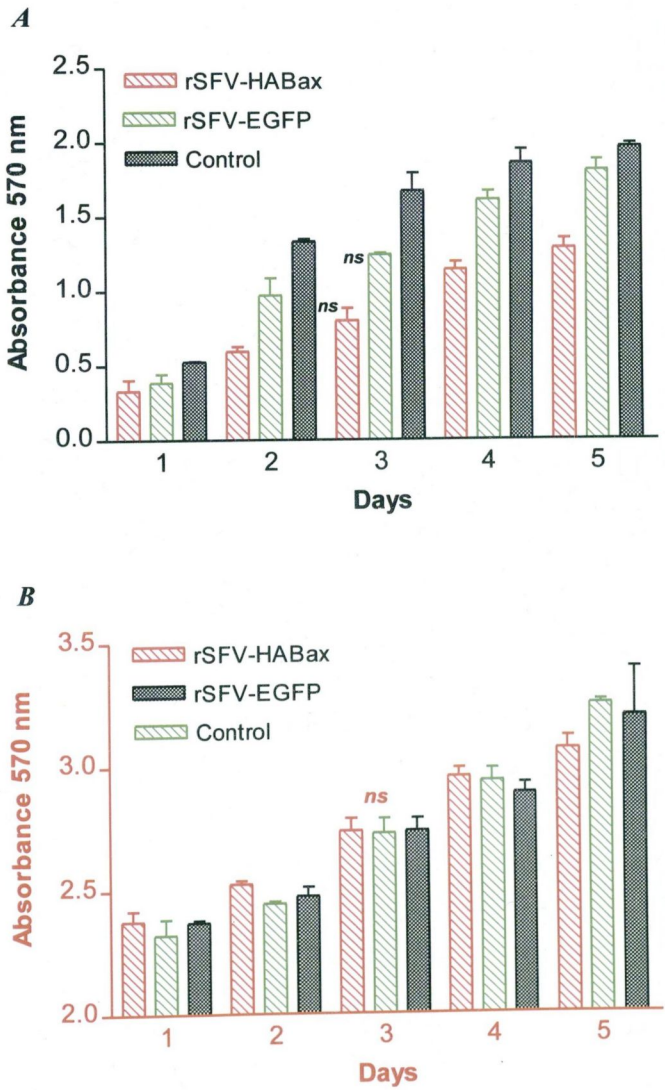


Figure 5.45- Viability of AT3-Neo and AT3-Bcl-2 cells following infection with rSFV-HABax particles, as determined by sulphorhodamine B colorimetric analysis.

Figure 5.46- **Viability of AT3-Neo (*A*) and AT3-Bcl-2 (*B*) cells following infection with rSFV-HABax particles, as determined by ^{3}H thymidine incorporation.** AT3 cells were plated at densities of 1 x 10^{4} cells/well in 6-well plates, and infected with rSFV-HABax virus (moi 30), rSFV-EGFP virus (moi 30) or medium alone as a control. At each indicated timepoint p.i., medium from triplicate wells, for both cells lines, was replaced with medium containing methyl-^{3}H thymidine. Following a 24 h incubation, cells were removed, and ^{3}H incorporation was measured using a liquid scintillation counter. *Points*; means, *bars*; SD for a single experiment.

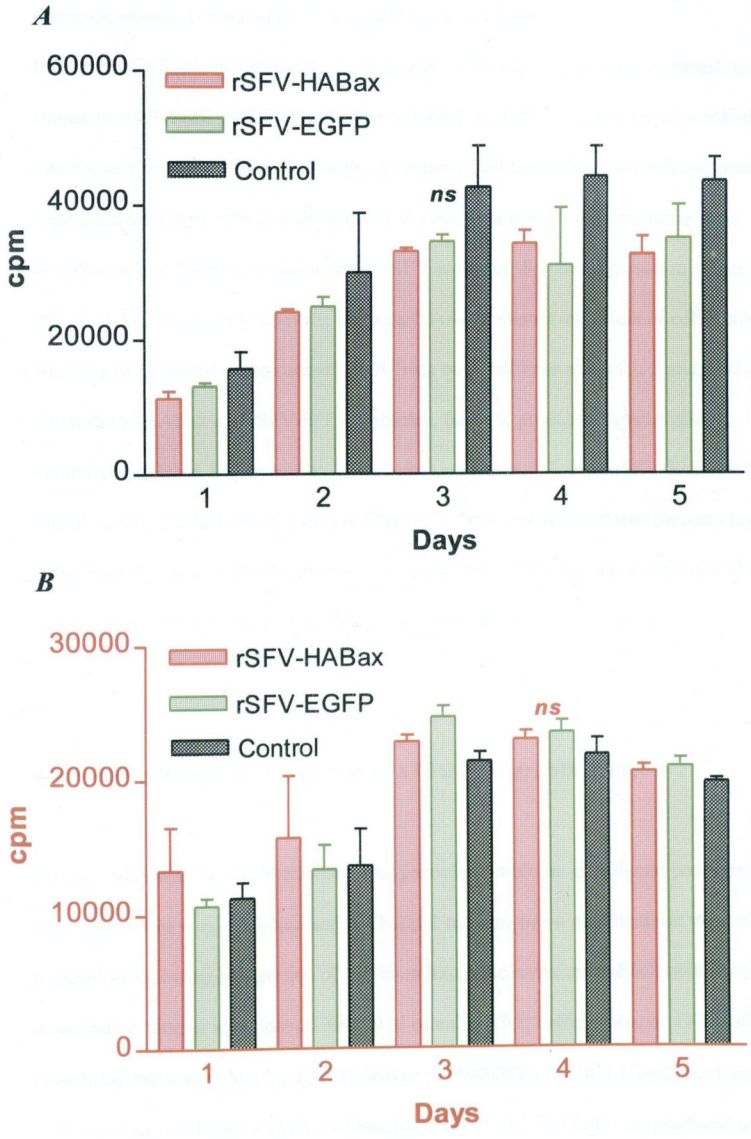


Figure 5.46- Viability of AT3-Neo and AT3-Bcl-2 cells following infection with rSFV-HABax particles, as determined by ^{3}H thymidine incorporation.

overexpression of Bax protein within the AT3-Neo cells failed to accentuate these cytotoxic effects, compared to rSFV-EGFP virus infection.

Infection of AT3-Bcl-2 cells with HABax- and EGFP-expressing particles failed, at all stages, to inhibit cell proliferation (*Figures 5.44 B-5.46 B*). Section 5.3.10 described a much lower infection efficiency for the AT3-Bcl-2 cell line, which possibly explains the negligible inhibitory effects following rSFV virus infection at such low titres. This experiment also failed to reveal whether rSFV-mediated *Bax* overexpression within the AT3-Bcl-2 cell line could alleviate the initial *Bcl-2*-mediated inhibition of cell death. Analysis of extracted chromosomal DNA from both cell lines at days 1, 2 and 3 p.i., with either rSFV-HABax and rSFV-EGFP particles, failed to produce characteristic chromosomal DNA fragmentation (*not shown*), observed following rSFV-EGFP virus infection at 200-fold higher titres (*see Figure 5.37*). It was assumed that the very low infection efficiency of rSFV particles, coupled with the 200-fold lower viral inoculum, was responsible for the lack of AT3-Bcl-2 growth inhibition.

5.3.15 rSFV-HABax viral inhibition of AT3 tumour growth *in vivo*.

To determine whether rSFV-HABax virus particles inhibit the growth and proliferation of AT3 tumours *in vivo*, AT3-Neo and AT3-Bcl-2 tumours of ~4 mm diameter were allowed to develop following sc injection of cell lines into male *nu/nu* mice. Each tumour received direct intratumoural injections of 50-100 µl of either TNE buffer alone, or TNE buffer containing rSFV-HABax (1×10^7 I.U./ml) or rSFV-EGFP (1×10^7 I.U./ml), each on days 1, 2, 3 and days 7, 8 and 9. rSFV-HABax particles of ~10^7 I.U./ml were produced using the high titre particle production procedure, but remained ~200-times lower than conventional rSFV-EGFP particle titres used for *in vivo* studies. rSFV-EGFP particles were therefore diluted in TNE buffer and used at ~10^7 I.U./ml also. Five mice were used per treatment group and tumours were measured daily for 20 days. Results for both

Figure 5.47- **Effects of rSFV-HABax virus treatment on AT3 tumour growth *in vivo*.** AT3-Neo (*A*) and AT3-Bcl-2 (*B*) cell lines (5×10^4) were injected subcutaneously into Balb/C *nu/nu* mice. On reaching tuomour diameters of ~4 mm (approximately 4 days), tumours received six intratumoural injections of rSFV-HABax particles (5×10^5), rSFV-EGFP particles (5×10^5 I.U.) or TNE buffer. Five mice were used per treatment group, for both cell lines. Arrows indicate days of treatment. Tumour diameters were measured in two orthogonal directions, and tumour volume was calculated by assuming a spherical shape. *Points*; means, *bars*; SD, for a single experiment.

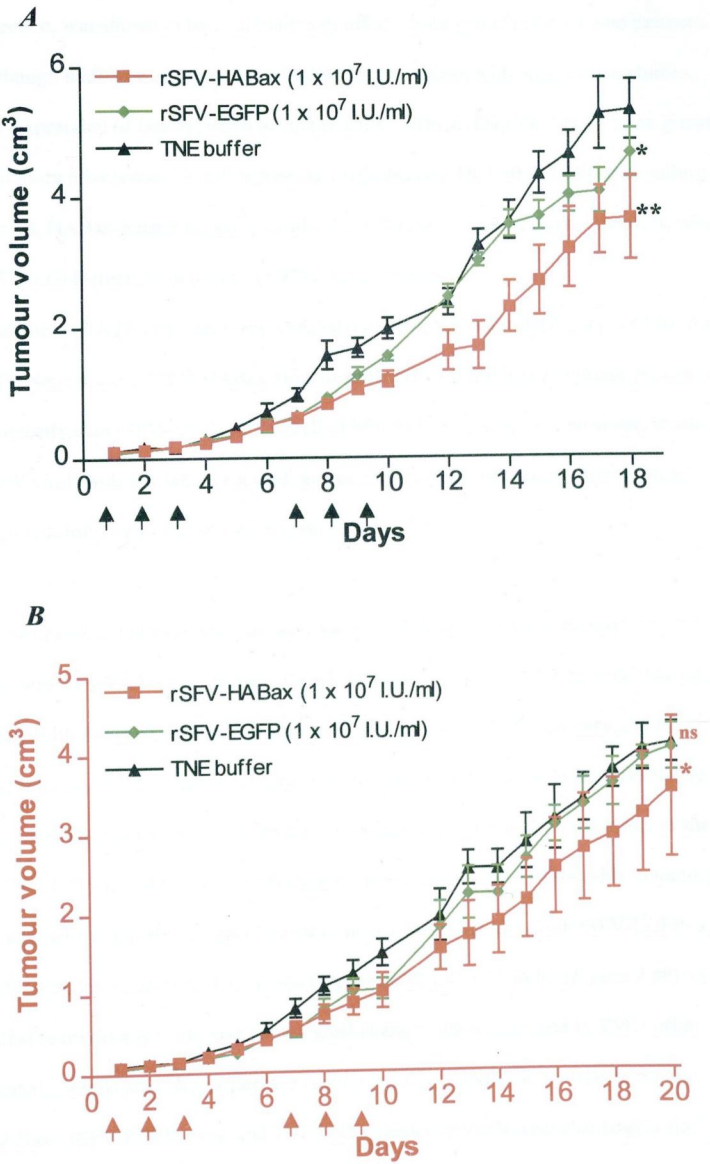


Figure 5.47- Effects of rSFV-HABax virus treatment on AT3 tumour growth *in vivo*.

tumours types are illustrated in Figure 5.47. rSFV-HABax virus treatment, at ~10^6 I.U. per injection, was shown to have an inhibitory effect on the growth of AT3-Neo tumours. Although inhibition appeared to be limited in comparison with other *in vivo* studies, overexpression of Bax appeared to significantly enhance (Day 18, $P<0.002$) the growth inhibitory effects over EGFP-expressing particles (Day 18, $P<0.012$). Prior to culling on day 18, HABax-treated tumours remained at 64% the volume of control tumours, whereas rSFV-EGFP-treated tumours were 87% that of controls.

Treatment of AT3-Bcl-2 tumours revealed a more complex result (*Figure 5.47 B*). As with AT3-Neo tumours, rSFV-HABax virus treatment ($P<0.02$) inhibited tumour growth more efficiently than rSFV-EGFP particles ($P<0.05$). At latter time-points however, levels of rSFV viral inhibition were obscured, as treated tumours continued to show signs of regrowth following cessation of treatment.

As with earlier analyses, tumours were taken at defined intervals post-treatment and assessed for pathological changes. Frozen AT3-Neo and AT3-Bcl-2 cryosections were analysed for either EGFP or HABax expression, by direct epifluorescence and ICC, respectively. The very low viral titres administered to each tumour were reflected by the lack of foreign gene expression. EGFP expression could not be detected in any of the rSFV-EGFP-treated tumours, and HABax expression was barely detectable in tumours treated with rSFV-HABax particles (*not shown*). Histologically, both rSFV-EGFP- and rSFV-HABax virus-treated AT3-Neo (*Figure 5.48*) and AT3-Bcl-2 (*Figure 5.49*) tumours failed to reveal any distinctive pathological changes when compared to TNE buffer-treated controls analysed earlier (*see section 5.3.13*). TUNEL reactivities in rSFV-HABax-, rSFV-EGFP virus- and TNE buffer-treated controls were also largely similar, when sampled at identical timepoints to those used for histology (*not shown*). Thus when assessed pathologically, overexpression of HABax at these very low titres *in vivo* failed to create any cytocidal advantage over the *EGFP*-expressing SFV system.

Figure 5.48- **Histology of AT3-Neo tumours following treatment with rSFV-HABax particles.** (*A*) AT3-Neo tumour, 24 h following six daily intratumoural injections with TNE buffer. Photographed at x 100 magnification (*see Figure 5.42 A*). (*B, C*) AT3-Neo tumours, 24 h following direct intratumoural injections with rSFV-EGFP and rSFV-HABax particles (5 x 10^6 I.U./ml), respectively. The extent of necrotic cell death observed following treatment with rSFV-HABax particles (*C; arrow*), did not appear to differ substantially from levels of endogenous necrosis observed within other areas of the TNE buffer- and rSFV-EGFP virus-treated tumours (*not shown*). Photographed at x 100 and x 200 magnification, respectively.

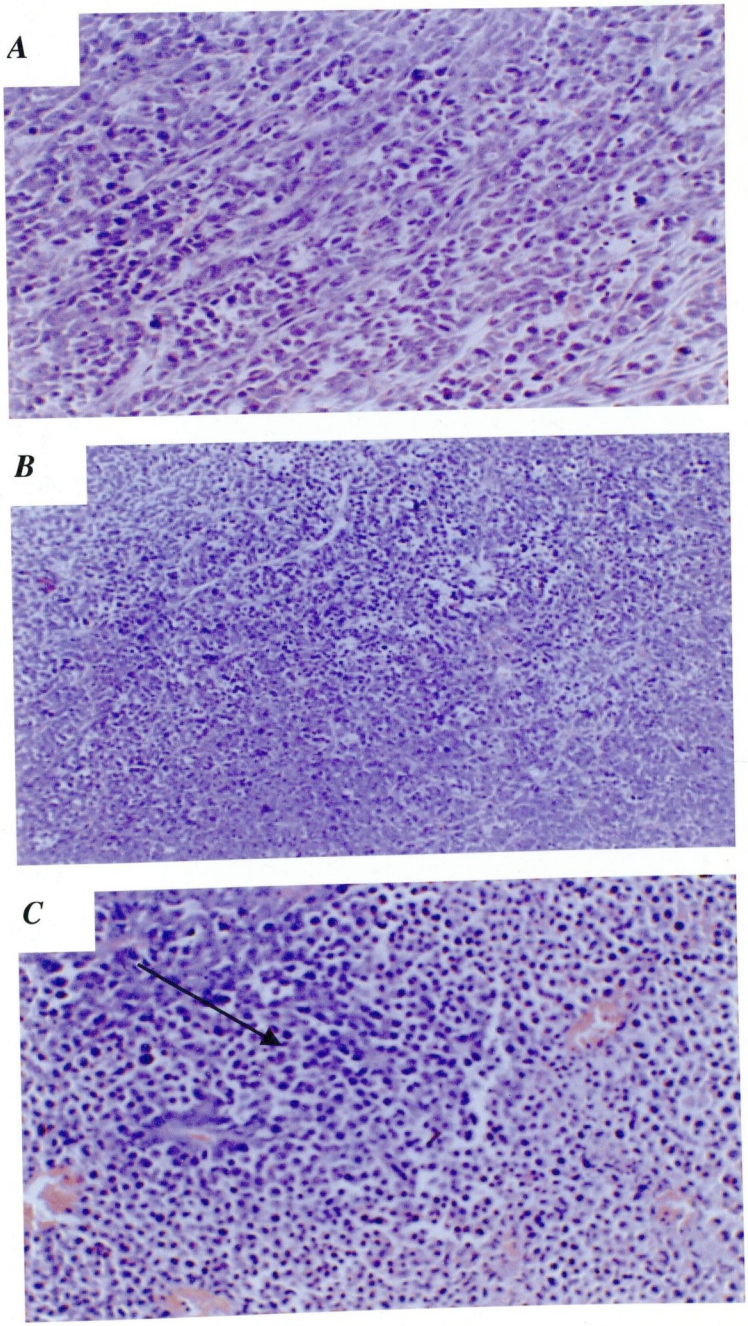


Figure 5.48- Histology of AT3-Neo tumours following treatment with rSFV-HABax particles.

Figure 5.49- **Histology of AT3-Bcl-2 tumours following treatment with rSFV-HABax particles.** (*A*) AT3-Bcl-2 tumour, 24 h following six daily intratumoural injections with TNE buffer (*see Figure 5.42 B*). (*B, C*) AT3-Bcl-2 tumours, 24 h following direct intratumoural injections with rSFV-EGFP and rSFV-HABax particles (5 x 10^6 I.U./ml), respectively. As in AT3-Neo tumours, the extent of necrotic cell death observed following treatment with rSFV-HABax virus (*C; arrow*), did not appear to differ substantially from levels of endogenous necrosis observed following treatment with TNE buffer or the vector control. Photographed at x 200 magnification.

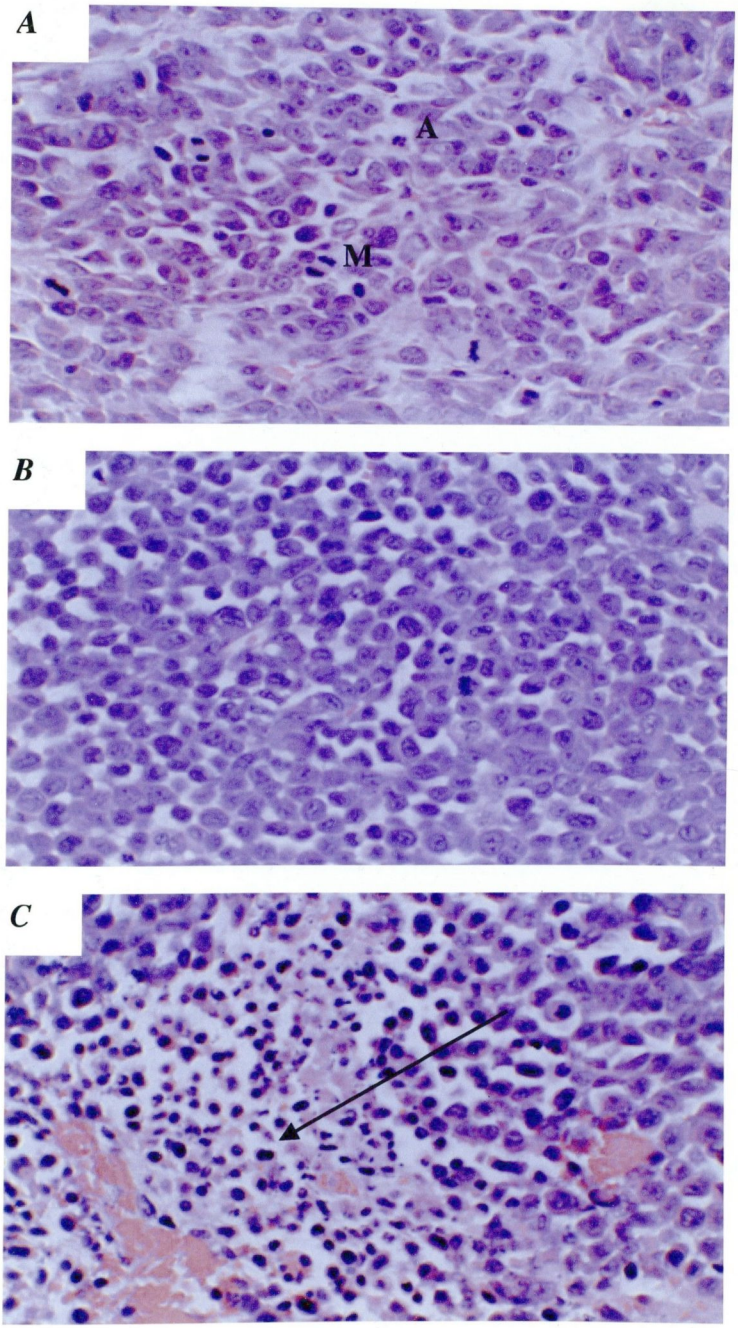


Figure 5.49- Histology of AT3-Bcl-2 tumours following treatment with rSFV-HABax particles.

5.3.16 Electroporation of SFV-HABax RNA counteracts *Bcl-2*-mediated inhibition of AT3-Bcl-2 cell death.

Due to the dramatic nature of cell death within BHK-21 cells following transfection with RNA derived from pSFV-HABax clones (*section 5.3.3*), we assessed whether transfection of AT3 cells with SFV RNA would produce a more powerful inhibitory effect on tumour cell growth, than infection with recombinant rSFV-HABax particles (*section 5.3.14*). Electroporation efficiencies for both AT3 cell lines was firstly optimised for SFV RNA transfection using SFV-EGFP RNA (*not shown*). Two pulses at 0.90 kV was determined as optimal for SFV transfection, with efficiencies of 30-40% for both tumour cell lines. In terms of AT3-Bcl-2 cells, electroporation of SFV RNA was a more efficient mechanism of facilitating viral entry, compared to ~10% infection efficiencies with rSFV-EGFP virus particles (*see section 5.3.10*). As before, cells were plated at densities of $\sim 10^4$ cells/well, in 6-well plates following electroporation with RNA transcribed from either pSFV-HABax, pSFV-EGFP plasmids, or PBS alone as a mock-transfection control. Cells transfected with SFV-HABax RNA were assessed for morphological alterations in comparison to SFV-EGFP- and PBS-transfected cells at 24 h p.e. (*Figures 5.50-5.51*). Cell viability was assessed over a 5-day period using the standard trypan blue (*Figure 5.52*), sulphorhodamine B (*Figure 5.53*) and thymidine incorporation (*Figure 5.54*) assays. In the results presented below, the optical densities of each RNA solution used to transfect cells was assumed identical by visualisation of ethidium bromide-stained RNA gels. All three experiments revealed that electroporation of RNA from pSFV-HABax plasmids inhibited AT3-Neo cell proliferation more efficiently (Day 3, $P<0.01$), than SFV-EGFP RNA ($P<0.035$). Electroporation control cells failed to show any growth inhibitory effects at any of the above time-points, and continued to grow and proliferate until fully confluent. These results also indicated that at later time-points, non-SFV RNA transfected cells survived and continued to proliferate, although not to the same intensity as control cells. Figure 5.55 *A* indicates apoptosis induction within the AT3-Neo cell population at

Figure 5.50- Cytopathic effect in AT3-Neo cells following transfection with SFV-HABax RNA. AT3-Neo cells were grown until ~90% confluent, trypsinised and transfected with RNA, *in vitro*-transcribed from recombinant pSFV-HABax (*A*), pSFV-EGFP plasmids (*B*) or PBS alone as a mock transfection control (*C*). Following electroporation, cells were placed into 6-well plates and analysed for cytopathic effect at 24 h p.e. Cells were observed by inverted light microscopy. Photographed at x 100 magnification.

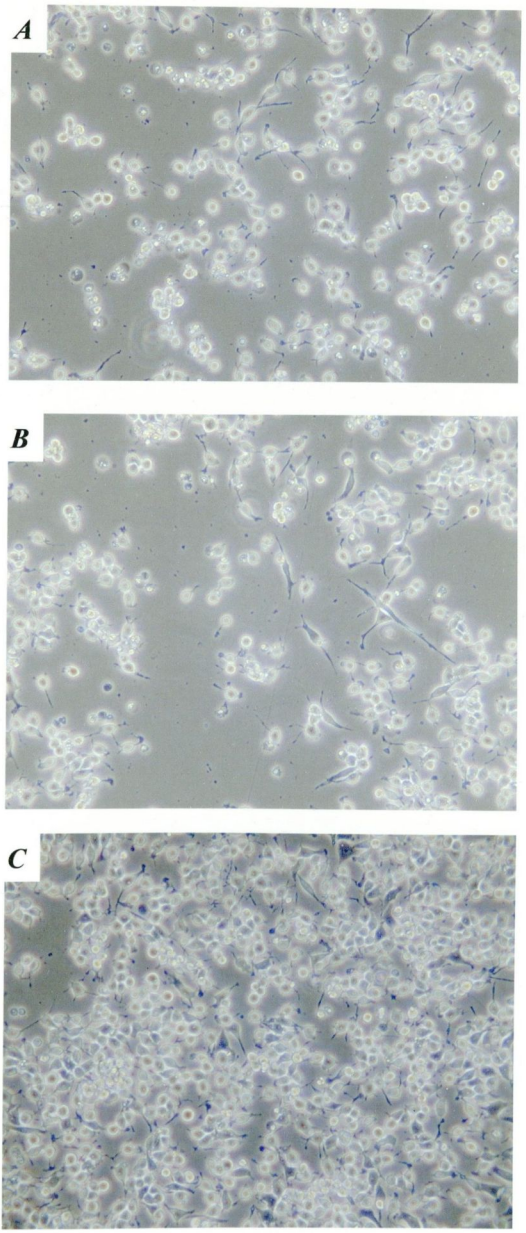


Figure 5.50- Cytopathic effect in AT3-Neo cells following transfection with SFV-HABax RNA.

Figure 5.52- **Viability of AT3-Neo (*A*) and AT3-Bcl-2 (*B*) cells following transfection with SFV-HABax RNA, as determined by trypan blue exclusion.** AT3 cells were washed, trypsinsined and mixed with *in vitro*-transcribed SFV-HABax, SFV-EGFP RNA, or PBS alone as a control, and pulsed twice at 0.90 kV. Cells were plated in normal medium, at densities of $1x10^4$ cells/well in 6-well plates. At each indicated timepoint p.i., triplicate wells for both cell lines, were trypsinsied and counted using trypan blue exclusion criteria. *Points*; means, *bars*; SD for a single experiment.

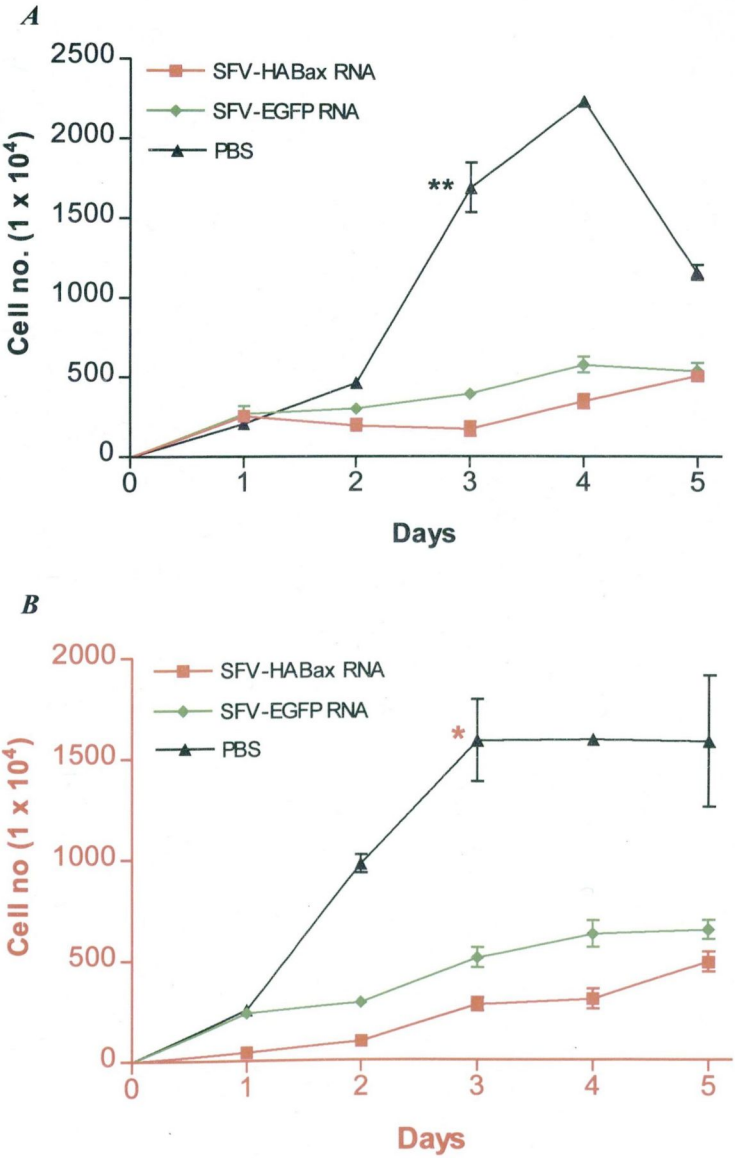


Figure 5.52- Viability of AT3-Neo and AT3-Bcl-2 cells following transfection with SFV-HABax RNA, as determined by trypan blue exclusion.

Figure 5.53- **Viability of AT3-Neo (*A*) and AT3-Bcl-2 (*B*) cells following transfection with SFV-HABax RNA, as determined by sulphorhodamine B colorimetric analysis.** AT3 cells were washed, trypsinised and mixed with *in vitro*-transcribed SFV-HABax, SFV-EGFP RNA, or PBS alone as a control, and pulsed twice at 0.90 kV. Cells were plated in normal medium, at densities of $1x10^4$ cells/well in 6-well plates. At each indicated timepoint p.i., cells were fixed in TCA, stained with sulphorhodamine B, and the surviving cells were measured colorimetrically using an ELISA reader. *Points*; means, *bars*; SD for a single experiment.

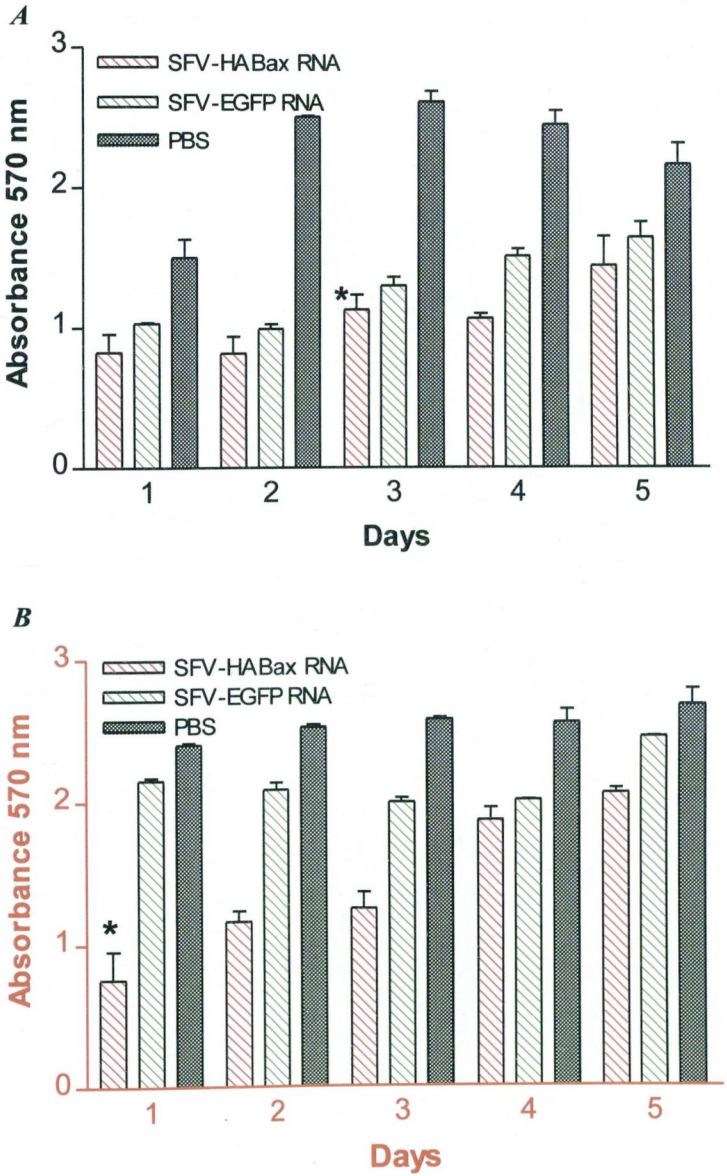


Figure 5.53- Viability of AT3-Neo and AT3-Bcl-2 cells following transfection with SFV-HABax RNA, as determined by sulphorhodamine B colorimetric analysis.

Figure 5.54- **Viability of AT3-Neo (*A*) and AT3-Bcl-2 (*B*) cells following transfection with SFV-HABax RNA, as determined by ^{3}H thymidine incorporation.** AT3 cells were washed, trypsinised and mixed with *in vitro*-transcribed SFV-HABax, SFV-EGFP RNA, or PBS alone as a control, and pulsed twice at 0.90 kV. Cells were plated in normal medium, at densities of $1x10^{4}$ cells/well in 6-well plates. At each indicated timepoint p.i., medium from triplicate wells, for both cells lines, was replaced with medium containing methyl-^{3}H thymidine. Following a 24 h incubation, cells were removed, and ^{3}H incorporation was measured using a liquid scintillation counter. *Points*; means, *bars*; SD for a single experiment.

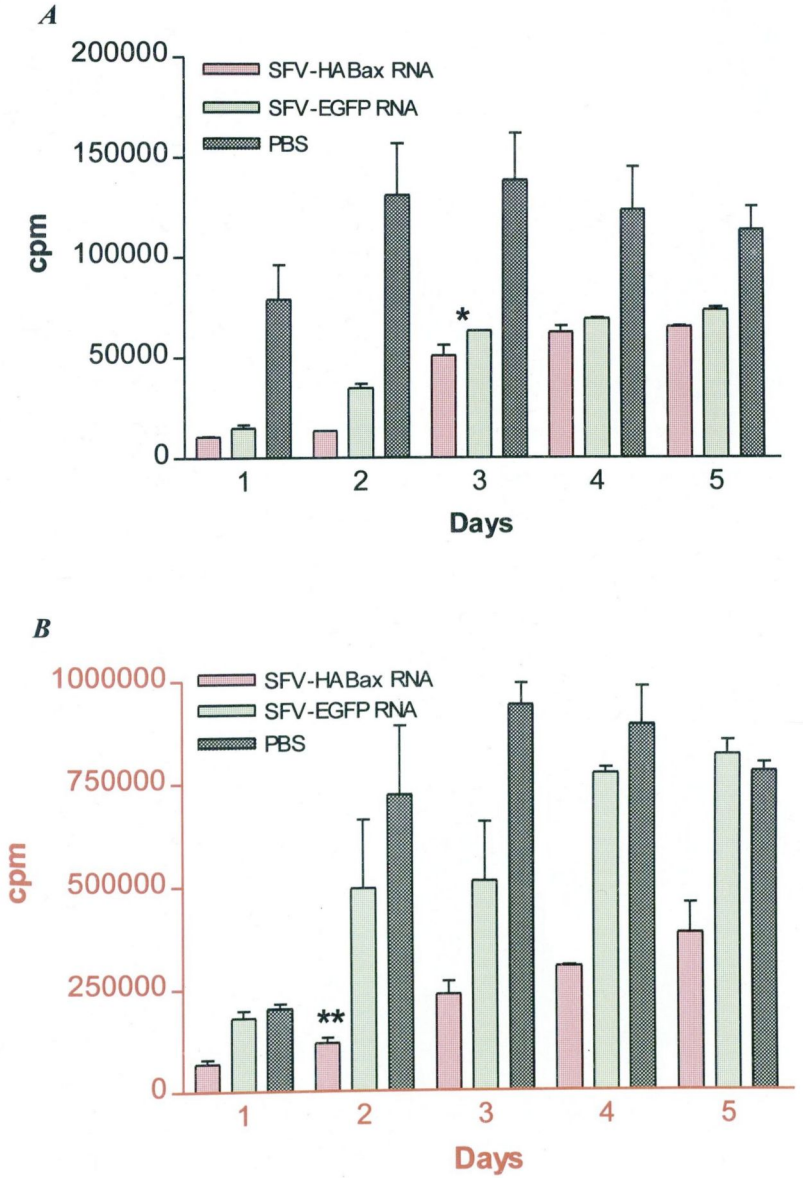


Figure 5.54- Viability of AT3-Neo and AT3-Bcl-2 cells following transfection with SFV-HABax RNA, as determined by ^{3}H thymidine incorporation.

Figure 5.55- Apoptosis induction in AT3-Neo (*A*) and AT3-Bcl-2 (*B*) cells following transfection with SFV-HABax RNA. AT3 cells were washed, trypsinised and mixed with *in vitro*-transcribed SFV-HABax, SFV-EGFP RNA, or PBS alone as a control, and pulsed twice at 0.90 kV. Cells were plated in normal medium, in 75 cm^2 culture flasks and incubated. At 24 h intervals following electroporation, cells were lysed and DNA was released by enzymatic digestion. Cellular DNA from transfected cells was analysed for fragmentation into oligonucleosomal-size fragments, indicative of cell death, by agarose gel electrophoresis. (*A*) AT3-Neo cells. *Lanes 1, 4 and 7*; DNA from SFV-HABax RNA-transfected AT3-Neo cells, at 24, 48 and 72 h p.e., respectively. *Lanes 2, 5 and 8*; DNA from SFV-EGFP RNA-transfected AT3-Neo cells, at 24, 48 and 72 h p.e., respectively. *Lanes 3, 6 and 9*; DNA from mock-transfected control AT3-Neo cells, at 24, 48 and 72 h p.e., respectively. *Lane 10;* λ (*Hind 111* and *EcoR1*) DNA molecular weight markers. (*B*) AT3-Bcl-2 cells. *Lanes 1, 4 and 7*; DNA from SFV-HABax RNA-transfected AT3-Bcl-2 cells, at 24, 48 and 72 h p.e., respectively. *Lanes 2, 5 and 8*; DNA from SFV-EGFP RNA-transfected AT3-Bcl-2 cells, at 24, 48 and 72 h p.e., respectively. *Lanes 3, 6 and 9*; DNA from mock-transfected control AT3-Bcl-2 cells, at 24, 48 and 72 h p.e., respectively. *Lane 10;* λ (*Hind 111* and *EcoR1*) DNA molecular weight markers.

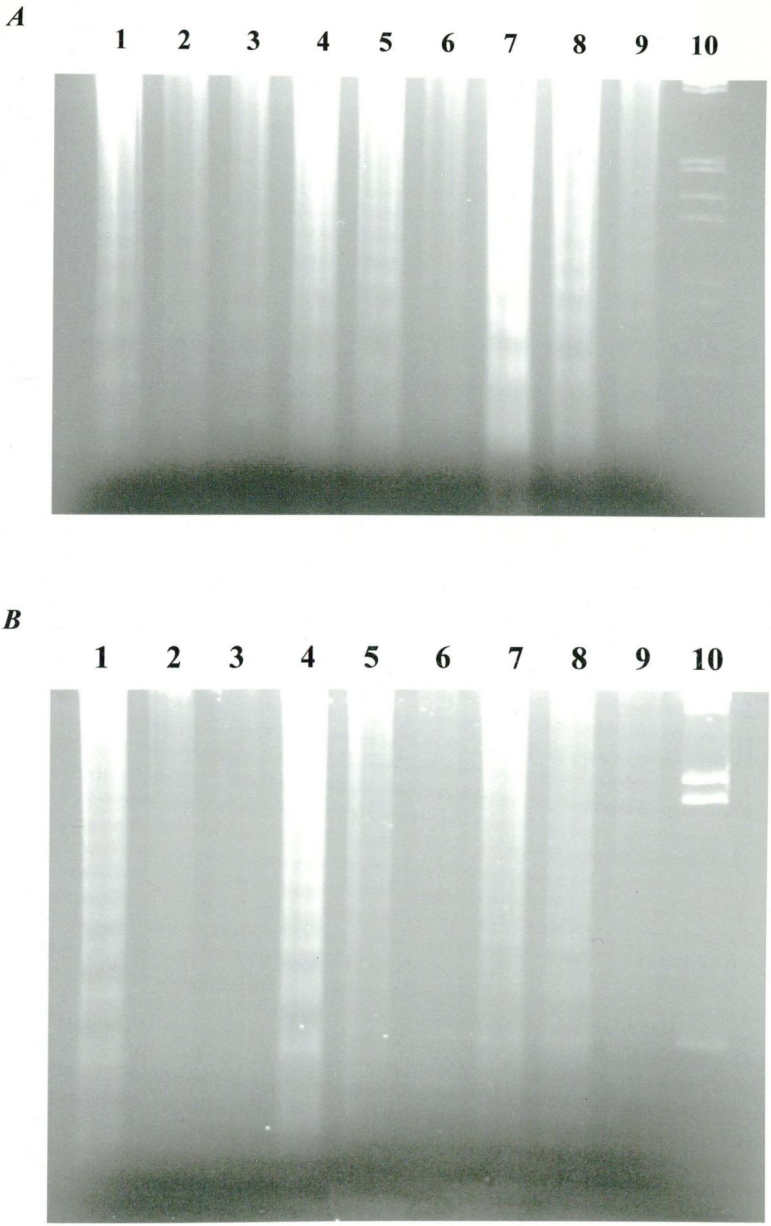


Figure 5.55- Apoptosis induction in AT3-Neo and AT3-Bcl-2 cells following transfection with SFV-HABax RNA.

Figure 5.56- **SFV-HABax RNA-induced programmed cell death in AT3-Neo cells, as assessed by chromosomal DNA fragmentation, using TUNEL.** AT3-Neo cells were washed, trypsinised and mixed with *in vitro*-transcribed RNA from SFV-HABax (*A*), SFV-EGFP (*B*), or PBS alone (*C*), as a mock-transfection control. Cells were plated onto glass coverslips in 6-well plates and incubated. At 48 h p.e., cell monolayers were fixed and fragmented chromosomal DNA labelled with TdT and horse-radish peroxidase. Colorimetric detection was performed using DAB. Normal cells were counterstained with methyl green. *A*; AT3-Neo cells, 48 h following electroporation with SFV-HABax RNA. *B*; AT3-Neo cells, 48 h following electroporation with SFV-EGFP RNA. *C*; Mock-transfected AT3-Neo cells. Note brown, $TUNEL^{+}$ peroxidase staining within apoptotic nuclei, and apoptotic bodies in the SFV RNA-transfected cell monolayers (*A, B*). Photographed at x 400 magnification.

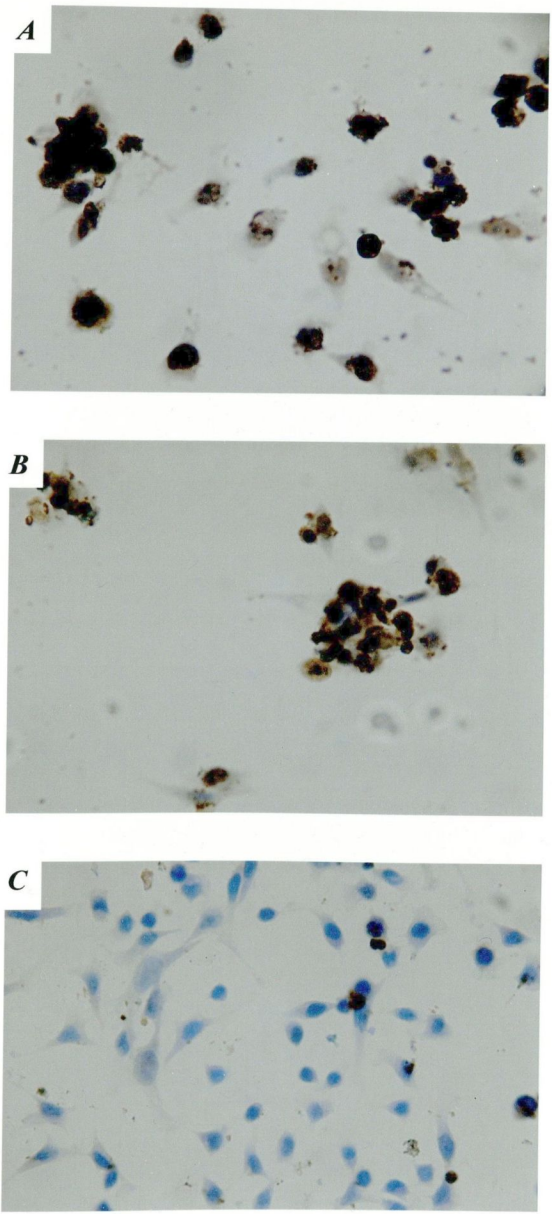


Figure 5.56- SFV-HABax RNA-induced programmed cell death in AT3-Neo cells, as assessed by chromosomal DNA fragmentation, using TUNEL.

Figure 5.57- **SFV-HABax RNA-induced programmed cell death in AT3-Bcl-2 cells, as assessed by chromosomal DNA fragmentation, using TUNEL.** AT3-Bcl-2 cells were washed, trypsinised and mixed with in vitro-transcribed RNA from SFV-HABax (*A*), SFV-EGFP (*B*), or PBS alone (*C*), as a mock-transfection control. Cells were plated onto glass coverslips in 6-well plates and incubated. At 18 h p.e., cell monolayers were fixed and fragmented chromosomal DNA labelled with TdT and horse-radish peroxidase. Colorimetric detection was performed using DAB. Normal cells were counterstained with methyl green. *A*; AT3-Neo cells, 18 h following electroporation with SFV-HABax RNA. *B*; AT3-Neo cells, 18 h following electroporation with SFV-EGFP RNA. *C*; Mock-transfected AT3-Neo cells. Note brown, $TUNEL^{+}$ peroxidase staining within apoptotic nuclei in the SFV-transfected cell monolayers (*A, B*). Photographed at x 400 magnification.

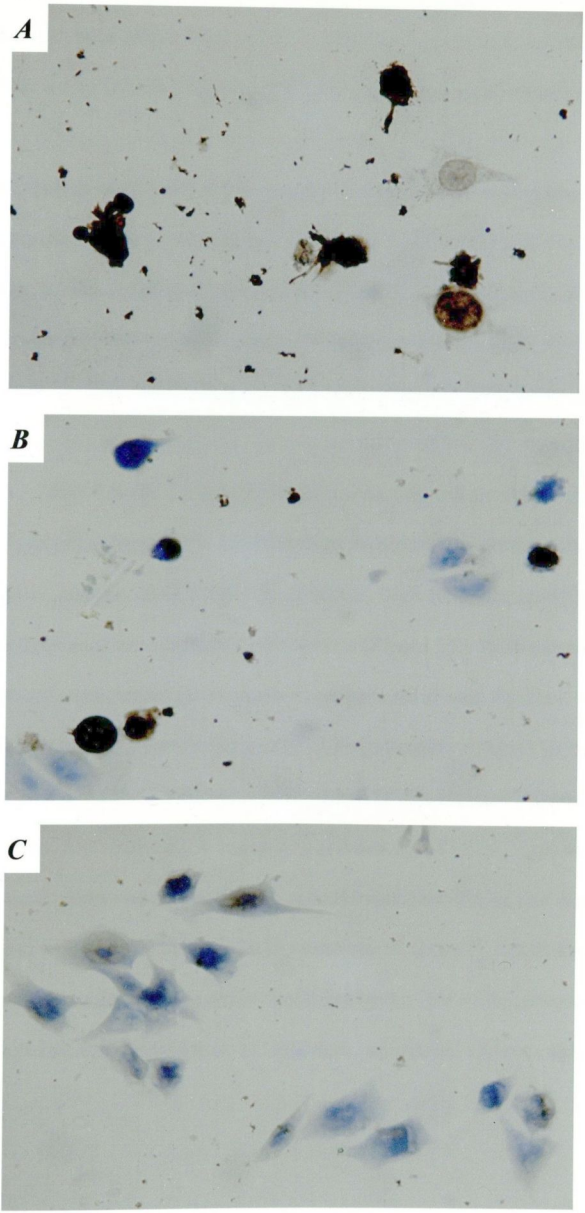


Figure 5.57- SFV-HABax RNA-induced programmed cell death in AT3-Bcl-2 cells, as assessed by chromosomal DNA fragmentation, using TUNEL.

24 h p.e. with both SFV-HABax and SFV-EGFP RNA constructs, and this continued at 48 h, as detected by TUNEL (*Figure 5.56*). Control cells appeared normal throughout.

Finally, analysis of AT3-Bcl-2 cell growth following electroporation demonstrated that overexpression of Bax protein within RNA transcribed from the pSFV-HABax plasmid overcame the *Bcl-2*-mediated inhibition of AT3-Bcl-2 cell death, a scenario which does not occur in SFV-EGFP RNA-transfected cells (*Figures 5.52 B-5.54 B*). The *Bax*-overexpressing RNA construct decreased AT3-Bcl-2 cell viability by up to 92% of controls, as early as 24 h p.e., and was not observed in SFV-EGFP-transfected cells (*Figure 5.52 B*). The Bax-mediated inhibition of tumour cell growth spanned the entire 5 days of analysis, whereas SFV-EGFP-mediated inhibition did not become evident until day 2-3 p.e. Analysis of AT3-Bcl-2 chromosomal DNA following transfection with SFV-HABax RNA confirmed the above observations (*Figure 5.55 B*). In comparison to SFV-EGFP transfection, where apoptosis did not occur until at least day 2 p.i., SFV-mediated overexpression of Bax protein induced DNA fragmentation within AT3-Bcl-2 cells as early as 24 h p.e. This was further confirmed by TUNEL analysis (*Figure 5.57*) at 18 h p.e. Whereas SFV-EGFP RNA-transfected and control AT3-Bcl-2 cells appeared healthy, with normal round/oval nuclei, those transfected with SFV-HABax RNA revealed significant levels of cpe, shown to be characteristic of apoptotic cell death.
Thus, overexpression of Bax protein, facilitated by the SFV vector, overcame the initial 24-48 h *Bcl-2*-mediated inhibition of cell death, and induced vigorous apoptotic cell death *in vitro*.

5.4 DISCUSSION

Cancer of the prostate is the most common malignancy and second greatest cause of cancer-related deaths in men. The American Cancer Society revealed that the estimated incidence of prostate cancer (PCa) in the US increases by up to 100,000 new cases each year, with more than 30,000 deaths. Most PCa patients present with advanced disease and are not generally conducive to curative surgical resection due to the high metastatic nature of prostate malignancy (Emmett *et al*, 1960). Therapeutic intervention usually begins by reducing serum testosterone levels, or androgen ablation (Roehrborn *et al*, 1991). Castration initiates the regression of the malignancy through a process involving the loss of the vast majority of cells by means of apoptosis, although it is known that basal epithelial cells, in contrast to secretory cells, remain resistant to apoptosis induced by androgen ablation (Gjertsen *et al*, 1999). However, the majority of patients who exhibit an initial therapeutic response relapse within 2-3 years, with androgen-independent carcinoma, which is rapidly fatal (Shina *et al*, 1977). The molecular events associated with conversion from androgen-dependent carcinoma to androgen-independent carcinoma are largely unknown. Recently, upregulation of the anti-apoptotic Bcl-2 protein expression has been identified as a molecular alteration of importance in androgen-independent PCa (McDonnell *et al*, 1992; Berchem *et al*, 1995), as well as mutations in the *p53* tumour suppressor gene (Navone *et al*, 1993), and less frequent alterations in apoptosis-related proteins such as pRB and $p21^{WAF1/CIP1}$ (Gjertsen *et al*, 1999).

Bcl-2 expression, which is poorly detected within the majority of newly-diagnosed PCa patients, is upregulated in PCa cells after androgen ablation (Beham *et al*, 1998). Thus, expression of *Bcl-2* in prostate cancer is not a primary event, but rather a secondary event associated with an apoptosis-resistance phenotype within the malignant cell population. In terms of prognostic indications, *Bcl-2*-overexpression is correlated with tumour recurrences, resistance to chemotherapeutic intervention (Mackey *et al*, 1998), and

is a predictive marker for poor response to therapy. Consequently, there is widespread interest in developing therapeutic interventions that will abrogate the survival advantage imparted by *Bcl-2*.

The primary mechanism for PCa intervention involves chemotherapeutic drugs such as taxols and vincristine, which phosphorylate and inactivate the Bcl-2 protein (Reed, 1997c). Further studies on the kinases and phosphatases responsible for Bcl-2 phosphorylation may provide additional new therapeutic avenues also (Gjertsen *et al*, 1999; Srivastava *et al*, 1998). Numerous alternate startegies are currently being developed to overcome the cytoprotective effects of *Bcl-2* in PCa. Antisense oligonucleotides have already proved useful in down-regulating Bcl-2 activity, particularly in patients with non-Hodgkins lymphoma (Webb *et al*, 1997). Antisense oligonucleotides have also proved significant in the downregulation of the oncogene in an androgen-independent Shinonogi PCa model, as an adjuvant to doxetaxel treatment (Gleave *et al*, 1999). In a separate study, catalytic antisense RNAs or ribozyme strategies have been shown to sensitise PCa cells to PCD induction (Dorai *et al*, 1997).

The identification of other key members of the *Bcl-2* superfamily, known to bind to and counteract Bcl-2 activity *in vivo*, have provided an opportunity for novel gene transfer therapeutics. Of most interest is the pro-apoptotic member of the *Bcl-2* family, *Bax* (Oltvai *et al*, 1993). The rheostat model of cell death susceptibility predicts that the ratio of Bax to Bcl-2, rather than the absolute levels of either protein within the cells, is the critical determinant in apoptotic cell death induction in PCa (Oltavai *et al*, 1993; Perlmann *et al*, 1999). The *Bax* gene promoter has been shown to possess consensus p53-binding sites and to be transcriptionally activated by the p53 tumour suppressor protein (Miyashita & Reed, 1995), functioning as a tumour suppressor molecule, at least in a subset of prostate and other cancers (Rampino *et al*, 1997). Bax can also activate apoptotic cell death pathways via direct effects on mitochrondrial function (Khaled *et al*, 1999; Jürgensmeier *et al*, 1998), or by facilitating cleavage of caspase-3 activation (Cregan *et al*,

1999), or indirectly by lowering the apoptotic threshold in response to certain chemotherapeutic agents (Pawlowski & Kraft, 2000). Numerous *Bax* gene transfer studies have been indicated for ovarian (Tai *et al*, 1999), breast (Sakakura *et al*, 1996), lung, head and neck cancers (Guo *et al*, 2000) and leukaemia (Kobayashi *et al*, 1998), and as an adjuvant to chemotherapeutic (Xiang *et al*, 2000) and radiotherapeutic treatment (Arafat *et al*, 2000). All studies suggest that overexpression of Bax protein alone, or in combination with chemo/radiotherapy, may have potential therapeutic applications for human cancers. An additional advantage in comparison with *p53* tumour suppressor gene transfer studies is the fact that the Bax protein can effectively suppress tumour growth in both *p53*-sensitive and *p53*-resistant cancer cell types (Kagawa *et al*, 2000). To the best of our knowledge, viral vector-mediated *Bax* overexpression has not been utilised as a therapeutic avenue for PCa gene therapy.

Despite extensive knowledge and documentation of *Bcl-2* overexpression in human NSCLC (Groeger *et al*, 1999; Ohsaki *et al*, 1996), to date, we were unable to locate any natural *Bcl-2*-overexpressing established NSCLC cell line, either from ATCC or in the literature. As it was initially sought to study *Bcl-2* overexpression in NSCLC, four NSCLC cell lines from ATCC were assessed for *Bcl-2* overexpression, using an anti-human Bcl-2 antibody. All four cell lines were negative for *Bcl-2* overexpression. As positive and negative controls for the ICC studies, we also had available at rat prostatic adenocarcinoma cell line, AT3, which was previously engineered by Levine and coworkers (1993), to overexpress the *Bcl-2* oncogene, producing the stable transfected AT3-Bcl-2 cell lines. AT3-Bcl-2 cells proved positive for *Bcl-2* overexpression by ICC, whereas the negative control AT3-Neo cells were completely negative. Thus for the remainder of the study, the pro-apoptotic properties of Bax overexpression were studied on the rat PCa AT3-Bcl-2 cell line, with AT3-Neo cells as a *Bcl-2*-negative control.

As a prerequisite for therapeutic intervention studies, it was necessary to determine whether both cell lines formed solid tumours in the *in vivo nu/nu* mouse xenograph model. Both AT3-Neo and AT3-Bcl-2 cell lines rapidly developed sc tumours, detectable as early as 24 h post-inoculation and grew vigorously for about 20 days only, at which time tumour volumes reached maximum levels. *Bcl-2* overexpression within AT3-Bcl-2 cells was shown to be maintained *in vivo*, and pathological examination revealed highly aggressive tumour growth, with extensive vascularisation, haemorrhage and large areas of acute ischemic necrosis. The localised nature of tumour growth and absence of secondary tumours made both AT3 cell lines highly amenable towards therapeutic intervention studies.

The AT3-Neo and AT3-Bcl-2 cell lines have been previously utilised to demonstrate *Bcl-2*-mediated suppression of virally-induced cell death in infected cells. Levine *et al*, (1993), revealed that infection with SV induced apoptosis in AT3-Neo cells upon infection, whereas *Bcl-2* oncogene overexpression suppressed apoptotic cell death, establishing a persistently infected cell line. In a more relevant study, Scallan *et al* (1997) showed that *Bcl-2* overexpression within the AT3-Bcl-2 cell line inhibited wild-type SFV virus-mediated apoptosis following infection with both avirulent A7 and virulent L10 strains of the virus, again leading to a persistent infection. Ubol *et al*, (1994), indicated that a single amino acid change (Gln^{55}-His^{55}) within the E2 glycoprotein, enabled SV to induce apoptosis in the AT3-Bcl-2 cell line, but no similar mutations have been identified for SFV. This scenario indicates the possible advantage of natural *Bcl-2* overexpression within long-lived cells, such as post-mitotic neurons, sustaining irreplaceable cells following viral infection, or as a consequence of other pro-apoptotic stimuli.

In this study, the pro-apoptotic properties of a third SFV strain of infectiou virus, SFV-4, derived from the virulent L10 strain, was assessed using the AT3 cell lines. As with SFV virus vius strains A7 and L10 (Scallan *et al*, 1997), SFV-4 induced rapid inhibition of AT3-Neo cell proliferation following infection in culture, shown to be as a

result of apoptosis induction. Following the first 24-36 h of SFV-4 infection, AT3-Bcl-2 cells remained healthy, and continued to proliferate at similar levels to mock-infected controls, as was demonstrated for A7 and L10 strains of the virus (Scallan *et al*, 1997). Analysis of chromosomal DNA also failed to indicate the characteristic features of apoptotic cell death at these time-points. It appears that Bcl-2 functions at the level of viral entry, or at the early stages of SFV viral replication (Scallan *et al*, 1997), to block the apoptotic pathway, a scenario that was not observed in AT3-Neo cells. However, at all subsequent timepoints following this 24-36 h delay, AT3-Bcl-2 cells infected with SFV-4 virus in this study, revealed initial signs of growth inhibition, as determined by three independent viability assays, and revealed characteristic features of apoptotic cell death, in comparison to mock-infected controls.

To a lesser extent, infection with the suicide rSFV-EGFP particles, which undergo one round of replication, indicated an identical response to infectious SFV-4 virus, in both AT3-Neo and AT3-Bcl-2 cells in culture. Viability of AT3-Neo cells was dramatically decreased compared to controls as early as 24 h p.i., and at 48 h p.i. in AT3-Bcl-2 cells. Analysis of chromosomal DNA following infection with the vector indicated a similar level of apoptosis induction to SFV-4 virus infection, following a 24-36 h delay in AT3-Bcl-2 cells. With rSFV-EGFP virus infection however, non-transfected cells, which occupied approximately 50-90% of the total AT3-Neo and AT3-Bcl-2 cell population respectively, explained why both cell lines eventually recovered and began to proliferate following cessation of rSFV-EGFP *in vitro* treatment. This was in contrast to infectious SFV-4 virus, that has similar infection efficiencies, but are replication-competent, and produce progeny virions following infection.

The fact that SFV virus replication can overcome *Bcl-2*-mediated apoptosis inhibition, was also demonstrated by Grandgirard *et al* (1998). Three *Bcl-2*-overexpressing cell lines were shown to undergo apoptosis following infection with both SFV and SV, facilitated by direct caspase-3-mediated cleavage of the pro-apoptotic

protein Bcl-2. This cleavage releases the essential BH4 and/or BH3 domains of the protein, responsible for conferring cell death protection. In this study, *Bcl-2* overexpression delayed apoptotic cell death for as little as 4 h p.i. in comparison to controls, before succumbing to caspase-3 activation, Bcl-2 cleavage and apoptotic cell death. Grandgirard *et al* (1998), proposed that a virally-encoded factor, particularly the viral capsid protein, known to contain endogenous protease activities, was responsible for caspase-3 cleavage. The fact that rSFV-EGFP virus particles, which lack capsid gene expression, also conferred apoptotic cell death in *Bcl-2*-overexpressing cells, suggests that other host or virally-encoded factors also play a role in Bcl-2 cleavage.

Although tumour cell growth in two-dimensional cell culture conditions differs markedly to growth in solid tumours *in vivo*, AT3-Bcl-2 tumours were similarly inhibited following infection with rSFV-EGFP particles in nude mice. Six intratumoural injections were chosen as the treatment protocol, based on earlier successes with the NSCLC model in Chapter 4. Six injections with high titre rSFV-EGFP particles inhibited AT3-Neo tumour growth by up to 30% that of mock-infected control tumours. AT3-Bcl-2 tumours similarly remained less than 75% the volume of control tumours at the end of analysis. The *Bcl-2*-mediated delay in apoptotic cell death and tumour growth inhibition were more difficult to assess *in vivo*. However, apoptosis as detected *in situ* by TUNEL, was more prevalent following rSFV-EGFP virus treatment, as were the pathological indications. In comparison to successes with rSFV-EGFP virus-mediated NSCLC inhibition and regression in Chapter 4, the much lower infection efficiencies of both AT3 cell lines, coupled with the extremely vigorous nature of tumour cell growth impeded the potential growth suppressive effects of the rSFV vector *in vivo*, compared to a slower-growing H358a NSCLC model.

Having demonstrated the pro-apoptotic properties of the rSFV vector in *Bcl-2*-overexpressing cells *in vitro* and *in vivo*, we next assessed whether the vector could be

further developed as a cytotoxic therapy agent for cancer, by overexpression of the pro-apoptotic protein Bax. In order to assess the pro-apoptotic effects of SFV vector-mediated Bax overexpression, the *Bax* gene was cloned into the multicloning site of the SFV vector. The human *Bax-α* gene was provided within the pSG5 vector backbone (Cheng *et al*, 1996), but any knowledge of the *Bax-α* flanking sequences for PCR amplification and cloning, were not provided. In order to clone the *Bax-α* gene, consensus sequences from the literature and from GenBank, were used to design *Bax*-specific primers for PCR amplification from the vector, but all attempts failed. Instead, *Bax-α* was sequenced directly from pSG5-Bax, using PCR primers specific for pSG5 vector backbone sequences, further upstream and downstream of the *Bax-α* insertion site. Direct sequencing provided the primers specific for *Bax-α* amplification, and included a *Xma I* site, in both forward and reverse primers, to facilitate ligation with the multicloning site of the SFV expression vector. Recombinant pSFV1-Bax clones were screened using a specific anti-human Bax antibody, in BHK-21 cells transfected with RNA transcribed from SFV-Bax clones. Whereas overexpression of Bax was immediately detected 18 h following transfection, this was complicated by endogenous low-level Bax expression within SFV1-Bax antisense clones, and in mock-transfected control BHK-21 cells. This was obviated by expression detection in the *Bax*-null cell line, HL-60, but the endogenous expression in Bax-positive cell lines, such as BHK-21 cells, would only further complicate downstream analyses, such as rSFV-Bax particle titrations, and *in vivo* studies.

An alternative was provided in a second pSG5 plasmid, containing the *Bax-α* gene, fused to the influenza virus haemagglutinin (HA) epitope. The HA Tag is not expressed in mammalian cells and offered a more feasible detection method, using anti-HA epitope antibodies. As with the pSG5-Bax vector, the sequence of the HA epitope remained elusive. Numerous HA epitope sequences were present in the database, and therefore, the *HA* tag sequence was obtained as before, using primers specific for upstream and downstream pSG5 flanking sequences. The HABax fusion protein was

cloned into the SFV expression vector using *Xma I* restriction digestion as before, and clones were selected using anti-HA antibodies in BHK-21 cells transfected with RNA transcribed from SFV-HABax clones. In this procedure, both antisense HABax constructs and mock-transfected controls remained negative for HA epitope expression. Analysis of SFV1-HABax-transfected cells indicated 100% infection efficiencies and a massive induction of cpe, shown to be apoptotic, as early as 8-9 h p.e. This was attributable only to Bax overexpression, as antisense RNAs failed to produce this vigorous cell death, inducing the standard SFV-mediated apoptotic phenotype at approximately 24 h p.e. Thus, SFV-mediated HABax expression proved amenable to specific detection *in situ*, and greatly enhanced the capacity of the SFV system to induce apoptotic cell death *in vitro*.

Transfection of AT3-Neo and AT3-Bcl-2 cells with RNA transcribed from the pSFV-HABax plasmid provided similar levels of cell death *in vitro*. Taking into consideration that RNA quantities were identical (neither O.D. readings not DNase treatments were carried out), the viability of AT3-Neo cells were reduced at 24 h p.e. with SFV-HABax and SFV-EGFP RNAs, as determined by three independent viability studies, and apoptosis was detected at 24 h p.e., using both agarose gel electrophoresis and TUNEL analyses. *HABax* overexpression was shown to be more potent at inducing AT3-Neo cell death, than SFV-EGFP RNA alone, but non-transfected cells, which totalled approximately 40% of the AT3-Neo population, did shown signs of recovery and proliferation at latter stages of analysis.

In terms of AT3-Bcl-2 cell death, shown to be delayed in all instances following infectious SV, SFV A7, SFV L10, SFV-4 viruses and rSFV-EGFP virus particle infections, was abolished *in vitro* following transfection with SFV RNA overexpressing the Bax protein. AT3-Bcl-2 cell growth was inhibited by up to 90% that of mock-transfected controls as early as 24 h p.e. with SFV-HABax RNA, and transfected cells revealed classical signs of apoptotic cell death at 24 h p.e., as determined by agarose gel electrophoresis and TUNEL. This was not observed following transfection with SFV-

EGFP RNA, which did not reveal cell death induction until day 2-3 p.e. *Bax* overexpression within AT3-Bcl-2 cells presumably counteracted the *Bcl-2*-mediated suppression of SFV-induced cell death, shown in previous studies to be due to Bcl2-Bax heterodimerisation, or via direct pro-apoptotic effects on cellular mitochondria (Khaled *et al*, 1999; Cregan *et al*, 1999). *Bcl-2*-mediated suppression of SFV-induced cell death was abolished, and cells rapidly sucumbed to programmed cell death. Obviously due to the complex nature of apoptotic cell death pathways *in vivo*, other, as yet undetermined mechanisms of *Bax*-induced apoptosis and *Bcl-2* suppression in virally infected cells, may be responsible for what was observed.

The potent cytotoxicity of the Bax protein however, proved to be an unexpected hindrance in terms of rSFV-HABax particle production. rSFV particle titres, usually in the range of 1-5 x 10^8 I.U./ml for *LacZ*- and *EGFP*-expressing virus, were reduced by up to 200 times in the parallel production of rSFV-HABax particles. Analysis of particle-producing BHK-21 cells during the 24 h incubation period prior to particle harvest identified the reason for these low titres. Due to the vigorous and rapid nature of *Bax*-mediated apoptosis induction, particle-producing BHK-21 cells, which were transfected with RNA transcribed from pSFV-HABax, plasmids, as well as the helper RNA species, underwent rapid cell death compared to the non-cytotoxic *EGFP*-expressing RNA. Thus, the particle-producing BHK-21 cells did not survive long enough to produce the quantities of rSFV particles normally attained during the 24 h incubation period.

Infection of both AT3-Neo and AT3-Bcl-2 cells with rSFV-HABax virus particles proved to have little effect on cell growth *in vitro*. The low titres used to infect the cells, coupled with the low rSFV virus infection efficiencies of AT3 cells proved responsible for this lack of cytotoxicity. The numbers of infected AT3-Neo and AT3-Bcl-2 cells proved to be minimal, particularly at the low moi of 10-50 virions per cell, and grew at rates similar to mock-infected controls, or those infected with rSFV-EGFP particles at a similar

concentration. This was confirmed in three independent viability assays, and apoptotic cell death was not detected at any stage in the analysis.

For *in vivo* studies, both AT3-Neo an AT3-Bcl-2 tumours received direct intratumoural injections of rSFV-HABax and rSFV-EGFP particles, or TNE buffer alone, as mock-infection controls. Although high concentration particle preparation was used, titres of rSFV-HABax particles remained 200 times lower than high-titre *EGFP*-expressing particles, thereby immediately limiting the effect. It was shown that rSFV-HABax particles at 10^7 I.U./ml, indeed significantly inhibited AT3-Neo tumour growth, and to a lesser extent, AT3-Bcl-2 tumour growth *in vivo*. AT3-Neo tumours were up to 64% the size of TNE treated controls, and AT3-Bcl-2 tumours 87% that of TNE-treated controls at 11 days following cessation of treatment. The localised nature of *in vivo* treatments may explain why a significant rSFV-HABax virus response was observed *in vivo* and not *in vitro*. It was inevitable however, that due to the low viral treatment inoculum, that treated tumours would reveal signs of recovery, and grow to sizes similar to control levels following cessation of treatment.

In terms of improvement, it would be far more suitable to initially begin with a cell line derived from NSCLC, as these tumours are known to grow at much reduced rates compared to the AT3 cells in this study. Slower-growing NSCLC tumours would also have higher rSFV transduction efficiencies and thus, more amenable to treatment. In terms of the vector, the potent pro-apoptotic properties of *Bax* overexpression should be curtailed until necessary for cell death induction, presumably using an inducible promoter system (Xiang *et al*, 2000). This strategy has been overcome in DNA viral vectors such as Ads, to produce significantly higher virus titres, such as a tetracycline-resistant promoter (Kagawa *et al*, 2000a), Gal4 response element (Kagawa *et al*, 2000b), or a Cre-LoxP system (Arafat *et al*, 2000). Due to difficulties in providing an inducible promoter for an RNA expression vector, the rSFV-HABax particles could be produced in an apoptosis-

resistant cell line. A *Bax*-unresponsive apoptosis-inhibiting protein overexpressed in a BHK-21 cell line, in which SFV infection efficiencies have been optimised to 100%, would indeed be ideal.

It has been reported that *Bax* is up to 50% more toxic to transfected cells than wild-type *p53* overexpression (Kagawa *et al*, 2000b). Furthermore, the potent pro-apoptotic properties of the SFV-HABax system could be used as an adjuvant to chemotherapeutic studies, as Bax protein has been shown to sensitise malignant cell lines to chemotherapeutic agents such as cisplatin, taxols and vincristine (Gjertsen *et al*, 1999) and to radiotheraeutic (Reed, 1997b) interventions.

Chapter 6

General Discussion

6.1 DISCUSSION

The field of gene therapy for cancer is progressing considerably and is rapidly gaining medical and scientific acceptance. There have been impressive advances in our understanding of the molecular pathogenesis of cancer, providing an ever-increasing range of genes with important roles in malignant progression, rendering more and more tumour types amenable to gene therapy. One of the more crucial limiting factors to gene therapy success at present however, is the lack of suitable and efficient gene delivery systems to mediate the therapeutic effect.

In this study, the potential of the rSFV vector was investigated and developed for cancer gene therapy. Although the molecular biology and vaccine delivery potential of this system were well established at the outset of this study (*see section 1.5*), a gene therapy application for the recombinant virus had not been examined. SFV offers several advantages over adenoviral and retroviral vector systems (*see section 1.3*) for gene therapy. The SFV system can accommodate up to 5 kb of foreign DNA and produce large amounts of recombinant protein (for SFV, 25% of total cellular protein) (Liljeström & Garoff, 1991). Unlike the retroviral system, alphaviruses infect a broad range of host species and cell types, regardless of their mitotic status (Strauss & Strauss, 1994). Also, rSFV particles are much more stable, and titres of 10^{10} I.U./ml can be generated (Berglund *et al*, 1993). Unlike first generation adenoviral vectors, rSFV does not generate significant anti-vector immune responses *in vivo*, since only genome replication occurs, and no structural proteins are produced in host cells (Zhou *et al*, 1995); and most mammalian species have no pre-existing immunity against the virus (Atkins *et al*, 2000). Biosafety concerns have been alleviated following the generation of a 'split helper' packaging system (Smerdou & Liljeström, 1999), which brings the potential of SFV replication-competent virus

contamination, widely observed in Ad, AAV and Rv systems, to negligible values. rSFV functions directly as an mRNA encoding its own replicase, and is thus, a transient expression system. Its episomal maintenance obviates any nuclear complications, such as random chromosomal integration and adventitious splicing, as well as limitations in nuclear transcription factors, mRNA transport and efficient capping. The long-term expression of foreign proteins by the Rv systems following chromosomal integration could be seen as an advantage over transient-based systems (Roth *et al*, 1996). However, where the mainstay of cancer therapy is the elimination of the malignant cell, long-term gene expression is not necessary and may be undesirable.

The most significant advantage of the alphaviral system, particularly in terms of cancer therapy, is its endogenous cytolytic property. Alphaviruses have been clearly shown to induce PCD in cultured cells (Glasgow *et al*, 1997, Scallan *et al*, 1997, Levine *et al*, 1993). The pro-apoptotic function has also been shown to reside in the non-structural region of SFV RNA molecules (Glasgow *et al*, 1998), and in infectious rSFV particles, in this study (*Chapter 2*). Thus, rSFV particles can infect tumour cells in culture and mediate a cytotoxic effect in the absence of foreign pro-apoptotic protein expression, unlike the more conventional, non-cytopathic Rv and AAV vector systems, which rely exclusively on foreign gene expression to mediate a therapeutic effect. Wild-type adenoviruses have been shown to possess pro-apoptotic capabilities in infected cells (Teodoro *et al*, 1995). However, the main region of the genome that contains this pro-apoptotic function, identified as the *E1A* gene region, is usually deleted in the recombinant vector to create space for insertion of the heterologous gene (Engelhardt *et al*, 1994). In fact a second adenoviral protein, E1B (19K and 55K) is known to be a potent suppressor of apoptotic cell death (Farrow *et al*, 1995; Rao *et al*, 1992).

The molecular mechanisms governing alphaviral-induced cell death remain to be fully elucidated. Recently, pseudoaspartate caspase inhibitors have shown that alphaviral-induced apoptosis proceeds via a similar pathway to that of FasL and TNFα-induced apoptosis (Nava *et al*, 1998), and can induce cleavage of the anti-apoptotic protein Bcl-2 (Grandgirard *et al*, 1998; Lundstrom *et al*, 1997), via the induction of caspase-3. In other instances however, Bcl-2 overexpression successfully delays the onset of both SV- and SFV-induced apoptosis, creating persistently infected cell lines (Scallan *et al*, 1997; Levine *et al*, 1993; Mastrangelo *et al*, 2000). SFV-induced cell death is not dependent on wild-type *p53* expression, as *p53*-deleted H358a cells undergo apoptosis in a similar fashion to a *p53*-positive, non-tumourigenic cell line following infection with the virus (Glasgow *et al*, 1998).

A number of investigators have analysed the pro-apoptotic factors involved in SV-induced PCD (Jan *et al*, 2000; Jan & Griffin, 1999; Joe *et al*, 1998; Ubol *et al*, 1994) (*see section 1.4.4*). However, delineation of the main mechanisms of SFV-induced apoptosis is largely unknown. Most recently, Grandgirard *et al*, (2000) identified a mitochondrial role in SFV-induced cell death, involving cytochrome *c* release and caspase 9 activation, offering yet another location for cell death modulation by Bcl-2. The autoproteolytic activities of SFV capsid protein were postulated as the main inducer of caspase cleavage and apoptosis induction (Grandgirard *et al*, 1998). However, Glasgow *et al*, (1998) showed that for SFV, the capsid protein is not necessary, and deletion of all SFV structural proteins fails to abrogate apoptosis induction, suggesting instead that apoptosis occurs directly via a non-structural protein-induced mechanism, or indirectly, as a consequence of viral replication.

Alphaviral replication results in the formation of dsRNA intermediates, a process that does not occur in uninfected mammalian cells (Favre *et al*, 1996), and functions to activate the dsRNA-dependent serine/threonine protein kinase

PKR. This gene, which can also be induced by type-1 interferons, exists as a 68kDa and 65kDa protein in humans and mice respectively (Muers *et al*, 1990; Icely *et al*, 1991). Phosphorylation and activation of PKR in turn, functions to phosphorylate and inhibit the action of the α-subunit of eukaryotic initiation factor 2α (eIF2α), and consequently inhibits host macromolecular synthesis (Lee & Esteban, 1994). Recent studies have shown that $PKR^{-/-}$ mice are resistant to dsRNA-induced apoptosis, whereas overexpression of the protein can trigger apoptosis in HeLa and U937 cells (Yeung *et al*, 1996). PKR is also reported as a secondary messenger in a number of signal transduction pathways including PDGF, TNFα, STAT-1, IL-3 (Kumar *et al*, 1994; Mundschau & Faller, 1995; Yang *et al*, 1995) and NFκB, known to be a necessary component of SV-induced apoptosis (Lin *et al*, 1998; Lin *et al*, 1995). Although it is possible that PKR activation may inhibit the translation of some cellular transcripts, it is plausible that activation of PKR triggers apoptosis via mechanisms independent of translational regulation. More recently, PKR has been shown to function directly as a key receptor/inducer of dsRNA-mediated apoptosis (Balachandran *et al*, 1998). This appears to be a consequence of an upregulation in the expression of members of the TNFR family, including Fas, TNFR-1, FADD and FLICE. It is also possible that SFV-induced apoptosis relies on more than one of the above apoptotic triggers, the outcome from which depends on a number of important cellular factors.

In this study, the cytolytic properties of rSFV particles were assessed in the context of gene therapy for cancer. rSFV particles were shown to inhibit the proliferation and induce apoptotic cell death in both *p53*-deleted and *Bcl-2*-overexpressing cell lines *in vitro* and *in vivo*, using the tumour xenograft nude mouse model. In both NSCLC (*Chapters 3 & 4*) and prostate cancer (PCa)

(*Chapter 5*) studies, the recombinant virus contained no pro-apoptotic transgene, but *EGFP*, a non-cytopathic protein, that was present simply to facilitate detection of the vector *in situ* (Chalfie *et al*, 1994). Thus, rSFV relied on the lytic ability of this suicide vector to kill cells directly. The *p53*-deleted H358a NSCLC cell line showed approximately 50% reduction in viability at 24 h following rSFV-EGFP treatment, with as little as 10% survival after one week. The cells actively underwent rSFV-induced apoptosis, independently of the *p53* status of infected cells.

Infection of the AT3-Neo and AT3-Bcl-2 PCa cell lines revealed similar pathologies, but with less efficiency, mainly due to much lower rSFV transfection efficiencies, particularly with the apoptosis-resistant AT3-Bcl-2 cells. Bcl-2 overexpression in the PCa cell line efficiently blocked infection with both replication-competent SFV-4 virus and suicide rSFV-EGFP particles, for at least 36 h compared to AT3-Neo controls. It is unclear on which level the block of SFV transduction existed. The very low transfection efficiencies of rSFV (~11%) for the AT3-Bcl-2 cell line, in comparison to the AT3-Neo counterpart (~90%), suggests that productive infection is blocked at the level of viral attachment and/or uncoating, and prior to transcription of viral RNA (Scallan *et al*, 1997), since the AT3-Bcl-2 cells that are infected, express the *EGFP* transgene at levels comparable to that of AT3-Neo. This indicates that SFV replication is fully supported by the AT3-Bcl-2 cells that contain the SFV replicon (Mastrangelo *et al*, 2000; Wahlfors *et al*, 2000; Scallan *et al*, 1997).

Recent studies by Joe *et al* (2000) indicate that the primary event in SV-induced apoptosis is at the level of viral attachment and internalisation, followed by ceramide release during endosomal membrane fusion. Bcl-2, or a Bcl-2-regulated anti-apoptotic factor may modulate the efficiency of this internalisation process, thereby delaying alphaviral replication and cytopathic effects.

The cytolytic efficiency of rSFV-EGFP was also assessed on both NSCLC and PCa tumours *in vivo*. Subcutaneous implantation of tumour cell suspensions was used to initiate tumour growth in the nude mice. Tumours with an average diameter of 4 mm were determined as optimal for therapeutic intervention, although the kinetics of the H358a and AT3 tumours differed considerably. Based on earlier successes with Ad systems in cervical and lung cancer xenograph models (Hamada *et al*, 1996; Fujiwara *et al*, 1994b), a total of six rSFV intratumoural injections were administered during the first 9 days of treatment, and tumours were assessed for regrowth for the remainder of the experiment.

The NSCLC study was very successful (*Chapter 4*), with up to 95% reduction in tumour volumes following high titre rSFV-EGFP treatment, in comparison to buffer-treated controls, in the absence of any apparent toxicity to normal surrounding tissue. In almost 50% of cases, the tumours regressed entirely, and no tumour regrowth was observed when mice were maintained for over 3 months after treatment.

In the PCa study (*Chapter 5*), both AT3-Neo and AT3-Bcl-2 tumours showed approximately 40-50% reduction in tumour growth following high titre rSFV-EGFP treatment, and thus, *Bcl-2* overexpression appeared to be inadequate in inhibiting the cytolytic properties of rSFV *in vivo*. However, the extremely rapid nature of AT3 tumour growth, and lower transfection efficiencies observed *in vitro*, may explain why both AT3 tumour types recovered following cessation of treatment. Recently, Hardy *et al* (2000) identified a number of other human PCa cell lines that are more amenable to rSFV infection and therefore, treatment. The *Bcl-2* status of these PCa cells was not discussed however.

Bystander effects may have been of crucial importance in establishing the degree of rSFV-mediated tumour kill *in vivo*, particularly when low tumour cell

transfection efficiencies were observed *in vitro*. This bystander effect, which has been observed with other vector systems (Yang *et al*, 1998; Rizk *et al*, 1999; Fujiwara *et al*, 1994a), can be either local or systemic, but in both *in vivo* studies presented here, it appears that a bystander effect stemming from rSFV-mediated disruption of the tumour vascular network and subsequent ischemic necrosis, may be the determining factor in tumour regression.

Differences in the kinetics and morphology of H358a and AT3 tumour growth also aim to explain the discrepancy in rSFV-EGFP treatment success. On gross and histologic examination, the NSCLC tumours were solid, compact lobular aggregates of carcinoma cells, surrounded by layers of connective/stromal tissue. The compact and encapsular nature of the H358a tumour created an amenable environment for direct intratumoural injections with the virus, compared to a much softer, more gelatinous AT3 tumour, which had high levels of endogenous necrosis and haemorrhage.

The success of rSFV-EGFP cytolytic therapy for cancer differs from treatments with the conventional Rv, Ad and AAV systems. In all previous H358 tumour therapy studies, the viral vector mediated a therapeutic effect by virtue of wild-type gene replacement (Fugiwara *et al*, 1994a; Quazilbash *et al*, 1997; Fujiwara *et al*, 1994b). In both Rv and Ad studies, direct intratumoural injections resulted in H358 tumour growth inhibition, but tumours regrew after only 7 (Rv) and 12 (Ad) days post-treatment. Also, Ad-*wtp53* therapy was only successful in mediating a therapeutic effect on the tumour when used in conjunction with cisplatin (Fujiwara *et al*, 1994b). AAV-*wtp53* treatment appeared to hold more promise, but is limited due to low viral titres for intratumoural injection. As almost 70% of all NSCLC are defective in *p53* function (Takahashi *et al*, 1989), it is reasonable to assume that inclusion of *wt-p53* into the rSFV system would

further enhance the cytolytic properties of rSFV for *p53*-deleted or mutated lung and other tumours.

Bcl-2 overexpression is widely associated with the progress of androgen-independent PCa, and is also an important prognostic indicator (McDonnell *et al*, 1992; Ozen & Pathak, 2000). In previous gene therapy studies for *Bcl-2*-overexpressing prostate and other cancer therapies, conventional vectors have predominantly utilised anti-Bcl-2 molecules, such as ASO's and ribozymes (*see section 1.2.3.1*) to downregulate oncogene expression and mediate a therapeutic effect (Webb *et al*, 1997; Gibson *et al*, 2000; Leech *et al*, 2000). In this study, overexpression of *Bax*, whose gene product is known to play a key role in Bcl-2 inhibition and induction of apoptosis *in vivo*, was expressed. *Bax* may be a more suitable transgene than ASO's, as it is known to play a role in *p53*-mediated apoptosis (Miyashita & Reed, 1995), and sensitises a number of tumour cell lines to both radio- and chemotherapeutic agents (Kobayashi *et al*, 1998; Sakakura *et al*, 1996). This strategy was initiated as the cytolytic properties of rSFV-EGFP alone proved inadequate for cytolysis of the *Bcl-2*-overexpressing PCa cell line AT3-Bcl-2.

SFV-mediated HABax overexpression was shown to greatly reduce AT3-Bcl-2 cell proliferation, abolishing the Bcl-2-mediated delay in SFV-induced apoptosis, resulting in 90% inhibition of AT3-Bcl-2 cell growth at 24 h following transfection with the recombinant SFV-HABax RNA molecule. In contrast, rSFV-HABax particles were limited in their effects *in vitro* and *in vivo*, due to very low particle titres. The inclusion of a tumour-specific or inducible promoter as in DNA viruses (Kagawa *et al*, 2000; Tai *et al*, 1999; Komatsu *et al*, 2000), or the use of a more apoptosis-resistant particle-producing cell line, may serve to increase rSFV-HABax particle titres, creating a highly potent cytolytic cancer therapy agent for the elimination of more apoptosis-resistant tumours.

Because *Bax* (and possibly *p53*) overexpression in the SFV system during particle production seriously limits viral titre, other anti-tumour factors which do not result in cell lysis in producer cells could be much more successful for rSFV tumour therapy. Of significant potential are the inhibitors of tumour angiogenesis. The AT3 PCa tumours examined in this study indicated the profound importance of angiogenesis in tumour progression. A number of anti-angiogenic factors are being discovered (O'Reilly *et al*, 1997; O'Reilly *et al*, 1994; Hlatky *et al*, 1996), and a limited number of studies, primarily using the Ad and AAV systems, have demonstrated significant tumour regression via its vascular network, following delivery of potent anti-angiogenic factors such as angiostatin, endostatin or anti-sense molecules to downregulate the expression of vascular endothelial growth factor (Nguyen *et al*, 1998; Feldman *et al*, 2000).

Other applications for rSFV tumour therapy include the enhancement of immune responses to the tumour (Ying *et al*, 1999; Colmenero *et al*, 1999; Leitner *et al*, 2000) by administration of rSFV containing potent antigenic transgenes, which induce a more systemic anti-tumour effect in immuno-competent mice.

rSFV therapy, as with other vectors, could be combined with conventional treatments to generate more significant responses. There is a correlation between the *p53*, *Bax* and *Bcl-2* status of tumour cells with chemo- and radio-sensitivity (Roth & Cristiano, 1997; Vile *et al*, 2000). In nude mice studies, the synergistic effect of vector-mediated transgene expression (*wt-p53*, *Bax* and antisense *Bcl-2*), and intraperitoneal administration of chemotherapeutic agents such as etoposide, 5'-FU and adriamycin, have resulted in improved tumour responses above that of either regime alone (Arafat *et al*, 2000; Owaga *et al*, 1997; Sakakura *et al*, 1996; Chung-Faye *et al*, 2000; Lee *et al*, 2000).

One of the most important limitations of gene therapy for cancer continues to be the specificity of therapeutic gene expression. Administration of viral vectors to animal models or to patients in clinical trials is limited in the majority of cases to local or regional tumours, since current vectors are not approved for systemic delivery. Although viral vectors do have some specificity that results from normal tissue tropism, vector-specific tumour re-targeting is currently being developed at two main levels, namely vector targeting and tumour-specific promoters.

AAV and SV vectors have been successfully re-targeted for gene delivery by attachment of antibodies that react with specific cell surface antigens. In the SV system, an envelope chimera with the *Staphlococcus* protein A was used in conjunction with Mabs that react with specific cell surface antigens, infecting target cells specifically and with high efficiency (Ohno *et al*, 1997). As protein A binds to the Fc portion of the Mab, it allows flexibility with regard to the targeting elements, and a variety of Mabs and tumour antigens can be selected. The tropism of AAV was also redirected to infect a human leukaemia cell line by means of a bispecific $F(ab'\gamma)_2$, where one $Fab'\gamma$ arm recognises the cell surface receptor, and the other recognises the AAV capsid protein (Bartlett *et al*, 1999).

The next level of specificity that can be generated is by the use of tissue/tumour-specific promoters. Promoters for human *α-fetoprotein* and *CEA* genes have been incorporated into vectors to successfully direct transgene expression to a number of cancer types (DiMaio *et al*, 1994; Gazit *et al*, 1995). The identification of truly universal cancer-specific promoters has been difficult due to the heterogeneity of cancer types.

The trailblazer of self-limiting, cancer-specific vectors has been the ONYX-015 virus, an Ad with a deleted *E1B 55kDa* gene. Where the major function of Ad E1B 55kDa is to bind and inactivate p53 (Rao *et al*, 1992), Bischoff *et al* (1996) postulated that this *E1B 55kDa*-defective virus would fail to

replicate in cells with *wt-p53*, and would thus, be uniquely selective for *p53*-deleted cells, observed in a myriad of cancer types. Although the exact mechanism of ONYX-015-induced cytolysis was initially disputed (Lane, 1998), both Phase I and II clinical trials have shown selective intratumoural replication and tumour-selective tissue destruction in tumours deficient in one or more elements of the *p53* signalling pathways (Kirn *et al*, 1998; Ganly *et al*, 2000). More recently, ONYX-015 therapy has resulted in therapeutic responses following intratumoural administration in combination with 5'FU, in patients with recurrent head and neck cancer (Khuri *et al*, 2000). Similar to rSFV, ONYX-015 has no therapeutic transgene itself and relies on the lytic ability of the replicating Ad to kill cells directly.

Gene therapy for cancer is still at an early stage of development. The results from numerous pre-clinical and Phase 1 trials show great potential for virus vector-based therapy, either alone, or as an adjunct to pharmaceutical and radiotherapeutic agents. The recent death of a young patient following adenoviral gene therapy raises many ethical and technical issues regarding safety, which must be resolved before these therapies ever reach routine clinical application.

Increased understanding of the molecular aspects of cancer and in the development of targeted, safer and more efficient gene transfer systems, particularly with reference to transient-based vectors, such as rSFV described here, provide future potential for substantial progress in gene-based therapeutic strategies for human cancer treatment.

Chapter 7

References

7. *References*

Abramovitch, R., Meir, G., & Neeman, M. 1995. Neovascularization induced growth of implanted C6 glioma multicellular spheroids: Magnetic resonance microimaging. *Can. Res.* 55:1956-1962.

Adams, J. M. and Cory, S. 1998. The Bcl-2 protein family: arbitraters of cell survival. *Science.* 281:1322-1325.

Ahola, T. and Kaariainen, L. 1995. Reaction in alphavirus mRNA capping: formation of a covalent complex of nonstructural protein nsP1 with 7-methyl-GMP. *Proc. Natl. Acad. Sci. USA.* 92:507-511.

Alnemri, E. S., Livingston, D. L., Nicholson, D. W., Salvesen, G., Thornberry, N. A., Wong, W. W., & Yuan, J. 1996. Human ICE/CED-3 protease nomenclature. *Cell.* 87:171.

Alperti, G. and Schlesinger, M. J. 1978. Evidence for an autoprotease activity of Sindbis virus capsid protein. *Virology.* 90:366-369.

Amor, S., Scallan, M. F., Morris, M. M., Dyson, H., Fazakerley, J. F. 1996. Role of immune responses in protection and pathogenesis during Semliki Forest virus encephalitis. *Jnl. Gen. Virol.* 77:281-291.

Annonymous. 1982. The World Health Organisation histological typing of lung cancers. *Amer. Jnl. Clin. Pathol.* 77:123-136.

Arafat, W. O., Gomez-Navarro, J., Xiang, J., Barnes, M. N., Mahasreshti, P., *et al.* 2000. An adenovirus encoding proapoptotic Bax induces apoptosis and enhances the radiation effect in human ovarian cancer. *Mol. Ther.* 1:545-554.

Argos, P. 1988. A sequence motif in many polymerases. *Nucl. Acids Res.* 16:9909-9916.

Asher, A. L., Mule, J. J., Kasid, A., Restifo, N. P., Salo, J. C., Reichert, C. M., *et al.* 1991. Murine tumour cells transduced with the gene for tumour necrosis factor alpha. Evidence for paracrine immune effects of tumour necrosis factor against tumours. *Jnl. Immunol.* 254:3227-3234.

Ashkenazi, A. and Dixit, V. M. 1998. Death receptors: signalling and modulation. *Science.* 281:1305-1309.

Asselin-Paturel, C., Lassau, N., Guinebretiere, J-M, Zhang, J., Gay, F., Bex, F., Hallez, S., Leclere, J., Peronnea P., Mami-Chouaib, F., Chouaib, S. 1998. Transfer of the murine interleukin-12 gene *in vivo* by a Semliki Fores virus vector induces B16 tumor regression through inhibition of tumor blood vessel formation monitored by Doppler ultrasonography. *Gene Ther.* 5:606-615.

Atkins, G. J., Sheahan, B, J., Mooney, D. A. 1990. Pathogenicity of Semliki Forest virus for the rat central nervous system and primary rat neural cell cultures-possible implications for the pathogenesis of multiple sclerosis. *Neuropathol. Appl. Neurobiol.* 16:57-68.

Atkins, G. J., Sheahan, B. J., Liljestrom, P. 2000. The molecular pathogenesis of Semliki Forest virus: a model virus made useful. *Jnl. Gen. Virol.* 80:2287-2297.

Austin, E. A. and Huber, B. E. 1993. A first step in the development of gene therapy for colorectal cancer; cloning, sequencing and expression of *Escherichia coli* cytosine deaminase. *Mol. Pharmacol.* 43:380-387.

Baillie-Johnston, H., Twentyman, P. R., Fox, N. E., Walls, G. A., *et al.* 1985. Establishment and characterisation of cell lines from patients with small-cell lung cancer. *Br. Jnl. Cancer.* 52;495-504.

Balachandran, S., Kim, C. N., Yeh, W.-C., Mak, T. W., Bhalla, K., Barber, G. N. 1998. Activation of the dsRNA-dependent protein kinase, PKR, induces apoptosis through FADD-mediated death signalling. *EMBO J.* 17:6888-6902.

Balluz, I. M., Glasgow, G. M., Killen, H. M., Mabruk, M. J. E., M. F., Sheahan, B. J., Atkins, G. J. 1993. Virulent and avirulent strains of Semliki Forest virus show similar cell tropism for the murine central nervous sytem but differ in the severity and rate of induction of cytolytic damage. *Neuropathol. Appl. Neurobiol.* 19:233-239.

Barth, B.-U., Wahlberg, J.M., Garoff, H. 1995. The oligomerization reaction of the Semliki Forest virus membrane protein subunits. *Jnl. Cell. Biol.* 128:283-291.

Bartlett, J. S., Kleinschmidt, J., Boucher, R. C., Samulski, R. J. 1999. Targeted adeno-associated virus vector transduction of nonpermissive cells mediated by a bispecific F(ab'y)2 antibody. *Nature Biotech.* 17:181-186.

Beattie, E., Tartaglia, J., Paoletti, E. 1991. Vaccinia virus-encoded eIF-2 alpha homolog abrogates the antiviral effect of interferon. *Virology.* 183:419-422.

Beg, A. A. and Baltimore, D. 1996. An essential role for NF-kappaB in preventing TNF-alpha-induced cell death. *Science.* 274:782-784.

Beham, A. W., Sarkiss, M., Brisbay, S., Tu, S. M., von Eschenbach, A. C., McDonnell, T. J. 1998. Molecular correlates of Bcl-2-enhanced growth following androgen-ablation in prostate carcinoma cells *in vivo*. *Int. Jnl. Mol. Med.* 1:953-959.

Bejcek, B. E., Wang, D., Bervan, E., Pennell, C. A., Peiper, S. C., Popperna, S., Uckun, F. M., Kersey, J. H. 1995. Development and characterisation of three recombinant single chain antibody fragments (scFvs) directed against the CD19 antigen. *Can. Res.* 55:2346-2351.

Belani, C. P. 1993. Multimodality management of regionally advanced non-small-cell lung cancer. *Semin. Oncol.* 20:302-314.

Berchem, G. J., Bosseler, M., Sugars, L.Y., Voeller, J., Zeitlin, S., Gelmann, E. P. 1995. Androgens induce resistance to Bcl-2-mediated apoptosis in LNCaP prostate cancer cells. *Can Res.* 55:735-738.

Berglund, P., Sjoberg, M., Atkins, G. J., Sheahan, B. J., Garoff, H., Liljestrom, P. 1993. Semliki Forest virus expression systems: Production of conditionally infectious recombinant particles. *Bio/Technol.* 11:916-920.

Berglund, P., Tubulekas, I., Liljestrom, P. 1996. Alphaviruses as vectors for gene delivery. *TIBTECH.* 14:130-134.

Berglund, P., Quesada-Rholander, P., Putkonen, P., Biberfeld, G., Thorstensson, R., Liljestrom, P. 1997. Outcome of immunisation of cynomolgus monkeys with recombinant Semliki Forest virus encoding human immunodeficiency virus type 1 envelope protein and challenge with a high dose of SHIV-4 virus. *AIDS Res. Hum. Retrovir.* 13:1487-1495.

Berglund, P., Smerdou, C., Fleeton, M. N., Tubulekas, I., Liljestrom, P. 1998. Enhancing immune responses using suicidal DNA vaccines. *Nature Biotech.* 16:562-565.

Bernardi, P., Scorrano, L., Colonna, R., Petronelli, V., di Lisa, F. 1999. Mitochondria and cell death: mechanistic aspects and methological issues. *Eur. Jnl. Biochem.* 264:687-701.

Bi, W. L., Parysek, L. M., Warnick, R., Stambrook, P. J. 1993. *In vitro* evidence that metabolic cooperation is responsible for the bystander effect observed with HSV*tk* retroviral gene therapy. *Hum. Gene Ther.* 4:725-731.

Bilbao, G., Feng, M., Rancourt, C., Jackson, W. H., Curiel, D. T. 1997. Adenoviral/retroviral vector chimeras: a novel strategy to achieve high-efficiency stable transduction *in vivo*. *FASEB Jnl.* 11:624-634.

Bischoff, J. R., Kirn, D. H., Williams, A., Heise, C., Horn, S., *et al.* 1996. An adenovirus mutant that replicates selectively in *p53*-deficient human tumour cells. *Nature.* 274:373-376.

Bishop, J. M. 1992. The molecular biology of cancer. *Science.* 235:305-311.

Bissonnette, R. P., Echeverri, F., Mahboudi, A., Green, D. R. 1992. Apoptotic cell death induced by *c-myc* is inhibited by *Bcl-2*. *Nature*. 359:552-554.

Boise, L. H., Gonzalez-Garcia, M., Postema, C. E., Ding, L., Lindsten, T., Turka, L. A., Mao. X., Nunez, G., Thompson, C. B. 1993. *Bcl-x*, a *bcl-2*-related gene that functions as a dominant regulator of apoptotic cell death. *Cell.* 74:597-608.

Boldin, M. P., Goncharov, T. M., Goltsev, Y. V., Wallach, D. 1996. Involement of MACH, a novel MORT1/FADD-interacting protease, in Fas/APO-1-and TNF receptor-induced cell death. *Cell.* 85:803-815.

Boulakia, C. A., Chen, G., Ng, F. W. H., Teodoro, J. G., Branton, P. E., Nicholson, D. W., Poirier, G. G., Shore, G. C. 1996. Bcl-2 and adenovirus E1B 19kDa protein prevent E1A processing of CPP32 and cleavage of poly(ADP-ribose) polymerase. *Oncogene*. 12:529-535.

Bouvet, M., Ellis, L. M., Nishizakii, M., Fujiwara, T. *et al*. 1998. Adenovirus-mediated *p53* gene transfer downregulates vascular endothelial growth factor expression and inhibits angiogenesis in human colon cancer. *Can. Res*. 58:2288-2292.

Boyd, J. M., Gallo, G. J., Elangovan, B., Houghtan, A. B., Malstrom, S., Avery, B. J., *et al*. 1995. Bik, a novel death-inducing protein shares a distinct sequence motif with Bcl-2 family proteins and interacts with viral and cellular survival-promoting proteins. *Oncogene*. 11:1921-1928.

Bradish, C. J., Allner, K., Maberm H. B. 1971. The virulence of original and derived strains of Semliki Forest virus for mice, guinea pigs and rabbits. *Jnl. Gen. Virol.* 12:141-162.

Brady, H. J., Gil-Gomez, G., Kirberg, J., Berns, A. J. 1996. Bax alpha perturbs T cell development and affects cell cycle entry of T cells. *EMBO J.* 15:6991-7001.

Bredenbeek, P. J., Frolov, I., Rice, C. M., Schlesinger, S. 1993. Sindbis virus expression vectors: packaging of RNA replicons by using defective helper RNAs. *Jnl. Virol.* 67:6439-6446.

Brojatsch, J., Naughton, J., Rolls, M. M., Zingler, K., Young, J. A. 1996. CAR1, a TNFR-related protein, is a cellular receptor for cytopathic avian leukosis-sarcoma virus and mediates apoptosis. *Cell.* 87:845-855.

Brower, M., Carney, D. N., Oie, H. K., Gazdar, A. F., Minna, J. D. 1986. Growth of cell lines and clinical specimens of human non-small cell lung cancer in a serum-free defined medium. *Can Res.* 46:798-806.

Cai, D. W., Mukhopadhyay, T., Liu, Y., Fujiwara, T., Roth, J. A. 1993. Stable expression of the wild-type *p53* gene in human lung cancer cells after retrovirus-mediated gene therapy. *Hum. Gene Ther.* 4:617-624.

Casciola-Rosen, L. A., Miller, D. K., Anhalt, G. J., Rosen, A. 1994. Specific cleavage of the 70-kDa protein component of the U1 small nuclear ribonucleoprotein is a characteristic biochemical feature of apoptotic cell death. *Jnl. Biol. Chem.* 269:30757-30760.

Chalfie, M., Tu, Y., Euskirchen, G., Ward, W. W., Prasher, D. C. 1994. Green Fluorescent Protein as a marker for gene expression. *Science.* 263:802-805.

Chamberlain, R. W. 1980. Epidemiology of arthropod-borne togaviruses; the role of arthropods as vectors, and of vertrbrate hosts in natural transmission cycles. p175-227. *In*, Togaviruses: biology, structure and replication. R. W. Schlesinger (*ed*). Academic Press, Inc, Orlando, FLA.

Chang, B. S., Minn, A. J., Muchmore, S. W., Fesik, S. W., Thompson, C. B. 1997. Identification of a novel regulatory domain in Bcl-X(L) and Bcl-2. *EMBO J.* 16:968-977.

Chen, P.-L., Chen, Y., Bookstein, R., Lee, W.-H. 1990. Genetic mechanisms of tumour suppression by the human *p53* gene. *Science.* 250:1576-1579.

Cheng, E. H.-Y., Levine, B., Boise, L. H., Thompson, C. B., Hardwick, J. M. 1996. Bax-independent inhibition of apoptosis by Bcl-xl. *Nature.* 379:554-556.

Cheng, E. H., Kirsch, D. G., Clem, R. J., Ravi, R., Kastan, M. B., Bedi, A., Ueno, K., Hardwick, J. M. 1997. Conversion of Bcl-2 to a Bax-like death effector by caspases. *Science.* 278:1966-1968.

Chinnaiyan, A. M., O'Rourke, K., Tewari, M., Dixit, V. M. 1995. FADD, a novel death domain-containing protein, interacts with the death domain of Fas and initiates apoptosis. *Cell.* 81:505-512.

Chinnaiyan, A. M., O'Rourke, K., Duan, H., Poirier, G. G., Dixit, V. M. 1996. Molecular ordering of the cell death pathway. *Jnl. Biol. Chem.* 271:4573-4576.

Chinnaiyan, S., Tepper, C. G., Seldin, M. F., O'Rourke, K., Kischkel, F. C., *et al.* 1996. FADD/MORT1 is a common mediator of CD95 (Fas/APO-1) and Tumor Necrosis Factor Receptor-induced apoptosis. *Jnl. Biol. Chem.* 271:4961-4965.

Chirmule, N., Propert, K., Magosin, S., Qian, Y., Qian, R, Wilson, J. 1999. Immune responses to adenovirus and adenoassociated virus in humans. *Gene Ther.* 6:1574-1583.

Chittenden, Y., Harrington, E. A., O'Connor, R., Flemington, C., Lutz, R. J., Evan, G. I., Guild, B. C. 1995. Induction of apoptosis by the Bcl-2 homologue Bak. *Nature*. 374:733-736.

Choi, R. H., Kuhn, R. J., Olson, N. H., Rossman, M. G., Choi, H.-K., Smith, T. J., Baker, T. S. 1991. Structure of Sindbis virus core protein reveals a chymotypsin-like serine proteinase and the organisation of the virion. *Nature*. 354:37-43.

Choi, S. S., Park, I. C., Yun, J. W., Sung, Y. C., Hong, S. I., Shin, H. S. 1995. A novel Bcl-2 related gene, *Bfl-1*, is overexpressed in stomach cancer and preferentially expressed in bone marrow. *Oncogene*. 11:1693-1698.

Chong, H., Todryk, S., Hutchinson, G., Hart, I. R., Vile, R. G. 1998. Tumour cell expression of B7 costimulatory molecules and IL-12 or GM-CSF induces a local antitumour response that may generate systematic immunity. *Gene Ther*. 5:223-232.

Chung-Faye, G. A., Kerr, D. J., Young, L. S., Searle, P. F. 2000. Gene therapy strategies for colon cancer. *Molec. Med. Today*. 6:82-87.

Clarke, A. R., Purdie, C. A., Harrison, D. J., Morris, R. G., Bird, C. C., Hooper, M. L., Wyllie, A. H. 1993. Thymocyte apoptosis induced by *p53*-dependent and independent pathways. *Nature*. 362:849-852.

Clemens, M. J. and Elia, A. 1997. The double-stranded RNA-dependent protein kinase PKR: structure and function. *Jnl. Interf. Cytokine Res*. 17:503-524.

Cohen, G. M. 1997. Caspases: the executioners of apoptosis. *Biochem. Jnl*. 326:1-16.

Colmenero, P., Liljestrom, P., Jondal, M. 1999. Induction of P815 tumour immunity by recombinant Semliki Forest virus expressing the *P1A* gene. *Gene Ther*. 6:1728-1733.

Conry, R., *et al*. 1995. Breaking tolerance to CEA with a rV virus vaccine in man. (Abstr.). *Proc. Am. Assoc. Can. Res*. 36:492.

Cregen, S. P., MacLaurin, J. G., Crais, C. G., Robertson, G. S., Nicholson, D. W., Park, D. S., Slack, R. S. 1999. Bax-dependent caspase-3 activation is a key determinant in *p53*-induced apoptosis in neurons. *Jnl. Neurosci*. 19:7860-7869.

Criekinge, W. V., Beyaert, R., Van de Craen, M., Vandenbeele, P., Schotte, P., De Valck, D., Fiers, W. 1996. Functional characterisation of the prodomain of interleukin-1B-converting enzyme. *Jnl. Biol. Chem*. 271:27245-27248.

Cryns, V. L., Bergeron, L., Zhu, H., Li, H., Yuan, J. 1996. Specific cleavage of α-Fodrin during Fas- and Tumor necrosis factor-induced apoptosis is mediated by an interleukin-1b-converting enzyme/Ced-3 protease distinct from the Poly(ADP-ribose) polymerase protease. *Jnl. Biol. Chem.* 271:31277-31282.

Cryns, V. L. and Yuan, J. 1998. The cutting edge: caspases in apoptosis and disease. p177-210. *In*, When cells die. R. A. Lockshin, Z. Zakeri and J. L. Tilly (*eds*). Wiley-Liss, Inc.

Curiel, D. T., Agarwal, S., Wagner, E., Cotten, M. 1991. Adenovirus enhancement of transferrin polylysine mediated gene delivery. *Proc. Natl. Acad. Sci. USA*. 88:8850-8854.

Curiel, D. T., Agarwal, S., Romer, S., Wagner, M. U., Cotton, M., Birnsteil, M. L., Boucher, R. C. 1992. Gene transfer to respiratory epithelial cells via the receptor-mediated endocytosis pathway. *Am. Jnl. Respir. Cell Mol. Biol.* 6:247-252.

Dangles, V., Femenia, F., Laine, V., Berthelemy, M., Le Rhun, D., Poupon, M.-F., Levy, D., Schwartz-Cornil, I. 1997. Two- and three-dimensional cell structures govern epidermal growth factor survival function in human bladder carcinoma cell lines. *Can. Res.* 57:3360-3364.

Davies, A. M. 1995. The Bcl-2 family of prteins, and the regulation of neuronal survival. *TINS.* 18:355-359.

Davis, B. M., Koc, O. N., Lee, K., Gerson, S. L. 1996. Current progess in the gene therapy of cancer. *Curr. Opin. Oncol.* 8:499-508.

Davis, N. L., Willis, L. V., Smith, J. F., Johnston, R. E. 1989. *In vitro* synthesis of infectious Venezuelan equine encephalitis virus RNA from a cDNA clone: analysis of a viable deletion mutant. *Virology*. 171:189-204.

Debbas, M. and White, E. 1993. Wild-type *p53* mediates apoptosis by E1A, which is inhibited by E1B. *Genes Dev.* 7:546-554.

deCurtis, I. and Simons, K. 1988. Dissection of Semliki Forest virus glycoprotein delivery from the trans-Golgi network to the cell surface in permeabilised BHK-21 cells. *Proc. Natl. Acad. Sci. USA*. 85:8052-8056.

del Peso, L., Gonzalez-Garcia, M., Page, C., Herrara, R., Nunez, G. 1997. Interleukin-3-induced phosphorylation of BAD through the protein kinase Akt. *Science*. 278:687-689.

Despres, P., Griffin, J. W., Griffin, D. E. 1995. Effects of anti-E2 monoclonal antibody on Sindbis virus replication in AT3 cells expressing Bcl-2. *Jnl. Virol.* 69:7006-74.

DeTuello, L. and Kirchausen, T. 1998. The clathrin endocytic pathway in viral infection. *EMBO J.* 17:4585-4593.

Deveraux, Q. L., Takahashi, R., Salvesen, G. S., Reed, J. C. 1997. X-linked IAP is a direct inhibitor of cell-death proteases. *Nature.* 388:300-304.

Dillman, R. O., Herndon, J., Seagren, S. L., Eaton, W. L. Jr., Green, M. R. 1996. Improved survival in stage 111 non-small-cell lung cancer: seven-year follow-up of cancer and leukemia group B (CALGB) 8433 trial. *Jnl. Natl. Can. Instit.* 88:1210-1215.

DiMaio, J. M., Clary, B. M., Via, D. F., Coveney, E., Pappas, T. N., Lyerly, H. K. 1994. Directed enzyme pro-drug gene therapy for pancreatic cancer *in vivo*. *Surgery.* 116:205-213.

Ding, M., and Schlesinger, M. J. 1989. Evidence that Sindbis virus *nsP2* is an autoprotease which processes the virus nostructural polyprotein. *Virology.* 171:280-284.

Donnelly, S. M., Sheahan, B. J., Atkins, G. J. 1997. Long-term effects of Semliki Forest virus infection in the mouse central nervous system. *Neuropathol. Appl. Neurobiol.* 23:235-241.

Dorai, T., Olsson, C. A., Katz, A. E., Buttyan, R. 1997. Development of a hammerhead ribozyme against Bcl-2. 1. Preliminary evaluation of a potential gene therapeutic agent for hormone-refractory human prostate cancer. *Prostate.* 32:246-258.

Duan, H. and Dixit, V. M. 1997. RAIDD is a new 'death" adaptor molecule. *Nature.* 385:86-89.

Dubuisson, J. and Rice, C. M. 1993. Sindbis virus attachment: isolation and characterisation of mutants with impaired binding to vertebrate cells. *Jnl. Virol.* 67:3363-3374.

Dulic, V., Kaufmann, W. K., Wilson, S. J., Tlsty, T. D., Lees, E., Harper, J. W., Elledge, S. J., Reed, S. I. 1994. *p53*-dependent inhibition of cyclin-dependent kinase activities in human fibroblasts during radiation-induced G1 arrest. *Cell.* 76:1013-1023.

Ellis, H. M. and Horovitz, H. R. 1986. Genetic control of programmed cell death in the nematode *C. elegans*. *Cell.* 44:817-829.

Emmett, J. L., Greene, L. F., Papantoniou, A. 1960. Endocrine therapy in carcinoma of the prostate gland: ten year survival studies. *Jnl. Urol.* 83:471-484.

Enari, M., Sakahira, H., Yokoyama, H., Okawa, K., Iwamatsu, A., Nagata, S. 1998. A caspase-activated DNase that degrades DNA during apoptosis, and its inhibitor ICAD. *Nature*. 391:43-50.

Engelhardt, J. F., Ye, X., Doranz, B., Wilson, J. M. 1994. Ablation of *E2A* in recombinant adenoviruses improves transgene persistence and decreases inflammatory response in mouse liver. *Proc. Natl. Acad. Sci. USA*. 91:6196-6200.

Everett, H. and McFadden, G. 1999. Apoptosis: and innate immune response to virus infection. *Trends Microbiol*. 7:160-165.

Fallaux, F. J., Bout, A., van den Velde, I. van der Wollenberg, D. J. *et al*. 1998. New helper cells and matched early region 1-deleted adenovirus vectors prevent generation of repliaction-competent adenovirus. *Hum. Gene Ther*. 9:1909-1917.

Fang, B., Eisensmith, R. C., Wang, H., Kay, M. A., Cross, R. E., Landen, C. N., *et al*. 1995. Gene therapy for hemophilia B; host immunosuppression prolongs the therapeutic effect of adenovirus-mediated factor IX expression. *Hum. Gene Ther*. 6:1039-1044.

Farrow, S. N., White, J. H., Martinou, I., Raven, T., Pun, K. T., Grinham, C. J., Moutinov, J. C., Brown, R. 1995. Cloning of a *bcl-2* homologue by the interaction with adenovirus E1B19K. *Nature*. 374:431.

Favre, D., Studer, E., Michel, M. R. 1996. Semliki Forest virus caspid protein inhibits the initiation of translation by upregulating the double-stranded RNA-activated protein kinase (PKR). *Biosci. Reports*. 16:485-511.

Fazakerley, J. K. and Webb, H. E. 1987. Semliki Forest virus-induced, immune-mediated demyelination: adoptive transfer studies and viral persistence in nude mice. *Jnl. Gen. Virol*. 68:377-386.

Fazakerley, J. K., Pathak, S., Scallan, M., Amor, S. Dyson, H. 1993. Replication of the A7(74) strain of Semliki Forest virus is restricted in neurons. *Virology*. 195:627-637.

Fazakerley, J. K. and Buchmeier, M. J. 1993. Pathogenesis of virus-induced demyelination. *Adv. Virus Res*. 42:249-324.

Fearon, E. R., Pardoll, D. M., Itaya, T., Golumbek, P., Levitsky, H. I., Simons, J. O., *et al*. 1990. Interleukin-2 production by tumour cells bypassess T helper function in the generation of an antitumour response. *Cell*. 60:397-403.

Feldman, A. L., Restifo, N. P., Alexander, H. R., Bartlett, D. L., Hwu, P., Seth, P., Libutti, S. K. 2000. Antiangiogenic gene therapy of cancer utilising a recombinant adenovirus to elevate systemic endostatin levels in mice. *Can. Res.* 60:1503-1506.

Felgner, P. L., Gadek, T. R., Holm, M., Roman, R., Chan, H. W., Wenz, M., Northrop, J. P., Ringold, G. M., Danielsen, M. 1987. Lipofection: a highly efficient, lipid-mediated DNA-transfection procedure. *Proc. Natl. Acad. Sci. USA.* 84:7413-7417.

Feng, M., Jackson, W. H., Goldman, C. K., Rancourt, C., Wang, M., Dusing, S. K., Siegel, G., Curiel, D. T. 1997. Stable *in vivo* gene transduction via a novel adenoviral/retroviral chimeric vector. *Nature Biotech.* 15:866-870.

Fernandes-Alnemri, T., Armstrong, R. C., Krebs, J., Srinivasula, S. M., Wang, L., *et al.* 1996. *In vitro* activation of CPP32 and Mch3 by Mch4, a novel human apoptotic cysteine protease containing two FADD-like domains. *Proc. Natl. Acad. Sci. USA.* 93:7464-7469.

Fernandes, R. S. and Cotter, T. G. 1993. Activation of a calcium magnesium independent endonuclease in human leukemic cell apoptosis. *Antican. Res.* 13:1253-1259.

Ferrari, F. K., Xiao, X. McCarty, D., Samulski, R. J. 1997. New developments in the generation of Ad-free, high-titer rAAV gene therapy vectors. *Nature Med.* 3:1295-1297.

Fleeton, M. N., Sheahan, B. J., Gould, E. A., Atkins, G. J., Liljestrom, P. 1999. Recombinant Semliki Forest virus particles encoding the prME or NS1 proteins of louping ill virus protect mice from lethal challenge. *Jnl. Gen. Virol.* 80:1189-1198.

Fleeton, M. N., Liljestrom, P., Sheahan, B. J., Atkins, G. J. 2000. Recombinant Semliki Forest virus particles expressing louping ill virus antigens induce a better protective response than plasmid-based DNA vaccines or an inactivated whole particle vaccine. *Jnl. Gen. Virol.* 81:749-758.

Forsell, K., Suomalainen, M., Garoff, H. 1995. Structure-function relation of the NH2-terminal domain of the Semliki Forest virus capsid protein. *Jnl. Virol.* 69:1556-1563.

Forstova, J., Krauzewicz, N., Sandig, V., Elliot, J., Palkova, Z., Strauss, M. *et al.* 1995. Polyoma virus pseudocapsids as efficient carriers of heterologous DNA into mammalian cells. *Hum. Gene Ther.* 6:297-306.

Frankel, A., Buckman, R., Kerbel, R. S. 1997. Abrogation of Taxol-induced G2-M arrest and apoptosis in human ovarian cancer cells grown as multicellular tumor spheroids. *Can. Res.* 57:2388-2393.

Frederik, M. J., Holton, P. R., Hudson, M., Wang, M., Clayman, G. L. 1999. Expression of apoptosis-related genes in human head and neck squamous cell carcinomas undergoing *p53*-mediated programmed cell death. *Clin. Can. Res.* 5:361-369.

Freeman, S. M., Abboud, C. N., Whartenby, K. A., Packman, C. H., Koeplin, D. S., Moolten, F. T., Abraham, G. N. 1993. The "bystander effect": tumour regression when a fraction of the tumour mass is genetically modified. *Can. Res.* 53:5274-5283.

Freyer, P. J., and Sutherland, R. M. 1980. Selective dissociation and characterization of cells from different regions of multicell tumor spheroids. *Can. Res.* 40:3956-3965.

Frolov, I. and Schlesinger, S. 1994. Translation of Sindbis virus mRNA: effects of sequences downstream of the initiating codon. *Jnl. Virol.* 68:8111-8117.

Frolov, I. H., T. A., Pragai, B. M., Dryga, S. A., Huang, H. V., Schlesinger, S., Rice, C. M. 1996. Alphavirus-based expression vectors: strategies and applications. *Proc. Natl. Acad. Sci. USA.* 93:11371-11377.

Froshauer, S., Kartenbeck, J., Helenius, A. 1988. Alphavirus RNA replicase is located on the cytoplasmic surface of endosomes and lysosomes. *Jnl.Cell Biol.* 107:2075-2086.

Fujiwara, T., Grimm, E. A., Mukhopadhyay, T., Cai, D. W., Owen-Schaub, L. B., Roth, J. A. 1993. A retroviral wild-type *p53* expression vector penetrates human lung cancer spheroids and inhibits growth by inducing apoptosis. *Can. Res.* 53:4129-4133.

Fujiwara, T., Cai, D. W., Georges, R. N., Mukhopadhyay, T., Grimm, E. A., Roth, J. A. 1994a. Therapeutic effect of a retroviral wild-type *p53* expression vector in an orthotopic lung cancer model. *Jnl. Natl. Can. Inst.* 86:1458-1462.

Fujiwara, T., Grimm, E. A., Mukhopadhyay, T., Zhang, W.-W., Owen-Schaub, L. B., Roth, J. A. 1994b. Induction of chemosensitivity in human lung cancer cells *in vivo* by adenovirus-mediated transfer of the wild-type *p53* gene. *Can. Res.* 54:2287-2291.

Fujiwara, T., Grimm, E. A., Roth, J. A. 1994c. Gene therapeutics and gene therapy for cancer. *Curr. Opin. Oncol.* 6:96-105.

Gajewski, T. F. and Thompson, C. B. 1996. Apoptosis meets signal transduction: elimination of a BAD influence. *Cell.* 87:589-592.

S. Galbraith, Dept. Microbiology, Trinity College, Dublin 2, Ireland.

Gale, M. J. J., Korth, M. J., Tang, N. M., Tan, S. L., Hopkins, D. A., *et al.* 1997. Evidence that hepatitis C virus resistance to interferon is mediated through repression of the PKR protein kinase by the nonstructural 5A protein. *Virology*. 230:217-227.

Ganly, I., Eckhardt, S. G., Rodriguez, I., Sontar, D. S., *et al.* 2000. A Phase 1 study of ONYX-015, an E1B attenuated adenovirus, administered intratumourally to patients with recurrent head and neck cancer. *Clin. Can. Res*. 6:798-806.

Gansbacher, B., Bannerji, R., Daniels, B., Zier, K., Cronin, K., Gilboa, E. 1990. Retroviral vector-mediated gamma interferon gene trasfer into tumour cells generates potent and long-lasting antitumour immunity. *Can. Res*. 50:7820-7825.

Garoff, H., Simons, K., Renkonen, O. 1974. Isolation and characterisation of the membrane proteins of Semliki Forest virus. *Virology*. 61:493-504.

Garoff, H. and Simons, K. 1974. Location of the spike glycoproteins in the Semliki Forest virus membrane. *Proc. Natl. Acad. Sci. USA*. 71:3988-3992.

Garoff, H., Huylebroeck, D., Robinson, A., Tillman, U., Liljestrom, P. 1990. The signal sequence of the p62 protein of Semliki Forest virus is involved in iniation but not in completing chain translocation. *Jnl. Cell Biol*. 111:867-876.

Gatalica, Z. and Miettinen, M. 1994. Distribution of carcinoma antigens CA-19-9 and CA-15-3; and immunohistochemical study of 400 tumours. *Appl. Immunohistochem*. 2:205.

Gavrieli, Y., Sherman, Y, Ben-Sasson, S. A. 1992. Identification of programmed cell death *in situ* via specific labelling of nuclear DNA fragmentation. *Jnl. Cell Biol*. 119:1559-1563.

Gazdar, A. 1994. Cell culture of lung cancers. p121-160. *In*, Atlas of human tumour cell lines. Academic Press.

Gazdar, A. F., Carney, D. N., Russell,, E. K., Sims, H. L., Baylin, S. B., *et al.* 1980. Establishment of continuos, clonable cultures of small-cell carcinoma of lung which have amine precursor uptake and decarboxylation cell properties. *Can. Res*. 40:3502-3507.

Gazdar, A. F. and Linnoila, R. I. 1988. The pathology of lung cancer-changing concepts and newer diagnostic techniques. *Sem. Oncol*. 15; p215-225.

Gazdar, A. F., Linnoila, R. I., Kurita, Y., Oie, H. K., Mulshine, J. L., Clark, J. C., Whitsett, J. A. 1990. Peripheral airway cell differentiation in human lung cancer cell lines. *Can. Res*. 50:5481-5487.

Gazit, G., Kane, S. E., Nichols, P. Lee, A. S. 1995. Use of the stress-inducible grp78/BiP promoter in targeting high level gene expression in fibrosarcoma *in vivo*. *Can. Res.* 55:1660-1663.

Georges, R. N., Mukhopadhyay, T., Zhang, Y., Yen, N., Roth, J. A. 1993. Prevention of orthtopic human lung cancer growth by intratracheal instillation of a retroviral antisense K-ras construct. *Can. Res.* 53:1743-1746.

Ghazizadeh, S., Carroll, J. M., Taichman, L. B. 1997. Repression of retrovirus-mediated transgene expression by interferons: Implications for gene therapy. *Jnl. Virol.* 71:9163-9169.

Gibson, L., Holmgreen, S. P., Huang, D. C., Bernard, O., Copeland, N. G., Jenkins, N. A., *et al.* 1996. Bcl-w, a novel member of the Bcl-2 family, promotes cell survival. *Oncogene.* 13:665-675.

Gibson, S. A., Pellenz, C., Hutchison, R. E., Davey, F. R., Shillitoe, E. J. 2000. Induction of apoptosis in oral cancer cells by an anti-Bcl-2 ribozyme delivered by an adenovirus vector. *Clin. Can. Res.* 6:213-222.

Gillet, G. and Brun, G. 1996. Viral inhibition of apoptosis. *Trends Microbiol.* 4:312-316.

Gjertsen, B. T., Logothetis, C. L., McDonnell, T. J. 1999. Molecular regulation of cell death and therapeutic strategies for cell death induction in prostate carcinoma. *Cancer Meta. Rev.* 17:345-351.

Glanville, N., Ranki, M., Morser, J., Kaariainen, L., Smith, A. E. 1976. Initiation of translation directed by 42S and 26S RNAs from Semliki Forest virus *in vitro*. *Proc. Natl. Acad. Sci. USA.* 73:3059-3063.

Glasgow, G. M. Dept. Microbiology, Trinity College, Dublin 2, Ireland.

Glasgow, G. M., Sheahan, B. J., Atkins, G. J., Wahlberg, J. M., Salminen, A., Liljestrom P. 1991. Two mutations in the envelope glycoprotein E2 of Semliki Forest virus affecting the maturation and entry patterns of the virus attenuates pathogenicity. *Virology.* 185:741-748.

Glasgow, G. M., McGee, M. M., Sheahan, B. J., Atkins, G. J. 1997. Death mechanisms in cultures cells infected by Semliki Forest virus. *Jnl. Gen. Virol.* 78:1559-1563.

Glasgow, G. M., McGee, M. M., Tarbatt, C. J., Mooney, D. A., Sheahan, B. J., Atkins, G. J. 1998. The Semliki Forest virus vector induces *p53*-independent apoptosis. *Jnl. Gen. Virol.* 79:2405-2410.

Gleave, M. E., Miayake, H., Goldie, J., Nelson, C., Tolcher, A. 1999. Targeting the *Bcl-2* gene to delay androgen-independent progression and enhance chemosensitivity in prostate cancer using antisense Bcl-2 oligodeoxynucleotides. *Urology*. 54:36-46.

Goddard, M. J., Wilson, B., Grant, J. W. 1991. Comparison of commercially available cytokeratin antibodies in normal and neoplastic adult epithelial and non-epithelial tissues. *Jnl. Clin. Pathol.* 44:660-663.

Golstein, P. 1997. Cell death: TRAIL and its receptors. *Curr. Biol.* 7:R750-R753.

Golumbek, P. T., Lezerby, A. J., Levitsky, H. I., Jaffee, L. M., Karasuyama, H., Baker, M., *et al.* 1991. Treatment of established renal cancer by tumour cells engineered to secrete IL-4. *Science.* 254:713-716.

Gorbalenya, A. E., Koonin, E. V. 1989. Viral proteins containing the purine NTP-binding sequence pattern. *Nucl. Acids Res.* 17:8413-8430.

Gould, V. E. and Warren, W. H. 1989. Epithelium neoplasms. p77-93. *In*, Thoracic Oncology. J. A. Roth, J. C. Ruckdeschel, T. H. Weisenburg (*eds*). Philadelphia Saunders.

Grandgirard, D., Studer, E., Monney, L., Belser, T., Fellay, I., Borner, C., Michel, M. R. 1998. Alphaviruses induce apoptosis in Bcl-2-overexpressing cells: evidence for a caspase-mediated, proteolytic inactivation of Bcl-2. *EMBO J.* 17:1268-1278.

Grandgirard, D., Gianinazzi, C., Monney, L., Borner, C., Michel, M. R. 2000. Apoptosis induced by the alphavirus Semliki Forest is associated with mitochondrial cytochrome *c* release. *Manuscript.*

Green, N. K., Youngs, D. J., Neoptolemos, J. P., *et al.* 1997. Sensitisation of colorectal and pancreatic cancer cell lines to the prodrug 5-(aziridin-1-yl)-2, 4-dinitrobenzamide (CD1954) by retroviral transduction and expression of the E. coli nitroreductase gene. *Can. Gene Ther.* 4:229-238.

Green, D. R. and Reed, J. C. 1998. Mitochondria and apoptosis. *Science.* 281:1309-1312.

Green, D. and Kroemer, G. 1998. The central executioners of apoptosis: caspases or mitochondria? *Trends Cell Biol.* 8:267-271.

Griffin, D. E. 1998. A review of alphavirus replication in neurons. *Neurosci. Biobehav. Rev.* 22:721-723.

Groeger, A. M., Caputi, M., Esposito, V., De Luca, A., Salat, A., Murabito, M., Giordano, G. G., Baldi, F., Giordano, A., Wolner, E. 1999. Bcl-2 protein expression correlates with nodal status in non small cell lung cancer. *Antican. Res.* 19:821-824.

Gunji, Y., Tagawa, M., Matsubara, H., Takenaga, K., *et al.* 1996. Antitumour effect induced by the expression of granulocyte macrophage-colony stimulating factor gene in murine colon carcinoma cells. *Cancer Lett.* 101:257-261.

Guo, M. and Hay, B. A. 1999. Cell proliferation and apoptosis. *Curr. Opin. Cell Biol.* 11:745-752.

Guo, B., Cao, S., Toth, K., Azrak, R. G., Rustum, Y. M. 2000. Overexpression of Bax enhances antitumour activity of chemotherapeutic agents in human head and neck squamous cell carcinoma. *Clin. Can. Res.* 6:718-724.

Hahn, Y. S., Grakoui, A., Rice, C. M., Strauss, E. G., Strauss, J. H. 1989. Mapping of RNA temperature-sensitive mutants of Sindbis virus: complementation group F mutants have lesions in *nsP4*. *Jnl. Virol.* 63:1194-1202.

Hahn, C. S., Hahn, Y. S., Braciale, T. J., Rice, C. M. 1992. Infectious Sindbis virus transient expression vectors for studying antigen processing and presentation. *Proc. Natl. Acad. Sci. USA.* 89:2679-2683.

Hamada, K., Alemany, R., Zhang, W.-W., Hittelman, W. N., Lotan, R., Roth, J. A., Mitchell, M. F. 1996. Adenovirus-mediated transfer of a wild-type *p53* gene and induction of apoptosis in cervical cancer. *Can. Res.* 56:3047-3054.

Hamilton, G. 1998. Multicellular spheroids as an *in vitro* tumor model. *Cancer Lett.* 131:29-34.

Hanai, N., Shitara, K., Furuya, A., Yoshida, H., Dohi, T., Nudelman, E., Hakomori, S., Satoh, S. 1990. Detailed characterisation of reactivities of anti-gastric cancer monoclonal antibodies to carbohydrate antigen. *Antican. Res.* 10:1579-1586.

Harding, F. A., McAurthur, J. G., Gross, J. A., Raulet, D. H., *et al.* 1992. CD-28-mediated signalling costimulates murine T cells and prevents induction of anergy in T cell clones. *Nature.* 356:607-609.

Hardy, W. R., and Strauss, J. H. 1988. Processing of the nonstructural polypoteins of Sindbis virus: study of the kinetics *in vivo* using monospecific antibodies. *Jnl. Virol.* 62:998-1007.

Hardy, P. A., Mazzini, M. J., Schweitzer, C., Lundstrom, K., Glode, L. M. 2000. Recombinant Semliki Forest virus infects and kills human prostate cancer cell lines and prostatic duct epithial cells *ex vivo*. *Int. Jnl. Mol. Med.* 5:241-245.

Harris, M. P., Sutjipto, S., Wills, K. N., Hancock, W., Cornell, D. 1996. Adenovirus-mediated *p53* gene transfer inhibits growth of human tumour cells expressing mutant p53 protein. *Can. Gene Ther.* 3:121-130.

Helenius, A., Morein, B., Fries, E., Simons, K., Robinson, P., Schirrmacher, V., *et al.* 1978. Human (HLA-A and HLA-B) and murine (H-2K and H2-D) histocompatibility antigens are cell surface receptors for Semliki Forest virus. *Proc. Natl. Acad. Sci. USA.* 75:3846-3850.

Henderson, S., Huen, D., Rowe, M., Dawson, C., Johnson, G ., Rickinson, A. 1993. Epstein-Barr virus-coded BHRF1 protein, a viral homologue of Bcl-2, protects human B cells from programmed cell death. *Proc. Natl. Acad. Sci. USA.* 90:8479-8483.

Hengartner, M. O. and Horvitz, H. R. 1994. *C. elegans* cell survival gene *ced-9* encodes a functional homolog of the mammailian proto-oncogene *Bcl-2*. *Cell.* 76:665-676.

Hlatky, L., Hahnfeldt, P., Tsionou, C., Coleman, C. N. 1996. Vascular endothelial growth factor: environmental controls and and effects in angiogenesis. *Br. Jnl. Cancer.* 27:S151-S156.

Hock, H., Dorsch, M., Diamantstein, T., Blackstein, T. 1991. Interleukin-7 induces CD4+ T cells-dependent tumour rejection. *Jnl. Exp. Med.* 174:1291-1298.

Hockenbery, D., Nunez, G., Milliman, C., Schreiber, R. D., Korsmeyer, S. J. 1990. Bcl-2 is an inner mitochondrial membrne protein that blocks programmed cell death. *Nature.* 348:334-336.

Hodge, J. W., Abrams, S., Schlou, J., Kantor, J. A. 1994. Induction of antitumour immunity by recombinant Vaccinia virus expressing B7-1 and B7-2 costimulatory molecules. *Can. Res.* 54:5552-5555.

Hofmann, K., Bucher, P., Tschopp, J. 1997. The CARD domain: a new apoptotic signalling motif. *Trends Biochem Sci.* 22:155-156.

Hollenstein, M., Sidransky, D., Vogelstein, B. Harris, C. C. 1991. *p53* mutations in human cancers. *Science.* 253:49-53.

Horwitz, M. S. 1990. p1679-1721. *In*, Fields virology. B. N. Fields et al (*eds*). Lippincott-Raven publishers, Philadelphia.

Hsu, H., Xiong, J., Goeddel, D. V. 1995. The TNF receptor 1-associated protein TRADD signals cell death and NF-kappa B activation. *Cell*. 81:495-504.

Hsu, H., Huang, J., Shu, H. B., Baichwal, V., Goeddel, D. V. 1996. TNF-dependent recruitment of the protein kinase RIP to the TNF receptor-1 signalling complex. *Immunity*. 4:387-396.

Huang, D. C., Adams, J. M., Cory, S. 1998. The conserved N-terminal BH-4 domain of Bcl-2 homologues is essential for inhibition of apoptosis and interaction with ced-4. *EMBO J.* 17:1029-1039.

Huber, B. E., Austin, E. A., Richards, C. A., Davis, S. T., Good, S. S. 1994. Metabolism of 5'-Fluorocytosine to 5'Fluorouracil in human colorectal tumour cells transduced with the *cytosine deaminase* gene; significant antitumour effects when only a small percentage of tumour cells express cytosine deaminase. *Proc. Natl. Acad. Sci. USA*. 91:8302-8306.

Hwang, H. C., Smythe, W. R., Elshami, A. A., Kucharczuk, J. C. Amin, K. M., *et al.* 1995. Gene therapy using adenovirus carrying the Herpes Simplex *thymidine kinase* gene to treat *in vivo* models of human malignant mesothelioma and lung cancer. *Am. Jnl. Resp. Cell Mol. Biol*. 13:7-16.

Icely, P. L., Gros, P., Bergeron, J. J., Devault, A., Afar, D. E., Bell, J. C. 1991. TIK, a novel serine/throenine kinase, is recognised by antibodies directed against phosphotyrosine. *Jnl. Biol. Chem*. 266:16073-16077.

Inohara, N., Ding, L., Chen, S., Nunez, G. 1997. *Harakiri*, a novel regulator of cell death, encodes a protein that activates apoptosis and interacts selectively with the survival-promoting proteins Bcl-2 and Bcl-XL. *EMBO J.* 16:1686-1694.

Irmler, M., Hofmann, K., Vaux, D, Tschopp, D. 1997a. Direct physical interaction between *C. elegans* 'death protein' Ced-3 and Ced-4. *FEBS Lett*. 406:189-190.

Irmler, M., Thorne, M., Hahne, M. *et al.* 1997b. Inhibition of death receptor signals by cellular FLIP. *Nature*. 388:190-195.

Ivanova, L. and Schlesinger, M. J. 1993. Site-directed mutations in the Sindbis virus E2 glycoprotein identify palmitoylation sites and affect virus budding. *Jnl. Virol*. 67:2546-2551.

Jacobs, B. L. and Langland, J. O. 1996. When two strands are better than one: the mediators and modulators of the cellular responses to double-stranded RNA. *Virology*. 219:339-349.

Jacobson, M. D., Weil, M., Raff, M. C. 1997. Programmed cell death in animal develpoment. *Cell.* 88:347-354.

Jan, J. T. and Griffin, D. E. 1999. Induction of apoptosis by Sindbis virus occurs at cell entry and does require virus replication. *Jnl. Virol.* 73:10296-10302.

Jan, J. T., Chatterjee, S., Griffin, D. E. 2000. Sindbis virus entry into cells triggers apoptosis by activating sphingomylinase, leading to the release of ceremide. *Jnl. Virol.* 74:6425-6432.

Janeway, C. A., Travers, P., Walport, M., Capra, J. D. 1999. Immunobiology; the immune system in health and disease, 4th edition. P. Austin and E. Lawrence (*eds*). Elsevier Science Ltd/Garland Publishing.

Jia, W. W.-G., McDermott, M., Goldie, J., Cynader, M., Tan, J., Tufaro, F. 1994. Selective destruction of gliomas in immunocompetent rats by *thymidine kinase*-defective HSV-1. *Jnl. Natl. Can. Inst.* 86:1209-1215.

Jin, X., Nguyen, D., Zhang, W. W., Kyritsis, A. P., Roth, J. A. 1995. Cell cycle arrest and inhibition of tumour cell proliferation by the p16INK-4 gene mediated by an adenovirus vector. *Can. Res.* 55:3250-3253.

Joe, A. K., Foo, H. H., Kleeman, L. Levine, B. 1998. The transmembrane domains of Sindbis virus envelope glycoproteins induce cell death. *Jnl. Virol.* 72:3935-3943.

Johnson, R. E. and Peters, C. J. 1996. Alphaviruses. p843-898. *In*, Fields virology, 3rd edition. B. N. Fields, D. N. Knipe, P. M. Howley *et al* (*eds*). Lippincott-Raven publishers, Philadelphia.

Jurgensmeier, J. M., Xie, Z., Deveraux, Q., Ellerby, L., Bredesen, D., Reed, J. C. 1998. Bax directly induces release of cytochrome *c* from isolated mitochondria. *Proc. Natl. Acad. Sci. USA.* 95:4997-5002.

Kaariainen, L., Takkinen, K., Keranen, S., Soderlund, H. 1987. Replication of the genome of Alphaviruses. *Jnl. Cell Sci.* 7:231-250.

Kagawa, S., Gu, J., Swisher, S. G., Ji, L., Roth, J. A., Lai, D., Stephens, L. C., Fang, B. 2000a. Antitumour effect of adenovirus-mediated *Bax* gene transfer on *p53*-sensitive and p53-resistant cancer lines. *Can. Res.* 60:1157-1161.

Kagawa, S., Pearson, S. A., Ji, L., Xu, K., McDonnell, T. J., Swiaher, S. G., Roth, J. A., Fang, B. 2000b. A binary adenoviral vector system for expressing high levels of the proapoptotic gene *bax*. *Gene Ther*. 7:75-79.

Kantor, J., Irivne, K., Abrams, S., Kaufman, H., *et al*. 1992. Antitumour activity and immune responses induced by a recombinant carcinoembryonic antigen-vaccinia virus vaccine. *Jnl. Natl. Can. Inst*. 84:1084-1091.

Kaplan, J. M., St.George, J. A., Pennington, S. E., Keyes, L. D. *et al*. 1996. Humoural and cellular immune responses of non-human primates to long-term repeated lung exposure to Ad2-CFTR. *Gene Ther*. 3:117-127.

Kaplan, D. and Sieg, S. 1998. Role of the Fas/Fas ligand apoptotic pathway in human immunodeficiency virus type 1 disease. *Jnl. Virol*. 72:6279-6282.

Kastan, M. B., Zhan, Q., el-Diery, W. S., Carrier, F *et al*. 1992. A mammalian cell cycle checkpoint pathway utilising p53 and GADD45 is defective in ataxia-telangiectasia. *Cell*. 71:587-597.

Kaufmann, S. H., Desnoyers, S., Ottaviano, Y., Davidson, N. E., Poirier, G. G. 1993. Specific proteolytic cleavage of Poly(ADP-ribose) polymerase: An early marker of chemotherapy-induced apoptosis. *Can. Res*. 53:3976-3985.

Kelekar, A., Chang, B. S., Harlan, J. E., Fesik, S. W., Thompson, C. B. 1997. Bad is a BH3 domain-containing protein that forms an inactivating dimer with Bcl-XL. *Mol. Cell Biol*. 17:7040-7046.

Kelekar, A. and Thompson, C. B. 1998. Bcl-2-family proteins: the role of the BH3 domain in apoptosis. *Trends Cell Biol*. 8:324-330.

Kelly, W. R., Blakemore, W. F., Jagelman, S., Webb, H. E. 1982. Demyelination induced in mice by avirulent Semliki Forest virus. II. An ultrastructural study of focal demyelination in the brain. *Neuropathol. Appl. Neurobiol*. 8:43-53.

Keranen, S. and Kaariainen, L. 1975. Proteins synthesised by Semliki Forest virus and its 16 temperature sensitive mutants. *Jnl. Virol*. 16:388-396.

Khaled, A. R., Kim, K., Hofmeister, R., Muegge, K., Durum, S. K. 1999. Withdrawal of IL-7 induces Bax translocation from cytosol to mitochondria through a rise in intracellular. *Proc. Natl. Acad. Sci. USA*. 96:14476-14481.

Khuri, F. R., Nemunaitis, J., Ganly, I., *et al.* 2000. A controlled trial of intratumoural ONYX-015, a selectively-replicating adenovirus, in combination with cisplatin and 5'fluorouracil in patients with recurrent head and neck cancer. *Nature Med.* 6:879-885.

Kirn, D. *et al.* 1998. A Phase 11 trial of intratumoural injection with ONYX-015, in patients with recurrent, refractory head and neck cancer. *Proc. Am. Soc. Clin. Oncol.* (abstr) 17:391a.

Kischkel, F. C., Hellbardt, S., Behrman, I., Germer, M., Pawlita, M., Krammer, P. H., Peter, M. E. 1995. Cytotoxicity-dependent APO-1 (Fas/CD95)-associated proteins form a death-inducing signalling complex (DISC) with the receptor. *EMBO J.* 14:5579-5588.

Klein, D., and Gunzburg, W. H. 1997. Comparison of viral vectors: Implications for gene therapy. *BIOforum Int.* 2:104-109.

Kobayashi, T., Ruan, S., Clodi, K., Kliche, K. O., Shiku, H., Andreeff, M., Zhang, W. 1998. Overexpression of *Bax* gene sensitises K562 erythroleukemia cells to apoptosis induced by selective chemotherapeutic agents. *Oncogene.* 16:1587-1591.

Komatsu, K., Suzuki, S., Shimosegawa, T., Miyazaki, J. I., Toyota, T. 2000. Cre-lox-P-mediated *Bax* gene activation reduces growth rate and increases sensitivity to chemotherapeutic agents in human gastric cancer cells. *Can. Gene Ther.* 7:885-892.

Korff, T., and Augutin, H. G. 1998. Integration of endothelial cells in multicellular spheroids prevents apoptosis and induces differentiation. *Jnl. Cell Biol.* 143:1341-1352.

Korsmeyer, S. J., Shutter, J. R., Veis, D. J., Merry, D. E., Oltavi, Z. N. 1993. Bcl-2/Bax: a rheostat that regulates an anti-oxidant pathway and cell death. *Sem. Can. Biol.* 4:327-332.

Kothakota, S., Azuma, T., Reinhard, C., Klippel, A., Tang, J., Chu, K., McGarry, T. J., *et al.* 1997. Caspase-3-generated fragment of gelsolin: Effector of morphological change in apoptosis. *Science.* 278:294-298.

Kozopas, K. M., Yang, T., Buchan, H. L., Zhou, P., Craig, R. W. 1993. MCL-1, a gene expressed in programmed myeloid cell differentiation, has sequence similarity to Bcl-2. *Proc. Natl. Acad. Sci. USA.* 90:3516-3520.

Krajewski, S., Tanaka, S., Takayama, S., Schibler, M. J., Fenton, W., Reed, J. C. 1993. Investigation of the subcellular distribution of the bcl-2 oncoprotein: residence in the nuclear envelope, endoplasmic reticulum, and outer mitochondrial membranes. *Can. Res.* 53:4701-4714.

Kuerbitz, S. J., P., Walsh, W. V., Kastan, M. B. 1992. Wild-type *p53* is a cell cycle checkpoint determinant following irradiation. *Proc. Natl. Acad. Sci. USA*. 89:7491-7495.

Kumar, A., Haque, J., Lacoste, J., Hiscott, J., Williams, B. R. 1994. ds-RNA-dependent protein kinase activates transcription factor NF-kappa B by phosphorylating I kappa B. *Proc. Natl. Acad. Sci. USA*. 91:6288-6292.

Lachmi, B.-E. and Kaariainen, L. 1976. Sequential translation of nonstructural proteins in cells infected with Semliki Forest virus mutant. *Proc. Natl. Acad. Sci. USA*. 73:1936-1940.

Laird, A. D., Brow, P. I., Fausto, N. 1994. Inhibition of tumour growth in liver epithelial cells transfected with a transforming growth factor and antisense gene. *Can. Res*. 54:4224-4232.

Lane, D. P. 1998. Killing tumour cells with viruses- a question of specificity. *Nature Med*. 4:1012-1013.

LaStarza, M. W., Grakoui, A., Rice, C. M. 1994. Deletion and duplication mutations in the C-terminal nonconserved region of Sindbis virus *nsP3*: effects on phosphorylation and on virus replication in vertebrate and invertebrate cells. *Virology*. 202:224-232.

Latchman, D. S. 1994. Herpes Simplex virus vectors for gene therapy. *Mol. Biotech*. 2:179-195.

Laucet, F. R. *et al*. 1995. Mutations in Fas associated with human lymphoproliferative syndrome and autoimmunity. *Science*. 268:1347-1349.

Lazebnik, Y. A., Kaufmann, S. H., Desnoyers, S., Poirier, G. G., Earnshaw, W. C. 1994. Cleavage of poly(ADP-ribose) polymerase by a proteinase with properties like ICE. *Nature*. 371:346-347.

Ledley, F. D. 1994. Non-viral gene therapy. *Curr. Opin. Biotech*. 5:626-636.

Lee, J. M. *et al*. 1993. *p53* mutations increase resistance to ionising radiation. *Proc. Natl. Acad. Sci. USA*. 90:5742-5746.

Lee, S. B., and Esteban, M. 1994. The interferon-induced double-stranded RNA-activated protien kinase induces apoptosis. *Virology*. 199:491-496.

Lee, A., DeJong, G., Guo, J., Bu, X., Jia, W. W. 2000. Bax expressed from a herpes viral vector enhances the efficacy of N, N'-bis(2-hydroxyethyl)-N-nitrosourea treatment in a rat glioma model. *Can. Gene Ther*. 7:1113-1119.

Leech, S. H., Olie, R. A., Gautschi, O., Simoes-Wust, P., Tschopp, S., Haner, R., *et al.* 2000. Induction of apoptosis in lung-cancer cells follwoing bcl-xL antisense treatment. *Int. Jnl. Cancer.* 86:570-576.

LeGouill, C. and Diery, C. V. 1991. A rapid procedure for the screening of recombinant plasmids. *Nucl. Acids Res.* 19:6655.

Leitner, W. W., Ying, H., Driver, D. A., Dubensky, T. W., Restifo, N. P. 2000. Enhancement of tumour-specific immune response with plasmid DNA replicon vectors. *Can. Res.* 60:51-55.

Levine, A. J., Momand, J., Finlay, C. A. 1991. The *p53* tumour suppressor gene. *Nature.* 351:453-456.

Levine, B., Huang, Q., Isaacs, J. T., Reed, J. C., Griffin, D. E., Hardwick, J. M. 1993. Conversion of lytic to persistent alphavirus infection by the *bcl-2* cellular oncogene. *Nature.* 361:739-742.

Levine, B., Goldman, J. E., Jiang, H. H., Griffin, D. E., Hardwick, J. M. 1996. Bcl-2 protects mice against fatal alphavirus encephalitis. *Proc. Natl. Acad. Sci. USA.* 93:4810-4815.

Levine, A. J. 1997. *p53*, the cellular gatekeeper for growth and division. *Cell.* 88:323-331.

Levis, R., Weiss, B. G., Tsiang, M., Huang, H., Schlesinger, S. 1986. Deletion mapping of Sindbis virus DI RNAs derived from cDNAs defines the sequences assential for replication and packaging. *Cell.* 44:137-145.

Lewis, J., Oyler, G. A., Ueno, K., Fannjiang, Y. R., Chau, B. N., Korsmeyer, S. J., Zou, S., Hardwick, J. M. 1999. Inhibition of virus-induced neuronal apoptosis by Bax. *Nature Med.* 5:832-835.

Li, Q. T., Kay, M. A., Firegold, M., Stratford-Perricaudet, L. D., Woo, S. L. 1993. Assessment of recombinant adenoviral vectros for hepatic gene therapy. *Hum. Gene Ther.* 4:403-409.

Li, F., Srinivasan, A., Wang, Y., Armstrong, R. C., Tomaselli, K. J., Fritz, L. C. 1997a. Cell-specific induction of apoptosis by microinjection of cytochrome *c*. *Jnl. Biol. Chem.* 272:30299-30305.

Li, J.-H., Li, P., Klamut, H., Liu, F.-F. 1997b. Cytotoxic effects of Ad5CMV-p53 expression in two human nasopharyngeal carcinoma cell lines. *Clin. Can. Res.* 3:507-514.

Li, P., Nijhawan, D., Budihardjo, I., Srinivasula, S. M., Ahmad, M., Alnemri, E. S., Wang, X. 1997c. Cytochrome *c* and ATP-dependent formation of Apaf-1/caspase-9 complex initiates an apoptotic protease cascade. *Cell.* 91:479-489.

Li, H., Zhu, H., Xu, C. J., Yuan, J. 1998. Cleavage of BID by caspase 8 mediates the mitochondrial damage in the Fas pathway of apoptosis. *Cell*. 94:491-501.

Li, S. and Huang, L. 2000. Nonviral gene therapy: promises and challenges. *Gene Ther*. 7:31-34.

Liang, X. H., Kleeman, L. K., Jiang, H. H., Gordon, G., Goldman, J. E., Berry, G., Herman, B., Levine, B. 1998. Protection against fatal Sindbis virus encephalitis by beclin, a novel Bcl-2-interacting protein. *Jnl. Virol*. 72:8586-8596.

Lichenbeld, H., Harvard University, Boston, USA.

Lieubeau-Tillet, B., Rak, J., Jothy, S., Iliopoulos, O., Kaelin, W., Kerbel, R. S. 1998. von Hippel-Lindau gene-mediated growth suppression and induction of differentation in renal cell carcinoma cells grown as multicellular tumor spheroids. *Can. Res*. 58:4957-4962.

Liljestron, P., Karolinska Institute, Stockholm, Sweden.

Liljestrom, P., and Garoff, H. 1991. A new generation of animal cell expression vectors based on the Semliki Forest virus replicon. *BIO/TECHNOLOGY*. 9:1356-1361.

Liljeström, P. and Garoff, H. 1994. Expression of proteins using Semliki Forest virus vectors, p16.20.11-16.20.16. *In*, Current protocols in molecular biology, Vol 2F. M. Ausebel, R. Brent, R. E. Kingston, D. D. Moore, J. A. Smith, J. G. Seidman and K. Struhl (*eds*). Greene Publishing associates and Wiley Interscience, New York.

Liljestrom, P., Lusa, S., Huylebroeck, D., Garoff, H. 1991. *In vitro* mutagenesis of a full-lenght cDNA clone of Semliki Forest virus: the small 6,000-molecular-weight membrane protein modulates virus release. *Jnl. Virol*. 65:4107-4113.

Lin, K. I., Lee, S. H., Narayanan, R., Baraban, J. M., Hardwick, J. M., Ratan, R. R. 1995. Thiol agents and Bcl-2 identify an alphavirus-induced apoptotic pathway that requires activation of the transcription factor NF-kappa B. *Jnl. Cell Biol*. 131:1149-1161.

Lin, K. I., DiDonata, J. A., Hoffman, A., Hardwick, J. M., Ratan, R. R. 1998. Suppression of steady-state, but not stimulus-induced NF-kappa B activity inhibits alphavirus-induced apoptosis. *Jnl. Cell Biol*. 141:1479-1487.

Liu, T.-J., El-Nagger, A. K., McDonnell, T. J., Steck, K. D., Wang, M., Taylor, D. L., Clayman, G. L. 1995. Apoptosis induction mediated by wild-type *p53* adenoviral gene transfer in squamous cell carcinoma of the head and neck. *Can. Res*. 55:3117-3122.

Liu, X., Kim, C. N., Yang, J., Jemmerson, R., Wang, X. 1996. Induction of apoptotic program in cell-free extracts: requirement for dATP and cytochrome *c*. *Cell*. 86:147-157.

Liu, X., Zou, H., Slaughter, C., Wang, X. 1997. DFF, a heterodimeric protein that functions downstream of caspase-3 to trigger DNA fragmentation during apoptosis. *Cell*. 89:175-184.

Lobigs, M., and Garoff, H. 1990. Fusion function of the Semliki Forest virus spike is activated by proteolytic cleavage of the envelope glycoprotein p62. *Jnl. Virol*. 64:1233-1240.

Lowe, S. W., Ruley, H. E., Jacks, T., Housman, D. E. 1993. *p53*-dependent apoptosis modulates the cytotoxicity of anticancer agents. *Cell*. 74:957-967.

Lowndes, N. F. and Murguia, J. R. 2000. Sensing and responding to DNA damage. *Curr. Opin. Genet. Dev*. 10:17-25.

Ludwig, R. L., Bates, S., Vousden, K. H.,. 1996. Differential activation of target cellular promoters by *p53* mutants with impaired apoptotic function. *Mol. Cell Biol*. 16:4952-4960.

Lundstrom, K., Pralong, W., Martinou, J.-C. 1997. Anti-apoptotic effect of Bcl-2 overexpression in RIN cella infected with Semliki Forest virus. *Apoptosis*. 2:189-191.

Lusa, S., Garoff, H., Liljestrom, P. 1991. Fate of the 6K membrane protein of Semliki Forest virus during virus assembly. *Virology*. 185:843-846.

Mackey, T. J., Borkowski, A., Amin, P., Jacobs, S. C., Kyprianou, N. 1998. Bcl-2/Bax ratio as a predictive marker for therapeutic response to radiotherapy in patients with prostate cancer. *Urology*. 52:1085-1090.

Majno, G. and Joris, I. 1995. Apoptosis, oncosis and necrosis. *Am. Jnl. Pathol*. 146:3-15.

Manji, G. A., Hozak, R. R., LaCount, D. J., Friesen, P. D. 1997. Baculovirus inhibition of apoptosis functions at or upstream of the apoptotic suppressor *p35* to prevent programmed cell death. *Jnl. Virol*. 71:4509-4516.

Mann, S., University Toronto, Canada.

Markowitz, D., Goff, S., Bank, A. 1988. Construction and use of a safe and efficient amphotropic packaging cell line. *Virology*. 167:400-406.

Marquardt, M. T., Phalen, T., Kielian, M. 1993. Cholesterol is required in the exit pathway of Semliki Forest virus. *Jnl. Cell Biol.* 123:57-65.

Marshall, C. J. 1991. How does p21ras transform cells? *Trends Genet.* 7:91-95.

Marsters, S. A., Sheridan, J. P., Pitti, R. M., Brush, J., Goddard, A., Ashkenazi, A. 1998. Identification of a ligand for the death-domain-containing receptor Apo3. *Curr. Biol.* 8:525-528.

Mastrangeli, A., Harvey BG, Yao J, Wolff G, Kovesdi I, Crystal RG, Falck-Pedersen E. 1996. "Sero-switch" adenovirus-mediated *in vivo* gene transfer: circumvention of anti-adenovirus humoral immune defenses against repeat adenovirus vector administration by changing the adenovirus serotype. *Hum. Gene Ther.* 7:79-87.

Mastrangelo, A. J., Hardwick, J. M., Bex, F.,Betenbaugh, M. J. 2000. Part 1. Bcl-2 and Bcl-xL limit apoptosis upon infection with alphavirus vectors. *Biotechnol. Bioeng.* 67:544-554.

May, C., Gunther, R., McIvor, R. S. 1995. Protection of mice from lethal doses of methothrexate by transplantation with transgenic marrow expressing drug-resistant dihydrofolate-reductase activity. *Blood.* 86:2439-2448.

McDonnell, T. J., Troncoso, P., Brisbay, S. M., Logothetis, C., Chung, L. W., *et al.* 1992. Expression of the protooncogene bcl-2 in the prostate and its associateion with the emergence of androgen-independent prostate cancer. *Can. Res.* 52:6940-6944.

McIntosh, B. M., Brookworth, C and Kokernot, R. H. 1961. Semliki Forest virus from *Aedes* (Aedinorphus) *argenteopunctatus* (Theobald) collected in Japanese East Africa. *Trans. Royal Soc. Trop. Med. Hygiene.* 55:192-198.

Mehtali, M. 1996. *Cytotechnology.* 19:43-54.

Melancon, P. and Garoff, H. 1987. Processing of Semliki Forest virus structural polyprotein: role of the capsid protease. *Jnl. Virol.* 61:1301-1309.

Mesnil, M., Piccoli, C., Tiraby., G., Willecke, K., Yamasaki, H. 1996. Bystander killing of cancer cells by herpes simplex virus *thymidine kinase* gene is mediated by connexins. *Proc. Natl. Acad. Sci. USA.* 93:1831-1835.

Metiskko, K. and Garoff, H. 1990. Oligomers of the cytoplasmic domain of the p62/E2 membrane protein of Semliki Forest virus bind to the nucleocapsid *in vitro*. *Jnl. Virol.* 64:4678-4683.

Mickisch, G. H., Aksentijevich, I., Scholenlein, P. V., Goldstein, L. J., Galski, H., *et al.* 1992. Transplantation of bone marrow cells *in vivo* after retroviral transfer of the human MDR-1 gene. *Blood.* 79:1087-1093.

Miller, D. G., Adam, M. A., Miller, A. D. 1990. Gene transfer by retrovirus vectors occurs only in cells that are actively replicating at the time of infection. *Mol. Cell. Biol.* 10:4239-4242.

Minn, A. J., Boise, L. H., Thompson, C. B. 1996. Bcl-xS antagonises the protective effects of Bcl-xL. *Jnl. Biol. Chem.* 271:6306-6312.

Minna, J. D., Glatstein, E. J., Pass, H. I., Ihde, D. C. 1989. Cancer of the lung. p591-705. *In*, Cancer; principles and practice in oncology. V. T. DeVita, S. Hellman and S. A. Rosenberg. (*eds*). Lippincott, Philadelphia.

Miura, M., Zhu, H., Rotello, R., Hartweig, E. A., Yuan, J. 1993. Induction of apoptosis in fibroblasts by IL-1B-converting enzyme, a mammalian homologue of the *C. elegans* cell death gene Ced-3. *Cell.* 75:653-660.

Miyashita, T. and Reed, J. C. 1995. Tumour suppressor *p53* is a direct transcriptional activator of the human *bax* gene. *Cell.* 80:293-299.

Mokhtarian, F., Wesselingh, S., Choi, S., Maeda, A., Griffin, D. E., Sobel, R. A., Brob, D. 1996. Production and role of cytokines in the CNS of mice with acute viral encephalitis. *Jnl. Neuroimmunol.* 66:11-22.

Moll, R., Franke, W. W., Schiller, D. L., Geiger, B., Kepler, R. 1982. The catalog of human cytokeratins: patterns of expression in normal epithelia, tumours and cultured cells. *Cell.* 31:11-24.

Monaghan, P. E. and Samulski, R. J. 2000. AAV vectors; is clinical success on the horizon? *Gene Ther.* 7:24-30.

Moolten, F. L. 1994. Drug sensitivity ('suicide') genes for selective cancer chemotherapy. *Can. Gene Ther.* 1:279-287.

Moritz, T., MacKay, W., Glassner, B. J., Williams, D. A., Samson, L. 1995. Retrovirus-mediated expression of a DNA repair protein in bone marrow protects hematopoietic cells from nitrosourea-induced toxicity in vitro and in vivo. *Can. Res.* 55:2608-2614.

Morris-Downes, M. M., Phenix, K. V., Sheahan, B. J., Lilquist, S., Mooney, D. A., Liljestrom, P., Todd, D. and Atkins, G. J. 2000. Biosafety studies on SFV vector-based vaccines; persistence, distribution and pathological analysis in two animal systems. *Vaccine. In press.*

Mossman, S. P., Bex, F., Berglund, P., Arthos, J., O'Neill, L. S. P., Riley, D., Maul, D. H., *et al.* 1996. Protection against lethal simian immunodeficiency virus disease by a recombinant Semliki Forest virus gp160 subunit vaccine. *Jnl. Virol.* 70:1953-1960.

Mountain, A. 2000. Gene Therapy: the first decade. *TIBTECH.* 18:119-128.

Muchmore, S. W., Sattler, M., Liang, H., Meadows, R. P., Harlan, J. E., Yoon, H. S. *et al* 1996. X-ray and NMR structure of human Bcl-XL, and inhibitor of programmed cell death. *Nature.* 381:335-341.

Mueller-Kleiser, W. 1997. Three-dimensional cell cultures: from molecular mechanisms to clinical applications. *Am. Jnl. Phys.* 273:C1109-C1123.

Muers, E. F., Chong, K., Galabru, J., Thomas, N. S., Kerr, I. M., Williams, B. R., Hovanessian, A. G. 1990. Molecular cloning and characterisation of the human double-stranded RNA-activated protein kinase induced by interferon. *Cell.* 62:379-390.

Mukhopadhyay, T., Tainsky, M., Cavender, A. C., Roth, J. A. 1991. Specific inhibition of K-ras expression and tumorigenicity of lung cancer cells by antisense RNA. *Cancer Res.* 51:1744-1748.

Mundschau, L. J.,and Faller, D. V. 1995. Platelet-derived growth factor signal transduction through the interferon-inducible PKR immediate early gene transduction. *Jnl. Biol. Chem.* 270:3100-3106.

Muzio, M., Chinnayian, A. M., Kischkel, F. C., O'Rourke, K., Shevchenko, A., Ni, J., *et al.* 1996. FLICE, a novel FADD-homologous ICE/CED-3-like protease, is recruited to the CD95 (Fas/APO-1) death-inducing signalling complex. *Cell.* 85:817-827.

Muzio, M., Stockwell, B. R., Stennicke, H. R., Salvesen, G. S., Dixit, V. M. 1998. An induced proximity model for caspase-8 activation. *Jnl. Biol. Chem.* 273:2926-2730.

Nagata, S. and Goldstein, P. 1995. The Fas death factor. *Science.* 267:1449-1455.

Nagata, S. 1997. Apoptosis by death factor. *Cell.* 88:355-365.

Nava, V. E., Rosen, A., Veliuona, M. A., Clem, R. J., Levine, B., Hardwick, J. M. 1998. Sindbis virus induces apoptosis through a caspase-dependent, CrmA-sensitive pathway. *Jnl. Virol.* 72:452-459.

Navone, N. M., Tronscoso, P., Pisters, L. L., Goodrow, T. L., Palmer, J. L., Nichols, W. W., *et al.* 1993. p53 protein accumulation and gene mutation in the progression of human prostate carcinoma. *Jnl. Natl. Cancer Inst.* 85:1657-1669.

Neamati, N., Fernandez, A., Wright, S., Keifer, J., McConkey, D. J. 1995. Degradation of Lamin B1 preceded oligonucleosomal DNA fragmentation in apoptotic thymocytes and isolated thymocyte nuclei. *Jnl. Immunol.* 154:3788-3795.

Nerrouche, Y., Negrier, S., Bain, C., Combaret, V., Mercateelo, A., *et al.* 1995. Clinical application of retoviral gene transfer in oncology; resulst of a french study with tumour infiltrating lymphocytes transduced with the gene for neomycin resistance. *Jnl. Clin. Oncol.* 13:410-418.

Nesterova, M.and Cho-Chung, Y. S. 1995. A single-injection protein kinase-A directed antisense treatment to inhibit tumour growth. *Nature Med.* 1:538-533.

Nevins, J. R. 1992. E2F: a link between the Rb tumor suppressor protein and viral oncoproteins. *Science.* 258:424-429.

Nguyen, J. T., Wu, P., Clouse, M. E., Hlatky, L., Terwilliger, E. F. 1998. Adeno-associated virus-mediated delivery of antiangiogenic factors as an antitumour strategy. *Can. Res.* 58:5673-5677.

North, S. and Hainut, P. 2000. *p53* and cell cycle control: a finger in every pie. *Pathol Biol.* 48:255-270.

Nunez, G., London, L., Hockenbery, D., Alexander, M., McKearn, J., Korsmeyer, S. J. 1990. Deregulated Bcl-2 gene expression selectively prolongs survival of growth factor-deprived hemopoietic cell lines. *Jnl. Immunol.* 144:3602-3604.

O'Connor, L., Strasser, A., O'Reilly, L. A., Hausmann, G., Adams, J. M., Cory, S., Huang, D. C. 1998. Bim: a novel member of the Bcl-2 family that promotes apoptosis. *EMBO J.* 17:384-395.

O'Malley, B. W., Chen, S.-H., Schwartz, M. R., Woo, S. L. C. 1995. Adenovirus-mediated gene therapy for human head and neck squamous cell cancer in a nude mouse model. *Can. Res.* 55:1080-1085.

O'Reilly, M. S., Holmgreen, L., Shing, Y., Chen, C., Rosenthal, R. A., Moses, M., Lane, W. S., Cao, Y., Sage, E. H., Folkman, J. 1994. Angiostatin: a novel angiogenesis inhibitor that mediates the suppression of metastases by a Lewis lung carcinoma. *Cell.* 79:315-328.

O'Reilly, M. S., Boehm, M., Shing, Y., Naomi, F., Vasios, G., Lane, W. S., Flynn, E., Birkgead, J. R., Olsen, B. R., Folkman, J. 1997. Endostatin: an endogenous inhibitor of angiogenesis and tumour growth. *Cell*. 88:277-285.

Obeid, L., Linardic, C. M., Karolak, L. A., Hannun, Y. A. 1993. Programmed cell death induced by ceremide. *Science*. 259:1769-1772.

Ohno, K., Sawai, K., Iijima, Y., Levin, B., Meruelo, D. 1997. Cell-specific targeting of sindbis virus vectors displaying IgG-binding domains of Protein A. *Nature Biotech.* 15:763-767.

Ohsaki, Y., Toyoshima, E., Fujiuchi, S., Matsui, H., Hirata, S., Miyokawa, N., Kubo, Y., Kikuchi, K. 1996. Bcl-2 and p53 protein expression in non-small cell lung cancers: correlation with survival time. *Clin. Can. Res*. 2:915-920.

Oldstone, M. B. A., Tishon, A., Dutko, F. J., Kennedy, S. I. T., Holland, J. J., Lampery, P. W. 1980. Does the major hiostocompatibility complex serve as a specific receptor for Semliki Forest virus? *Jnl. Virol*. 34:256-265.

Oliver, K. R., Scallan, M. F., Dyson, H., Fazakerley, J. K. 1997. Susceptibility to a neurotropic virus and its changing distribution in the developing brain is a function of CNS maturity. *Jnl. Neurovirol.* 3:38-48.

Oltavai, Z. N., Milliman, C. L., Korsmeyer, S. J. 1993. Bcl-2 heterodimerizes *in vivo* with a conserved homolog, Bax, that accelerates programmed cell death. *Cell.* 74:609-619.

Osaki, T., Tanio, Y., Tachibana, I., Hosoe, S., Kumagai, T., Kawase, I., *et al.* 1994. Gene therapy for carcinoembryonic antigen-producing human lung cancer cells by cell type-specific expression of Herpes Simplex virus *thymidine kinase* gene. *Can. Res*. 54:5258-5261.

Owaga, N. *et al.* 1997. Novel combination for human colon cancer with Adenovirus-mediated wild-type *p53* gene transfer and DNA-damaging chemotherapeutic agents. *Int. Jnl. Cancer*. 73:367-370.

Owen, K. E., Kuhn, R. J. 1996. Identification of a region in the Sindbis virus nucleocapsid protein that is involved in specificity of RNA encapsidation. *Jnl. Virol*. 70:2757-2763.

Ozen, M. and Pathak, S. 2000. Genetic alterations in human prostate cancer: a review of current literature. *Antican. Res*. 20:1905-1912.

Pahl, H. L. and Baeuerle, P. A. 1997. The ER-overload response: activation of NF-kappa B. *Trends Biochem. Sci.* 22:63-67.

Palese, P. 1998. RNA virus vectors: Where are we and where do we need to go? *Proc. Natl. Acad. Sci. USA*. 95:12750-12752.

Palmero, I., Pantojia, C., Serrano, M. 1998. p19ARF links the tumour suppressor *p53* to *Ras*. *Nature*. 395:125-126.

Pan, G., Ni, J., Wei, Y. F., Yu, G., Dixit, V. M. 1997. An antagonist decoy receptor and the death domain-containing receptor for TRAIL. *Science*. 277:815-818.

Pan, H., Yin, C., Van Dyke, T. 1997. Apoptosis and cancer mechanisms. *Cancer Surv*. 29:305-327.

Pan, G., Ni, J., Yu, G., Wei, Y. F. and Dixit, V. M. 1998. TRUNDD, a new member of the TRAIL receptor family that antagonizes TRAIL signalling. *FEBS Lett*. 424:41-45.

Parker, S. L., Tong, T., Bolden, S., Wingo, P. A. 1997. Cancer statistics. CA *Cancer J. Clin.* 47:5-27.

Pawlowski, J., and Kraft, A. S. 2000. Bax-induced apoptotic cell death. *Proc. Natl. Acad. Sci. USA*. 97:529-531.

Peranen, J., Takkinen, K., Kalkkinen, N., Kaariainen, L. 1988. Semliki Forest virus-specific non-structural protein nsP3 is a phosphoprotein. *Jnl. Gen. Virol*. 69:2165-2178.

Peranen, J. R., M., Liljestrom, P. and Kaariainen. L. 1990. Neclear localisation of the Semliki Forest virus-specific non-structural protein nsP2. *Jnl. Virol*. 64:1888-1896.

Peranen, J. 1991. Localisation and phosphorylation of Semliki Forest virus non-structural protein nsP3 expressed in COS cells from a cloned cDNA. *Jnl. Gen. Virol*. 72:195-199.

Peranen, J. and Kaariainen, L. 1991. Biogenesis of type 1 cytopathic vacuoles in Semliki Forest virus-infected BHK cells. *Jnl. Virol*. 65:1623-1627.

Peranen, J., Laakkonen, P., Hyvonen, M., Kaariainen, L. 1995. The alphavirus replicase protein nsP1 is membrane associated and has affinity to endocytic organelles. *Virology*. 208:610-620.

Perlman, H., Zhang, X., Chen, M. W., Walsh, K., Buttyan, R. 1999. An elevated Bax/Bcl-2 ratio corresponds with the onset of prostate epithelial cell apoptosis. *Cell Death Differ*. 6:48-54.

Pezzella, F., Turley, H., Kuzu, I., Tungekar, M. F., Dunnill, M. S., Pierce, C. B., Harris, A., Gatter, K. C., Mason, D. Y. 1993. Bcl-2 protein in non-small cell lung cancer. *N. Engl. Jnl. Med.* 329:690-694.

Phenix, K. V., McKenna, B. M., Fitzpatrick, R., Vaughan, L., Atkins, G. J., Liljestrom, P., Todd, D. 1999. Evaluation of the Semliki Forest virus expression system as a novel approach for antigen delivery and expression in fish. *Marine Micro. in press.*

Piche, A., Grim, J., Rancourt, C., Gomez-Navarro, J., Reed, J. C., Curiel, D. T. 1998. Modulation of Bcl-2 protein levels by an intracellular anti-Bcl-2 single-chain antibody increases drug-induced cytotoxicity in the breast cancer cell line MCF-7. *Can. Res.* 58:2134-2292.

Plautz, G. E., Yang, Z. Y., Wu, B. Y., Gao, X., Huang, L., Nabel, G. J. 1993. Immunotherapy of malignancy by *in vivo* gene transfer into tumours. *Proc. Natl. Acad. Sci. USA.* 90:4645-4649.

Polo, J. M., Belli, B. A., Driver, D. A., Frolov, I., Sherrill, S., Harihan, M. J., *et al.* 1999. Stable alphavirus packaging cell lines for Sindbis virus- and Semiliki Forest virus-derived vectors. *Proc. Natl. Acad. Sci. USA.* 96:4598-4603.

Polyak, K., Xia, Y., Zweier, J. L., Kinzler, K. W., Vogelstein, B. 1997. A model for *p53*-induced apoptosis. *Nature.* 389:300-305.

Prasher, D. C., Eckenrode, V. K., Ward, W. W., Prendergast, F. G., Cormier, M. J. 1992. Primary structure of the Aequorea victoria green-fluorescent protein. *Gene.* 111:229-233.

Pritchard, H. and Micklem, H. S. 1974. The nude (*nu/nu*) mouse as a model of thymus and T-lymphocyte deficiency. p127-139. *In*, Proceedings of the first workshop on nude mice. J. Rygaard and C. O. Povlsen (*eds*). Stuttgardt: Gustav Fisher Verlay.

Prives, C. 1998. Signalling to *p53*: breaking the mdm-2-p53 circuit. *Cell.* 95:5-8.

Pugachev, K. V., Mason, P. W., Shope, R. E., Frey, T. K. 1995. Double-stranded Sindbis virus recombinants expressing immunogenic proteins of Japanese Encephalitis virus induce significant protection in mice against lethal JEV infection. *Virology.* 212:587-594.

Pushko, P., Parker, M., Ludwig, G. V., Davis, N. L., Johnston, R. E., Smith, J. F. 1997. Replicon-helper systems from attenuated Venezuelan equine encephalitis virus-Expression of heterologous genes *in vitro* and immunisation against heterologous pathogens *in vivo*. *Virology.* 239:389-401.

Qin, H., Srinivasula, S. M., Wu, G., Fernandes-Alnemri, T., Alnemri, E. S., Shi, Y. 1999. Structural basis of procaspase-9 recruitment by the apoptotic protease-activating factor 1. *Nature.* 399:549-557.

Quazilbash, M. H., Xiao, X., Seth, P., Cowan, K. H., Walsh, C. E. 1997. Cancer gene therapy using a novel adeno-associated virus vector expressing human wild-type *p53. Gene Ther.* 4:675-682.

Raju, R. and Huang, H. V. 1991. Analysis of Sindbis virus promoter recognition *in vivo*, using novel vectors with two subgenomic mRNA promoters. *Jnl. Virol.* 65:2501-2510.

Raju, R., Subramanian, S. V., Hajjou, M. 1995. Genesis of Sindbis virus by *in vivo* recombination of non-replicative RNA precursors. *Jnl. Virol.* 69:7391-7401.

Rampino, N., Yamamoto, H., Ionov, Y., Li, Y., Sawai, H., Reed, J. C., Perucho, M. 1997. Somatic frameshift mutations in the *Bax* gene in colon cancers of the microsatellite mutator phenotype. *Science.* 275:967-969.

Rao, L., Debbas, M., Sabbatini, P., Hockenbery, D., Korsmeyer, S., White, E. 1992. The adenovirus E1A proteins induce apoptosis, which is inhibited by the E1B 19-kDa and Bcl-2 proteins. *Proc. Natl. Acad. Sci. USA.* 89:7742-7746.

Ray, C. A., Black, R. A., Kronheim, S. R., Greenstreet, T. A., Sleath, P. R., Salvesen, G. S., Pickup, D. J. 1992. Viral inhibition of inflammation: cowpox virus encodes an inhibitor of the interleukin-1 beta converting enzyme. *Cell.* 69:597-604.

Ray, R. B., Meyer, K., Ray, R. 1996. Suppression of apoptotic cell death by Hepatitis C virus core protein. *Virology.* 226:176-182.

Razvi, E. S., and Welsh, R. M. Apoptosis in viral infections. *Adv. Virus Res.* 45:1-60.

Reed, J. C. 1997a. Double identity for proteins of the BCL-2 family. *Nature.* 387:773-778.

Reed, J. C. 1997b. Bcl-2 family proteins: strategies for overcoming chemoresistance in cancer. *Adv. Pharmacol.* 41:501-532.

Reed, J. C. 1997c. Bcl-2 family proteins: Regulators of apoptosis and chemoresistance in hematologic malignancies. *Sem. Hematol.* 34:9-19.

Renkonen, O., Kaariainen, L., Simons, K., Bahmbeg, C. G. 1971. The lipid class composition of Semliki Forest virus and plasma membranes of the host cells. *Virology.* 46:318-326.

Rice, C. M., Levis, R. Strauss, J. H., Huang, H. V. 1987. Production of infectious RNA transcripts from Sindbis virus cDNA clones: Mapping of lethal mutations, rescue of a temperature-sensitive marker, and *in vitro* mutagenesis to generate defined mutants. *Jnl. Virol.* 61:3809-3819.

Rizk, N. P., Chang, H. Y., El Kouri, C., Seth, P., Kaiser, L. R., Albelda, S. M. Amin, K. M. 1999. The evaluation of adenoviral *p53*-mediated bystander effect in gene therapy of cancer. *Can. Gene Ther.* 6:291-301.

Roehrborn, C. G. Oncogenes and growth factors in prostate cancer. p97-122. *In*, Mechanisms and progression to hormone-independent growth of breast and prostatic cancer. P. M. M. J. Berns, J. C. Ronijn, J. C. and F. A. Schoder. (*eds*). Parthenon publishing group, Park Ridge, NJ.

Rosenfeld, M. A., Siegfried, W., Yoshimura, K., Yoneyama, K., Fukayama, M., Stier, L. E., *et al.* 1991. Adenovirus-mediated transfer of a recombinant α-antitrypsin gene to the lung epithelium *in vivo*. *Science*. 252:430-434.

Roth, J. A., Nguyen, D., Lawrence, D. D., Kemp, B. L., Carrassco, C. H., Ferson, D. Z., *et al.* 1996. Retrovirus-mediated wild-type *p53* gene transfer to tumors of patients with lung cancer. *Nature Med.* 2:985-991.

Roth, J. A. and Cristiano, R. J. 1997. Gene therapy for cancer: what have we done and where are we going? *Jnl. Natl. Cancer Inst.* 89:21-39.

Rothe, M., Wong, S. C., Henzel, W. J., Goeddel, D. V. 1994. A novel family of putative signal transducers associated with the cytoplasmic domain of the 75kDa tumour necrosis factor receptor. *Cell.* 78:681-692.

Roy, S., Katze, M. G., Parkin, N. T., Edery, I., Hovanessian, A. G., Sonenberg, N. 1990. Control of the interferon-induced 68-kilodalton protein kinase by the HIV-1 *tat* gene product. *Science*. 247:1216-1219.

Sakakura, C., Hagiwara, A., Tsujimoto, H. *et al.* 1995. Inhibition of colon cancer cell proliferation by antisense olignucleotide targeting the messenger RNA of the Ki-ras gene. *Anti-Can. Drugs*. 6:553-561.

Sakakura, C., Sweeney, F. A., Shirahama, T., Igarashi, Y., Hakomori, S., Nakatani, H., *et al.* 1996. Overexpression of bax sensitises human breast cancer MCF-7 cells to radiation-induced apoptosis. *Int. Jnl. Cancer*. 67:101-105.

Salminen, A., Wahlberg, J. M., Lobigs, M., Liljestrom, P., Garoff, H. 1992. Membrane fusion process of Semliki Forest virus 11: Cleavage dependant reorganization of the spike protein complex controls virus entry. *Jnl. Cell. Biol.* 116:349-357.

Samuel, C. E. 1991. Antiviral actions of interferon. Interferon-regulated cellular proteins and their surprisingly selective antiviral activities. *Virology*. 183:1-11.

Samulski, R. J., Zhu, X., Xiao, X., Brook, J. D., Housman, D. E., Epstein, N., Hunter, L. A. 1991. Targeted integration of adeno-associated virus (AAV) into human chromosome 19. *EMBO J.* 10:3941-3950.

Santagati, M. G., Maatta, L. A., Itaranta, P. V., Salmi, A. A., Hinkkanen, A. E. 1995. The Semliki Forest virus *E2* gene as a virulence determinant. *Jnl. Gen. Virol.* 76:47-52.

Sariola, M., Saraste, J.,Kuismanen, E. 1995. Communication of post-Golgi elements with early endocytic pathway: regulation of endoproteolytic cleavage of Semliki Forest virus p62 precursor. *Jnl. Cell Sci.* 108:2465-2475.

Sattler, M., Liang, H., Nettesheim, D., Meadows, R. P., Harlan, J. E., Eberstadt, M., *et al.* 1997. Structure of Bcl-xL-Bak peptide complex: recognition between regulators of apoptosis. *Science*. 275:983-986.

Sawicki, C. L. and Gamatos, P. J. 1976. Replication of Semliki Forest virus: polyadenylation in plus-strnad RNA and polyuridylate in minus-strand RNA. *Jnl. Virol.* 20:446-464.

Sawicki, D. L., Kaariainen, L., Lambek, C., Gomatos, P. J. 1978. Mechanism for control of synthesis of Semliki Forest virus 26S and 42S RNA. *Jnl. Virol.* 25:19-27.

Sawicki, D. L. and Sawicki, S. G. 1985. Functional analysis of the A complmentation group, mutant of Sindbis large HR virus. *Virology*. 144:20-34.

Scallan, M. F., Allsopp, T. E., Fazakerley, J. K. 1997. Bcl-2 acts early to restrict Semliki Forest virus replication and delays virus-induced programmed cell death. *Jnl. Virol.* 71:1583-1590.

Schiedner, G. *et al.* 1998. Genomic DNA transfer with high capacity adenovirus vector in improved *in vivo* gene expression and decreased toxicity. *Nat. Genet.* 18:180-183.

Schlesinger, S. and Schlesinger, M. J. 1996. Togaviridae: the viruses and their replication. p825-868. *In*, Fields virology 3rd edition. B. N. Fields, D. M. Knipe, P. M. Howley *et al* (*eds*). Lippincott-Raven publishers, Philadelphia.

Schuler, M., Rochlitz, C., Horowitz, J. A., Schlegel, J., Peruchoud, A. P., Kommoss, F., *et al.* 1998. A phase 1 study of adenovirus-mediated wild-type *p53* gene transfer in patients with advanced non-small-cell lung cancer. *Hum. Gene Ther.* 9:2075-2082.

Sentman, C. L., Shutter, J. R., Hockenbery, D., Kanagawa, O., Korsmeyer, S. J. 1991. Bcl-2 inhibits multiple forms of apoptosis but not negative selection in thymocytes. *Cell.* 67:879-888.

Sharkey, F. E. and Fogh, J. 1984. Considerations in the use of nude mice for cancer research. *Can. Meta. Rev.* 3:341-360.

Sheahan, B. J. Veterinary Pathology Dept., University College, Ballsbridge, Dublin 4, Ireland.

Shimizu, S., Eguchi, Y., Kosaka, H., Kamiike, W., Matsuda, H., Tsujimoto, Y. 1995. Prevention of hypoxia-induced cell death by Bcl-2 and Bcl-xL. *Nature.* 374:811-813.

Shina, A. A., Blackard, C. E, Seal, U. S. 1977. A critical analysis of tumour morphology and hormone treatments in the untreated and estrogen-treated responsive and refractory human prostatic carcinoma. *Cancer* (Phila.). 40:2836-2850.

Shisler, J., Yang, C., Walter, B., Ware, C. F., Gooding, L. R. 1997. The adenovirus E3-10.4K/14.5K complex mediates loss of cell surface Fas (CD95) and resistance to Fas-induced apoptosis. *Jnl. Virol.* 71:8299-8306.

Shweiki, D., Neeman, M., Itin, A., Keshet, E. 1995. Induction of vascular endothelial growth factor expression by hypoxia and glucose deficiency in multicell spheroids: Implications for tumor angiogenesis. *Proc. Natl. Acad. Sci. USA.* 92:768-772.

Simons, K. and Garoff, H. 1980. The budding mechanisms of enveloped animal viruses. *Jnl. Gen. Virol.* 50:1-21.

Singh, I. and Helienius, A. 1992. Role of ribosomes in Semliki Forest virus nucleocapsid uncoating. *Jnl. Virol.* 66:7049-7058.

Sjoberg, E. M., Suomalainen, M., Garoff, H. 1994. A significantly improved Semliki Forest virus expression system based on translational enhancer segments from the viral capsid gene. *Bio/Technology.* 12:1127-1131.

Sjoberg, E. M. and Garoff, H. 1996. The translation-enhancing region of the Semliki Forest virus subgenome is only functional in the virus-infected cell. *Jnl. Gen. Virol.* 77:1323-1327.

Skehan, P., Storeng, R., Scudiero, D., Monks, A., McMahon, J., Vistica, D., Warren, J. T., Bokesch, H., Kenney, S., Boyd, M. R. 1990. New colorimetric cytotoxicity assay for anticancer-drug screening. *Jnl. Natl. Can. Inst.* 82:1107-1112.

Skoging, U., Vihinen, M., Nilsson, L., Liljestrom, P. 1996. Aromatic interactions define the binding of alphavirus spike to its nucleocapsid. *Structure*. 4:519-529.

Slebos, R. J., Lee, M. H., Plunkett, B. S., Kessis, T. D., Williams, B. O., Jacks, T., *et al.* 1994. *p53*-dependent G1 arrest invloves pRB-related proteins and is disrupted by the human papillomavirus 16 E7 oncoprotein. *Proc. Natl. Acad. Sci. USA*. 91:5320-5324.

Smeekens, S. P. 1993. Processing of portein precursors by a novel family of subtilisin-related mammalian endoproteases. *Bio/Technology*. 11:182-186.

Smerdou, C., and Liljestrom, P. 1999. Two-helper RNA system for production of recombinant Semliki Forest virus particles. *Jnl. Virol*. 73:1092-1098.

Smithburn, K. C. and Haddow, A. J. 1944. Semliki Forest virus. I. Isolation and pathogenic properties. *Jnl. Immunol*. 49:141-157.

Smyth, J. M. B., Sheahan, B. J., Atkins, G. J. 1990. Multiplication of virulent and demyelinating Semliki Forest virus in the mouse central nervous system: consequences in Balb/C and SJL mice. *Jnl. Gen. Virol*. 71:2575-2583.

Sobol, R. and Scanlon, K. J. 1995. Clinical protocol lists. *Can. Gene Ther*. 2:225-234.

Soderland, H., von Bonsdorff, C.-H., Ulmanen, I. 1979. Comparison of the structural properties of Sindbis and Semliki Forest virus nucleocapsids. *Jnl. Gen. Virol*. 45:15-26.

Soilu-Hanninen, M., Eralinna, J.-P., Hukkanen, V., Roytta, M., Salmi, A. A., Salonen, R. 1994. Semliki Forest virus infects mouse brain endothelial cells and causes blood-brain barrier damage. *Jnl. Virol*. 68:6291-6298.

Song, Q., Lees-Miller, S. P., Kumar, S., Zhang, Z., Chan, D. W., Smith, G. C., Jackson, S. P., *et al.* 1996. DNA-dependent protein kinase catalytic subunit: a target for an ICE-like protease in apoptosis. *EMBO J.* 15:3238-3246.

Song, Z. and Steller, H. 1999. Death by design: mechanism and control of apoptosis. *TIBS*. 24:49-52.

Sorrentino, B. P., Brandt, S. J., Bodine, D., Gottesman, M., pastar, I., Cline, A., *et al.* 1992. Selection of drug-resistant bone marrow cells *in vivo* after retoviral transfer of the human MDR-1 gene. *Science*. 257:98-103.

Srivastava, R. K., Srivastava, A. R., Korsmeyer, S. J., Nesterova, M., *et al.* 1998. Involvement of microtubules in the regulation of Bcl-2 phosphorylation and apoptosis through cyclic AMP-dependent protein kinase. *Mol. Cell Biol.* 18:3509-3517.

Stein, C. S., Pemberton, J. L., van Rooijen, N., Davidson, B. L. 1998. Effects of macrophage depletion and anti-CD40 ligand on transgene expression and redosing with recombinant adenovirus. *Gene Ther.* 5:431-439.

Strasser, A., Harris, A. W., Jacks, T., Cory, S. 1994. DNA damage can induce apoptosis in proliferating cells via *p53*-independent mechanisms inhibitable by Bcl-2. *Cell.* 79:329-339.

Strauss, E., Rice, C. M., Strauss, J. H. 1983. Sequence coding for the alphavirus nonstructural proteins is interrupted by an opal termination codon. *Proc. Natl. Acad. Sci. USA.* 80:5271-5275.

Strauss, J. H. and Strauss, E. G. 1994. The Alphaviruses: gene expression, replication and evolution. *Microbiol. Rev.* 58:491-562.

Subak-Sharpe, I., Dyson, H., Fazakerley, J. F. 1993. *In vivo* depletion of CD8+ T cells prevents lesions of demyelination in Semliki Forest virus infection. *Jnl. Virol.* 67:7629-7633.

Sumantran, V. N., Ealovega, M. W., Nunez, G., Clarke, M. F., Wicha, M. S. 1995. Overexpression of Bcl-xS sensitises MCF-7 cells to chemotherapy-induced apoptosis. *Can. Res.* 55:2507-2510.

Suomalainen, M. P., Liljestrom, P., Garoff, H. 1992. Spkie protein- nucleocapsid interactions drive the budding of alphaviruses. *Jnl. Virol.* 66:4737-4747.

Susin, S. A., Lorenzo, H. K., Zamzami, N., Marzo, I., Snow, B. E., Brothers, G. M., *et al.* 1999. Molecular characterisation of mitochondrial apoptosis-inducing factor. *Nature.* 397:441-445.

Sutherland, R. M., McCredie, J. A.,Inch, W. R. 1971. Growth of multicell spheroids in tissue culture as a model of nodular carcinomas. *Jnl. Natl. Can. Inst.* 46:113-120.

Sutherland, R. M., Sordat, B., Bamat, J., Gabbert, H., Bourrat, B., Mueller-Kleiser, W. 1986. Oxygenation and differentiation in multicelular spheroids of human colon carcinoma. *Can. Res.* 46:5320-5329.

Sutherland, R. M. 1988. Cell and environment interactions in tumor microregions: The multicell spheroid model. *Science.* 240:177-184.

Swisher, S. G., Roth, J. A., Nemunaitis, J., Lawerence, D. D., Kemp, B. L., Carrasco, C. H., *et al.* 1999. Adenovirus-mediated *p53* gene transfer in advanced non-small cell lung cancer. *Jnl. Natl. Can. Inst.* 91:763-771.

Symonds, H., Krall, L., Remington, L., Saenz-Robles, M., Lowe, S., Jacks, T.,Van Dyke, T. 1994. *p53*-dependent apoptosis suppresses tumour growth and progression *in vivo*. *Cell.* 78:703-711.

Tai, Y. T., Strobel, T., Kufe, D., Cannistra, S. A. 1999. *In vivo* cytotoxicity of overian cancer cells through tumour-selective expression of the BAX gene. *Can. Res.* 59:2121-2126.

Takahashi, T., Nau, M. M., Chiba, I., Birrer, M. J., Rosenberg, R. K., Vinocour, M., Levitt, M., Pass, H., Gazdar, A., Minna, J. D. 1989. *p53*: A frequent target for genetic abnormalities in lung acncer. *Science*. 246:491-494.

Takkinen, K., Peranen, J., Keranen, S., Soderland, H., Kaariainen, L. 1990. The Semliki Forest virus-specific non-structural protein nsP4 is an autoproteinase. *Eur. Jnl. Biochem*. 189:33-38.

Takkinen, K., Peranen, J., Kaariainen, L. 1991. Proteolytic processing of Semliki Forest virus-specific non-structural polyprotein. *Jnl. Gen. Virol*. 72:1627-1633.

Tan, X., Martin, S. J., Green, D. R., Wang, J. Y. J. 1997. Degradation of retinoblastoma protein in tumor necrosis factor- and CD95-induced cell death. *Jnl. Biol. Chem*. 272:9613-9616.

Tartaglia, L. A. and Goeddel, D. V. 1992. Two TNF receptors. *Immunol. Today*. 13:151-153.

Tartaglia, L. A., Ayres, T. M., Wong, G. H., Goeddel, D. V. 1993. A novel domain within the 55kd TNF receptor signals cell death. *Cell*. 74:845-853.

Teodoro, J. G., Shore, G. C., Branton, P. E. 1995. Adenovirus E1A proteins induce apoptosis by both *p53*-dependent and *p53*-independent mechanisms. *Oncology*. 11:467-474.

Teodoro, J. G. and Branton, P. E. 1997. Regulation of apoptosis by viral gene products. *Jnl. Virol*. 71:1739-1746.

Thierry, A. R., Rabinovich, P., Peng, B., Mahan, L. C., Bryant, J. L., Gallo, R. C. 1997. Characterization of liposome-mediated gene delivery: expression, stability and pharmacokinetics of plasmid DNA. *Gene Ther.* 4:226-237.

Thompson, C. B. 1995. Apoptosis in the pathogenesis and treatment of disease. *Science*. 267:1456-1462.

Thornberry, N. A. and Laznebnik, Y. 1998. Caspases: enemies within. *Science*. 281:1312-1317.

Todryk, S. and Lemoine, N. 1998. Can immunotherapy by gene transfer tip the balance against colorectal cancer? *Gut*. 43:445-449.

Trono, D. 2000. Lentiviral vectors: turning a deadly foe into a therapeutic agent. *Gene Ther*. 7:20-23.

Trump, T. F., Berezesky, I. K., Chang, S. H. Phelps, P. C. 1997. The pathways of cell death: oncosis, apoptosis, and necrosis. *Toxicol. Pathol*. 25:82-88.

Tschopp, J., Thome, M., Hofmann, K., Meinl, E. 1998. The fight of viruses against apoptosis. *Curr. Opin. Genet. Dev*. 8:82-87.

Tucker, P. C., Griffin, D. E., Choi, S., Biu, N., Wesselingh, S. 1996. Inhibition of nitric oxide synthesis increases mortality in Sindbis virus encephalitis. *Jnl. Virol*. 70:3972-3977.

Tuittila, M. Y., Santagati, M. G., Roytta, M., Maatta, J. A, Hinkkanen, A. E. 2000. Prototype Semliki Forest virus *nsP3/nsP4* gene region expressed by avirulent SFVA7(74) confers lethal neurovirulence. *Manuscipt*.

Turell, M. J. 1988. Horizontal and vertical transmission of viruses by insect and tick vectors.p127-152. *In*, The arboviruses; epidemiology and ecology. T. P. Monath (*ed*). CRC Press, Inc, Boca Raton, FLA.

Tyler, K. L., Squier, M. K., Rodgers, S. E., Schneider, B. E., Oberhaus, S. M., *et al*. 1995. Differences in the capacity of reovirus strains to induce apoptosis are determined by the viral attachment protein sigma 1. *Jnl. Virol*. 69:6972-6979.

Ubol, S., Tucker, P. C., Griffin, D. E., Hardwick, J. M. 1994. Neurovirulent strains of Alphavirus induce apoptosis in bcl-2-expressing cells: Role of a single amino acid change in the E2 glycoprotein. *Proc. Natl. Acad. Sci. USA*. 91:5202-5206.

Ulmanen, I., Soderland, H., Kaariainen, L. 1976. Semliki Forest virus capsid protein associated with the 60S ribosomal subunit in infected cells. *Jnl. Virol*. 20:203-210.

Vanags, D. M., Porn-Ares, M. I., Coppola, S., Burgess, D. H., Orrenius, S. 1996. Protease involvement in fodrin cleavage and phosphatidylserine exposure in apoptosis. *Jnl. Biol. Chem*. 271:31075-31085.

Vaughan, L. M., Fitzpatrick, R. M., McKenna, B. and Atkins, G. J. 1998. Molecular approaches to fish vaccine design. p161-166. *In*, Methodology in fish disease research. A. Barnes, G. Davidson, M. Hiney and D. McIntosh (*eds*). Aberdeen Albion Press.

Vaux, D. L., Weissman, I. L., Kim, S. K. 1992. Prevention of programmed cell death in *Caenorhabditis elegans* by human bcl-2. *Science.* 258:1955-1957.

Vaux, D. L. and Korsmeyer, S. J. 1999. Cell death in development. *Cell.* 96:245-254.

Vile, R. G., Nelson, J. A., Castleden, S., Chong, H., Hart, I. R. 1994. Systemic gene therapy of mure melanoma using tissue specific expression of HSV*tk* gene involves an immune component. *Can. Res.* 54:6228-6234.

Vile, R. G., Russell, S. J., Lemoine, N. R. 2000. Cancer Gene Therapy: hard lessons and new courses. *Gene Ther.* 7:2-8.

Vincenz, C. and Dixit, V. M. 1997. Fas-associated death domain protein interleukin-1beta-converting enzyme 2 (FLICE2), anICE/CED-3 homologue, is proximally involved in CD95- and p55-mediated death signalling. *Jnl. Biol. Chem.* 272:6578-6583.

von Borndorff, C.-H. and Harrison, S. C. 1975. Sindbis virus glycoproteins form a regular icosahedral surface lattice. *Jnl. Virol.* 16:141-145.

Wahlberg, J. M., Bron, R., Wilschut, J., Garoff, H. 1992. Membrane fusion of Semliki Forest virus involves homotrimers of the fusion protein. *Jnl. Virol.* 66:7309-7318.

Wahlfors, J. J., Zullo, S. A., Loimas, S., Nelson, D. M., Morgan, R. A. 2000. Evaluation of recombinant alphaviruses as vectors in gene therapy. *Gene Ther.* 7:472-480.

Walker, N. P. C., Talanian, R. V., Hammill, L. D., Herzog, L. *et al.* 1994. Crystal structure of the cysteine protease interleukin-1B-converting enzyme; a (p20/p10)2 homodimer. *Cell.* 78:343-352.

Wang, K.-S., Schmaljohn, L., Kuhn, R. J., Strauss, J. H. 1991. Anti-idiotypic antibodies as probes for the Sindbis virus receptor. *Virology.* 181:694-702.

Wang, K. S., Kuhn, R. J., Strauss, E. G., Ou, S., Strauss, J. H. 1992. High-affinity laminin receptor is a receptor for Sindbis virus in mammalian cells. *Jnl. Virol.* 66:4992-5001.

Wang, H. G., Miyashita, T., Takayama, S., Sato, T., Torigoe, T., Krajewski, S., Tanaka, S., Hovey, L., Troppmair, J., Rapp, U. R. *et al.* 1994a. Apoptosis regulation by interaction of Bcl-2 protein and Raf-1 kinase. *Oncogene*. 9:2751-2756.

Wang, Y.-F., Sawicki, S. G., Sawaicki, D. L. 1994b. Alphavirus *nsP3* functions to form replication complexes transcribing negative-strand RNA. *Jnl. Virol*. 68:6466-6475.

Webb, A., Cunningham, D., Cotter, F., Clarke, P. A., di Stefano, F., Ross, P., Corbo, M., Dziewanowska, Z. 1997. BCL-2 antisense therapy in patients with non-Hodgkin lymphoma. *Lancet*. 349:1137-1141.

Welch, W. J. and Sefton, B. M. 1980. Characterisation of a small non-structural viral polypeptide present late during infection of BHK cells by Semliki Forest virus. *Jnl. Virol*. 33:230-237.

Welch, W. J., Sefton, B. M., Esch, F. S. 1981. Amino-terminal sequence analysis of alphavirus polypeptides. *Jnl. Virol*. 38:968-972.

Wengler, G. and Wengler, G. 1976. Localisation of the 26S RNA sequence on the viral genome type 42S RNA isolated from SFV-infected cells. *Virology*. 73:190-199.

White, C. L., Thomson, M., Dimmock, N. J. 1998. Deletion analysis of a defective interfering Semliki Forest virus RNA genome defines a region in the *nsP2* sequence that is required for efficient packaging of the genome into virus particles. *Jnl. Virol*. 72:4320-4326.

Wolter, K. G., Hsu, Y.-T., Smith, C. L., Nechushtan, A., Xi, X.-G., Youle, R. J. 1997. Movement of Bax from the cytosol to mitochondria during apoptosis. *Jnl. Cell Biol.* 139:1281-1292.

Wyllie, A. H. 1995. The genetic regulation of apoptosis. *Curr. Opin. Genet. Dev*. 5:97-104.

Xiang, J., Gomez-Navarro, J., Arafat, W., Liu, B., Barker, S. D., Alvarez, R. D., Siegel, G. P., Curiel, D. T. 2000. Pro-apoptotic treatment with an adenovirus encoding Bax enhances the effect of chemotherapy in ovarian cancer. *Jnl. Gene. Med.* 2:97-106.

Xu, H. J., Zhou, Y., Seigne, J., Perng, G. S., Mixon, M., Zhang, C. *et al.* 1996. Enhanced tumour suppressor gene therapy via a replication-deficient adenovirus vector expressing an N-terminal truncated retinoblastoma protein. *Can. Res*. 56:2245-2249.

Xu, M., Kumar, D., Srinivas, S., Detolla, L. J., Yu, S. F., Stass, S. A., Mixson, A. J. 1997. Parenteral gene therapy with *p53* inhibits human breast tumours *in vivo* through a bystander mechanism without evidence of toxicity. *Hum. Gene Ther*. 8:177-185.

Yam, P., Chow, W., Zaia, J. A., Yee, J. K. 1995. Comparison of pseudotype and amphotrophic retroviral mediated gene transfer into human hematopoietic progenitors and cell lines. *Can. Gene Ther.* 2:323.

Yamabe, K., Shimizu, S., Ito, T., Yoshioka, Y., Nomura, M., Narita, M., Saito, I., Kanegae, Y., Matsuda, H. 1999. Cancer gene therapy using a pro-apoptotic gene, caspase-3. *Gene Ther.* 6:1952-1959.

Yang, Y., Trinchieri, G., Wilson, J. M. 1995a. Recombinant IL-12 prevents formation of blocking IgA antibodies to recombinant adenovirus and allows repeated gene therapy to mouse lung. *Nature Med.* 1:890-893.

Yang, Y. L., Reis, L. F., Pavlovic, J., Agguzi, A., Schafer, R., Kumar, A., Williams, B. R., Aguet, M., Weissman, C. 1995b. Deficient signalling in mice devoid of double-stranded RNA-dependent protein kinase. *EMBO J.* 14:6095-6106.

Yang, E., and Korsmeyer, S. J. 1996. Molecular thanopsis: a discourse on the BCL2 family and cell death. *Blood.* 88:386-401.

Yang, J., Liu, X., Bhalla, K., Kim, C. N., Ibrado, A. M., Cai, J., Peng, T. I., Jones, D. P., Wang, X. 1997. Prevention of apoptosis by Bcl-2: a release of cytochrome *c* from mitochondria blocked. *Science.* 275:1129-1132.

Yang, L., Chiang, Y., Lenz, H.-J., Danenberg, K., Spears, C. P., *et al.* 1998. Intracellular communication mediates the bystander effect during Herpes Simplex thymidine kinase/gancyclovir-based gene therapy of human gastrointestinal tumour cells. *Hum. Gene Ther.* 9:719-728.

Yeung, M. C., Liu, J., Lau, A. S. 1996. An essential role for the interferon-inducible, double-stranded RNA-activated protein kinase PKR in the tumor necrosis factor-induced apoptosis in U937 cells. *Proc. Natl. Acad. Sci. USA.* 93:12451-12455.

Yin, X. M., Oltvai, Z. N., Korsmeyer, S. J. 1994. BH1 and BH2 domains of Bcl-2 are reqiured for inhibition of apoptosis and heterodimerisation with Bax. *Nature.* 369:321-323.

Ying, H., Zaks, T. Z., Wang, R.-F., Irvine, K. R., Kammula, U. S., Marincola, F. M., Leitner, W. W., Restifo, N. P. 1999. Cancer therapy using a self-replicating RNA vaccine. *Nature Med.* 5:823-827.

Yuan, J. *et al.* 1993. The *C. elegans* cell death gene *ced-3* encodes a protein similar to mammalian interleukin-1B-converting enzyme. *Cell.* 75:641-652.

Chapter 8

Publications and Presentations

8.1 Publications

Papers

1. Murphy, A-M., Morris-Downes, M. M., Sheahan, B. J., and Atkins, G. J. 2000. Inhibition of human lung carcinoma cell growth by apoptosis induction using Semliki Forest virus recombinant particles. *Gene Therapy*. Vol 7 (17), p1477-1482.

2. Murphy, A-M., Sheahan, B. J. and Atkins, G. J. 2000. Induction of apoptosis in Bcl-2-expressing prostate cancer cells using the Semliki Forest virus vector. *Jnl. Natl. Cancer Inst.*. Submitted for publication.

3. Fleeton, M. F., Chen, M., Berglund, P., Rhodes, G., Parker, S., **Murphy, A-M.**, Atkins, G. J. and Liljeström, P. 2000. Self-replicating RNA vaccines elicit protection against Influenza A virus, Respiratory Syncytial virus and a tick-borne encephalitis virus. *Journal of Infectious Diseases*. In press.

Abstracts

1. Murphy, A-M., Morris-Downes, M. M., Sheahan, B. J. and Atkins, G. J. 2000. Apoptosis induction and tumour regression mediated by recombinant Semliki Forest virus particles in non-small cell lung cancer. *Proc. Amer. Assoc. Can. Res.* April, p732.

8.2 Presentations

1. *Induction of apoptosis in human lung carcinoma cells by the Semliki Forest virus vector and inhibition of tumour growth in nude mice.*

A-M. Murphy, M. M., Morris-Downes, B. J. Sheahan and G. J. Atkins.

Oral presentation at the virus group session of the 145th Society of General Microbiology (SGM) meeting, in the University of Surrey, UK, on Thursday 6 January 2000.

2. *Apoptosis induction and tumour regression mediated by recombinant Semliki Forest virus particles in non-small cell lung cancer.*

A-M. Murphy, M. M. Morris-Downes, B. J. Sheahan and G. J. Atkins.

Poster presentation at the 91st annual American Association for Cancer Research (AACR) meeting, at the Moscone Centre, San Francisco, CA, USA, on Wednesday 5 April 2000.

3. *Apoptosis induction and tumour regression mediated by recombinant Semliki Forest virus particles in non-small cell lung cancer.*

A-M. Murphy, M. M. Morris-Downes, B. J. Sheahan and G. J. Atkins.

Poster presentation at the Irish Diagnostic Virology Group (IDVG) annual meeting, in Belfast NI, on Friday 19 May 2000.

Gene Therapy (2000) 7, 1477–1482
© 2000 Macmillan Publishers Ltd All rights reserved 0969-7128/00 $15.00
www.nature.com/gt

ACQUIRED DISEASES RESEARCH ARTICLE

Inhibition of human lung carcinoma cell growth by apoptosis induction using Semliki Forest virus recombinant particles

A-M Murphy[1], MM Morris-Downes[1], BJ Sheahan[2] and GJ Atkins[1]
[1]Department of Microbiology, Moyne Institute of Preventive Medicine, Trinity College, Dublin; and [2]Department of Veterinary Pathology, Faculty of Veterinary Medicine, University College, Ballsbridge, Dublin, Ireland

We have utilised cell cultures and growth of tumours in nude mice to assess further the potential of the Semliki Forest virus (SFV) vector as a cancer therapy agent. This vector is a transient RNA-based expression vector, and we have previously shown that SFV and its derived vector can induce p53-independent apoptosis by expression of the nonstructural region of the virus genome. Apoptosis induction is therefore an inherent property of the vector and is not dependent on heterologous gene expression. SFV recombinant suicide particles (rSFV) were shown to induce apoptosis in H358a cells, which are human non-small cell lung carcinoma cells deleted in p53. EGFP-expressing rSFV also inhibited the growth of developing H358a spheroids. Direct injection of rSFV into H358a tumours subcutaneously implanted as xenografts in nu/nu mice inhibited tumour growth, and in some cases caused complete regression. It is concluded that tumour growth suppression induced by rSFV was due to apoptosis induction and that the vector has an inherent cell death-promoting and antitumour activity. These results, as well as previous work by other authors on targeting and immune stimulation using alphavirus vectors, indicate that SFV recombinant particles in particular have considerable potential for further exploitation as a cancer therapy agent. Gene Therapy (2000) **7**, 1477–1482.

Keywords: *cancer gene therapy; lung carcinoma; virus vector; apoptosis; alphavirus; Semliki Forest virus*

Introduction

Several types of virus vector are currently under development as tumour therapy agents. Previous studies have indicated that *p53* gene replacement strategies, using recombinant viral vectors, can induce apoptosis and suppress tumour growth in p53-defective tumour cells. Adenovirus and retrovirus vectors have been the leading candidates for cancer gene therapy,[1,2] and adeno-associated virus has also proved successful in the transduction of this tumour suppresser gene.[3] Inactivation of *p53* has been implicated in many types of tumour,[4] and non-small cell lung carcinoma (NSCLC) is one of the most common human cancers in which *p53* mutations have been frequently identified. However, not all tumours are amenable to therapy with p53, and there is a need for the development of vectors which induce apoptosis independently of p53. In this report, we further evaluate the potential of a newly developed system, Semliki Forest virus recombinant particles (labelled rSFV), as a cancer therapy agent. This vector system may have several advantages over the retro- and adenovirus systems currently under development, particularly its inherent capacity to induce p53-independent apoptosis.

SFV, an enveloped positive-sense RNA virus, has been developed as a transient expression vector,[5–7] and has been utilised in the development of prototype recombinant vaccines.[7–9] In the vector, the SFV structural proteins, which are formed in large amounts in infected cells by a gene amplification mechanism, are replaced with a polylinker sequence, which facilitates insertion of a heterologous gene. This does not affect the replication capacity of the vector and structural proteins are supplied *in trans* by helper RNAs to form recombinant encapsidated particles. Such particles can be produced at high titres, and will infect cells and express a heterologous gene cloned into the multicloning site of the vector. They are capable of only one round of multiplication upon infection, and are thus suicide particles. In terms of cancer therapy, SFV offers an important advantage over other vectors, since previous studies show that SFV induces apoptosis in cultured cells,[7,10,11] and this can occur in the absence of viral structural protein genes and independently of the *p53* status of infected cells.[11] Thus, unlike alternative vectors, rSFV does not depend solely on the heterologous gene for apoptosis induction.

In this study, we used encapsidated rSFV particles to infect *p53*-deleted human NSCLC cells to determine the effects on tumour cell growth *in vitro* and *in vivo*. The multicloning site contained the reporter gene *EGFP* to facilitate detection of the vector *in situ*. The results indicate that SFV recombinant particles can inhibit the growth of human lung carcinoma cells and induce tumour regression by apoptosis induction, in the absence of heterologous gene expression.

Correspondence: GJ Atkins, Department of Microbiology, Moyne Institute, Trinity College, Dublin 2, Ireland
Received 14 April 2000; accepted 30 May 2000

Results

Transduction of H358a cells

The conditions for optimal viral transduction of the H358a lung carcinoma cell line with SFV recombinant particles were determined by infecting cells with EGFP-expressing rSFV particles (rSFV-EGFP) using a range of different MOIs (Figure 1). A linear relationship existed between the number of infected cells and the MOI used, up to a MOI of 100. At MOI 400, almost 50% of H358a cells were positive for the vector, and this was improved using multiple infections (data not shown).

Effects of rSFV particles on cell growth in vitro

H358a cells were incubated with rSFV-EGFP, rSFV-1 or medium alone for 1 h and the medium replaced. rSFV-1 particles lack a reporter gene and contain the vector backbone only. Cell growth and viability were estimated by cell count (Figure 2a) and colorimetric assays (Figure 2b). In both assays, mock-infected cells continued to grow and proliferate, whereas the survival rate of rSFV-EGFP-infected cells was greatly reduced, with less than 50% of cells surviving after 1 day and only 10% after 1 week. Tumour cell growth was similarly inhibited on infection with rSFV-1. Values for both assays were reproduced in four independent experiments. Similar results were obtained with rSFV-LacZ particles (data not shown). Thus, infection with rSFV particles suppresses H358a cell growth and this occurs independently of the heterologous gene.

Due to the marked decrease in H358a cell viability on infection with rSFV, we examined if this were due to the induction of apoptosis. Chromosomal DNA was extracted from cells infected with rSFV-EGFP (Figure 2c) or medium alone, and was analysed by agarose gel electrophoresis. The appearance of 180–200-bp DNA fragments and their multiples, formed by internucleosomal cleavage, is characteristic of apoptotic cell death. This was demonstrated at 24 and 48 h after infection with rSFV-EGFP particles (Figure 2d). Fragmented DNA was not observed in mock-infected controls. These results were confirmed using TUNEL staining (not shown), and were similar to those obtained previously using transfected vector RNA.[11]

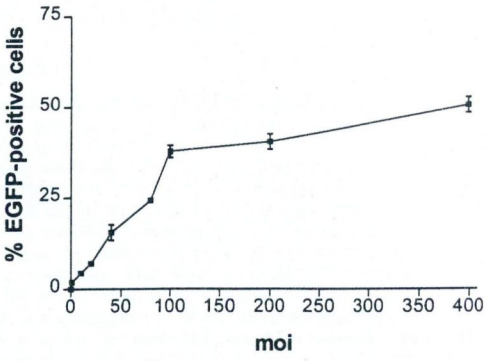


Figure 1 *Transduction efficiency of NSCLC cell line H358a. Recombinant SFV particles expressing EGFP (rSFV-EGFP) were used to infect cells at different MOIs ranging from 1 to 400. The percentages of EGFP-expressing cells were obtained by scoring 600 cells, each on triplicate dishes, error bars indicate standard deviation.*

Effect of rSFV infection on spheroids

Multicellular spheroids are composed of tumour cells growing in culture as three-dimensional structures, simulating the growth and microenvironmental conditions of tumours *in vivo*.[12] The cytotoxic efficiency of rSFV particles was further evaluated in H358a cells growing as tumour spheroids. Following 36 h in culture, individual H358a spheroids were placed in medium alone, or medium containing rSFV-EGFP. We then compared the relative abilities of these spheroids to proliferate. At 24 h after treatment, mock-infected spheroids incorporated at least eight times the amount of ^{3}H-thymidine compared with those treated with the vector (Figure 3a). The results of the MTS viability assay were similar to those of the cell proliferation assay (Figure 3b). A four-fold difference in spheroid viability was demonstrated after 6 days in culture. Similar results were obtained in three separate experiments.

Effect of rSFV administration on tumour growth in nude mice

To address the potential therapeutic efficiency of the rSFV particles *in vivo*, H358a cells were injected subcutaneously into *nu/nu* mice to form xenografts, and tumours of 4 mm in diameter were allowed to develop. Mice received a direct intratumoral injection of 50 µl of either TNE buffer alone, or TNE buffer containing rSFV-EGFP particles (1×10^{10} IU/ml) daily for 3 days (Figure 4a). In mice treated with TNE buffer, tumours continued to grow rapidly throughout the treatment. Mice treated with rSFV-EGFP showed a marked inhibition of tumour growth as early as day 4 after treatment. At 30 days after injection, tumour growth was reduced five-fold in comparison to controls.

The growth inhibitory effect was more pronounced after two treatment cycles (Figure 4b). Mice received intratumoral injections of TNE buffer or rSFV-EGFP particles each on days 1, 2, 3 and days 7, 8 and 9. Six injections with rSFV-EGFP reduced the size of tumours by 95% in comparison to controls. Three of the seven treated tumours showed complete regression on macroscopic examination, and no signs of regrowth were observed, even at 135 days after treatment. Similar results were observed in two separate experiments.

Histopathological examination of tumours injected with TNE buffer only revealed well-demarcated, densely cellular nodular masses located in the subcutis. The tumour cells had distinct cell borders and oval hyperchromatic nuclei with prominent nucleoli. Numerous mitotic figures and apoptotic forms were present together with occasional small foci of oncotic necrosis. Tumours treated once with rSFV-EGFP and sampled at 4 days after treatment were characterised by large coalescent areas of oncotic necrosis (Figure 4d); apoptosis was also common. Small aggregates of lymphoid cells and neutrophils were present among fibroblastic cells that partially encircled the tumour nodules. The vector was detected by EGFP fluorescence in treated tumours no earlier than 16 h after injection and persisted for 3 days (Figure 4c). Positive TUNEL reactivity was detected as early as 8 h after treatment with the vector, reaching maximum reactivity at 24

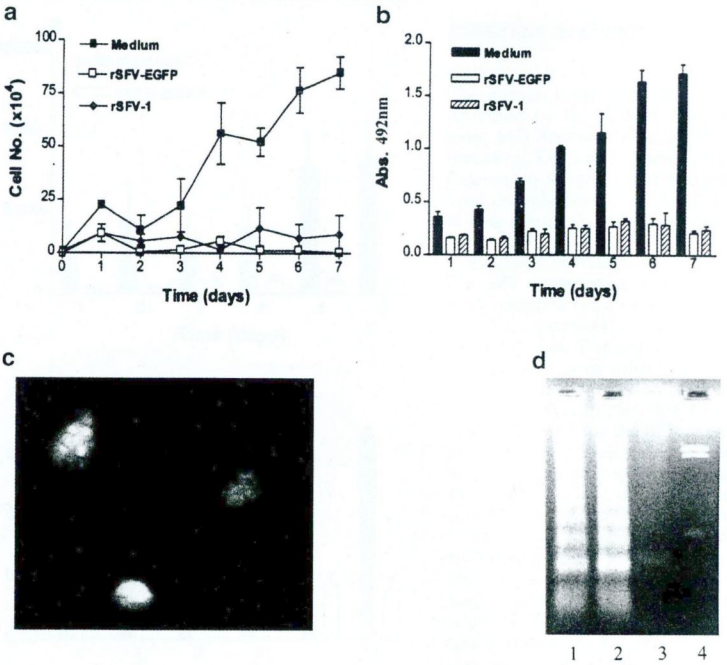


Figure 2 Cell viability and apoptosis induction in H358a cells following infection with rSFV-EGFP. (a and b) H358a cells were incubated at densities of 1 × 10⁴ cells/well in six-well plates, and infected with rSFV-EGFP, rSFV-1 (MOI = 100) or medium alone. (a) Cell count assay. At each indicated time-point, triplicate wells were trypsinised and counted by trypan blue exclusion. (b) Cells from triplicate wells were fixed, stained and surviving cells were measured colorimetrically using an ELISA reader. (c) Expression of EGFP in H358a cells 16 h after infection with rSFV-EGFP (× 400). (d) DNA fragmentation analysis of control and rSFV-EGFP-infected cells. DNA was extracted from cells and analysed by agarose gel electrophoresis. Lanes 1 and 2, DNA from rSFV-EGFP-infected cells at 24 and 48 h after infection, respectively; lane 3, DNA from mock-infected control cells at 24 h; lane 4, λ HindIII DNA molecular weight markers.

h and approached control levels after 1 week (Figure 4c, e). Control tumours exhibited neither EGFP fluorescence nor large areas of TUNEL reactivity.

Discussion

As an expression system, rSFV has already proved successful in treating murine tumours via the anti-angiogenic effects of interleukin-12.[13] In this study, we have shown that direct infection with rSFV particles can inhibit tumour growth and induce regression in the *p53*-deleted human NSCLC cell line H358a. Growth suppression and tumour regression have been previously demonstrated in this cell line by restoring wild-type *p53* activity and inducing apoptosis. This was achieved using adenoviral,[14] retroviral[15] and adeno-associated[3] viral vectors. SFV-induced apoptosis can occur independently of *p53* expression, and in our study rSFV particles contained the reporter gene *EGFP*. Expression of this gene did not contribute to the induction of apoptosis but was necessary to facilitate detection of the vector *in situ*. Pathological analysis of rSFV-treated tumours indicated that inhibition of tumour growth was not due to the induction of an immune response, but was consistent with an initial induction of apoptosis followed by a large depletion of tumour cells by oncotic necrosis.[16]

SFV also offers several other advantages over retrovirus and adenovirus vector systems. It is a transient RNA-based expression system, and this obviates nuclear complications such as random RNA splicing or host chromosomal integration. rSFV particles are very stable and can be concentrated to titres exceeding 10^{10} infectious units per millilitre. The vector also has the ability to infect both dividing and non-dividing cells. The treated mice in this study remained healthy, and no gross lesions were detected in the tissue surrounding the tumour. This may be because rSFV particles adsorb rapidly to cells at the injection site and are capable of one round of multiplication only. Our unpublished results indicate that dispersal of rSFV particles from the injection site to other organs is transient, and that no detectable tissue damage occurs. Unlike DNA vectors, which disperse in the host and persist for many weeks following administration,[17] rSFV vector RNA persists for 7 days only as detected by RT-PCR (MM Morris-Downes and GJ Atkins, unpublished results).

This study and previous work by other authors has promising implications for tumour therapy. We have

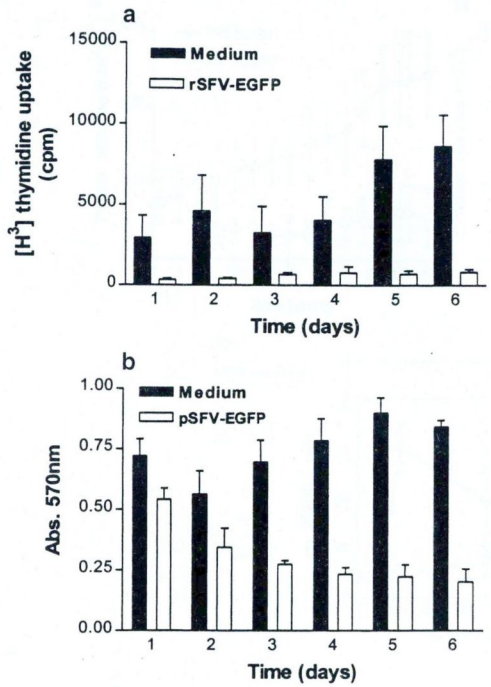


Figure 3 Effects of rSFV-EGFP on the growth of H358a spheroids as assessed by (a) ^{3}H-thymidine incorporation; and (b) cell viability (MTS) assay. On day 0, spheroids were exposed to rSFV-EGFP (MOI = 100) or medium alone for 24 h, and spheroid viability was monitored daily for 6 days. Points represent the means of triplicate wells.

shown here that the SFV vector has inherent cell death-promoting and antitumour activity which acts independently of p53. However, the cell killing ability of the vector in its present form is relatively low, necessitating multiple treatments to induce efficient cell killing of cultured cells. In tumour tissue, cell killing may be enhanced by a possible bystander effect, or an effect on angiogenesis leading to oncotic necrosis. Replacing the reporter gene *EGFP* with a known pro-apoptotic gene such as *bax* could serve to augment further the cell death-promoting capability of this vector in NSCLC and other tumours, and may serve to counteract the action of anti-apoptotic genes such as *bcl-2*. As has been recently shown with both naked SFV RNA and rSFV particles, it may also be possible to augment antitumour immune responses by expression of immunogenic proteins.[18,19] Attempts have been made with other vectors, including the Sindbis vector (an alphavirus-based vector like SFV), to target vectors to tumour cells by modification of viral structural proteins.[20] This strategy could also be applied to the SFV system, possibly by modification of the viral E2 protein to recognise tumour-specific receptors. We feel that the unique properties of SFV could be further exploited to develop a safe and effective vector for cancer gene therapy.

Materials and methods

Cells

The human lung carcinoma cell line H358a was kindly provided by Dr JA Roth (Department of Thoracic Surgery, MD Anderson Cancer Center, University of Texas, Houston, TX, USA). These cells contain a homozygous deletion in the *p53* gene[4] and were propagated in RPMI 1640 supplemented with 10% heat-inactivated foetal bovine serum (Life Technologies, Paisley, UK).

Preparation of recombinant SFV vector

The SFV vector system, and a vector expressing *EGFP*, were obtained from Professor P Liljeström, Microbiology and Tumorbiology Center, Karolinska Institute, Stockholm, Sweden. The production of recombinant SFV RNA and generation of fully infectious vector particles have been described previously.[6] Briefly, BHK-21 cells were cotransfected with rSFV RNA and two helper RNAs, one of which codes for the SFV capsid protein, the other for the envelope proteins. These RNAs were transcribed *in vitro* from the appropriate plasmids; particles expressing *EGFP* (rSFV-EGFP), or with no heterologous cloned gene (ie vector alone, rSFV-1), were produced. After 24 h incubation, fully infectious virus particles containing the recombinant gene were harvested. Titration was performed by direct (rSFV-EGFP) or indirect epifluorescence using antiserum to the SFV non-structural proteins (rSFV-1). For *in vivo* experiments, virus particles were concentrated by ultracentrifugation through a 20% (w/v) sucrose cushion (Beckman SW40 rotor; 25000 r.p.m. for 1.5 h at 4°C; Beckman Coulter, Fullerton, CA, USA). Virus pellets were resuspended in TNE buffer (50 mM Tris-HCL, pH 7.4, 100 mM NaCl, 0.1 mM EDTA) and titres were determined as before.

Cell death analysis

To measure growth and cytotoxicity in cultured cells, H358a cells were plated at a density of 1×10^4 cells per well in six-well plates and infected with rSFV-EGFP or rSFV-1 particles (MOI = 100). Medium alone was used as a mock-infection control. Cells were harvested and counted daily for 7 days. Cell viability was determined by trypan blue exclusion and each sample was counted in triplicate. The cytotoxicity of both vector constructs was also assessed using a colorimetric assay.[21] H358a cells (1×10^4) in six-well dishes were infected as before. At 24 h intervals, cells were fixed in 5% trichloroacetic acid, washed, air dried, and stained for 20 min with 0.4% (w/v) sulphorhodamine B (Sigma Chemical, St Louis, MO, USA) in 1% acetic acid. Absorbance values were measured at 492 nm using an ELISA reader, and were directly related to the total number of surviving cells.

To detect the internucleosomal DNA fragments characteristic of apoptosis, DNA was isolated from rSFV-EGFP-infected and mock-infected H358a cells at 24 h and 48 h after infection. Cells were treated with lysis buffer (20 mM EDTA, 100 mM Tris, pH 8, 0.8% w/v sodium lauryl sarcosinate), followed by ribonuclease A (10 mg/ml; Sigma) at 37°C for 2 h and proteinase K (20 mg/ml; Sigma) digestion for 18 h. Samples were subjected to electrophoresis on a 1.5% agarose gel and visualised by ethidium bromide staining. TUNEL staining, characteristic of apoptosis *in situ*, was performed as described previously.[11] Cells were fixed in 4% paraformaldehyde, per-

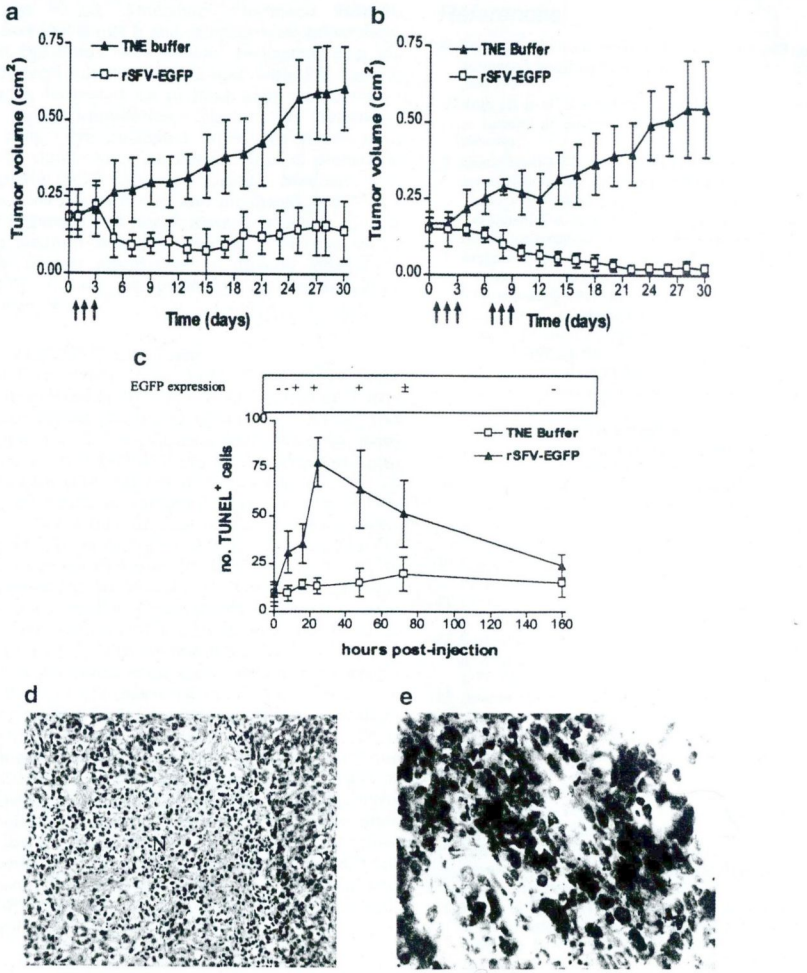


Figure 4 *Effects of rSFV-EGFP treatment on tumour growth in vivo. (a and b) H358a cells (10^6) were injected subcutaneously into Balb/c nu/nu mice. On reaching diameters of 4 mm (approximately 15–20 days), tumours received (a), three, or (b) six intratumoral injections of rSFV-EGFP (5×10^8 IU) or TNE buffer. Tumour diameters were measured without knowledge of treatment groups. Five to seven mice were used per treatment group; arrow, day of treatment. (c) Composite representation of EGFP expression and TUNEL staining after one intratumoral injection. (d and e) Histology and TUNEL staining of tumours. (d) Tumour 4 days after treatment with rSFV-EGFP. An area of oncotic necrosis (N) is surrounded by tumour cells. H&E, × 200. (e) TUNEL staining of a treated tumour 24 h after treatment with rSFV-EGFP. An intense area of TUNEL staining (black) is shown (× 400).*

meabilized in 0.1% Triton X-100 solution and labelled using terminal transferase and horseradish peroxidase (Boehringer Mannheim, Indianapolis, IN, USA). Colorimetric detection was performed using diaminobenzidine.

Spheroid culture

Multicellular spheroids were prepared by the liquid overlay technique.[22] A total of 10^4 H358a cells in 0.1 ml of complete medium were plated in 96-well plates, whereas 10^5 cells in 1 ml were used in 24-well plates. To prevent cell attachment, plates were coated with 1% medium agar. After 1–2 days incubation, aggregates formed in each well, with all suspended cells contributing to the formation of a single spheroid. To determine the proliferation of H358a cells as three-dimensional spheroids, cells were plated in 24-well plates for 36 h and then infected with rSFV-EGFP (MOI = 100) or with medium alone. The spheroids were then incubated with ^{3}H-thymidine (2

μCi/well in 50 μl; Amersham Pharmacia Biotech, Uppsala, Sweden) for 24 h and samples were taken daily for 6 days. Spheroids were washed, resuspended in 1% sodium dodecyl sulfate, precipitated with 5% trichloroacetic acid, harvested on to filter mats and counted using a liquid scintillation counter. To determine viability, cells were incubated in 96-well plates with additions as above. After incubation, 20 μl of phenazine methosulphate (MTS reagent; Promega, Madison, WI, USA) was added to each well and incubated at 37°C for 4 h. MTS is bioreduced into formazan which is soluble in culture medium and was detected at 570 nm using an ELISA reader; absorbance is directly related to cell viability. Results are presented as the means of triplicate samples.

Inhibition of tumour growth in vivo

Female Balb/c *nu/nu* mice aged 50–60 days were obtained from Harlan (Bicester, UK), and were maintained under barrier conditions with sterilised food and water supplied *ab libitum*, in accordance with the principles set down in SI 17/94 European Communities regulations, 1994 for care and use of laboratory animals. To determine inhibition of tumour growth *in vivo*, H358a cells (1×10^6 in 0.4 ml complete medium) were injected into the right flank of each mouse to form xenografts. On reaching a diameter of 4 mm, 50 μl of TNE buffer alone or TNE containing rSFV-EGFP (1×10^{10} IU/ml) was injected intratumorally. Three separate analyses were performed; one with a single injection (on day 1), three injections (days 1, 2, 3) or six injections (days 1, 2, 3, and 7, 8, 9). Five to seven mice were used per treatment group. Tumours were measured every 2 days with calipers in two perpendicular diameters without knowledge of the treatment groups. Tumour volume was calculated by assuming a spherical shape, with the average tumour diameter calculated as the square root of the product of the cross-sectional diameters. Tumours which received one injection only were harvested from 8 h to 8 days after infection for pathological examination. Direct epifluorescence and TUNEL were performed on paraformaldehyde-fixed tumour cryosections. Haematoxylin and eosin (H&E) staining was performed on formalin-fixed, paraffin-embedded sections.

Acknowledgements

We thank Dr Marina Fleeton and Professor Peter Liljeström for providing the vectors used in this study and for help with the vector system, and Ms Marie Moore for her assistance with pathological studies. We are also grateful to Ms Deborah Mansfield and Dr Jack Roth for providing the H358a cells. This work was supported by the Cancer Research Advancement Board of the Irish Cancer Society, the Irish Health Research Board, BioResearch Ireland, the Wellcome Trust and the European Union Biotechnology Programme.

References

1 Swisher SG *et al*. Adenovirus-mediated p53 gene transfer in advanced non-small-cell lung cancer. *J Natl Cancer Inst* 1999; **91**: 763–771.
2 Roth JA *et al*. Retrovirus-mediated wild-type *p53* gene transfer to tumors of patients with lung cancer. *Nature Med* 1996; **2**: 985–991.
3 Quazilbash MH *et al*. Cancer gene therapy using a novel adeno-associated virus vector expressing human wild-type *p53*. *Gene Therapy* 1997; **4**: 675–682.
4 Takahashi T *et al*. p53: A frequent target for genetic abnormalities in lung cancer. *Science* 1989; **246**: 491–494.
5 Berglund P *et al*. Semliki Forest virus expression system: production of conditionally infectious recombinant particles. *Bio/Technology* 1993; **11**: 916–920.
6 Smerdou C, Liljeström P. Two-helper RNA system for production of recombinant Semliki Forest virus particles. *J Virol* 1999; **73**: 1092–1098.
7 Atkins GJ, Sheahan BJ, Liljeström P. The molecular pathogenesis of Semliki Forest virus: a model virus made useful? *J Gen Virol* 1999; **80**: 2287–2297.
8 Berglund P *et al*. Immunization with recombinant Semliki Forest virus induces protection against influenza challenge in mice. *Vaccine* 1999; **17**: 497–507.
9 Fleeton MN *et al*. Recombinant Semliki Forest virus particles expressing louping ill virus antigens induce a better protective response than plasmid-based DNA vaccines or an inactivated whole particle vaccine. *J Gen Virol* 2000; **81**: 749–758.
10 Glasgow GM *et al*. Death mechanisms in cultured cells infected by Semliki Forest virus. *J Gen Virol* 1997; **78**: 1559–1563.
11 Glasgow GM *et al*. The Semliki Forest virus vector induces *p53*-independent apoptosis. *J Gen Virol* 1998; **79**: 2405–2410.
12 Sutherland RM. Cell and environment interactions in tumor microregions: the multicell spheroid model. *Science* 1988; **240**: 177–184.
13 Asselin-Paturel C *et al*. Transfer of the murine interleukin-12 gene *in vivo* by a Semliki Forest virus vector induces B16 tumor regression through inhibition of tumor blood vessel formation monitored by Doppler ultrasonography. *Gene Therapy* 1998; **5**: 606–615.
14 Fujiwara T *et al*. Induction of chemosensitivity in human lung cancer cells *in vivo* by adenovirus-mediated transfer of the wild-type *p53* gene. *Cancer Res* 1994; **54**: 2287–2291.
15 Fujiwara T *et al*. Therapeutic effect of a retroviral wild-type p53 expression vector in an orthotopic lung cancer model. *J Natl Cancer Inst* 1994; **86**: 1458–1462.
16 Majno G, Joris I. Apoptosis, oncosis, and necrosis. An overview of cell death. *Am J Pathol* 1995; **146**: 3–15.
17 Donnelly JJ *et al*. DNA vaccines. *Ann Rev Immunol* 1997; **15**: 617–626.
18 Ying H *et al*. Cancer therapy using a self-replicating RNA vaccine. *Nature Med* 1999; **5**: 823–827.
19 Colmenero P *et al*. Induction of P815 tumor immunity by recombinant Semliki Forest virus expressing the P1A gene. *Gene Therapy* 1999; **6**: 1728–1733.
20 Ohno K *et al*. Cell-specific targeting of Sindbis virus vectors displaying IgG-binding domains of Protein A. *Nature Biotech* 1997; **15**: 763–768.
21 Skehan P *et al*. New colorimetric cytotoxicity assay for anticancer-drug screening. *J Natl Cancer Inst* 1990; **82**: 1107–1112.
22 Korff T, Augustin HG. Integration of endothelial cells in multicellular spheroids prevents apoptosis and induces differentiation. *J Cell Biol* 1998; **143**: 1341–1352.